Medicinal Chemistry Division, Cardiff school of Pharmacy and Pharmaceutical Sciences, Cardiff University

Development of Novel Antibacterial Agents through the Design and Synthesis of Aminoacyl tRNA Synthetase (AaRS) Inhibitors

A thesis submitted in accordance with the conditions governing candidates for the degree of

Philosophiae Doctor in Cardiff University

Hanadi Asiri

Supervisors:

Dr. Claire Simons

Dr. Efi Mantzourani

December 2020

Acknowledgements

Thanks **God Almighty** for good health, peace of mind and the strength to finish this research despite the difficult situations. Thanks God, for giving me chance to know **Dr. Claire Simons**.

I would like to express my sincere gratitude to my supervisor **Dr. Claire Simons** for her continuous support, guidance, teaching, patience, enthusiasm and endless helping throughout my PhD journey. The completion of this thesis could not have been possible without her valuable experience.

I would like to thank **Dr. Efi Mantzourani** for her support and valuable advice throughout the course of this research.

Thanks to the EPSRC mass spectrometry service centre, **Shaun Reeksting** from Bath University and Medac Ltd. for the accurate mass, HPLC measurements and the microanalysis determination.

A Big thank to **Jennifer Richard**, **Dr. Mandy Wootton**, **Casey Hughes** and **Dr. James Bullard** for the antimicrobial screening test and aminoacylation assay results.

Finally, many thanks to all the members in **Cardiff University** who help and encourage me and do not forget to thank my mum (Aminah Al-Anbar), sisters (Al-Anoud and Alaa Asiri), brother (Abdullah Asiri), children (Amal, Yaser, Yazen and Nouf) and my husband (Musaad Al-Makhilib) for their unconditional support, love and encouragement.

In the name of God, most gracious, most Merciful

This thesis is dedicated to my supervisor (**Claire Simons**) for her support

Read! In the Name of your Lord who has created ❶ He has created man from a clot ❷ Read! And your Lord is the most Generous ❸ Who has taught (the writing) by the pen ❹ He has taught man that which he knew not ❺ Nay! Verily, man does transgress (in disbelief and evil deed) ❻ Because he considers himself self-sufficient ❼ Surely, to your Lord is the return❽

Surah Al-Alag (The Clot) (96)

Abstract

Antimicrobial resistance is a global public health issue which significantly threatens human life. There are approximately 50,000 deaths in the USA and Europe per year owing to antimicrobial resistance infections. This burden of resistance has increased resulting in an increase in morbidity and mortality in clinical and community setting. Thus, global collaborative action is needed for developing effective strategies to combat antimicrobial resistance. International and local approaches including antimicrobial surveillance, guidelines for treatment of bacterial infections, regulation of the availability of antibiotics, improving hand hygiene, understanding the mechanism of bacterial resistance and development of new antimicrobial agents have been advised.

Aminoacyl tRNA synthetases are valuable targets for antibiotic development as they have a fundamental role at a cellular level during the translation process of the genetic code. Mupirocin (Bactroban ®) is an approved isoleucine tRNA synthetase inhibitor which is used for the treatment of methicillin resistant *Staphylococcus aureus* (MRSA). High and low level of mupirocin resistance has been demonstrated in most *S. aureus* isolates due to acquired plasmid-mediated mupA, which encodes a novel IleRS and mutation, respectively. Thus, the design of multitarget aminoacyl tRNA synthetases inhibitors could be an effective way to make significant reductions in the biological fitness of bacteria leading to a reduction in drug resistant microorganisms.

Class IIb aminoacyl tRNA synthetases of which AspRS and AsnRS belong is a target of the project in *Staphylococcus aureus* and *Enterococcus faecalis*. A computational study of both enzymes in both microorganisms including homology modelling, validation techniques, molecular dynamics and docking of the natural substrates (aa-AMP) were used to be a platform for the design of dual site inhibitors containing a sulphamoyl linkage which mimic aa-AMP in both enzymes. Different series of AspRS/AsnRS inhibitors were designed to occupy both pockets of the target enzymes then synthesised after optimisation their synthetic routes. The minimum inhibitory concentration of compounds against a panel of microorganisms were evaluated compared with ciprofloxacin as the standard and one compound showed good inhibitory activity against *Enterococcus faecalis* (MIC = 2 µg/mL).

Content

Figures

Tables

Schemes

Abbreviations

AdT: Aminotransferases

AMR: antimicrobial resistance

CA-MRSA: Community acquired MRSA

DNA: Deoxyribonucleic acid

GDP: Gross Domestic Product

GIT: Gastrointestinal tract

GPs: general practices

HA-MRSA: Hospital acquired MRSA

ICU: Intensive care unit

MHRA: The Medicines and Healthcare Products Regulatory Agency

MOE: Molecular Operating Environment

MRSA: Methicillin resistant *Staphylococcus aureus*

ND: non-discriminated

NHS: National Health Service

NICE: National Institute for Health and Care Excellence

ORFs: Open reading frames

RNA: Ribonucleic acid

tRNA: Transfer RNA

VMD: The Veterinary Medicines Directorate

WHO: World Health Organisation

UTI: Urinary tract infection

Chapter 1: Introduction

1. Introduction

1.1. Antimicrobial resistance (AMR)

Antimicrobial resistance is a global public health issue with significant implications on human life. That burden of resistance has increased resulting in an increase in mortality and morbidity in clinical and community setting. There are approximately 50,000 deaths in the United States of America (USA) and Europe per year with many hundreds of thousands more dying in other areas of the world owing to antimicrobial resistance infections (1, 2). It is reported that there are almost 2 million cases of infection in the USA as a direct consequence of resistant bacteria infection with total cost of $20 billion (3). In addition, there are about 4,000,000 surgical procedures which are performed in England and using antibiotics for most of them is essential to prevent infections either pre or post operation (4). One fourth of births in the United Kingdom (UK) are delivered by caesarean section where antibacterial agents are used for infant and mother protection. Also, the majority of females in the UK suffer from urinary tract infection (UTI) at some point in their lives and they need antibiotic for infection treatment (4). AMR has become a global concern because most of microorganisms have a great adaptability to resists not only the current antibiotics, but also, the new antibacterial agents. While in the 1960s, 70s, and 80s, resistance was not a clinical problem as a large number of new antibiotics had appeared on the market, that diversity of antibacterial agents is no longer available and rapid antibacterial drug discovery has been deprioritised with the most new antibacterial agents based on chemical structures discovered 30 or more years ago (Figure 1). For example, the latest registered new antibacterial agents are linezolid, daptomycin, and the topical medications retapamulin and tavaborole which were introduced in 2000, 2003, 2007 and 2014 respectively, but their chemical classes -oxazolidinones, acid lipopeptides, pleuromutilins and aminoacyl tRNA synthetases- were first reported in 1978, 1987, 1952 and 1988 respectively (5,6,7,8). This reflects considerably on human and economic cost, with the continuous rise in resistance reported to lead to 10 million people dying every year and by 2050, Gross Domestic Product (GDP) may be reduced by 2% to 3.5% costing the world up to 100 trillion USD (4, 9). The ability to treat general infectious disease will be reduced causing a greater risk of complications and prolonged illness beside compromising advances in other medical fields such as organ

transplantation, cancer chemotherapy and major surgery. All of these AMR consequences will increase the economic burden on health care system, families and societies (2). Thus, the aim of the October 2017 call in Berlin is for a global action against antibiotic resistance included a review focussed on the collaborative work to understand the implications of AMR and proposed international solutions for addressing AMR (1, 10). As antimicrobial resistance is a natural phenomenon, it is accelerated by several actions, such as inappropriate prescribing, poor infection control practices and the use of antimicrobial agents in agriculture (9). The lack of public awareness and understanding of how the misuse of antibiotic contributes to AMR was highlighted by work conducted by both the WHO (11) and the Wellcome Trust (12). The work of the WHO and Wellcome Trust confirmed that there was a notable gap in public understanding with two third of people not understanding how AMR could affect even though they know it is an issue and participants in the research also believing that antibiotics are just for colds and flu treatment. The majority of participants thought that the body becomes resistant to antibiotics not bacteria and the problem comes from using them regularly (12). In general, the participants did not have an idea about the proper use of antibiotics in terms of the treatment course with some participants skipping doses or sharing with others when they feel a little improvement (13). With these misconceptions and absence of infection control practice, the AMR problem is exacerbated especially in cases of poor diagnosis. Seventy-six percent of general practices (GPs) prescribe antibiotics without checking if the infection is due to bacteria or not (14). Using antibiotics in agriculture is furthermore driving the resistance in the same way that it does in humans, with the extensive use of antibiotics in agriculture considered as a risk to human health owing to transmission of the resistant microbes to human (15). In the USA, animals consume 70%, and humans 30% of the medically antibiotics (15). As a consequence, the environment is significantly affected by resistance that comes from human, animal and antibiotic waste. Resistance has been observed in terrestrial and aquatic environments as well as in UK wildlife as a result of widespread manufacture of antibiotics (16). International and local approaches for effective strategies to combat antimicrobial resistance are needed including antimicrobial surveillance, guidelines for bacterial infections treatment, regulation of the availability of antibiotics, reduction in

the unnecessary use of antimicrobials in agriculture, a global public awareness campaign on AMR, improving hand hygiene, understanding the mechanism of bacterial resistance, and development of new antimicrobial agents (10). In the UK, the role has been played by the government is essential in continuing international work on AMR through focusing on three strategic aims; improvement in the understanding and knowledge of AMR, ensuring existing treatments stay effective and new anti-infective agents to slow the spread and development of AMR. The National Health Service (NHS), National Institute for Health and Care Excellence (NICE) and the Medicines and Healthcare Products Regulatory Agency (MHRA) are responsible for leading on the strategy while the Veterinary Medicines Directorate (VMD) (2, 16) regulates the use of medicines in agriculture and aquaculture. Research development is additionally supported, and the UK considers international intergovernmental co-operation to be essential in the development of new antibiotics (2).

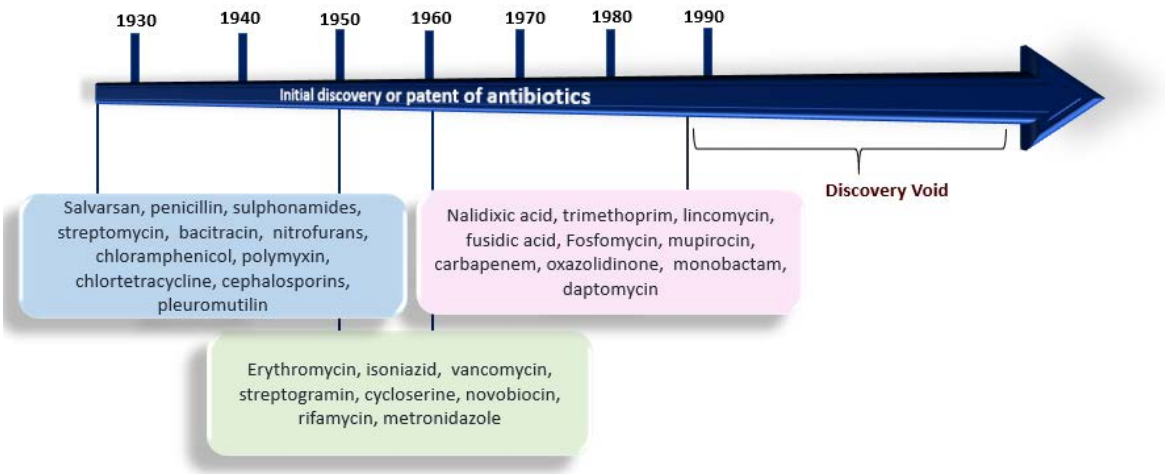

Figure 1: Dates related to antibiotics discovery with an illustration of the discovery void. Figure modified from L. Silver (17).

1.2. Mechanism of bacterial resistance

Antibacterial resistance is a natural phenomenon that is categorised as arising either endogenously by selection and mutation or due to exogenous factor through horizontal gene transmission (HGT) from environmental microorganisms such as commensals, antibiotic producers and nonhuman pathogens to human pathogens (18-25). A better understanding of the bacterial cell and different types of available antibiotics will help in identification of the mechanism of bacterial resistance which in

turn regulates the way of using antibiotics in different situation (26). Antibiotics are classified into five major classes based on their mechanisms of action; inhibition of cell wall synthesis, interference with protein synthesis, inhibition of nucleic acid synthesis, interference with a metabolic pathway and disruption of bacterial membrane (Figure 2) (27). β-Lactams drugs such as penicillin, carbapenem, cephalosporins, and monobactam work by inhibiting bacterial cell wall synthesis through disrupting the enzyme required for the synthesis of the peptidoglycan layer, while glycopeptides including teicoplanin and vancomycin bind to the terminal D-alanyl D-alanine portion of the peptide side chain of the precursor peptidoglycan subunit leading to inhibition of the cross-linking steps required for the thickness and stability of the bacterial cell wall (27, 28). Antibiotics that work by inhibiting protein synthesis such as tetracycline, aminoglycosides, macrolides, chloramphenicol, streptogramins and oxazolidinones are selective for bacteria owing to the difference between the bacterial ribosome and human counterpart. Tetracyclines and aminoglycosides bind to the 30S subunit of the ribosome whereas others bind to the 50S subunit (29). Fluoroquinolones inhibit bacterial DNA gyrase leading to disruption of DNA synthesis during DNA replication, while trimethoprim and sulphonamide block the pathway for folic acid synthesis and finally inhibit DNA synthesis (30-32). The fifth class includes polymyxins that increases bacterial membrane permeability inducing leakage of bacterial content. The cyclic lipopeptide daptomycin also disrupts the bacterial membrane through inserting its lipid tails resulting in membrane depolarisation and eventual death of bacterium (33, 34).

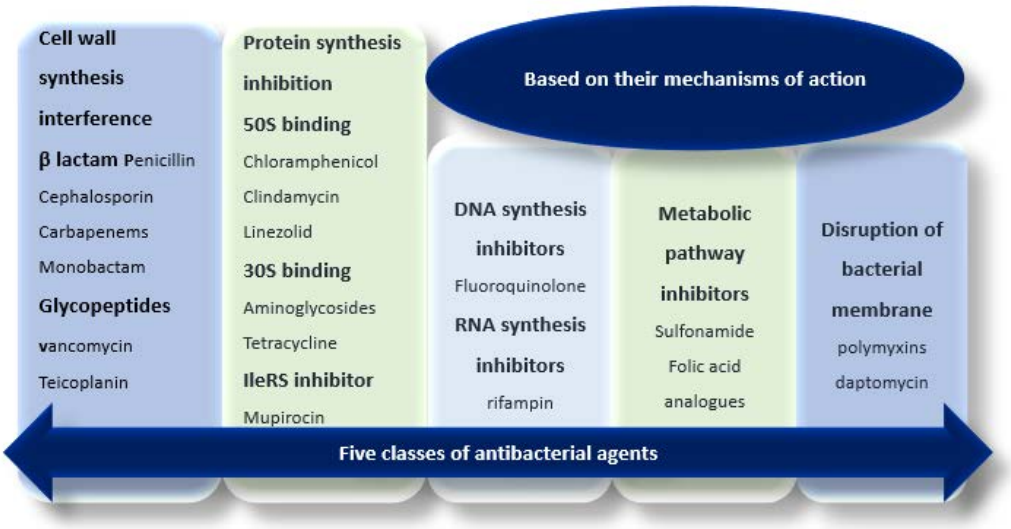

Figure 2: Mechanism of action of antibacterial agents. DNA = deoxyribonucleic acid, RNA = ribonucleic acid, tRNA = transfer RNA.

Regarding the mechanism of bacterial resistance, there are three main biochemical mechanisms for development of acquired resistance. Antibiotic inactivation, which can be occurred by the action of three main enzymes; β-lactamases, aminoglycoside-modifying enzymes, and chloramphenicol acetyltransferases (CAT) (35). Nearly all β-Lactams are hydrolysed by β-lactamases as they have an ester and amide bond and to date there are around 300 known β-lactamases which are classified into structural and functional enzymes (36). Class A β-lactamases (penicillinase) have little or no activity against cephalosporin and their actions are halted by β-lactamases inhibitors such as sulbactam, tazobactam or clavulanic acid (37). Class B β-lactamases (metallo-β-lactamases) are inhibited by chelating agents as they require heavy metal for catalysis and they are resistant to carbapenems, sulbactam, aztreonam and clavulanate (38). Class C β-lactamases (cephalosporinases) are produced by all Gram-negative bacteria except *Salmonella* and *Klebsiella* which have the ability to hydrolyse all β-lactams and cephalosporins including the broad spectrum ones, with the exception of carbapenems and their actions are not inhibited by clavulanic acid (39). Class D β-lactamases (oxacillin hydrolysing enzymes) are found in *Enterobacteriaceae* and in *Pseudomonas aeruginosa* which are resistant to penicillin, cloxacillin, oxacillin, and methicillin and weakly inhibited by clavulanic acid (40). In the case of aminoglycosides, they are inactivated by phosphoryl-transferases, nucleotidyl-transferases or adenylyl-transferases and the binding affinity of aminoglycosides or any modified molecules to

the 30S ribosomal subunit is reduced resulting in extended spectrum resistance to them. These phosphoryl-transferases, nucleotidyl-transferases or adenylyl-transferases enzymes are found in *S. pneumoniae*, *E. faecalis*, and *S. aureus* strains (41, 42). However, chloramphenicol-acetyltransferases are found in few Gram positive and negative bacteria and a number of *Haemophilus influenzae* strains and they work by acylating the chloramphenicol hydroxyl groups to impair its ability and any modified chloramphenicol to bind with the 50S ribosomal subunit properly (43).

The second common mechanism of resistance is a target molecule modification and it often results either from spontaneous mutation of a bacterial gene on the chromosome or from plasmid carrying antibiotics resistance genes. Just minor changes in the target can affect its binding with antibiotics. To illustrate, the 50S subunit of ribosome is altered by the action of plasmid coded gene (*erm* gene) leading to resistance to drugs targeting bacterial protein synthesis. The *erm* gene results in methylation of adenine at position 2058 of the 50S rRNA and this result in reduced binding affinity of antibiotics such as macrolides (44-46). Another example of resistance referable to target modification is that caused by the gene mec A, which is found in the mobile genetic element (Staphylococcal cassette chromosome mec). This gene is responsible for penicillin binding protein (PBP) modification making Gram positive bacteria resistant to β-lactams antibiotics through encoding a new penicillin binding protein (PBP2a) (36, 47). Also, glycopeptides drugs lose effectiveness against Gram positive bacteria owing to alteration in the terminal D-alanyl-alanine amino acid sequence of transpeptidase to D-alanyl-lactate preventing glycopeptides from cross linking. *Enterococcus faecium* and *Enterococcus faecalis* strains show three types of resistance; Van A resistance against vancomycin and teicoplanin, and Van B and Van C resistance against only vancomycin (48, 49). The mutation can furthermore occur in enzymes that are targeted by antibiotics such as topoisomerase IV and DNA gyrase resulting in bacteria resistant to quinolones drugs; these mutations are encoded by gyr A, gyr B, par C and par E genes to disrupt the DNA replication (50).

The third mechanism of resistance is by preventing the accumulation of antibiotics either by increasing active efflux of the antimicrobial from the cell or decreasing uptake. The aim of increasing efflux is to pump antibiotics out of the cell before they can do any damage (51). For example, small hydrophilic compounds such as

quinolones and β-lactams use the pore forming porins to gain access to the cell interior while hydrophobic compounds such as aminoglycosides diffuse across the lipid bilayer (52). Porins are present in the outer membrane while the pumps responsible for efflux mechanisms are present in the cytoplasmic membrane (44). The outer membrane (OM) of most Gram negative bacteria has an essential role of providing an extra protection layer to the organisms without compromising the exchange of material needed for maintaining life (52). Thus, in resistant strains of bacteria, the OM permeability is changed to the lower level decreasing the number of porin channels and as a result the entry of antibiotics such as β-lactams will be decreased. Due to low OM permeability, there is acquired resistance to all antibacterial agents classes in *Pseudomonas aeruginosa* (49). Efflux pumps are membrane proteins, which are responsible for exporting antibiotics from the cell to keep their low-intracellular concentration. Efflux pumps can be specific to antibiotics as they are activated by a specific substrate, but most efflux pumps are multidrug transporters having the ability to pump a broad range of antibiotics and are considered as the main cause of multidrug resistant (MDR) (51, 49). For those antibiotics that work by inhibiting the metabolic pathway such as sulphonamides, resistance comes in the form of alteration of the metabolic pathway. For example, resistant bacteria to sulphonamides do not use para-amino benzoic acid as a precursor for the formation of folic acid and instead they use preformed folic acid (53).

Therefore, horizontal gene transfer is the primary mechanism for the spread of antimicrobial resistance and phylogenetic analysis predicts that the rapid transfer of antibiotic resistant genes to pathogenic and commensal bacteria is most probably attributed to the accelerated horizontal transfers within bacteria in the antibiotic era (51, 54, 55). Transformation, transduction and conjugation are three mechanisms of HGT to transfer resistant genes from one bacterial species to another species (56- 58).

1.3. Gram positive bacteria

Staphylococcus aureus (*S. aureus*) and *Enterococcus faecalis* (*E. faecalis*) as Gram-positive bacteria are major bacterial human pathogens owing to their high ability to resist antibiotics (59). *S. aureus* is the most isolated strain at 29.1% of the isolated Gram positive bacterial population and as one of the ESKAPE pathogens can cause

both nosocomial-associated or community-associated infections and these infections are reported all over the world (60-62). *E. faecalis* is the second frequently isolated Gram-positive bacteria at 19.5% and it is found in re-infected root canal treated teeth in a percentage ranging from 30% to 90% of the cases (59, 63). Both are commensal bacteria found in human and mammals and their resistant strains are multidrug resistant (64, 65).

1.3.1. *Staphylococcus aureus*

S. aureus is one of the major pathogens that induce human diseases with various degrees of severity and a high rate of mortality. *S. aureus* is a commensal bacterium that presents in the nose, respiratory system and on the skin and nearly a third of the population is predicted to be asymptomatically colonised with this microorganism (66). Bacteraemia, infective endocarditis, pleuropulmonary infections, skin and soft tissue infections are mainly caused by *S. aureus* (67).

1.3.1.1. Structure of *Staphylococcus aureus*

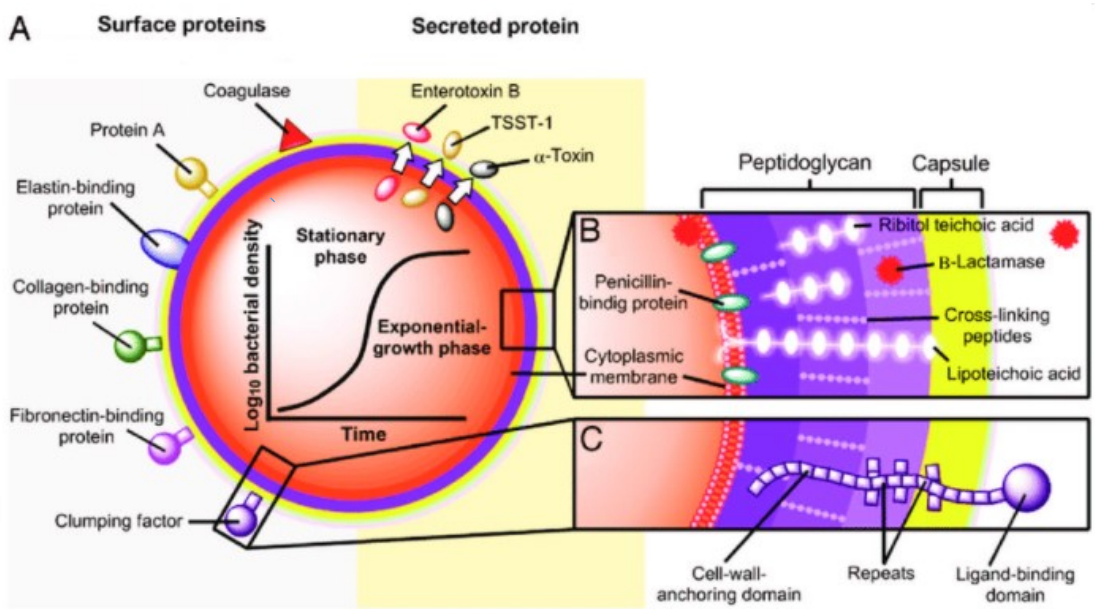

Figure 3: Structure of *Staphylococcus aureus* (68). Reproduced with permission from (68), Copyright Massachusetts Medical Society.

S. aureus has a thick peptidoglycan cell wall with an inner lipid membrane layer, and it is also surrounded by a polysaccharide capsule to increase its resistance against the phagocytosis process of the host cell (Figure 3) (69). In addition to the basic

characteristic features of Gram-positive bacteria, it has genetic materials in the form of circulate DNA and plasmid, which are responsible for some of the resistant genes. *S. aureus* is a facultative anaerobe that can grow in the absence of oxygen and its surface layer contains different types of proteins to protect and assist the microorganism in the invasion process (70). The first protein is called protein A, which protects the bacteria from destruction inside the host cell through binding to antibodies. Also, it has adhesins which are fibronectin and collagen binding proteins in order to adhere the cell to human extracellular matrix components and serum proteins allowing the cell to be invaded (71). In addition to these general features that assist *S. aureus* invasion, there are other specific factors that are known as virulence factors such as secreted enzymes and toxins. Regarding them, *S. aureus* has six different types of enzymes with different functions. Coagulase enzyme either bonded or free is essential to avoid phagocytosis through using fibrin substance to coat the surface of cell, this coagulation process is one of the main defence strategies to protect *S. aureus* (72). Hyaluronidase, staphylokinase, deoxyribonuclease and lipase enzymes are responsible for dissolving hyaluronic acid, fibrin, DNA and lipids respectively in an attempt to aid the spreading of the pathogen while the penicillinase enzyme, β-lactamase, has a substantial role in resistance and inactivation of β-lactams antibiotics (73). Secreted exotoxins are based on the type of *S. aureus* strains and many of them are leading causes of diseases. They are classified into three groups namely: superantigens, exfoliative toxins (ETs) and others. The first group includes toxic shock syndrome toxin 1 (TSST-1) and enterotoxin type B, which induce toxic shock syndrome (TSS) and gastroenteritis respectively. The second one has two distinct serotypes which are designated as ETA and ETB, both are responsible for scalded skin syndrome (SSS) in infants but ETA is the most produced toxin in around 80% of *S. aureus* strains in Europe, the USA and Africa while ETB produces strains are more prevalent in Japan than those expressing ETA (74). The third group involves alpha toxin, beta toxin, delta toxin, and some of bicomponent toxins (70).

1.3.1.2. Methicillin resistant *Staphylococcus aureus* (MRSA)

The first appearance of the methicillin resistant strain was in the 1960s (71) and was one of the main problems in hospital acquired infections due to its ability to resist treatment. Since that first emergence in hospitals, another form of MRSA that has

substantially increased in several countries. This type is community acquired MRSA (CA-MRSA), which is more susceptible to numerous non-beta lactam antibiotics than the first form (HA-MRSA) (75).CA-MRSA usually induces skin and soft tissue infections and in some cases, it can induce pneumonia. The route of CA-MRSA transmission is by contact with patients who are infected or who have open wounds in the community, especially in crowded areas or by sharing personal items and equipment that has been touched by infected skin. Thus, people in crowded places are at risk such as school students and staff, athletes and military personnel. Regarding the treatment of CA-MRSA, it can be treated despite its virulence but if left untreated, its infection will become severe (76). One study has shown that the incidence of CA-MRSA infection has increased based on the increased number of mortality and morbidity reports, which include details about re-emergence of severe *S. aureus* sepsis syndrome, a higher incidence of pulmonary complications along with bone and joint infections, a longer duration of fever and prolonged hospitalisation (77). By contrast, HA-MRSA is considered as a burden on patients and health care staff because it can be transmitted by direct contact with infected wounds or contaminated hands leading to an increase in the cost of hospitalisation as well as the rate of morbidity and mortality (78). There are many studies to show that problems, which are related to MRSA appear in large tertiary care hospitals with patients in burn (79) and in post-operative facilities (80). HA-MRSA can lead to severe complications such as sepsis and death if not treated quickly (70). Due to the ability of these strains to resist the first line of treatment, the availability of safe alternatives is needed.

1.3.1.3. Diseases related to *Staphylococcus aureus*

1.3.1.3.1. *Staphylococcus aureus* bacteraemia (SAB)

S. aureus is one of the major causes that leads to community-acquired and hospital-acquired bacteraemia (67). In the case of MRSA, the mortality rate is higher, and death can occur within 30 days if the treatment fails (81, 82). Regarding bacteraemia epidemiology, it is reported that there was an incidence of SAB in around 10 to 30 per 100,000 persons per year in the industrial world (83). Although there was a 50% reduction in the rates of methicillin resistant *S. aureus* bacteraemia (MRSAB) in the United Kingdom in 2011 (84), there were a total of 16.242 *S. aureus* bloodstream

infections recorded between November 2015 and November 2016. (85). A total of 12,878 *S. aureus* bacteraemia cases were registered in Public Health England (PHE) in 2018/19 through both the MRSA bacteraemia and MSSA bacteraemia surveillance schemes. This represents a 0.6% increase in the numbers of bacteraemia cases caused by *S. aureus* from 2017/18 and a 30.3% increase from 2011/12 (68). There are risk factors that contribute to the increasing incidence of SAB for example, age, gender, ethnicity and health condition (87).

1.3.1.3.2. Infective endocarditis

Infective endocarditis is a disease that is predominantly caused by *S. aureus* in various industrialised countries based on many studies (88). By contrast, infective endocarditis is caused by *Streptococci* in the non-industrialised and newly industrialised countries (89-93).

1.3.1.3.3. Pleuropulmonary infection

S. aureus is one of the predominant causes of three major types of pneumonia: ventilator-associated pneumonia (VAP), health care-associated pneumonia (HCAP), and hospital-acquired pneumonia (HAP) (94). A 2013 study showed that in 31 American community hospitals 40% of culture positive HCAP cases and 28% of VAP cases were owing to MRSA infection (95). Additionally, other study showed a new clinical case of severe necrotising pneumonia was induced by the emergence of a distinct *S. aureus* strain (96). Recently, *S. aureus* is not the most common pathogen isolated in patients suffering from respiratory symptoms, *P. aeruginosa* becomes prevalent and *S. aureus* still plays a significant role as a cause of exacerbations (97). Smokers or people who have a history of chronic liver disease, diabetes, and pneumonia are at risk of infection. Also, patients who have a history of hospitalisation, history of surgery and history of long-term care residence can be infected by MRSA (98).

1.3.1.3.4. Skin and soft tissue infection

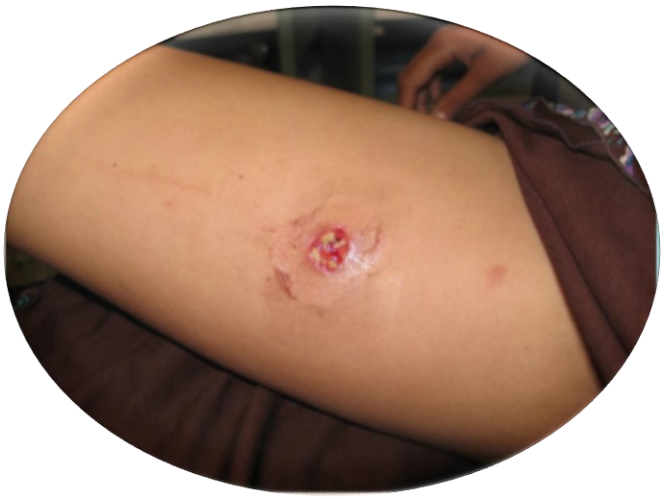

Figure 4: *Staphylococcus aureus* skin and soft tissue infections (abscess) (67).

Different types of infections either mild or severe are caused by *S. aureus* which is the most common microorganism found in cutaneous abscesses (figure 4), surgical site infections (SSIs), and purulent cellulitis (99). Although skin and mucous membranes are effective barriers to protect the body, damaged skin is a good environment to carry bacteria into underlying tissue and bloodstream (100). Once *S. aureus* penetrates the skin, neutrophils and macrophages act as a primary defence mechanism of the body and aggregate at the site of infection trying to eliminate the bacteria by phagocytosis but *S. aureus* evades this response by multiple ways, involving sequestering host antibodies, hiding from detection through formation of polysaccharide capsule or biofilm, and resisting destruction after ingestion by phagocytes (67). A high rate of skin and soft tissue infections was recorded in Australia and UK in a period between 2010 and 2012 (101, 102). The percentage of skin and soft tissue infections cases has increased from 16.4% in 2007/08 to 33.4% in 2018/19 (97).

1.3.1.3.5. Osteoarticular infection

Osteomyelitis (OM), prosthetic joint infection and native joint septic arthritis are three types of osteoarticular infections which are predominantly induced by *S. aureus* (103-105). Although osteoarticular infections are normal in children, they have distinctive clinical features in young patients. OM leads to inflammatory destruction and necrosis of bone because of infected bones (106) and according to a nationwide Japanese study, there was an increase in the incidence of osteomyelitis from 5.3 per 100.000 person-year in 2007 to 7.4 per 100,000 person-years in 2010 (107). Advancing age,

diabetes mellitus and immunosuppression are main risk factors of osteomyelitis (108-110). Native joint septic arthritis, which is rare in industrialised countries, but its incidence was higher in non-industrialised countries with exactly 29.1 per 100,000 person-years in aboriginal Australians and 13.8 per 100,000 person-years in children in Cambodia (111). In prosthetic joint infection, the percentage of infection was about 2% of hip and knee arthroplasties based on data from a large U.S. Medicare data set (112). In 8-year period (2007-2015), 123 children with CA-SA osteoarticular infections were admitted to the main tertiary paediatric hospitals of Athens and MRSA accounted for 44 of these (35.8 %). Those with MRSA infection had a remarkably higher admission rate to the ICU and longer duration of hospitalization (113).

1.3.2. *Enterococcus faecalis*

E. faecalis is a natural inhabitant of the human gastrointestinal tract (GIT) and through faecal contamination is found in food, water, sewage, and soil. *E. faecalis* is an opportunistic pathogen, which is a main cause of life threatening infections such as urinary tract infections, bacteraemia and infective endocarditis (64, 114). As a Gram positive bacterium, it shares most of the general features with *S. aureus* including cytoplasmic lipid membrane, thick peptidoglycan cell wall and polysaccharide capsule (115).

1.3.2.1. Resistance in *Enterococcus faecalis*

Resistance in *E. faecalis* can be categorised as intrinsic resistance, tolerance and acquired resistance. Intrinsic resistance is encoded within the core genome of all members of *Enterococci* species. *E. faecalis* is naturally tolerant to the bactericidal activity of antibiotics that target the cell wall, such as β–lactams and vancomycin which means it is not inhibited by clinically achievable concentrations (116). This type of tolerance can be treated by combining one of the cell wall inhibitors with aminoglycoside to confer a synergistic bactericidal activity, but the mechanism is still unknown. Based on in vitro data, the combined treatment with both a cell wall inhibitor and aminoglycosides results in a higher concentration of aminoglycosides inside the cell indicating that the cell wall inhibitor promotes uptake of aminoglycoside (116). Acquired resistance is present in only some members of the species and occurs owing to the horizontal exchange of mobile genetic elements. As commensal bacteria

in human, they are incidentally exposed to the course of antibiotic therapy for other bacterial infections suggesting about the existence of resistance determinants (115). For example, the genetic mechanism of glycopeptides resistance suggests that resistance is not owing to the acquisition of only one gene and each phenotype of resistance is related to a complex cluster of genes, which are generally grouped in operons and are located in a plasmid having the ability to transfer between species (115). Glycopeptides resistance results from nine distinct gene clusters (Van genes) and based on their physical locations, they are genetically and phenotypically different. They are encoded either on a mobile genetic element or in the core genome (115, 116). The Van gene clusters are commonly classified based on the ligases they encode (Van A, Van B, Van C, and so on). Van A and Van B types are the most common among the clinical isolates. Vancomycin and teicoplanin are glycopeptides antibiotics and the resistance toward them is different based on the type of cluster. For example, Van A determinant confers a high level of resistance to teicoplanin and vancomycin while Van B determinant causes moderate to high-level resistance to vancomycin but not to teicoplanin. Vancomycin resistance is widespread in *E. faecium*, although it remains relatively rare in E. *faecalis* (115).

1.4. Aminoacyl tRNA synthetases

Aminoacyl tRNA synthetases (aaRSs) have an essential role at a cellular level during the translation process of the genetic code. They specifically catalyse the binding of amino acids and their cognate tRNAs in the presence of an ATP molecule to create charged tRNAs, which are required to transfer the correct amino acid to the growing polypeptide chain (117).

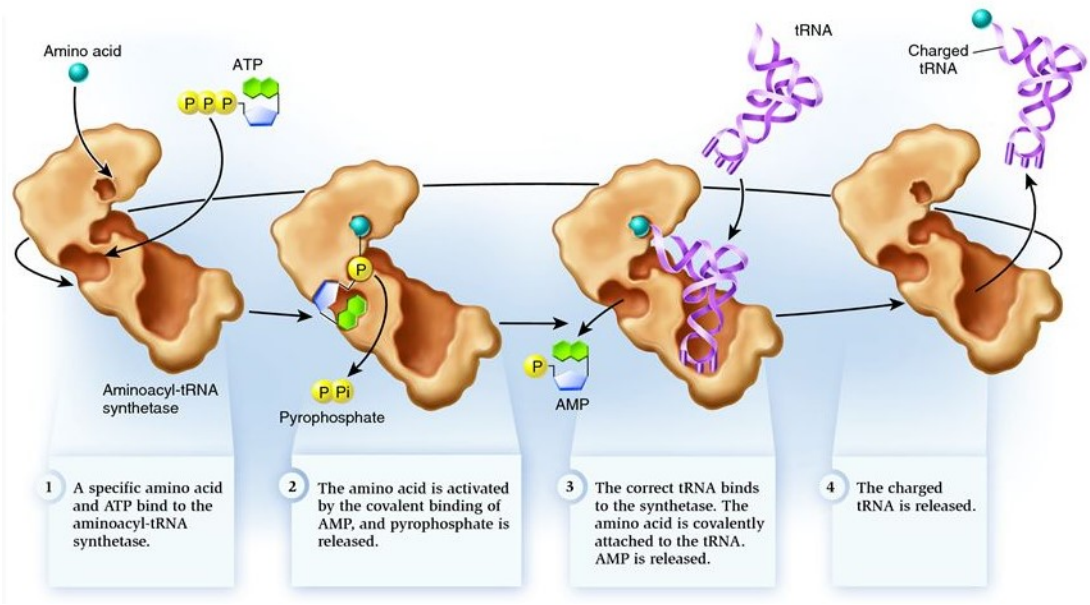

Figure 5: Mechanism of tRNA charging by aminoacyl tRNA synthetases (118).

This attachment is evolutionarily conserved and occurs in two important steps (Figure 5). First, aminoacyl tRNA synthetase catalyses the covalent binding between the carboxyl end of a specific amino acid and adenosine triphosphate (ATP) molecule through a nucleophilic attack on the α phosphate group of ATP (Scheme 1) in the presence of magnesium ion. As a result, the enzyme bound aminoacyl adenylate (aa-AMP) is produced involving a penta-coordinated phosphorus transition state and pyrophosphate is released. This binding with ATP is essential for the formation of the energy-rich aminoacyl-adenylate (aa-AMP) (117, 119).

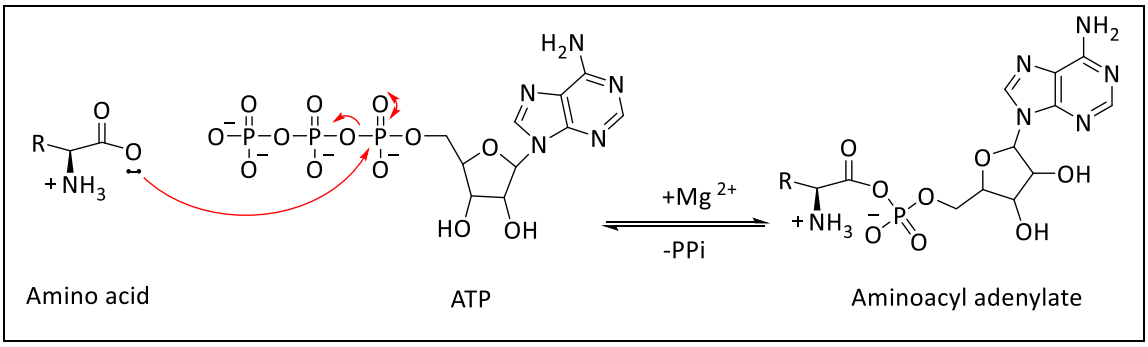

Scheme 1: Mechanism of aminoacylation reaction (first step).

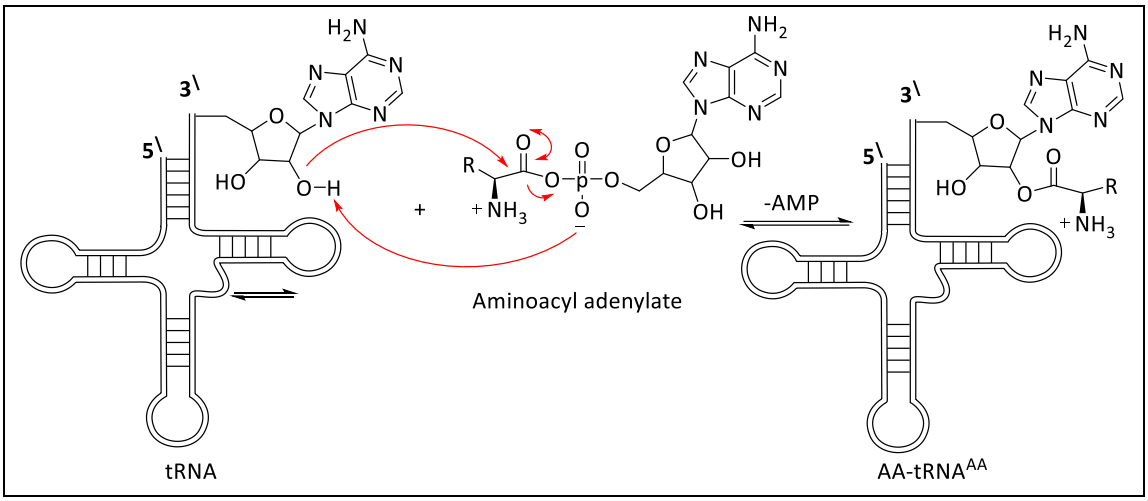

Scheme 2: Mechanism of transferring amino acid to its cognate tRNA molecule (second step), tRNA is in secondary structure.

Secondly, this ligase enzyme binds its corresponding tRNA to transfer the active amino acid from the intermediate to the 2- ´or 3- ´hydroxyl group of the terminal ribose at the 3´- end of the tRNA molecule (120). This occurs by nucleophilic attack of the hydroxyl group in the terminal adenosine of the tRNA on the carbonyl group of the intermediate to form aminoacyl-tRNA (aa-tRNA^{aa}) (Scheme 2). Aminoacyl tRNA synthetases are a group of 20 enzymes, each of which can specifically bind a specific amino acid with its cognate tRNA molecule under the same mechanism of action (121). However, the strategy for the specific recognition of the amino acid and tRNA substrates is unique to each synthetase (119). Amino acid sequence, size, three-dimensional (3D) structure and oligomeric state are the main differences between each aaRS (122).

1.4.1. Classification of aminoacyl tRNA synthetases

There are two classes of aminoacyl tRNA synthetases, class I and class II, based on the high-resolution crystal structures. Class I enzymes cover eleven amino acids while class II specifies ten amino acids, of note is that lysine tRNA ligase is present in both classes (123). The aminoacylation site, catalytic domain and signature motifs, ATP conformation and tRNA acceptor approach are four characteristic features that contribute to aaRSs classification (Table 1). Regarding the aminoacylation site of the terminal ribose of adenosine of tRNA molecules, the acylation of class I enzymes occurs at the 2'- OH position while class II enzymes acylate amino acids at the 3'- OH site with an exception of phenyl tRNA synthetase (PheRS). This may be explained by

the differences in the manner by which the enzymes approach the acceptor stem of tRNAs. To illustrate, Class I synthetases bind the minor groove side of tRNA molecules whereas class II synthetases approach the major groove side (124). Another reason for the ability of class I aminoacyl tRNA synthetases to approach the minor groove side of their cognate tRNA molecules is their open pocket binding sites that charge the bulkier amino acids. Biologically, class I synthetases are more complicated in their mechanism of action than class II enzymes because the ribosome, which is responsible for protein synthesis termination is not be able to recognise amino acids that ligate the 2'-hydroxyl group during the translation process. Thus, transesterification occurs as a third step after aminoacylation and transferring amino acids to their cognate tRNA molecules in order for them to be at the 3' hydroxyl group position (125). It is proposed that through the action of any base, the 3'- hydroxyl group of the terminal ribose is deprotonated. Then, the nucleophilic oxygen attacks the electrophilic centre of the amino acid to cleave the ester linkage between the amino acid and the 2'- hydroxyl group of the terminal ribose (Scheme 3). Additionally, the variation in the spatial charge distribution of ATP either extended or bent conformation and the architecture of the catalytic domain are attributed to the difference between the two classes (126) (Figure 6).

Table 1: The characteristic features of class I and class II aminoacyl tRNA synthetases.

Characteristic features	Class I aminoacyl tRNA synthetases	Class II aminoacyl tRNA synthetases
Site of aminoacylation	2' OH group of terminal ribose at 3' end of tRNA molecules	3' OH group of terminal ribose at 3' end of tRNA molecules
Catalytic domain	Rossmann fold	Anti-parallel β sheet
Consensus sequences	HIGH, KMSKS	Motif 1, motif 2 and motif 3
ATP conformation	Extended conformation	Bent conformation
tRNA acceptor approach	Minor groove	Major groove

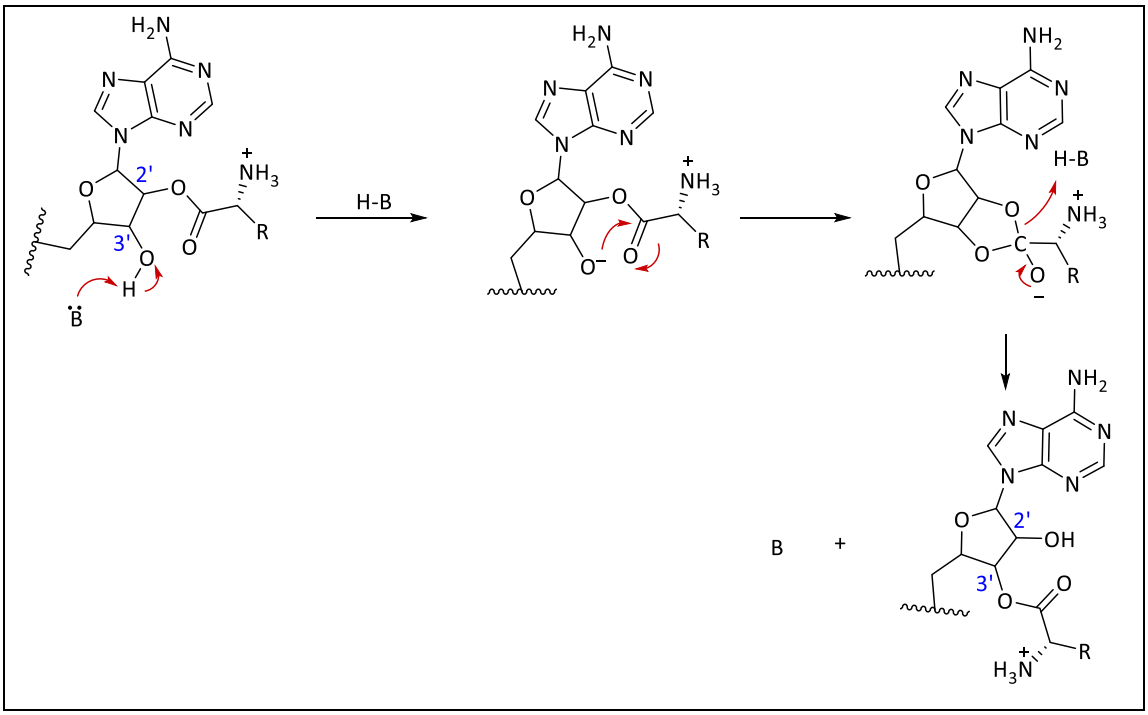

Scheme 3: Proposed mechanism of transesterification.

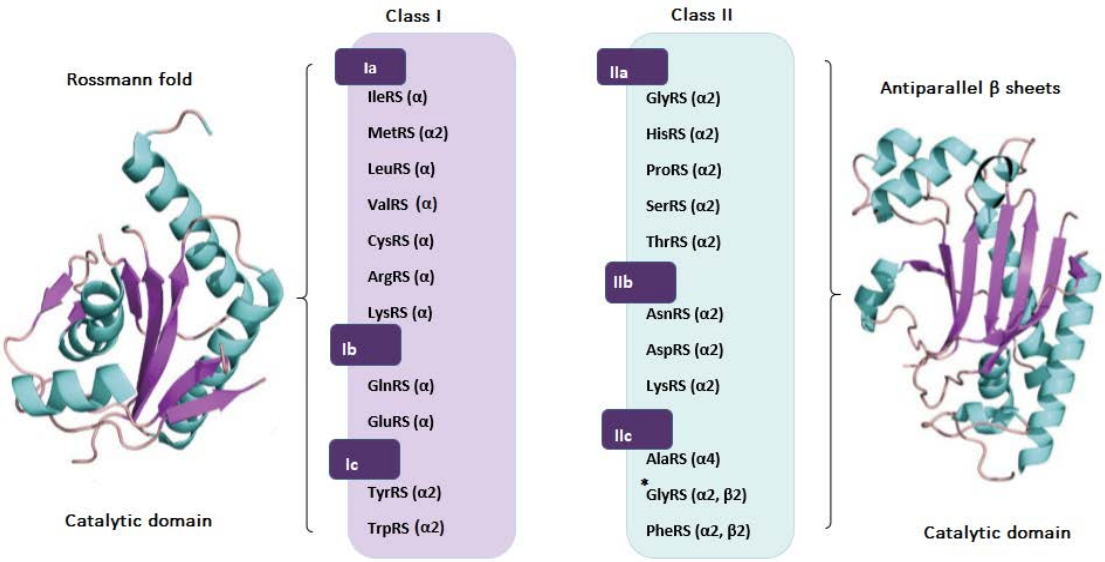

Figure 6: Class I and II aminoacyl tRNA synthetases with illustration of protein subunits (115, 119). IleRS: Isoleucyl tRNA synthetase, MetRS: Methionyl tRNA synthetase, LeuRS: Leucyl tRNA synthetase, ValRS: Valyl tRNA synthetase, CysRS: Cysteinyl tRNA synthetase, ArgRS: Arginyl tRNA synthetase, LysRS: Lysyl tRNA synthetase, GlnRS: Glutaminyl tRNA synthetase, GluRS: Glutamyl tRNA synthetase, TyrRS: Tyrosyl tRNA synthetase, TrpRS: Tryptophanyl tRNA synthetase, GlyRS: Glycyl tRNA synthetase, HisRS: Histidyl tRNA synthetase, ProRS: Prolyl tRNA synthetase, SerRS: Seryl tRNA synthetase, ThrRS: Threonyl tRNA synthetase, AsnRS: Asparaginyl tRNA synthetase,

AspRS: Aspartyl tRNA synthetase, AlaRS: Alanyl tRNA synthetase, PheRS: Phenylalanine tRNA synthetase. *GlyRS (α2, β2) is a specific form of enzyme found in few bacteria.

Based on the structural data, class I aaRSs are generally monomeric, with the exception of MetRS, TyrRS, and TrpRS, and their active site adopts a Rossmann fold consisting of a five-stranded parallel β sheet flanked by α helices. Structurally class II enzymes are dimeric or multimeric characterised by a seven-stranded antiparallel β sheet connected by α helices (127) (Figure 2). The presence of these enzymes in dimer or multimeric form could be related to their active sites, which are different than that of class I aaRSs. The isolated subunit may not by itself have the capacity to organise spatially in a functionally active conformation (128). Thus, the (α2) and (α2, β2) configuration should be considered as an integral structural necessity for a functional antiparallel nucleotide binding site. Aminoacyl tRNA synthetases display consensus signature sequences as a part of the active site that are conserved amino acid residues in all living organism aaRSs (129). The Rossmann fold of class I aaRSs consists of HIGH (His–Ile–Gly-His) and KMSKS (Lys-Met-Ser-Lys-Ser), which are present near to the ATP pocket for catalysis assistance (122, 124, 130-132). Specifically, the HIGH motif locates in the loop between the first β-strand and the subsequent α-helix (strand A and helix B) while the KMSKS motif exists in the loop immediately behind the fifth β strand (strand E) (Figure 3) (123, 133). The adenine base of the ATP is correctly positioned through the interaction of HIGH motif with phosphate and the second Lys in the KMSKS motif contributes to stabilise the transition state of the amino acylation step (134). Once the KMSKS motif is open, recognition and binding amino acids will take place in the catalytic site and it is closed after the formation of the active intermediate (aa-AMP) (135-137). In class II aaRSs, the catalytic core consists of three conserved motifs namely; motif 1, motif 2 and motif 3. Motif 1 consists of an α helix followed by a β strand involving a conserved Pro residue that has a role in homodimerisation (128). Arg and Phe in motif 2 and Arg in motif 3 are highly conserved amino acid residues that have an essential role in catalytic activity. Motif 2 participates in the coupling of ATP to the amino acid and also in transferring of the amino acid to the tRNA molecule while motif 3 binds ATP molecule. Binding of the amino acid to tRNA molecule causes

a specific conformational change to individual aaRSs owing to their substantial diversity within the subclasses (133, 138).

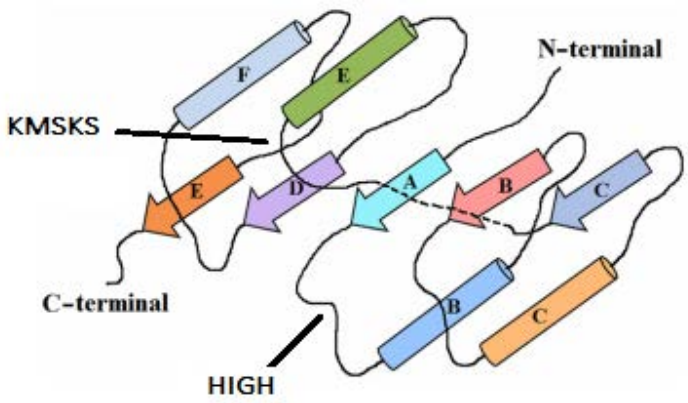

Figure 7: Schematic diagram of Rossmann fold with identification of HIGH and KMSKS positions (123), permission license number 4830490160491.

Each class of aaRSs is subdivided into subclasses based on the sequence homology, domain architecture and structural similarities as enzymes in each subclass recognise their cognate amino acids based on the similarity in their chemical properties (124, 130) (Figure 7). Class I aaRSs are generally subdivided into three subclasses in most studies except one study which classifies them into five subclasses namely; Ia, Ib, Ic, Id, and Ie based on their chemical properties for amino acid recognition (123, 139, 140). The members of the first subclass are IleRS, MetRS, LeuRS, and ValRS, which recognise hydrophobic amino acids having aliphatic groups, while CysRS, GluRS, and GlnRS belong to subclass Ib enzymes having charged amino acid as their substrates. Subclass Ic enzymes recognise tyrosine and tryptophan, which are aromatic amino acids and the subdivision of ArgRS alone in Id subclass is owing to the dissimilarity of its structure with other subclasses. Despite the structural similarity between LysRS with subclass Ib enzymes, it is classified in subclass Ie because there is a unique α helix cage in its structure making it distinctive from other subclasses (141). Most class I aaRSs bind to their corresponding tRNA molecules before starting the aminoacylation reaction (142). Also, they are sharing other general domains such as stem contact fold (SC fold), an α helical anticodon binding domain, and other domain for proofreading containing connective peptides 1 (CP1) and 2 (CP2) (143). CP1 exists at the end of strand D of the Rossmann fold whereas CP2 is found between strand D and the beginning of the Rossmann fold. This editing domain is for post transfer editing

activities of mischarged tRNAs and is present in IleRS, ValRS, LeuRS, MetRS and CysRS. CP1 consists of about 250–275 amino acid residues in IleRS, ValRS and LeuRS which is slightly larger than that in MetRS and CysRS (100 and 50 amino acids respectively) (143). Class II aaRSs are subdivided into three subclasses designated as IIa, IIb, and IIc. Subclass IIa synthetases include HisRS, SerRS, GlyRS, ProRS, and ThrRS which specify their N-terminal domains for aminoacylation reaction while the aminoacylation domain of subclass IIb synthetases, AspRS, AsnRS, and LysRS, is structurally identical to the C-terminal aminoacylation domain. Furthermore, there is a variation in the anticodon binding domains of class II synthetases especially between subclasses a and b enzymes, for subclass IIa, the anticodon binding domain consists of an alpha/ beta fold while subclass IIb enzymes, it consists of a five stranded beta barrel fold known as an oligomer binding (OB) fold (144). AlaRS, human GlyRS, and PheRS are members of subclass IIc, which exist in tetrameric conformation, however they all share the three conserved motifs in their catalytic domains.

Interestingly, LysRS is found in both classes according to its occurrence. Most archaea and a few bacteria use LysRS as class I while class II LysRS is found in most of the bacteria and eukaryotes, However, *M. barkeri* and *M. Acetivorans* as archaea genus *Methanosarcina*, *Nitrosococcus oceani* and *Bacillus cereus* have both subclasses of LysRS (145-147). Both enzymes recognise the same amino acid (Lys) and the same tRNA molecule ($tRNA^{Lys}$) *in vitro* and *in vivo* although they differ in their structures (Figure 8) (141, 142), however, class I LysRS is more specific than class II LysRS for their $tRNA^{Lys}$ anticodon according to the structural and functional data (148, 149). The main difference between them in aminoacylation is that class I LysRS has to bind uncharged $tRNA^{Lys}$ prior to the formation of lysyl- adenylate complex as class I aaRSs while class II LysRS needs only ATP and Lys to create an enzyme bound aminoacyl adenylate complex as required for all other class II aaRSs (142, 150, 151). LysRS class I is a distinctive enzyme because it has an α-helix cage, which is uncommon domain not found in all protein structures identified to date (149) (Figure 8). The α helix cage is reported to have a fundamental role in recognition of the tRNA molecule through using bases C34 and U35 of class I LysRS to recognise the anticodon of $tRNA^{Lys}$ (141). In *Escherichia coli* (*E. coli*), LysRS is found in two isoforms called Lys S and Lys U, both have the same topology characteristic of the catalytic domain found in class II

synthetases sharing a high degree of identity (88%). Lys S is produced under normal growth condition while the other isoform, Lys U, is formed under extreme physiological conditions such as heat shock when silent gene is overexpressed. Thus, it is proposed that the Lys U isoform acts as a modulator of the heat shock response and stress response through production of a number of adenyl dinucleotides (152).

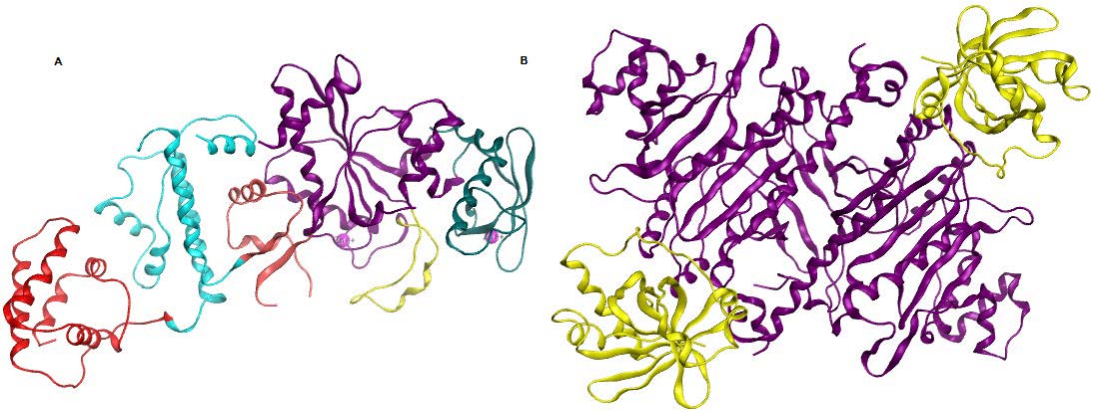

Figure 8: A = class I LysRS (pdb: 1IRX), B = class II LysRS (pdb: 1LYL). In LysRS I, Rossmann fold is coloured purple, CP domain teal, SC fold domain pink, α cage helix red, α helix bundle cyan, the helical insertion yellow. LysRS II (pdb: 1LYL) is in a dimer form. Active sites are coloured purple and the N-terminal domain yellow (123, 141, 152).

Glycinyl tRNA synthetase is also found in two distinct forms, one is present in a few bacteria such as *E. coli* while the other form is more common in eukaryotes, archaea and the remaining bacteria (153). Both forms of GlyRS share a similar structural catalytic domain belonging to class II aaRSs, however their anticodon binding domains are different in both sequence and structure. The first GlyRS is a hetero tetramer (α2β2) containing α and β subunits (Figure 6) and its active site has the shortest sequence among class II aaRSs (154, 155). The anticodon binding domain of the tetramer GlyRS is in a β subunit and has a role in the interaction with the tRNA molecule, but there is no similarity with the anticodon recognition domain of the more general GlyRS, which resembles ArgRS belonging to class I aaRSs in sequence (156). The α and β subunits in tetrameric GlyRS are encoded by two open reading frames (ORFs), the catalytic domain is encoded in the α subunit, however the anticodon binding domain is encoded in the N-terminal domain of the β subunit. In contrast, the second form of GlyRS is a dimeric form (α2) that has similarity with ProRS in its structure and both catalytic domain and anticodon recognition domains are in the α

subunit which is encoded by a single ORF as most of the class II synthetases, but both different oligomeric types of GlyRSs recognise the same $tRNA^{Gly}$ (155, 157).

1.4.2. Aminoacylation proofreading

Aminoacyl tRNA synthetases are crucial for the fidelity of the genetic code, thus the aminoacylation reaction for corresponding amino acids is specifically catalysed by their catalytic and anticodon recognition domains (124, 155, 158). The stereospecific interaction between aminoacyl tRNA synthetases, their cognate tRNAs, and amino acids contributes in achieving accuracy in protein synthesis. Without aminoacylation proofreading, many neurological diseases such as encephalopathy, neuropathy, and cerebellar ataxia result in human and cell death in microbes (159-161). For the purpose of maintaining the accuracy of the translation process and normal cellular function, several synthetases have an additional editing domain which confers a proofreading process via two mechanisms to avoid increasing the number of incorrectly amino acylated tRNA (162). The first one is pre-transfer editing to hydrolyse amino acid and AMP in case of misactivated aminoacyl adenylate occurred while in the post-transfer editing, the incorrect amino acid and tRNA molecule are hydrolysed in case of incorrectly aminoacylated tRNA formation (163). The proofreading activity of aaRSs is determined by the presence of two different pockets, catalytic active site and editing site, which act as double sieve editing cores (164). To illustrate, the first sieve is made by the catalytic site of aaRSs to exclude the amino acids having bigger size or others that are not appropriate for the interaction with the active site. That means, all smaller amino acids can fit into the pocket and escape from the first sieve to be incorrectly activated but the editing site is able to hydrolyse the misactivated amino acids (124). In 1998, the accuracy of IleRS to distinguish between isoleucine and valine was reported, a difference of just one methyl group in isoleucine was studied by using X-ray studies of IleRS isolated from *Thermus thermophilus* and the co-crystal structures of complexes with isoleucine and valine (165). As a result, the first active site activates both amino acids, isoleucine and valine to aminoacyl-AMP, but the second active site hydrolysed the valine-acyl-AMP into valine and AMP owing to the smaller size of valine than that of isoleucine and only isoleucine is sterically occluded. The percentage of the accuracy is high, and the double sieve mechanism enables an error frequency of around 1 mistake in 40,000 aminoacylation reactions (166, 167). Based on the

biochemical and structural studies, 50% of the aminoacyl tRNA synthetases have a totally different domain with a hydrolytic pocket for amino acid editing (168). Owing to the relative position of the catalytic and editing domains, it is predicted that the aaRSs will undergo a conformational change to allow tRNA to translocate between the domains as demonstrated in subclass Ia (169).

In class II aaRSs, the editing domain is distinctive in both structure and position. For example, the editing domain of phenyl tRNA synthetase (PheRS) is located between β3 – β4 domain to hydrolyse the misacylated tyrosine-$tRNA^{Phe}$, while ProRS contains an insertion domain (INS) found between motif 2 and motif 3 for hydrolysing the misacylated Ala-$tRNA^{Pro}$ (170, 171). That hydrolytic action is due to the presence of Lys297 in the INS domain (172). Furthermore, the editing domain of threonyl tRNA synthetase (ThrRS) is similar to that internal editing domain in alanyl tRNA synthetase (AlaRS) but it is positioned at its N terminus and it is not found in most of mitochondrial and archaeal ThrRS. This repositioned domain is called N-terminal N2 domain (NTD) and is responsible for cleaving any bond formed between tRNA and D-amino acid (170, 173, 174). In spite of the similarity in the editing domains of AlaRS and ThrRS, AlaRS has a distinct C-Ala domain tethered to the C-terminal end of its editing domain to recognise the elbow of $tRNA^{Ala}$. Thus, the catalytic and editing domains bind to the $tRNA^{Ala}$ acceptor stem at the same time for collaborative editing and aminoacylation (174, 175). In some cases, there is an additional protein in several aaRSs that mediates the hydrolysis of the misacylated tRNAs such as YbaK protein in *Haemophilus influenzae*. The YbaK protein hydrolyses Cys-$tRNA^{Pro}$ to Cys and $tRNA^{Pro}$ by the action of its Lys46 residue and the substitution of that Lys will reduce the editing activity of *E. coli* ProRS (176-178). Regarding class I aaRSs, it is known that the binding of tRNA molecules to their cognate aaRSs is an important step for aminoacylation and that will serve in the editing activity although class Ia synthetases share a similar domain (150, 179, 180). Also, the study of *S. aureus* IleRS predicts a different tRNA-dependent shuttling mechanism between the two active sites for misactivation and misacylation correction (151).

1.4.3. Indirect pathway of aminoacylation

As well as a direct pathway of aminoacylation to charge tRNA molecules, there is an indirect aminoacylation pathway that is used by archaea and bacteria that are missing some open reading frames (ORFs) in their genes encoding aminoacyl tRNA synthetase. In the indirect pathway, a non-discriminated (ND) synthetase forms a mischarged aminoacyl tRNA pair to be modified by aminotransferases (AdT), which is a specific RNA dependent enzyme. Glutaminyl and asparaginyl tRNA synthetases (GlnRS and AsnRS) are generally not encoded by some bacterial genomes but Gln and Asn can be synthesised by the indirect method and the mechanism is clarified in Scheme 4 (123). This mischarged tRNA does not affect the fidelity of translation as they are not recognised by the translational elongation factors (181). Although the structure of GluRS and GlnRS is different, Glu and Gln are connected together owing to their biosynthetic pathways with Glu as the precursor of Gln (182), while the lack of recognition of the last anticodon nucleotide (C36 and U36) in $tRNA^{Asp}$ and $tRNA^{Asn}$ respectively, the ability of the ND AspRS is increased to recognise both tRNA molecules. This refers to the similarity between them in both structure and function and that double specificity charging of $tRNA^{Asp}$ and $tRNA^{Asn}$ has been detected in eubacterium (*Thermus thermophilus*) and archaea (*Haloferax volcanii*) (183, 184).

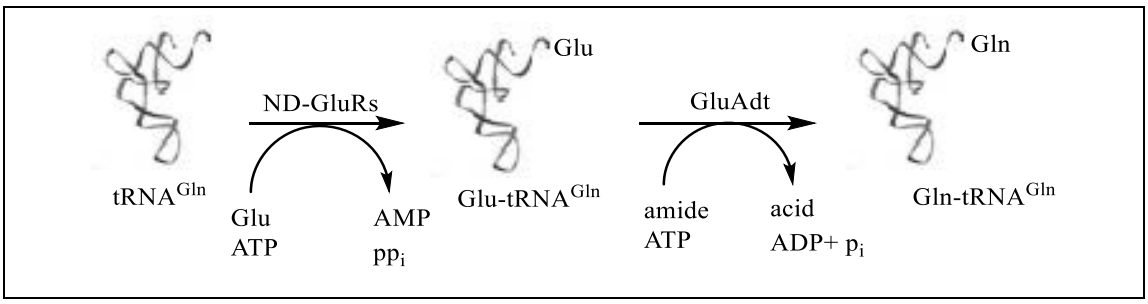

Scheme 4: Mechanism of $tRNA^{Gln}$ charging used by *S. aureus* and other microorganisms that do not have GluRS or AsnRS.

1.4.4. Other functions of aminoacyl tRNA synthetases

Both pathways of aminoacylation as well as editing functions are considered as canonical functions of aaRSs which are highly conserved throughout the three kingdoms. However, they have domains normally attached to the amino or carboxy terminus that are responsible for noncanonical activities unrelated to aminoacylation (185) such as, angiogenesis, cell migration, signal transduction, tumourigenesis, inflammation, translation control, and transcription regulation. Any mistakes in either

canonical or noncanonical aaRSs functions induce human diseases, cancer as an example is potentially associated with aaRSs upregulations (186, 187).

1.4.5. Aminoacyl tRNA synthetases inhibitors

Although there are many known natural and synthetic compounds that act competitively with aminoacyl adenylate to bind the same active site of aaRSs, only a few have reached to the stage of clinical development (124). However, these enzymes are valuable targets for the development of anti-infective agents as exemplified by the two approved drugs mupirocin (Figure 9) and tavaborole (Figure 9) that inhibit IleRS and LeuRS respectively (188, 189). Both are topical anti-infective drugs with mupirocin used for the treatment of MRSA infection and tavaborole used as an antifungal medication for onychomycosis treatment (190, 191). Mupirocin shows high selectivity for pathogenic aaRS over human aaRS (192) and its use is restricted to local treatment because of its low bioavailability resulting from rapid hydrolysis in the blood and tissue (192). Tavaborole is able to fully penetrate through the human nail by the addition of ethyl acetate and propylene glycol (193). Tavaborole is a non-competitive inhibitor of LeuRS, which works by binding to the editing site of the LeuRS and works by trapping $tRNA^{Leu}$ through the formation of two covalent bonds between boron and the 2`- and 3`- hydroxyl groups of the 3` terminal adenosine of $tRNA^{Leu}$ with formation of an acyclic borate structure (194). Despite the presence of many analogues of mupirocin, none of them have reached clinics yet. SB-234764 (Figure 9) is the most successful analogue, which combined structural features of IleRS and mupirocin, but with poor selectivity (195) while CB-432 (figure 9) was modified to increase its selectivity for *E. coli* IleRS through replacing the adenine by a phenyl tetrazole moiety, although It was not subjected to further development owing to its high binding ability with albumin (196, 197). Icofungipen (Figure 10) inhibits fungal IleRS with accumulation in yeast cells up to 200-fold of the extracellular concentration (6), however, there is evidence for the rapid development of resistance although its potency is comparable with amphotericin B (198). SB-203207 (Figure 10) is a non- selective IleRS inhibitor with poor antibacterial activity (190, 200). The natural furanomycin compound (Figure 10) is an alternative IleRS substrate that was found to bind *E. coli* IleRS with the same binding affinity of Ile and it was activated, aminoacylated and readily incorporated into protein, however, it was found to be highly toxic for mammals (201, 202). Thiomarinol

(Figure 10), produced by the marine bacterium Alteromonas rava species, is another IleRS natural inhibitor consisting of a terminal chromophoric holothin group with higher inhibitory activity against Gram positive and negative bacteria (203, 204). The synthetic NSC70442 compound (Figure 10) was effective in the treatment of *Trypanosoma brucei* infected mice and had the ability to cross the blood brain barrier, but there is no complete data about its toxicity in human (205). Thiaisoleucine (Figure 10) is a weak IleRS inhibitor that inhibits growth of malarial parasites but has a poor therapeutic index (206).

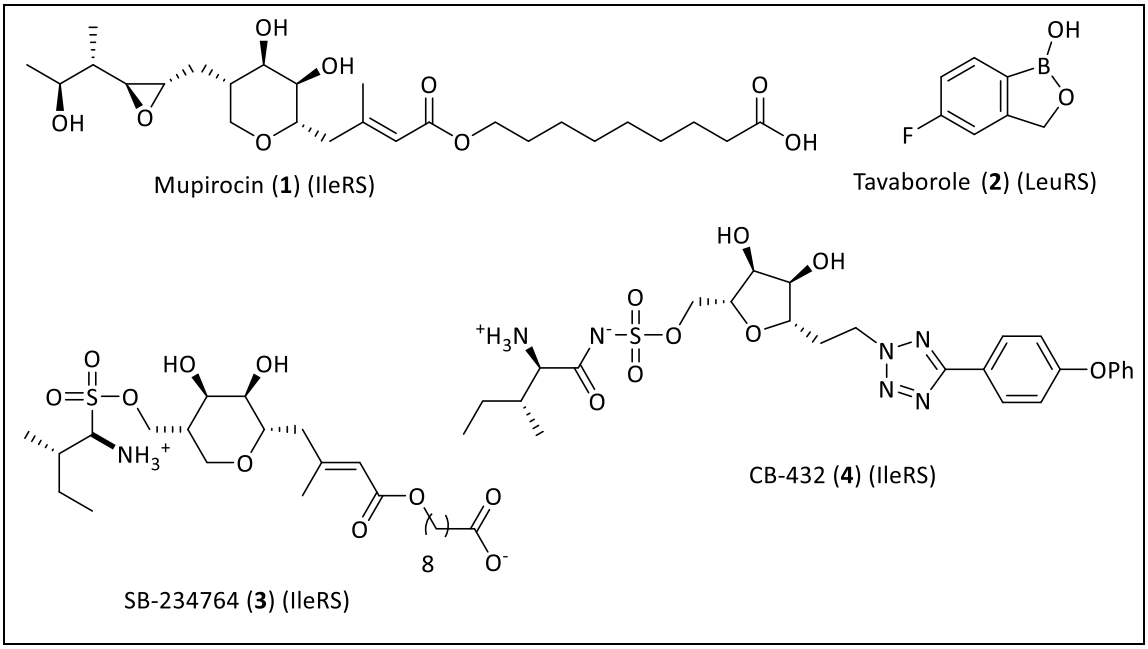

Figure 9: Chemical structures of IleRS and LeuRS inhibitors.

The non-hydrolysable analogues of aminoacyl-AMP form the biggest class of potentially active compounds against aaRSs (207). For example, Agrocin 84 (Figure 11) is a LeuRS inhibitor used to inhibit the formation of plant tumours caused by *Agrobacterium tumefaciens*. Agrocin 84 contains a D-glucofuranosyloxyphosphoryl moiety, which is essential for pathogen uptake as well as the structure of leucine adenylate (117, 208-210). By contrast, granaticin (Figure 11) is a natural compound produced by *Streptomyces olivaceus* acting potently against LeuRS with high mammalian toxicity (211). Based on the chemical structure of tavaborole (Figure 9), benzooxaborole derivatives (Figure 11, compounds 13, 14 and 15) have been developed to target protozoal tRNA synthetases with good activity as LeuRS inhibitors

showing *T. brucei* parasite growth inhibition activity (212). However, Epetraborole was halted in phase I clinical trials owing to rapid resistance development (213).

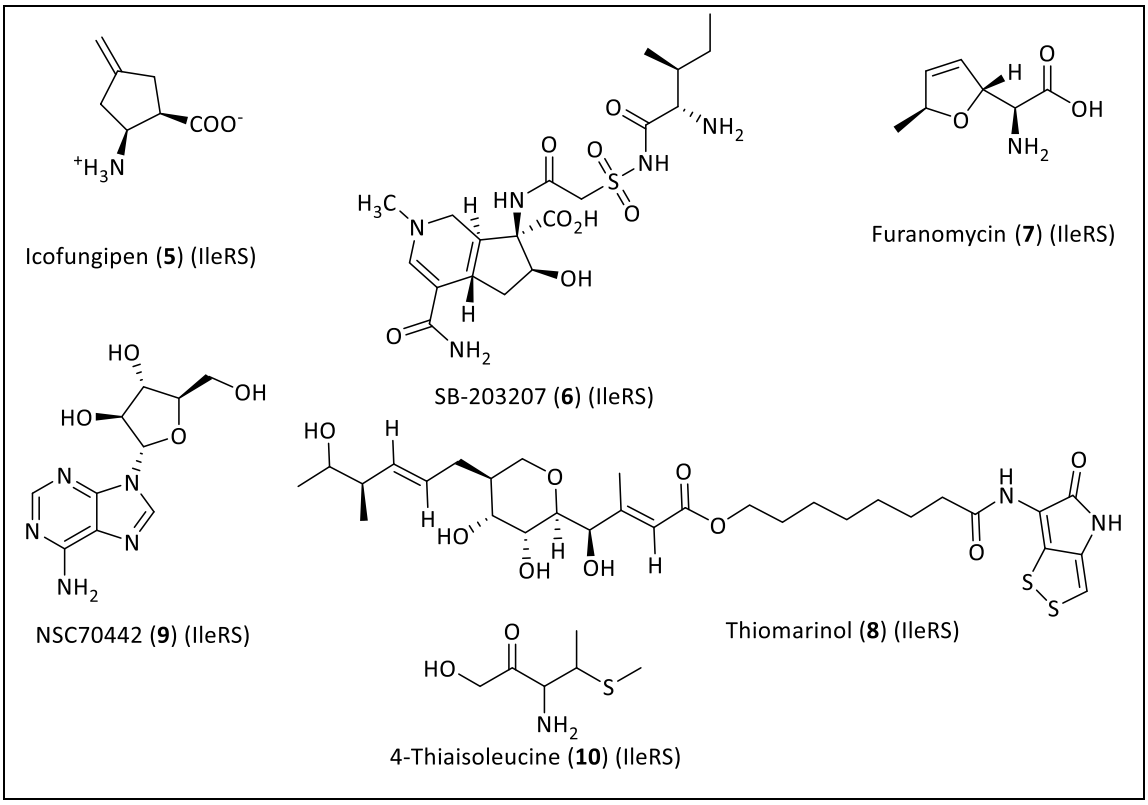

Figure 10: Chemical structures of IleRS inhibitors.

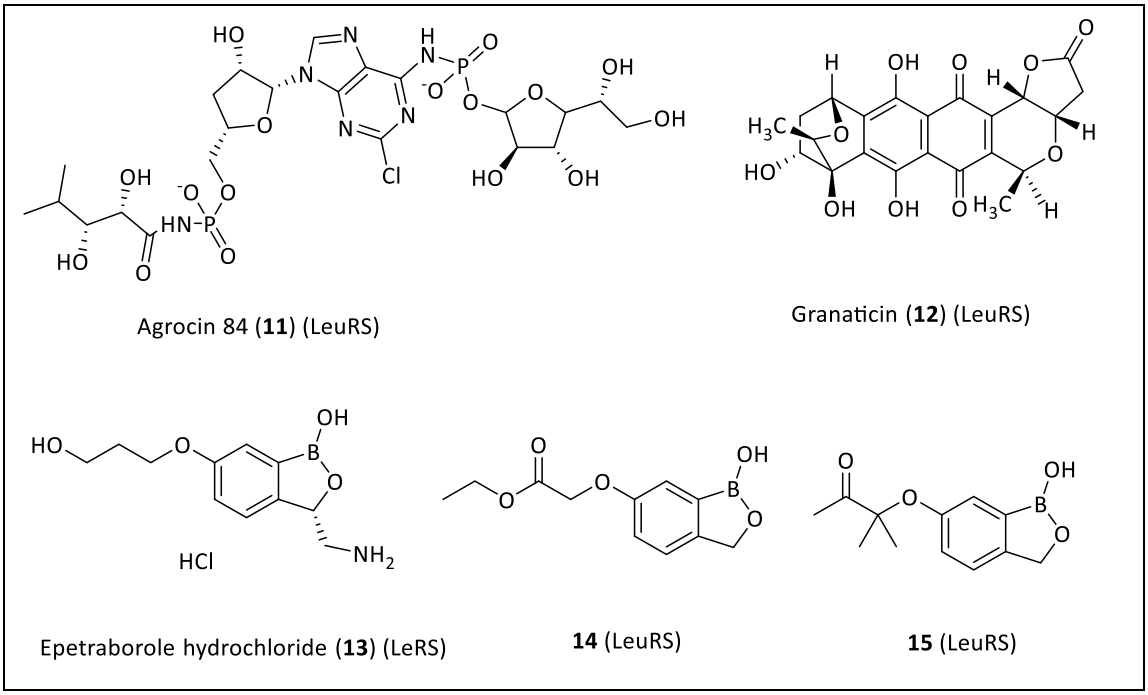

Figure 11: Chemical structures of LeuRS inhibitors.

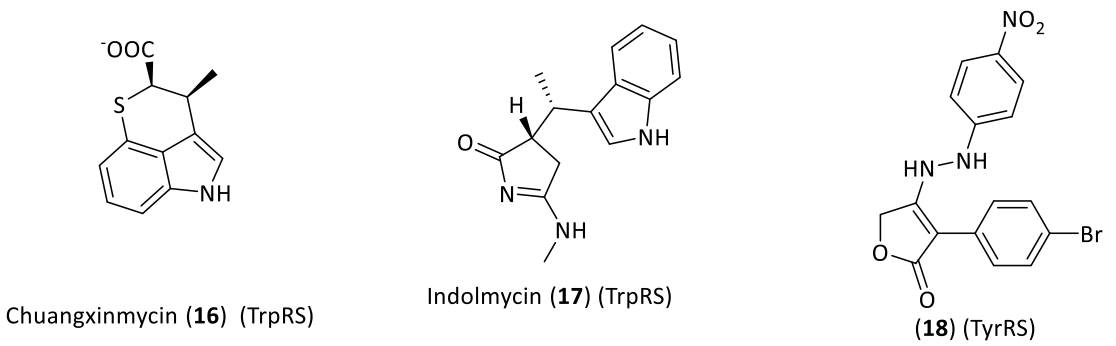

Figure 12: Chemical structures of TrpRS and TyrRS inhibitors.

Two TrpRS inhibitors with activity against range of Gram negative and Gram positive bacteria have been described. The first one is chuanginmycin (Figure 12), which is natural compound and in spite of its potency, there are no reports on further development (130), while the second one is indolmycin (Figure 12), which is a biosynthetic derivative of TrpRS. The cellular uptake of indolmycin is impaired owing to its hydrophobicity and recent studies showed that indolmycin was not sufficiently active against the most of commonly occurring pathogenic bacteria (133, 214) but it has a bacteriostatic activity against *S. aureus* (215). The 3-aryl-4-alkylaminofuran derivative (Figure 12, compound 18) is a potent *S. aureus* TyrRS inhibitor with MIC_{50} 0.42 µg/mL and through a docking study was shown to fit well in the active site (216).

Ascamycin (Figure 13) is another example of natural antibiotic, which is also an aa-AMP analogue, formed by *Streptomyces* and bearing a 2-chloroadenine moiety. Ascamycin inhibits the binding of phenylalanine in *Xanthomonas citri* and *Xanthomonas oryzae* (217-219). The chlorinated dihydroisocoumarin acid with a phenyl alanine moiety (ochratoxin AS) (Figure 13) is also natural compound produced by *Aspergillus*, however, it was found to be toxic for mammals (220, 221).

Cispentacin, phosmidosin, febrifugine and halofuginone (Figure 14) are ProRS natural inhibitors. Cispentacin is a cyclic β-amino acid effective against Candida albicans species, however, it was found to be toxic (133, 222). Phosmidosin is a proline -AMP analogue, which acts as an antifungal nucleotide inhibitor preventing the spore production of Botrytis cinerea (223). Febrifugine and halofuginone have antimalarial activity and mammalian toxicity, however, halofuginone is approved by the FDA to suppress coccidiosis in poultry because it inhibits all three stages of malaria (224- 227).

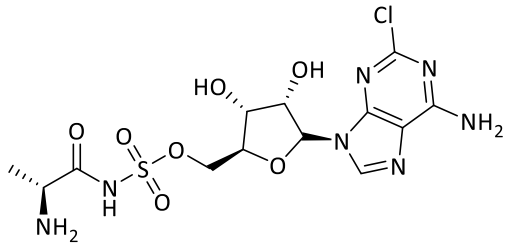

Ascamycin (**19**) (PheRS)

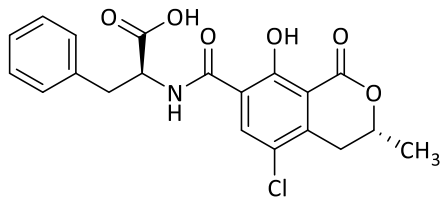

Ochratoxin AS (**20**) (PheRS)

Figure 13: Chemical structures of PheRS inhibitors.

In the case of ThrRS, borrelidin and its derivative BC194 (Figure 14) are natural compounds, which are allosteric inhibitors that act on threonine and ATP binding leading to impairment of catalytic conformational changes as well as the angiogenesis inhibitory effect of BC194 (228). The mammalian toxicity of BC194 is lower than borrelidin toxicity and both have antifungal, antiviral and antibacterial properties as well as inhibition of Plasmodium growth (140, 229-231). REP8839 (Figure 15) is a fully synthetic inhibitor of MetRS, which blocks methionine activation. REP8839 is a fluorvinylthiophene connected to 1,3 diaminopropane with quinolone and is more potent that its analogue (Figure 15, compound 28). REP8839 is currently in phase I clinical trials for the treatment of skin and wound infections of *S. aureus* (232) and also showed good activity against *Streptococcus* pyogenes as well as against several of other *Staphylococci* and *Enterococci* (232). However, it is a relatively selective agent that binds to human cytoplasmic and mitochondrial MetRS with K_m values around three- to six-fold higher than *S. aureus* MetRS, and well tolerated when used as an intranasal ointment (232, 233).

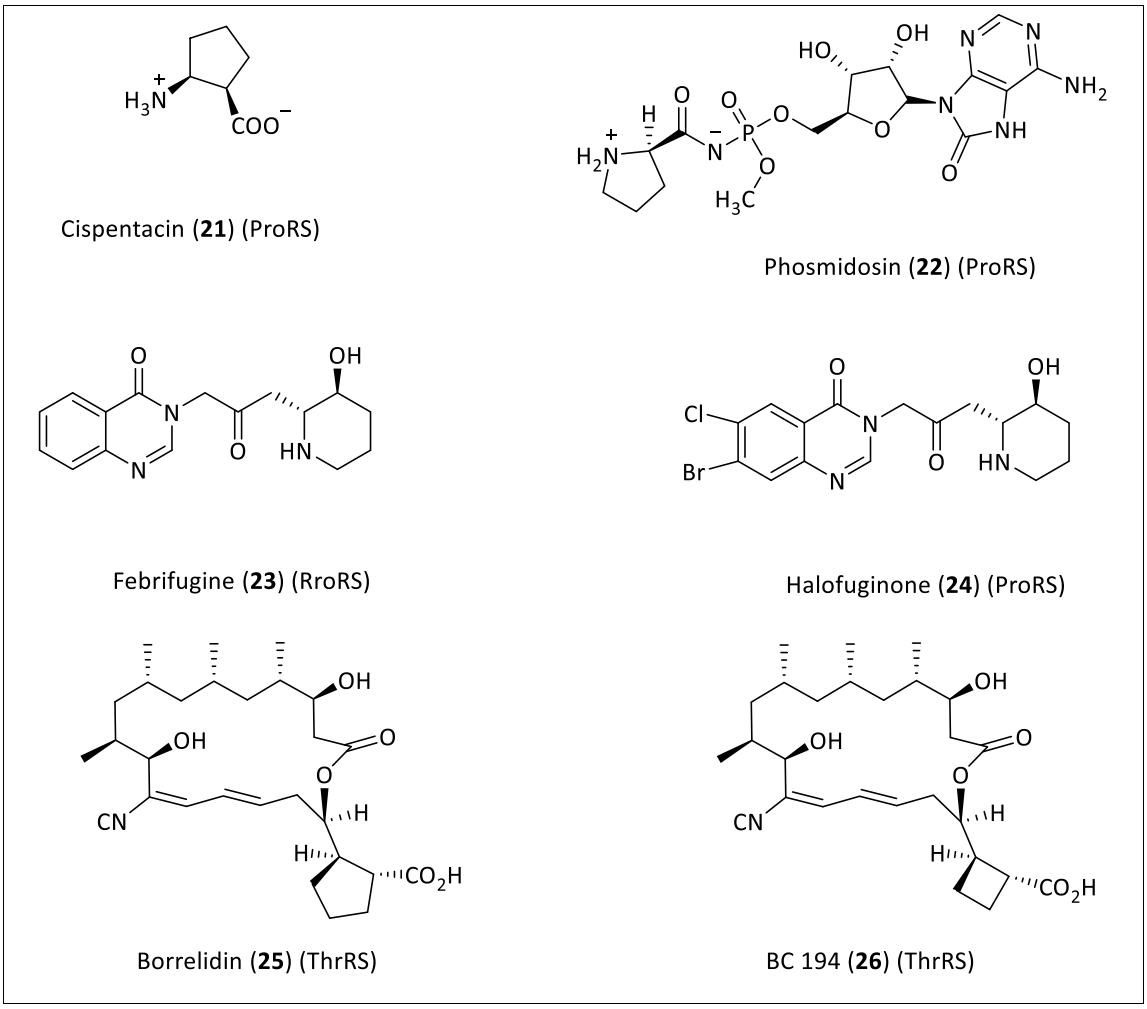

Figure 14: Chemical structures of ProRS and ThrRS inhibitors.

In contrast, Albomycin (Figure 15) is a trojan horse compound consisting of an iron binding targeting region (siderophore like moiety connected to an aminoacyl-thioribosyl pyrimidine) to trick the bacteria into taking up the warhead. The tetrapeptide siderophore attaches the thiosugar warhead enabling the compound to cross the phospholipid bilayer and this SerRS inhibitor was under investigation to determine the method of the bacterial inactivation via thiosugar and the transportation of the molecule inside the bacteria (196, 200, 234, 235). The high antimicrobial activity of the albomycin is believed to be owing to the siderophore-dependent iron acquisition systems of the bacterial targets (236). Albomycin is hydrolytically digested by peptidase once it is transported into the bacterial cell to deliver the active antimicrobial agent, which inhibits SerRS (236). Albomycin exhibited an MIC value of 5 ng/mL against *Escherichia co*li and 10 ng/mL against *Streptococcus pneumoniae* which is almost tenfold more potent than penicillin and 8-fold more potent than ciprofloxacin (237, 238). Albomycin also inhibited *S. aureus* USA 300 strain

NRS38441, a virulent MRSA strain, with an MIC of 0.125 µg/mL, and was 16-fold more potent than ciprofloxacin (238). Thus, further studies to evaluate albomycin as a potentially effective and safe antibiotic are ongoing (238). In contrast, another study reported that there was no toxicity showed during in vivo studies of albomycin and it was well tolerated and safe up to a maximum dose evaluated in mice as well as it has been successfully used to treat human bacterial infections (239).

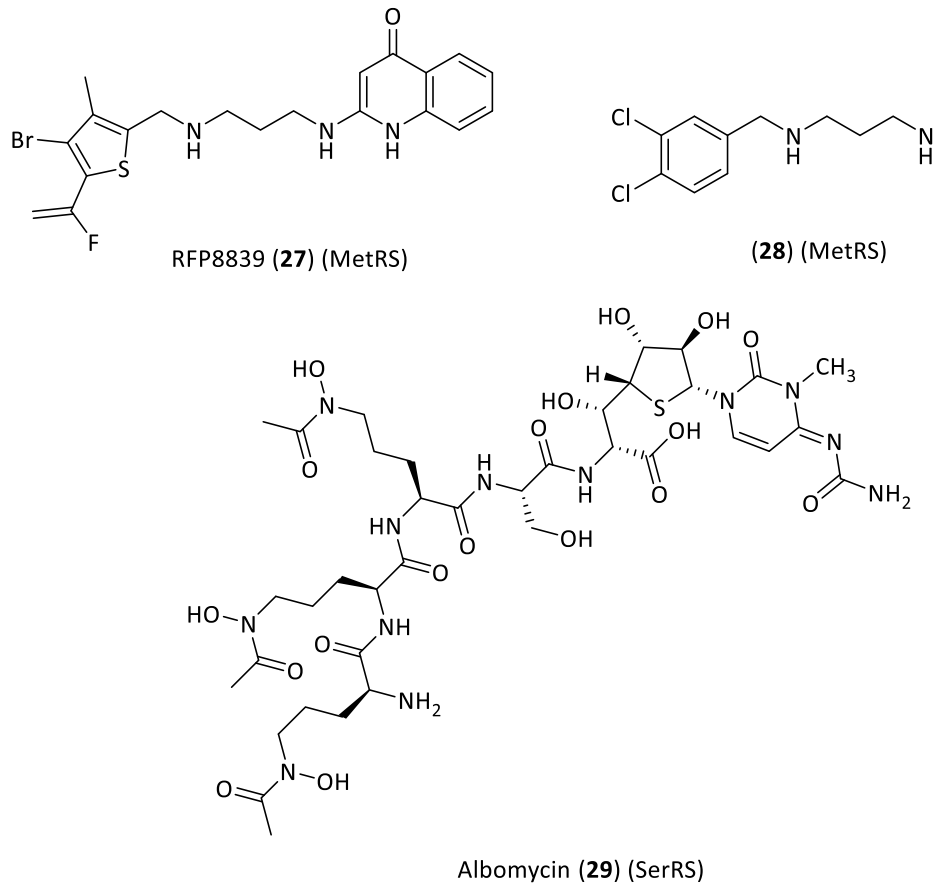

Figure 15: Chemical structures of MetRS and SerRS inhibitors.

Cladosporin and BC-K-YH16899 (Figure 16) are LysRS inhibitors, Cladosporin is a natural compound which is selective for pathogenic over mammalian LysRS, with antifungal, antibacterial, inflammatory and insecticidal activity as well as plant growth regulatory effect (240). Cladosporin also inhibits *Plasmodium falciparum* blood and liver stage proliferation (240, 241). BC-K-YH16899 is a synthetic compound that inhibits the interaction of LysRS with the laminin receptor (67L) and the metastasis in mouse models is suppressed, however its potential as an antimetastatic therapeutic target has not reported (242, 243). The carboxamide and acetamide derivatives (Figure 16) are *Pseudomonas aeruginosa* ND-AspRS inhibitors, which are resulted from

screening 1690 natural and synthetic compounds for AspRS inhibitory activity. BT02A02 and BT02C05 have shown broad spectrum antibacterial activity and also inhibit growth of efflux and hypersensitive strains of *Pseudomonas aeruginosa*. However, BT02A02 and BT02C05 were not effective against the wild-type strains of *E. coli* and *P. aeruginosa*, suggesting that both compounds are pumped out of the bacterial cell before reaching an effective concentration. Both derivatives do not compete with either aspartic acid or ATP binding sites of AspRS, indicating that their mechanism of actions occur outside the aminoacylation site and potentially in blocking the formation of Asp-tRNA^{Asp} or Asn-tRNA^{Asn} complexes during protein biosynthesis (244).

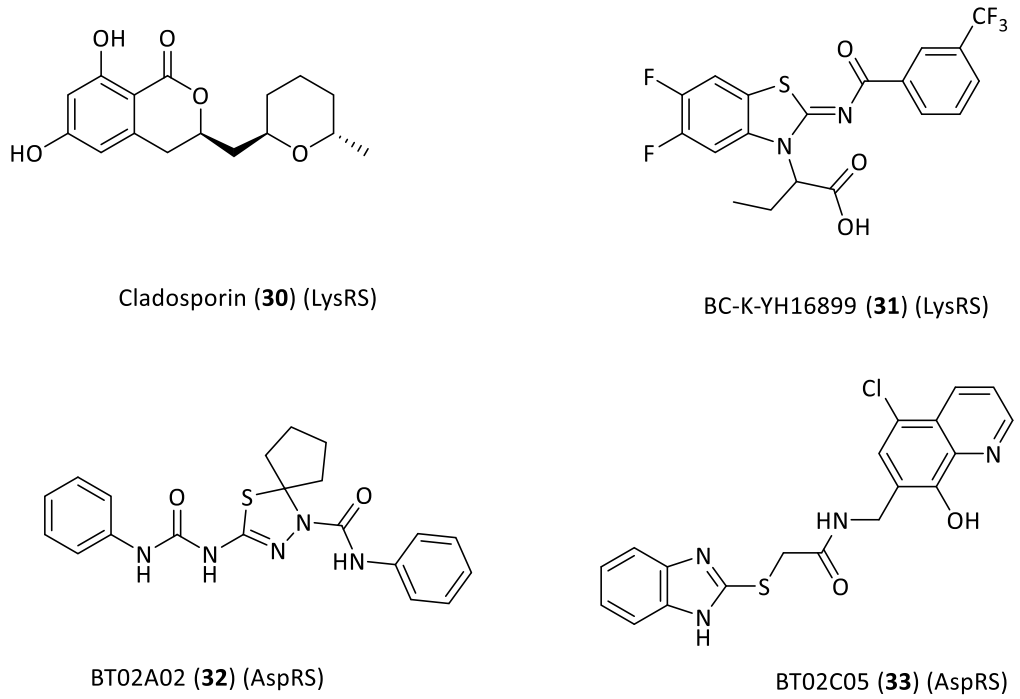

Figure 16: Chemical structures of LysRS and AspRS inhibitors.

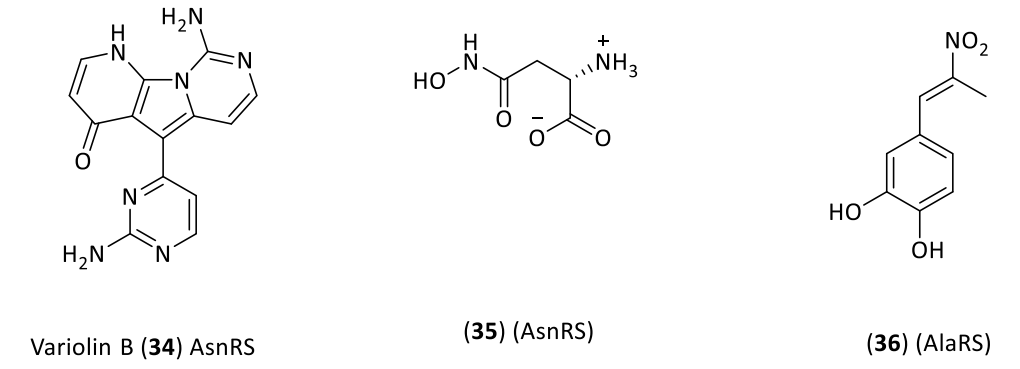

Figure 17: Chemical structures of AsnRS and AlaRS inhibitors.

Variolin B (Figure 17) is a *Brugia malayi* AsnRS inhibitor, which was identified from *in slico* screening (245) while the oxobutanoate derivative (L-aspartate β-hydroxamate) (Figure 17) is a natural AsnRS that inhibits the pre-transfer editing of the *Brugia malayi* AsnRS (245). The catechol derivative (Figure 17) was also found through *in silico* docking against *Plasmodium falciparum* AlaRS and inhibited parasite growth in culture (245, 246).

In conclusion, antibiotic resistance is a global public health issue, which has a significant negative impact on GDP owing to the effect on health and economy. Increased mortality and morbidity, as deaths and prolonged periods of sickness respectively attributable to antibiotic resistance, will reduce the size of the working age population and productivity. As a result, there has been extensive research on antibiotic development including aaRSs inhibitors. With around 20 aaRS enzymes, aaRS inhibitors, which interfere with bacterial protein synthesis, have been well investigated producing potent anti-infective agents (247). With the purpose of developing of new multitarget inhibitors, the similarity of *S. aureus* and *E. faecalis* aaRSs in term of their protein sequences of the active catalytic sites and significant motifs, was a focus to find the most similar enzymes that can be targeted by one inhibitor. *S. aureus* is one of the antibiotic-resistant pathogenic bacteria in the WHO published priority list owing to its ability to resist multiple antibiotics for example MRSA (239). However, *E. faecalis* is the major pathogen responsible for human nosocomial infections, accounting for 85–90% of *Enterococci* infections (248) and the toxicity induced by *E. faecalis* infection is exacerbated by its cytolysin production leading to a 5-fold increase in mortality of nosocomial bacteraemia (249).

1.5. Aim and objectives

As aaRSs are important target in the bacterial world with intensive research focused on their inhibitors as potential antibiotics owing to their crucial role in protein synthesis, the aim of the project was to design antibacterial aaRSs inhibitors effective against *S. aureus* and *E. faecalis*. The similarity in the protein sequences of aaRSs specifically in their conserved catalytic sites and significant motifs makes the design of multitarget inhibitors a viable option. By using a multitarget hypothesis, the bacterial fitness will be significantly affected leading to a reduction in bacterial resistance development. However, the FDA approved aaRSs inhibitors, Bactroban® and Kerydin®, target only one aaRS enzyme and resistance against them is detected (188, 189).

For the purpose of identifying the most similar aaRSs in *S. aureus* and *E. faecalis*, a study and analysis of aaRSs in both microorganisms was the main objective to fully understand their evolutionary relationships defining their common domains and signature motifs, and also to understand their stereospecificity with respect to amino acid and ATP bindings. The design of the dual AspRS and AsnRS inhibitors of the target microorganisms was performed as described in three main stages;

- Computational studies of the target enzymes with their natural substrates including molecular modelling, docking studies, molecular dynamics simulations and binding affinity to provide valuable data in the design process and therefore to determine the optimal compounds for synthesis.
- Synthesise of the selected compounds through optimisation of the synthetic schemes and subsequent purification using chromatography techniques and analysis.
- Assessment of inhibitory activity with an initial preliminary screen against a panel of microorganisms to determine MIC values. Further evaluation of inhibitory activity against target aaRS enzymes to determine IC_{50} values.

Chapter 2: Computational studies

2. Introduction

The prediction of binding interactions between proposed molecules and active site of a target enzyme is the most fundamental goal in drug design. Additionally, the estimation of binding strength and small molecules conformational changes inside a target are essential to afford a more detailed understanding of binding affinity (250). Thus, computational approaches have recently used in a computer aided drug design (CADD) assists in the analysis, development and discovery of drugs and similar biologically active molecules (251). These tools can determine and elaborate the strength of interactions between ligands and targets for identification of lead molecules from databases (252). CADD can be generally classified into two classes, namely: ligand-based drug design (LBDD) and structure-based drug design (SBDD). LBDD focuses on the knowledge of a structure activity relationship (SAR) of known ligands for a target and chemical similarity criteria in order to establish a relationship between their physicochemical properties and their activities for optimisation or designing compounds with improved activity (252, 253). When structural information of a biological target is missing (254), a set of reference structures collected from known compounds is used to interact with the target of interest and analysis of their two-dimensional (2D) or three-dimensional (3D) structures allows prediction of the nature and strength of binding interaction. By using quantum chemistry methods or density functional theory, the optimised parameters are delivered for the molecular mechanics calculation to anticipate the conformation of the small molecules and to model conformational changes in the biological target that may occur when the small molecule binds to it (255). Furthermore, the estimation of the electronic properties, such as electrostatic potential and polarisability can be provided of the drug candidate that will influence binding affinity (251). SBDD is a direct molecular modelling approach based on the knowledge of the 3D structure of the biological target, which is determined by X-ray crystallography and NMR spectroscopy (251). By analysing the 3D structural information of a biological macromolecular target, the important binding sites and interactions are identified for their respective biological functions. Such information can then be utilised to design novel drugs that can compete with essential interactions involving the target and thus interrupt the biological pathways essential for survival of the targeted microorganism (251). There is increased availability of

resolved protein structures in the last few years, increasing the possibility of using SBDD (254). As a result, these innovative computational tools are used to bridge the gap between the number of known sequences and that of 3D models (256). Because the percentage of experimentally known 3D models is currently less than 1%, template-based protein structure modelling techniques are used as a comparative tool to determine 3D-protien folding and to build a full atom model from a possible set of available templates (257). Despite the fact that 3D structures of proteins from the same family are more conserved than their amino acid sequences, the structural similarity between two proteins can be assumed if the similarity of their sequences is detectable (258, 259). The benefit of using computational modelling in chemistry and biology is to save numerous time and cost as it is a fast, cheap, and reliable workhorse for making predictions concerning biomolecular systems. (260-262). There are several computational programs and web servers, which automate the comparative modelling process. Molecular Operating Environment (MOE) (263) is a drug discovery software, which is mainly applied for ligand, structure and fragment- based designs, pharmacophore discovery, medicinal chemistry applications, antibody and biologics design, protein, DNA/RNA and antibody modelling, 3D molecular visualisation, structural bioinformatics, molecular simulations, structure activity relationship (SAR) explorer and virtual screening (263). Additionally, it runs on many operating systems (Windows, MAC and Unix) to serve as a platform of combining visualisation, modelling and simulations, as well as methodology development in one package (264, 265). On the other hand, there are free structural bioinformatics web servers that integrate programs and databases required for protein structure modelling in a web-based workspace such as the SWISS-MODEL server (266). In terms of the quality of generating models between MOE and the SWISS MODEL server, the latter one automatically decreases gaps between the sequences. Thus, its accuracy to generate reliable 3D protein structure models is higher than those generated from MOE. SWISS-MODEL uses ProMod3, an inhouse comparative modelling engine based on open structure. ProMod3 extracts initial structural information from the template structure and Insertions and deletions, as defined by the sequence alignment, are resolved by first searching for viable candidates in a structural database. Final candidates are then selected using statistical potentials of mean force scoring methods (267). By using

SBDD, computational studies in this project are summarised in five essential steps including (Figure 18);

(i) similarity search for proteins with known 3D structures that are similar in their sequences to the target sequence

(ii) alignment of the protein sequences of the closest 3D template with the query protein to identify conserved regions and generate a homology model

(iii) evaluation of the constructed models to determine stereochemical and overall protein structure quality and also validate the compatibility of 3D model with its amino acids 1D sequence

(iv) determination the key amino residues in the active site and identification of the binding interactions of the natural substrate through docking studies, and

(v) molecular dynamics simulations to predict ligand–receptor interactions and the conformational changes that a protein or ligand may undergo under different conditions (256, 268).

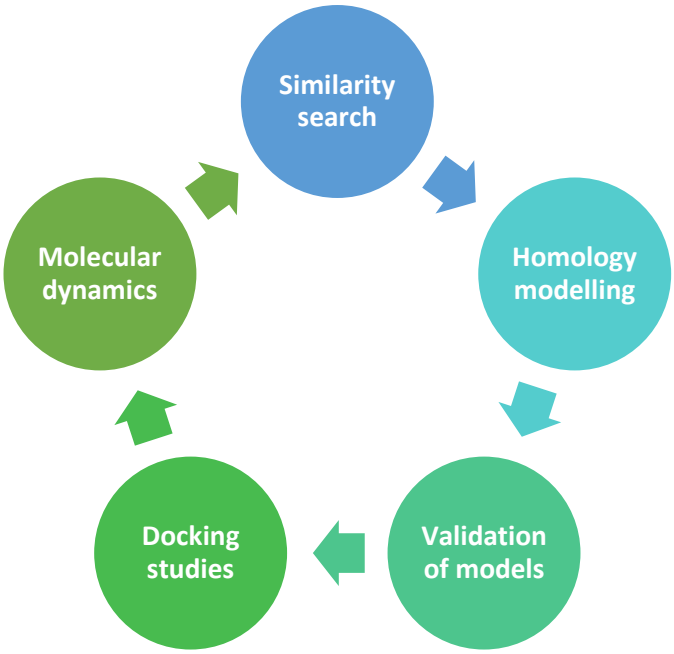

Figure 18: The main five stages of the computational studies.

2.1. *Staphylococcus aureus* aminoacyl tRNA synthetases

Studying aaRSs in the target microorganisms contributed to better understanding of similarities and differences between them, thus the UniProtKB server (269) was used to obtain *S. aureus* aaRSs and their protein sequences, with Uniprot identifiers provided in Tables 2 and 3. Additionally, by using basic local alignment search tool (BLAST) analysis, the active sites, conserved signatures, motifs and dimer interface amino acid residues were determined (Tables 2 and 3) (270). In *S. aureus*, there are 19 aaRSs responsible for 19 amino acids. GlnRS is missing, thus synthesis of Gln-tRNA^{Gln} is made by an indirect aminoacylation pathway as previously described (Section 1.4.3).

2.1.1. Class I *S. aureus* aminoacyl tRNA synthetases

From 19 *S. aureus* aaRS enzymes, nine of them represent class I. LeuRS, TyrRS and TrpRS are dimeric enzymes while others are monomers (Table 2).

Table 2: Class I *S. aureus* aaRSs with clarification of the position of active sites, HIGH and KMSKS signatures.

Enzymes	Accession No. [a]	Length [a]	HIGH region [b]	KMSKS region [b]
CysRS	Q2G2M6	466	30-40	265-269
Active site [b]	Cys28, Gly29, Pro30, Thr31, His37, Gly39, Asn40, Pro43, Ala44, Asn66, Thr68, Trp204, Cyc208, Gly225, Gly226, Asp228, Leu229, His233, Gly257, Phe258, Ile259			
IleRS	Q2FZ82	917	57-67	595-599
Active site [b]	Pro56, Pro57, Tyr58, His64, Gly66, His67, Asn70, Arg440, Trp528, Ser531, Glu554, Gly555, Ser556, Asp557, Gln558, Arg560, Trp562, His585, Gly586, Phe587, Val588, Met589, Gly593, Lys594, Lys595, Met596, S597, Lys598, Asp623			
LeuRS	Q2FXH2	805	41-52	577-581
Active site [b]	Phe40, Tyr42, His49, His52, Asp80, Gln88, Gly531, Glu533, His534, His538, Gln567			
Dimer interface	Phe39, Tyr41, His48, His51, Asp79, Gly532, Glu534, His535, His535, His539, Gln567, Ile570, Met578, Lys580			
ValRS	Q2FXR8	876	44-54	520-524

Active site [b]	Pro42, Pro43, Pro44, Asn45, His51, Gly53, His54, Asp58, Asp83, Typ447, Ser450, Thr479, Gly480, Asp482, Ile483, Trp487, His510, Gly511, Leu512, Val513, Met521			
MetRS	Q2G1R9	657	13-23	308-312
Active site [b]	Pro11, Ile12, Tyr14, Asp51, Trp237, Ala240, Leu241, Tyr244, Ile273, His277			
TyrRS	Q2FXJ5	420	41-50	231-235
Active site [b]	Tyr36, Cys37, Gly38, Ala39, Asp40, His47, Gly49, His50, Pro53, Phe54, Leu71, Thr76, Asn125, Tyr169, Gln173, Asp176, Gln190, Gly192, Gly193, ASP195, Gln196, Asn199, Leu123, Lys131, Phe132, Lys134			
Dimer interface	Gly74, Met77, Leu133, Ile134, Ser135, Phe136, Leu137, Arg138, Gly141, Lys142, Val144, Gly145, Val146, Asn147, Met148, Leu149, Thr165, Phe167, Thr168, Ile171, Leu172			
TrpRS	Q2FZ Q7	329	10-18	193-197
Active site [b]	Phe5, Ser6, Gly7, Ile8, Gln9, Thr15, Gly17, Asn18, Gly21, Cys38, His43, Gln81, Tyr128, Met132, Asp135, Val144, Gly145, Asp147, Gln148, His151, Arg183, Lys193, Met194, Lys196			
Dimer interface	Gln42, Ile45, Thr46, His86, Val87, Ala90, Gly19, Trp92, Thr95, Thr96, Ser99, Val100, Gly101, Leu103, Glu104, Gly123, Leu125, Thr126, Pro129, Leu130			
ArgRS	Q2G0F8	553	130-140	380-384
Active site [b]	Glu126, Ser129, Asn131, His139, His142, Tyr314, Asp318, His341, Tyr344			
GluRS	Q2G241	484	11-21	252-256
Active site [b]	Arg9, Ala11, Pro12, Ser13, Gly21, Asn22, Arg24, Thr25, Glu45, Tyr205, Val209, Arg223, Gly224, Asp226, His227, Ser243, Leu244, Lys252, Leu253.			

a http://www.uniprot.org/uniprot/ b www.ncbi.nlm.nih.gov

2.1.2. Class II *S. aureus* aminoacyl tRNA synthetases

Most of class II *S. aureus* aaRS enzymes are dimeric except AlaRS and PheRS and LysRS is only found as class II in this microorganism. Key amino acid residues are identified for active sites, motifs, dimer interface and polypeptide binding sites (Table 3).

Table 3: Class II *S. aureus* aaRSs with clarification of the position of active sites, dimer interface and conserved motifs.

Enzyme	Accession No. [a]	Length [a]	Motif 1[b]	Motif 2[b]	Motif 3[b]
AlaRS	Q2FXV9	876	Val23, Glu24, Pro25, Ser27, Ala28	Ile70, Arg71, Thr72	Gly228, Met229, Gly230, Leu231, Glu232, Arg233
Active site [b]	Tyr53, Asp55, Arg71, Phe88, Met90, Gly92, Asn93, Phe94, Glu203, Val204, Val208, Asn224, Ile225, Met229, Gly230				
HisRS	Q2FXU4	420	Tyr35, Lys36, Glu37, Ile38, Arg39, Thr40, Pro41, Ile42, Phe43	Phe111, Arg112, Tyr113, Glu114, Arg115	Gly305, Phe306, Ala307, Leu308, Ser309, Arg312
Active site [b]	Glu80, Thr82, Arg112, Glu114, Tyr121, Phe124, Gln126, Glu130, Arg257, Leu259, Tyr261, Tyr262, Thr283, Gly288, Phe306, Ser309, Arg312				
Dimer interface	Arg20, Phe32, Glu37, Ile38, Arg39, Thr40, Pro41, Ile42, Phe43, Phe66, Lys67, Glu79, Thr81, Arg86, Ser87, Glu90, His91, Arg122, Gln123, Glu130, Ser138, Glu142, Ala145, Gly287, Gly305, Phe306				
GlyRS	Q2FY08	463	Val61, Gly62, Ile63, Asp64, Ala65, Ala66, Ile67, Leu68	Phe205, Arg206, Asn207, Glu208	Gly334, Ala335, Asp336, Arg337
Active site [b]	Glu174, Ala176, Arg206, Glu208, Phe216, Arg217, Thr218, Phe221, Gln223, Glu225, Glu290, Leu291, Arg297, Glu320, Ser322, Glu324, Arg327				
Dimer interface	Gly16, Lys42, Trp50, Gln56, Gly62, Ile63, Ala66, Ile67, Leu68, Asn70, Phe155, Lys156, Thr157, Phe158, Asn185, Ser189, Glu220, Lys304				
ProRS	Q2G1Z4	567	Ser66, Val67, Glu68, Ile69, Leu70, Met71, Pro72, Ala73	Phe139, Arg140, Asp141, Glu142	Gly441, Ile442, Gly443, Ile444, Ser445, Arg446
Active site [b]	Thr109, Glu111, Arg140, Glu142, Leu150, Arg151, Glu152, Phe155, Met157, Lys158, Asp159, Glu411, Glu413, Val414, Gln416, Cys439, Tyr440, Glu441, Glu443, Arg446				

Dimer interface	Lys33, Gln34, Ser41, Tyr42, Leu43, Pro44, Asn51, Glu68, Ile69, Leu70, Pro72, Ala73, Leu94, Arg96, Leu97, Gln98, Asp99, Arg100, Ile118, Ser138, Glu155				
SerRS	P95689	428	Thr192, Glu193, Met194, Met195, Val196, Pro197, Gln198, Leu199	Phe261, Arg262, Ser263, Glu264	Gly387, Leu388, Ala389, Arg391
Active site [b]	Ala162, Thr231, Ala233, Arg262, Ala264, Arg271, Arg273, Ile276, Leu278, Phe281, Lys282, Glu284, Glu349, Ile350, Ser351, Ser352, Asn382, Ser384, Arg391				
Dimer interface	Arg154, Ala155, Ala156, Lys157, Val158, Ser159, Arg162, Phe163, Val164, Tyr165, Leu166, Thr167, Asn168, Gln172, Glu174, Ala176, Asn179, Thr192, Glu193, Met194, Met195, Pro197, Gln198, Leu199, Asn201, Phe219, Lys220, Glu222, Leu226, Pro235, Phe239, Glu243, Ala259, Gln281, Phe416, Met417				
ThrRS	Q2FXP7	645	Asp291, His292, Val293, Tyr294, Thr295, Pro296, Val297, Leu298	His364, Arg365, Tyr366, Glu367	Ser522, Thr523, Met524, Glu525, Arg526
Active site [b]	Lys244, Leu258, His309, Tyr312, Asp315, Met316, Pro330, Arg365, Glu367, Ser369, Gly370, Ala371, Gln376, Arg377, Val378, Met381, Leu383, Lys482, Thr485, Leu486, Gln490, Ser522, Thr523, Arg526				
Dimer interface	Glu249, Asn255, Gln257, Leu258, Val259, Ala261, Leu263, Leu265, Trp266, Pro268, Ala271, Val286, Ser287, Asp291, His292, Tyr294, Pro296, Val297, Leu298, Asn300, Phe318, Pro319, Pro320, Gln322, Leu323, Asp324, Glu325, Met329, Met341, Ile342, Asn345, Lys346, Pro347, Ser349, Tyr350, Arg351, His364, Tyr366, Ser369, Arg379, Gly380, Ile408, Glu453, Leu454, Gly455, Ile505, Gln507				
AspRS	Q2FXU5	588	Pro169, Val170, Leu171, Thr172, Lys173	Phe222, Arg223, Asp225, Glu225	Gly537, Leu538, Asp539, Arg540

Active site [b]	Glu177, Gly178, Ala179, Ser199, Gln201, Lys204, Arg223, Glu225, Asp230, Arg231, Gln232, Phe235, Gln237, His451, His452, Glu485, Gly488, Arg492, Ile534, Ala535, Gly537, Arg540				
Dimer interface	Arg147, His148, Gln149, Arg152, Arg155, Gln156, Asp159, Gly162, Phe163, Phe164, Asp165, Glu167, Thr168, Pro169, Val170, Leu171, Thr172, Lys173, Arg180, Leu183, Val184, Pro185, Ser186, Arg187, Gly191, Glu192, Phe193, Tyr194, Ile209, Ser210, Asp213, Lys214, Lys220, Asp224, Glu234, Phe244, Asp249, Phe519, Asp522, Ala523, Lys525, Tyr526, Gly527, Ala528, Ala556, Phe557, Lys559				
AsnRS	Q2FYH6	430	Pro155, Ile156, Leu157, Thr158, Ala159	Phe205, Arg206, Ala207, Glu208	Gly401, Leu402, Glu403, Arg404
Active site [b]	Arg206, Glu208, Arg213, His214, Glu351, Gly354, Gly401, Arg404				
Dimer interface	His116, H118, Arg122, His127, Arg133, Asn134, Ile137, Tyr141, Gly148, Lys151, Asp153, Pro155, Ile156, Leu157, Ala159, His170, Thr171, Tyr172, Phe173, Asp174, Tyr186, Ala189, Met192, Ala193, His194, Gly195, Ile216, Glu217, Ala226, Phe227, Glu232, Asp386, Arg389, Tyr390, Gly391, Ser392				
LysRS [c]	Q2G0Q3	495	Pro201, Met202, Met203, His204, Gln205	Phe254, Arg255, Asn256, Glu257	Gly469, Ile470, Asp471, Arg472
Active site [b]	Glu233, Arg255, Glu257, His263, Phe267, Glu406, Glu413, Asn416, Glu420, Arg472				
Dimer interface	Gly65, Arg66, Asp83, Leu84, Ile113, Thr139, Leu142, Arg143, Pro144				
PheRS	P68849	352	Tyr128, Glu129, Ile130, Val131, Asn132, Gly133, Tyr134	Tyr199, Arg200, Arg201, Asp202	Gly313, Met314, Gly315, Pro316, Asp317, Arg318
Active site [b]	Asp156, Met157, Gln158, His172, Ser174, Gln177, Arg200, Asp202, Thr207, His208, Ser209, Phe212, Gln214, Glu216, Phe254, Phe256, Thr257, Glu285, Ile286, Leu287, Gly288, Ala289, Gly290, Phe312, Gly313, Met314, Gly315, Arg318, Ile329				

Polypeptide binding	αHis110, αThr113, αIle116, αGlu117, αLeu124, αGlu129, αIle130, αAsn131, αGly132, αTyr133, αSer150, αAsp155, αSer159, αPhe160, αTyr161, αIle162, αThr163, αAsp164, αThr180, αPro188, αVal189, αLys196, αTyr198, αArg200, αSer208, αMet225, αSer226, αAsp227, αLys229, αGly230, αPro251, αGlu258, αPro259, αSer260, αGlu262, αHis293, αPro294, αTyr333, αAsn335, αAsp336, αVal337, βGlu508, βGlu511, βLeu515, βGln517, βIle519, βIle520, βTyr521, βIle539, βAsp540, βLeu541, βLeu542, βArg553, βAsn567, βLeu577, βAsn582, βPhe585, βAla587, βGln596, βVal627

a http://www.uniprot.org/uniprot/ b www.ncbi.nlm.nih.gov , c = LysRS is only found as class II in *S. aureus*

2.2. *Enterococcus faecalis* aminoacyl tRNA synthetases

As found for *S. aureus*, *E. faecalis* has 19 aaRSs responsible for 19 amino acids, with Gln-tRNA^{Gln} synthesised through the indirect aminoacylation pathway. By using BLAST analysis, the active sites, conserved signatures, motifs and dimer interface residues were determined (Tables 4 and 5).

2.2.1. Class I *E. faecalis* aminoacyl tRNA synthetases

From 19 *E. faecalis* aaRS enzymes, nine of them represent class I. TyrRS and TrpRS are dimeric enzymes while others are monomers (Table 4).

Table 4: Class I *E. faecalis* aaRSs with clarification of the position of active sites, HIGH and KMSKS signature.

Enzyme	Accession No.[a]	Length [a]	HIGH region [b]	KMSKS region [b]
CysRS	A0A1X3ALU9	470	37-40 (HIGN)	270-274
Active site [b]	Cys28, Gly29, Pro30, Thr31, His37, Gly39, Asn40, Ser43, Ala44, Asn66, Thr68, Trp207, Cys211, Gly228, Gly229, Asp231, Leu232, His236, Gly260, Trp261, Val262			
IleRS	A0A1Q1FSR4	926	64-67 (HLGH)	593-597
Active site [b]	Pro56, Pro57, Tyr58, His64, Gly66, His67, Asn70, Arg438, Trp526, Ser529, Glu552, Gly553, Ser554, Asp555, Gln556, Arg558, Trp560, Gln581, Gly582,			

	Met583, Val584, Leu585, Gly587, Arg588, Lys589, Met590, Ser591, Lys591, Asp628			
LeuRS	A0A1B4XLV7	804	48-51 (HVGH)	576-580
Active site [b]	Phe39, Tyr41, His48, His51, Asp79, Gln87, Gly530, Glu532, His533, His537, Gln566, Ile569, Met577, Lys579			
ValRS	A0A2R6U726	880	55-58 (HLGH)	524-528
Active site [b]	Pro46, Pro47, Pro48, Asn49, His55, Gly57, His58, Asp61, Asp86, Trp451, Ser454, Thr483, Gly484, Asp486, Ile487, Trp491, His514, Gly515, Leu516, Ile517, Met525			
MetRS	A0A1G1S8M1	669	21-24 (HIGN)	309-313
Active site [b]	Pro12, Ile13, Tyr15, Asp52, Trp238, Ala241, Leu242, Tyr245, Ile274, His278			
TyrRS	A0A1B4XLC0	418	45-48	228-232 (KFGKT)
Active site [b]	Tyr34, Gly36, Val37, Asp38, His45, Gly45, His48, Tyr166, Gln170, Asp173, Gln186, Gly188, Gly189, Gln192, Leu220, Met221, Lys228, Phe229, Gly230, Lys231			
Dimer interface	Gly72, Thr75, Ile76, Leu129, Leu130, Phe132, Leu133, Arg134, Gly137, Lys138, Phe150, Asn141, Val142, Asn143, Met145, Leu146, Thr162, Phe164, Thr165, Ile168, Leu169			
TrpRS	A0A2T5D6I6	336	15-18 (TIGN)	198-202
Active site [b]	Phe5, Ser6, Gly7, Ile8, Gln9, Thr15, Gly17, Asn18, Gly21, Cys38, His43, Gln81, Trp128, Met132, Asp135, Val143, Val145, Gly146, Asp148, Gln149, His152, Arg187, Lys198, Met199, Lys201			
Dimer interface	Glu42, Ile45, Thr46, His86, Ala87, Ala89, Gly90, Trp91, Gln94, Cys95, Thr97, Ser98, Ile99, Gly100, Leu102, Glu103, Gly123, Leu125, Thr126, Pro129, Leu130			
ArgRS	A0A3N3ZCS8	563	129-132 (SMGH)	372-375 (LSTR)
Active site [b]	Asp118, Ser120, Asn122, Ser128, His131, Trp307, Asp311, Gln336, His339			
GluRS	A0A1J6YUN6	485	17-20 (HIGN)	253-257 (KLSKR)
Active site [b]	Arg7, Ala9, Pro10, Ser11, Gly19, Asn20, Arg22, Thr23, Glu43, Tyr196, Val200, Arg214, Gly215, Asp217, His218, Thr243, Leu244, Lys253, Leu254			

a http://www.uniprot.org/uniprot/ b www.ncbi.nlm.nih.gov ,

2.2.2. Class II *E. faecalis* aminoacyl tRNA synthetases

Most of class II *E. faecalis* aaRSs are dimeric enzymes except AlaRS and PheRS and LysRS is found only as class II in this microorganism (Table 5).

Table 5: Class II *E. faecalis* aaRSs with clarification of the position of active sites, dimer interface and conserved motifs.

Enzyme	Accession No. [a]	Length [a]	Motif 1[b]	Motif 2[b]	Motif 3[b]
AlaRS	A0A1G1SE70	880	Val24, Glu25, Pro26, Ser27, Ala28	Ile70, Arg71, Thr72	Gly229, Met230, Gly231, Leu232, Glu233, Arg234
Active site [b]	Tyr51, Asp53, Arg71, Phe88, Met90, Gly92, Asn93, Phe94, Glu202, Ile203, Val207, Asn226, Ile227, Met231, Gly232, Arg235				
HisRS	A0A1Q1FV24	433	Tyr36, Gln37, Glu37, Ile38, Arg40, Thr41, Pro42, Ile43, Phe45	Phe113, Arg114, Tyr115, Glu116, Arg117	Gly306, Phe307, Gly308, Met309, Gly310, Arg313
Active site [b]	Glu81, Thr83, Arg115, Glu117, Leu124, Phe127, Gln129, Glu133, Arg259, Leu261, Tyr263, Tyr264, Thr284, Gly289, Phe307, Gly310, Arg313				
Dimer interface	Gln21, Asp33, Glu38, Ile39, Arg40, Thr41, Pro42, Ile43, Phe44, Phe68, Tyr69, Glu81, Thr83, Arg88, Ala89, Glu92, Asn93, Arg124, Gln125, Glu132, Ala140, Glu144, Ala147, Gly288, Gly306, Phe307				
GlyRS	A0A1Q1FVX2	302	Cys23, Met24, Leu25, Met26, Gln27, Ala28, Tyr29, Asp30	Arg61, Arg62, Pro63, Ala64	Gly164, Leu165, Glu166, Arg167
Active site [b]	Ala35, Thr37, Arg62, His78, Gln80, Gln82, Val83, Val84, Glu139, Ile140, Thr144, Glu160, Ile161, Tyr163, Gly164, Glu166, Arg167				
Dimer interface	Gln8, Leu12, Lys16, Met24, Leu25, Gln27, Tyr29, Asp30, Thr31, Glu32, Gly48, Val57, Arg61, Gln77, Trp183, Pro196, Glu199, His200, Ile207, Asn209, Met212, Glu215, Asn216, Lys219, Phe220, Glu223, Arg226, Glu230, Leu232, Val233, His234, Pro235, Asp238, Lys242				

ProRS	Q831W7	572	Ala66, Val67, Glu68, Met69, Leu70, Met71, Pro72, Ala73	Tyr139, Arg140, Asp141, Glu142	Gly442, Ile443, Gly444, Val445, Ser446, Arg447
Active site [b]	Thr110, Glu111, Arg140, Glu142, Leu150, Gly152, Phe155, Met157, Asp159, Gly405, Glu407, Ile408, His410, Cys440, Tyr441, Gly442, Gly444, Arg447				
Dimer interface	Arg33, Gln34, Ile54, Tyr42, Leu43, Pro44, Glu51, Glu68, Met69, Leu70, Pro72, Ala73, Leu93, Arg95, Leu96, Lys97, Asp98, Arg99, Leu117, Thr137, Glu154				
SerRS	A0A1B4XSE9	423	Thr192, Glu193, Met194, Ile195, Thr196, Pro197, Tyr198, Ile199	Phe261, Arg262, Ser263, Glu264	Gly385, Leu386, Ala387, Arg390
Active site [b]	Ser161, Thr231, Glu233, Arg262, Glu264, Arg271, Arg274, Ile277, Leu279, Phe282, Lys284, Glu286, Glu350, Ile351, Ser352, Ser353, Asn383, Ser385, Arg391				
Dimer interface	Arg154, Gly155, Ala156, Lys157, Val158, Ala159, Arg162, Phe162, Phe163, Val164, Tyr165, Tyr166, Lys167, Gly168, Arg172, Ala176, Asn179, Thr192, Glu193, Met194, Ile195, Pro197, Tyr198, Ile199, Asn201, Phe219, Gln220, Gln222, Leu226, Pro235, Tyr239, Glu243, Pro259, Gln280, Tyr415, Met416				
ThrRS	A0A3N3SQX9	647	Gln291, His292, Val293, Tyr294, Thr295, Pro296, Ile297	His364, Arg365, Tyr366, Glu367	Se523r, Thr524, Met525, Glu526, Arg527
Active site [b]	Lys245, Glu258, His309, Tyr313, Asp316, Met317, Pro333, Arg365, Glu367, Ser369, Gly370, Ala371, Gln376, Arg377, Val378, Met381, Leu383, Thr482, Thr485, Leu486, Gln490, Ser523, Thr524, Arg527				
Dimer interface	Glu249, Val255, Pro257, Glu258, Val259, Ser261, Leu263, Phe265, Trp266, Pro268, Ala271, Val286, Ser287, Gln291, His292, Try294, Pro296, Ile297, Met298, Asp300, Phe318, Pro319, Pro320, Gly324, Asp325, Gly326, Glu327, Leu329, Met341, Val342, Asn345, Thr346, Ile347, Ser349, tyr350, Arg351,				

	His364, Tyr366, Ser368, Arg379, Glu380, Val407, Glu454, Leu455, Glu456, Val504, Glu506				
AspRS	Q833I2	589	Pro168, Tyr169, Leu170, Gly171, Lys172	Phe221, Arg222, Asp223, Glu224	Gly535, Leu536, Asp537, Arg538
Active site [b]	Glu176, Gly177, Ala178, Ser198, GLN200, Lys203, Arg222, Glu224, Asp229, Arg230, Gln231, Phe234, Gln236, His449, His450, Glu483, Gly486, Arg490, Ile532, Ala533, Gly535, Arg538				
Dimer interface	Arg146, His147, Gln148, Lys151, Arg154, His155, Asp158, Asp161, Phe162, Leu163, Asp164, Glu166, Thr167, Pro168, Tyr169, Leu170, Gly171, Lys172, Arg179, Leu182, Val183, Pro184, Ser185, Arg186, Gly190, His191, Phe192, Tyr193, Gly208, Ala209, Asp212, Arg213, Arg219, Asp223, Glu233, Phe243, Glu248, Phe517, Asp520, Ala521, Asp523, Tyr524, Gly525, Phe226, Ala554, Phe555, Lys557				
AsnRS	A0A3N3KT82	450	Pro170, Ile171, Leu172, Thr173, Gly174	Phe220, Arg221, Ala222, Glu223	Gly421, Leu422, Glu423, Arg424
Active site [b]	Arg221, Glu223, Arg228, His229, Glu371, Gly374, Gly421, Arg424				
Dimer interface	His131, His133, Arg137, His142, Arg148, Asn149, Ile152, Tyr156, Gly163, Lys166, Asp168, Pro170, Ile171, Leu172, Gly174, Glu185, Thr186, Tyr188, Phe189, Gly190, Tyr202, Ala205, Met208, Ala209, Phe210, Gly211, Thr232, Glu233, Ala242, Tyr243, Glu248, Asp406, Lys409, Tyr410, Gly411, Ser412, Arg443, Met444, Ile445				
LysRS [c]	AOA1G1SBV2	498	Pro206, Val207, Leu208, His209, Asn210	Phe259, Arg260, Asn261, Glu262	Gly474, Ile475, Asp456, Arg477
Active site [b]	Glu238, Arg260, Glu262, His268, Phe272, Glu411, Glu418, Asn421, Glu425, Arg477				
PheRS	A0A3N3RQX8	345	Tyr28, Gln29, Ile30, Val31, Glu32, Gly33, Tyr34	Phe200, Arg201, Arg202, Asp203	Gly214, Leu215, Gly216, Pro217, Asp218, Arg219

Active site [b]	Asp156, Met157, Gln158, His172, Ser174, Gln177, Arg201, Pro203, Thr208, His209, Ser210, Phe213, Gln215, Glu217, Phe255, Phe257, Thr258, Glu285, Ile286, Leu287, Gly288, Ala289, Gly290
Polypeptide binding site	αHis110, αThr113, αMet116, αGlu117, αVal124, αGln129, αIle130, αGlu132, αGly133, αTyr134, αAsp151, αAsp156, αThr160, αPhe161, αTyr162, αIle163, αSer164, αAsp165, αThr179, αAla189, αLeu190, αArg191, αPro195, αLys197, αPhe199, αArg201, αSer209, αMet227, αGly228, αAsp229, αLys231, αGly232, αPro253, αGlu260, αPro261, αSer262, αGlu264, αHis294, αPro295, αTyr334, αAsn336, αAsp337, αLeu338.βGln501, βHis502, βSer509, βGlu512, βThr513, βGlu516, βIle518, βSer519, βTyr520, βThr539, βArg540, βLeu541, βAla542, βArg553, βAsn569

a http://www.uniprot.org/uniprot/ b www.ncbi.nlm.nih.gov , c = LysRS is only found as class II in *E. faecalis*

2.3. Result and discussion

2.3.1. Computational analysis of *S. aureus* aminoacyl tRNA synthetases.

In order to identify which of the aaRS enzymes of *S. aureus* would be optimal to target in a multitarget drug design approach, a similarity search was performed for class I and class II aaRSs separately using Clustal Omega (271), available at the European bioinformatics Institute (EMBL-EBI) (272). From the percent identity matrix results of class I aaRSs, the closet similarity was shown for subclass Ia members (Figure 19), followed by subclass IIb aaRSs (Figure 20). Inhibitors of subclass Ia aaRSs have been the main focus of research to date (see section aaRSs inhibitors, Chapter 1), therefore inhibitors of subclass IIb aaRSs, namely AspRS and AsnRS were the focus of the research presented here.

1: sp|Q2G241|	GLU	100.00	15.29	13.45	18.13	17.01	13.99	13.49	18.42	17.51
2: tr|Q2FZQ7|	TRP	15.29	100.00	15.95	16.26	16.67	11.47	16.21	14.78	14.64
3: sp|Q2FXJ5|	TYR	13.45	15.95	100.00	14.07	20.40	14.05	16.98	19.01	16.22
4: sp|Q2G0F8|	ARG	18.13	16.26	14.07	100.00	17.44	20.32	14.01	19.16	16.43
5: sp|Q2FXH2|	LEU	17.01	16.67	20.40	17.44	100.00	18.81	23.37	26.12	27.30
6: sp|Q2G2M6|	CYS	13.99	11.47	14.05	20.32	18.81	100.00	18.27	20.18	21.16
7: tr|Q2G1R9|	MET	13.49	16.21	16.98	14.01	23.37	18.27	100.00	22.30	25.20
8: sp|Q2FZ82|	ILE	18.42	14.78	19.01	19.16	26.12	20.18	22.30	100.00	25.80
9: sp|Q2FXR8|	VAL	17.51	14.64	16.22	16.43	27.30	21.16	25.20	25.80	100.00

Figure 19: Percent identity matrix of class I *S. aureus* aminoacyl tRNA synthetases, the % of similarity in subclass Ia enzymes shows in blue shaded boxes of LeuRS, green shaded boxes of IleRS and pink shaded boxes of ValRS.

1: sp|P95689|	SER	100.00	25.41	10.24	10.53	14.46	12.06	15.76	12.11	15.25	13.11
2: sp|Q2FXP7|	THR	25.41	100.00	15.00	16.39	21.75	16.71	15.06	14.83	14.58	15.59
3: sp|P68849|	PHE	10.24	15.00	100.00	25.17	16.48	11.85	14.53	9.09	18.55	12.50
4: sp|Q2FXV9|	ALA	10.53	16.39	25.17	100.00	18.64	18.55	12.80	11.21	18.03	14.71
5: sp|Q2G1Z4|	PRO	14.46	21.75	16.48	18.64	100.00	15.53	18.62	13.36	17.99	17.46
6: sp|Q2FY08|	GLY	12.06	16.71	11.85	18.55	15.53	100.00	18.21	12.10	19.33	16.76
7: sp|Q2FXU4|	HIS	15.76	15.06	14.53	12.80	18.62	18.21	100.00	16.53	21.66	17.90
8: sp|Q2FYH6|	ASN	12.11	14.83	9.09	11.21	13.36	12.10	16.53	100.00	25.24	24.32
9: sp|Q2FXU5|	ASP	15.25	14.58	18.55	18.03	17.99	19.33	21.66	25.24	100.00	25.50
10: sp|Q2G0Q3|	LYS	13.11	15.59	12.50	14.71	17.46	16.76	17.90	24.32	25.50	100.00

Figure 20: Percent identity matrix of class I *S. aureus* aminoacyl tRNA synthetases. the % of similarity in subclass IIb enzymes shows in blue shaded boxes of AsnRS, green shaded boxes of AspRS and pink shaded boxes of LysRS.

2.3.1.1 Construction of *S. aureus* AspRS and AsnRS models

2.3.1.1.1 Homology search of *S. aureus* AspRS and AsnRS

A basic local alignment search tool (BLAST) analysis (273, 274) was performed for the initial screening for all possible templates of *S. aureus* AspRS and AsnRS amino acid sequences using the ExPASy proteomic server (275) against the PDB resolved structures (276). Four structures were identified for each as possible templates (Table 6, 7). All chosen templates are wild type, that is they are not mutants or engineered, and have the same function but are from different bacteria. The criteria of selection are based on the reasonable sequence identity with both *S. aureus* AspRS and AsnRS. The AspRS enzyme of *Thermus thermophilus* (pdb: 1EFW) was chosen as the best template for *S. aureus* AspRS with 50.59% identity (277). The presence of the Glu177 as an important amino residue for the binding site in the outlier region of the *E. coli* based model in Ramachandran plot is excluded the AspRS *E coli* template (pdb: 1EQR) (278). *Pseudomonas aeruginosa* (pdb: 4WJ3) (279) as an asparagine transamidosome was unfavourable as a template owing to its slightly different enzyme function (280).

Therefore, selected *Thermus thermophilus* (pdb: 1EFW) was the best template for AspRS model building. *Thermus thermophilus* AsnRS (pdb: 5ZG8) (281) was the optimal template for homology modelling of *S. aureus* AsnRS owing to the high percentage of similarity (Table 7), however, the crystal structure was incomplete with two-8 amino acid residue gaps (161-168 and 209-216). The first gap is near to the catalytic site and the second gap is an important region for the active site (Figure 21) therefore *Pyrococcus horikoshii* AsnRS (pdb: 1X54) (282), with 45.83 % homology, was chosen as a template to build the *S. aureus* AsnRS homology model.

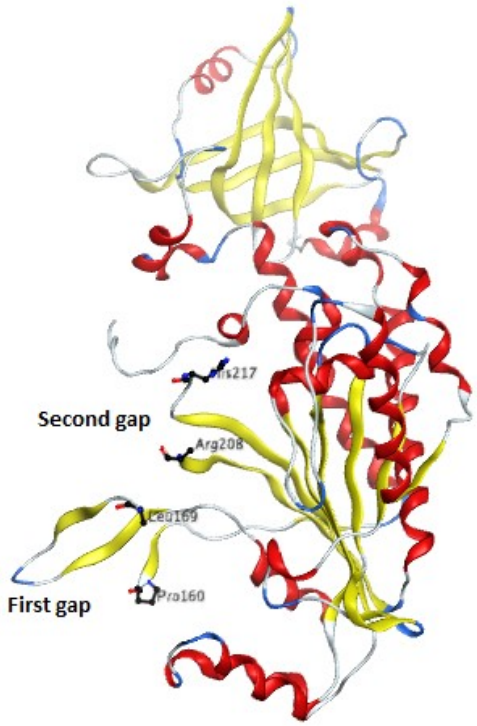

Figure 21: 3D structure of *Thermus thermophilus* AsnRS (pdb: 5ZG8) with two-8 amino acid residues gaps (161-168 and 209-216) identified. Stick and ball representation in black colour of each two amino acids residues shows the missing sequence.

Table 6: The first four hits in the *S. aureus* AspRS BLAST results.

Organisms	PDB code	BLAST score [a]	Sequence identity [b]	Sequence identity %	Positive %	Chain length	E-Value
E coli	1EQR	659	321/589	54.50	72	590	0.0
Pseudomonas aeruginosa	4WJ3	622	312/590	52.88	71	599	0.0
Thermus thermophilus	1EFW	566	298/589	50.59	68	580	0.0
Mycolicibacterium smegmatis	4O2D	531	270/595	45.38	62	620	0.0

[a] The BLAST score for an alignment is calculated by summing the scores of each aligned position and the scores of gaps. [b] (number of identical residues)/ (length of sequence fragment identified by PSI/BLAST)

Table 7: The first four hits in the *S. aureus* AsnRS BLAST results.

Organisms	PDB code	BLAST score [a]	Sequence identity [b]	Sequence identity %	Positive %	Chain length	E-Value
Thermus thermophilus	5ZG8	495	238/438	54.34	72	438	2e-174
Pyrococcus horikoshii	1X54	399	198/432	45.83	65	434	2e-136
Elizabethkingia anopheles	6PQH	273	168/478	35.15	54	490	2e-86
Thermococcus kodakarensis	3NEL	248	158/430	36.74	54	438	1e-77

[a] The BLAST score for an alignment is calculated by summing the scores of each aligned position and the scores of gaps. [b] (number of identical residues)/ (length of sequence fragment identified by PSI/BLAST)

To obtain more information, the phylogeny server (283) was used to conduct a phylogenetic tree using AspRS protein sequence from different organisms to determine the relative distances between these enzymes and the query sequence (Figure 22) and the same was done for AsnRS (Figure 23). The phylogenetic tree determines the different evolutionary branching of the prokaryotic and eukaryotic AspRS and AsnRS enzymes. The closet protein sequences to *S. aureus* AspRS in this

group of species are *E. coli* (ECOLI) followed by *Pseudomonas aeruginosa* (PSEAE) and *Thermus thermophilus* (THETH) while *Enterococcus faecalis* (ENTFL) and *Thermus thermophilus* (THETH) followed by *Pyrococcus horikoshii* (PYRHO) are the closet for *S. aureus* AsnRS. The least homologous are *Mycobacterium smegmatis* (MYCSE) for *S. aureus* AspRS and *Elizabethkingia anopheles* (9FLAO), and *Thermococcus kodakarensis* (THEKO) for *S. aureus* AsnRS. The difference of bacterial aaRSs than their human counterparts is clearly shown in the phylogenetic trees (Figures 22 and 23). Clustal analysis and percent identity matrix results (Figures 24 and 25) provide further validation.

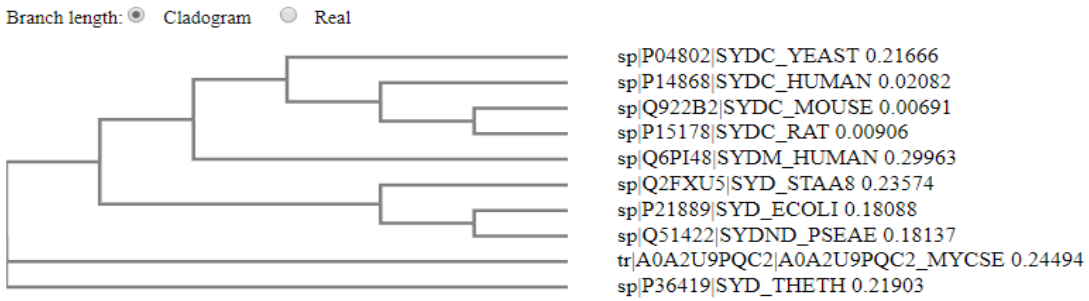

Figure 22: The phylogenetic tree of *S. aureus* AspRS (Q2FXU5) in relation to AspRS from other organisms: *Saccharomyces cerevisiae* (yeast) (P04802), *Homo sapiens* (cytoplasmic) (P14868), *Mus musculus* (mouse) (Q922B2), *Rattus norvegicus* (rat) (P15178), *Homo sapiens* (mitochondria) (Q6PI48), *E coli* (P21889), *Pseudomonas aeruginosa* (Q51422), *Mycolicibacterium smegmatis* (A0A2U9PQC2) and *Thermus thermophilus* (P36419).

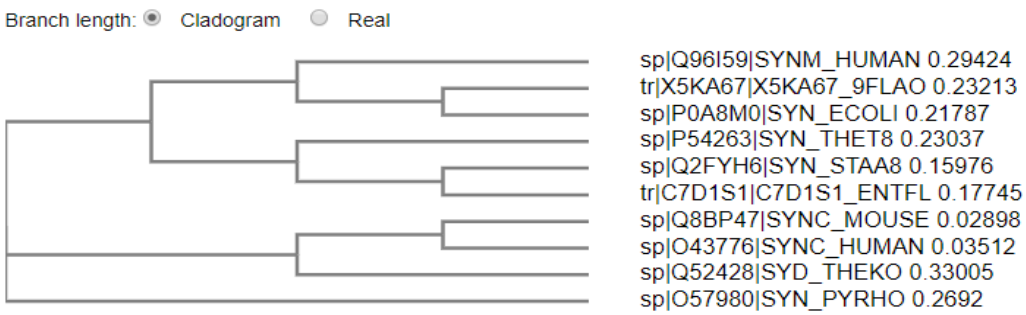

Figure 23: The phylogenetic tree of *S. aureus* AsnRS (Q2FYH6) in relation to AsnRS from other organisms: *Homo sapiens* (mitochondria) (Q96I59), *Elizabethkingia anopheles* (X5KA67), *E coli* (P0A8M0), *Thermus thermophilus* (P54263), *Enterococcus faecalis* (C7D1S1), *Mus musculus* (mouse) (Q8BP47), *Homo sapiens* (cytoplasmic) (O43776), *Thermococcus kodakarensis* (Q52428) and *Pyrococcus horikoshii* (O57980).

Percent Identity Matrix - created by Clustal2.1

1: sp|P04802|SYDC_YEAST	100.00	56.69	56.49	56.29	24.69	26.67	26.59	27.46	25.96	26.80
2: sp|P14868|SYDC_HUMAN	56.69	100.00	96.01	95.61	23.73	26.87	27.78	26.82	25.52	26.61
3: sp|Q922B2|SYDC_MOUSE	56.49	96.01	100.00	98.40	23.94	27.10	27.08	26.82	26.21	26.83
4: sp|P15178|SYDC_RAT	56.29	95.61	98.40	100.00	23.52	26.64	27.08	26.59	26.21	26.83
5: sp|Q6PI48|SYDM_HUMAN	24.69	23.73	23.94	23.52	100.00	41.52	45.41	41.11	41.87	40.59
6: tr|A0A2U9PQC2|A0A2U9PQC2_MYCSE	26.67	26.87	27.10	26.64	41.52	100.00	53.60	45.64	49.57	50.52
7: sp|P36419|SYD_THETH	26.59	27.78	27.08	27.08	45.41	53.60	100.00	50.87	50.62	51.49
8: sp|Q2FXU5|SYD_STAA8	27.46	26.82	26.82	26.59	41.11	45.64	50.87	100.00	54.66	53.01
9: sp|P21889|SYD_ECOLI	25.96	25.52	26.21	26.21	41.87	49.57	50.62	54.66	100.00	63.78
10: sp|Q51422|SYDND_PSEAE	26.80	26.61	26.83	26.83	40.59	50.52	51.49	53.01	63.78	100.00

Figure 24: The percent identity matrix of *S. aureus* AspRS (Q2FXU5) in relation to AspRS from other different organisms: *Saccharomyces cerevisiae* (yeast) (P04802), *Homo sapiens* (cytoplasmic) (P14868), *Mus musculus* (mouse) (Q922B2), Rattus *norvegicus* (rat) (P15178), *Homo sapiens* (mitochondria) (*Q6PI48*), *Mycolicibacterium smegmatis* (A0A2U9PQC2), *Thermus thermophilus* (P36419), *E coli* (P21889) and *Pseudomonas aeruginosa* (Q51422), the closet similar AspRSs sequences is observed in blue shaded boxes.

Percent Identity Matrix - created by Clustal2.1

1: sp|Q96I59|SYNM_HUMAN	100.00	42.47	43.32	29.61	28.02	29.13	31.80	34.06	35.87	34.38
2: tr|X5KA67|X5KA67_9FLAO	42.47	100.00	55.00	26.46	26.23	30.38	33.89	36.26	37.11	36.68
3: sp|P0A8M0|SYN_ECOLI	43.32	55.00	100.00	27.06	26.35	30.48	37.44	39.05	38.61	37.00
4: sp|Q8BP47|SYNC_MOUSE	29.61	26.46	27.06	100.00	93.59	32.93	37.56	31.35	33.57	32.24
5: sp|O43776|SYNC_HUMAN	28.02	26.23	26.35	93.59	100.00	32.45	37.32	31.12	33.09	31.29
6: sp|Q52428|SYD_THEKO	29.13	30.38	30.48	32.93	32.45	100.00	38.00	33.65	34.75	33.41
7: sp|O57980|SYN_PYRHO	31.80	33.89	37.44	37.56	37.32	38.00	100.00	45.92	45.79	41.40
8: sp|P54263|SYN_THET8	34.06	36.26	39.05	31.35	31.12	33.65	45.92	100.00	54.65	53.10
9: sp|Q2FYH6|SYN_STAA8	35.87	37.11	38.61	33.57	33.09	34.75	45.79	54.65	100.00	66.28
10: tr|C7D1S1|C7D1S1_ENTFL	34.38	36.68	37.00	32.24	31.29	33.41	41.40	53.10	66.28	100.00

Figure 25: The percent identity matrix of *S. aureus* AsnRS in relation to AsnRS from other organisms: *Homo sapiens* (mitochondria) (Q96I59), *Elizabethkingia anopheles* (X5KA67), *E coli* (P0A8M0), *Mus musculus* (mouse) (Q8BP47), *Homo sapiens* (cytoplasmic) (O43776), *Thermococcus kodakarensis* (Q52428), *Pyrococcus horikoshii* (O57980), *Thermus thermophilus* (P54263), and *Enterococcus faecalis* (C7D1S1), the closet similar AsnRSs sequences is observed in green shaded boxes.

2.3.1.2. Multiple sequence and structure alignment

The preferred *S. aureus* AspRS and AsnRS templates sequences and the *S. aureus* query sequences were aligned using Clustal Omega (271) to observe the conserved amino acid residues. The conservation is clearly observed in most amino residues between *S. aureus* sequence and the most related template *Thermus thermophilus* sequence in AspRS (Figure 26) and between *S. aureus* and *Pyrococcus horikoshii* sequences for AsnRS (Figure 27). Both enzymes contain three conserved sequence motifs (motif 1, motif 2 and motif 3) at the C-terminal catalytic domain, which are typical for class II b

aaRS (284). Motifs 2 and 3 have an important role in the aminoacylation process, as they are responsible for active site formation, while motif 1 has a fundamental role in dimerisation of the two α subunits (284). In the active pockets, the amino acid is activated using ATP then transferred to its cognate tRNA molecule through esterification reaction with the 3` hydroxyl group of the ribose in terminal nucleotide in its acceptor stem. PSIPRED (285) secondary structure prediction for *S. aureus* AspRS showed that motif 1 (169-173) is a fold in the form of a coil then short strand followed by coil, motif 2 (222-225) folds mainly in coils and motif 3 (537-540) is a short coil followed by helices (Figure 28). These motifs are similar in their structures to those found in *Thermus thermophilus* 3D crystal structure (1EFW) indicating good agreement with the prediction of the PSIPRED for the query sequence. Also, the agreement in motifs structure; motif 1 (155-159), motif 2 (205-208), and motif 3 (401-404) is clear in AsnRSs between *S. aureus* and its template *Pyrococcus horikoshii* (1X54) (Figure 29).

```
CLUSTAL O(1.2.4) multiple sequence alignment

tr|A0A2U9PQC2|A0A2U9PQC2_MYCSE      -MLRTHAAGSLRPADAGQTVTLAGWVARRRDHGGVIFIDLRDASGVSQVVFREG---DVL      56
sp|P36419|SYD_THETH                 -MRRTHYAGSLRETHVGEEVVLEGWVNRRRDLGGLIFLDLRDREGLVQLVAHPAS--PAY      57
sp|Q2FXU5|SYD_STAA8                 MSKRTTYCGLVTEAFLGQEITLKGWVNNRRDLGGLIFVDLRDREGIVQVVFNPAFSEEAL      60
sp|P21889|SYD_ECOLI                 --MRTEYCGQLRLSHVGQQVTLCGWVNRRRDLGSLIFIDMRDREGIVQVFFDPDRA-DAL      57
sp|Q51422|SYDND_PSEAE               -MMRSHYCGQLNESLDGQEVTLCGWVHRRRDHGGVIFLDVRDREGLAQVVFDPDRA-ETF      58
                                       *:  .* :  :  *: :.* *** .*** *.:**:*:** .*: *:.        .

tr|A0A2U9PQC2|A0A2U9PQC2_MYCSE      AAAHRLRAEFCVAVTGVVEVRPEGNENPEIPTGQIEVNATELTVLGESAPLPFQLDEQ--      114
sp|P36419|SYD_THETH                 ATAERVRPEWVVRAKGLVRLRPE--PNPRLATGRVEVELSALEVLAEAKTPPFPVDAGWR      115
sp|Q2FXU5|SYD_STAA8                 KIAETVRSEYVVEVQGTVTKRDPETVNPKIKTGQVEVQVTNIKVINKSETPPFSINEE--      118
sp|P21889|SYD_ECOLI                 KLASELRNEFCIQVTGTVRARDEKNINRDMATGEIEVLASSLTIINRADVLP--LDSN--      113
sp|Q51422|SYDND_PSEAE               AKADRVRSEFVVKITGKVRLRPEGARNPNMASGSIEVLGYELEVLNQAETPPFPLDEY--      116
                                      *  :* *: :   * *  *     *  : :* :**    : :: .:   *  ..
                                                                                   Motif 1
tr|A0A2U9PQC2|A0A2U9PQC2_MYCSE      ------AGEEARLKYRYLDLRREGPGNALRLRSKVNAAARSVLAEHDFVEIETPTLTRST      168
sp|P36419|SYD_THETH                 GEEEKEASEELRLKYRYLDLRRRRMQENLRLRHRVIKAIWDFLDREGFVQVETPFLTKST      175
sp|Q2FXU5|SYD_STAA8                 ---NVNVDENIRLKYRYLDLRRQELAQTFKMRHQITRSIRQYLDDEGFFDIETPVLTKST      175
sp|P21889|SYD_ECOLI                 ---HV-NTEEARLKYRYLDLRRPEMAQRLKTRAKITSLVRRFMDDHGFLDIETPMLTKAT      169
sp|Q51422|SYDND_PSEAE               ---SD-VGEETRLRYRFIDLRRPEMAAKLKLRARITSSIRRYLDDNGFLDVETPILGRPT      172
                                           *: **:**::****      :: * ::       :  ..*.::*** * . *
                                                                                   Motif 2
tr|A0A2U9PQC2|A0A2U9PQC2_MYCSE      PEGARDFLVPARLQPGSFYALPQSPQLFKQLLMVAGMERYYQIARCYRDEDFRADRQPEF      228
sp|P36419|SYD_THETH                 PEGARDFLVPYRHEPGLFYALPQSPQLFKQMLMVAGLDRYFQIARCFRDEDLRADRQPDF      235
sp|Q2FXU5|SYD_STAA8                 PEGARDYLVPSRVHDGEFYALPQSPQLFKQLLMISGFDKYYQIVKCFRDEDLRADRQPEF      235
sp|P21889|SYD_ECOLI                 PEGARDYLVPSRVHKGKFYALPQSPQLFKQLLMMSGFDRYYQIVKCFRDEDLRADRQPEF      229
sp|Q51422|SYDND_PSEAE               PEGARDYLVPSRTYPGHFFALPQSPQLFKQLLMVAGFDRYYQIAKCFRDEDLRADRQPEF      232
                                    ******:*** *   * *:***********:**::*:::*:**.:*:****:******:*
```

```
tr|A0A2U9PQC2|A0A2U9PQC2_MYCSE   TQLDMEMSFVEADDVIAISEQVLKAVWAT-IGYDLPLPLPRISYEEAMRRFGSDKPDLRF   287
sp|P36419|SYD_THETH              TQLDLEMSFVEVEDVLELNERLMAHVFREALGVELPLPFPRLSYEEAMERYGSDKPDLRF   295
sp|Q2FXU5|SYD_STAA8              TQVDIEMSFVDQEDVMQMGEEMLKKVVKEVKGVEINGAFPRMTYKEAMRRYGSDKPDTRF   295
sp|P21889|SYD_ECOLI              TQIDVETSFMTAPQVREVMEALVRHLWLEVKGVDL-GDFPVMTFAEAERRYGSDKPDLRN   288
sp|Q51422|SYDND_PSEAE            TQIDIETSFLDESDIIGITEKMVRQLFKEVLDVEF-DEFPHMPFEEAMRRYGSDKPDLRI   291
                                 **:*:* **:   ::  : * ::  :     . ::   :* : : ** .*:****** *

tr|A0A2U9PQC2|A0A2U9PQC2_MYCSE   GIELVECTEYFKDTTFRVFQAPY------VGAVVMPGGASQPRRTLDGWQEFAKQRGHKG   341
sp|P36419|SYD_THETH              GLELKEVGPLFRQSGFRVFQEAES-----VKALALP--KALSRKEVAELEEVAKRHKAQG   348
sp|Q2FXU5|SYD_STAA8              EMELIDVSQLGRDMDFKVFKDTVENDGEIKAIVAKGAAEQYTRKDMDALTEFVNIYGAKG   355
sp|P21889|SYD_ECOLI              PMELTDVADLLKSVEFAVFAGPANDPKGRVAALRVPGGASLTRKQIDEYGNFVKIYGAKG   348
sp|Q51422|SYDND_PSEAE            PLELVDVADQLKEVEFKVFSGPANDPKGRVAALRVPGAASMPRSQIDDYTKFVGIYGAKG   351
                                  :** :     :.  * **             :          *  :    :..     :*

tr|A0A2U9PQC2|A0A2U9PQC2_MYCSE   LAYVLVGED----GTLGGPVAKNLSDAERDGLVAHVGANPGDCIFFAAGPAKGARALLGA   397
sp|P36419|SYD_THETH              LAWARVEE-----GGFSGGVAKFLEP-VREALLQATEARPGDTLLFVAGPRKVAATALGA   402
sp|Q2FXU5|SYD_STAA8              LAWVKVVE-----DGLTGPIGRFFETENVETLLTLTGAEAGDLVMFVADKPNVVAQSLGA   410
sp|P21889|SYD_ECOLI              LAYIKVNERAKGLEGINSPVAKFLNAEIIEDILDRTAAQDGDMIFFGADNKKIVADAMGA   408
sp|Q51422|SYDND_PSEAE            LAYIKVNERAKGVEGLQSPIVKFIPEANLNVILDRVGAVDGDIVFFGADKAKIVCDALGA   411
                                 **:  * *       : . : : :     : ::  . *  ** ::* *.  : .   :**

tr|A0A2U9PQC2|A0A2U9PQC2_MYCSE   TRIEIAKRLDLIDPNAWAFTWVVDFPMFEAADEATAAGDVAVGSGAWTAMHHAFTAPKPD   457
sp|P36419|SYD_THETH              VRLRAADLLGLKR-EGFRFLWVVDFPLLEWDEE----------EEAWTYMHHPFTSPHPE   451
sp|Q2FXU5|SYD_STAA8              LRVKLAKELGLIDETKLNFLWVTDWPLLEYDED----------AKRYVAAHHPFTSPKEA   460
sp|P21889|SYD_ECOLI              LRLKVGKDLGLTDESKWAPLWVIDFPMFEDDGE-----------GGLTAMHHPFTSPKDM   457
sp|Q51422|SYDND_PSEAE            LRIKVGHDLKLLT-REWAPMWVVDFPMFEENDD-----------GSLSALHHPFTSPKC-   458
                                  *:. .. * *         ** *:*::*   :                 ** **:*:

tr|A0A2U9PQC2|A0A2U9PQC2_MYCSE   SVDTFDSDPGNALSDAYDIVCNGNEIGGGSIRIHRRDIQERVFAMMGIDHDEAQEKFGFL   517
sp|P36419|SYD_THETH              DLPLLEKDPGRVRALAYDLVLNGVEVGGGSIRIHDPRLQARVFRLLGIGEEEQREKFGFF   511
sp|Q2FXU5|SYD_STAA8              DIAKLGTAPEEAEANAYDIVLNGYELGGGSIRIHDGELQEKMFEVLGFTKEQAQEQFGFL   520
sp|P21889|SYD_ECOLI              TAAELKAAPENAVANAYDMVINGYEVGGGSVRIHNGDMQQTVFGILGINEEEQREKFGFL   517
sp|Q51422|SYDND_PSEAE            TPAELEANPGAALSRAYDMVLNGTELGGGSIRIHDKSMQQAVFRVLGIDEAEQEEKFGFL   518
                                     :   *  . : ***:* ** *:****:***   :*  :* ::*: . : .*:***:
                                                Motif 3
tr|A0A2U9PQC2|A0A2U9PQC2_MYCSE   LDAFSYGAPPHGGIAFGWDRITALLAGVDSIREVIAFPKSGGGVDPLTDAPAPITPQQRK   577
sp|P36419|SYD_THETH              LEALEYGAPPHGGIAWGLDRLLALMTGSPSIREVIAFPKNKEGKDPLTGAPSPVPEEQLR   571
sp|Q2FXU5|SYD_STAA8              LDAFKYGAPPHGGIALGLDRLVMLLTNRTNLRDTIAFPKTASATCLLTNAPSEVSDKQLE   580
sp|P21889|SYD_ECOLI              LDALKYGTPPHAGLAFGLDRLTMLLTGTDNIRDVIAFPKTTAAACLMTEAPSFANPTALA   577
sp|Q51422|SYDND_PSEAE            LDALKYGAPPHGGLAFGLDRLVMLMTGASSIREVIAFPKTQSAGDVMTQAPGSVDGKALR   578
                                 *:*:.**:***.*:* * **:  *::.  .:*:.*****.  .   :* **.

tr|A0A2U9PQC2|A0A2U9PQC2_MYCSE   ESGIDAKPREDKPKEDAKSKA        598
sp|P36419|SYD_THETH              ELGLMVVRP------------        580
sp|Q2FXU5|SYD_STAA8              ELSLRIRH-------------        588
sp|P21889|SYD_ECOLI              ELSIQVVKKAENN--------        590
sp|Q51422|SYDND_PSEAE            ELHIRLREQPKAE--------        591
                                 *  :
```

Figure 26: Sequence alignment of *S. aureus* AspRS with the most similar templates: *Mycolicibacterium smegmatis* (UNIPROT: A0A2U9PQC2), *T. Thermophilus* (UNIPROT: P36419)*, E. coli* (UNIPROT*:* P21889) *and P. Aeruginosa* (UNIPROT*:* Q51422) using Clustal Omega in which ¨ * ¨ means that the residues are identical, ¨ : ¨ means that conserved substitutions have been observed, ¨ . ¨ means that semi-conserved substitutions are observed. The residues are coloured according to their chemical properties where red, small hydrophobic *(*AVFPMILWY); blue, acidic (DE); purple, basic (RHK); green, hydroxyl + amine + basic (STYHCNGQ), motifs: motif 1 PVLTK (169-173), motif 2 FDRE (222-225) and motif 3 GLDR (537-540) are observed in yellow shaded boxes.

```
CLUSTAL O(1.2.4) multiple sequence alignment

tr|X5KA67|X5KA67_9FLAO      -MHKQTIKEVLENYKKFLHHDITVYGWVRAFRSN---RFIALNDGSTINNLQIVVDFENF      56
sp|Q52428|SYD_THEKO         MYRTHYSSEIT---EELNGQKVKVAGWVWEVKDLGGIKFLWIRDRDGIV--QITAPKKKV      55
sp|O57980|SYN_PYRHO         MIEKVYCQEVK---PELDGKKVRLAGWVYTNMRVGKKIFLWIRDSTGIV--QAVVAKNVV      55
sp|Q2FYH6|SYN_STAA8         --MKTTIKQAK---DHL-NQDVTIGAWLTNKRSSGKIAFLQLRDGTGFM--QGVVVKSEV      52
sp|P54263|SYN_THET8         --MRVFIDEIA---RHV-DQEVELRGWLYQRRSKGKIHFLILRDGTGFL--QATVVQGEV      52
                                   .:      ..  :.: : .*:          *: :.*   :   * ..    .

tr|X5KA67|X5KA67_9FLAO      DEN---LIKNINTASSLKIVGEVVESQGAGQTVEIIAKKIIVLGDNFTEELQNTILQPK-      112
sp|Q52428|SYD_THEKO         DPELFKLIPKLRSEDVVAVEGVVNFTPKAKLGFEILPEKIVVLNRAET----PLPLDPTG      111
sp|O57980|SYN_PYRHO         GEETFEKAKKLGRESSVIVEGIVKADERAPGGAEVHVEKLEVIQA-VSEF--PIPENPE-      111
sp|Q2FYH6|SYN_STAA8         DEEVFKLAKEITQESSLYVTGTITEDNRSDLGYEMQVKSIEVISE-AHDY----PITPK-      106
sp|P54263|SYN_THET8         PEAVFREADHLPQETALRVWGRVREDRRAPGGFELAVRDLQVVSRPQGEY----PIGPK-      107
                                  .:     : : * :     :    *:  ..: *:                  *
                                                                                Motif 1
tr|X5KA67|X5KA67_9FLAO      --KHSLEKLREQAHLRFRTNLFGAVFRVRHAVSFAIHSFFNDRQFFYLNTPVITGADAEG      170
sp|Q52428|SYD_THEKO         KVKAELDTRLDNRFMDLRRPEVMAIFKIRSSVFKAVRDFFHENGFIEIHTPKIIATATEG      171
sp|O57980|SYN_PYRHO         --QASPELLLDYRHLHIRTPKASAIMKVKETLIMAAREWLLKDGWHEVFPPILVTGAVEG      169
sp|Q2FYH6|SYN_STAA8         --NHGTEFLMDHRHLWLRSKKQHAVMKIRNEVIRATYEFFNKDGFTKVDPPILTASAPEG      164
sp|P54263|SYN_THET8         --EHGIDFLMDHRHLWLRHRRPFAVMRIRDELERAIHEFFGERGFLRFDAPILTPSAVEG      165
                              :   :   :  .: :*     *:::::  :  *  .:: .  :  .  * :     **

tr|X5KA67|X5KA67_9FLAO      AGEMFGVTNFDLDNIPRNEDGAIDYTQDFFGRKTNLTVSGQLEGETA-AMGLGRIYTFGP      229
sp|Q52428|SYD_THEKO         GTELFPMKYFEE--------------------DAFLAQSPQLYKQIMMASGLDRVYEIAP      211
sp|O57980|SYN_PYRHO         GATLFKLKYFDK--------------------YAYLSQSAQLYLEAA-IFGLEKVWSLTP      208
sp|Q2FYH6|SYN_STAA8         TSELFHTKYFDQ--------------------DAFLSQSGQLYLEAA-AMAHGKVFSFGP      203
sp|P54263|SYN_THET8         TTELFEVELFDGE-------------------KAYLSQSGQLYAEAG-ALAFAKVYTFGP      205
                                 :*    *:                     : *: * **  :     .  ::: : *
                            Motif 2
tr|X5KA67|X5KA67_9FLAO      TFRAENSNTTRHLAEFWMVEPEVAFNNLE-DNIDLAEDFLKYVIQYVLDKCKDDLEFLDK      288
sp|Q52428|SYD_THEKO         IFRAEEHNTTRHLNEAWSIDSEMAFIEDEEEVMSFLERLVAHAINYVREHNAKELDILNF      271
sp|O57980|SYN_PYRHO         SFRAEKSRTRRHLTEFWHLELEAAWMDLW-DIMKVEEELVSYMVQRTLELRKKEIEMFRD      267
sp|Q2FYH6|SYN_STAA8         TFRAEKSKTRRHLIEFWMIEGEMAFTNHA-ESLEIQEQYVTHVVKSVLENCKLELKILER      262
sp|P54263|SYN_THET8         TFRAERSKTRRHLLEFWMVEPEVAFMTHE-ENMALQEELVSFLVARVLERRSRELEMLGR      264
                             ****. .* *** * * :: * *:     : : . *  : . :  . :    ::.::

tr|X5KA67|X5KA67_9FLAO      RFAEEQKQKPEKERAKEGLIEKLENVVAKRFKRVSYTEAIDILLNSKENKKGKFVYPVEK      348
sp|Q52428|SYD_THEKO         EL------------------EE----PKLPFPRVSYDKALEILGDL---------GKEIP      300
sp|O57980|SYN_PYRHO         DL------------------TTLKN-TEPPFPRISYDEAIDILQSK---------GVNVE      299
sp|Q2FYH6|SYN_STAA8         DT------------------SKLEKVA-TPFPRISYDDAIEFLKAE-----G---FDDIE      295
sp|P54263|SYN_THET8         DP------------------KALEPAAEGHYPRLTYKEAVALVNRIAQEDPE---VPPLP      303
                                                          : *::* .*: ::

tr|X5KA67|X5KA67_9FLAO      WGADLQSEHER----YLVEKHFECPVVLFDYPAEIKAFYMRLNEDNKTV-AAMDVLF-PG      402
sp|Q52428|SYD_THEKO         WGEDIDTEGERLLGKYMMENENAPLYFLYQYPSEAKPFYIMKYDNKPEICRAFDLE--YR      358
sp|O57980|SYN_PYRHO         WGDDLGADEERVLTE-----EFDRPFFVYGYPKHIKAFYMKEDPNDPRKVLASDMLAPEG      354
sp|Q2FYH6|SYN_STAA8         WGEDFGAPHETAIAN-----HYDLPVFITNYPTKIKPFYMQPNPENEETVLCADLIAPEG      350
sp|P54263|SYN_THET8         YGEDFGAPHEAALSR-----RFDRPVFVERYPARIKAFYMEPDPEDPELVLNDDLLAPEG      358
                            :* *: :  *          .     .:  ** . * **:    :.      *:
                                                                          Motif 3
tr|X5KA67|X5KA67_9FLAO      IGEIIGGSQREERLDVLKKKMDDMHVDQEELWWYLDTRKFGSVPHSGFGLGLERLVLFVT      462
sp|Q52428|SYD_THEKO         GVEISSGGQREHRHDILVEQIKEKGLNPESFEFYLKAFRYGMPPHGGFGLGAERLIKQML      418
sp|O57980|SYN_PYRHO         YGEIIGGSQREDDYDKLLNRILEEGMDPKDYEWYLDLRRYGSVPHSGFGLGVERLVAWVL      414
sp|Q2FYH6|SYN_STAA8         YGEIIGGSERVDDLELLEQRVKEHGLDEEAYSYYLDLRRYGSVPHCGFGLGLERTVAWIS      410
sp|P54263|SYN_THET8         YGEIIGGSQRIHDLELLRRKIQEFGLPEEVYDWYLDLRRFGSVPHSGFGLGLERTVAWIC      418
                              ** .*.:* .  : * .:: :  :  :   :**.  ::*  ** ***** ** :  :

tr|X5KA67|X5KA67_9FLAO      GMTNIRDVIPFPRTPKSAEF        482
sp|Q52428|SYD_THEKO         DLPNIREVILFPRDRRRLTP        438
sp|O57980|SYN_PYRHO         KLDHIRWAALFPRTPARLYP        434
sp|Q2FYH6|SYN_STAA8         GVEHVRETAPFPRLLNRLYP        430
sp|P54263|SYN_THET8         GLAHVREAIPFPRMYTRMRP        438
                             : ::* .  ***
```

Figure 27: Sequence alignment of *S. aureus* AsnRS with the most similar templates: *Elizabethkingia anopheles* (UNIPROT: X5KA67), *Thermococcus kodakaraensis* (UNIPROT: Q52428), *Pyrococcus horikoshii* (UNIPROT: O57980) and *Thermus thermophilus* (UNIPROT: p54263) using Clustal Omega in which ¨ * ¨ means that the residues are identical, ¨ : ¨ means that conserved substitutions have been observed, ¨ . ¨ means that semi-conserved substitutions are observed. The residues are coloured according to their chemical properties where red, small hydrophobic *(*AVFPMILWY);

blue, acidic (DE); purple, basic (RHK); green, hydroxyl + amine + basic (STYHCNGQ), motifs: motif 1 PILTA (155-159), motif 2 FRAE (205-208) and motif 3 GLER (401-404) are observed in yellow shaded boxes.

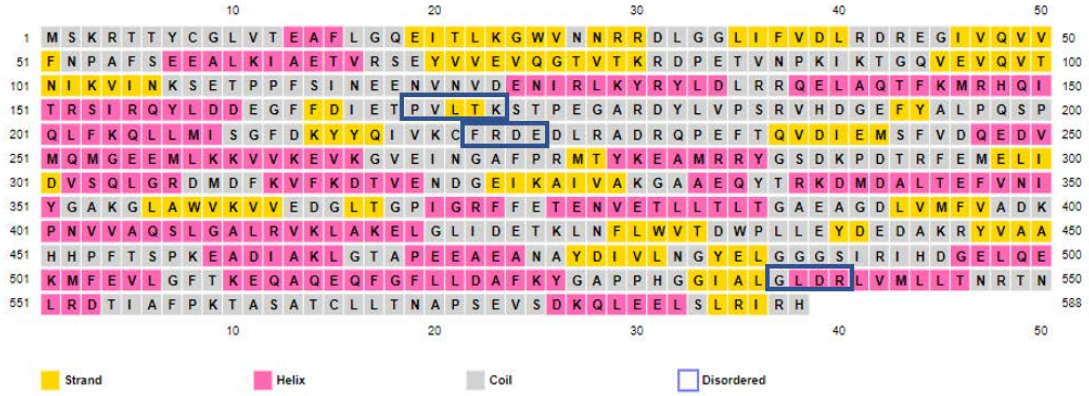

Figure 28: PSIPRED secondary structure prediction for *S. aureus* AspRS with three conserved motifs, motifs 1, 2 and 3 identified in blue squares.

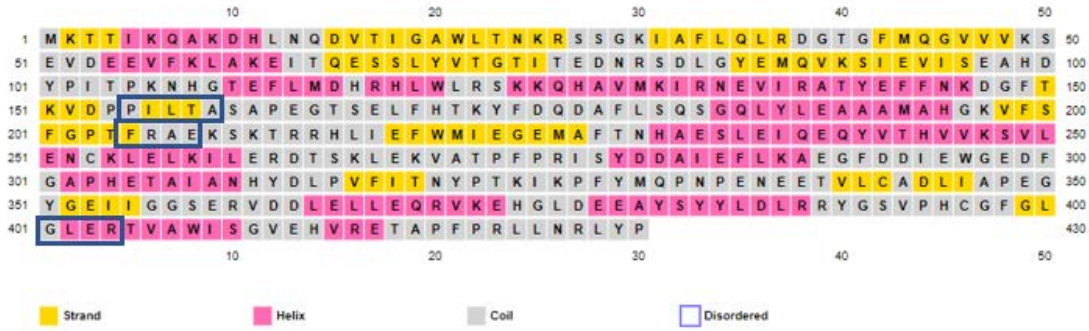

Figure 29: PSIPRED secondary structure prediction for *S. aureus* AsnRS with three conserved motifs, motifs 1, 2 and 3 identified in blue squares.

2.3.1.3. 3D *S. aureus* AspRS and AsnRS models building and validation

The molecular modelling experiment for building the 3D *S. aureus* AspRS and AsnRS models was performed using MOE software (263) and SWISS-MODEL server (266). In both programmes, the protein sequences of *S. aureus* AspRS and AsnRS were used in a FASTA format which were obtained from the ExPASy proteomics server at the Swiss Bioinformatics Institute (275), with the Uniprot identifiers Q2FXU5 (SYD_STAA8) and Q2FYH6 (SYN_STAA8) respectively (286, 287). The AspRS and AsnRS homology models were constructed using *Thermus thermophilus* AspRS (pdb: 1EFW) (277) and *Pyrococcus horikoshii* AsnRS (pdb: 1X54) (264) crystal structures respectively. MOE and SWISS-MODEL constructed models for both enzymes were subjected to a number of checks to assess their qualities. Stereochemical quality was evaluated by

Ramachandran plots using the RAMPAGE server (288) and the compatibility of 3D models with their amino acids 1D sequence was validated using Verify 3D (289), while overall protein structures were evaluated using ProSA (290). By using the templates for comparison, validation results would propose that MOE and SWISS-MODEL performed well but SWISS-MODEL gave the best evaluation results in the case of *S. aureus* AspRS. In the Ramachandran plot, the main chain dihedral ϕ and ψ angles in both MOE and SWISS-MODEL AspRS models were reasonably accurate with a total of 85.1% and 92.8% amino acids residues were in the favoured region of the respective MOE and SWISS-MODEL compared with their template 1EFW (87.9%) (Figure 30, 31). Only 20 and 4 amino acid residues of MOE and SWISS AspRS models respectively were found in the outlier region, which are away from the active sites and would not be expected to affect enzymes function (Table 8). Regarding the constructed MOE and SWISS AsnRS models, they display also good results with a total of 90.2% and 95.6% amino acids residues respectively in the favoured region of the plot compared with the AsnRS template 1X54 (97.9%) (Figures 32 and 33) with just 8 and 2 amino acids residues in the outlier region of the Ramachandran plot of the respective MOE and SWISS-MODEL AsnRS models (Table 9) (291).

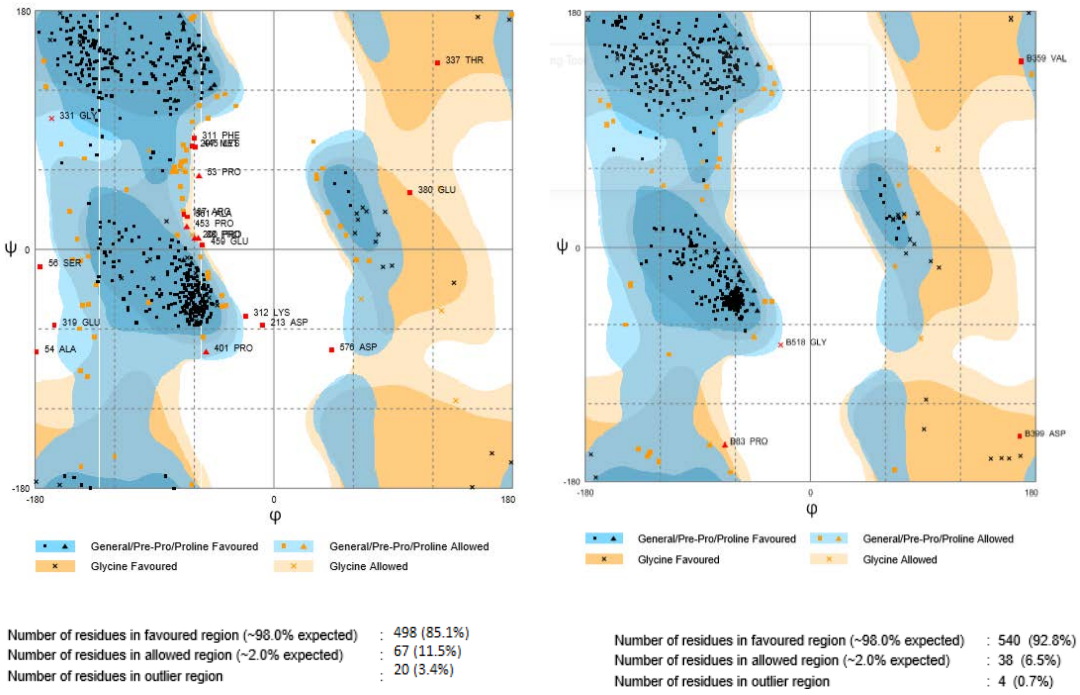

Figure 30: Ramachandran plots of the MOE and SWISS-MODEL AspRS models. The left plot is for MOE model and the right one is for SWISS-MODEL.

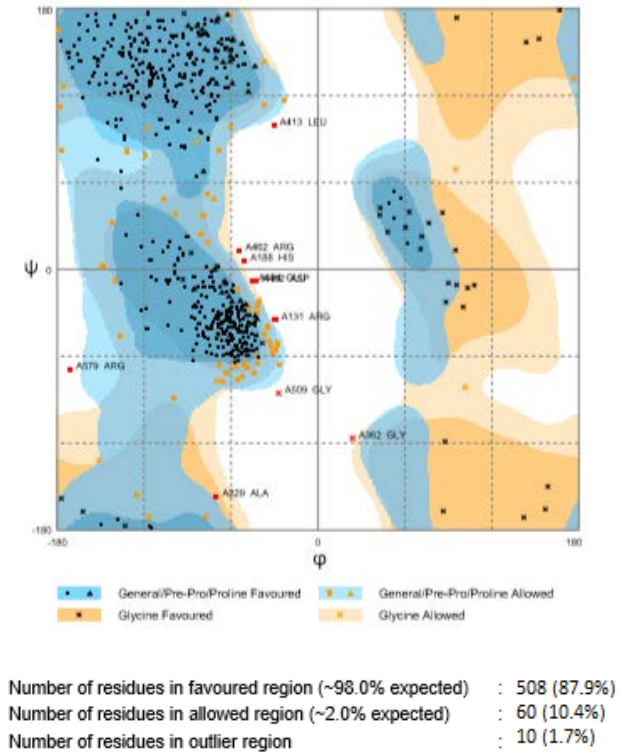

Figure 31: Ramachandran plot for *Thermus thermophilus* AspRS template (pdb: 1EFW).

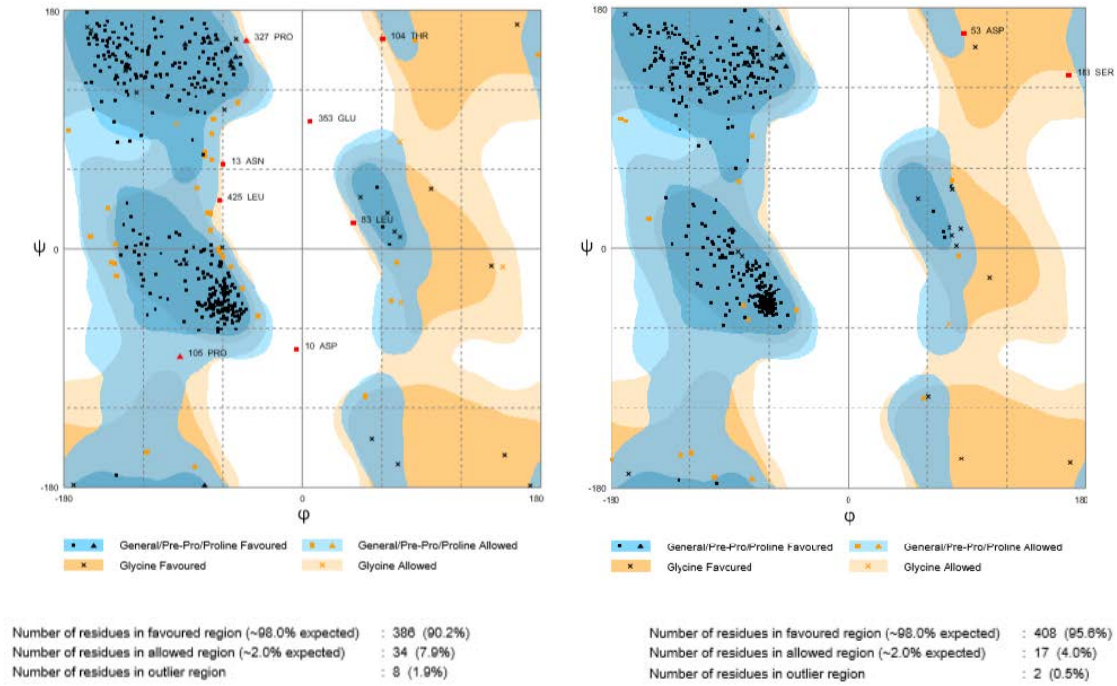

Figure 32: Ramachandran plots of the MOE and SWISS-MODEL AsnRS models. The left plot is for MOE model and the right one is for SWISS-MODEL.

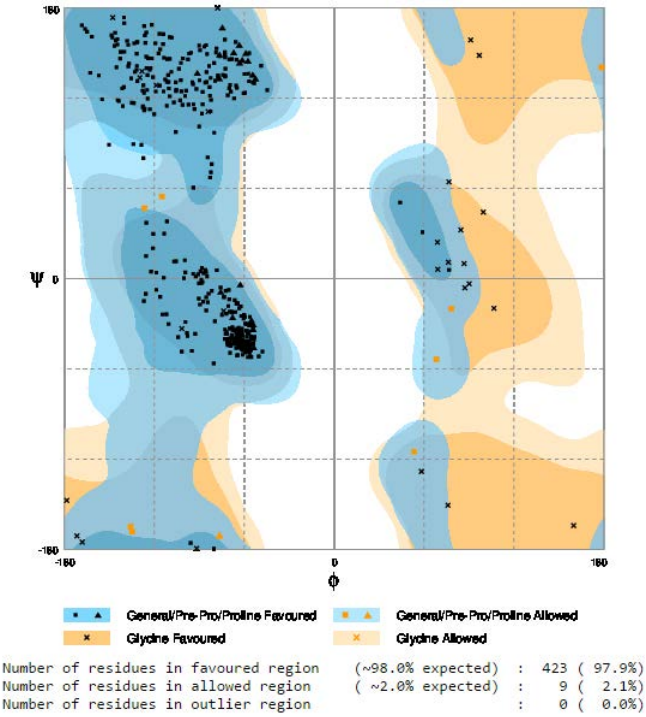

Figure 33: Ramachandran plot for *Pyrococcus horikoshii* AsnRS template (pdb: 1X54).

Table 8: Ramachandran plot results of *T. Thermophilus* AspRS and the constructed MOE and SWISS-MODEL *S. aureus* models.

AspRS	No. of amino acid residues in			Amino acid residues in outlier region
	favoured region	allowed region	outlier region	
T. thermophilus (pdb: 1EFW)	508	60	10	Arg131, His188, Ala229, Gly362, Leu413, Glu434, Asp452, Arg462, Gly509 and Arg579
MOE AspRS model	489	67	20	Pro53, Ala54, Ser56, Pro88, Arg187, Pro200, Asp213, Met297, Phe311, Lys312, Glu319, Gly331, Thr337, Glu380, Pro401, Lys445, Pro453, Glu459, Ala561 and Asp576
SWISS AspRS model	540	38	4	Pro83, Val359, Asp399 and Gly518

Table 9: Ramachandran plot results of *P. horikoshii* AsnRS and the constructed MOE and SWISS-MODEL *S. aureus* models.

AsnRS	No. of amino acids residues in			Amino acid residues in outlier region
	favoured region	allowed region	outlier region	
P. horikoshii AsnRS (pdb: 1X54)	423	9	0	
MOE AsnRS model	386	34	8	Asp10, Asn13, Leu83, Thr104, Pro105, Pro327, Glu353 and Leu425
SWISS AsnRS model	408	17	2	Asp53 and Ser183

Verify 3D was used to determine the compatibility of an atomic model (3D) with its own amino acid sequence (1D) by assigning a structural class based on its location and environment and other parameters such as secondary structures, degree of buried surface area and fraction of side chain area covered by polar atoms for each residue in both structures (289). The correlation was calculated between this set of observed parameters and the ideal parameters of the amino acid type to which it has been assigned. Verify 3D should stay above 0.2 and not fall under zero (289). The percentage of residues, which are more than 0.2 was 85.69%, 86.8% and 91.72% for the *S. aureus* AspRS MOE, SWISS-MODEL models and the *Thermus thermophilus* (pdb: 1EFW) template respectively (Figure 34), while it was 98.37%, 96.50% and 91.24% for the *S. aureus* AsnRS MOE, SWISS-MODEL models and *P. horikoshii* AsnRS (pdb: 1X54) template. For both models, the residues that fall under zero are far from the active sites (Figure 35).

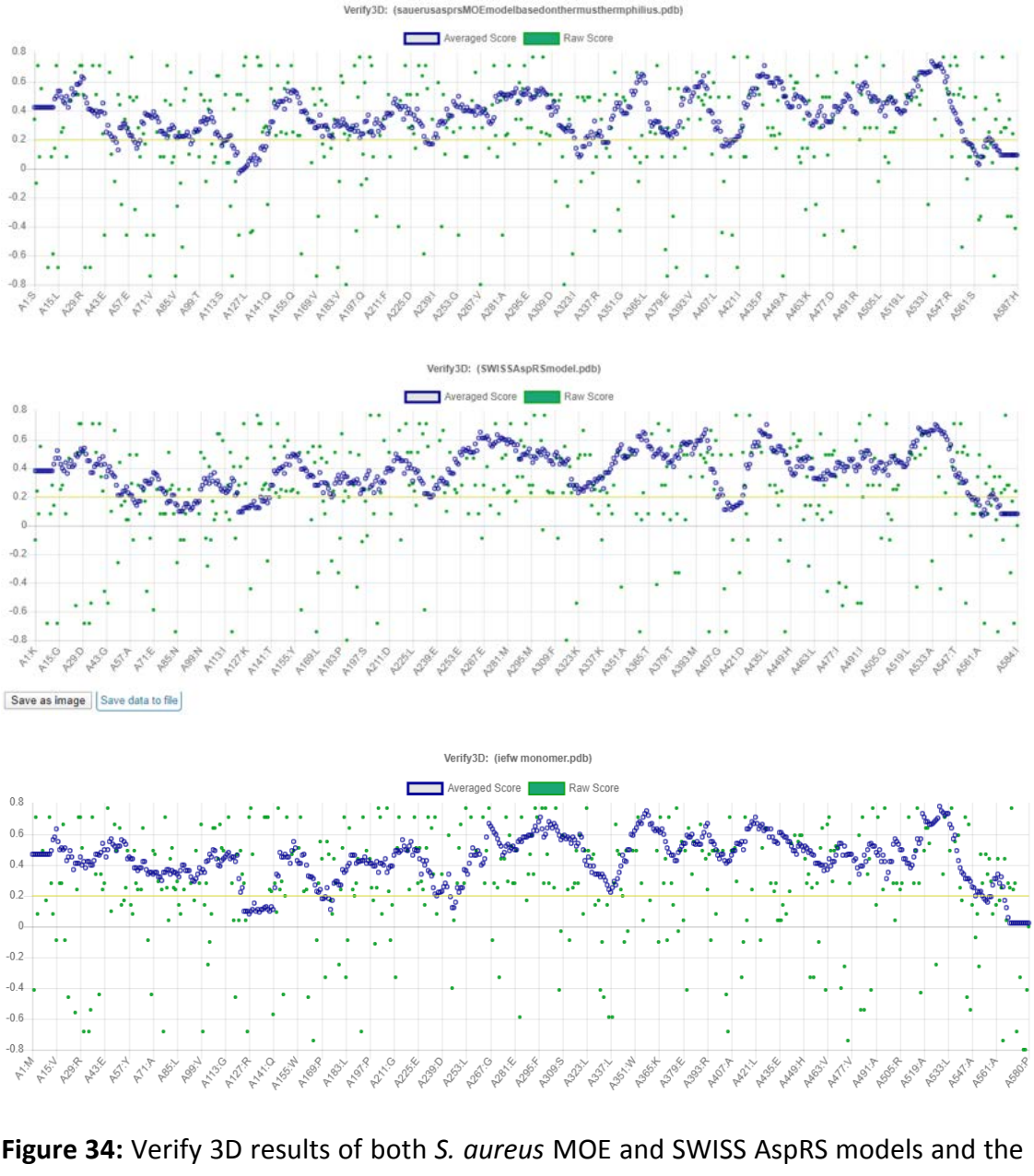

Figure 34: Verify 3D results of both *S. aureus* MOE and SWISS AspRS models and the template (pdb: 1EFW). Each graph is titled and the percentage of amino acid residues that have averaged 3D-1D score of more than 0.2 is 85.69%, 86.8% and 91.72% respectively.

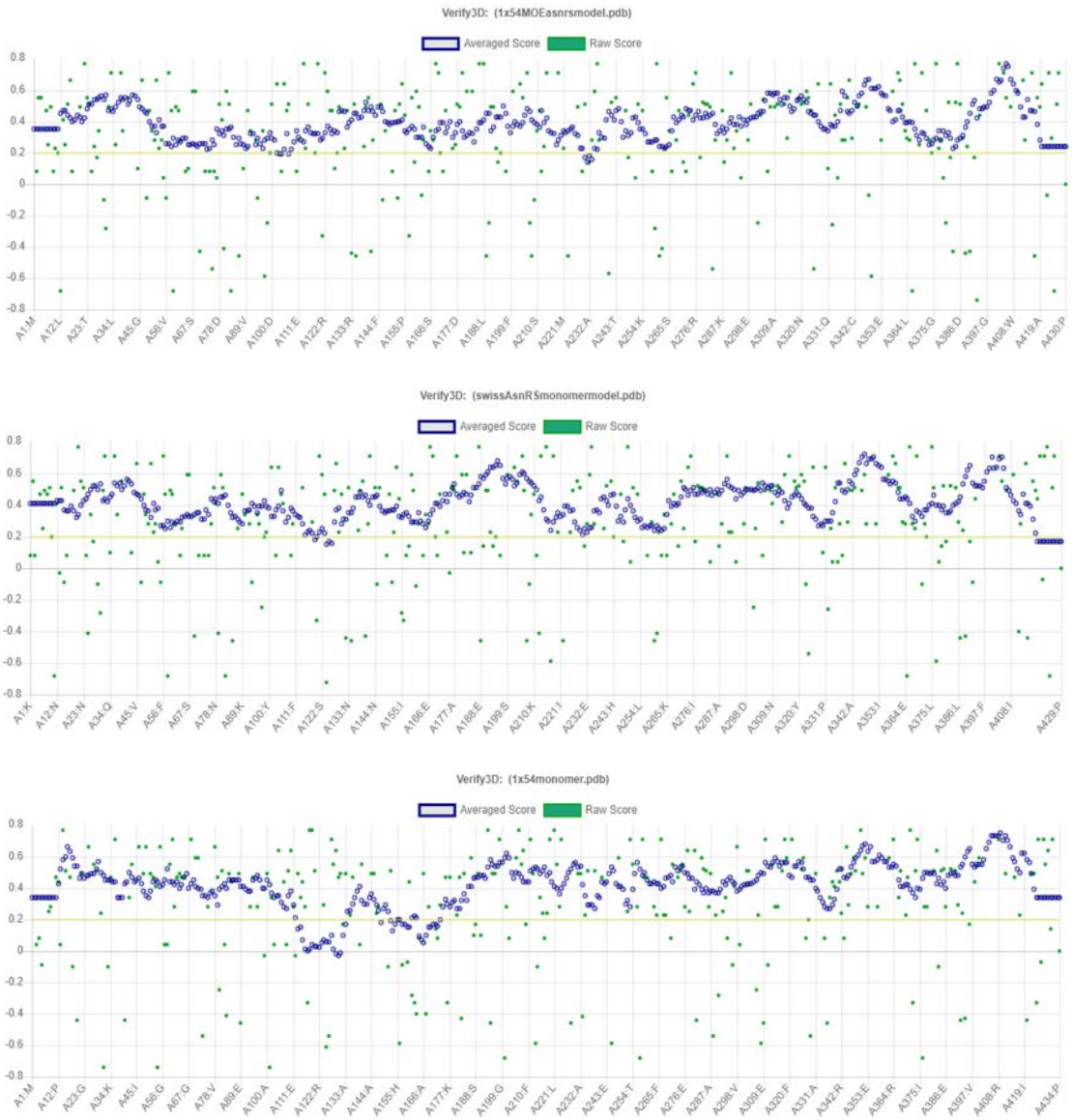

Figure 35: Verify 3D results of both *S. aureus* MOE and SWISS AsnRS models and the template (pdb: 1X54). Each graph is titled and the percentage of amino acid residues that have averaged 3D-1D score of more than 0.2 is 98.37%, 96.50% and 91.24% respectively.

Protein statistical analysis (ProSA) (290) was the third method was used to validate the models, ProSA checks the local and overall model quality through providing two plots; the first one (Figures 36a, 37a, 38a and 39a) shows the local model quality by plotting energies as a function of amino acid sequence position generally positive values relate to erroneous parts of the input structure. The second plot (Figures 36b, 37b, 38b and 39b) displays the Z- score as an indicator of the overall model quality through calculating the Z-score of all experimentally determined protein chains in the current PDB identified by X-ray crystallography or NMR spectroscopy, a negative value

indicates a good model while a positive score shows errors. The Z-score of the MOE and SWISS-MODEL AspRS models was -8.87 and - 10.8 respectively compared with the Z-score of the template 1EFW - 9.84. The Z-score of the MOE and SWISS-MODEL AsnRS models and their template 1X54 was - 9.07, - 9.16 and - 9.69 respectively. In addition, superimposition of the models with their main templates showed low root-mean-square deviation (RMSD) values of 1.05 Å for MOE AspRS model and its template 1EFW, and 0.88 Å for the SWISS-MODEL one with the same template (Figure 40). RMSD was 0.60 Å and 0.23 Å for the MOE and SWISS-MODEL AsnRS model with the template 1X54 respectively indicating a high degree of similarity (Figure 41). Ramachandran plot, Verify 3D and ProSA validation methods indicates that the SWISS-MODEL AspRS and MOE AsnRS models were good in terms of quality of backbone and side chain stereochemistry for both *S. aureus* AspRS and AsnRS compared with their templates (Table 10). Additional validation of the active site architecture of both models was performed by docking experiments with natural substrates and ligands.

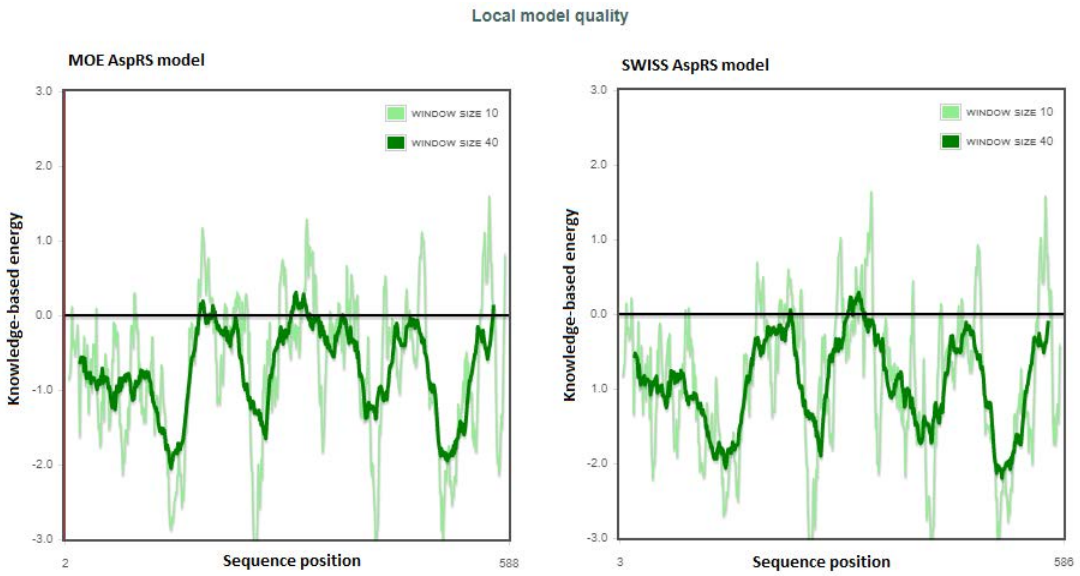

Figure 36a: ProSA output for the *S. aureus* AspRS model. The graph shows the local model quality by plotting energies as a function of amino acid sequence position.

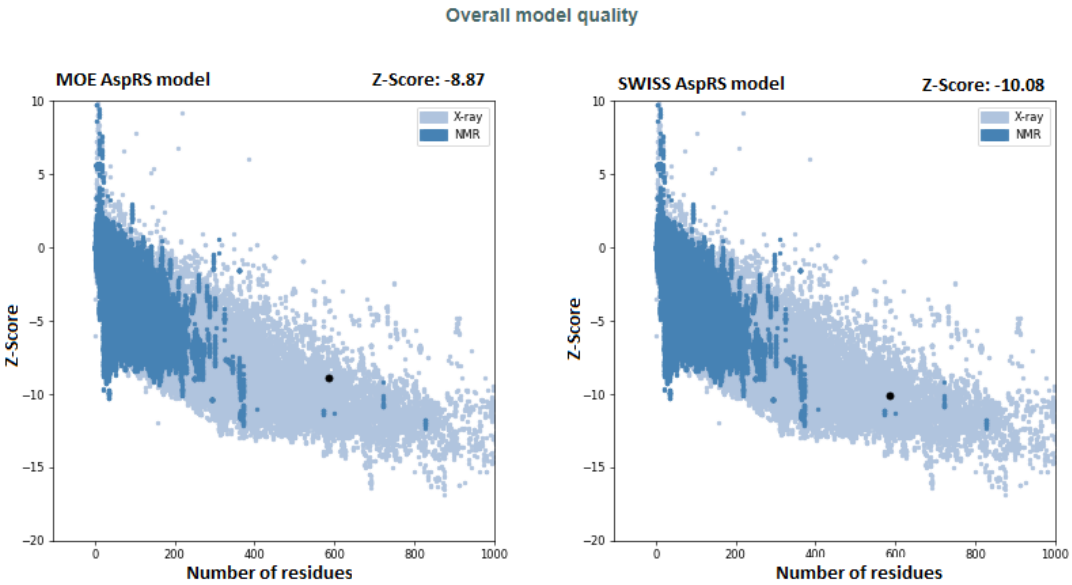

Figure 36b: ProSA output for the *S. aureus* AspRS model. The plot shows the overall model quality by calculating Z-score (dark spot).

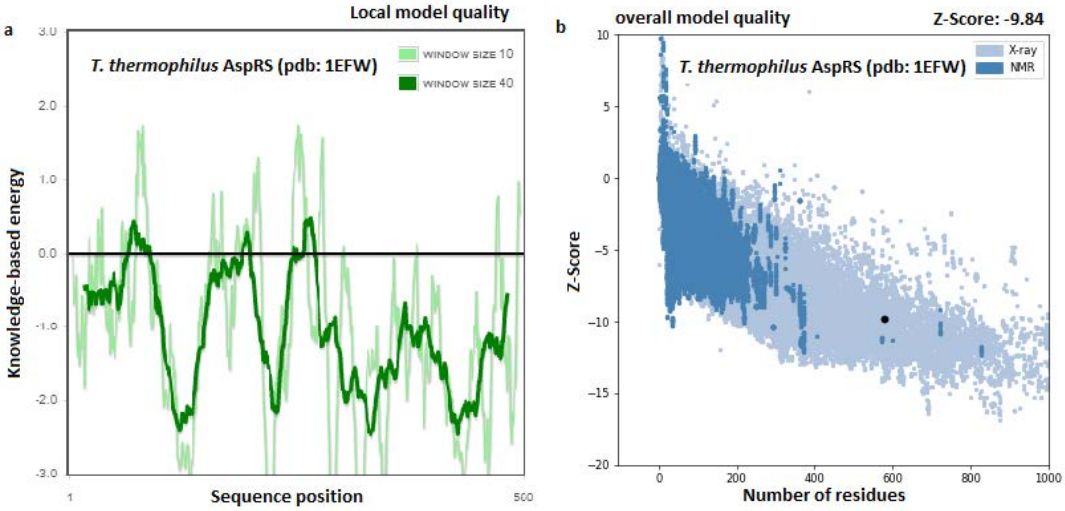

Figure 37: ProSA output for the *T. thermophilus* AspRS. a: shows the local model quality by plotting energies as a function of amino acid sequence position b: shows the overall model quality by calculating Z-score (dark spot).

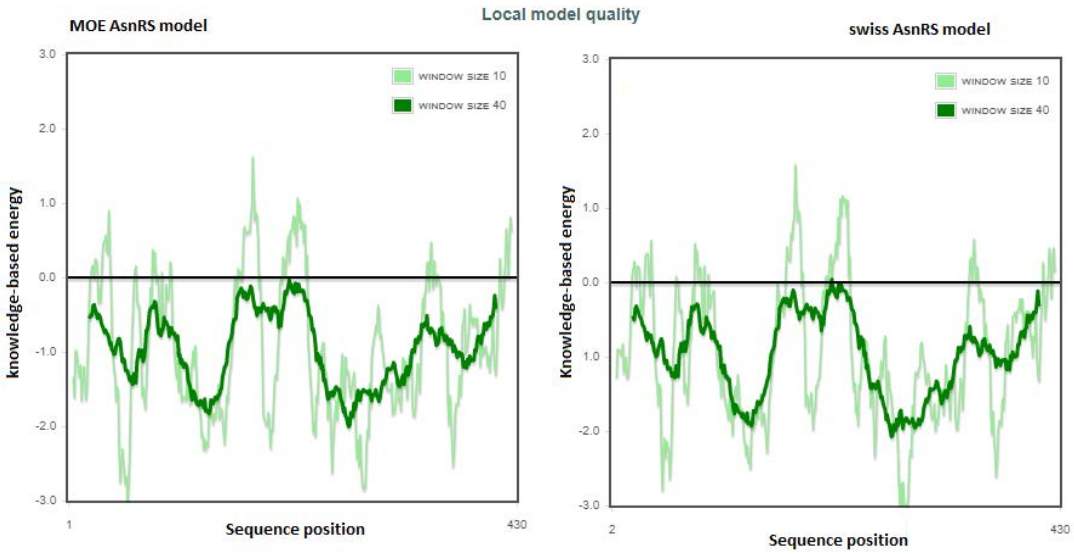

Figure 38a: ProSA output for the *S. aureus* AsnRS model. The graph shows the local model quality by plotting energies as a function of amino acid sequence position.

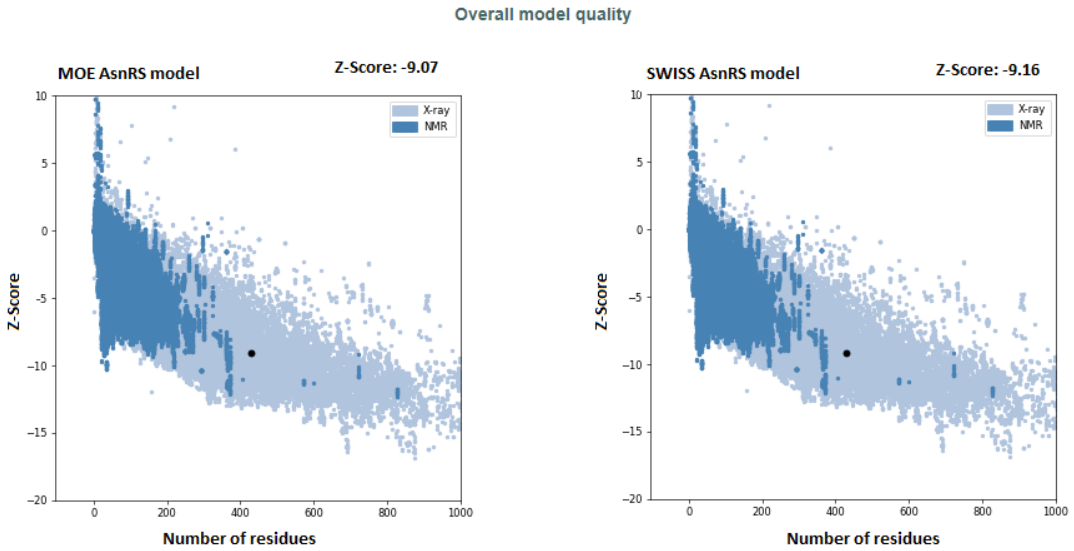

Figure 38b: ProSA output for the *S. aureus* AsnRS model. The plot shows the overall model quality by calculating Z-score (dark spot).

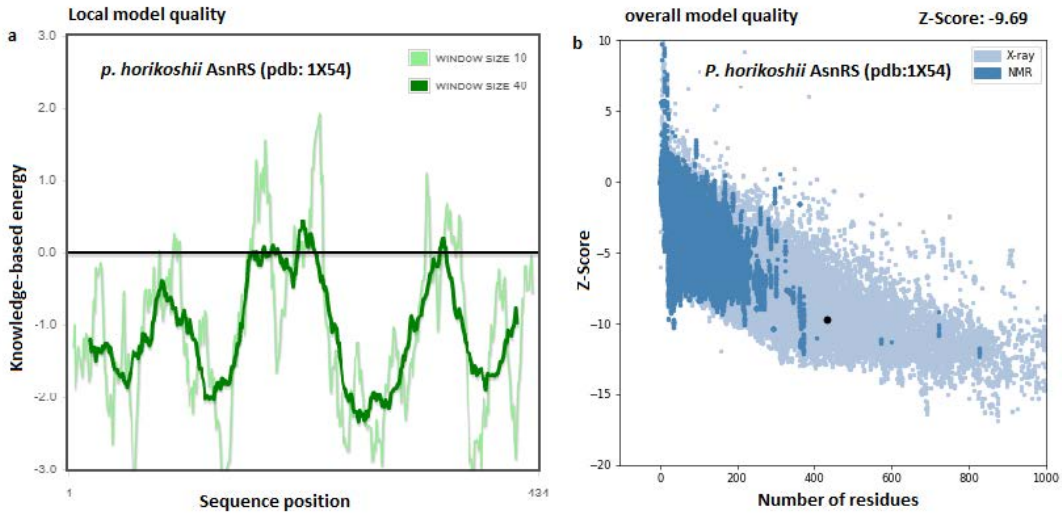

Figure 39: ProSA output for the *P. horikoshii* AsnRS. a: shows the local model quality by plotting energies as a function of amino acid sequence position b: shows the overall mode l quality by calculating Z-score (dark spot).

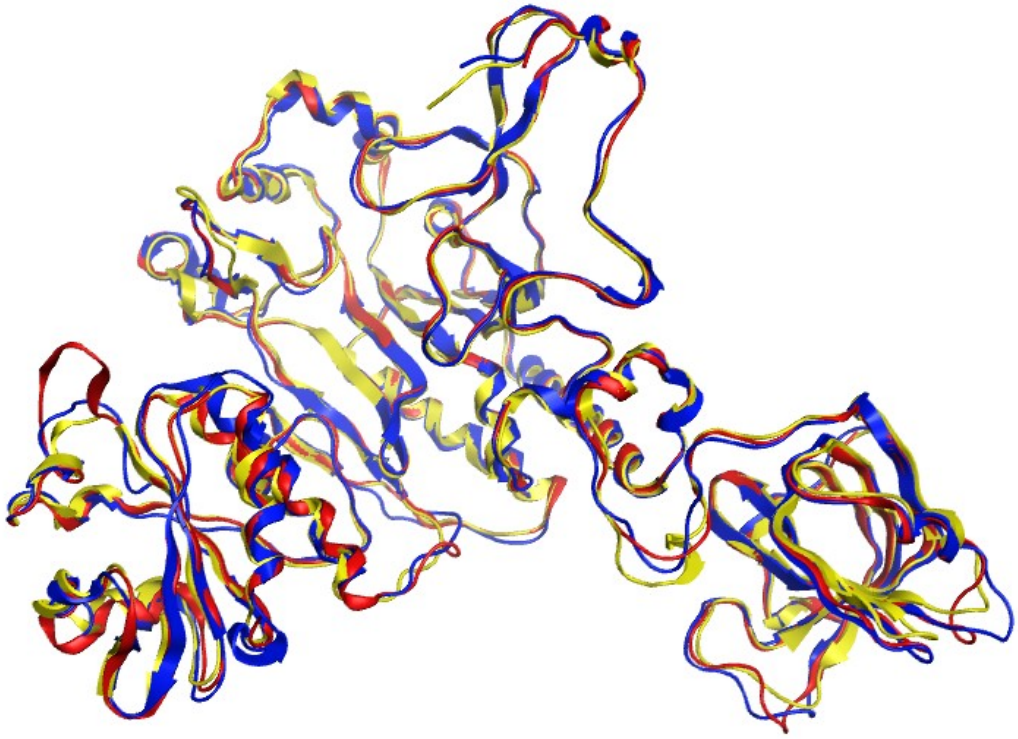

Figure 40: Superimposition of the constructed *S. aureus* MOE (blue) and SWISS-MODEL (red) AspRS models with the X-ray structure of template 1EFW (yellow), RMSD= 1.05 Å and 0.88 Å of MOE and SWISS AspRS model respectively with the template (pdb: 1EFW).

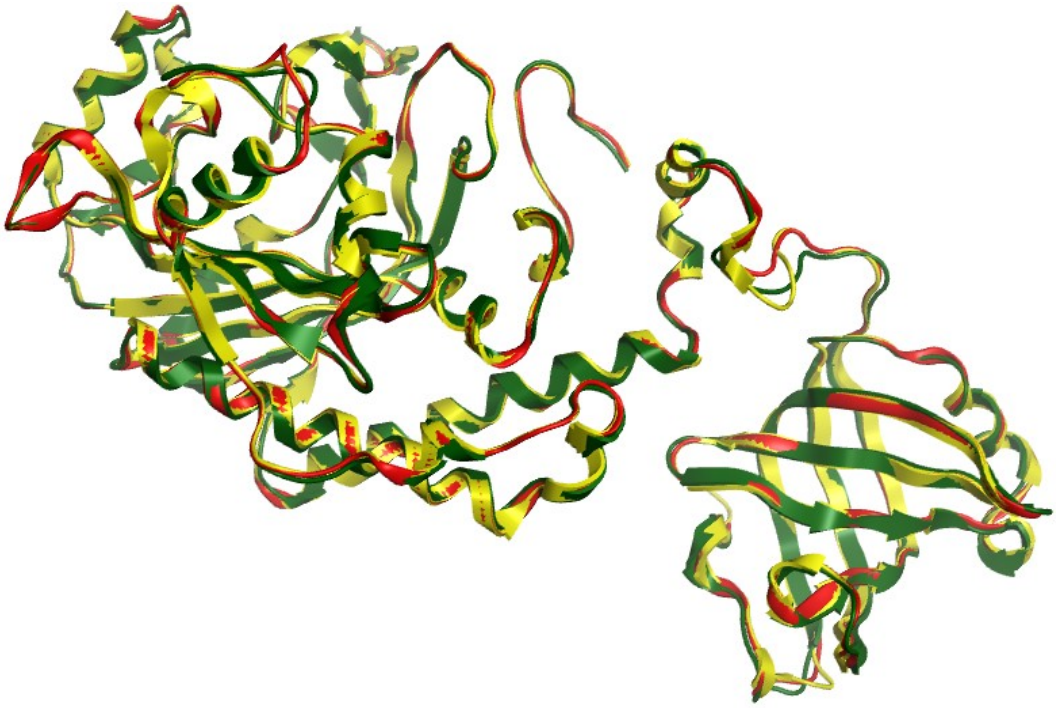

Figure 41: Superimposition of the constructed *S. aureus* MOE (green) and SWISS-MODEL (red) AsnRS models with the X-ray structure of template 1X54 (yellow). RMSD= 0.60 Å and 0.23 Å of MOE and SWISS AsnRS model respectively with the template (pdb: 1X54).

Table 10: Validation results of the MOE and SWISS constructed *S. aureus* AspRS and AsnRS models.

Validation methods	*S. aureus* AspRS		Template	*S. aureus* AsnRS		Template
	MOE AspRS	SWISS AspRS	1EFW	MOE AsnRS	SWISS AsnRS	1x54
Ramachandran plot (outlier region)	20	4	10	8	2	N
ProSA (Z-Score)	-8.87	-10.8	-9.84	-9.07	-9.16	-9.69
Verify 3D	85.69%	86.8%	91.72%	98.37%	96.50%	91.24%
RMSD	1.05 Å	0.88 Å	-	0.60 Å	0.23 Å	-

2.3.1.4. Docking study of *S. aureus* AspRS and AsnRS models

2.3.1.4.1. Active site identification

The initial validation of the predicted active site was assessed through the protein BLAST tool (273, 274) using the query protein sequence in FASTA format against all known class IIb aaRSs to identify the conserved domains (Figures 42 and 43) (271, 292). Both enzymes have hydrophobic pockets as shown in the 3D ligand binding interactions (Figures 44a and 45a). Colours indicate the chemical nature and type of bonds that could be established with ligands green colour is for hydrophobic interactions, while pink and red colours are for hydrogen bonding and electrostatic interactions. The active site of AspRS is formed by the following amino residues Glu177, Gly178, Ala179, Ser199, Gln201, Lys204, Arg223, Glu225, Asp230, Arg231, Gln232, Phe235, Gln237, His451, His452, Glu485, Gly488, Arg492, Ile534, Ala535, Gly537 and Arg540 while the active site of AsnRS consists of Arg206, Glu208, Arg214, His215, Glu353, Gly356, Gly401, Arg404. Both active sites were further validated using the MOE alignment tool for docking the natural substrates into the selected AspRS and AsnRS models. For *S. aureus* AspRS, the model built using SWISS-MODEL was selected for the docking study owing to higher validation results than its MOE counterpart. In the docking study, the 3D structure of *Mycolicibacterium smegmatis* MC2 155 AspRS co-crystallised with aspartic acid (pdb: 4O2D) and the 3D structure of *E coli* AspRS with the natural substrate (pdb: 1C0A) were used to identify which key amino residues in the AspRS model active site bound with aspartic acid and aspartyl-adenylate respectively. For *S. aureus* AspRS, Gln201, Lys204, His452, Gly488, Ser490 and Arg492 bind aspartic acid through a network of hydrogen bonds while the water molecule bridge between aspartic acid and Asp239 is characteristic and observed in others AspRS enzymes (Figure 44b) (293). The adenosine monophosphate (AMP) moiety is generally positioned by class II invariants (Arg223, Phe235 and Arg540) and by AspRSs conserved residues (Gln232, Gln237 and Glu485). Phe235 and Arg540 as class II conserved motif 2 and motif 3 respectively are key residues to augment the interactions of the adenine main chain (Figure 45b). Among the residues responsible for the recognition of the aspartyl adenylate, Gln237 is specific for eubacteria and interacts with the α-phosphate O and carbonyl atom of the aspartyl adenylate. This interaction is observed with Gln231 and Gln237 in *E coli* and *Thermus thermophilus*

AspRSs respectively, but it is not present in archaeal or eukaryotic AspRSs (293, 294). Regarding *S. aureus* AsnRS, the constructed MOE model was used for the docking study of the natural substrate because in the Ramachandran plot of the SWISS-MODEL model, Ser183, which is near the active site, is in the outlier region. By using the MOE alignment service (263), the co-crystal structure of *Pyrococcus horikoshii* AsnRS was used to study the binding interaction of the *S. aureus* AsnRS model with asparaginyl-adenylate. Due to the close similarity between AspRS and AsnRS, AsnRS is missing in many bacterial and archaeal taxa. In these organism, non-discriminating AspRS misacylate $tRNA^{Asn}$ with aspartic acid then the Asp-$tRNA^{Asn}$ is converted to Asn-$tRNA^{Asn}$ by the action of amidotransferase. Thus, it is believed that AsnRS has originated from a primordial AspRSs after the branching of the three major divisions of life (295, 296). Despite that, AsnRS has the ability to discriminate its cognate asparagine from the non-cognate protonated aspartic acid (297). From studying the asparagine binding site in *Thermus thermophilus* AsnRS, only two amino acid residues; Glu225 and Arg368 are involved in the asparagine recognition, which interact with though one of the amide protons and carbonyl groups respectively. However, it is proposed that the existence of water molecules has a role in recognising the second proton atom of the asparagine amide group (298). The crystal structure of *Pyrococcus horikoshii* AsnRS complexed with the substrate proved that Glu228 and Arg364 are important to recognise asparagine as well as the role of water molecules that contribute through directly binding with the asparagine amide and carbonyl groups and also constraining the amino acid orientation avoiding incorrect AspRS/Asp-AMP like binding (299). These water molecules are conserved in most of AsnRSs because the eight amino acid residues that form the active site are not able to form a pocket complementary to the shape of the asparagine side chain (299) and this was observed during the study of the constructed AsnRS model. In the docking study of *S. aureus* AsnRS model with asparaginyl-adenylate, a strong electron density peak observed proximal to the phosphate group could be assigned to a magnesium ion as described in the interaction of *Pyrococcus horikoshii* AsnRS with the substrate (299). Water molecules have a crucial role in asparagine recognition especially two of them were found to fill the voids between the amino acid residues and asparagine side chain (Figure 46). By analysing the 30 poses of the docking study, Glu223 and Arg360 interact with the

asparagine side chain and could play a role in defining the asparagine specificity, as they make direct hydrogen bonding interactions with the asparagine amide and carbonyl groups respectively (Figure 46). Clustal alignments of *S. aureus* AsnRS with *T. Thermophilus* and *P. Horikoshii* AsnRSs furthermore proved the position of Glu223 and Arg360 corresponding to Glu225, Arg368 and Glu228, Arg364 respectively in both organisms (Figure 47).

```
Feature 1                                          ###                    # #  #
query      144 FKMRHQITRSIRQYLDDE     GFFDIETPVLTKSTPEGARDYLVPSR.[3].GEFYALPQSPQLFKQLLMISGFDKYY 216
1IL2_A     138 LKTRAKITSLVRRFMDDH     GFLDIETPMLTKATPEGARDYLVPSR.[3].GKFYALPQSPQLFKQLLMMSGFDRYY 210 Escherichia coli
1G51_A     144 LRLRHRVIKAIWDFLDRE     GFVQVETPFLTKSTPEGARDFLVPYR.[3].GLFYALPQSPQLFKQMLMVAGLDRYF 216 Thermus thermophilus
Q9X1F4     138 IILRYRISKIIRDYFDEL     GFLEIETPFLTRSTPEGARDFLVPSR.[3].GKFYALPQSPQLFKQILMISGFDRYF 210 Thermotoga maritima
P73851     144 LQLRHQVVKAMRRFLEDQ.[1].NFLEIETPILTRSTPEGARDYLVPSR.[3].GEWYALPQSPQLFKQLLMVAGMDRYY 217 Synechocystis sp. PCC 6803
O67589     149 LIFRHRVYQITRNFFTKE     GFIEIETPFLTKSTPEGARDFLVPSR.[3].GKFYALPQSPQLFKQILMIAGFDRYF 221 Aquifex aeolicus
O32038     144 MQLRHNVTKAVRSFLDEN     GFLDIETPILTGSTPEGARDYLVPSR.[3].GEFYALPQSPQLFKQLLMVSGIERYY 216 Bacillus subtilis
NP_711861  150 MIKRHEFIFAIRNYLNKR     KFVEIETPILNKSTPEGARDFLVPSR.[3].NQFYALPQSPQIFKQILMVGGMERYF 222 Leptospira interrogans ...
Q8XJ28     147 FKIRHKTTKAIRDYLDQN     GFLEMETPILTKSTPEGARDYLVPSR.[3].GMFYALPQSPQLFKQLLMVSGFDRYF 219 Clostridium perfringens
CAA19270   159 LRQRSRLAYQVHSFFNDR     EFCEVETPLLFKSTPEGAREFVVPSR.[3].GKFYALPQSPQQYKQILMASGIGNYY 231 fission yeast

Feature 1            # #    ###  # #
query      217 QIVKCFRDEDLRADRQPEFTQVDIEMSFV     DQEDVMQMGEEMLKKVVKEV.[6].GAFPRMTYKEAMRRYG 287
1IL2_A     211 QIVKCFRDEDLRADRQPEFTQIDVETSFM     TAPQVREVMEALVRHLWLEV.[5].GDFPVMTFAEAERRYG 280 Escherichia coli
1G51_A     217 QIARCFRDEDLRADRQPDFTQLDLEMSFV     EVEDVLELNERLMAHVFREA.[6].LPFPRLSYEEAMERYG 287 Thermus thermophilus
Q9X1F4     211 QIVRCFRDEDLRADRQPEFTQVDVEMSFV     DVEDVLNVSEGMVSRVFKES.[6].VPFDRIPYDDAMEKYG 281 Thermotoga maritima
P73851     218 QIARCFRDEDLRADRQPEFTQLDMEMSFM     GQEEILDLNEALICHIFKVV.[6].RPFPRLTYQESMAKYG 288 Synechocystis sp. PCC 6803
O67589     222 QIVKCFRDEDLRADRQPEFTQIDYEMSFV     SEEEVMDVAERLIATLFKEL.[6].TPFERISYREAMEKYG 292 Aquifex aeolicus
O32038     217 QIARCFRDEDLRADRQPEFTQIDIEMSFM     SQEDIMSLAEEMMAKVMRET.[6].LPLPRMTYDEAMNKYG 287 Bacillus subtilis
NP_711861  223 QIVKCFRDEDLRADRQPEFTQLDMEFSFV     SQEEILSEIEGLVETIYKEV.[6].IPFPRMTYNTAMEEYG 293 Leptospira interrogans serov...
Q8XJ28     220 QIVKCFRDEDLRANRQPEFTQVDLEMSFV     EQDDVMALNEGLIKHVFKEV.[6].TPIKRMTFKDAMEKYG 290 Clostridium perfringens
CAA19270   232 QIARCFRDEDLRFDRQPEFTQIDLEMSFV.[1].KPHEIMEVVEDLLVRLVSFA.[6].KPFQHITYQHAIDKYG 303 fission yeast

Feature 1                                     ##                                  #  #
query      288 .[139].LNFLWVTDWPLLEYDE.[2].KRYVAAHHPFTSPKE.[ 5].LGTAPE.[ 2].EANAYDIVLNGYELGGGSI 491
1IL2_A     281 .[144].WAPLWVIDFPMFEDDG.[1].GGLTAMHHPFTSPKD.[ 5].LKAAPE.[ 2].VANAYDMVINGYEVGGGSV 488 Escherichia coli
1G51_A     288 .[130].FRFLWVVDFPLLEWDE.[2].EAWTYMHHPFTSPHP.[ 5].LEKDPG.[ 2].RALAYDLVLNGVEVGGGSI 482 Thermus thermophilus
Q9X1F4     282 .[138].FDVLWVVDFPYFEWSE.[2].ERFVARHHPFTMPVL.[ 2].LGDDYT.[ 2].RAKAYDLVINGYEVGGGSI 481 Thermotoga maritima
P73851     289 .[145].INLLWITDFPMFEWNS.[2].KRFEALHHPFTAPHP.[ 2].LGDLKT.[ 1].RAQAYDLVMNGVEIGGGSL 494 Synechocystis sp. PCC 6803
O67589     293 .[137].WDVFWIVDFPLMEWDE.[2].ERFVSLHHPFTMPRE.[ 5].LKEALE.[14].RARAYDMVLNGEEIGGGSI 506 Aquifex aeolicus
O32038     288 .[139].FNFLWVIDWPLLEHDP.[2].GRFYAAHHPFTMPVR.[ 5].IETAPE.[ 2].KAQAYDLVLNGYELGGGSI 491 Bacillus subtilis
NP_711861  294 .[139].INITWIVDFPMFEWNK.[2].KRWDALHHPFTSPSD.[11].LQKNAG.[ 2].TAKAYDLVMNGVEIGGGSI 503 Leptospira interrogans ...
Q8XJ28     291 .[139].FNFTWITEFDLLEYDE.[2].GRYFAAHHPFTMPMD.[ 5].LDTDPG.[ 2].RAKAYDLVLNGEELGGGSI 494 Clostridium perfringens
CAA19270   304 .[139].LKFVWVVDFPLFSPTE.[3].QSITSTHHPFTAPHW.[ 5].LEKKPL.[ 2].RGLHYDIVVNGIELGGGSI 508 fission yeast

Feature 1     #                                   ## #  #
query      492 RIHDGELQEKMFEVLG.[7].EQFGFLLDAFKYGAPPHGGIALGLDRLVMLLTNRTNLRDTIAFPKTAS 562
1IL2_A     489 RIHNGDMQQTVFGILG.[7].EKFGFLLDALKYGTPPHAGLAFGLDRLTMLLTGTDNIRDVIAFPKTTA 559 Escherichia coli
1G51_A     483 RIHDPRLQARVFRLLG.[7].EKFGFFLEALEYGAPPHGGIAWGLDRLLALMTGSPSIREVIAFPKNKE 553 Thermus thermophilus
Q9X1F4     482 RIHRRDIQEKIFELLG.[7].KKFGFFLEAFRYGVPPHGGIAFGLDRLVSIIAGESSIREVIAFPKTGN 552 Thermotoga maritima
P73851     495 RIYQREVQEKVFATIG.[7].EKFGFLLDAFEYGTPPHGGIAYGLDRLVMLLAKEDSIRDVIAFPKTQQ 565 Synechocystis sp. PCC 6803
O67589     507 RIHRRDIQEVVFKLLG.[7].EKFGFLLEALKYGAPPHGGLAFGLDRVVALMLGLDSIRDTIAFPKTQR 577 Aquifex aeolicus
O32038     492 RIFEKDIQEKMFALLG.[7].EQFGFLLEAFEYGAPPHGGIALGLDRLVMLLAGRTNLRDTIAFPKTAS 562 Bacillus subtilis
NP_711861  504 RIHSREIQNKVFQILG.[7].EKFGFLLEALEFGAPPHGGLAFGIDRMLMLLTGGKSIRDVIAFPKTQK 574 Leptospira interrogans serovar lai...
Q8XJ28     495 RIHDTKLQEKMFEVLG.[7].ERFGFLLEAFKFGPPPHGGLAFGLDRMIMFLAGTENIKDVITFPKNQN 565 Clostridium perfringens
CAA19270   509 RIHNPDIQRFVLKDVL.[7].ATFEHLIRVLSSGCPPHGGIALGFDRLAALLTNAPGIREVIAFPKTSS 579 fission yeast
```

Figure 42: Sequence alignments of the *S. aureus* AspRS with other AspRSs for active site identification. The active sites of *S. aureus* AspRS consist of Glu177, Gly178, Ala179, Ser199, Gln201, Lys204, Arg223, Glu225, Asp230, Arg231, Gln232, Phe235, Gln237, His451, His452, Glu485, Gly488, Arg492, Ile534, Ala535, Gly537 and Arg540.

```
Feature 1                                                  # #     ##
query      168 ELFEVELFDgEKAYLSQSGQLYAEAGALA-FAKVYTFGPTFRAErSKTRRHLLEFWMVEPEVAFmt-hEENMALQEELVS 245
1B8A_A     174 ELFPMKYFE-EDAFLAESPQLYKEIMMASgLDRVYEIAPIFRAEeHNTTRHLNEAWSIDSEMAFiedeEEVMSFLERLVA 252 Thermococcus kodak...
NP_476609  263 NVFTVSYFK-DSAYLAQSPQLYKQMAIAAdFDKVYTVGAVFRAEdSNTHRHLTEFVGLDLEMAFkyhyHEVLHTIGNTFT 341 fruit fly
AAH42227   262 NVFTVSYFK-TSAYLAQSPQLYKQMCICAdFEKVFCIGPVFRAEdSNTHRHLTEFVGLDIEMAFnyhyHEVVDEIADTLV 340 African clawed frog
O29342     172 ELFPISYFE-KEAFLNQSPQLYKQVLMAAgFEKVFEIGPIFRAEeHNTTRHLNEAISIDIEMSFtd-hNGVMDVLERLVQ 249 Archaeoglobus fulg...
Q9Y9U7     176 EVFPVVYFD-KTAFLAQSPQFYKQFAVIAgLERVFEIGPVFRAEpHHTSRHLNEYHSLDIEVGFiesyNDVMNYVEGFMR 254 Aeropyrum pernix
AAO51772   306 SVFKLNYFN-THAYLAQSPQLYKQMAICAdFNKVFEIGPVFRAEnSNTHRHLTEFVGLDLEMTFkdhyHEALDTLDRLMT 384 Dictyostelium disc...
P58692     192 IDYSQDFFA-KPTYLTVSGQLEAEVMAMA-FSNVYTFGPTFRAEnSNTSRHLAEFWMVEPEMAFcd-lEGDMDLAEAFLK 268 Nostoc sp. PCC 7120
NP_585835  206 NLFSVDYFK-RKAFMAQSPQLYKQMAIVGgFKRVYEIGHVYRAEeSNINRYLSEFVGLDMEMEIctdyNDVIRFIHSMLV 284 Encephalitozoon cu...
P38707     288 TLFKMNYYG-EEAYLTQSSQLYLETCLAS-LGDVYTIQESFRAEkSHTRRHLSEYTHIEAELAFlt-fDDLLQHIETLIV 364 baker's yeast

Feature 1                                                  #  #
query      321 -----dRPVFVERYPAr-IKAFYMEPDPedpeLVLNDDLLAPeGyGEIIGGSQRIHDLELLRRKIQEFglpeevydwyLD 394
1B8A_A     318 menenaPLYFLYQYPSeaKPFYIMKYDNkp-eICRAFDLEYR-G-VEISSGGQREHRHDILVEQIKEKglnpesfefyLK 394 Thermococcus kodak...
NP_476609  411 kakydtDFYILDKFPLa-IRPFYTMPDPnnpvYSNSYDMFMR-G-EEILSGAQRIHDPEYLIERAKHHgidtskiaayIE 487 fruit fly
AAH42227   410 kekydtDFYILDKYPLa-VRPFYTMPDPnnpkYSNSYDMFMR-G-EEILSGAQRVHDPQLLTDRATHHgidlekikayID 486 African clawed frog
O29342     315 -----gGLYFITDWPTe-SKPFYAMPYEdrpeISKSFDLMHG-W-LELSSGAQRIHLYDMLVESIKAKgmepesfgfyLE 386 Archaeoglobus fulg...
Q9Y9U7     322 geeldsDFVFIVEYPWk-VRPFYTMRKDdepsWTYSFDLLYR-G-LEIVTGGQREHRYHRLLENLRDKgldaesfqfyLD 398 Aeropyrum pernix
AAO51772   456 kekfgvDFFIVDKFHVe-VRPFYTMPDPnnpqWANAYDLFMR-G-EEICSGAQRIHDPELLEKSAKSHgvviediqgyID 532 Dictyostelium disc...
P58692     347 f----kKPVIVTDYPAq-IKAFYMRLSDde-kTVRAMDVLAP-KiGEIIGGSQREERLDVLERRVLAQgmqpedlwwyLD 419 Nostoc sp. PCC 7120
NP_585835  354 rrmhgvDIFVIKDYPIs-TRPFYTYRDEek-gITRSYDFILR-G-QEILSGAQRVSIYKDLVKYVEEHgispsslggyLE 429 Encephalitozoon cu...
P38707     438 -----gVPIFLTRFPVe-IKSFYMKRCSddprVTESVDVLMP-NvGEITGGSMRIDDMDELMAGFKREgidtdayywfID 510 baker's yeast
Feature 1                    #  #
query      395 LRRFGSVPHSGFGLGLERTVAWICGLAHVREAIPFPR 431
1B8A_A     395 AFRYGMPPHGGFGLGAERLIKQMLDLPNIREVILFPR 431 Thermococcus kodakaraensis
NP_476609  488 SFRYGCPPHAGGGIGMERVVMLYLGLDNIRKTSMFPR 524 fruit fly
AAH42227   487 SFRFGAPPHAGGGIGLERVTMLYLGLHNVRQTSMFPR 523 African clawed frog
O29342     387 AFRYGMPPHAGWGLGAERLIMSMLGLKNVREAVLFPR 423 Archaeoglobus fulgidus
Q9Y9U7     399 FFKHGAPPHGGAGMGLERIVMQTLKLENIREARMLPR 435 Aeropyrum pernix
AAO51772   533 SFKYGCSQHAGGGVGLERVVMLYLGLGNIRKASFCPR 569 Dictyostelium discoideum
P58692     420 LRRYGTVPHAGFGLGFERLVQFITGMGNIRDVIPFPR 456 Nostoc sp. PCC 7120
NP_585835  430 SFKYGAPPHGGCGIGLERLMKAYFGMGDIRCFSLFPR 466 Encephalitozoon cuniculi
P38707     511 QRKYGTCPHGGYGIGTERILAWLCDRFTVRDCSLYPR 547 baker's yeast
```

Figure 43: Sequence alignments of the *S. aureus* AsnRS with other AsnRSs for active site identification. The active sites consist of Arg206, Glu208, Arg214, His215, Glu353, Gly356, Gly401, Arg404.

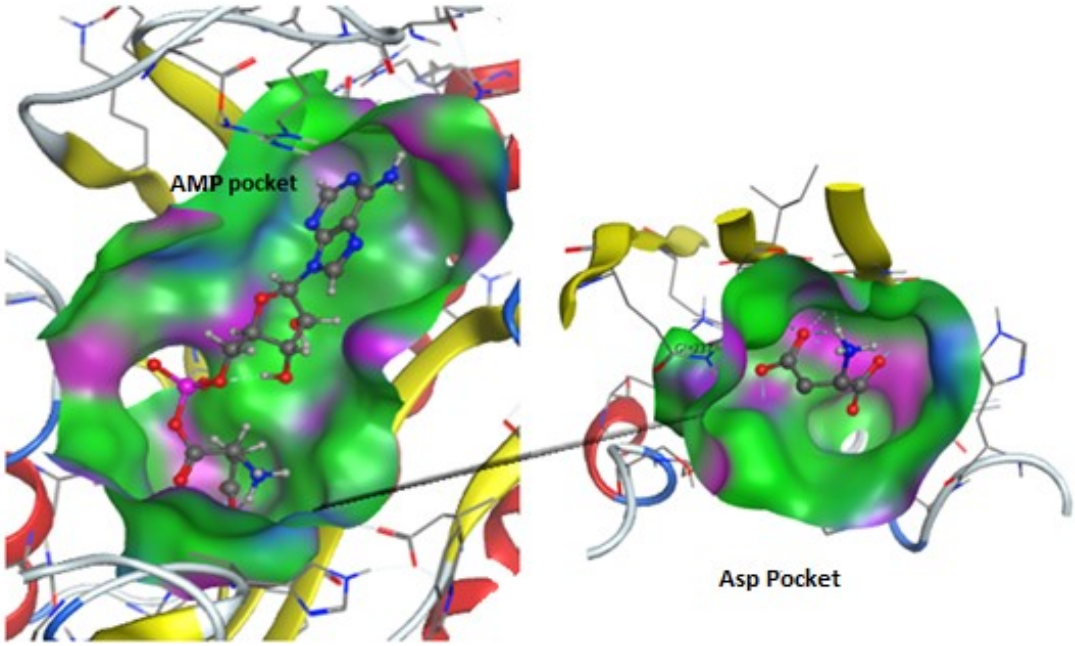

Figure 44a: 3D structure of the docking of the natural substrate (aspartyl-adenylate) in the *S. aureus* AspRS SWISS-MODEL model with ATP and aspartic acid pockets identified. The active sites are coloured based on the chemical type of bonds that could be established with ligands: hydrophobic (green); hydrogen bonds (pink); mild polar area (red).

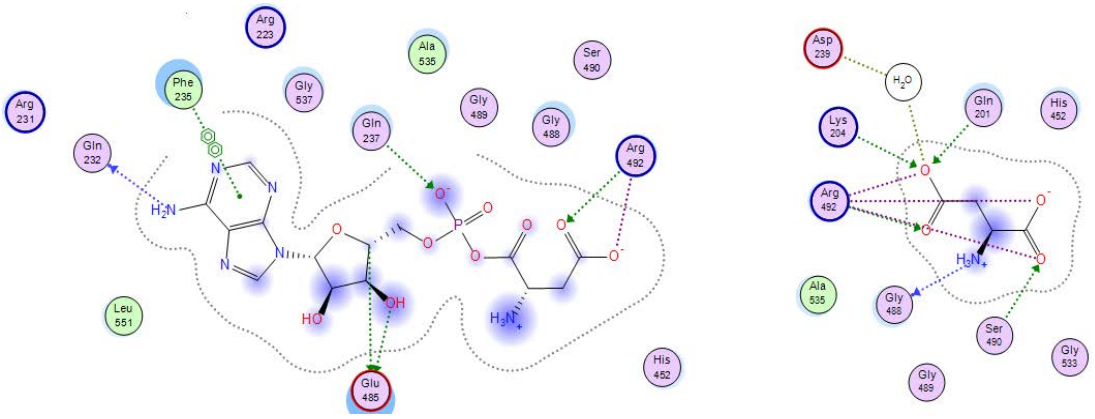

Figure 44b: 2D binding interactions of aspartyl-adenylate and aspartic acid in *S. aureus* AspRS SWISS-MODEL model active sites.

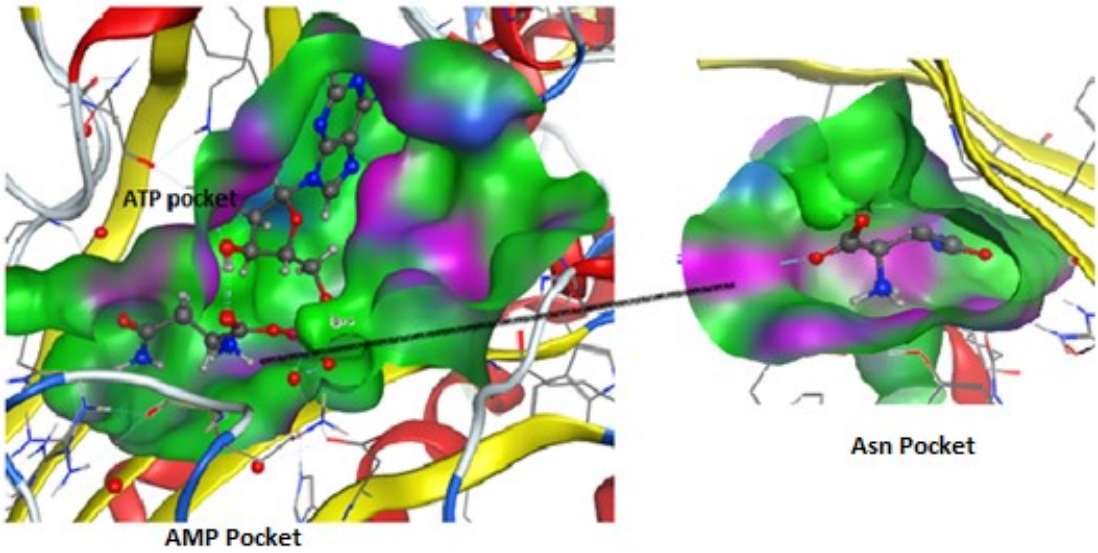

Figure 45a: 3D structure of the docking of the natural substrate (asparaginyl-adenylate) in the *S. aureus* AsnRS MOE model with ATP and asparagine pockets identified. The active sites are coloured based on the chemical type of bonds that could be established with ligands: hydrophobic (green); hydrogen bonds (pink); mild polar area (red).

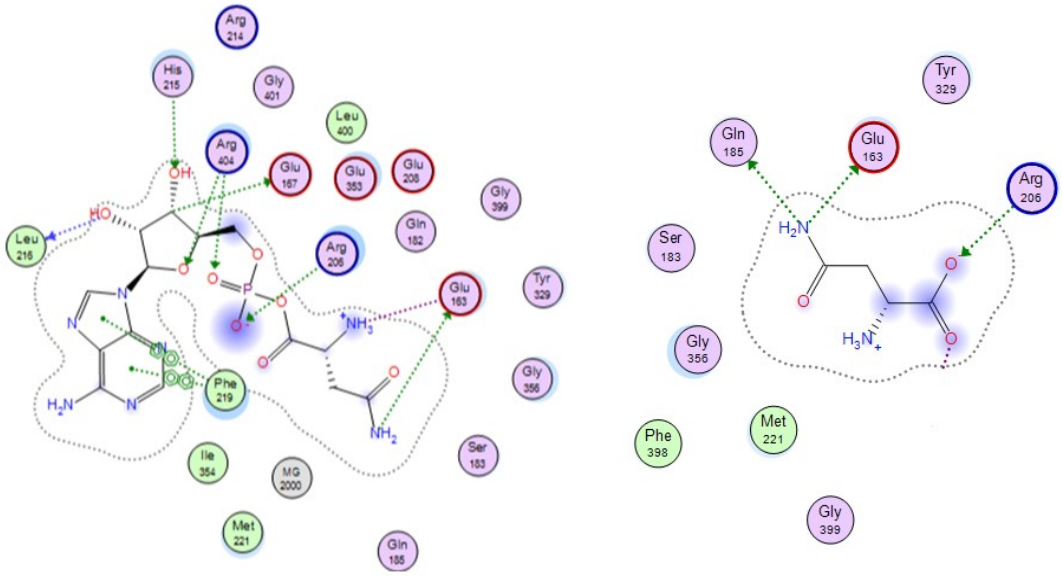

Figure 45b: 2D binding interactions of asparaginyl-adenylate and asparagine in *S. aureus* AsnRS MOE model active sites.

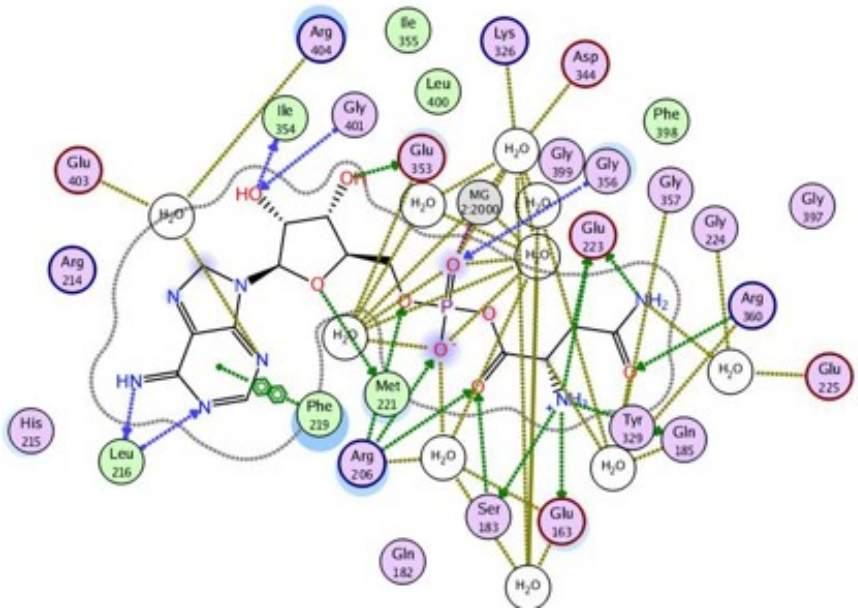

Figure 46: 2D binding interactions of asparaginyl-adenylate in the *S. aureus* AsnRS active site identified water-mediated asparagine recognition and the two amino acids residues contributed in asparagine recognition (Glu223 and Arg360).

```
sp|O57980|SYN_PYRHO     MIEKVYCQEVKPELDGKKVRLAGWVYTNMRVGKKIFLWIRDSTGIVQAVVAKNVVGEETF   60
sp|P54263|SYN_THET8     --MRVFIDEIARHV-DQEVELRGWLYQRRSKGKIHFLILRDGTGFLQATVVQGEVPEAVF   57
sp|Q2FYH6|SYN_STAA8     --MKTTIKQAKDHL-NQDVTIGAWLTNKRSSGKIAFLQLRDGTGFMQGVVVKSEVDEEVF   57
                           :.  .:   .: .:.* : .*:  .   **  ** :**.**::*..*.:. * * .*

sp|O57980|SYN_PYRHO     EKAKKLGRESSVIVEGIVKADERAPGGAEVHVEKLEVIQA-VSEFPIPENPEQASPELLL   119
sp|P54263|SYN_THET8     READHLPQETALRVWGRVREDRRAPGGFELAVRDLQVVSRPQGEY--PIGPKEHGIDFLM   115
sp|Q2FYH6|SYN_STAA8     KLAKEITQESSLYVTGTITEDNRSDLGYEMQVKSIEVISE-AHDY--PITPKNHGTEFLM   114
                        . *..: :*::: * * :  *.*:  * *: *..::*:.    ::  *  *:: . ::*:

sp|O57980|SYN_PYRHO     DYRHLHIRTPKASAIMKVKETLIMAAREWLLKDGWHEVFPPILVTGAVEGGATLFKLKYF   179
sp|P54263|SYN_THET8     DHRHLWLRHRRPFAVMRIRDELERAIHEFFGERGFLRFDAPILTPSAVEGTTELFEVELF   175
sp|Q2FYH6|SYN_STAA8     DHRHLWLRSKKQHAVMKIRNEVIRATYEFFNKDGFTKVDPPILTASAPEGTSELFHTKYF   174
                        *:*** :*  :  *:*:::: :  *  *:: : *: ..  ***. .* ** : **. : *

sp|O57980|SYN_PYRHO     DK-YAYLSQSAQLYLEAAIFGLEKVWSLTPSFRAEKSRTRRHLTEFWHLEIEAAWMDLWD   238
sp|P54263|SYN_THET8     DGEKAYLSQSGQLYAEAGALAFAKVYTFGPTFRAERSKTRRHLLEFWMVEFEVAFMTHEE   235
sp|Q2FYH6|SYN_STAA8     DQ-DAFLSQSGQLYLEAAAMAHGKVFSFGPTFRAEKSKTRRHLIEFWMIEGEMAFTNHAE   233
                        *   *:****.*** **. :.  **::: *:****:*:***** *** :* * *:    :

sp|O57980|SYN_PYRHO     IMKVEEELVSYMVQRTLELRKKEIEMFRDDLTTLKN-TEPPFPRISYDEAIDILQSK---   294
sp|P54263|SYN_THET8     NMALQEELVSFLVARVLERRSRELEMLGRDPKALEPAAEGHYPRLTYKEAVALVNRIAQE   295
sp|Q2FYH6|SYN_STAA8     SLEIQEQYVTHVVKSVLENCKLELKILERDTSKLEKVA-TPFPRISYDDAIEFLKAE---   289
                         : ::*: *:.:*  .**  . *::::  * . *:  :   :**::*.:*: :::

sp|O57980|SYN_PYRHO     ---GVNVEWGDDLGADEERVLTEEFDRPFFVYGYPKHIKAFYMKEDPNDPRKVLASDMLA   351
sp|P54263|SYN_THET8     DPEVPPLPYGEDFGAPHEAALSRRFDRPVFVERYPARIKAFYMEPDPEDPELVLNDDLLA   355
sp|Q2FYH6|SYN_STAA8     --GFDDIEWGEDFGAPHETAIANHYDLPVFITNYPTKIKPFYMQPNPENEETVLCADLIA   347
                              : :*:*:** .* .::..:* *.*:  ** :** ***: :*:: . **  *::*

sp|O57980|SYN_PYRHO     PEGYGEIIGGSQRIDDYDKLLNRILEEGMDPKDYEWYLDLRRYGSVPHSGFGLGVERLVA   411
sp|P54263|SYN_THET8     PEGYGEIIGGSQRIHDLELLRRKIQEFGLPEEVYDWYLDLRRFGSVPHSGFGLGLERTVA   415
sp|Q2FYH6|SYN_STAA8     PEGYGEIIGGSERVDDLELLEQRVKEHGLDEEAYSYYLDLRRYGSVPHCGFGLGLERTVA   407
                        ***********  .* : * .:: * *:  : *.:******:*****.*****:** **
```

Figure 47: Sequence alignment of *P. Horikoshii* (SYN_PYRHO), *T. Thermophilus* (SYN_THET8) and *S. aureus* (SYN_STAA8) AsnRSs showed the conserved amino residues in blue squares which are responsible for asparagine side chain recognition. (Glu228, Arg364), (Glu225, Arg368) and (Glu223, Arg360) respectively.

2.3.1.4.2. Metal binding

Magnesium ions can act as a cofactor in numerous enzymatic reactions and plays a major role in class II aminoacyl tRNA synthetases (300). In AspRS, the co-substrate ATP binds preferentially with three associated magnesium cations in a bent geometry. These Mg^{2+} ions have a structural role in addition to their catalytically participation in the enzyme reaction to increase the discrimination of Asp-AMP over Asn-AMP (301). In AspRS and AsnRS, the adenylation reaction occurs in the absences of their cognate tRNA molecules once aspartic acid or asparagine and ATP are in their pockets (301). The amino acids backbone reacts with the α-phosphate through a nucleophilic displacement mechanism to form a pentacoordinate phosphorus transition state (293, 301). One of the Mg^{2+} cations increases the electropositivity of the α-phosphate

through withdrawing electrons and pulling its oxygen into a pentacoordinate geometry, which stabilises the pentavalent transition state via electrostatic reactions while other cations neutralise the leaving pyrophosphate product (301, 302). In general, there are two highly conserved amino residues to participate with Mg^{2+} cations in binding and coordination in class II aaRSs. Sequence alignment of *S. aureus* and other AspRSs, which have known bound amino residues with Mg^{2+} cations was used to identify the corresponding amino acids in the *S. aureus* AspRS model (Figure 48). By similarity, Glu485 and Gly488 amino residues could be responsible for Mg^{2+} cation binding in *S. aureus* AspRS whereas the same amino residues (Glu476, Gly479) and (Glu482, Gly485) are in *T. Thermophilus* and *E. coli* AspRSs respectively. As none of the similar 3D templates of *S. aureus* AspRS contain Mg^{2+} ion, the *Pyrococcus kodakaraensis* AspRS with Mg^{2+} ion (3NEM) (302) was used as a template to understand the interactions between the cation and the active site of *S. aureus* AspRS model. In the docking study of the model with the substrate in the presence of Mg^{2+} ion, Glu485 is bound with the cation over all poses (Figure 49). Due to the low similarity in the AspRS sequences in both organisms (30%), it is difficult to identify the role of Gly488 in that binding. Mg^{2+} cations are important in stabilising the released pyrophosphate, a docking study of the constructed model with ATP was favourably made to illustrate the role of Gly488. As a result, Gly489 and Asp478 participate in hydrogen binding with the O of γ phosphate via water molecules (Figure 50) not with Mg^{2+} cation. However, it has been reported that Asp478 and Glu485 are highly conserved amino acids residues bound with cation in class II aaRSs (301) and mutagenesis experiments have shown that both are functionally irreplaceable in AspRSs (300) and the role of Mg^{2+} cation in Asp/Asn discrimination by AspRS is clearly detected in *E coli*. When aspartic acid binds in its pocket of *E. coli* AspRS, the structural reorganisation is induced in two conserved loops: histidine loop (residues 436-449) and mobile flipping loop (residues 167- 173). As a result of that reorganization, His448 makes a hydrogen bond with aspartic acid and the flipping loop moves to a closer position over the amino acid binding site bringing the negative Glu171 close to the Asp ligand. As the flipping loop is conserved in eukaryal, eubacterial and archaebacterial AspRSs (282, 300, 303), residues 173- 179 could be the flipping loop in *S. aureus* while amino acids residues 438-452 form the histidine loop of *S. aureus* AspRS based on a

similarity search with *E. coli* and *T. Thermophilus* AspRSs. Docking studies of the model with aspartyl-adenylate showed that His452 binds with aspartic acid (Figure 49) and by similarity, Glu177 is one of the key amino acid residues in the active site beside its position in the flipping loop which may take the same role of Glu171 in *E coli* AspRS (Figure 42). To study the specificity of aspartic acid, a free energy simulation was used to compare aspartic acid and asparagine binding to *E. coli* AspRS in the presence of either bound ATP.Mg^{2+} or bound ATP.Mg_3^{2+} (304). In the case of aspartic acid, the discrimination is increased, and the positive charge is enhanced once ATP binds with its three associated Mg^{2+} cations. Both charged substrates and both short and long-range electrostatic interactions play a role. The His448 positive charge restores a large discrimination in favour of Asp. When asparagine replaces aspartic acid in the amino binding site, His448 loses its labile proton and become neutral (300). AspRS specificity is substrate-assisted and the binding of ATP with three Mg^{2+} ions and histidine charging allows AspRS to combine a moderate Asp binding affinity with a very strong Asp/Asn binding specificity (301). In case of *S. aureus* AsnRS, *Pyrococcus horikoshii* AsnRS template (1X54) was used to identify which amino acid residues bind with Mg^{2+} ion. MOE alignment and docking tools predict that Lys326 and Asp344 in *S. aureus* AsnRS constructed model bind the cation through water molecules, which correspond to Lys330 and Asp348 in *Pyrococcus horikoshii* AsnRS (Figure 46).

```
sp|P36419|SYD_THETH        PLLEKDPGRVRALAYDLVLNGVEVQGGSIRIHDPRLQARVFRLLGIGEEEQREKFGFFLE   513
sp|P21889|SYD_ECOLI        AELKAAPENAVANAYDMVINGVEVQGGSVRIHNGDMQQTVFGILGINEEEQREKFGFLLD   519
sp|Q2FXU5|SYD_STAA8        AKLGTAPEEAEANAYDIVLNGVELQGGSIRIHDGELQEKMFEVLGFTKEQAQEQFGFLLD   522
sp|Q9M084|SYDC2_ARATH      ------DNPLYSNSFDVFIRGEEISGAQRVHIPEVLEQRAGECGIDV----KTISTYID   514
sp|O07683|SYDND_HALSA      ------GDDVASRKFDLLYRGQELSSGGQREHDIERLTAKMREQGVEP----ENFEFYLD   392
tr|M0P2W5|M0P2W5_9EURY     ------GDEIASRKFDLIYKGQELSSGGQREHDVDRMVEVMEEEGVET----ANFEFYIE   390
sp|Q3IT59|SYDND_NATPD      ------D-GELSTGFDMMHPRMELVSGGQREHRREELIAGFEQQGLEP----EAFEYYTK   389
sp|Q8Q0R2|SYDND_METMA      ------DRPEFSKSFDMMHRTMELSSGAQRIHIPSLLKNRIESQGLNP----DGFEFYLK   400
sp|Q52428|SYD_THEKO        ------NKPEICRAFDLEYRGVEISSGGQREHRHDILVEQIKEKGLNP----ESFEFYLK   394
sp|O26328|SYDND_METTH      ------DDPERSHAFDLMYRDLEISSGAMRVHQHDLLVEKIKRQGLNP----DSFESYLS   393
                                  .  :*:     *  *. * *          *.       :    .
```

Figure 48: Part of sequence alignment of AspRSs in different organisms showing amino acid residues bound with Mg^{2+}: *Thermus thermophilus* (SYD_THETH), *Escherichia coli* (SYD_ECOLI), *Staphylococcus aureus* (SYD_STAA8), *Arabidopsis thaliana* (SYDC2_ARATH), *Halobacterium salinarum* (SYDND_HALSA), *Halorubrum lipolyticum* (M0P2W5_9EURY), *Natronomonas pharaonis* (SYDND_NATPD), *Methanosarcina mazei* (SYDND_METMA), *Thermococcus kodakarensis* (SYD_THEKO), *Methanothermobacter thermautotrophicus* (SYDND_METTH).

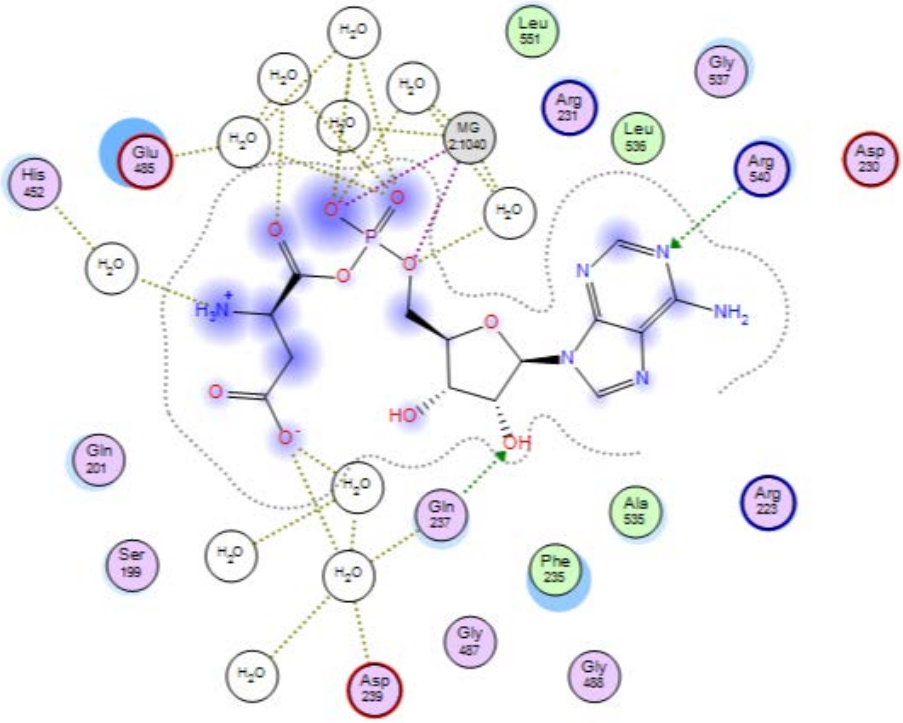

Figure 49: 2D binding interactions of aspartyl-adenylate in the *S. aureus* AspRS active site showing the interaction of His452 with aspartic acid in the presence of Mg^{2+} cation**.**

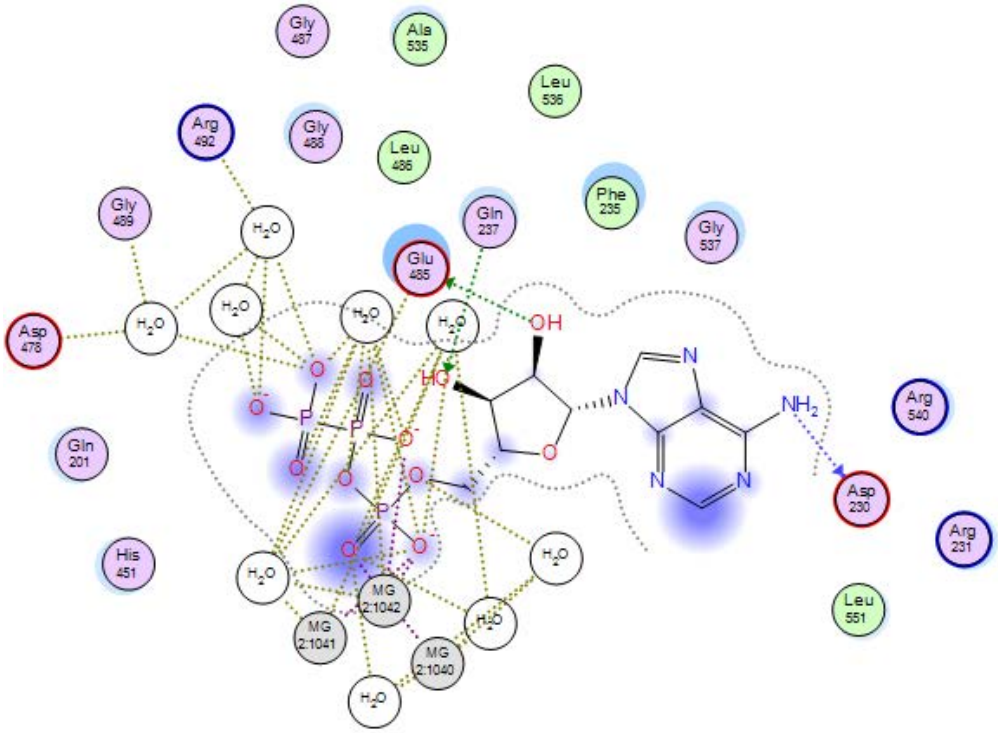

Figure 50: 2D binding interactions of *S. aureus* AspRS MOE model with ATP illustrating that Gly489 and Asp478 could participate in hydrogen binding with the O of γ phosphate via water molecules.

2.3.1.5. Molecular dynamic of *S. aureus* AspRS and AsnRS models

Because molecular recognition and drug binding are a very dynamic processes (305), using molecular dynamic as a simulation method for analysing the movement of ligand and its receptor was performed through Schrödinger platform (306). Root-Mean-Square-Deviation (RMSD) (Figure 51) and the Root-Mean-Square-Fluctuations (RMSF) (Figure 52) are common measures of structural fluctuations for conformational mobility. RMSD is used to measure the average change in displacement of a selection of atoms for a particular frame with respect to a reference frame while RMSF is useful for characterising local changes along the protein chain through measuring the displacement of a particular atom, or group of atoms, relative to the reference structure, averaged over the number of atoms (307). Monitoring the RMSD of the protein can indicate how large the conformational change of the protein is during the simulation time and how stable the ligand is with respect to the protein and its binding pocket. Figure 51 shows that the conformational change of *S. aureus* AspRS is larger than *S. aureus* AsnRS in 100 nano-second of simulation time whereas the natural substrate of the latter one is the most stable in its binding pocket. On the other hand, the RMSF figure 52 shows peaks that identify which areas of the protein fluctuated the most during the simulation (306).

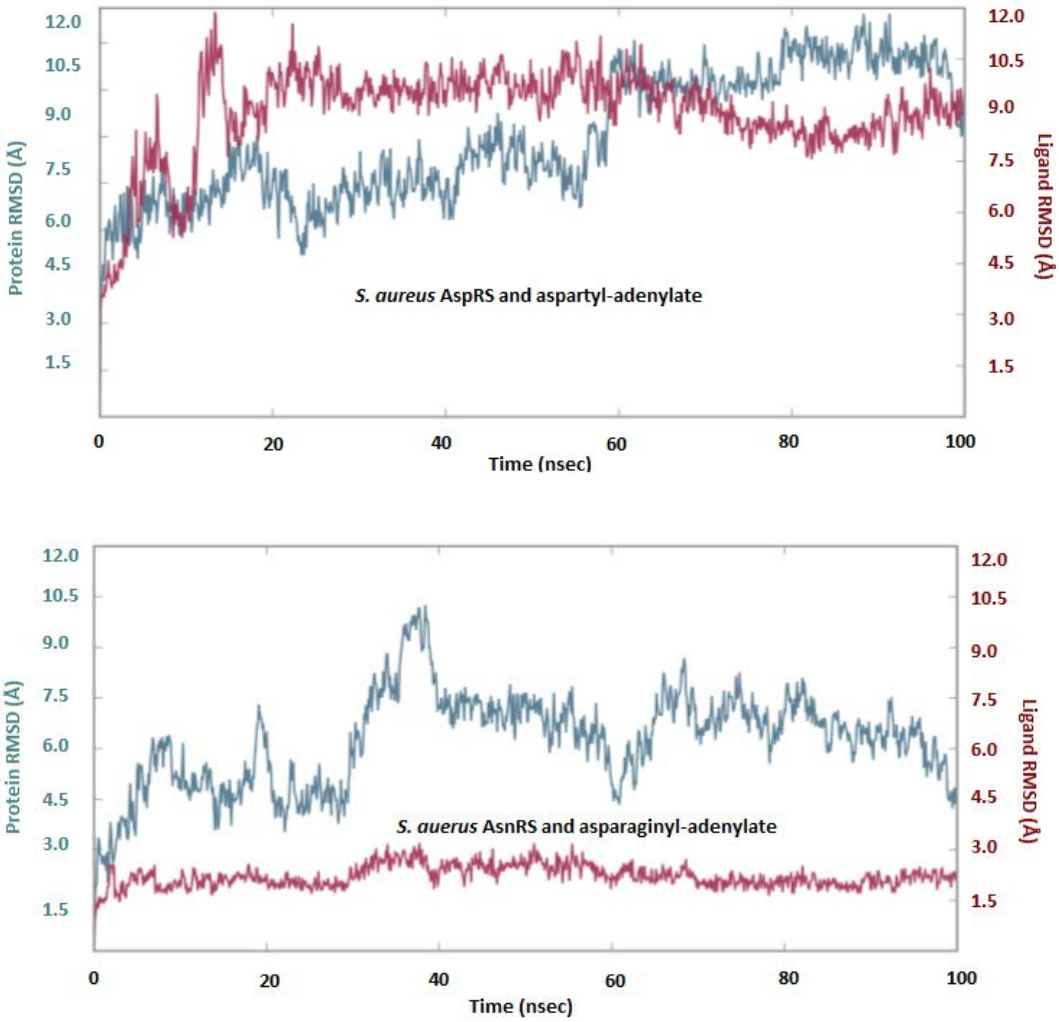

Figure 51: RMSD (in angstrom) plot with respect to time in nanoseconds during 100 ns MD simulation of *S. aureus* AspRS and AsnRS with their substrates.

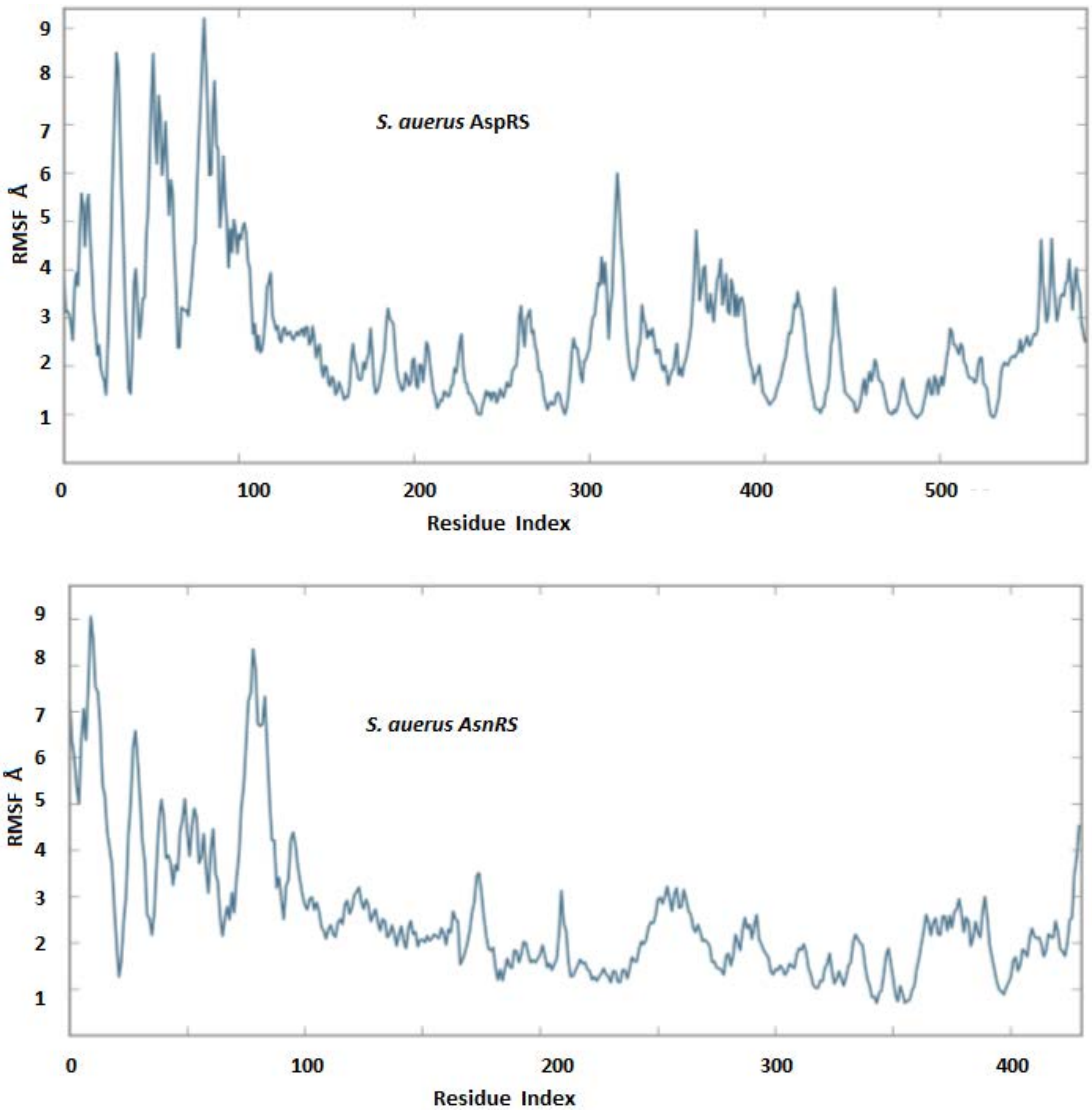

Figure 52: RMSF (in angstrom) plot of *S. aureus* AspRS and AsnRS amino acids residues.

Protein interactions with the ligand are also furthermore monitored during simulation time and characterised by type into four groups: hydrogen bonds, hydrophobic, ionic and water bridges with green, mauve, pink and blue colour respectively (Figure 53). The X-axis of both graphs represent the key amino acid residues of the targeting enzymes while the Y- axis is for the interactions fraction indicating the percentage of each specific interaction that is maintained during the simulation time. For example, Glu485 in *S. aureus* AspRS simulation interactions diagram formed a hydrogen bonds with the substrate for approximately 60% of the simulation time while throughout the simulation time there are hydrogen bonds mediated by water molecules. Any value above 1.0 indicates that residue may make multiple contacts of same subtype with the ligand.

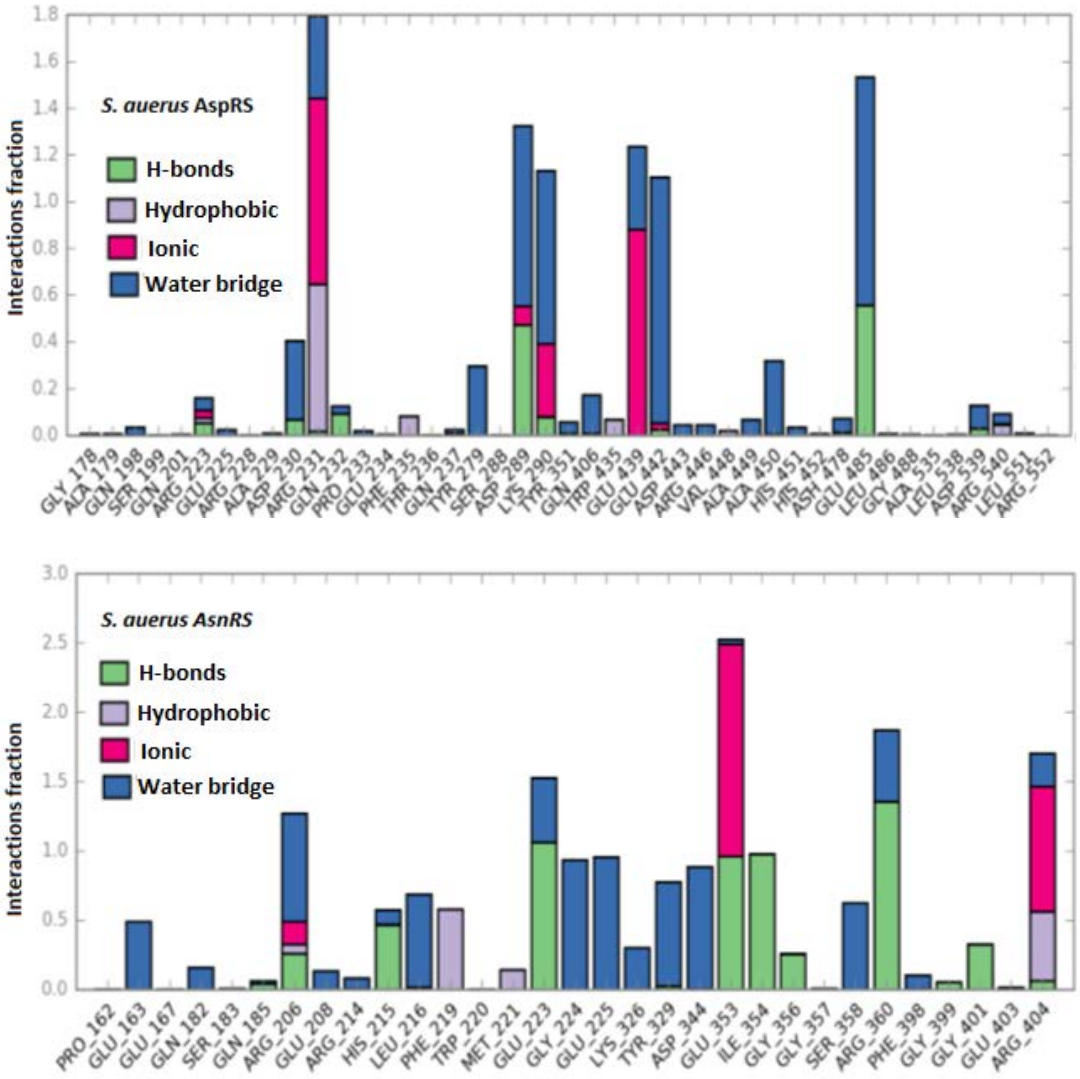

Figure 53: Simulation protein-ligand contact interactions over the 100ns trajectory diagram.

Studying molecular dynamic in Schrodinger also provides a direct prediction of small-molecule binding energies through using prime MM-GBSA (308) which generates energy properties including energies for the ligand, receptor, and complex structures in minimised and optimised free form. Thus, it can be used to estimate relative binding affinity for a list of ligands and there is a reasonable agreement of the ranking of the ligands based on the calculated binding energies with the result of ranking them based on experimental binding affinity (308). As the MM-GBSA binding energies are approximate free energies of binding, a more negative value indicates stronger binding (308). The binding free energy (Prime MMGBSA ΔG bind) is calculated with this equation:

ΔG (bind) = E_complex (minimised) - (E_ligand (minimised) + E_receptor (minimised))

The binding affinity of aspartyl-adenylate and asparaginyl-adenylate with their respective *S. aureus* enzymes is in positive value for AspRS and negative for AsnRS (Table 11) and that measurement could be used for understanding the binding affinity of designed *S. aureus* AspRS/AsnRS inhibitors.

Table 11: MM-GBSA binding energies of aspartyl-adenylate and asparaginyl-adenylate.

Binding affinity of natural substrates	*S. aureus* AspRS	*S. aureus* AsnRS
ΔG range (kcal/mol)	7.7972 to 52.882	-33.0909 to -9.3165
ΔG average (kcal/mol)	27.8939 ± 6.74	-22.5387 ± 4.93

2.3.1.6. Final constructed *S. aureus* AspRS and AsnRS models

The final built models of *S. aureus* AspRS and AsnRS have the same characteristic domains of subclass IIb aaRS enzymes where the C-terminal catalytic site is built around antiparallel β sheets (Figures 54 and 55). These enzymes are homodimers of two α subunits, with each monomer of AspRS contains four modules including the N-terminal domain for tRNA anticodon recognition, a small hinge domain, catalytic domain and large insertion domain which is characteristic of eubacterial AspRSs. However, the monomer of AsnRS consists of the first three modules and as they are members of class II aaRSs, they contain three conserved motifs (motifs 1, 2 and 3).

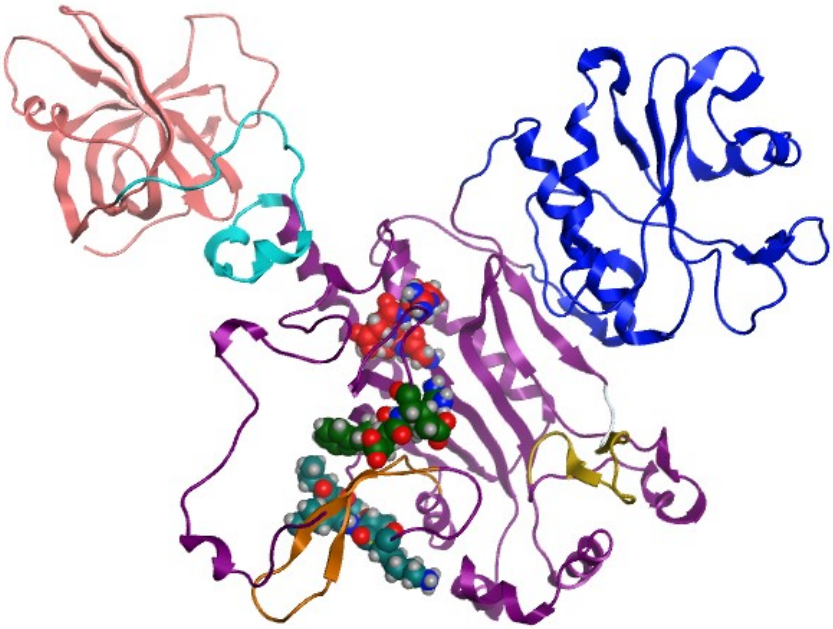

Figure 54: Final *S. aureus* AspRS homology model with characteristic domains and motifs: active site (purple), N-terminal anticodon binding domain (pink), insertion domain (blue), a small hinge domain (cyan), histidine loop (yellow), flipping loop (brown). Motifs represented in ball model structure are motif 1 (169-173) is in teal, motif 2 (222-225) in green and motif 3 (537-540) in red.

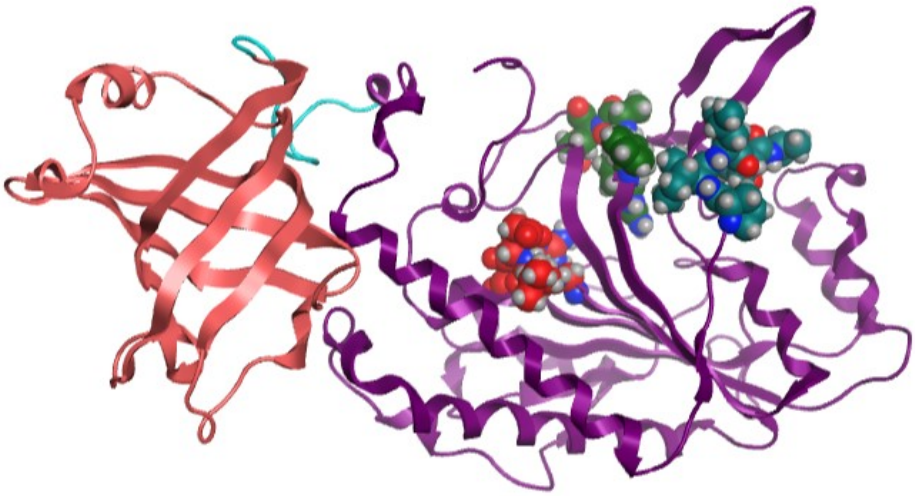

Figure 55: Final *S. aureus* AsnRS homology model with characteristic domains and motifs: C-terminal active site (purple), N-terminal anticodon binding domain (pink), hinge region (cyan). Motifs represented in ball model structure which motif 1 (155-159) is in teal, motif 2 (205-208) in green and motif 3 (401-404) in red.

2.3.2. *Computational analysis of E. faecalis aminoacyl tRNA synthetases*

E. faecalis AspRS and AsnRS with UNIPROT identifiers Q833I2 and Q831X4 respectively have high similarity in their protein sequences with *S. aureus* AspRS and AsnRS, which reaches to 63.82% and 66.28% respectively (Figures 56 and 57). By using the same computational analysis of *S. aureus* aaRSs, Clustal Omega (271) was used to perform a similarity search in *E. faecalis* aaRS enzymes. From the percent identity matrix results of class I aaRSs, the closet similarity was shown for subclass Ia (Figure 58), followed by subclass IIb aaRSs (Figure 59), therefore, this section focuses on *E. faecalis* AspRS and AsnRS.

```
Percent Identity  Matrix - created by Clustal2.1


  1: sp|Q833I2|SYD_ENTFA  100.00   63.82
  2: sp|Q2FXU5|SYD_STAA8   63.82  100.00
```

Figure 56: The percent identity matrix of *S. aureus* AspRS (SYD_STAA8) in relation to *E. faecalis* AspRS (SYD_ENTFA), with percentage of similarity is 63.82%.

```
Percent Identity  Matrix - created by Clustal2.1


  1: sp|Q831X4|SYN_ENTFA  100.00   66.28
  2: sp|Q2FYH6|SYN_STAA8   66.28  100.00
```

Figure 57: The percent identity matrix of *S. aureus* AsnRS (SYN_STAA8) in relation to *E. faecalis* AsnRS (SYN_ENTFA), with percentage of similarity is 66.28%.

1: tr|A0A1J6YUN6|A0A1J6YUN6_ENTFL	100.00	16.36	14.01	12.50	18.68	20.67	15.17	18.23	9.60
2: tr|A0A1B4XLV7|A0A1B4XLV7_ENTFL	16.36	100.00	17.31	15.38	23.99	25.73	23.35	13.76	14.29
3: tr|A0A1X3ALU9|A0A1X3ALU9_ENTFL	14.01	17.31	100.00	12.99	15.72	21.33	21.85	11.37	13.07
4: tr|A0A2T5D6I6|A0A2T5D6I6_ENTFL	12.50	15.38	12.99	100.00	19.59	16.78	17.11	7.64	6.45
5: tr|A0A1G1S8M1|A0A1G1S8M1_ENTFL	18.68	23.99	15.72	19.59	100.00	22.82	23.76	12.46	15.03
6: tr|A0A2R6U726|A0A2R6U726_ENTFL	20.67	25.73	21.33	16.78	22.82	100.00	26.51	17.44	12.37
7: tr|A0A1Q1FSR4|A0A1Q1FSR4_ENTFL	15.17	23.35	21.85	17.11	23.76	26.51	100.00	15.76	14.64
8: tr|A0A3N3ZCS8|A0A3N3ZCS8_ENTFL	18.23	13.76	11.37	7.64	12.46	17.44	15.76	100.00	19.72
9: tr|A0A1B4XLC0|A0A1B4XLC0_ENTFL	9.60	14.29	13.07	6.45	15.03	12.37	14.64	19.72	100.00

Figure 58: Percent identity matrix of class I *E. faecalis* aaRSs, the % of similarity in subclass Ia enzymes shows in blue shaded boxes of LeuRS, green shaded boxes of IleRS and pink shaded boxes of ValRS. GluRS: A0A1J6YUN6_ENTFL, LeuRS: A0A1B4XLV7_ENTFL, CysRS: A0A1X3ALU9_ENTFL, TrpRS: A0A2T5D6I6 _ENTFL, MetRS: A0A1G1S8M1_ENTFL, ValRS: A0A2R6U726_ENTFL, IleRS: A0A1Q1FSR4 _ENTFL, ArgRS: A0A3N3ZCS8_ENTFL, TyrRS: A0A1B4XLC0_ENTFL.

1:	tr|A0A1Q1FVX2|A0A1Q1FVX2_ENTFL	100.00	22.69	15.30	12.17	10.98	9.60	10.23	9.69	12.12	11.64
2:	tr|A0A1G1SE70|A0A1G1SE70_ENTFL	22.69	100.00	23.83	12.68	14.18	18.18	14.56	12.47	12.81	17.47
3:	tr|A0A1Q1FV24|A0A1Q1FV24_ENTFL	15.30	23.83	100.00	9.57	12.17	14.92	11.37	12.39	9.76	13.20
4:	sp|Q831X4|SYN_ENTFA	12.17	12.68	9.57	100.00	25.13	22.98	11.74	11.67	11.01	16.50
5:	tr|A0A1G1SBV2|A0A1G1SBV2_ENTFL	10.98	14.18	12.17	25.13	100.00	26.80	17.57	13.55	10.83	17.76
6:	sp|Q833I2|SYD_ENTFA	9.60	18.18	14.92	22.98	26.80	100.00	14.81	15.93	12.77	19.75
7:	tr|A0A1B4XSE9|A0A1B4XSE9_ENTFL	10.23	14.56	11.37	11.74	17.57	14.81	100.00	21.27	6.10	19.93
8:	tr|A0A3N3SQX9|A0A3N3SQX9_ENTFL	9.69	12.47	12.39	11.67	13.55	15.93	21.27	100.00	13.55	20.84
9:	tr|A0A3N3RQX8|A0A3N3RQX8_ENTFL	12.12	12.81	9.76	11.01	10.83	12.77	6.10	13.55	100.00	21.73
10:	sp|Q831W7|SYP_ENTFA	11.64	17.47	13.20	16.50	17.76	19.75	19.93	20.84	21.73	100.00

Figure 59: Percent identity matrix of class I *E. faecalis* aaRSs. the % of similarity in subclass IIb enzymes shows in blue shaded boxes of AsnRS, green shaded boxes of AspRS and pink shaded boxes of LysRS. GlyRS: A0A1Q1FVX2_ENTFL, AlaRS: A0A1G1SE70_ENTFL, HisRS: A0A1Q1FV24_ENTFL, AsnRS: Q831X4 (SYN_ENTFA), LysRS: A0A1G1SBV2_ENTFL, AspRS: Q833I2 (SYD_ENTFA), SerRS: A0A1B4XSE9_ENTFL, ThrRS: A0A3N3SQX9_ENTFL, PheRS: A0A3N3RQX8_ENTFL, ProRS: Q831W7 (SYP_ENTFA).

2.3.2.1. Construction of *E. faecalis* AspRS and AsnRS models

2.3.2.1.1. Homology search of *E. faecalis* AspRS and AsnRS

A BLAST analysis (273, 274) was also performed for the initial screening for all possible templates of *E. faecalis* AspRS and AsnRS amino acid sequences using the ExPASy proteomic server (275) against the PDB resolved structures. Four structures were identified for each as possible templates (Tables 12 and 13). As mentioned previous, the chosen templates are wild-type, that is they are not mutants or engineered and have the same function but are from different bacteria. They were selected based on the reasonable sequence identity with both *E. faecalis* AspRS and AsnRS. Due to the high percentage of similarity in proteins sequences between *S. aureus* and *E. faecalis* AspRS and AsnRS enzymes, the findings of homology search are the same in both enzymes. The AspRS enzyme of *Thermus thermophilus* (pdb: 6HHV) was the best template for *E. faecalis* AspRS with 51.27% identity (309). The Presence of the Pro175, Glu176 and Gln200 as important amino acid residues for the binding site in the outlier region of the *E coli* based SWISS-MODEL and MOE models in Ramachandran plot excludes *E coli* AspRS template (pdb: 1EQR) (278). *Pseudomonas aeruginosa* (pdb: 4WJ3) (279) as an asparagine transamidosome was unfavourable as a template owing to its slightly different enzyme function. Therefore, selected Thermus thermophilus (pdb: 6HHV) was the best template for AspRS model building. In the case of *E. faecalis* AsnRS, *Thermus thermophilus* AsnRS (pdb: 5ZG8) (281) has high percentage of

similarity with the *E. faecalis* query but because its incomplete protein sequence, AsnRS *Pyrococcus horikoshii* (pdb: 1X54) (282), with 45.83% homology, was selected as a template to build the *E. faecalis* AsnRS homology model.

Table 12: The first four hits in the *E. faecalis* AspRS BLAST results.

Organisms	PDB code	BLAST score [a]	Sequence identity [b]	Sequence identity %	Positive %	Chain length	E-Value
E coli	1EQR	629	314/590	53.22	70	590	0.0
Pseudomonas aeruginosa	4WJ3	602	303/586	51.71	70	599	0.0
Thermus thermophilus	6HHV	566	302/589	51.27	67	581	0.0
Mycolicibacterium smegmatis	4O2D	553	282/596	47.32	64	620	0.0

[a] The BLAST score for an alignment is calculated by summing the scores of each aligned position and the scores of gaps. [b] (number of identical residues)/ (length of sequence fragment identified by PSI/BLAST)

Table 13: The first four hits in the *E. faecalis* AsnRS BLAST results.

Organisms	PDB code	BLAST score [a]	Sequence identity [b]	Sequence identity %	Positive %	Chain length	E-Value
Thermus thermophilus	5ZG8	495	234/445	52.58	70	438	2e-167
Pyrococcus horikoshii	1X54	350	180/433	41.57	61	434	7e-117
Elizabethkingia anopheles	6PQH	270	162/477	33.96	53	490	4e-85
Thermococcus kodakarensis	3NEL	216	158/430	33.86	50	438	5e-65

[a] The BLAST score for an alignment is calculated by summing the scores of each aligned position and the scores of gaps. [b] (number of identical residues)/ (length of sequence fragment identified by PSI/BLAST)

The phylogeny server (283) was furthermore used to conduct a phylogenetic tree using AspRS protein sequence from different organisms to determine the relative

distances between these enzymes and the query sequence (Figure 60) and the same was done for AsnRS (Figure 61). The closet protein sequence to *E. faecalis* AspRS in this group of species are *E. coli* (ECOLI) followed by *Pseudomonas aeruginosa* (PSEAE) and *Thermus thermophilus* (THETH) while *Thermus thermophilus* (THETH) followed by *Pyrococcus horikoshii* (PYRHO) are the closet for *E. faecalis* AsnRS. The least homologous are *Mycolicibacterium smegmatis* (MYCSE) for *E. faecalis* AspRS and *Elizabethkingia anopheles* (9FLAO), and *Thermococcus kodakarensis* (THEKO) for *E. faecalis* AsnRS. The difference of bacterial aaRSs than their human counterparts is clearly shown in the phylogenetic trees (Figures 60 and 61). Clustal analysis and percent identity matrix results (Figures 62 and 63) provide further validation.

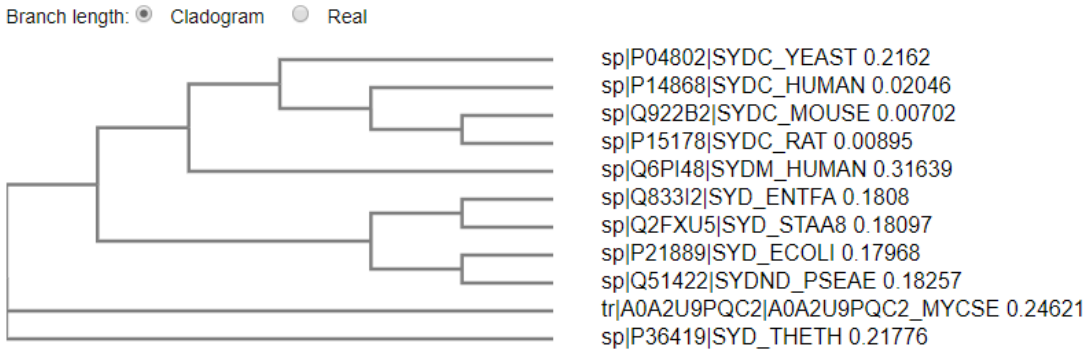

Figure 60: The phylogenetic tree of *E. faecalis* AspRS (Q833I2) in relation to AspRS from other organisms: *Saccharomyces cerevisiae* (yeast) (P04802), *Homo sapiens* (cytoplasmic) (P14868), *Mus musculus* (mouse) (Q922B2), *Rattus norvegicus* (rat) (P15178), *Homo sapiens* (mitochondria) (Q6PI48), *S. aureus* (Q2FXU5), *E coli* (P21889), *Pseudomonas aeruginosa* (Q51422), *Mycolicibacterium smegmatis* (A0A2U9PQC2) and *Thermus thermophilus* (P36419).

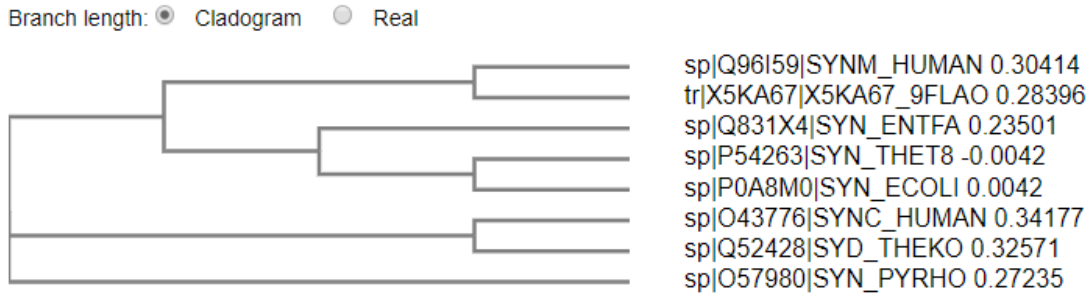

Figure 61: The phylogenetic tree of *E. faecalis* AsnRS (Q831X4) in relation to AsnRS from other organisms: *Homo sapiens* (mitochondria) (Q96I59), *Elizabethkingia anopheles* (X5KA67), *Thermus thermophilus* (P54263), *E coli* (P0A8M0), *Homo sapiens* (cytoplasmic) (O43776), *Thermococcus kodakarensis* (Q52428) and *Pyrococcus horikoshii* (O57980).

Percent Identity Matrix - created by Clustal2.1

1: sp|P04802|SYDC_YEAST	100.00	56.71	56.31	56.11	22.39	26.39	27.40	27.92	26.88	26.26	26.53
2: sp|P14868|SYDC_HUMAN	56.71	100.00	96.00	95.60	22.54	26.24	28.44	25.70	27.44	25.58	25.93
3: sp|Q922B2|SYDC_MOUSE	56.31	96.00	100.00	98.40	22.98	26.24	27.74	25.93	27.21	26.05	25.93
4: sp|P15178|SYDC_RAT	56.11	95.60	98.40	100.00	22.54	25.77	27.74	25.93	26.98	26.05	25.93
5: sp|Q6PI48|SYDM_HUMAN	22.39	22.54	22.98	22.54	100.00	39.54	43.73	41.26	40.28	40.88	38.88
6: tr|A0A2U9PQC2|A0A2U9PQC2_MYCSE	26.39	26.24	26.24	25.77	39.54	100.00	53.60	47.92	45.99	49.57	50.52
7: sp|P36419|SYD_THETH	27.40	28.44	27.74	27.74	43.73	53.60	100.00	52.26	51.05	50.62	51.49
8: sp|Q833I2|SYD_ENTFA	27.92	25.70	25.93	25.93	41.26	47.92	52.26	100.00	63.82	53.01	51.55
9: sp|Q2FXU5|SYD_STAA8	26.88	27.44	27.21	26.98	40.28	45.99	51.05	63.82	100.00	54.92	53.45
10: sp|P21889|SYD_ECOLI	26.26	25.58	26.05	26.05	40.88	49.57	50.62	53.01	54.92	100.00	63.78
11: sp|Q51422|SYDND_PSEAE	26.53	25.93	25.93	25.93	38.88	50.52	51.49	51.55	53.45	63.78	100.00

Figure 62: The percent identity matrix of *E. faecalis* AspRS (Q833I2) in relation to AspRS from other organisms: *Saccharomyces cerevisiae* (yeast) (P04802), *Homo sapiens* (cytoplasmic) (P14868), *Mus musculus* (mouse) (Q922B2), *Rattus norvegicus* (rat) (P15178), *Homo sapiens* (mitochondria) (Q6PI48), *Mycolicibacterium smegmatis* (A0A2U9PQC2), *Thermus thermophilus* (P36419), *S. aureus* (Q2FXU5), *E coli* (P21889) and *Pseudomonas aeruginosa* (Q51422), The closet similar AspRSs sequences is observed in blue shaded boxes.

Percent Identity Matrix - created by Clustal2.1

1: sp|Q96I59|SYNM_HUMAN	100.00	28.24	41.19	29.54	30.98	34.30	33.17	31.96
2: sp|O43776|SYNC_HUMAN	28.24	100.00	27.70	33.25	38.08	32.22	32.36	29.81
3: tr|X5KA67|X5KA67_9FLAO	41.19	27.70	100.00	31.50	33.89	37.32	37.26	36.74
4: sp|Q52428|SYD_THEKO	29.54	33.25	31.50	100.00	39.02	33.33	34.04	33.88
5: sp|O57980|SYN_PYRHO	30.98	38.08	33.89	39.02	100.00	41.49	45.45	45.24
6: sp|Q831X4|SYN_ENTFA	34.30	32.22	37.32	33.33	41.49	100.00	53.46	53.06
7: sp|P54263|SYN_THET8	33.17	32.36	37.26	34.04	45.45	53.46	100.00	100.00
8: sp|P0A8M0|SYN_ECOLI	31.96	29.81	36.74	33.88	45.24	53.06	100.00	100.00

Figure 63: The percent identity matrix of *E. faecalis* AsnRS in relation to AsnRS from other organisms: *Homo sapiens* (mitochondria) (Q96I59), *Homo sapiens* (cytoplasmic) (O43776), *Elizabethkingia anopheles* (X5KA67), *Thermococcus kodakarensis* (Q52428), *Pyrococcus horikoshii* (O57980), *Mus musculus* (mouse) (Q8BP47), *Thermus thermophilus* (P54263), and *E coli* (P0A8M0) the closet similar AsnRSs sequences is observed in green shaded boxes.

2.3.2.1.2. Multiple sequence and structure alignment

The protein sequences of *E. faecalis* AspRS and AsnRS were aligned with their respective templates by using Clustal Omega (271) to determine the conserved amino acid residues. The conservation is clearly observed in most amino residues between *E. faecalis* sequence and the most related template *Thermus Thermophilus* in AspRS (Figure 64) and between *E. faecalis* and *Pyrococcus horikoshii* sequences for AsnRS (Figure 65). As AspRS and AsnRS belong to class II aaRSs, they have three conserved sequence motifs (motif 1, motif 2 and motif 3) at their C-terminal catalytic domain (284). Identification of these motifs and analysing their positions and 2D structures were essentially performed using PSIPRED (285) owing to their important roles in the dimerisation of the two α subunits and in the aminoacylation process. As a result, motif 1 (168-172) in *E. faecalis* AspRS forms a fold containing coil then short strand followed by coil while motif 2 (221-224) is a coil and motif 3 (535-538) consists of short coil followed by helices (Figure 66). These motifs are similar in their structures to those found in *T. thermophilus* 3D crystal structure (6HHV) indicating good agreement with the prediction of the PSIPRED for the query sequence. In case of *E. faecalis* AsnRS, all motifs were identified and motif 1 (155-159) and motif 3 (401-404) are similar in the 2D structure with AspRS motifs whereas, motif 2 (205-208) starts by short strand then

coil (Figure 67). Also, the conserved motifs of *E. faecalis* AsnRS show agreement with those in the *Pyrococcus horikoshii* template (1X54).

```
CLUSTAL O(1.2.4) multiple sequence alignment

tr|A0A2U9PQC2|A0A2U9PQC2_MYCSE      -MLRTHAAGSLRPADAGQTVTLAGWVARRRDHGGVIFIDLRDASGVSQVVFREG---DVL      56
sp|P21889|SYD_ECOLI                 --MRTEYCGQLRLSHVGQQVTLCGWVNRRRDLGSLIFIDMRDREGIVQVFFDPDRA-DAL      57
sp|Q51422|SYDND_PSEAE               -MMRSHYCGQLNESLDGQEVTLCGWVHRRRDHGGVIFLDVRDREGLAQVVFDPDRA-ETF      58
sp|Q833I2|SYD_ENTFA                 MEKRTTYCGNVSAEFIEKEVVLKGWVQKRRDLGGVIFIDLRDREGIVQVVFNPEKSKEAW      60
sp|P36419|SYD_THETH                 -MRRTHYAGSLRETHVGEEVVLEGWVNRRRDLGGLIFLDLRDREGLVQLVAHPAS--PAY      57
                                       *:  .*.:      : *.* *** :*** *.:**:*:** .*: *:.        .

tr|A0A2U9PQC2|A0A2U9PQC2_MYCSE      AAAHRLRAEFCVAVTGVVEVRPEGNENPEIPTGQIEVNATELTVLGESAPLPFQLD----      112
sp|P21889|SYD_ECOLI                 KLASELRNEFCIQVTGTVRARDEKNINRDMATGEIEVLASSLTIINRADVLP--LD----      111
sp|Q51422|SYDND_PSEAE               AKADRVRSEFVVKITGKVRLRPEGARNPNMASGSIEVLGYELEVLNQAETPPFPLD----      114
sp|Q833I2|SYD_ENTFA                 EIADKCRSEYVIEVKGQVVYRDKEAINPKMKTGEFEVMATDITILNTAKTTPFTIE----      116
sp|P36419|SYD_THETH                 ATAERVRPEWVVRAKGLVRLR--PEPNPRLATGRVEVELSALEVLAEAKTPPFPVDAGWR      115
                                      * . * *: :  .* *  *     *  : :* .**    : ::  :   *  ..
                                                                                      Motif 1
tr|A0A2U9PQC2|A0A2U9PQC2_MYCSE      ----EQAGEEARLKYRYLDLRREGPGNALRLRSKVNAAARSVLAEHDFVEIETPTLTRST      168
sp|P21889|SYD_ECOLI                 --SNHVNTEEARLKYRYLDLRRPEMAQRLKTRAKITSLVRRFMDDHGFLDIETPMLTKAT      169
sp|Q51422|SYDND_PSEAE               --EYSDVGEETRLRYRFIDLRRPEMAAKLKLRARITSSIRRYLDDNGFLDVETPILGRPT      172
sp|Q833I2|SYD_ENTFA                 --DDNNVNDELRMKYRYLDLRRPSMTNNIKLRHQVTKTIRHYLDNHDFLDIETPYLGKST      174
sp|P36419|SYD_THETH                 GEEEKEASEELRLKYRYLDLRRRRMQENLRLRHRVIKAIWDFLDREGFVQVETPFLTKST      175
                                           :* *::**::****      :: * ::       :  ..*:::*** * : *
                                                                                      Motif 2
tr|A0A2U9PQC2|A0A2U9PQC2_MYCSE      PEGARDFLVPARLQPGSFYALPQSPQLFKQLLMVAGMERYYQIARCYRDEDFRADRQPEF      228
sp|P21889|SYD_ECOLI                 PEGARDYLVPSRVHKGKFYALPQSPQLFKQLLMMSGFDRYYQIVKCFRDEDLRADRQPEF      229
sp|Q51422|SYDND_PSEAE               PEGARDYLVPSRTYPGHFFALPQSPQLFKQLLMVAGFDRYYQIAKCFRDEDLRADRQPEF      232
sp|Q833I2|SYD_ENTFA                 PEGARDYLVPSRVHAGHFYALPQSPQLFKQLLMGAGFDRYYQIVRCFRDEDLRGDRQPEF      234
sp|P36419|SYD_THETH                 PEGARDFLVPYRHEPGLFYALPQSPQLFKQMLMVAGLDRYFQIARCFRDEDLRADRQPDF      235
                                    ******:*** *   * *:***********:** :*::**:**.:*:****:*.****:*

tr|A0A2U9PQC2|A0A2U9PQC2_MYCSE      TQLDMEMSFVEADDVIAISEQVLKAVWA-TIGYDLPLPLPRISYEEAMRRFGSDKPDLRF      287
sp|P21889|SYD_ECOLI                 TQIDVETSFMTAPQVREVMEALVRHLWLEVKGVDLG-DFPVMTFAEAERRYGSDKPDLRN      288
sp|Q51422|SYDND_PSEAE               TQIDIETSFLDESDIIGITEKMVRQLFKEVLDVEFD-EFPHMPFEEAMRRYGSDKPDLRI      291
sp|Q833I2|SYD_ENTFA                 TQIDIETTFLTPEEIQTYTENMLAEVMKETKGIEISVPFPRMSYDEAMARYGSDKPDTRF      294
sp|P36419|SYD_THETH                 TQLDLEMSFVEVEDVLELNERLMAHVFREALGVELPLPFPRLSYEEAMERYGSDKPDLRF      295
                                    **:*:* :*:   ::    * ::  :   . . ::   :* : : **  *:****** *

tr|A0A2U9PQC2|A0A2U9PQC2_MYCSE      GIELVECTEYFKDTTFRVFQAPYVG------AVVMP-GGASQPRRTLDGWQEFAKQRGHK      340
sp|P21889|SYD_ECOLI                 PMELTDVADLLKSVEFAVFAGPANDPKGRVAALRVP-GGASLTRKQIDEYGNFVKIYGAK      347
sp|Q51422|SYDND_PSEAE               PLELVDVADQLKEVEFKVFSGPANDPKGRVAALRVP-GAASMPRSQIDDYTKFVGIYGAK      350
sp|Q833I2|SYD_ENTFA                 AMELIDVAEVVKDVDFKVFQAALEN-GGHVKALNAKGAADKYSRKDMDNLGKYVSQFGAK      353
sp|P36419|SYD_THETH                 GLELKEVGPLFRQSGFRVFQEAESV-----K---ALALPKALSRKEVAELEEVAKRHKAQ      347
                                     :** :    .:.  * **                      *  :    : .     :

tr|A0A2U9PQC2|A0A2U9PQC2_MYCSE      GLAYVLVGED----GTLGGPVAKNLSDAERDGLVAHVGANPGDCIFFAAGPAKGARALLG      396
sp|P21889|SYD_ECOLI                 GLAYIKVNERAKGLEGINSPVAKFLNAEIIEDILDRTAAQDGDMIFFGADNKKIVADAMG      407
sp|Q51422|SYDND_PSEAE               GLAYIKVNERAKGVEGLQSPIVKFIPEANLNVILDRVGAVDGDIVFFGADKAKIVCDALG      410
sp|Q833I2|SYD_ENTFA                 GLAWLKVEE-----DGLKGPIAKFLTEV-SDELIAATNAEVGDILMFGADKPEIVAAALG      407
sp|P36419|SYD_THETH                 GLAWARVEE-----GGFSGGVAKFLEPV-REALLQATEARPGDTLLFVAGPRKVAATALG      401
                                    ***:  * *       : . :.* :     : ::  . *  ** ::* *.  : .   :*

tr|A0A2U9PQC2|A0A2U9PQC2_MYCSE      ATRIEIAKRLDLIDPNAWAFTWVVDFPMFEAADEATAAGDVAVGSGAWTAMHHAFTAPKP      456
sp|P21889|SYD_ECOLI                 ALRLKVGKDLGLTDESKWAPLWVIDFPMFEDDG-----------EGGLTAMHHPFTSPKD      456
sp|Q51422|SYDND_PSEAE               ALRIKVGHDLKLLT-REWAPMWVVDFPMFEEND-----------DGSLSALHHPFTSPKC      458
sp|Q833I2|SYD_ENTFA                 AVRTRLGKELGLIDESKFNFLWIVDWPLFEYDEE----------AGRYVSAHHPFTQPKA      457
sp|P36419|SYD_THETH                 AVRLRAADLLGLK-REGFRFLWVVDFPLLEWDEE----------EEAWTYMHHPFTSPHP      450
                                    * * . .. * *     :   *::*:*::*                    ** ** *:

tr|A0A2U9PQC2|A0A2U9PQC2_MYCSE      DSVDTFDSDPGNALSDAYDIVCNGNEIGGGSIRIHRRDIQERVFAMMGIDHDEAQEKFGF      516
sp|P21889|SYD_ECOLI                 MTAAELKAAPENAVANAYDMVINGYEVGGGSVRIHNGDMQQTVFGILGINEEEQREKFGF      516
sp|Q51422|SYDND_PSEAE               -TPAELEANPGAALSRAYDMVLNGTELGGGSIRIHDKSMQQAVFRVLGIDEAEQEEKFGF      517
sp|Q833I2|SYD_ENTFA                 EDVDRLATDPASVYAEAYDVVLNGYELGGGSLRIHTRELQEKMFETLGFTKEEAQDQFGF      517
sp|P36419|SYD_THETH                 EDLPLLEKDPGRVRALAYDLVLNGVEVGGGSIRIHDPRLQARVFRLLGIGEEEQREKFGF      510
                                         :   *  . : ***:* ** *:****:***   :*  :*  :*: . * .::***
```

Motif 3

```
tr|A0A2U9PQC2|A0A2U9PQC2_MYCSE    LLDAFSYGAPPHGGIAFGWDRITALLAGVDSIREVIAFPKSGGGVDPLTDAPAPITPQQR    576
sp|P21889|SYD_ECOLI               LLDALKYGTPPHAGLAFGLDRLTMLLTGTDNIRDVIAFPKTTAAACLMTEAPSFANPTAL    576
sp|Q51422|SYDND_PSEAE             LLDALKYGAPPHGGLAFGLDRLVMLMTGASSIREVIAFPKTQSAGDVMTQAPGSVDGKAL    577
sp|Q833I2|SYD_ENTFA               LLDALDYGFPPHGGIALGLDRLAMLLAGEENIREVIAFPKNGKAIDPMNNAPSLVSPLQL    577
sp|P36419|SYD_THETH               FLEALEYGAPPHGGIAWGLDRLLALMTGSPSIREVIAFPKNKEGKDPLTGAPSPVPEEQL    570
                                  :*:*:.** ***.*:* * **:  *::*  .**:******.  .   :. **.

tr|A0A2U9PQC2|A0A2U9PQC2_MYCSE    KESGIDAKPREDKPKEDAKSKA      598
sp|P21889|SYD_ECOLI               AELSIQVVKKAENN--------      590
sp|Q51422|SYDND_PSEAE             RELHIRLREQPKAE--------      591
sp|Q833I2|SYD_ENTFA               FELNIDVTAIDE----------      589
sp|P36419|SYD_THETH               RELGLMVVRP------------      580
                                   *  :
```

Figure 64: Sequence alignment of *E. faecalis* AspRS with the most similar templates: *Mycobacterium smegmatis* (UNIPROT: A0A2U9PQC2), *Escherichia coli* (UNIPROT: P21889), *Pseudomonas aeruginosa* (UNIPROT: Q51422) and *Thermus thermophilus* (UNIPROT: P36419) using Clustal Omega in which ¨ * ¨ means that the residues are identical, ¨ : ¨ means that conserved substitutions have been observed, ¨ . ¨ means that semi-conserved substitutions are observed. The residues are coloured according to their chemical properties where red, small hydrophobic *(*AVFPMILWY); blue, acidic (DE); purple, basic (RHK); green, hydroxyl + amine + basic (STYHCNGQ), motifs: motif 1 PYLGK (168-172), motif 2 FRDE (221-224) and motif 3 GLDR (535-538) are observed in yellow shaded boxes.

```
CLUSTAL O(1.2.4) multiple sequence alignment


tr|X5KA67|X5KA67_9FLAO    MHKQTIK---EVLENYKKFLHHDITVYGWVRAFRSN---RFIALNDGSTINNLQIVVDFE    54
sp|Q52428|SYD_THEKO       -----MYRTHYSSEITEELNGQKVKVAGWVWEVKDLGGIKFLWIRDRDGIV--QITAPKK    53
sp|O57980|SYN_PYRHO       -----MIEKVYCQEVKPELDGKKVRLAGWVYTNMRVGKKIFLWIRDSTGIV--QAVVAKN    53
sp|Q831X4|SYN_ENTFA       MNGETNVEQIQIIDSN-KHVGETVKIGAWIANKRSSGKIAFLQLRDGTAFF--QGVVFKP    57
sp|P54263|SYN_THET8       -------MRVFIDEIA-RHVDQEVELRGWLYQRRSKGKIHFLILRDGTGFL--QATVVQG    50
                                        :   .   . : : .*:          *: :.*   :   * ..

tr|X5KA67|X5KA67_9FLAO    NF--------DE---NLIKNINTASSLKIVGEVVESQGAGQTVEIIAKKIIVLGDNFTEE    103
sp|Q52428|SYD_THEKO       KV--------DPELFKLIPKLRSEDVVAVEGVVNFTPKAKLGFEILPEKIVVLNRAE-TP    104
sp|O57980|SYN_PYRHO       VV--------GEETFEKAKKLGRESSVIVEGIVKADERAPGGAEVHVEKLEVIQAVSEFP    105
sp|Q831X4|SYN_ENTFA       NFIEAFGEEAGTEKFQEIKHLSQETAVMVTGVIKEDSRSKFGYEMDITDLEVVGA-SE-D    115
sp|P54263|SYN_THET8       EV--------PEAVFREADHLPQETALRVWGRVREDRRAPGGFELAVRDLQVVSRPQG-E    101
                           .             .   ::     : : * :     :    *:   .: *:

tr|X5KA67|X5KA67_9FLAO    LQNTILQPK---KHSLEKLREQAHLRFRTNLFGAVFRVRHAVSFAIHSFFNDRQFFYLNT    160
sp|Q52428|SYD_THEKO       L---PLDPTGKVKAELDTRLDNRFMDLRRPEVMAIFKIRSSVFKAVRDFFHENGFIEIHT    161
sp|O57980|SYN_PYRHO       I---PENPE---QASPELLLDYRHLHIRTPKASAIMKVKETLIMAAREWLLKDGWHEVFP    159
sp|Q831X4|SYN_ENTFA       Y---PITPK---EHGTDFLMDHRHLWLRSSKQHAIMLVRNEIIRATYEFFNEQGFIKIDS    169
sp|P54263|SYN_THET8       Y---PIGPK---EHGIDFLMDHRHLWLRHRRPFAVMRIRDELERAIHEFFGERGFLRFDA    155
                                *    :   :   :  .: :*     *:: ::  :  *  .:: .  :  .
                          Motif 1
tr|X5KA67|X5KA67_9FLAO    PVITGADAEGAGEMFGVTNFDLDNIPRNEDGAIDYTQDFFGRKTNLTVSGQLEGET-AAM    219
sp|Q52428|SYD_THEKO       PKIIATATEGGTELFPMKYF--------------------EEDAFLAQSPQLYKQIMMAS    201
sp|O57980|SYN_PYRHO       PILVTGAVEGGATLFKLKYF--------------------DKYAYLSQSAQLYLEA-AIF    198
sp|Q831X4|SYN_ENTFA       PILTGSAPEGTTELFETDYF--------------------GQPAFLSQTGQLYAEA-GAM    208
sp|P54263|SYN_THET8       PILTPSAVEGTTELFEVELFD-------------------GEKAYLSQSGQLYAEA-GAL    195
                          * :    **   :*    *                     . : *: : **  :
```

```
                                Motif 2
tr|X5KA67|X5KA67_9FLAO      GLGRIYTFGPTFRAENSNTTRHLAEFWMVEPEVAFNNLE-DNIDLAEDFLKYVIQYVLDK      278
sp|Q52428|SYD_THEKO         GLDRVYEIAPIFRAEEHNTTRHLNEAWSIDSEMAFIEDEEEVMSFLERLVAHAINYVREH      261
sp|O57980|SYN_PYRHO         GLEKVWSLTPSFRAEKSRTRRHLTEFWHLELEAAWMDLW-DIMKVEEELVSYMVQRTLEL      257
sp|Q831X4|SYN_ENTFA         AFGKVFTFGPTFRAEKSKTRRHLTEFWMIEPEMAYTTHE-ESLDIQEAYVKHLIKSVLKN      267
sp|P54263|SYN_THET8         AFAKVYTFGPTFRAERSKTRRHLLEFWMVEPEVAFMTHE-ENMALQEELVSFLVARVLER      254
                            .: ::: : * ****. .* *** * * :: * *:     : : . *  : . :  . .

tr|X5KA67|X5KA67_9FLAO      CKDDLEFLDKRFAEEQKQKPEKERAKEGLIEKLENVVAKRFKRVSYTEAIDILLNSKENK      338
sp|Q52428|SYD_THEKO         NAKELDILNFELE----------------------EPKLPFPRVSYDKALEILGDLG---      296
sp|O57980|SYN_PYRHO         RKKEIEMFRDDLT------------------TL-KNTEPPFPRISYDEAIDILQSKG---      295
sp|Q831X4|SYN_ENTFA         QQYPLDVLERDTA------------------LLEKYVSEPFKRITYDDAIELLQKEE-A-      307
sp|P54263|SYN_THET8         RSRELEMLGRDPK------------------ALEPAAEGHYPRLTYKEAVALVNRIAQE-      295
                                ::.:                                : *::* .*: ::

tr|X5KA67|X5KA67_9FLAO      KGKFVYPVEKWGADLQSEHERYLVEKH----FECPVVLFDYPAEIKAFYMRLNEDNKTVA      394
sp|Q52428|SYD_THEKO         ------KEIPWGEDIDTEGERLLGKYMMENENAPLYFLYQYPSEAKPFYIMKYDNKPEIC      350
sp|O57980|SYN_PYRHO         ------VNVEWGDDLGADEERVLTEEF-----DRPFFVYGYPKHIKAFYMKEDPNDPRKV      344
sp|Q831X4|SYN_ENTFA         --NNDYDHIEWGEDFGSPHETFISNYY-----GVPTFILNYPKAIKAFYMKPHPTREDVV      360
sp|P54263|SYN_THET8         --DPEVPPLPYGEDFGAPHEAALSRRF-----DRPVFVERYPARIKAFYMEPDPEDPELV      348
                                     :* *: :  *  : .          .:  **   * **:

tr|X5KA67|X5KA67_9FLAO      -AMDVLF-PGIGEIIGGSQREERLDVLKKKMDDMHVDQEELWWYLDTRKFGSVPHSGFGL      452
sp|Q52428|SYD_THEKO         RAFDLE--YRGVEISSGGQREHRHDILVEQIKEKGLNPESFEFYLKAFRYGMPPHGGFGL      408
sp|O57980|SYN_PYRHO         LASDMLAPEGYGEIIGGSQREDDYDKLLNRILEEGMDPKDYEWYLDLRRYGSVPHSGFGL      404
sp|Q831X4|SYN_ENTFA         ICADLIAPEGYGEIIGGSERATDYDYLKEKVAEFGLSEEEYSWYLDLRKYGSVPHSGFGL      420
sp|P54263|SYN_THET8         LNDDLLAPEGYGEIIGGSQRIHDLELLRRKIQEFGLPEEVYDWYLDLRRFGSVPHSGFGL      408
                                  ** .*.:*    : * .:: :  :  :   :**.  ::*  **.****
                            Motif 3
tr|X5KA67|X5KA67_9FLAO      GLERLVLFVTGMTNIRDVIPFPRTPKSAEF      482
sp|Q52428|SYD_THEKO         GAERLIKQMLDLPNIREVILFPRDRRRLTP      438
sp|O57980|SYN_PYRHO         GVERLVAWVLKLDHIRWAALFPRTPARLYP      434
sp|Q831X4|SYN_ENTFA         GLERAVTFITGNEHIREAIPFPRMLNRIYP      450
sp|P54263|SYN_THET8         GLERTVAWICGLAHVREAIPFPRMYTRMRP      438
                            * ** :  :    ::* .  ***
```

Figure 65: Sequence alignment of *E. faecalis* AsnRS with the most similar templates: Elizabethkingia anopheles (UNIPROT: X5KA67), Thermococcus kodakaraensis (UNIPROT: Q52428), Pyrococcus horikoshii (UNIPROT: O57980) and *Thermus thermophilus* (UNIPROT: P54263) using Clustal Omega in which ¨ * ¨ means that the residues are identical, ¨ : ¨ means that conserved substitutions have been observed, ¨ . ¨ means that semi-conserved substitutions are observed. The residues are coloured according to their chemical properties where red, small hydrophobic *(*AVFPMILWY); blue, acidic (DE); purple, basic (RHK); green, hydroxyl + amine + basic (STYHCNGQ), motifs: motif 1 PILTG (170-174), motif 2 FRAE (220-223) and motif 3 GLER (421-424) are observed in yellow shaded boxes.

Figure 66: PSIPRED secondary structure prediction for *E. faecalis* AspRS with three conserved motifs, motifs 1, 2 and 3 identified in blue squares.

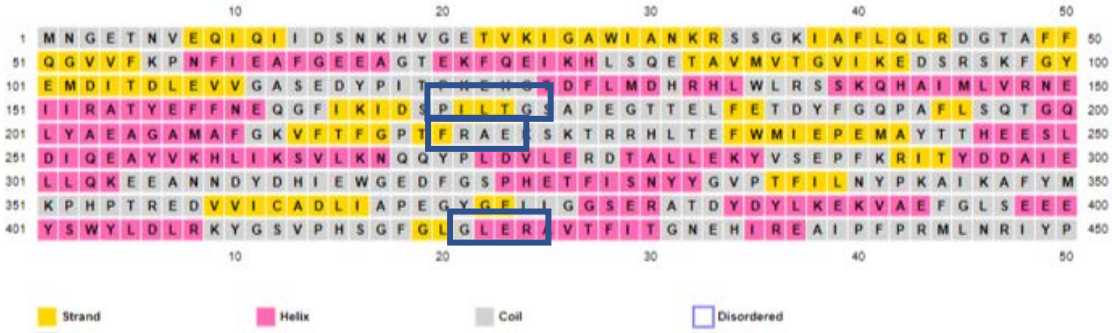

Figure 67: PSIPRED secondary structure prediction for *E. faecalis* AsnRS with three conserved motifs, motifs 1, 2 and 3 identified in blue squares.

2.3.2.1.3. 3D *E. faecalis* AspRS and AsnRS models building and validation

MOE (263) and SWISS-MODEL server (266) were also used to perform molecular modelling experiments for both *E. faecalis* AspRS and AsnRS. The FASTA format of their protein sequences were obtained from the ExPASy proteomics server at the Swiss Bioinformatics Institute (275), with the Uniprot identifiers Q833I2 (SYD_ENTFA) and Q831X4 (SYN_ENTFA) respectively (310). The *E. faecalis* AspRS and AsnRS homology models were built using *Thermus thermophilus* AspRS (pdb: 6HHV) (309) and *Pyrococcus horikoshii* AsnRS (pdb: 1X54) (282) crystal structures respectively. They were subjected to a number of checks to assess their qualities. Stereochemical quality was evaluated by Ramachandran plots using the RAMPAGE server (288) and the compatibility of 3D models with their amino acids 1D sequence was validated using Verify 3D (289), while overall protein structures were evaluated using ProSA (290). By using the templates for comparison, validation results would propose that SWISS-

MODEL AspRS and AsnRS models performed well and their stereochemical qualities are higher than those of MOE models.

In the Ramachandran plot (291), the main chain dihedral ϕ and ψ angles in SWISS-MODEL AspRS model was reasonably accurate with a total of 95.7% and 3.6% amino acids residues were in the favoured and allowed regions respectively compared with those in template 6HHV (98.2% and 1.8%) (Figures 68 and 69). Only 4 amino acid residues of the SWISS-MODEL model were found in the outlier region of the plot, which are a way from the active sites and would not be expected to affect enzyme function. However, the outlier region of the constructed MOE model consists of Ser198 in the Ramachandran plot and it is important in the binding interaction of *E. faecalis* AspRS with the natural substrate (Table 14). On the other hand, the main chain dihedral ϕ and ψ angles of the built AsnRS MOE and SWISS-MODEL models were accurate with a total of 87.6% and 94.6% amino acids residues respectively in the favoured region of the plot compared with the AsnRS template 1X54 (97.9%) (Figures 70 and 71), with just 10 and 1 amino acids residues in the outlier region of the Ramachandran plot of both respective models and they are away from the active site of *E. faecalis* AsnRS (Table 15).

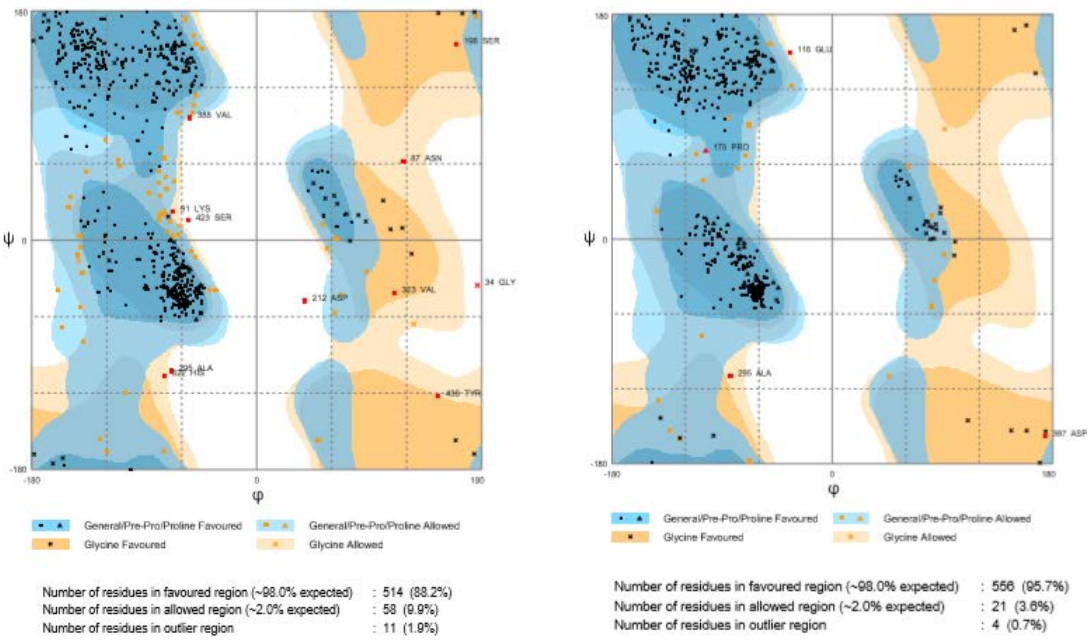

Figure 68: Ramachandran plots of the MOE and SWISS-MODEL AspRS models. The left plot is for MOE model and the right one is for SWISS-MODEL.

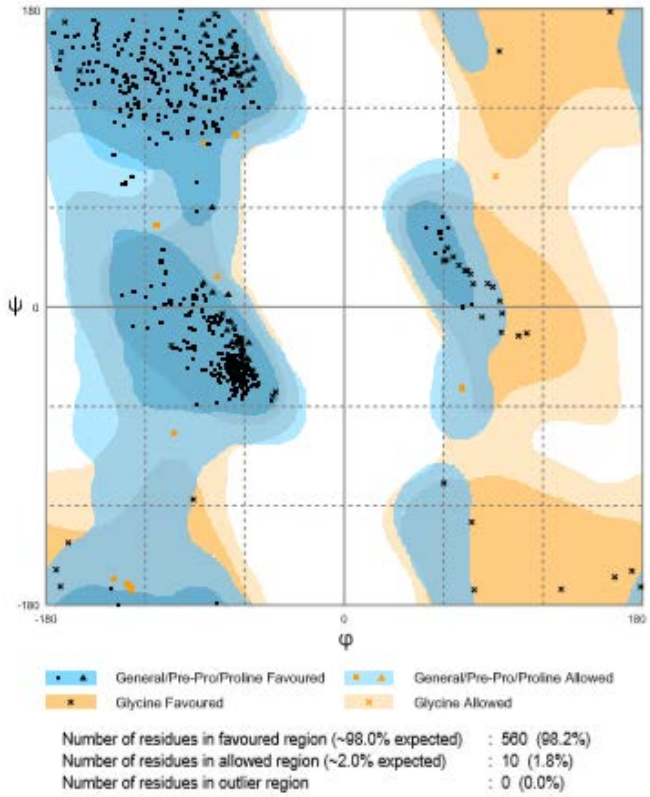

Figure 69: Ramachandran plot for *Thermus thermophilus* AspRS template (pdb: 6HHV).

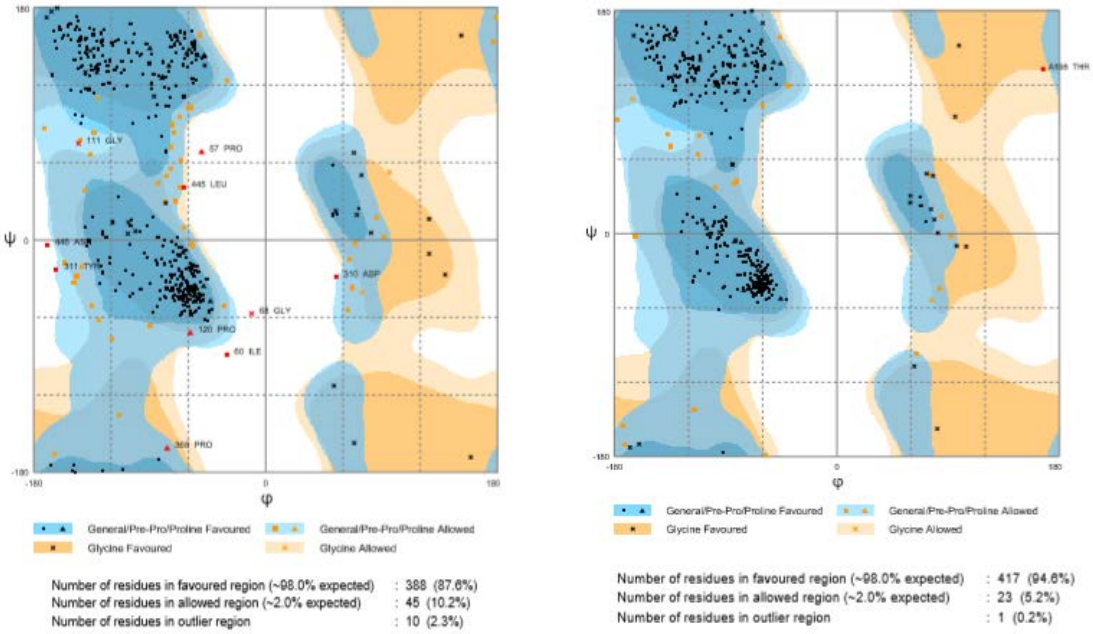

Figure 70: Ramachandran plots the of MOE and SWISS-MODEL AsnRS models. The left plot is for MOE model and the right one is for SWISS-MODEL.

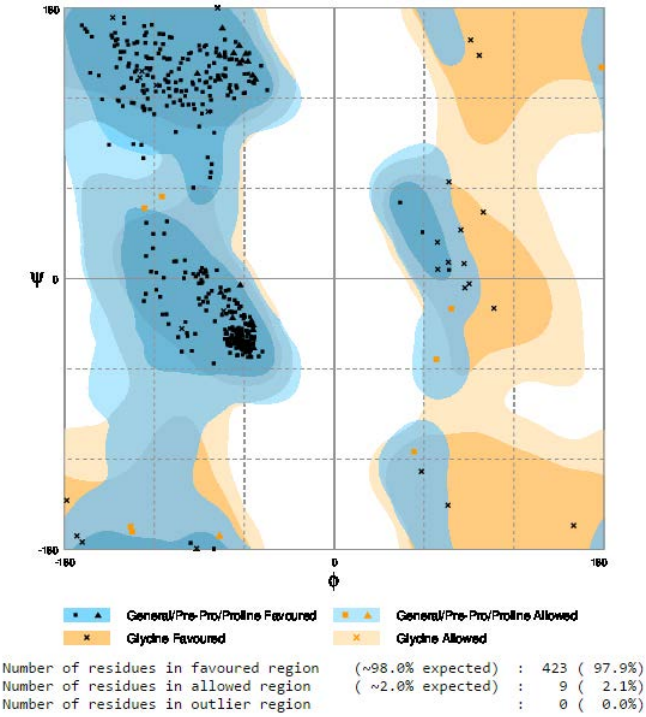

Figure 71: Ramachandran plot for *Pyrococcus horikoshii* AsnRS template (pdb: 1X54).

Table 14: Ramachandran plot results of *T. Thermophilus* AspRS and the constructed MOE and SWISS-MODEL *E. faecalis* models.

AspRS	No. of amino acid residues in			Amino acid residues in outlier region
	favoured region	allowed region	outlier region	
T. thermophilus (pdb: 6HHV)	560	10	0	
MOE AspRS model	514	58	11	Gly34, Asn87, Lys91, Ser198, Asp212, Ala295, His322, Val323, Val388, Ser423 and Tyr438
SWISS AspRS model	556	21	4	Glu116, Pro175, Ala295 and Asp397

Table 15: Ramachandran plot results of *P. horikoshii* AsnRS and the constructed MOE and SWISS-MODEL *E. faecalis* models.

AsnRS	No. of amino acids residues in			Amino acid residues in outlier region
	favoured region	**allowed region**	**outlier region**	
P. horikoshii AsnRS (pdb: 1X54)	423	9	0	
MOE AsnRS model	388	45	10	Pro75, Ile60, Gly68, Gly111, Pro120, Asp310, Tyr311, Pro368, Leu445 and Asn446
SWISS AsnRS model	417	23	1	Thr198

The compatibility of an atomic model (3D) with its own amino acid sequence (1D) was checked for MOE and SWISS-MODEL models of both enzymes using Verify 3D by assigning a structural class based on their locations and environment and other parameters such as secondary structures, degree of buried surface area and fraction of side chain area covered by polar atoms for each residue in both structures (289). The correlation was calculated between this set of observed parameters and the ideal parameters of the amino acid type to which it has been assigned. Verify 3D should stay above 0.2 and not fall under zero (289). The percentage of residues, which are more than 0.2 was 87.35%, 89.7% and 84.15% for the *S. aureus* AspRS MOE, SWISS-MODEL models and *T. Thermophilus* (pdb: 6HHV) template respectively (Figure 72) while it was 93.03%, 88.71% and 91.24% for *S. aureus* AsnRS MOE, SWISS-MODEL models and *P. horikoshii* AsnRS template. For both models, the residues of both enzymes that fall under zero are far from the active sites (Figure 73).

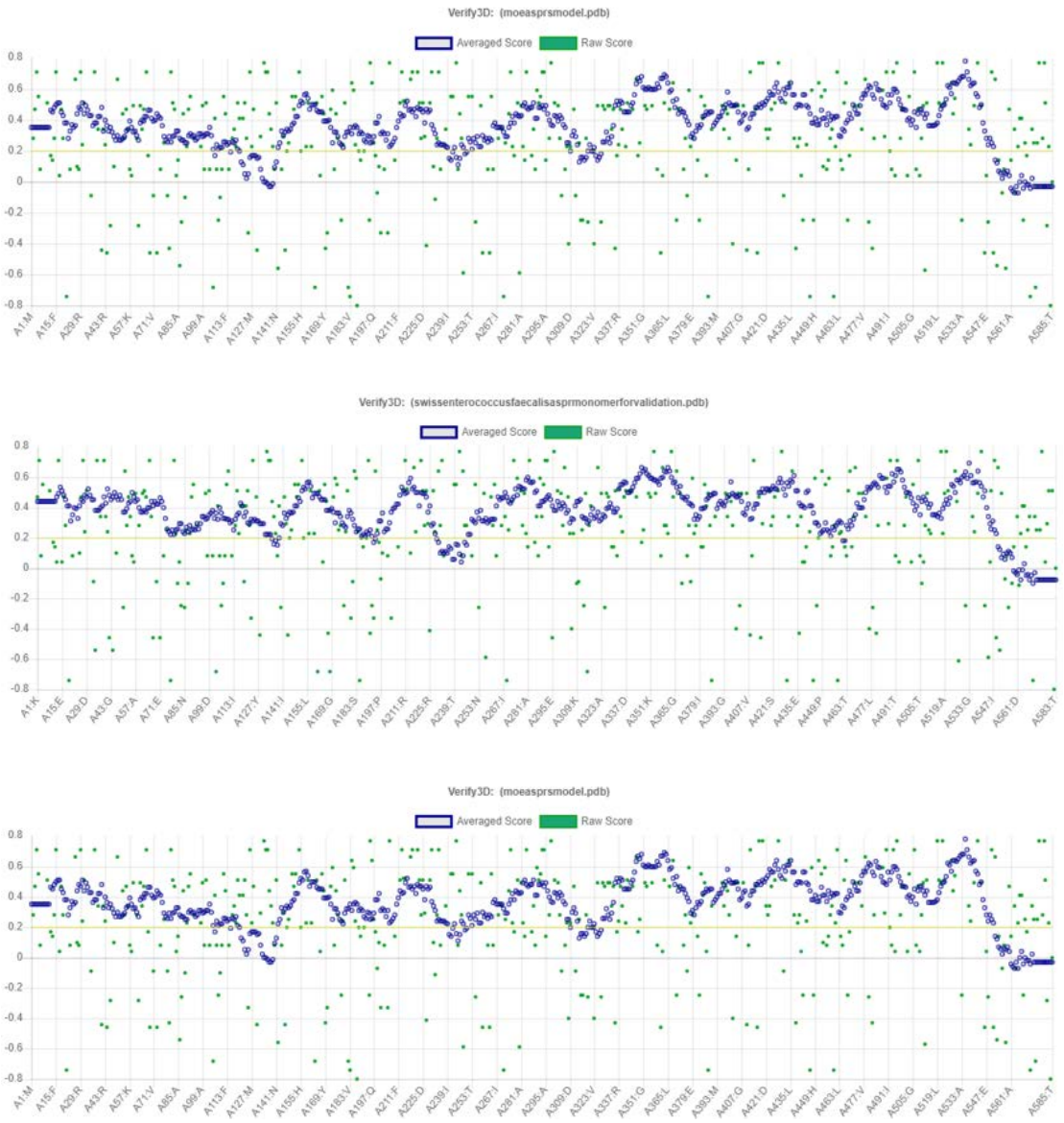

Figure 72: Verify 3D results of both *E. faecalis* MOE and SWISS-MODEL AspRS models and the template (pdb: 1EFW). Each graph is titled and the percentage of amino acid residues that have averaged 3D-1D score of more than 0.2 which is 87.35%, 89.7% and 84.15% respectively.

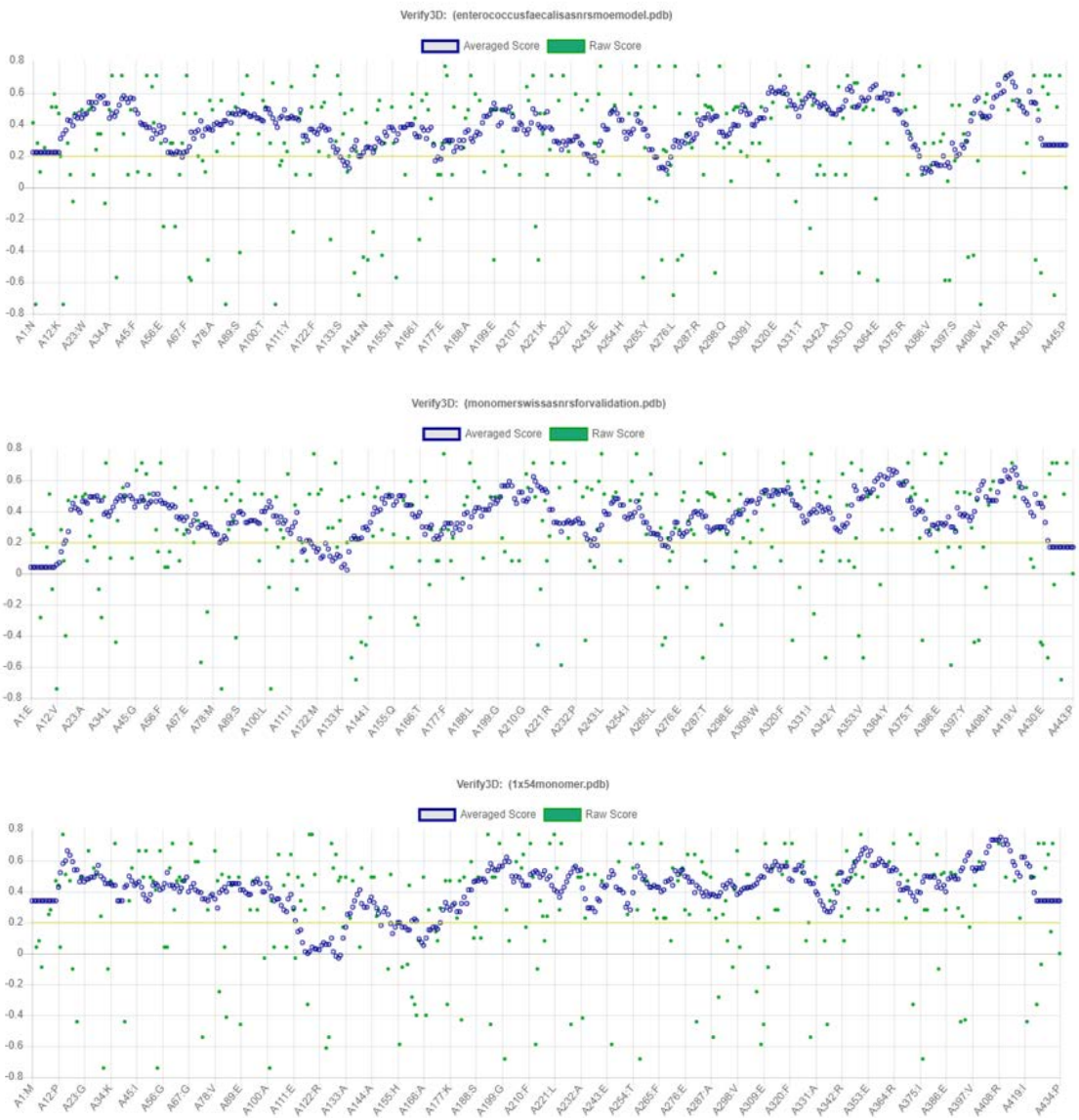

Figure 73: Verify 3D results of both *E. faecalis* MOE and SWISS-MODEL AsnRS models and the template (pdb: 1X54). Each graph is titled and the percentage of amino acid residues that have averaged 3D-1D score of more than 0.2 which is 93.03%, 88.71% and 91.24% respectively.

In addition, ProSA (290) was the third method used to validate the models. ProSA checks the local and overall model quality through providing two plots; the first one (Figures 74a, 75a, 76a and 77a) shows the local model quality by plotting energies as a function of amino acid sequence position generally positive values relate to erroneous parts of the input structure. The second plot (Figures 74b, 75b, 76b and 77b) displays the Z- score as an indicator of the overall model quality through calculating the Z-score of all experimentally determined protein chains in the current PDB identified by X-ray crystallography or NMR spectroscopy, a negative value

indicates a good model while a positive score shows errors. The Z-score of the MOE and SWISS-MODEL AspRS models was - 9.41 and - 10.28 respectively compared with the Z-score of the template 6HHV, which was - 9.36. The Z-score of the MOE and SWISS AsnRS models and their template 1X54 was - 8.58, - 9.09 and - 9.69 respectively. In addition, superimposition of the models with their main templates showed low RMSD values of 1.01 Å for MOE AspRS model and its template 6HHV, and 0.45 Å for the SWISS-MODEL model with the same template (Figure 78). RMSD was 1.00 Å and 0.33 Å for the MOE and SWISS AsnRS model with the template 1X54 respectively indicating a high degree of similarity (Figure 79). Ramachandran plot, Verify 3D and ProSA validation methods indicate that the models constructed using SWISS-MODEL server were good in terms of quality of backbone and side chain stereochemistry for both *E. faecalis* AspRS and AsnRS compared with their templates (Table 16). Additional validation of the active site architecture of both models was performed by docking experiments with natural substrates and ligands.

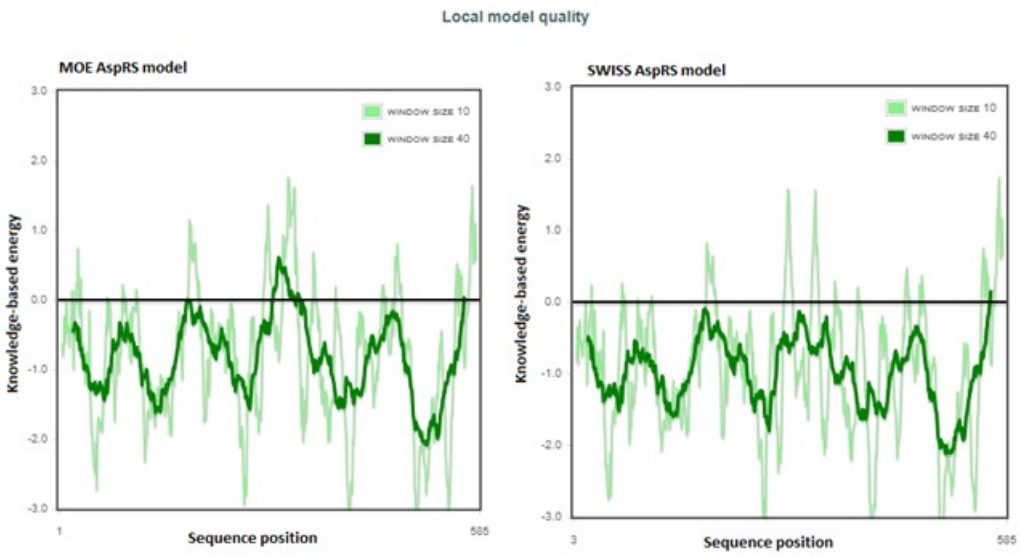

Figure 74a: ProSA output for the *E. faecalis* AspRS model. The graphs show the local model quality by plotting energies as a function of amino acid sequence position.

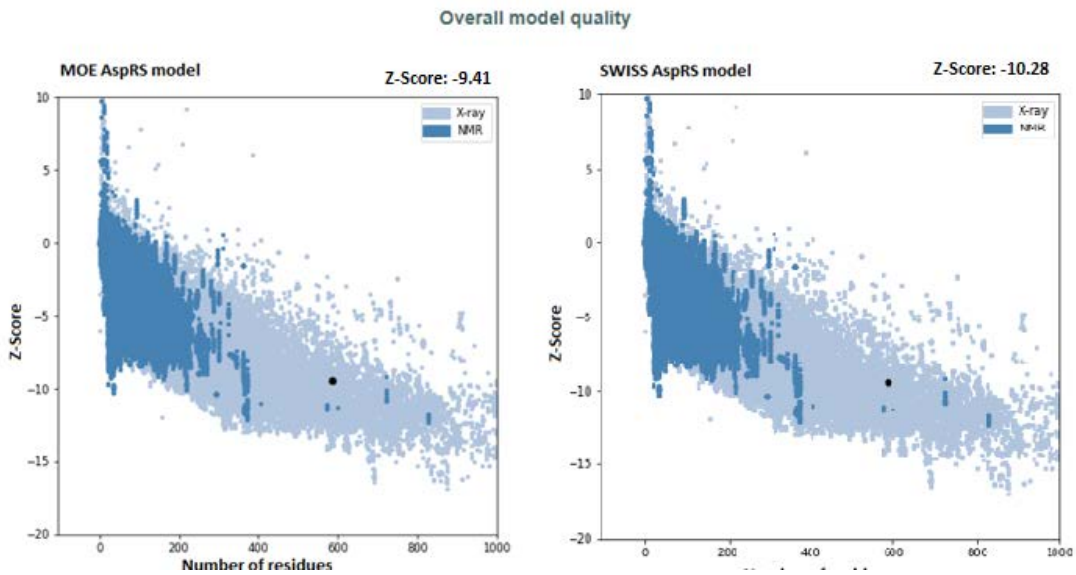

Figure 74b: ProSA output for the *E. faecalis* AspRS model. The plots show the overall model quality by calculating Z-score (dark spot).

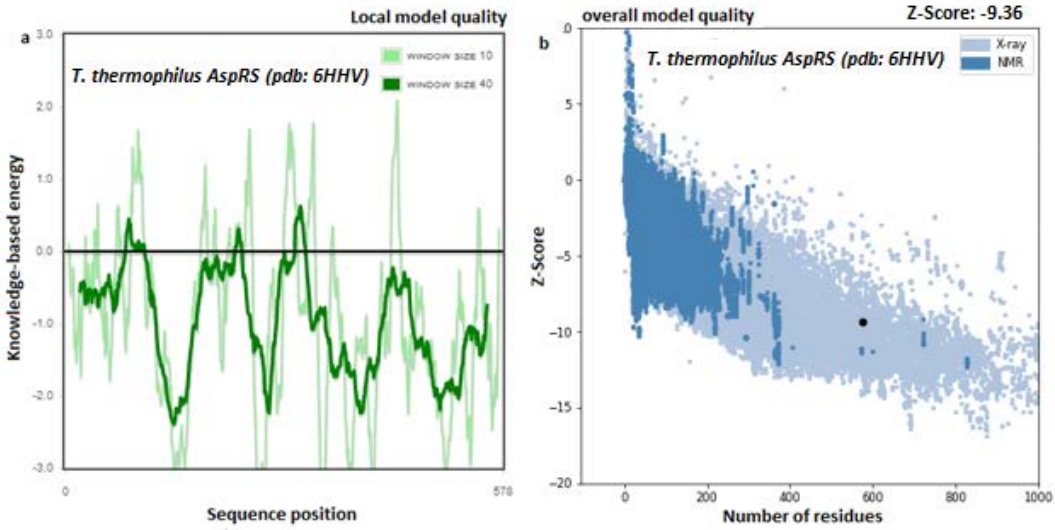

Figure 75: ProSA output for the *T. thermophilus* AspRS (pdb: 6HHV). a: shows the local model quality by plotting energies as a function of amino acid sequence position b: shows the overall model quality by calculating Z-score (dark spot).

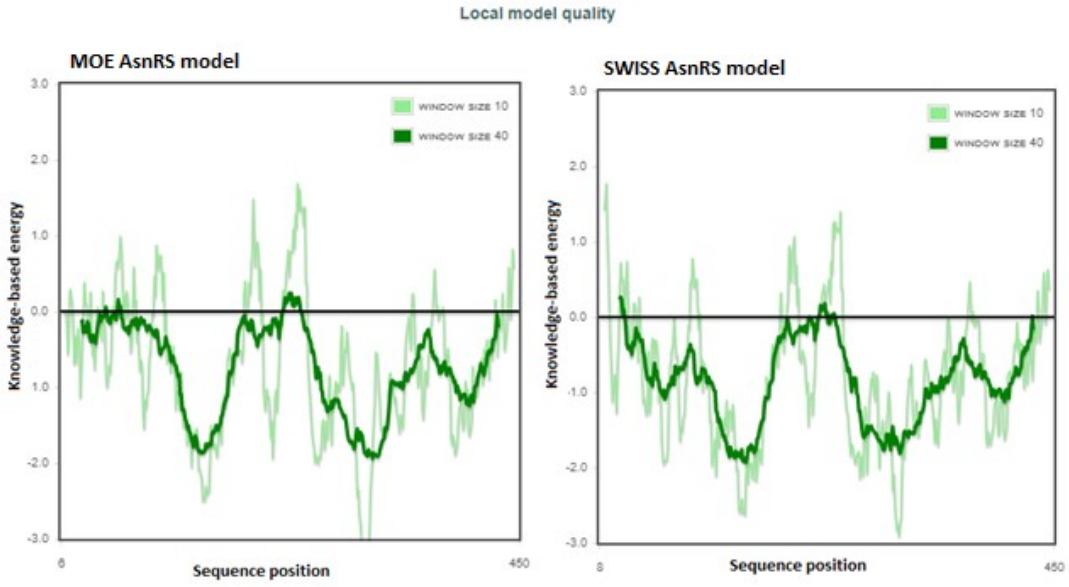

Figure 76a: ProSA output for the *E. faecalis* AsnRS model. The graphs show the local model quality by plotting energies as a function of amino acid sequence position.

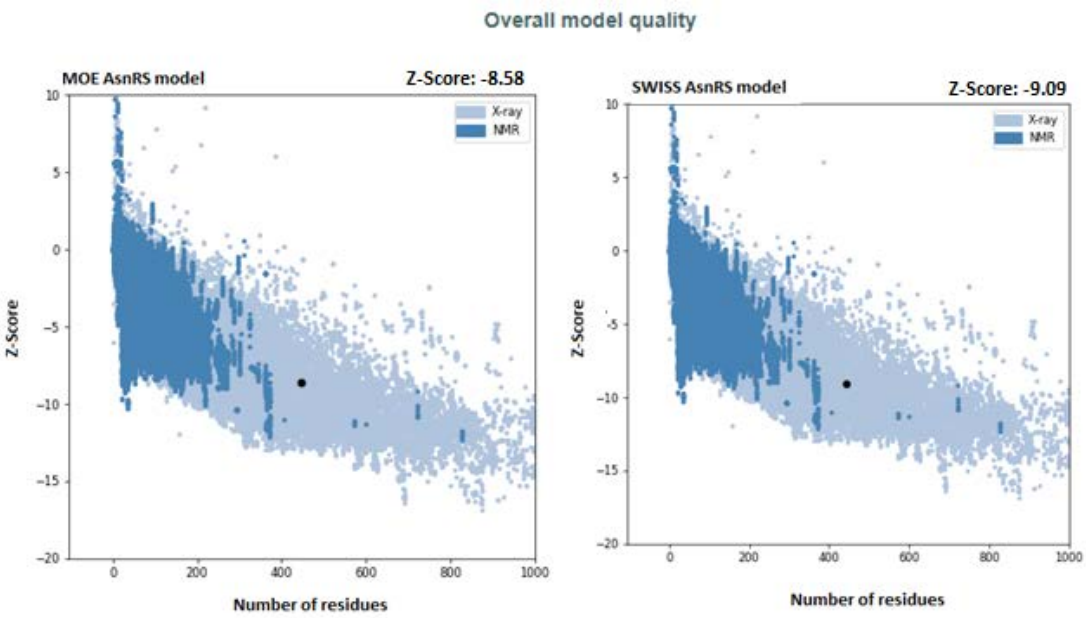

Figure 76b: ProSA output for the *E. faecalis* AsnRS model. The plots show the overall model quality by calculating Z-score (dark spot).

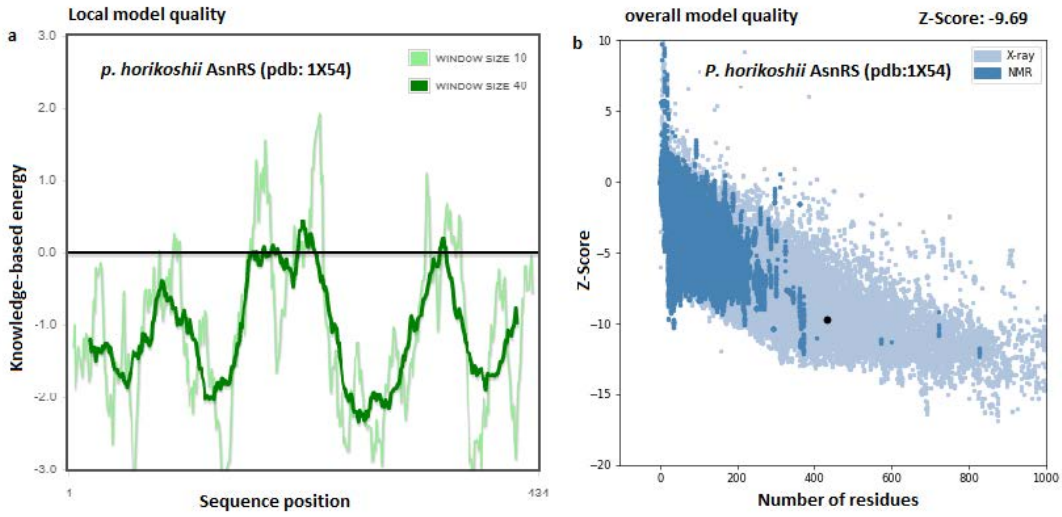

Figure 77: ProSA output for the *P. horikoshii* AsnRS (pdb: 1X54). a: shows the local model quality by plotting energies as a function of amino acid sequence position b: shows the overall model quality by calculating Z-score (dark spot).

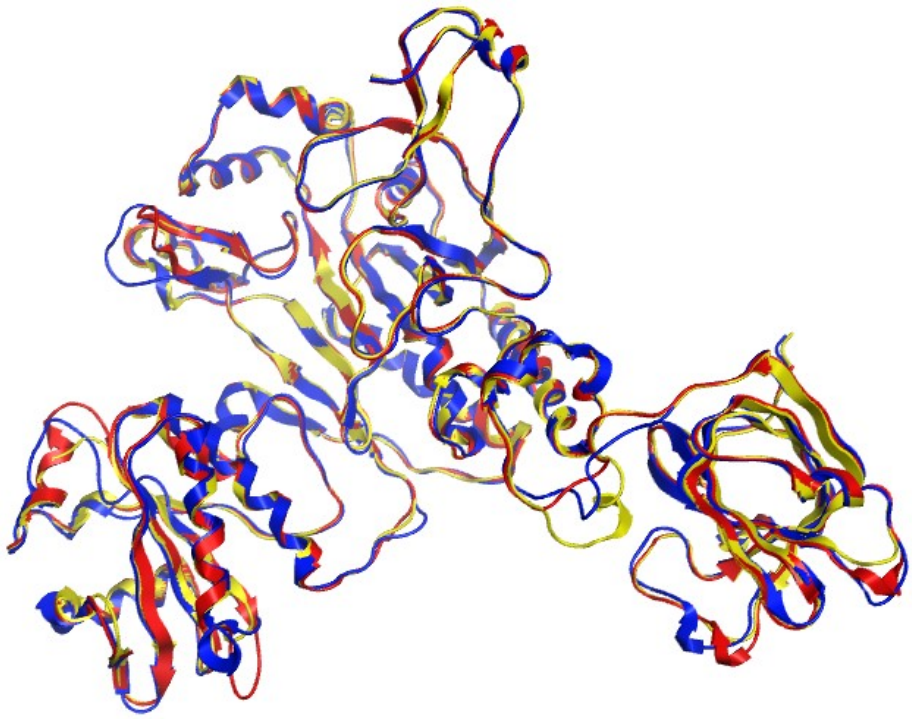

Figure 78: Superimposition of the constructed *E. faecalis* MOE (blue) and SWISS-MODEL (red) AspRS models with the X-ray structure of template 1EFW (yellow), RMSD= 0.45 Å and 1.01 Å of MOE and SWISS AspRS model respectively with the template (pdb: 6HHV).

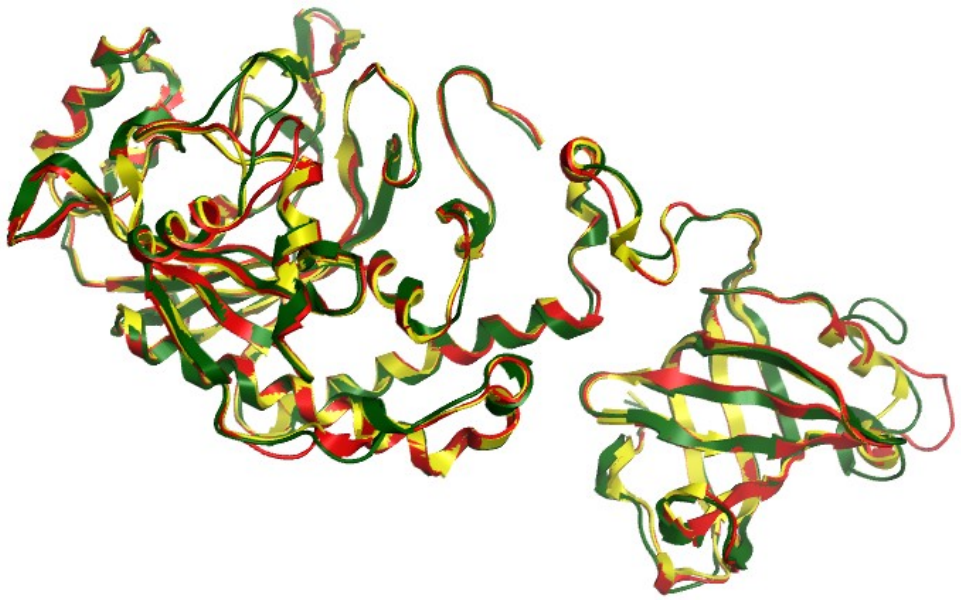

Figure 79: Superimposition of the constructed *E. faecalis* MOE (green) and SWISS-MODEL (red) AsnRS models with the X-ray structure of template 1X54 (yellow). RMSD= 0.60 Å and 0.23 Å of MOE and SWISS AsnRS model respectively with the template (pdb: 1X54).

Table 16: Validation results of the MOE and SWISS constructed *E. faecalis* AspRS and AsnRS models.

Validation methods	*E. faecalis* AspRS		Template	*E. faecalis* AsnRS		Template
	MOE AspRS	SWISS AspRS	6HHV	MOE AsnRS	SWISS AsnRS	1x54
Ramachandran plot (outlier region)	11	4	N	10	1	N
ProSA (Z-Score)	-9.41	-10.28	-9.36	-8.58	-9.09	-9.69
Verify 3D	87.35%	89.71%	84.15%	93.03%	88.71%	91.24%
RMSD	0.45 Å	1.01 Å	-	1.00 Å	0.33 Å	-

2.3.2.1.4. Docking study of *E. faecalis* AspRS and AsnRS models

2.3.2.1.4.1. Active site identification

The catalytic site of *E. faecalis* AspRS and AsnRS were identified using BLAST tool (273, 274) through alignment their protein sequences in FASTA format against all known class IIb aaRSs (Figures 80 and 81) (271, 292). *E. faecalis* AspRS and AsnRS have hydrophobic pockets as shown in the 3D ligand binding interactions (Figures 82a and 83a). Colours indicate the chemical nature and type of bonds that could be established with ligands green colour is for hydrophobic interactions, pink and red colours are for hydrogen bonding and electrostatic interactions respectively. The active site of *E. faecalis* AspRS consists of Glu176, Gly177, Ala178, Ser198, Gln200, Lys203, Arg222, Glu224, Asp229, Arg230, Gln231, Phe234, Gln236, His449, His450, Glu486, Arg490, Ile532, Ala533, Gly535, Arg538 while the catalytic core of *E. faecalis* AsnRS contains these key amino acid residues; Arg221, Glu223, Arg229, His230, Glu373, Gly376, Gly421, Arg424. Docking study of both enzymes selected SWISS-MODEL models with their natural substrates additionally validates the role of the identified amino acids residues in the binding interactions. For *E. faecalis* AspRS, the 3D structure of the same enzyme in *E. coli* and *Mycolicibacterium smegmatis* (pdb: 1C0A and pdb:4O2D) were used to investigate the biding interactions of the constructed model with ATP and aspartic acid. Glu176, Arg222, His449 and Arg490 are responsible for aspartic acid pocket and the binding of Asp238 with the carboxylic group of aspartic acid via water molecule is conserved in many AspRSs (Figure 82b) (293) while Arg222, Phe234, Gln231, Gln236, Glu483 and Arg538 are key amino acid residues for AMP moiety binding. In the case of *E. faecalis* AsnRS, the built SWISS-MODEL model was used for the docking study of asparaginyl-adenylate using alignment tool (263) with the 3D structure of *Pyrococcus horikoshii* AsnRS. As mentioned in the active site identification section of *S. aureus* AsnRS, only two amino acid residues are involved in the asparagine recognition and water molecules contribute in that through binding with asparagine amide and carbonyl groups. By similarity search and docking study of the SWISS-MODEL AsnRS model with the substrate, Glu238 and Arg380 could be the key amino acid residues which are responsible for asparagine recognition. They make direct hydrogen binding interactions with the asparagine amide and carbonyl groups respectively (Figure 83a). The role of water molecules in asparagine recognition is

conserved in most of AsnRSs (299) and is clearly shown in the same figure the importance of water molecules to fill the gap between the amino acid residues and asparagine side chain. Clustal alignments of *E. faecalis* AsnRS with *T. Thermophilus* and *P. horikoshii* AsnRSs furthermore identified the position of Glu238 and Arg380 corresponding to Glu225, Arg368 and Glu228, Arg364 respectively in both organisms (Figure 84).

```
Feature 1                                   ###                 # #  #
query      143 IKLRHQVTKTIRHYLDNH-DFLDIETPYLGKSTPEGARDYLVPSRvhaGHFYALPQSPQLFKQLLMGAGFDRYYQIVRCF 221
1IL2_A     138 LKTRAKITSLVRRFMDDH-GFLDIETPMLTKATPEGARDYLVPSRvhkGKFYALPQSPQLFKQLLMMSGFDRYYQIVKCF 216 Escherichia coli
1G51_A     144 LRLRHRVIKAIWDFLDRE-GFVQVETPFLTKSTPEGARDFLVPYRhepGLFYALPQSPQLFKQMLMVAGLDRYFQIARCF 222 Thermus thermophilus
Q9X1F4     138 IILRYRISKIIRDYFDEL-GFLEIETPFLTRSTPEGARDFLVPSRlrpGKFYALPQSPQLFKQILMISGFDRYFQIVRCF 216 Thermotoga maritima
P73851     144 LQLRHQVVKAMRRFLEDQeNFLEIETPILTRSTPEGARDYLVPSRvnpGEWYALPQSPQLFKQLLMVAGMDRYYQIARCF 223 Synechocystis sp. ...
O67589     149 LIFRHRVYQITRNFFTKE-GFIEIETPFLTKSTPEGARDFLVPSRlhpGKFYALPQSPQLFKQILMIAGFDRYFQIVKCF 227 Aquifex aeolicus
O32038     144 MQLRHNVTKAVRSFLDEN-GFLDIETPILTGSTPEGARDYLVPSRvheGEFYALPQSPQLFKQLLMVSGIERYYQIARCF 222 Bacillus subtilis
NP_711861  150 MIKRHEFIFAIRNYLNKR-KFVEIETPILNKSTPEGARDFLVPSRlnpNQFYALPQSPQIFKQILMVGGMERYFQIVKCF 228 Leptospira interro...
Q8XJ28     147 FKIRHKTTKAIRDYLDQN-GFLEMETPILTKSTPEGARDYLVPSRnypGMFYALPQSPQLFKQLLMVSGFDRYFQIVKCF 225 Clostridium perfri...
CAA19270   159 LRQRSRLAYQVHSFFNDR-EFCEVETPLLFKSTPEGAREFVVPSRlnpGKFYALPQSPQQVKQILMASGIGNYYQIARCF 237 fission yeast
Feature 1      # #    ###  # #
query      222 RDEDLRGDRQPEFTQIDIETTFL-TPEEIQTYTENMLAEVMKETkgieisVPFPRMSYDEAMARYGsdkpdtrfamelid 300
1IL2_A     217 RDEDLRADRQPEFTQIDVETSFM-TAPQVREVMEALVRHLWLEVkgv-dlGDFPVMTFAEAERRYGsdkpdlrnpmeltd 294 Escherichia coli
1G51_A     223 RDEDLRADRQPDFTQLDLEMSFV-EVEDVLELNERLMAHVFREAlgvelpLPFPRLSYEEAMERYGsdkpdlrfglelke 301 Thermus thermophilus
Q9X1F4     217 RDEDLRADRQPEFTQVDVEMSFV-DVEDVLNVSEGMVSRVFKESsgidlkVPFDRIPYDDAMEKYGtdkpdrrygmelrd 295 Thermotoga maritima
P73851     224 RDEDLRADRQPEFTQLDMEMSFM-GQEEILDLNEALICHIFKVVknidlpRPFPRLTYQESMAKYGndrpdtrfglelvd 302 Synechocystis sp. ...
O67589     228 RDEDLRADRQPEFTQIDYEMSFV-SEEEVMDVAERLIATLFKELlgvelkTPFERISYREAMEKYGtdkpdrrfglelie 306 Aquifex aeolicus
O32038     223 RDEDLRADRQPEFTQIDIEMSFM-SQEDIMSLAEEMMAKVMRETkgeelqLPLPRMTYDEAMNKYGsdkpdtrfdmlltd 301 Bacillus subtilis
NP_711861  229 RDEDLRADRQPEFTQLDMEFSFV-SQEEILSEIEGLVETIYKEVfniqlsIPFPRMTYNTAMEEYGsdkpdlrfgmklvd 307 Leptospira interro...
Q8XJ28     226 RDEDLRANRQPEFTQVDLEMSFV-EQDDVMALNEGLIKHVFKEVlgvdvkTPIKRMTFKDAMEKYGsdkpdlrfgmeitn 304 Clostridium perfri...
CAA19270   238 RDEDLRFDRQPEFTQIDLEMSFVdKPHEIMEVVEDLLVRLVSFAkgitlaKPFQHITYQHAIDKYGsdkpdirfelplkn 317 fission yeast

Feature 1                                                                                  ##
query      374 tevsdeliaatnaevgdilmfgadkpeivaaalgavrtrlgkelglideskFNFLWIVDWPLFEYDEe-aGRYVSAHHPF 452
1IL2_A     374 aeiiedildrtaaqdgdmiffgadnkkivadamgalrlkvgkdlgltdeskWAPLWVIDFPMFEDDGe--GGLTAMHHPF 451 Escherichia coli
1G51_A     367 lepvreallqatearpgdtllfvagprkvaatalgavrlraadllglkregFRFLWVVDFPLLEWDEe-eEAWTYMHHPF 445 Thermus thermophilus
Q9X1F4     369 kefrkiaetenmnegdvcliaahtdrnllnealgtlrleigkehfshlakgFDVLWVVDFPYFEWSEe-eERFVARHHPF 447 Thermotoga maritima
P73851     383 eaqvktllqltqaeagdlllfgagdtatvdkslsrlrlvlgeqlglidpdaINLLWITDFPMFEWNSd-eKRFEALHHPF 461 Synechocystis sp. ...
O67589     379 eeetqkllertkaepgdvilfsadkkemvykilgnlrlhlgkkyklideskWDVFWIVDFPLMEWDEe-eERFVSLHHPF 457 Aquifex aeolicus
O32038     376 eekqskliealdaaegdllfgadqfevvaaslgalrlklgkergliideklFNFLWVIDWPLLEHDPe-eGRFYAAHHPF 454 Bacillus subtilis
NP_711861  382 keeleaiskacgskegdmlffgadereivnhslgalrlklserfetpkeneINITWIVDFPMFEWNKd-hKRWDALHHPF 460 Leptospira interro...
Q8XJ28     379 eelnkiietmgaktgdlilivadknsvvlkalgelrlelsrkfdlvkdkseFNFTWITEFDLLEYDEe-eGRYFAAHHPF 457 Clostridium perfri...
CAA19270   392 qklqiginsivfmtnrpkylvsgttplgklrlllhellvkkkalpeldkdlLKFVWVVDFPLFSPTEeknQSITSTHHPF 471 fission yeast
Feature 1                                                        #  #   #
query      453 TQPKAedv------drLATDPAs------------vYAEAYDVVLNGYELGGGSLRIHTRELQEKMFETLGftkeeaqDQ 514
1IL2_A     452 TSPKDmta------aeLKAAPEn------------aVANAYDMVINGYEVGGGSVRIHNGDMQQTVFGILGineeeqrEK 513 Escherichia coli
1G51_A     446 TSPHPedl------plLEKDPGr------------vRALAYDLVLNGVEVGGGSIRIHDPRLQARVFRLLGigeeeqrEK 507 Thermus thermophilus
Q9X1F4     448 TMPVLe---------tLGDDYTk------------vRAKAYDLVINGYEVGGGSIRIHRRDIQEKIFELLGlseeeaqKK 506 Thermotoga maritima
P73851     462 TAPHPd---------dLGDLKTa-------------RAQAYDLVMNGVEIGGGSLRIYQREVQEKVFATIGlspeeahEK 519 Synechocystis sp. ...
O67589     458 TMPREeni------pkLKEALEeedlekkkeivhsvRARAYDMVLNGEEIGGGSIRIHRRDIQEVVFKLLGigeveaqEK 531 Aquifex aeolicus
O32038     455 TMPVRedl------elIETAPEd------------mKAQAYDLVLNGYELGGGSIRIFEKDIQEKMFALLGfspeeaaEQ 516 Bacillus subtilis
NP_711861  461 TSPSDesipffesmetLQKNAGn------------aTAKAYDLVMNGVEIGGGSIRIHSREIQNKVFQILGineeeakEK 528 Leptospira interro...
Q8XJ28     458 TMPMDedi------kyLDTDPGr------------vRAKAYDLVLNGEELGGGSIRIHDTKLQEKMFEVLGftqesawER 519 Clostridium perfri...
CAA19270   472 TAPHWddv------hlLEKKPLs------------vRGLHYDIVVNGIELGGGSIRIHNPDIQRFVLKDVLklpenryAT 533 fission yeast
Feature 1                          ## #  #
query      515 FGFLLDALDYGFPPHGGIALGLDRLAMLLAGEENIREVIAFPKNGK 560
1IL2_A     514 FGFLLDALKYGTPPHAGLAFGLDRLTMLLTGTDNIRDVIAFPKTTA 559 Escherichia coli
1G51_A     508 FGFFLEALEYGAPPHGGIAWGLDRLLALMTGSPSIREVIAFPKNKE 553 Thermus thermophilus
Q9X1F4     507 FGFFLEAFRYGVPPHGGIAFGLDRLVSIIAGESSIREVIAFPKTGN 552 Thermotoga maritima
P73851     520 FGFLLDAFEYGTPPHGGIAYGLDRLVMLLAKEDSIRDVIAFPKTQQ 565 Synechocystis sp. PCC 6803
O67589     532 FGFLLEALKYGAPPHGGLAFGLDRVVALMLGLDSIRDTIAFPKTQR 577 Aquifex aeolicus
O32038     517 FGFLLEAFEYGAPPHGGIALGLDRLVMLLAGRTNLRDTIAFPKTAS 562 Bacillus subtilis
NP_711861  529 FGFLLEALEFGAPPHGGLAFGIDRMLMLLTGGKSIRDVIAFPKTQK 574 Leptospira interrogans serovar lai str. 56601
Q8XJ28     520 FGFLLEAFKFGPPPHGGLAFGLDRMIMFLAGTENIKDVITFPKNQN 565 Clostridium perfringens
CAA19270   534 FEHLIRVLSSGCPPHGGIALGFDRLAALLTNAPGIREVIAFPKTSS 579 fission yeast
```

Figure 80: Sequence alignments of the *E. faecalis* AspRS with other AspRSs for active site identification. The active sites of *E. faecalis* AspRS consists of Glu176, Gly177, Ala178, Ser198, Gln200, Lys203, Arg222, Glu224, Asp229, Arg230, Gln231, Phe234, Gln236, His449, His450, Glu486, Arg490, Ile532, Ala533, Gly535, Arg538.

```
Feature 1                                          # #     ##
query      182 ELFETDYFGQPAFLSQTGQLYAEAGAMA-FGKVFTFGPTFRAEkSKTRRHLTEFWMIEPEMAYt-tHEESLDIQEAYVKH 259
1B8A_A     174 ELFPMKYFEEDAFLAESPQLYKEIMMASgLDRVYEIAPIFRAEeHNTTRHLNEAWSIDSEMAFiedEEEVMSFLERLVAH 253 Thermococcus kodak...
NP_476609  263 NVFTVSYFKDSAYLAQSPQLYKQMAIAAdFDKVYTVGAVFRAEdSNTHRHLTEFVGLDLEMAFkyhYHEVLHTIGNTFTS 342 fruit fly
AAH42227   262 NVFTVSYFKTSAYLAQSPQLYKQMCICAdFEKVFCIGPVFRAEdSNTHRHLTEFVGLDIEMAFnyhYHEVVDEIADTLVQ 341 African clawed frog
O29342     172 ELFPISYFEKEAFLNQSPQLYKQVLMAAgFEKVFEIGPIFRAEeHNTTRHLNEAISIDIEMSFt-dHNGVMDVLERLVQR 250 Archaeoglobus fulg...
Q9Y9U7     176 EVFPVVYFDKTAFLAQSPQFYKQFAVIAgLERVFEIGPVFRAEpHHTSRHLNEYHSLDIEVGFiesYNDVMNYVEGFMRA 255 Aeropyrum pernix
AAO51772   306 SVFKLNYFNTHAYLAQSPQLYKQMAICAdFNKVFEIGPVFRAEnSNTHRHLTEFVGLDLEMTFkdhYHEALDTLDRLMTS 385 Dictyostelium disc...
P58692     192 IDYSQDFFAKPTYLTVSGQLEAEVMAMA-FSNVYTFGPTFRAEnSNTSRHLAEFWMVEPEMAFc-dLEGDMDLAEAFLKH 269 Nostoc sp. PCC 7120
NP_585835  206 NLFSVDYFKRKAFMAQSPQLYKQMAIVGgFKRVYEIGHVYRAEeSNINRYLSEFVGLDMEMEIctdYNDVIRFIHSMLVS 285 Encephalitozoon cu...
P38707     288 TLFKMNYYGEEAYLTQSSQLYLETCLAS-LGDVYTIQESFRAEkSHTRRHLSEYTHIEAELAFl-tFDDLLQHIETLIVK 365 baker's yeast
Feature 1
query      260 LIKSVlknqqypldvle-----rdtallekyvsEPFKRITYDDAIELLQkeeann-dydhieWGEDFGSPHETFISNYy- 332
1B8A_A     254 AINYVrehnakeldi---------lnfeleepkLPFPRVSYDKALEILGdlgk------eipWGEDIDTEGERLLGKYmm 318 Thermococcus kodak...
NP_476609  343 IFKGLrdkyakeiesvg-----qqykvdafkflEPPLILQFADGVAMLReagv------etgDEEDLSTPNEKLLGRLvk 411 fruit fly
AAH42227   342 IFKGLqerfqteiqtvc-----kqfpcepfkflEPTLRLEYTEGVAMLReagv------emgDEEDLSTPNEKLLGRLvk 410 African clawed frog
O29342     251 VYEDVaekcerylgw---------levsleipeLPFPRITYDEAREIAArkge------eipWGEDLSTNALKLVGEEm- 314 Archaeoglobus fulg...
Q9Y9U7     256 IVRMLeedgrrvlel--------ygvelpripaSGIPKIPLRKAYEILEekyg-----kkveYGEDLDSEGERLMGAYag 322 Aeropyrum pernix
AAO51772   386 IFRGLetrfakeiesvn-----tqypfepfkftYPSPRFTFDEAAAMLAelndp----dyivKDNDFNTRQEKRLGKIik 456 Dictyostelium disc...
P58692     270 IFNHVlekcpedmeffnqridntvlataeniinNQFERLTYTDAIKLLEkadvkf--eypvsWGLDLQSEHERYLAEQlf 347 Nostoc sp. PCC 7120
NP_585835  286 IFDNLkkeygeeletir-----afhafedlkyrRDPVVLTHRECVDLLLnegv------emgYEDDFNSESEKKLGSVvr 354 Encephalitozoon cu...
P38707     366 SVQYVledpiagplvk-------qlnpnfkapkAPFMRLQYKDAITWLNehdikneegedfkFGDDIAEAAERKMTDTi- 437 baker's yeast
Feature 1                                                  #  #
query      333 ----gVPTFILNYPKa-IKAFYMKPHPtredVVICADLIAPeGyGEIIGGSERATDYDYLKEKVAEFglseeeyswyLDL 407
1B8A_A     319 enenaPLYFLYQYPSeaKPFYIMKYDNkp-eICRAFDLEYR-G-VEISSGGQREHRHDILVEQIKEKglnpesfefyLKA 395 Thermococcus kodak...
NP_476609  412 akydtDFYILDKFPLa-IRPFYTMPDPnnpvYSNSYDMFMR-G-EEILSGAQRIHDPEYLIERAKHHgidtskiaayIES 488 fruit fly
AAH42227   411 ekydtDFYILDKYPLa-VRPFYTMPDPnnpkYSNSYDMFMR-G-EEILSGAQRVHDPQLLTDRATHHgidlekikayIDS 487 African clawed frog
O29342     315 ----gGLYFITDWPTe-SKPFYAMPYEdrpeISKSFDLMHG-W-LELSSGAQRIHLYDMLVESIKAKgmepesfgfyLEA 387 Archaeoglobus fulg...
Q9Y9U7     323 eeldsDFVFIVEYPWk-VRPFYTMRKDdepsWTYSFDLLYR-G-LEIVTGGQREHRYHRLLENLRDKgldaesfqfyLDF 399 Aeropyrum pernix
AAO51772   457 ekfgvDFFIVDKFHVe-VRPFYTMPDPnnpqWANAYDLFMR-G-EEICSGAQRIHDPELLEKSAKSHgvviediqgyIDS 533 Dictyostelium disc...
P58692     348 ----kKPVIVTDYPAq-IKAFYMRLSDde-kTVRAMDVLAP-KiGEIIGGSQREERLDVLERRVLAQgmqpedlwwyLDL 420 Nostoc sp. PCC 7120
NP_585835  355 rmhgvDIFVIKDYPIs-TRPFYTYRDEek-gITRSYDFILR-G-QEILSGAQRVSIYKDLVKYVEEHgispsslggyLES 430 Encephalitozoon cu...
P38707     438 ----gVPIFLTRFPVe-IKSFYMKRCSddprVTESVDVLMP-NvGEITGGSMRIDDMDELMAGFKREgidtdayywfIDQ 511 baker's yeast

Feature 1                    #  #
query      408 RKYGSVPHSGFGLGLERAVTFITGNEHIREAIPFPR 443
1B8A_A     396 FRYGMPPHGGFGLGAERLIKQMLDLPNIREVILFPR 431 Thermococcus kodakaraensis
NP_476609  489 FRYGCPPHAGGGIGMERVVMLYLGLDNIRKTSMFPR 524 fruit fly
AAH42227   488 FRFGAPPHAGGGIGLERVTMLYLGLHNVRQTSMFPR 523 African clawed frog
O29342     388 FRYGMPPHAGWGLGAERLIMSMLGLKNVREAVLFPR 423 Archaeoglobus fulgidus
Q9Y9U7     400 FKHGAPPHGGAGMGLERIVMQTLKLENIREARMLPR 435 Aeropyrum pernix
AAO51772   534 FKYGCSQHAGGGVGLERVVMLYLGLGNIRKASFCPR 569 Dictyostelium discoideum
P58692     421 RRYGTVPHAGFGLGFERLVQFITGMGNIRDVIPFPR 456 Nostoc sp. PCC 7120
NP_585835  431 FKYGAPPHGGCGIGLERLMKAYFGMGDIRCFSLFPR 466 Encephalitozoon cuniculi
P38707     512 RKYGTCPHGGYGIGTERILAWLCDRFTVRDCSLYPR 547 baker's yeast
```

Figure 81: Sequence alignments of the *E. faecalis* AsnRS with other AsnRSs for active site identification. The active sites of *E. faecalis* AsnRS consists of Arg221, Glu223, Arg229, His230, Glu373, Gly376, Gly421, Arg424.

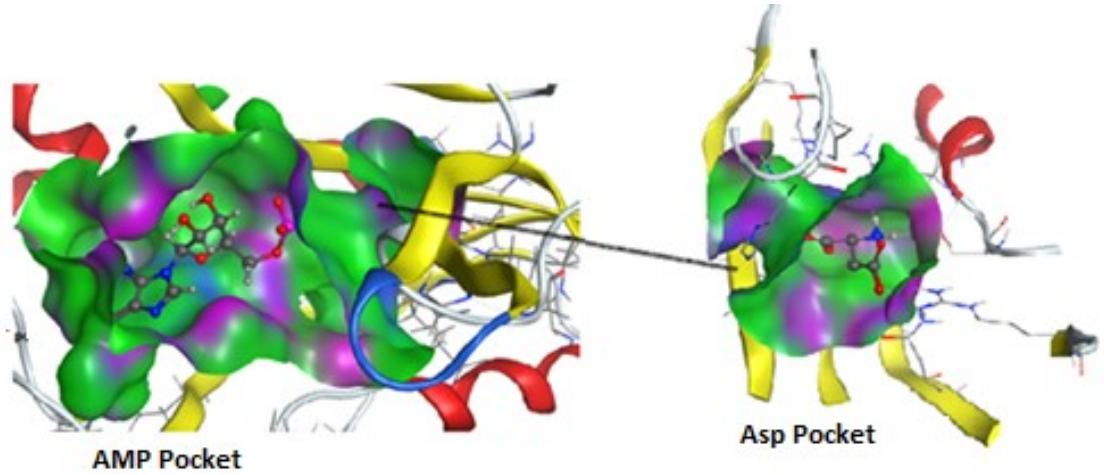

Figure 82a: 3D structure of the docking of the natural substrate (aspartyl-adenylate) in the *E. faecalis* AspRS SWISS-MODEL model with ATP and aspartic acid pockets identified. The active sites are coloured based on the chemical type of bonds that

could be established with ligands: hydrophobic (green), hydrogen bonds (pink), mild polar area (red).

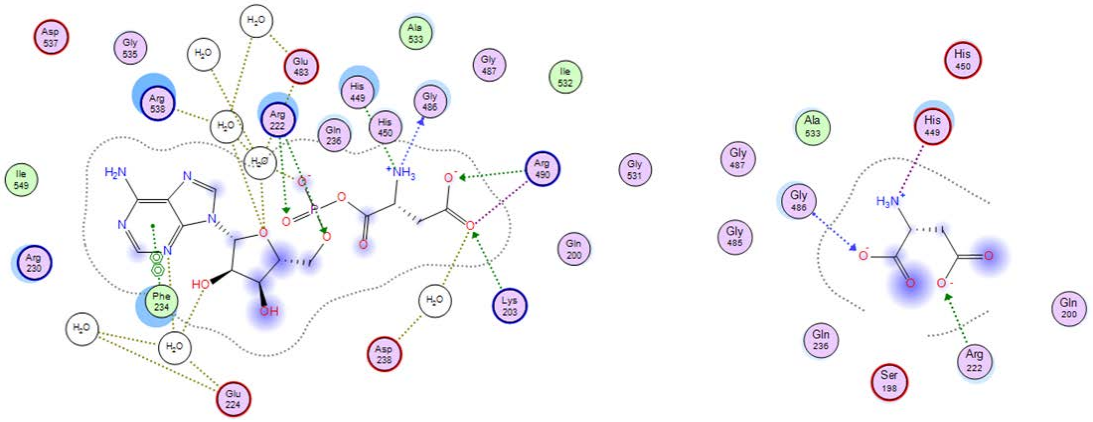

Figure 82b: 2D binding interactions of aspartyl-adenylate and aspartic acid in *E. faecalis* AspRS SWISS-MODEL model active sites.

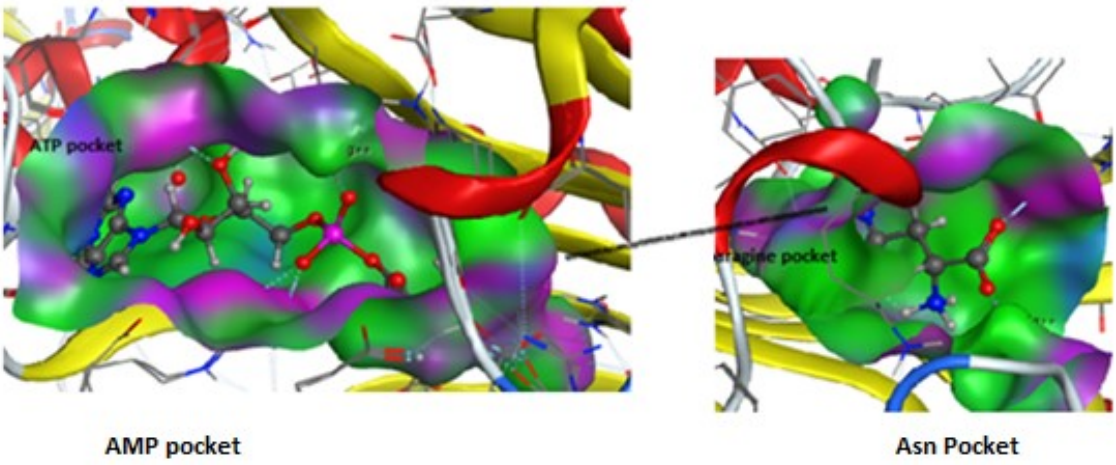

Figure 83a: 3D structure of the docking of the natural substrate (asparaginyl-adenylate) in *E. faecalis* AsnRS SWISS-MODEL model with ATP and asparagine pockets identified. The active sites are coloured based on the chemical type of bonds that could be established with ligands: hydrophobic (green), hydrogen bonds (pink), mild polar area (red).

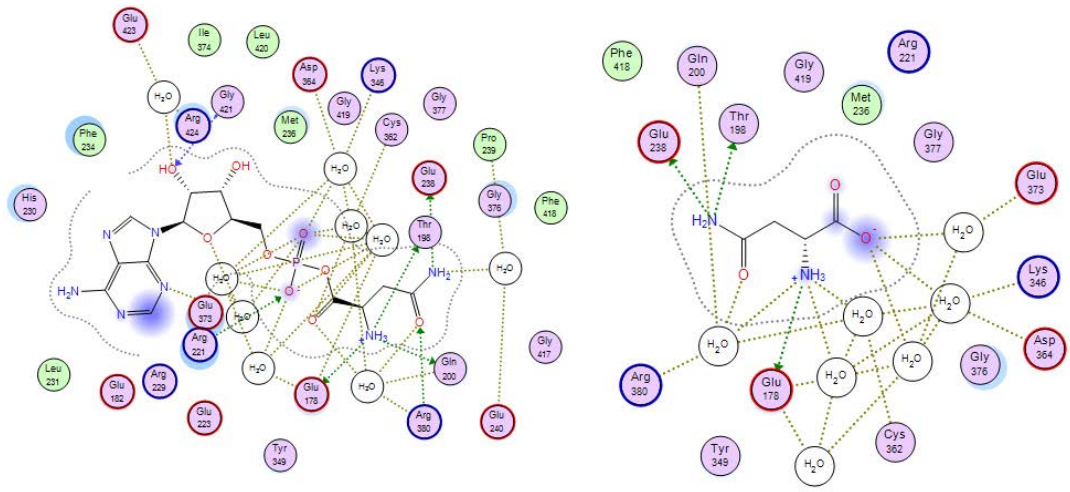

Figure 83b: 2D binding interactions of asparaginyl-adenylate and asparagine in *E. faecalis* AsnRS SWISS-MODEL model active sites.

```
CLUSTAL O(1.2.4) multiple sequence alignment


sp|O57980|SYN_PYRHO     -----MIEKVYCQEVKPELDGKKVRLAGWVYTNMRVGKKIFLWIRDSTGIVQAVVAKNVV   55
sp|Q831X4|SYN_ENTFA     MNGETNVEQIQIIDSN-KHVGETVKIGAWIANKRSSGKIAFLQLRDGTAFFQGVVFKPNF   59
sp|P54263|SYN_THET8     -------MRVFIDEIA-RHVDQEVELRGWLYQRRSKGKIHFLILRDGTGFLQATVVQGEV   52
                                ::   :   .  .: *.: .*:  .   **  ** :**.*.::*..* :  .

sp|O57980|SYN_PYRHO     --------GEETFEKAKKLGRESSVIVEGIVKADERAPGGAEVHVEKLEVIQAVSEFPIP   107
sp|Q831X4|SYN_ENTFA     IEAFGEEAGTEKFQEIKHLSQETAVMVTGVIKEDSRSKFGYEMDITDLEVVGA-SE-DYP   117
sp|P54263|SYN_THET8     --------PEAVFREADHLPQETALRVWGRVREDRRAPGGFELAVRDLQVVSRPQG-EYP   103
                                    *.: .:* :*::: * * :: * *:  * *: : .*:*:   .    *

sp|O57980|SYN_PYRHO     ENPEQASPELLLDYRHLHIRTPKASAIMKVKETLIMAAREWLLKDGWHEVFPPILVTGAV   167
sp|Q831X4|SYN_ENTFA     ITPKEHGTDFLMDHRHLWLRSSKQHAIMLVRNEIIRATYEFFNEQGFIKIDSPILTGSAP   177
sp|P54263|SYN_THET8     IGPKEHGIDFLMDHRHLWLRHRRPFAVMRIRDELERAIHEFFGERGFLRFDAPILTPSAV   163
                          *:: . ::*:*:*** :*  :  *:* ::: :  *  *:: : *: ..  ***. .*

sp|O57980|SYN_PYRHO     EGGATLFKLKYF-DKYAYLSQSAQLYLEAAIFGLEKVWSLTPSFRAEKSRTRRHLTEFWH   226
sp|Q831X4|SYN_ENTFA     EGTTELFETDYF-GQPAFLSQTGQLYAEAGAMAFGKVFTFGPTFRAEKSKTRRHLTEFWM   236
sp|P54263|SYN_THET8     EGTTELFEVELFDGEKAYLSQSGQLYAEAGALAFAKVYTFGPTFRAERSKTRRHLLEFWM   223
                        ** : **: . * .: *:***:.*** **. :.: **::: *:****:*:***** ***

sp|O57980|SYN_PYRHO     LELEAAWMDLWDIMKVEEELVSYMVQRTLELRKKEIEMFRDDLTTL-KNTEPPFPRISYD   285
sp|Q831X4|SYN_ENTFA     IEPEMAYTTHEESLDIQEAYVKHLIKSVLKNQQYPLDVLERDTALLEKYVSEPFKRITYD   296
sp|P54263|SYN_THET8     VEPEVAFMTHEENMALQEELVSFLVARVLERRSRELEMLGRDPKALEPAAEGHYPRLTYK   283
                        :* * *:    : : ::*  *.::  .*: :.  ::::  *   *   ..  : *::*.

sp|O57980|SYN_PYRHO     EAIDILQSKG------VNVEWGDDLGADEERVLTEEFDRPFFVYGYPKHIKAFYMKEDPN   339
sp|Q831X4|SYN_ENTFA     DAIELLQKEE-ANNDYDHIEWGEDFGSPHETFISNYYGVPTFILNYPKAIKAFYMKPHPT   355
sp|P54263|SYN_THET8     EAVALVNRIAQEDPEVPPLPYGEDFGAPHEAALSRRFDRPVFVERYPARIKAFYMEPDPE   343
                        :*: :::           : :*:*:*: .*  ::. :. * *:  **  ******: .*

sp|O57980|SYN_PYRHO     DPRKVLASDMLAPEGYGEIIGGSQREDDYDKLLNRILEEGMDPKDYEWYLDLRRYGSVPH   399
sp|Q831X4|SYN_ENTFA     REDVVICADLIAPEGYGEIIGGSERATDYDYLKEKVAEFGLSEEEYSWYLDLRKYGSVPH   415
sp|P54263|SYN_THET8     DPELVLNDDLLAPEGYGEIIGGSQRTHDLELLRRKIQEFGLPEEVYDWYLDLRRFGSVPH   403
                            *:  *::************:   * : * .:: * *:  : *.******::*****

sp|O57980|SYN_PYRHO     SGFGLGVERLVAWVLKLDHIRWAALFPRTPARLYP   434
sp|Q831X4|SYN_ENTFA     SGFGLGLERAVTFITGNEHIREAIPFPRMLNRIYP   450
sp|P54263|SYN_THET8     SGFGLGLERTVAWICGLAHVREAIPFPRMYTRMRP   438
                        ******:** *:::    *:* *  ***   *: *
```

Figure 84: Sequence alignment of *P. Horikoshii* (SYN_PYRHO), *E. faecalis* (SYN_ENTFA) and *T. Thermophilus* (SYN_THET8) and AsnRSs showed the conserved amino residues

in blue squares which are responsible for asparagine side chain recognition. (Glu228, Arg364), (Glu238, Arg380) and (Glu225, Arg368) respectively.

2.3.2.1.4.2. Metal binding

The specificity of AspRS is substrate-assisted and its binding with magnesium ion increases its discrimination of Asp-AMP over Asn-AMP (301). In bacterial AspRSs, there are two conserved amino acid residues which are generally bound with magnesium ion and contribute in stabilisation of the formed coordinate species. Thus, sequence alignment of *E. faecalis* AspRS with other AspRSs containing known bound amino acid residues with Mg^{2+} ion was performed to identify the corresponding ones in the target (Figure 85). By similarity, Glu483 and Gly486 amino acid residues could be responsible for mg^{2+} cation binding in *E. faecalis* AspRS as they conserved in all bacterial species but Gly486 is replaced with serine in other non-bacterial organisms (Figure 85). Docking study of *E. faecalis* AspRS with the substrate in the presence of Mg^{2+} cation was performed using *Pyrococcus kodakaraensis* AspRS (3NEM) (302) as a template to investigate the role of the cation in the active site of the *E. faecalis* AspRS model (Figure 86). As It has been reported that Asp476 is also highly conserved amino acids residue bound with cation in class II aaRSs (301) and the mutagenesis experiments have shown that is functionally irreplaceable beside Glu483 in AspRSs (300), that metal interaction is clearly shown in the same figure of the docking study. Based on similarity search of *E. faecalis*, *E. coli* and *T. Thermophilus* AspRSs, the discrimination of AspRS toward aspartic acid over asparagine substrate comes from the presence of mg^{2+} which induces structural reorganisation in mobile flipping loop (residues 172 - 178) and histidine loop (residues 436-450). This reorganisation is conserved in most AspRSs (264, 282, 285), which supposes making Glu176 and His449 close to Asp ligand (Figure 87). In the case of *E. faecalis* AsnRS, *Pyrococcus horikoshii* AsnRS template (1X54) was used to identify which amino acid residues bind with Mg^{2+} ion. MOE alignment and docking tools predict that Lys346 and Asp364 in *E. faecalis* AsnRS constructed model bind the cation through water molecules, which correspond to Lys330 and Asp348 in *Pyrococcus horikoshii* AsnRS (Figure 88).

```
sp|P21889|SYD_ECOLI        PKDMTAAELKAAPENAVANAYDMVINGYEVGGGSVRIHNGDMQQTVFGILGINEEEQREK    513
sp|Q833I2|SYD_ENTFA        PKAEDVDRLATDPASVYAEAYDVVLNGYEVGGGSLRIHTRELQEKMFETLGFTKEEAQDQ    514
sp|P36419|SYD_THETH        PHPEDLPLLEKDPGRVRALAYDLVLNGYEVGGGSIRIHDPRLQARVFRLLGIGEEEQREK    507
sp|O07683|SYDND_HALSA      QDVD--------GDDVASRKFDLLYRGQEVSGGQREHDIERLTAKMREQGVEP----EN    386
tr|M0P2W5|M0P2W5_9EURY     QDVE--------GDEIASRKFDLIYKGQEVSGGQREHDVDRMVEVMEEEGVET----AN    384
sp|Q3IT59|SYDND_NATPD      MDHE--------D-GELSTGFDMMHPRMEVVGGQREHRREELIAGFEQQGLEP----EA    383
sp|Q8Q0R2|SYDND_METMA      MPYE--------DRPEFSKSFDMMHRTMEVSGAQRIHIPSLLKNRIESQGLNP----DG    394
sp|Q52428|SYD_THEKO        MKYD--------NKPEICRAFDLEYRGVEVSGGQREHRHDILVEQIKEKGLNP----ES    388
sp|O26328|SYDND_METTH      MPDE--------DDPERSHAFDLMYRDLEVSGAMRVHQHDLLVEKIKRQGLNP----DS    387
sp|Q9M084|SYDC2_ARATH      MTCA--------DNPLYSNSFDVFIRGEEIIGAQRVHIPEVLEQRAGECGIDV----KT    508
sp|P14868|SYDC_HUMAN       MPDP--------RNPKQSNSYDMFMRGEEILGAQRIHDPQLLTERALHHGIDL----EK    451
                                        .  :*:     *  *. * *          *.
```

Figure 85: Part of sequence alignment of AspRSs in different organisms showing amino acid residues bound with Mg^{2+}: *E. coli* (SYD_ECOLI), *E. faecalis* (SYD_ENTFA), *T. Thermophilus* (SYD_THETH), Arabidopsis thaliana (SYDC2_ARATH), Halobacterium salinarum (SYDND_HALSA), Halorubrum lipolyticum (M0P2W5_9EURY), Natronomonas pharaonis (SYDND_NATPD), Methanosarcina mazei (SYDND_METMA), Thermococcus kodakarensis (SYD_THEKO), Methanothermobacter thermautotrophicus (SYDND_METTH) and Home sapiens (SYD_HUMAN).

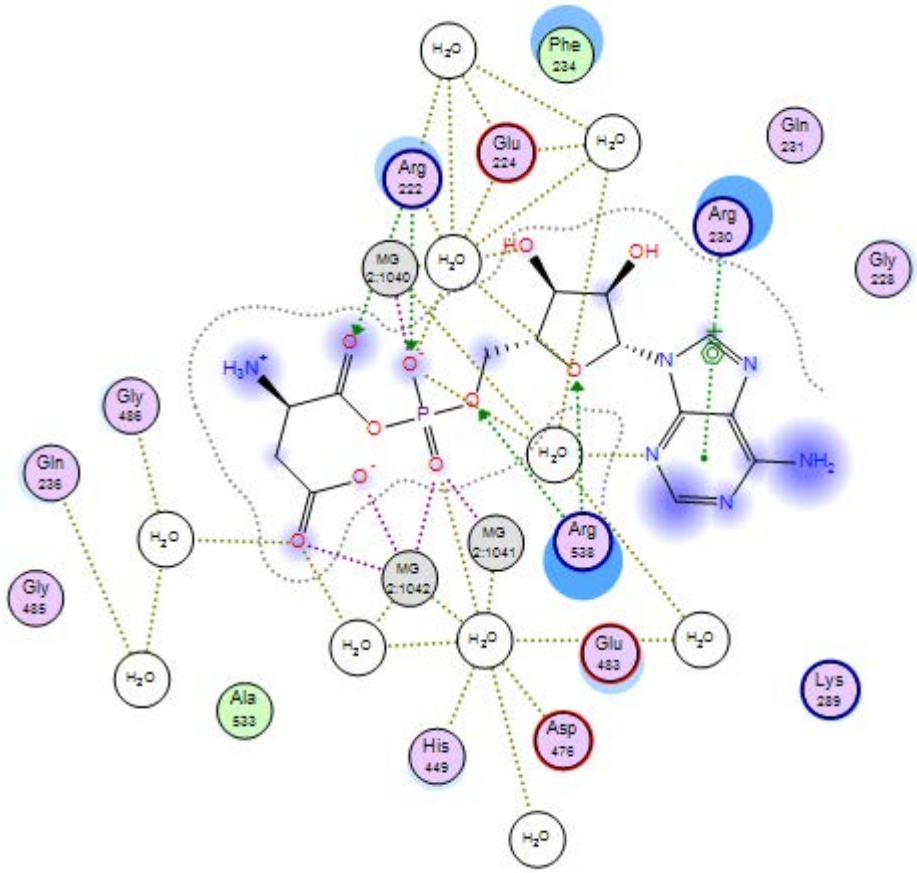

Figure 86: 2D binding interactions of aspartyl-adenylate in the *E. faecalis* AspRS active sites showing the interaction of His449 with aspartic acid in the presence of Mg^{2+}.

```
sp|P21889|SYD_ECOLI     ---NHVNTEEARLKYRYLDLRRPEMAQRLKTRAKITSLVRRFMDDHGFLDIETPMLTKAT   169
sp|Q833I2|SYD_ENTFA     --DDNNVNDELRMKYRYLDLRRPSMTNNIKLRHQVTKTIRHYLDNHDFLDIETPYLGKST   174
sp|P36419|SYD_THETH     GEEEKEASEELRLKYRYLDLRRRRMQENLRLRHRVIKAIWDFLDREGFVQVETPFLTKST   175
                           ::  .:* *:*********  * :.:: * :: . :  ::* ..*:::*** * ***

sp|P21889|SYD_ECOLI     PEGARDYLVPSRVHKGKFYALPQSPQLFKQLLMMSGFDRYYQIVKCFRDEDLRADRQPEF   229
sp|Q833I2|SYD_ENTFA     PEGARDYLVPSRVHAGHFYALPQSPQLFKQLLMGAGFDRYYQIVRCFRDEDLRGDRQPEF   234
sp|P36419|SYD_THETH     PEGARDFLVPYRHEPGLFYALPQSPQLFKQMLMVAGLDRYFQIARCFRDEDLRADRQPDF   235
                        *****:*** * . * *************:** :*:***:**.:********.****:*

sp|P21889|SYD_ECOLI     ALRLKVGKDLGLTDESKWAPLWVIDFPMFEDDGE-GGLTAMHHPFTSPKDMTAAELKAAP   466
sp|Q833I2|SYD_ENTFA     AVRTRLGKELGLIDESKFNFLWIVDWPLFEYDEEAGRYVSAHHPFTQPKAEDVDRLATDP   467
sp|P36419|SYD_THETH     AVRLRAADLLGLK-REGFRFLWVVDFPLLEWDEEEEAWTYMHHPFTSPHPEDLPLLEKDP   460
                        *:* : .. ***  .. :  **:: :.:: * *     . *****.*:      *   *
```

Figure 87: Parts of sequence alignment of AspRSs in *E. coli* (SYD_ECOLI), *E. faecalis* (SYD_ENTFA) and *T. Thermophilus* (SYD_THETH) showing the mobile and histidine loops.

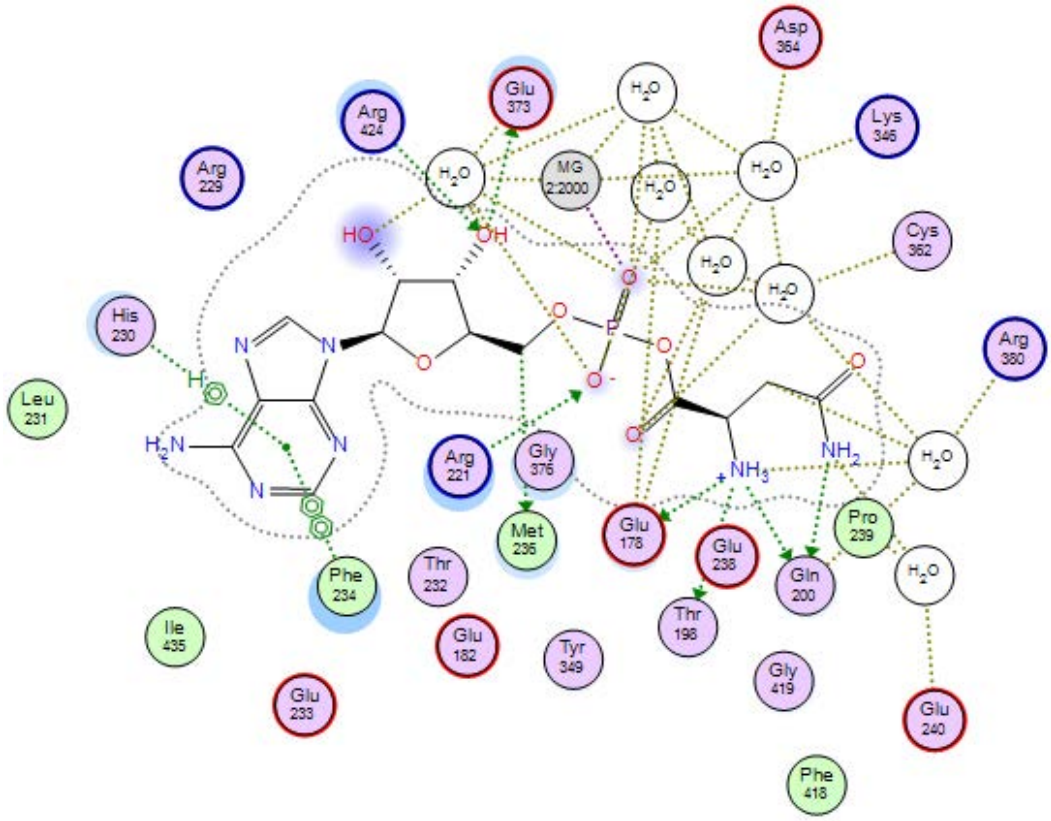

Figure 88: 2D binding interactions of asparaginyl-adenylate in the *E. faecalis* AsnRS active sites showing the binding interaction of Lys 346 and Asp364 with mg^{2+} cation.

2.3.2.1.5. Molecular dynamic of *E. faecalis* AspRS and AsnRS models

Because molecular recognition and drug binding are a very dynamic processes (305), using molecular dynamic as a simulation method for analysing the movement of ligand and its receptor was performed through Schrödinger platform (306). RMSD (Figure 89) and RMSF (Figure 90) are common measures of structural fluctuations for conformational mobility. RMSD is used to measure the average change in displacement of a selection of atoms for a particular frame with respect to a reference frame while RMSF is useful for characterising local changes along the protein chain through measuring the displacement of a particular atom, or group of atoms, relative to the reference structure, averaged over the number of atoms (307). Monitoring the RMSD of the protein can indicate how large the conformational change of the protein is during the simulation time and how stable the ligand is with respect to the protein and its binding pocket. Figure 89 shows that the conformational change of *E. faecalis* AspRS is larger than *E. faecalis* AsnRS in 100 nano-second of simulation time whereas the natural substrate of the latter one is the most stable in its binding pocket. On the other hand, the RMSF figure 90 shows peaks that identify which areas of the protein fluctuated the most during the simulation (306).

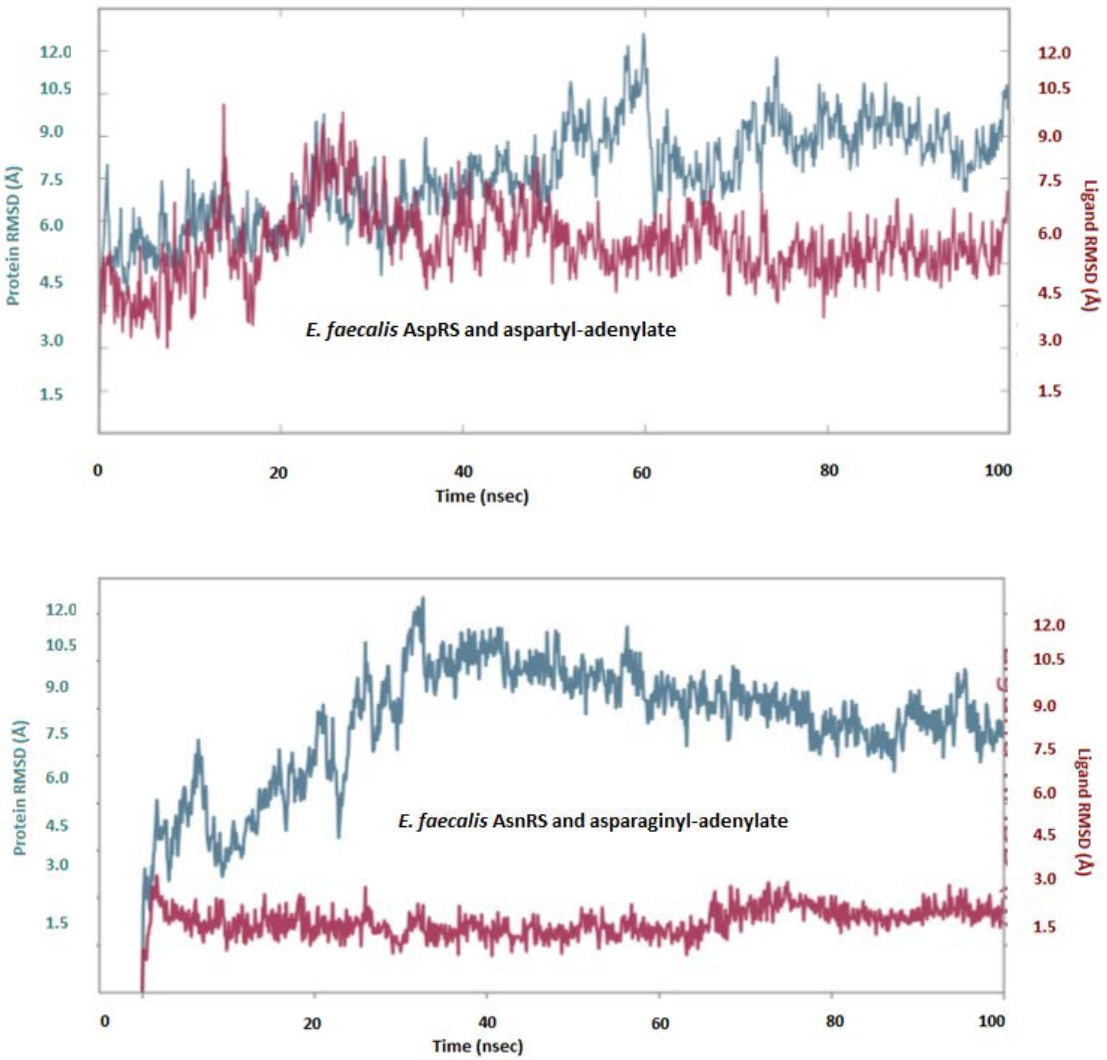

Figure 89: RMSD (in angstrom) plot with respect to time in nanoseconds during 100 ns MD simulation of *E. faecalis* AspRS and AsnRS with their substrates.

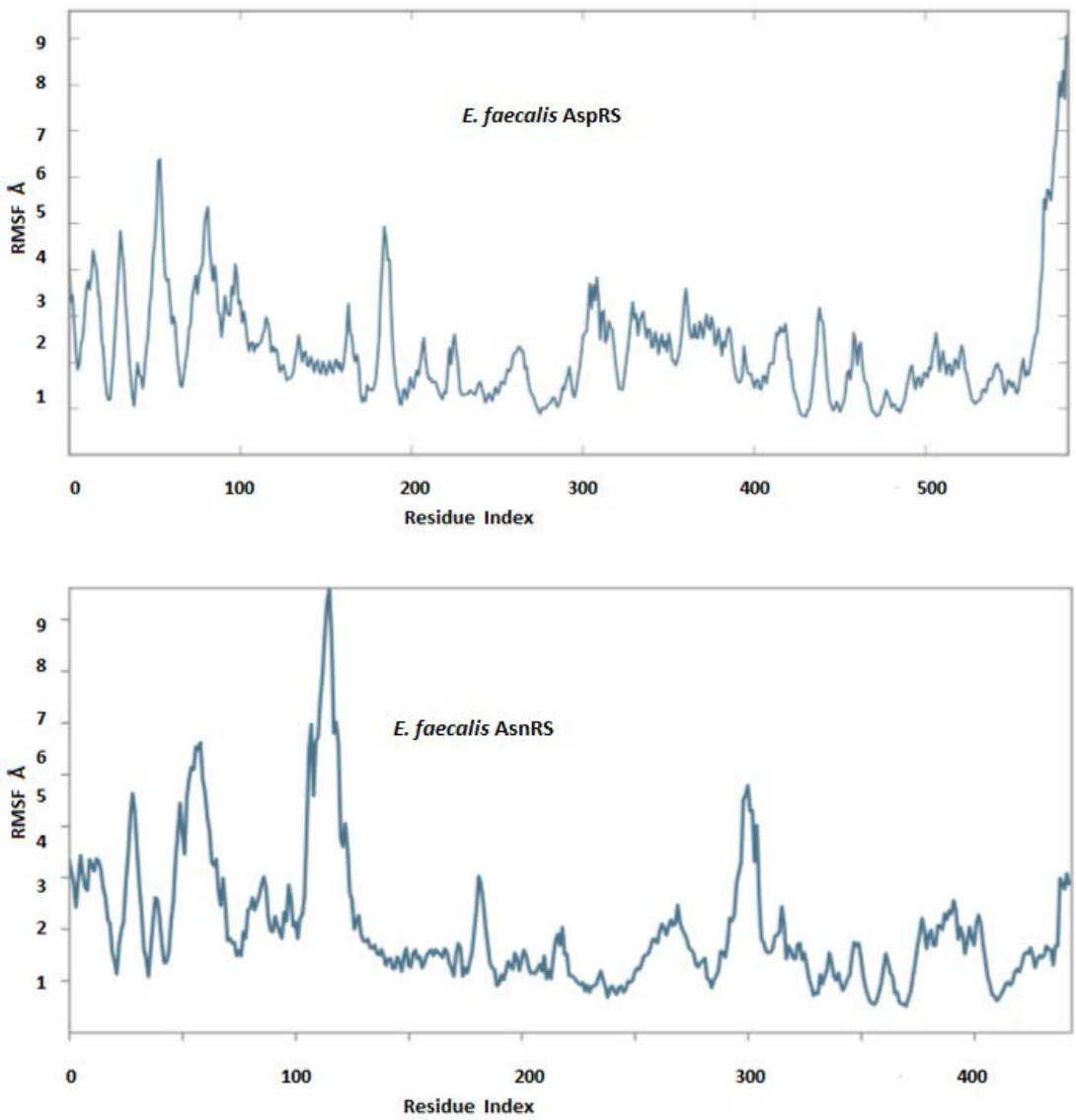

Figure 90: RMSF (in angstrom) plot of *S. aureus* AspRS and AsnRS amino acids residues.

Protein interactions with the ligand are also furthermore monitored during simulation time and characterised by type into four groups: hydrogen bonds, hydrophobic, ionic and water bridges with green, mauve, pink and blue colour respectively (Figure 91). The X-axis of both graphs represent the key amino acid residues of the targeting enzymes while the Y- axis is for the interactions fraction indicating the percentage of each specific interaction that is maintained during the simulation time. For example, ASP476 in *E. faecalis* AspRS simulation interactions diagram formed a hydrogen bonds with the substrate all the simulation time while throughout the simulation time there are hydrogen bonds mediated by water molecules. Any value above 1.0 indicates that residue may make multiple contacts of same subtype with the ligand.

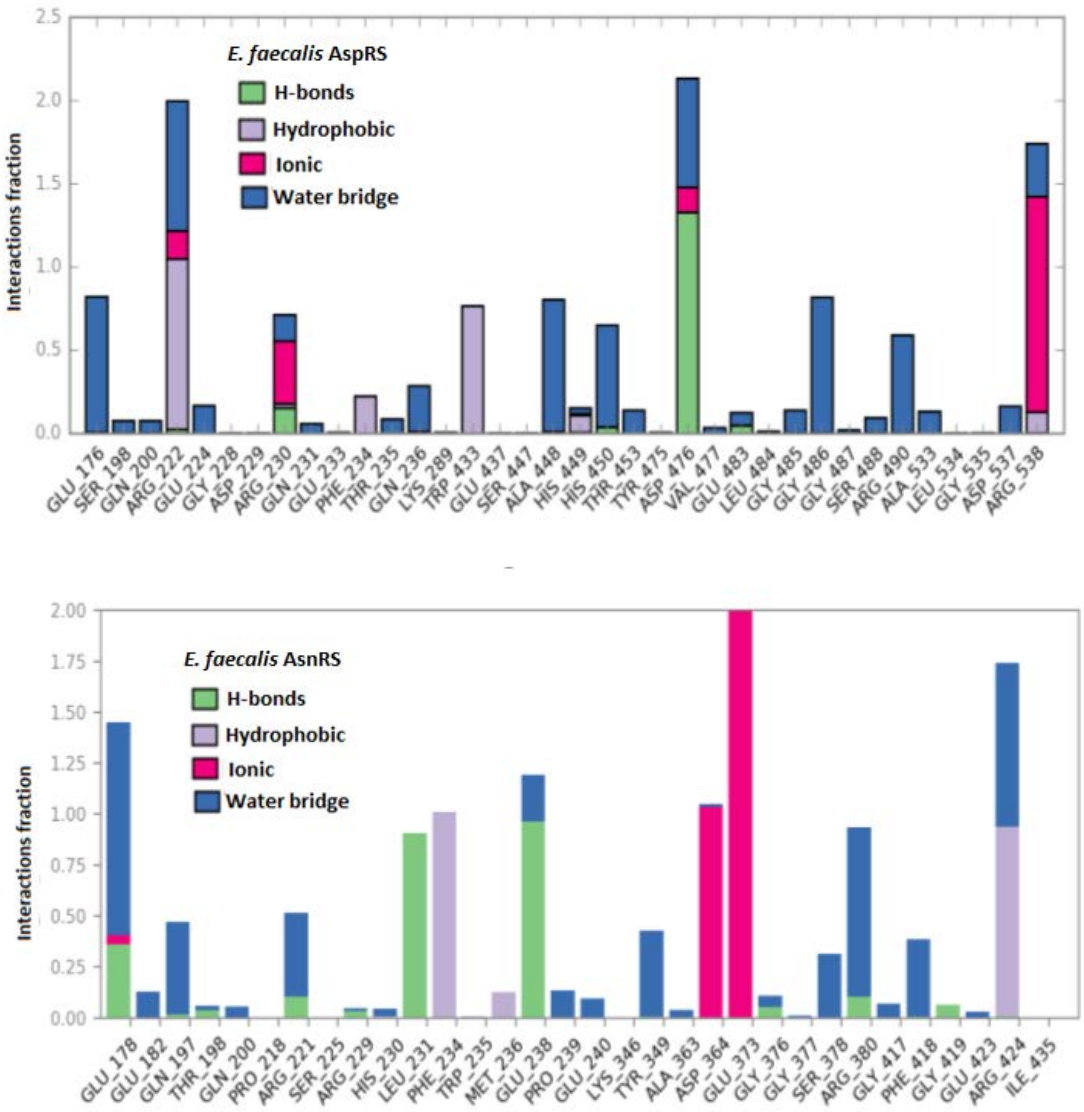

Figure 91: Simulation protein-ligand contact interactions over the 100ns trajectory diagram.

Studying molecular dynamic in Schrodinger also provides a direct prediction of small-molecule binding energies through using prime MM-GBSA (308) which generates energy properties including energies for the ligand, receptor, and complex structures in minimised and optimised free form. Thus, it can be used to estimate relative binding affinity for a list of ligands and there is a reasonable agreement of the ranking of the ligands based on the calculated binding energies with the result of ranking them based on experimental binding affinity (308). As the MM-GBSA binding energies are approximate free energies of binding, a more negative value indicates stronger binding (308). The binding free energy (Prime MMGBSA ΔG bind) is calculated with this equation:

ΔG (bind) = E_complex (minimised) - (E_ligand (minimised) + E_receptor (minimised))

The binding affinity of aspartyl-adenylate and asparaginyl-adenylate with their respective *E. faecalis* enzymes is in positive value for AspRS and negative for AsnRS (Table 17).

Table 17: MM-GBSA binding energies of aspartyl-adenylate and asparaginyl-adenylate.

Binding affinity of natural substrates	*E. faecalis* AspRS	*E. faecalis* AsnRS
ΔG range (kcal/mol)	-13.3773 - 57.8073	-8.4322 – 3.9545
ΔG average (kcal/mol)	10.4880 ± 13.11	-1.5024 ± 1.96

2.3.2.1.6. Final constructed *E. faecalis* AspRS and AsnRS models

The final constructed models of *E. faecalis* AspRS and AsnRS have the same characteristic domains of subclass IIb aaRS enzymes where the C-terminal catalytic site is built around antiparallel β sheets (Figures 92 and 93). These enzymes are homodimers of two α subunits, with each monomer of AspRS contains four modules including the N-terminal domain for tRNA anticodon recognition, a small hinge domain, catalytic domain and large insertion domain which is characteristic of eubacterial AspRSs. However, the monomer of AsnRS consists of the first three modules and as they are members of class II aaRSs, they contain three conserved motifs (motifs 1, 2 and 3).

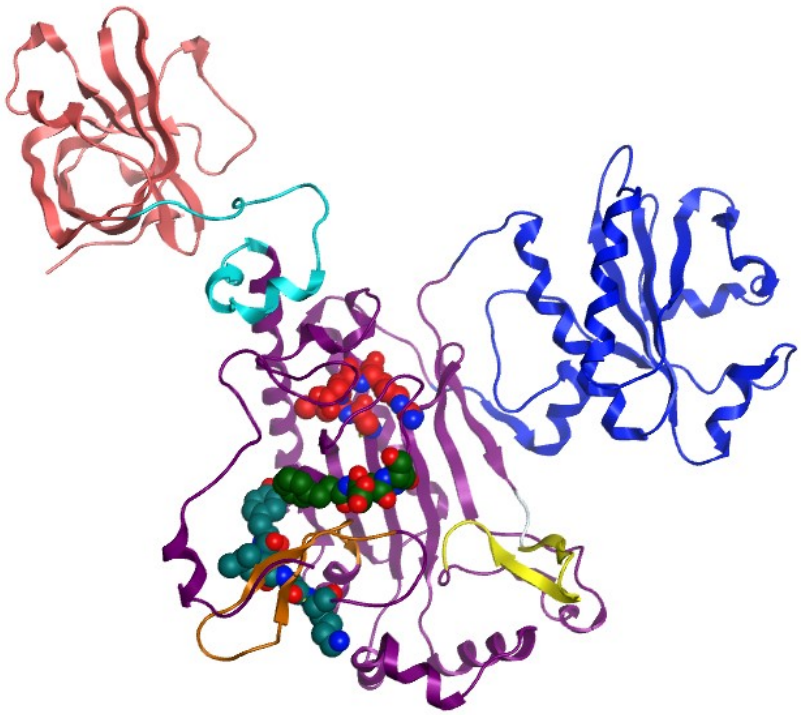

Figure 92: Final *E. faecalis* AspRS homology model with characteristic domains and motifs: active site (purple), N-terminal anticodon binding domain (pink), insertion domain (blue), a small hinge domain (cyan), histidine loop (yellow), flipping loop (brown). Motifs represented in ball model structure are motif 1 (168-172) is in teal, motif 2 (221-224) in green and motif 3 (535-538) in red.

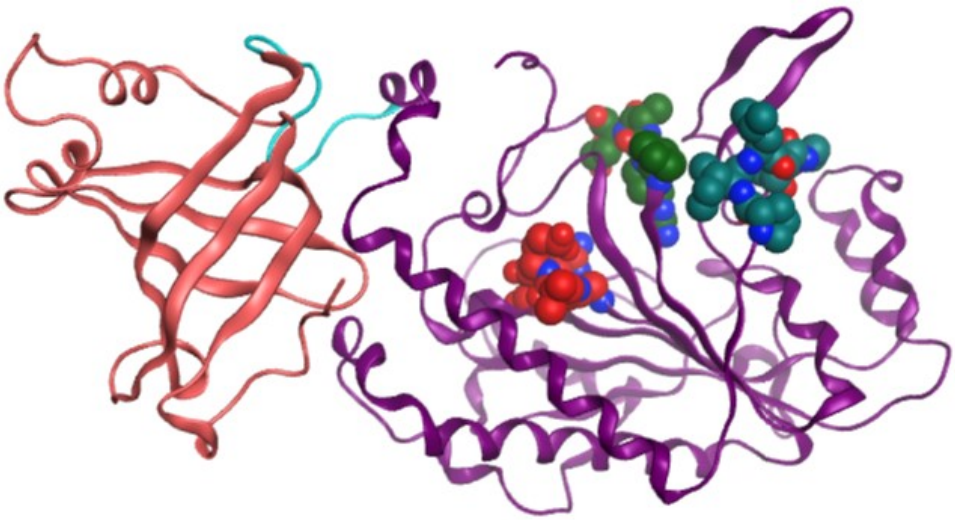

Figure 93: Final *E. faecalis* AsnRS homology model with characteristic domains and motifs: C-terminal active site (purple), N-terminal anticodon binding domain (pink), hinge region (cyan). Motifs represented in ball model structure which motif 1 (170-174) is in teal, motif 2 (220-223) in green and motif 3 (421-424) in red.

2.4. Selectivity study of *S. aureus* and *E. faecalis* AspRS and AsnRS with their human counterparts

The critical point of any proposed idea related to inhibitors drug design is aiming for targeting species only without affecting the host. Thus, the researched value of any new antibacterial agent is the range of its ability to be a selective molecule to the targeted receptor of species rather than the corresponding one in the human. The difference in protein sequences of *S. aureus* and *E. faecalis* AspRS and AsnRS than those of their human (mitochondrial and cytoplasmic) counterparts makes design selective inhibitors is possible. To illustrate, Clustal Omega (271) was used as a tool to determine the percentage of similarity between them. Mitochondrial and cytoplasmic AspRS with UNIPROT identifiers (Q6PI48, P14868) were used to identify the percent identity matrix with *S. aureus* (Q2FXU5) and *E. faecalis* (Q833I2) AspRSs (Figure 94). As a result, the protein sequences of *S. aureus* AspRS shares 40.53% and 29.30% similarity with the protein sequences of mitochondrial and cytoplasmic AspRSs respectively while the percentage of similarity in protein sequence of *E. faecalis* AspRS with its respective human counterparts is 41.70% and 25.41%. Both cytoplasmic and bacterial AspRSs are dimeric enzymes and each monomer consists of three modules: anticodon binding domain, hinge domain and catalytic domain but bacterial AspRS contains an extra insertion domain which is located between motif 2 and motif 3 of the catalytic site (293) and the cytosolic one also contains N-terminal extension which is a distinct domain in mammalian AspRSs and located next to anticodon binding domain (294). It is reported that the binding of the insertion domain to the cognate tRNA molecule is not sequence specific and all interactions are water mediated while the N-terminal extension of the cytosolic AspRS induces the nonspecific tRNA binding and gives a force to transfer its charged tRNA to elongation factor 1α (293, 294). The difference in the location of the two extra domains and proved the role of the N-terminal one in the cytoplasmic AspRS for tRNA binding suggests that insertion domain could contribute in the specificity of the bacterial AspRS active site. Regarding the mitochondrial AspRS, the percent of identity matrix with bacterial AspRSs is high owing to the closest similarity in their 3D architectures. However, the mitochondrial AspRS is distinctive by an enlarged catalytic groove, a more electropositive surface potential and an alternate interaction network at the subunits interface with absence of additional domains

(311). In the case of AsnRS, Mitochondrial (Q96I59) and cytoplasmic (O43776) AspRS were used to determine the percentage of similarity in their protein sequences with *S. aureus* (Q2FYH6) and *E. faecalis* (Q831X4) AspRSs (Figure 95). the protein sequences of *S. aureus* AsnRS shares 35.66% and 33.50% similarity with the protein sequences of mitochondrial and cytoplasmic AspRSs respectively while the percentage of similarity in protein sequence of *E. faecalis* AsnRS with its respective human counterparts is 34.43% and 31.79%. Due to the lack of data related to AsnRSs, the understanding of AsnRS is limited in term of the catalytic domain. Although Clustal Omega tool detects that there is a difference between *S. aureus*, *E. faecalis* and human AsnRSs, 3D structures of human counterpart (pdb: 5XIX and 4ZYA) are not useful for a comparison as they represent the N-terminal extension domain only (312). However, studies of bacterial AsnRSs are focusing on the discrimination between AspRS and AsnRS in term of aspartic acid and asparagine interactions with the active sites (295, 296, 299). There is one study of *T. Thermophilus* AsnRS clarified that there is an extra insertion domain between motif 2 and motif 3 in the catalytic domain similar to other members of subclass IIb which is characteristic for bacterial enzymes but small and less globular (313). This could make the binding of the substrate with bacterial AsnRS more selective than cytoplasmic AsnRS.

```
Percent Identity  Matrix - created by Clustal2.1


  1: sp|P14868|SYDC_HUMAN  100.00   25.05   29.30   25.41
  2: sp|Q6PI48|SYDM_HUMAN   25.05  100.00   40.53   41.70
  3: sp|Q2FXU5|SYD_STAA8    29.30   40.53  100.00   63.82
  4: sp|Q833I2|SYD_ENTFA    25.41   41.70   63.82  100.00
```

Figure 94: Similarity search of S. aureus (Q2FXU5) and E. faecalis (Q833I2) AspRSs with mitochondrial (Q6PI48) and cytoplasmic (P14868) AspRS. It shows in pink shaded boxes for *S. aureus* AspRS and in yellow shaded boxes for *E. faecalis* AspRS.

```
Percent Identity  Matrix - created by Clustal2.1


  1: sp|Q96I59|SYNM_HUMAN  100.00   28.21   35.66   34.43
  2: sp|O43776|SYNC_HUMAN   28.21  100.00   33.50   31.79
  3: sp|Q2FYH6|SYN_STAA8    35.66   33.50  100.00   66.28
  4: sp|Q831X4|SYN_ENTFA    34.43   31.79   66.28  100.00
```

Figure 95: Similarity search of *S. aureus* (Q2FYH6) and *E. faecalis* (Q831X4) AsnRSs with mitochondrial (Q96I59) and cytoplasmic (O43776) AsnRS. It shows in pink shaded boxes for *S. aureus* AspRS and in yellow shaded boxes for *E. faecalis* AspRS.

In conclusion, *S. aureus* and *E. faecalis* AspRS and AsnRS were selected as the targets of the project as the percentage of similarity in their protein sequences is high among other class II aaRS enzymes. Despite the fact that IleRS and LeuRS are most similar to each other in their protein sequences, they have been extensively studied (188-206). As there are no crystal structures for the target enzymes, two homology models were built for each enzyme using MOE software and SWISS-MODEL server. The homology modelling of *S. aureus* and *E. faecalis* AspRSs with respective Uniprot identifier numbers Q2FXU5 and Q833I2 was performed using *Thermus thermophilus* (pdb:1EFW and pdb:6HHV) as a template with 50.59% and 51.27% identity, respectively. However, *Pyrococcus horikoshii* AsnRS (pdb: 1X54) was used as a template for *S. aureus* and *E. faecalis* AsnRSs (Q2FYH6 and A0A3N3KT82) homology models with 45.83% identity of both enzymes. All used templates are wild-type not mutant or engineering having the same enzyme function while the stereochemical quality, compatibility of 3D models with their amino acids 1D sequence and overall protein structures were evaluated for all constructed models using Ramachandran plot, Verify 3D and ProSA. As a result, SWISS models of *S. aureus* AspRS and *E. faecalis* AspRS and AsnRS were used for the docking study as they are the most validated models while in the case of *S. aureus* AsnRS, the SWISS model was excluded owing to the presence of Ser183 as an important amino acid residue for the active site in the outlier region of the Ramachandran plot and the MOE model was used instead. Then, the key amino acid residues responsible for Asp/Asn and AMP pockets were identified using docking and molecular dynamic studies of the enzymes with their natural substrates in the presence of magnesium ions and water molecules. Furthermore, the binding affinity

of the natural substrates inside their active sites was measured using the Desmond programme of Schrödinger creating a platform for inhibitors design.

2.5. Methods

2.5.1. Homology search

The protein sequences of AspRS and AsnRS in both microorganisms were obtained from the UniProtKB serve (286), with the Uniprot identifiers Q2FXU5 (SYD_STAA8) (strain NCTC 8325) and Q2FYH6 (SYN_STAA8) (strain NCTC 8325), Q833I2 (SYD_ENTFA) (strain ATCC 700802 / V583) and Q831X4 (SYN_ENTFA) (strain ATCC 700802 / V583) for *S. aureus* and *E. faecalis* AspRS and AsnRS respectively. AspRS consists of 588 and 589 amino acid residues in each monomer of both respective microorganisms while AsnRS contains 430 and 450 amino acid residues of *S. aureus* and *E. faecalis* respectively (286, 287, 310). A homology search was performed using SIB BLAST service (273, 274) accessible from the ExPASy server (275), which was used to align the query sequences (AspRS and AsnRS) of both microorganisms against the sequences in the protein data bank (276) and thus their close homologous proteins were identified. The alignment parameters and the thresholds, used for screening expected homologues, were the default values and BLOSUM62 comparison matrix. The phylogeny server (283) was used to build phylogenetic trees for both query proteins with their homologous proteins from different organisms.

2.5.2. Multiple sequence and structure alignment

The sequences of the query enzymes were aligned with protein sequences of their most related AspRS and AsnRS templates using Clustal Omega (271). *E coli* (pdb: 1EQR), *Pseudomonas aeruginosa* (pdb: 4WJ3), *Thermus thermophilus* (pdb: 1EFW), *Mycobacterium smegmatis* (pdb: 4O2D) for *S. aureus* AspRS and *Thermus thermophilus* (pdb: 5ZG8), *Pyrococcus horikoshii* (pdb: 1X54), *Elizabethkingia anopheles* (pdb: 6PQH), *Thermococcus kodakarensis* (pdb: 3NEL) for *S. aureus* AsnRS. Due to the high similarity in protein sequence between *S. aureus* and *E. faecalis* AspRS and AsnRS, the closet similar templates of *E. faecalis* AspRS and AsnRS are the same ones which used for *S. aureus* enzymes just using *Thermus thermophilus* with pdb: 6HHV instead of that one has pdb: 1EFW. In addition, the secondary structure of *S. aureus* and *E. faecalis* AspRS and AsnRS were determined using PSIPRED v3.3b (285).

2.5.3. 3D model building

For 3D model building of *S. aureus* and *E. faecalis* AspRS and AsnRS, Molecular Operating Environment (MOE) 2014.0901 software (265) and SWISS-MODEL server (268) were used making two models for each enzyme for comparison purpose to select the most validated one for docking study. In MOE software, AMBER99 force field was used for building all models based on their protein sequences after aligning them with their most similar templates. However, SWISS-MODEL is accessible via a web server which is easily used through uploading the FASTA format of the query protein sequence. Then, a sequence database of protein in the PDB with BLAST is searched to construct a model for any PDB hits. The standard protocol of homologue identification, sequence alignment, determining the core backbone and modelling loops and side chains is followed in SWISS-MODEL server (314, 315). The final *S. aureus* AspRS and AsnRS homology models were constructed using Thermus thermophilus AspRS (pdb: 1EFW) and Pyrococcus horikoshii (pdb: 1X54) crystal structures respectively while the final *E. faecalis* AspRS and AsnRS homology models were constructed using Thermus thermophilus AspRS (pdb: 6HHV) and Pyrococcus horikoshii (pdb: 1X54) crystal structures respectively. Ten intermediate models were generated for each enzyme and the final models were taken as the cartesian average of all the intermediate models. All minimisations were performed until RMSD gradient of 0.05 kcal mol^{-1} $Å^{-1}$ with the specified forcefield and partial charges automatically calculated.

2.5.4. Model validation

Ramachandran plot was used for evaluation of the stereochemical quality of the polypeptide backbone and side chains through the RAMPAGE server (288), while the compatibility of the 3D models with their own amino acids 1D sequence were examined using Verify 3D (289). The ProSA server (290) was used to check defaults in the three-dimensional protein structure based on statistical analysis. Validation data for Thermus thermophilus AspRSs (pdb:1EFW) and (pdb: 6HHV) and Pyrococcus horikoshii (pdb:1X54) templates was used as the baseline of comparison to evaluate the respective models.

2.5.5. Docking study

Aspartyl-adenylate and asparaginyl-adenylate as the natural substrates of AspRS and AsnRS respectively were built as ligands using MOE-builder and the energy minimised for each ligand until a RMSD gradient of 0.01 Kcal mol^{-1} $Å^{-1}$ with MMFF94 forcefield and partial charges automatically calculated. These ligands were docked by running MOE-Dock with default setting: Placement: Triangular Matcher, Rescoring1: London ΔG, 30 poses were constructed for each ligand and the best scoring model-ligand complexes were selected. The ligand interactions were visualised using the MOE ligand interaction simulation (265).

2.5.6. Molecular dynamic

All molecular dynamic simulation studies were performed using Schrodinger 2017-4 platform in three following stages: structure preparation, ionization state correction and finally molecular dynamic. In the first step, the selected docked pose of enzyme with ligand is imported and prepared using default local host of protein preparation wizard in Maestro for overall optimisation including assigning bond orders, adding hydrogen, and correcting incorrect bond types. Then it is minimised after water and salt addition using OPLS3 force field for removing any atoms clashes, relaxing side chains and making other modifications. The orthorhombic water box (volume = 501882 Å3) allowed for a 10 Å buffer region between protein atoms and box sides. Overlapping water molecules were deleted, and the systems were neutralised with Na^+ ions and salt concentration 0.15 M. The simulation with Desmond was started after identification a 100 nano-second simulation time and selecting CPU processing unit to generate an approximate 1000 frames. Energy and trajectory atomic coordinate data were recorded at each 1.2 ns. RMSD plots were constructed and simulation interaction diagrams generated to examine binding interactions during the MD simulation.

2.5.7. Binding affinity (ΔG) calculations

Binding free energy of aspartyl-adenylate and asparaginyl adenylate with AspRS an AsnRS in both *S. aureus* and *E. faecalis* respectively were calculated using Prime/MMGBSA (306) which is available in Schrödinger Prime suite (308). The

calculation of the binding affinity (ΔG) is based on each frame from the point where the complex reached equilibrium to the final frame of the MD simulation.

Chapter 3: Sulphonyl piperazinyl methanone derivatives

(Series 1)

3. Introduction

To assist in the design of AspRS/AsnRS dual competitive inhibitors, an understanding of the natural substrate, aminoacyl adenylate (aa-AMP), is required. Aa-AMP is the natural substrate of all aaRS enzymes and consists of three main components; amino acid, linker and adenine base (Figure 96). The first component is essential for binding in the amino acid pocket while the other two components occupy the AMP pocket. Aa-AMP is a labile active intermediate and any general replacement by a non-hydrolysable bio-isostere would lead to a similar interaction with the enzyme (124). The replacement of aa-AMP by aminoacyl sulfamoyl adenylate (Figure 97, structure 37) (316, 317) or amino alkyl adenylate (Figure 97, structure 38) (318-320), or an amide linkage (321) are useful, however the phosphoramidate linkage found in some aaRSs inhibitors, such as, Agrocin 84 (Figure 11) is unstable in acidic and basic environments and in physiological conditions (322, 323). Those aaRS inhibitors bearing a sulfamoyl linkage are the most potent analogues described owing to the higher stability compared with the labile phosphoanhydride linkage (124). In addition, the electrons distribution of the sulfamoyl linkage closely resembles that of aa-AMP making the formation of the same hydrogen bonds possible in the hydrophilic cleft of aaRS enzymes (317). One of the important structural features for the binding of substrates with their cognate class II aaRS enzymes is the carbonyl group next to the amino acid. The presence of this group in a sulfamoyl linkage is not only crucial for recognition by class II aaRS enzymes but also for stabilisation of the transition state through its ability to delocalise the negative charge (316, 317, 321, 322). Therefore, the design of novel AspRS/AsnRS inhibitors focuses on exploiting the potency of the sulfamoyl linkage in the presence of the carbonyl group next to the amino acid or bio-isosteres (319). Regarding the adenine base, a large polar substituent or heterocycles such as tetrazole or thiazole can be useful as a replacement for adenine (196, 324, 325). However, any modifications of adenine base structure or replacement by other non-polar mimics can be effective in increasing the selectivity for bacterial class II aaRS enzymes (124). By mimicking the sulfamoyl adenosine structure, the designed compounds in this project consist of amino acid or a bio-isostere, a linker with variation in the length depending on its ability to completely fill the active site of the modelled enzyme, while the third group consists of aryl/biaryl moieties as replacements of the adenine base

(Figure 96) (Table 18). In addition, introduction of different substituents (R, see Table 18) in the non-polar adenine replacement that have different chemical properties will be important to evaluate and explore the overall pharmacodynamic and pharmacokinetic properties of the novel designed inhibitors, especially if the targeted enzymes have not been investigated yet. Any small addition to the designed molecules will affect the overall electronic properties, solubility and steric dimensions of the molecules, which may improve fit with the enzyme binding sites and enhance binding interactions (326).

This chapter is divided into five parts as follows:

- Results and discussion
- Docking studies
- Molecular dynamic studies
- Biological screening
- Methods

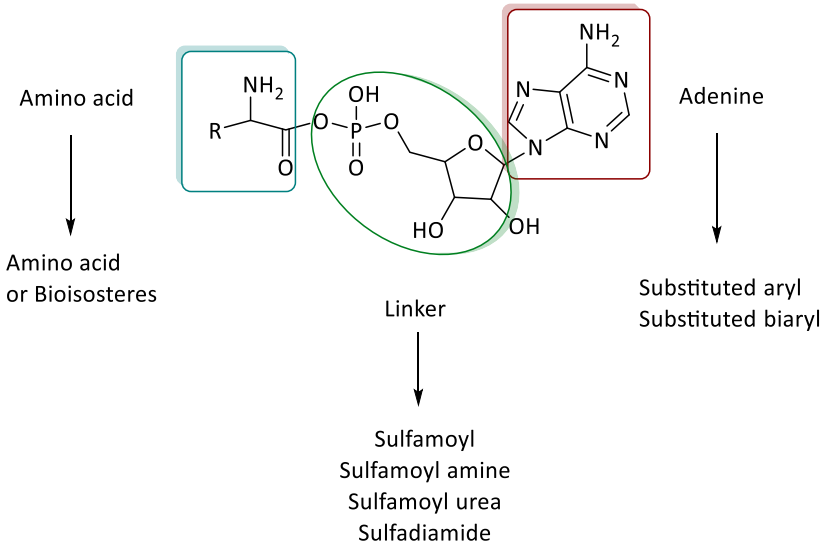

Figure 96: General structure of aminoacyl adenylate (aa-AMP).

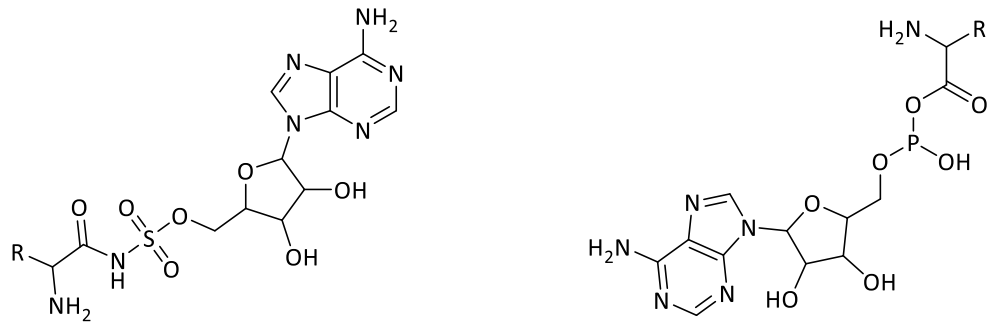

Figure 97: General chemical structure of aminoacyl sulfamoyl adenosine and amino alkyl adenylate.

Table 18: General chemical structures of scheme 1 AspRS and AsnRS inhibitors (**7**, **10** and **14**).

Series	General chemical structures	R groups
1	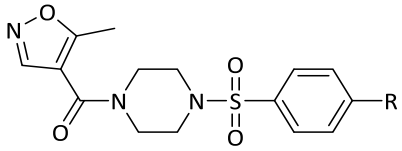	CH_3, NO_2, C_6H_5, $C_6H_4OCH_3$, C_6H_4F, C_6H_4Cl
1	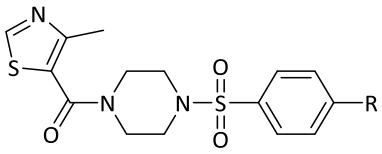	CH_3, NO_2, C_6H_5, $C_6H_4OCH_3$
1	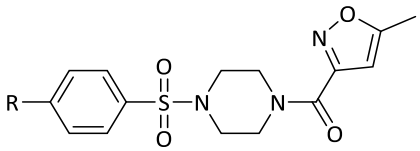	CH_3, NO_2, C_6H_5, $C_6H_4OCH_3$

3.1. Synthetic pathway for sulphonyl piperazinyl methanone derivatives (7, 10 and 14)

The first series consists of sulfamoyl piperazine derivatives bound to 4-carbonyl-5-methylthiazole, 3-carbonyl-5-methylisoxazole or 5-carbonyl-4-methylisoxazole. The amino acid component of aa-AMP is replaced by methyl-thiazole or methyl-isoxazole rings as classic bio-isosteres, combined with piperazine-sulfamoyl as the linker and substituted aryl or biaryl moieties instead of the adenine base. The synthetic pathways are shown in Schemes 5a-c and involved the following steps:

- Nucleophilic reaction of excess piperazine with substituted benzene sulfonyl chlorides (**3a**-**f**)
- Conversion of carboxylic acids to acid chlorides in the presence of thionyl chloride (**6**, **9**, **12**)
- Nucleophilic reaction of acid chlorides with sulfonyl piperazine derivatives (**7a**-**f** and **10a**-**d**)
- Amide bond formation using 1, 1'-carbonyldiimidazole (CDI) (**14a**-**d**)

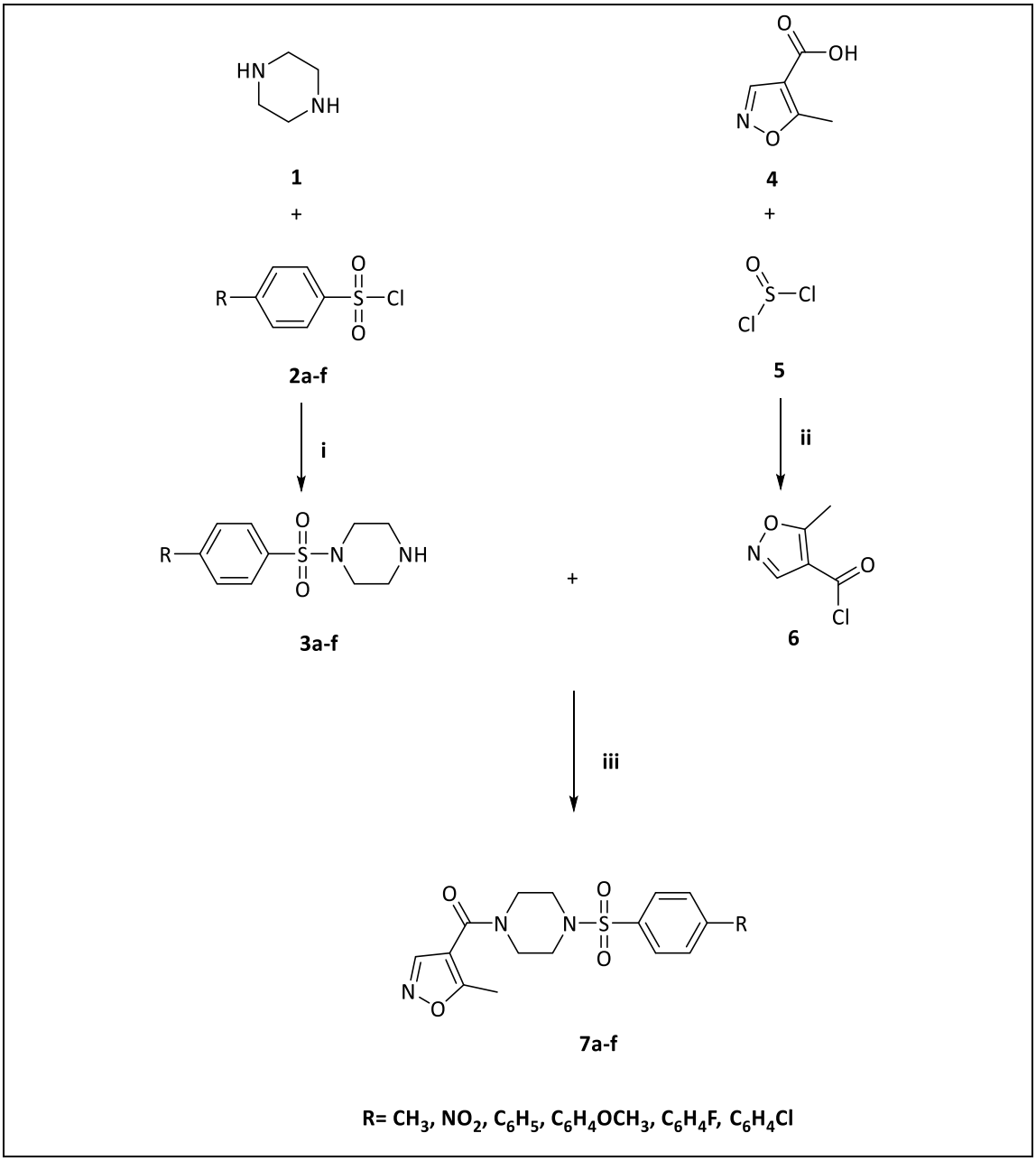

Scheme 5a: Synthetic pathway for (5-methylisoxazol-4-yl)(4-((4-phenyl)sulfonyl)piperazin-1-yl)methanone derivatives (**7a**-**f**). *Reagents and conditions*: (i) Et_3N, dry $CHCl_3$, 0 ^oC then rt 3-24 h, (ii) $SOCl_2$, 50 ^oC, 3 h, (iii) THF, 65 ^0C, 3-24 h.

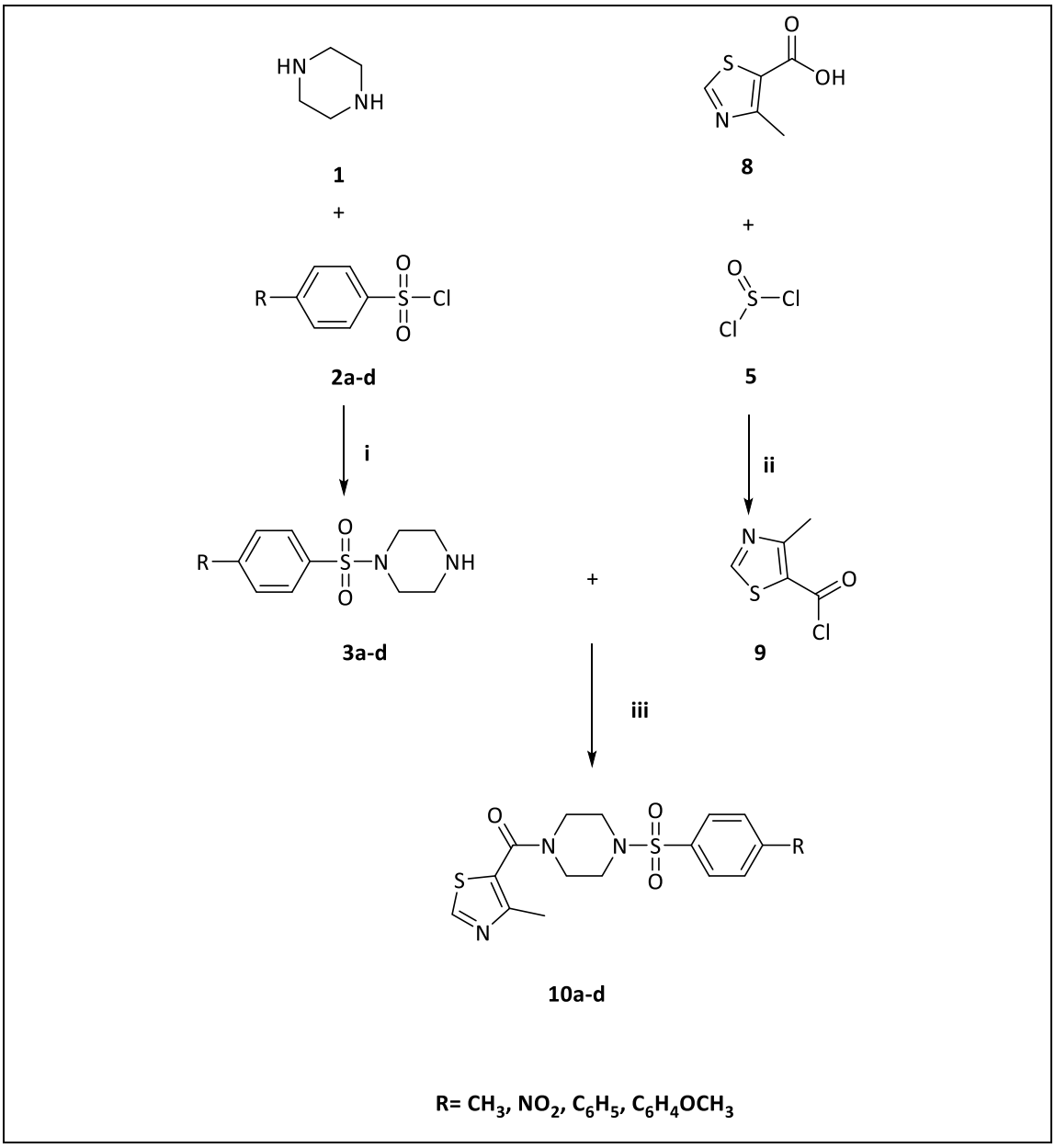

Scheme 5b: Synthetic pathway for (4-methylthiazol-5-yl)(4-((4-phenyl)sulfonyl)piperazin-1-yl)methanone derivatives (**10a-d**). *Reagents and conditions*: (i) Et_3N, dry $CHCl_3$, 0 ^oC then rt 3-24 h, (ii) $SOCl_2$, 50 ^oC, 3 h, (iii) THF, 65 ^0C, 3-24 h.

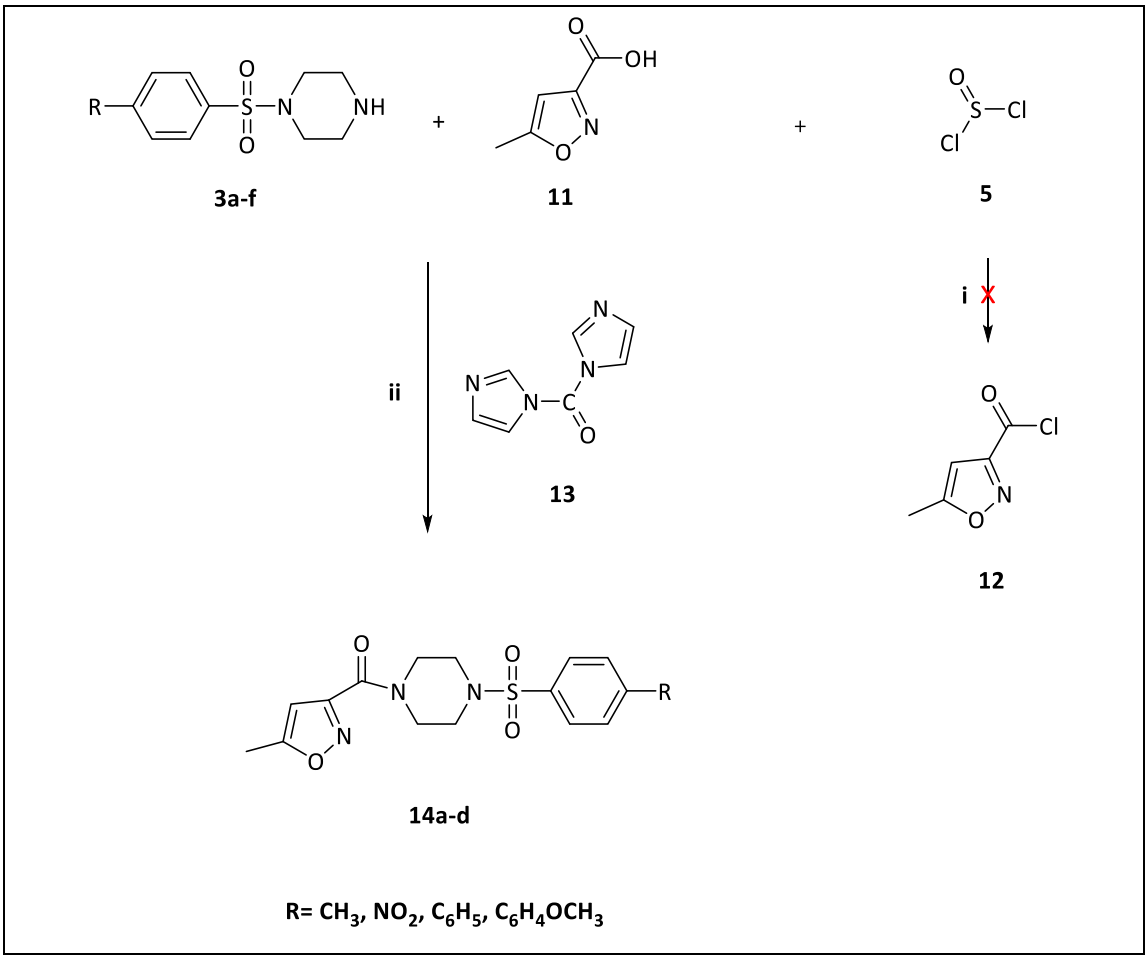

Scheme 5c: Synthetic pathway for (5-methylisoxazol-3-yl)(4-((4-phenyl)sulfonyl)piperazin-1-yl)methanone derivatives (**14a-d**). *Reagents and condition*: (i) $SOCl_2$, 50 °C, 3 h (ii) DMF, 1 h, rt then 0 °C, rt, 24 h.

3.1.1. Synthesis of sulfonyl piperazine derivatives (3a-f)

The sulfonyl piperazine derivatives were prepared by reaction of excess piperazine (**1**) with sulfonyl chloride derivatives (**2a-f**) in the presence of Et_3N as the base at room temperature for a period ranging from 3 hours to overnight (Scheme 5) (327). Using piperazine in excess is required to decrease the percentage of *N, N'*-disubstituted piperazine and increase the chemo-selectivity of the reaction (328, 329). Some of the produced compounds were pure enough after aqueous work-up and ready to proceed to the next step of the synthetic pathway while compounds **3e** and **3f** required an additional wash with acetonitrile to separate them from the disubstituted side product, resulting in lower yields (Table 19). High resolution mass spectrometry confirmed the molecular weight of the *N*-mono-substitution piperazine derivatives and ^{1}H NMR indicated the presence of the piperazine NH signal from 1 ppm to 2 ppm

in all compounds except **3b** and **3e**. Compound **3b** is previously described and the melting point confirmed that compound **3b** was successfully prepared (327). The chemical structure of compound **3e** was confirmed through ^{13}C NMR and high resolution mass spectrometry and the successful preparation of the next step is a further validation of their structures.

Table 19: Identification data for sulfonyl piperazine derivatives (**3a**-**f**).

Compd	R	Yield (%)	mp (^0C)	Appearance
3a	CH_3	96	104-106	White crystals
3b	NO_2	74	150-152	Yellow powder
3c	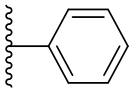	96	174-176	White powder
3d	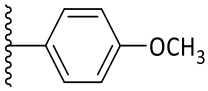	91	175-177	White powder
3e	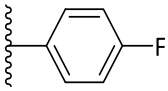	46	128-130	White powder
3f	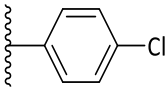	54	168-170	Shiny white powder

3.1.2. Synthesis of acid chlorides (6 and 9)

The second synthetic step generates acid chloride derivatives using thionyl chloride in excess as both the reagent and solvent (scheme 5a and 5b) (330). 5-Methylisoxazole-4-carbonyl chloride (**6**) and 4-methyl thiazole-5-carbonyl chloride (**9**) were successfully prepared in good yields using thionyl chloride method (Table 20). However, the preparation of 5-methylisoxazol-3-carbonyl chloride (**12**) using this method was unsuccessful possibly owing to reduced nucleophilicity of the hydroxyl group as a result of the inductive effect of the electronegative nitrogen atom. The N of 5-methylisoxazol-3-carboxylic acid (**11**) is positioned close to the carboxylic acid group reducing the availability of the lone pair on the carboxylic OH. By contrast, the presence of the electron donating methyl group of 5-methylisoxazole-4-carboxylic acid (**4**) is closer to the carboxylic acid, resulting, through delocalisation, in the lone pair of the OH being more available for nucleophilic reaction with thionyl chloride. Both acid chlorides, (**6** and **9**), were obtained in good yields (Table 20), however they were found to be very reactive so were used in the next step without any further purification.

Table 20: Identification data of acid chlorides (**6**-**12**).

Compd	Structure	Yield (%)	Appearance
6	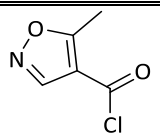	79	Yellow oil
9	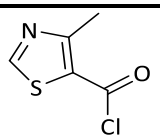	99	White powder
12	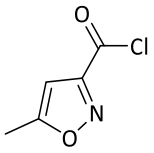	-	No reaction

3.1.3. Synthesis of sulfonyl piperazinyl methanone derivatives (7a-f, 10a-d and 14a-d)

The acid chlorides (**6** and **9**) were reacted with sulfonyl piperazine derivatives (**3a**-**f**) using tetrahydrofuran (THF) as solvent and the reaction mixture heated at 65 ^{O}C for a period of time ranging from 3 h to 24 h (Scheme 5a and 5b) (330). The products **7a**-**f** and **10a**-**d** were obtained in good yields and ^{1}H NMR, ^{13}C NMR spectra and either elemental analysis or HRMS confirmed the structures and purity. For example, the ^{1}H NMR spectrum of compound **7f** showed piperazine as two broad singlet peaks integrated for 4 protons each, isoxazole protons as two singlet peaks, one is for methyl group and other for *CH* while aromatic protons appear in the aromatic region as four doublet peaks, each integrated for 2 protons (Figure 98). As preparation of 5-methylisoxazole-3-carbonyl chloride (**12**) was unsuccessful, the sulfonyl piperazinyl methanone derivatives (**14**) were generated using an amide coupling reaction (Scheme 5c). Reaction of 5-methylisoxazol-3-carboxylic acid (**11**) and 1,1'-carbonyldiimidazole (CDI) (**13**) as a coupling reagent formed the acyl imidazole intermediate, this activated intermediate then reacted with the respective sulfonyl piperazines (**3a**-**d**) to form the final coupled compounds (**14**) (Scheme 6) (Table 21) (331-333).

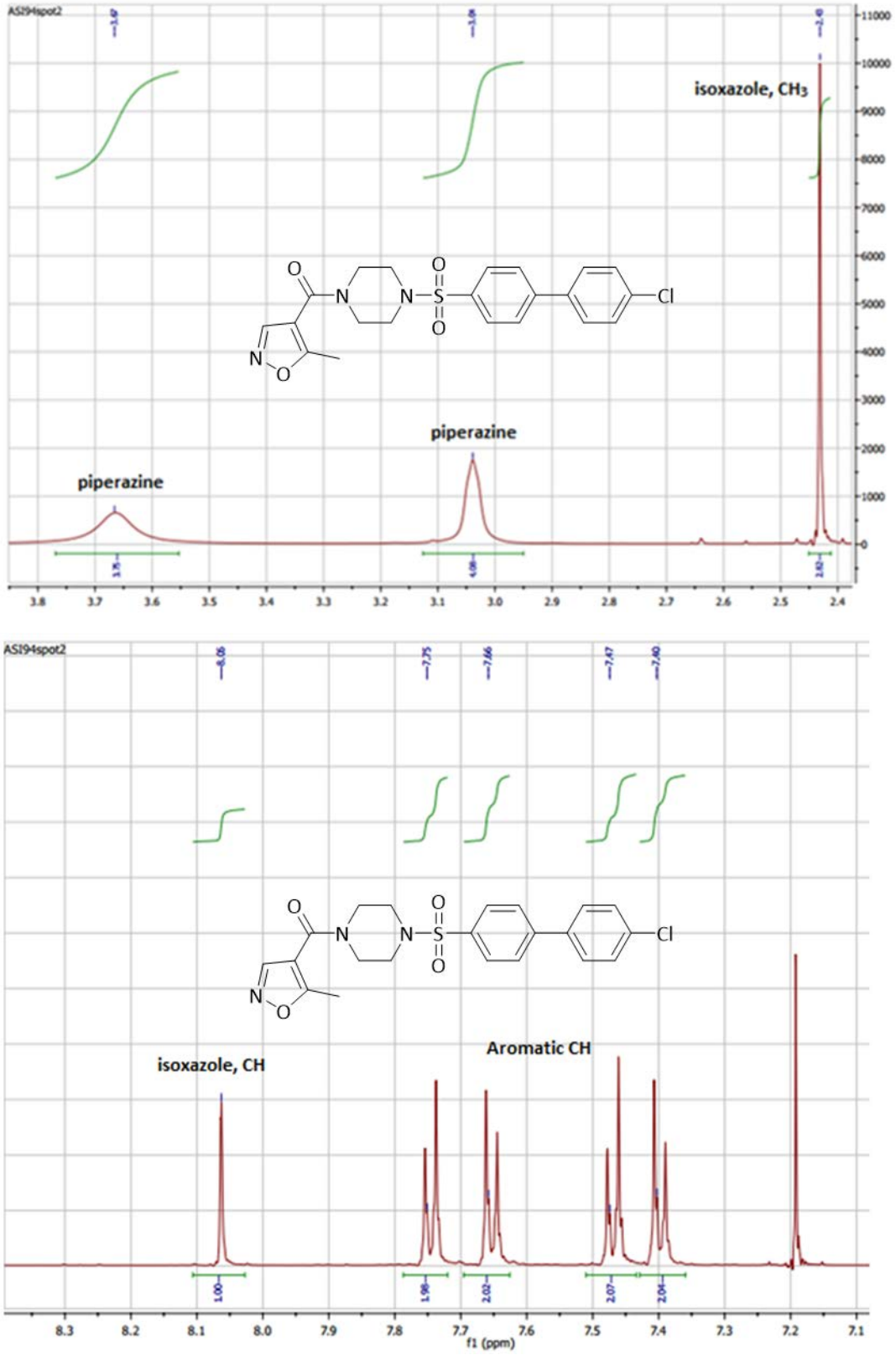

Figure 98: ^{1}H NMR spectrum of compound **7f**.

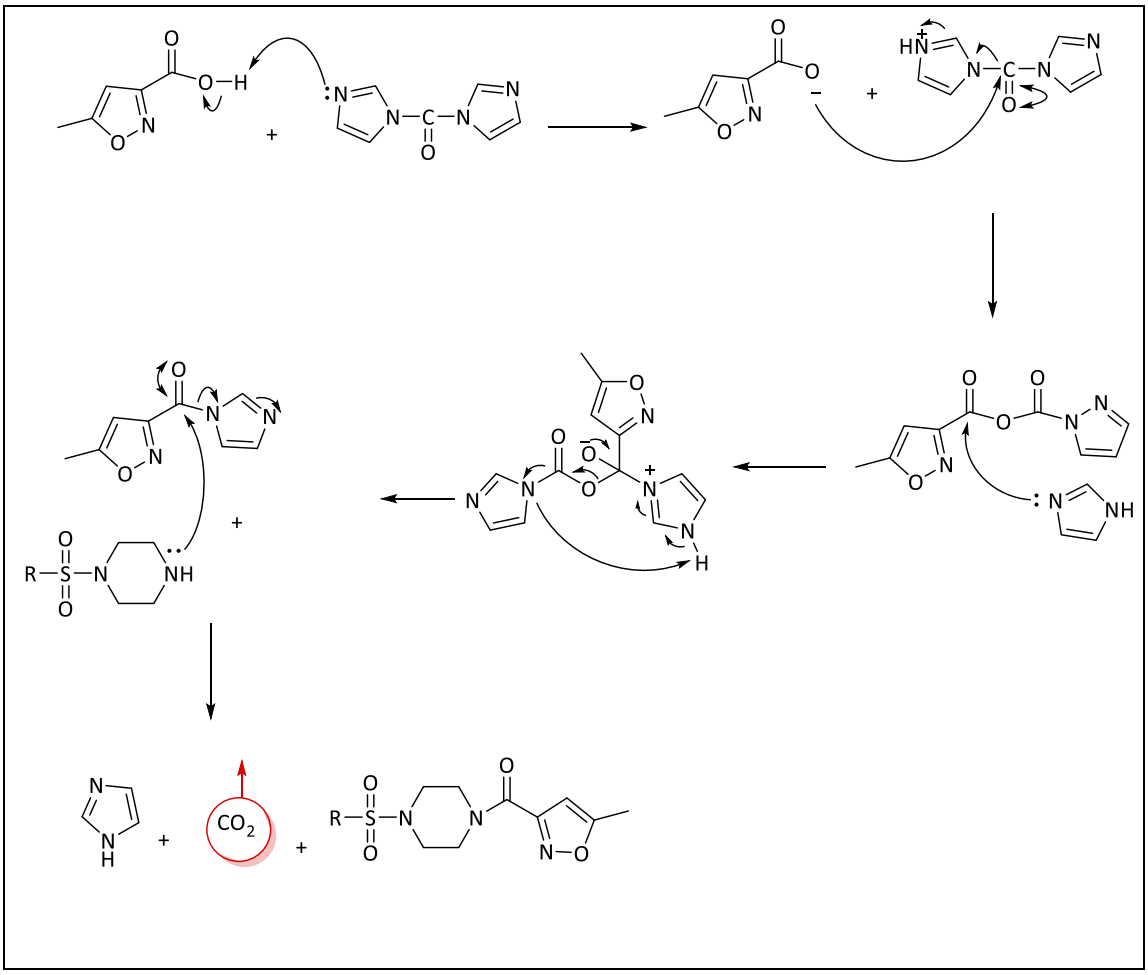

Scheme 6: Mechanism of coupling reaction using CDI.

Table 21: Identification data of sulfonyl piperazinyl methanone derivatives (**7a**-**f**, **10a**-**d** and **14a**-**d**).

Compd	R	Yield (%)	mp (^{O}C)	Appearance
7a	CH_3	88	138-140	White powder
7b	NO_2	99	168-170	Pale powder
7c	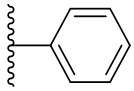	55	158-160	Crystalline solid
7d	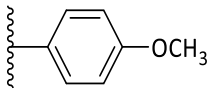	57	198-200	White powder
7e	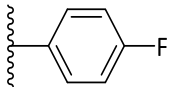	52	172-174	Colourless needles

7f	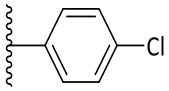	59	190-192	Pale yellow crystalline solid
10a	CH_3	86	143-144	Yellow powder
10b	NO_2	73	190-200	Yellow granules
10c	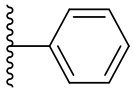	26	-	Yellow oil
10d	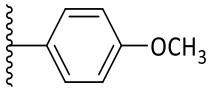	78	212-214	White crystals
14a	CH_3	68	148-150	Light brown crystalline solid
14b	NO_2	99	170-172	Pale yellow solid
14c	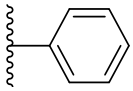	26	150-152	White powder
14d	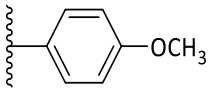	90	198-200	White powder

3.2. Docking studies

A docking study of the final compounds of series 1 with *S. aureus* and *E. faecalis* AspRSs and AsnRSs was performed to determine their binding interactions with the active sites of the respective aaRS enzymes. The docking study showed that the compounds interacted with the same amino acid residues observed for the aa-AMP natural substrates. Compounds **7a**-**b**, **10a**-**b** and **14a**-**b** were easily flipping inside the pockets owing to the smaller size and inability to completely fill the pocket. However, compounds **7c**-**f**, **10c**-**d** and **14c**-**d** showed a good fit within the pocket and hydrogen bonding interactions were observed.

3.2.1. Docking studies of *S. aureus* AspRS

By alignment of series 1 compounds with aspartyl adenylate inside the active site of *S. aureus* AspRS (Figure 99), the amino acid residues responsible for binding interactions were identified (Table 22). The carbonyl methyl isoxazole or thiazole moieties of series 1 compounds occupied the pocket of Asp and interacted with the same amino acid

residues observed for aspartic acid. Gln189, Ser199, Gln210, Asp239 and Gly488 made a network of hydrogen bonds with the isosteric group of Asp (Figures 100 and 101) while His452 and Gln237, which represent the histidine and flipping loops, are shown close to the isoxazole and thiazole rings indicating the successful recognition of them by the AspRS and selecting them for Asp replacement, which could be efficient for the activity (Figures 101-103). The phenyl sulfonyl piperazine derivatives in this series occupied the AMP pocket of *S. aureus* AspRS and bound with the key amino acid residues Glu485, Gly537, Asp539 and Arg540 (Figures 100-103). The benzene ring of the toluene moiety of compound **7a** interacted through cation-π interaction with Arg540 (Figure 100) while the nitro group in compounds **7b** and **10b** formed hydrogen bonds either direct or via a water molecule with the key amino acid residues responsible for the AMP pocket (Figures 101 and 102). In compound **7d**, the methoxy group was bound with Arg540 (Figure 103) while fluoro- and chloro- groups of compounds **7e** and **7f** did not show any type of interactions during the docking study. As Mg^{2+} ion is an important cofactor in aaRSs having structural and catalytic roles for stabilisation of the transition state of aminoacyl adenylate, the docking studies of series 1 compounds showed that Mg^{2+} ion was bound to the sulfamoyl linkage and/or the carbonyl group through water molecules in compounds **7a**, **7b**, **7d** and **10b** (Figures 100-103).

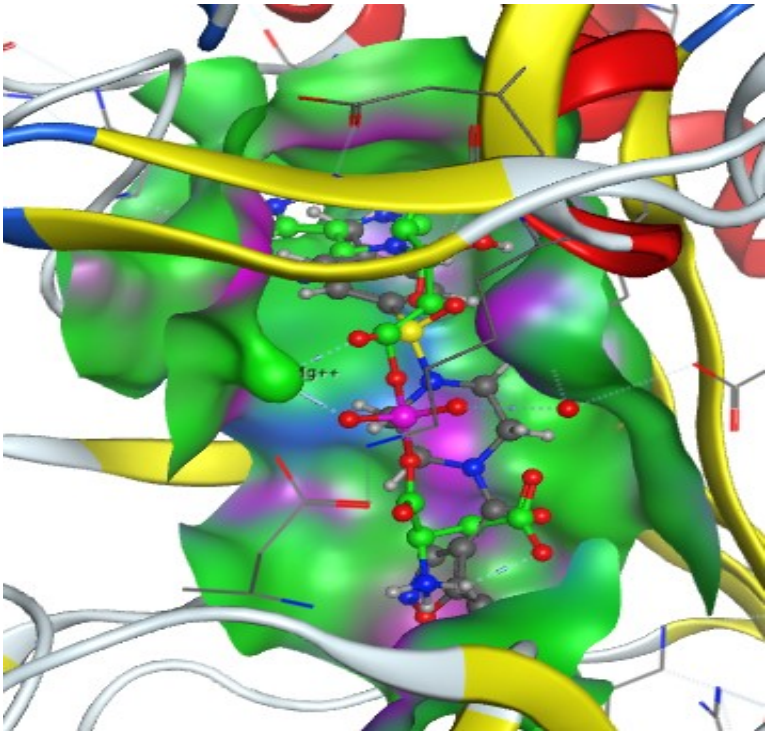

Figure 99: Alignment of compound **7a** (grey) with aspartyl adenylate (green) in the active sites of *S. aureus* AspRS.

Table 22: Binding interactions of series 1 compounds with the amino acid residues of the binding sites of *S. aureus* AspRS.

Ligands	Aspartic acid pocket	AMP pocket
Aspartyl-adenylate	Gln201, Lys204, His452, Gly488, Ser490, Arg492 and Asp239	Arg223, Phe235, Arg540, Gln232, Gln237 and Glu485
7a	Ser199, Gln201, Asp239, Gln237, Gly488 and His452	Arg223 and Arg540
7b	Ser199, Cys221, Asp239, Gln237 and Gly488	Arg223, Asp539 and Arg540
7c	Ser199, His452 and Gly488	Glu485 and Asp478
7d	Gln198, Ser199, Cys221, Asp239, Gln237, His451, His452 and Gly488	Arg540 and Glu485
7e	Ser199, Gln237, His451, Gly488, Gly489 and Arg492	Arg540

7f	Ser199, Asp239, Gln237, Gly488, His451 and His452	Phe235, Asp478, Glu485 and Arg540
10a	Ser199, Cys221, Asp239, Gln237, Gly488, His451 and His452	Arg223, Arg231, Phe235, Glu485 and Arg540
10b	Ser199, Cys221, Gln237 and Asp239	Gly537, Asp478, Glu485, Asp539 and Arg540
10c	Ser199, Gln237, His451, His452, Gly488, Gly489 and Arg492	Asp478 and Glu485
10d	Ser199, Gln201, Gln237, Asp239 His452 and Gly488	Arg231 and Glu485
14a	Ser199, Asp239, Gln237, Gly488 and His452	Glu485 and Arg540
14b	Ser199, Asp239, Gln237 and Gly488	Asp478, Glu485, Gly537 and Arg540
14c	Ser199, Asp239, Gln237, Gly488 and His452	Asp478 and Glu485
14d	Ser199, Gln237 Asp239, His451 and His452	Glu485, Arg540, Asp478 and Glu485

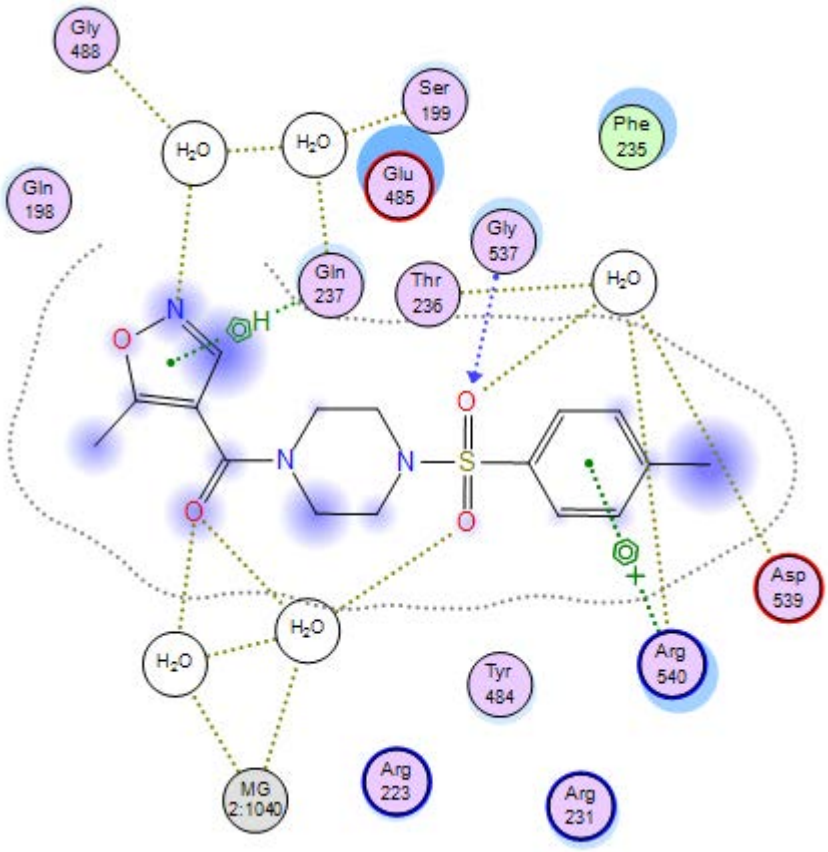

Figure 100: 2D binding interactions of compound **7a** with *S. aureus* AspRS.

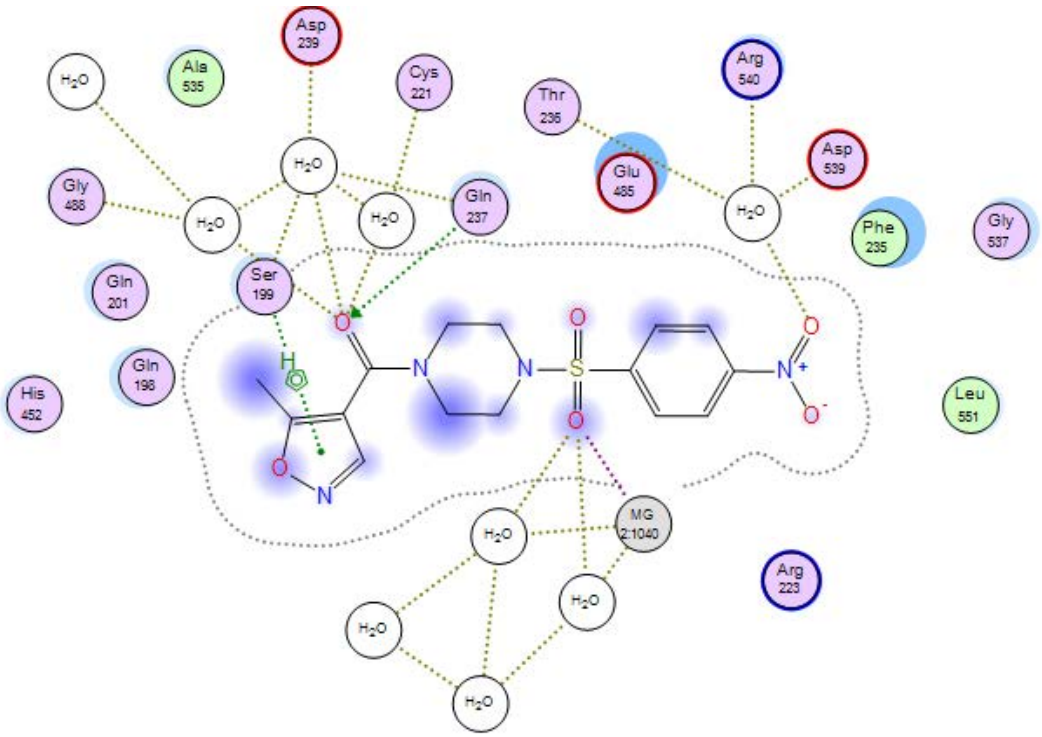

Figure 101: 2D binding interactions of compound **7b** with *S. aureus* AspRS.

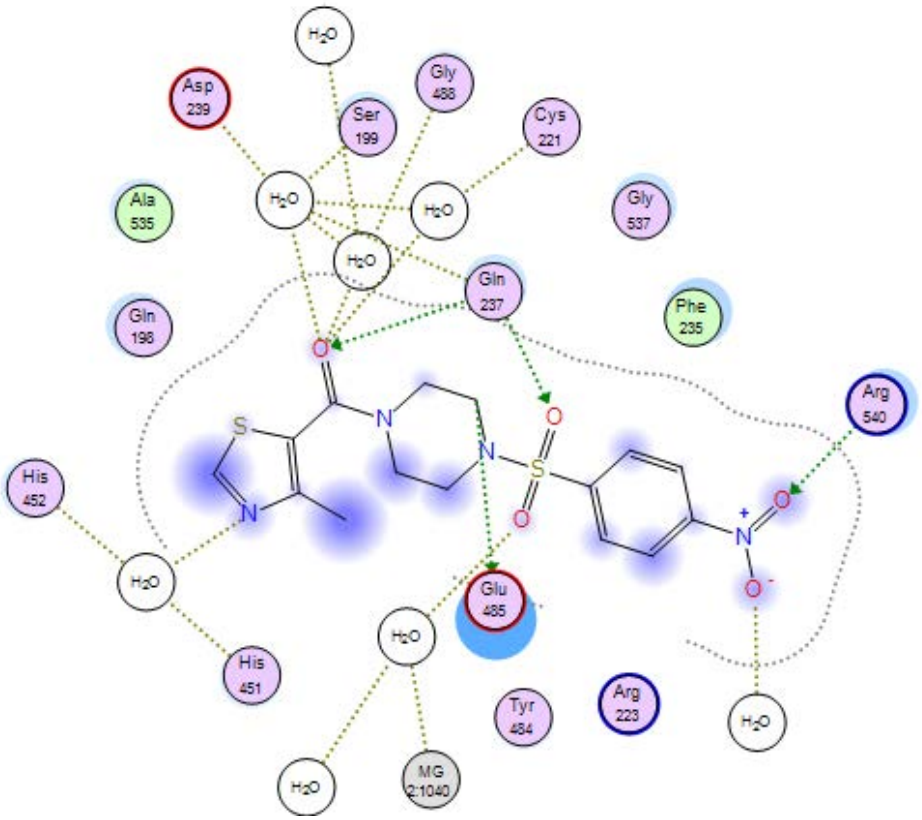

Figure 102: 2D binding interactions of compound **10b** with *S. aureus* AspRS.

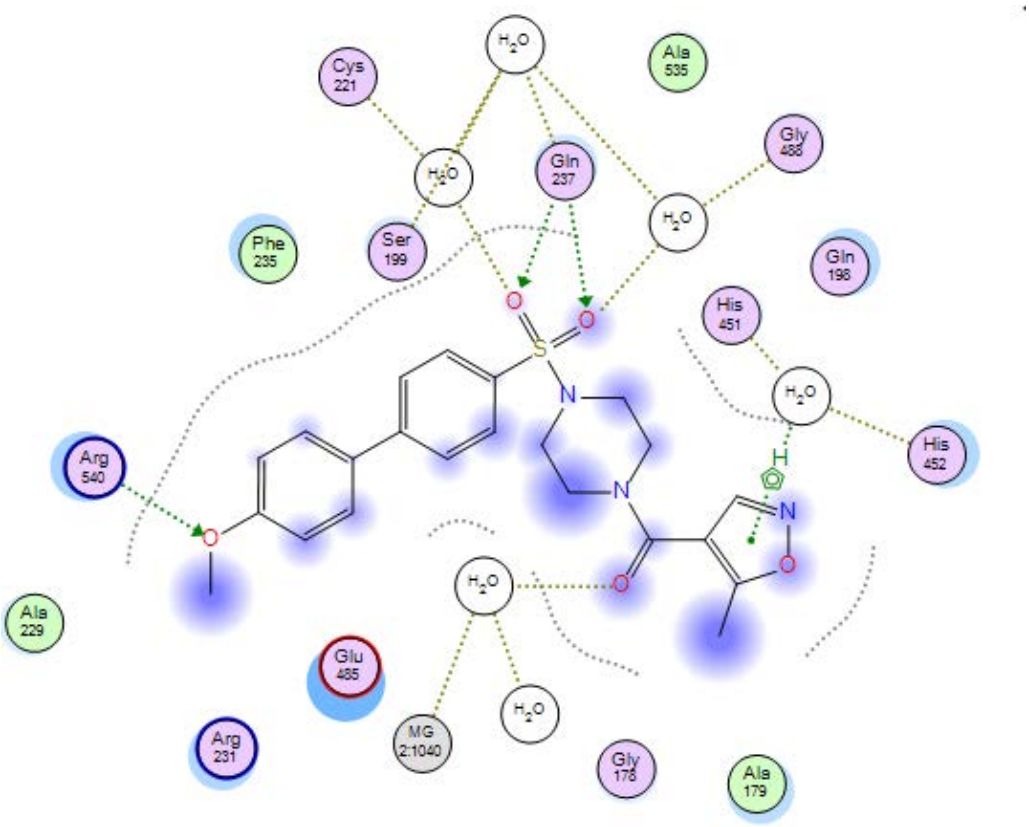

Figure 103: 2D binding interactions of compound **7d** with *S. aureus* AspRS.

3.2.2. Docking studies of *S. aureus* AsnRS

By alignment of series 1 compounds with asparaginyl adenylate inside the active site of *S. aureus* AsnRS (Figure 104), the amino acid residues responsible for binding interactions were identified (Table 23). The role of water molecules is important for assisting AsnRS for asparagine recognition, in the docking study of series 1, compound **7a** showed the network of water molecules interactions between the isosteric moiety of asparagine and the key amino acid residues inside asparagine active site more than that in compound **14a** (Figures 105 and 106). Glu163 and Gln185 interact via water molecules with isoxazole and thiazole rings in most series 1 compounds and the benzene ring of all derivatives showed good π-π stacking interaction with Phe219, which is a key amino residue in the adenine pocket (Figures 107 and 108). In the docking study of AsnRS with compounds **7a**-**e**, **10b**-**d** and **14d**, Arg360, one of the conserved amino acid residues for asparagine recognition formed a hydrogen bond with the amino acid isosteric moiety (Figures 108-110), while the docking study of compounds **7d** and **10b**-**d** showed that there was an additional hydrogen bonding interaction with the second key amino acid residue (Glu223) for asparagine recognition (Figure 109). The docking study of compounds **7d** and **10d** with *S. aureus* AsnRS showed that the methoxy group formed a hydrogen bonding interaction with Leu216 (Figure 110) but no interaction was observed with the fluoro and chloro groups of compounds **7e** and **7f** respectively. The docking studies of compounds **7c**, **7d** and **14a** showed the role of Mg^{2+} ion not only for stabilisation of the sulfamoyl linkage but also for binding the important amino acid residues (Lys326 and Asp344), which are responsible for Mg^{2+} ion binding interactions with asparaginyl adenylate intermediate in *S. aureus* AsnRS (Figures 106, 108 and 110).

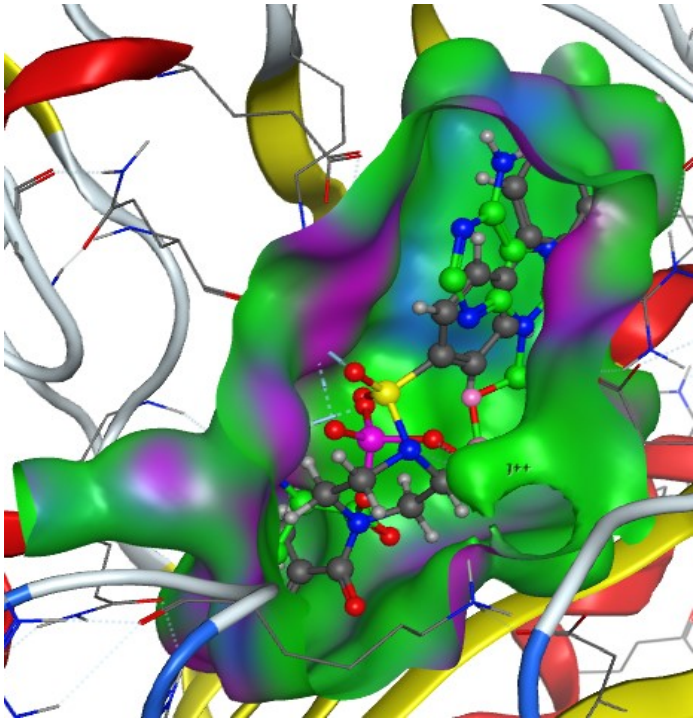

Figure 104: Alignment of compound **14d** (grey) with asparaginyl adenylate (green) in the active sites of *S. aureus* AsnRS.

Table 23: Binding interactions of series 1 compounds with the amino acid residues of the binding sites of *S. aureus* AsnRS.

Ligands	Asparagine pocket	AMP pocket
Asparaginyl-adenylate	Glu223 and Arg360	Arg206, Glu208, Arg214, His215, Phe219, Glu353, Gly356, Gly401 and Arg404
7a	Gln185, Gly224 and Arg360	His215, Phe219, Glu353, Gly356 and Arg404
7b	Gln185, Gly224 and Arg360	Glu163, Ser166, Glu167, Arg206, His215, Phe219, Asp299, Phe300, Asp344, Glu353 and Arg404
7c	Gln185 and Arg360	Glu163, Arg206, Phe219, Asp344, Glu353 and Arg404

7d	Gln185, Glu223 and Arg360	Glu163, Arg206, Leu216, Phe219, Asp344, Glu353 and Arg404
7e	Gln185 and Arg360	Glu163, Arg206, His215, Leu216 and Glu353
7f	Gln185 and Glu223	Glu163, Arg206, His215, Phe219, Glu353, Gly356 and Arg404
10a	Gln185 and Gly399	Leu216, Phe219, Arg206, Glu353 and Gly356
10b	Gln185, Glu223, Gly224 and Arg360	Glu163, Arg206, Phe219, Glu353 and Arg404
10c	Gln185, Glu223, Gly224 and Arg360	Arg206, Phe219, Glu353 and Gly356
10d	Gln185, Gly224, Glu223, Arg360 and Glys397	Glu163, Arg206, Leu216, Glu353, Gly401 and Arg404
14a	Asp344 and Lys326	Glu163, Phe219, Gly356 and Arg404
14b	Asp344 and Lys326	Glu163, Ser166, Glu167, Arg214, Phe219, Glu353 and Arg404
14c	Gln185, Glu223 and Ser358	Glu163, Arg206, His215, Phe219, Glu353 and Arg404
14d	Gln185, Ser358 and Arg360	Glu163, Arg206, His215, Phe219, Glu353 and Arg404

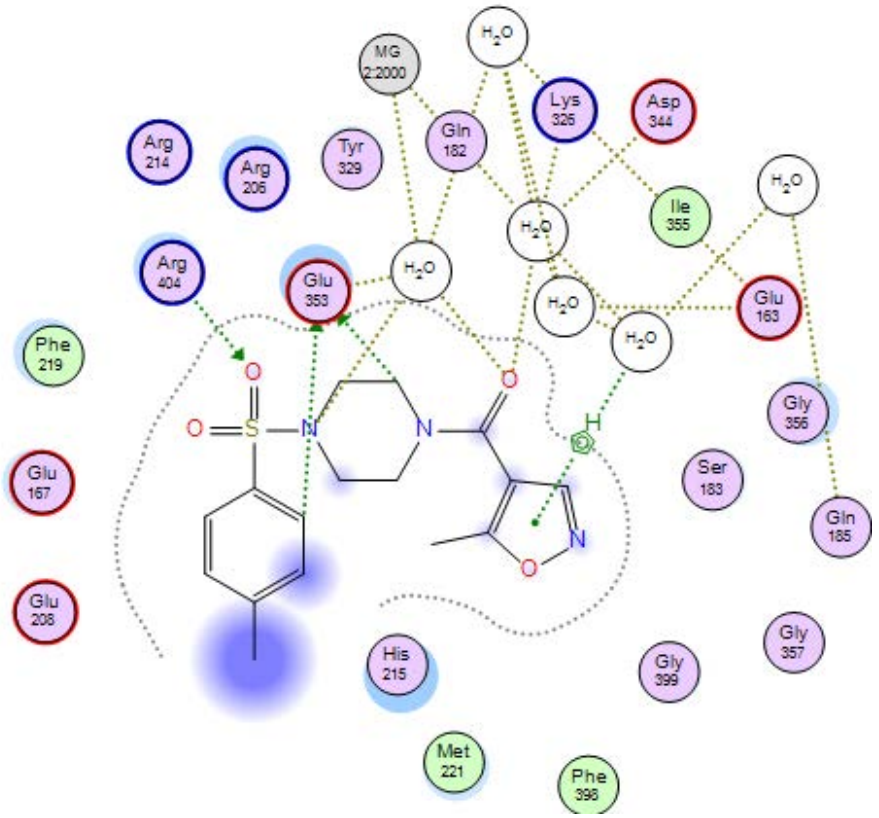

Figure 105: 2D binding interactions of compound **7a** with *S. aureus* AsnRS**.**

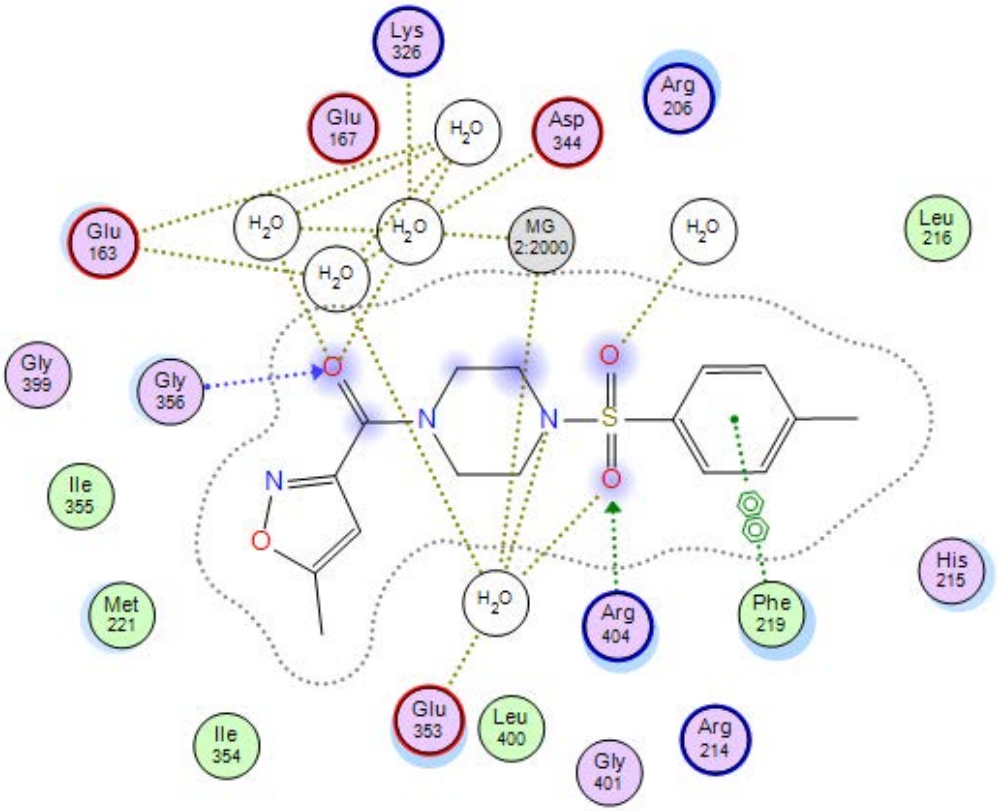

Figure 106: 2D binding interactions of compound **14a** with *S. aureus* AsnRS.

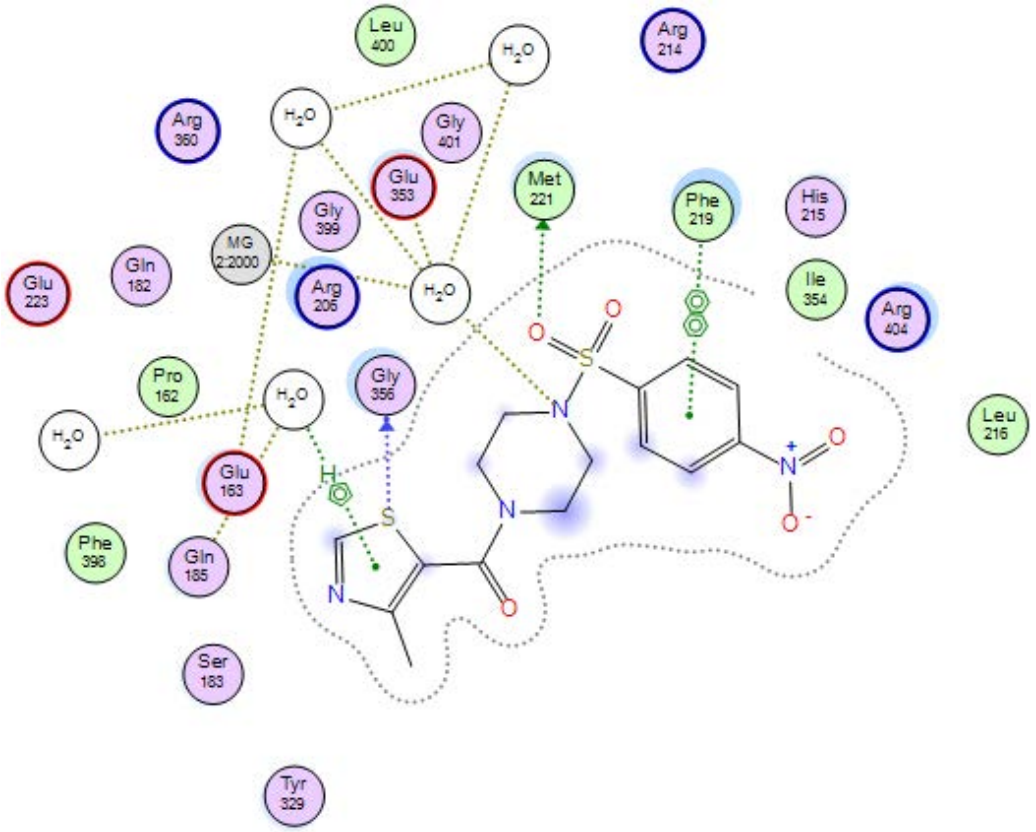

Figure 107: 2D binding interactions of compound **10b** with *S. aureus* AsnRS.

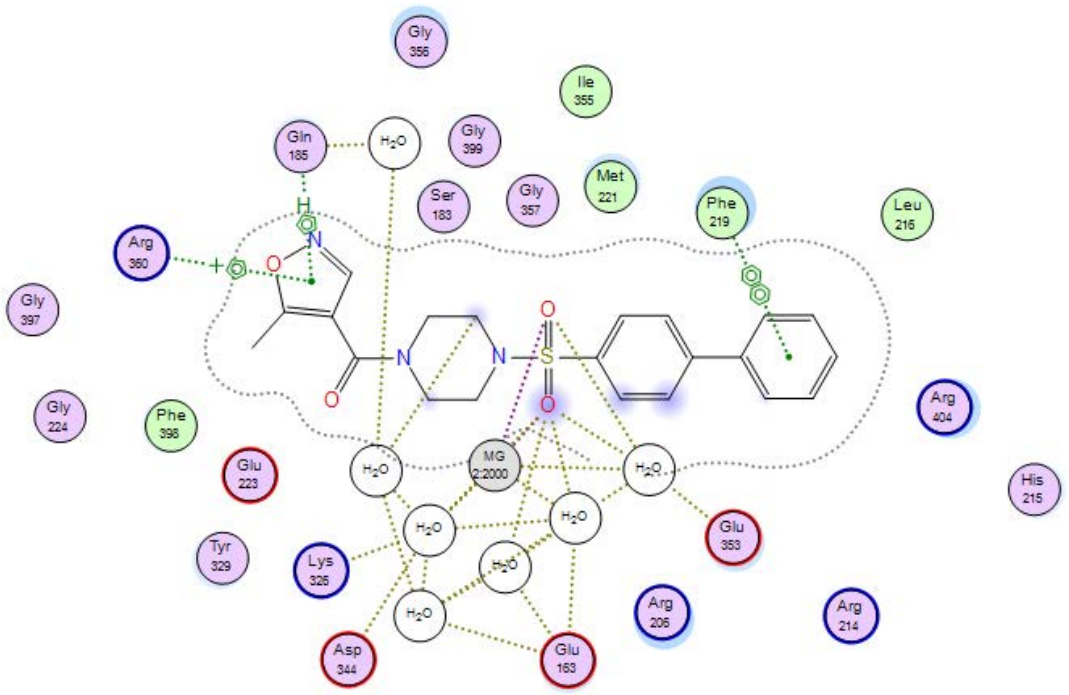

Figure 108: 2D binding interactions of compound **7c** with *S. aureus* AsnRS.

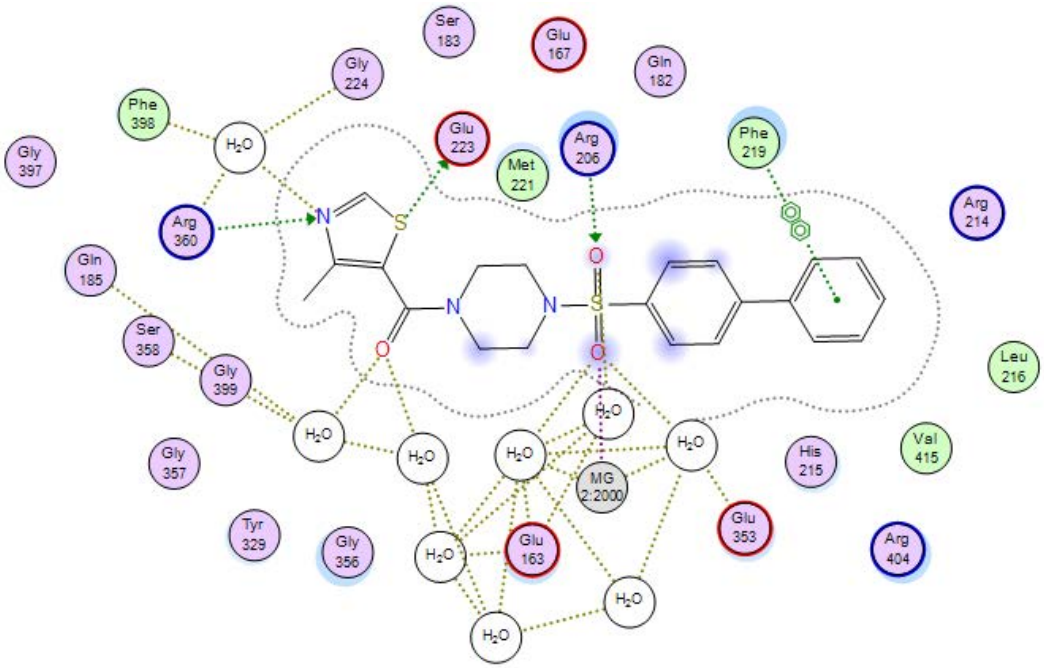

Figure 109: 2D binding interactions of compound **10c** with *S. aureus* AsnRS**.**

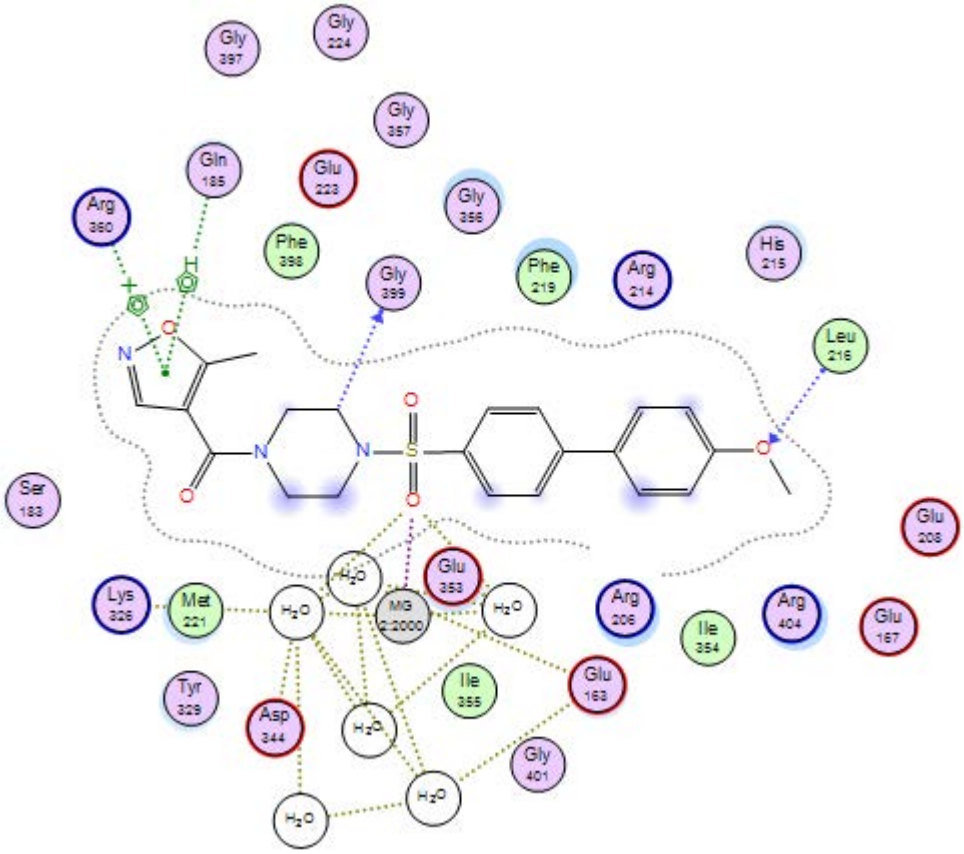

Figure 110: 2D binding interactions of compound **7d** with *S. aureus* AsnRS.

3.2.3. Docking studies of *E. faecalis* AspRS

The amino acid residues responsible for binding interactions with series 1 compounds were identified through alignment of series 1 compounds with aspartyl adenylate inside the active site of *E. faecalis* AspRS (Figure 111) (Table 24). The docking study of series 1 compounds with *E. faecalis* AspRS showed the same interactions observed with the natural substrate. Phe234 within the AMP pocket of *E. faecalis* AspRS forms a π-π stacking interaction with the benzene ring of some derivatives, while the nitro group of compounds **7b**, **10b** and **14b** formed hydrogen bonds with several amino acid residues including Gln236, Gly535 and Arg538 in *E. faecalis* AspRS (Figures 112-116). In the derivatives containing 4-carbonyl-5-methyl isoxazole, His449 and His450 from the histidine loop appeared to be close to the aspartic acid pocket indicating that this isosteric replacement for aspartic acid may be appropriate (Figure 112). There was no interaction with the methoxy group of compounds **7d**, **10d** and **14d** and with fluoro and chloro groups of compounds **7e** and **7f** respectively in the docking study of *E. faecalis* AspRS. The docking studies of series 1 compounds showed the role of Mg^{2+} in stabilisation of the sulfamoyl linkage. For example, compound **10b** and **14b** (Figure 113 and 114) but in compound **10b**, the docking study showed that the highly conserved amino acids residue (Asp476) interacted through a network of water molecules with Mg^{2+} ion as observed in the docking study of the natural substrate (Figure 113). However, some compounds such as **7c** and **10d** did not show any interactions with Mg^{2+} ion (Figures 115 and 116).

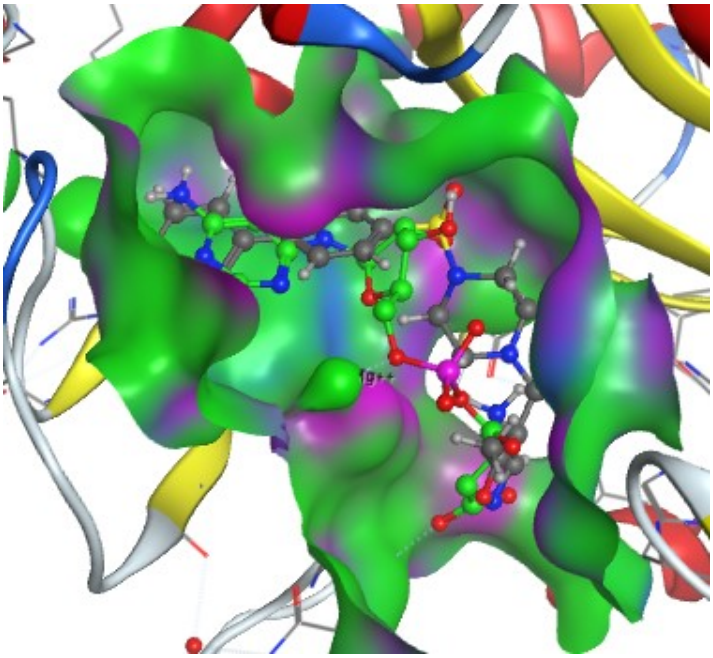

Figure 111: Alignment of compound **7c** (grey) with aspartyl adenylate (green) in the active sites of *E. faecalis* AspRS.

Table 24: Binding interactions of series 1 compounds with the amino acid residues of the binding sites of *E. faecalis* AspRS.

Ligands	Aspartic acid pocket	AMP pocket
Aspartyl-adenylate	Glu176, Arg230, His449, Arg490 and Asp238	Arg222, Phe234, Gln231, Gln236, Glu483 and Arg538
7a	His449, Asp476 and Gly486	Arg222, Arg230, Gln236, Glu483 and Arg538
7b	His449, Arg490, Gly486 and Gly487	Arg222, Glu224, Asp229, Arg230, Phe234, Gln236, Asp537 and Arg538
7c	Glu176, Gly177, Ser198, Asp238, His449, Arg490, Gly486 and Gly487	Arg222, Glu224, Arg230, Phe234, Gln236, Gly485 and Asp476
7d	Gly177, Ser198, Gly486 and His449	Arg222, Glu224, Arg230, Phe234, Gln236, Glu483 and Arg538

7e	Glu176, Gly177, Ala176, Asp23, His449 and Gly486	Arg222, Glu224, Phe234, Gln236, Glu483 and Arg538
7f	Ser198 and His449	Arg222, Glu224, Phe234 and Asp476
10a	Ser198, His449, Gly486, Gly487 and Arg490	Arg222, Glu224, Arg230 and Arg538
10b	Gln197, Ser198, His449, Gly486 and Gly487	Arg222, Glu224, Gln231, Arg230, Phe234, Gln236, Asp476, Glu535 and Arg538
10c	Gly177, His449 and Gly487	Arg222, Arg230, Phe234, Gln236, Asp476, Glu483 and Arg538
10d	Glu176, Ala176, Ser198 and His449	Arg222, Arg230, Phe234, Gln236, Glu483 and Arg538
14a	Ser198, His449, His450, Gly486 and Arg490	Arg222, Glu224, Arg230, Gln236, Glu483, Asp476 and Arg538
14b	-	Arg222, Glu224, Phe234, Gln236 and Arg538
14c	Ser198, His449 and Asp476	Arg222, Arg230, Phe234, Glu224 and Arg538
14d	Ser198 and His449	Arg222, Glu224, Arg230, Phe234, Glu483 and Arg538

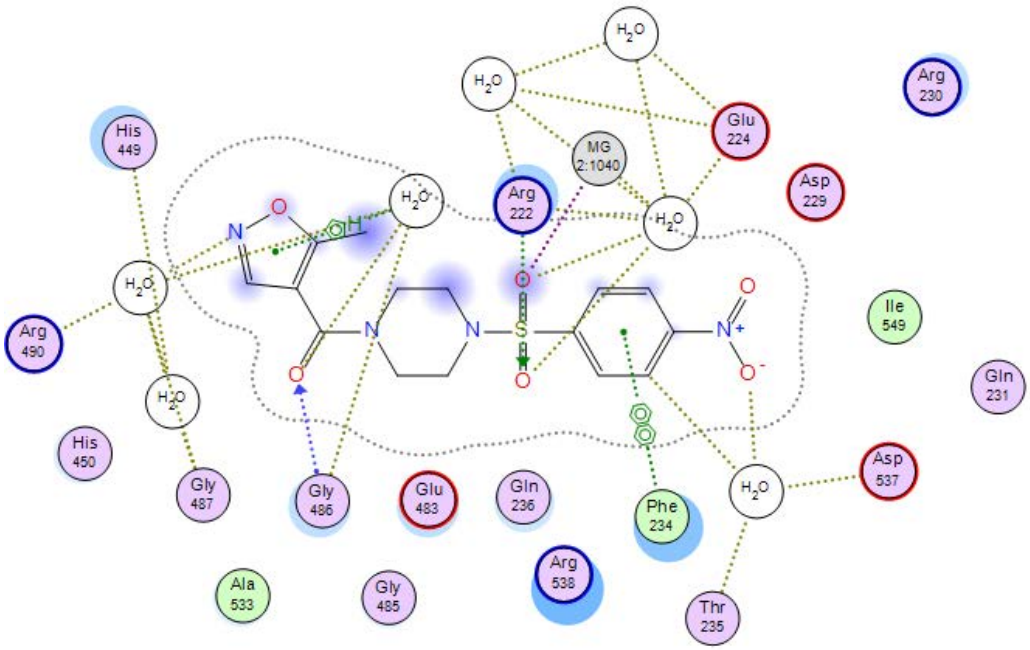

Figure 112: 2D binding interactions of compound **7b** with *E. faecalis* AspRS.

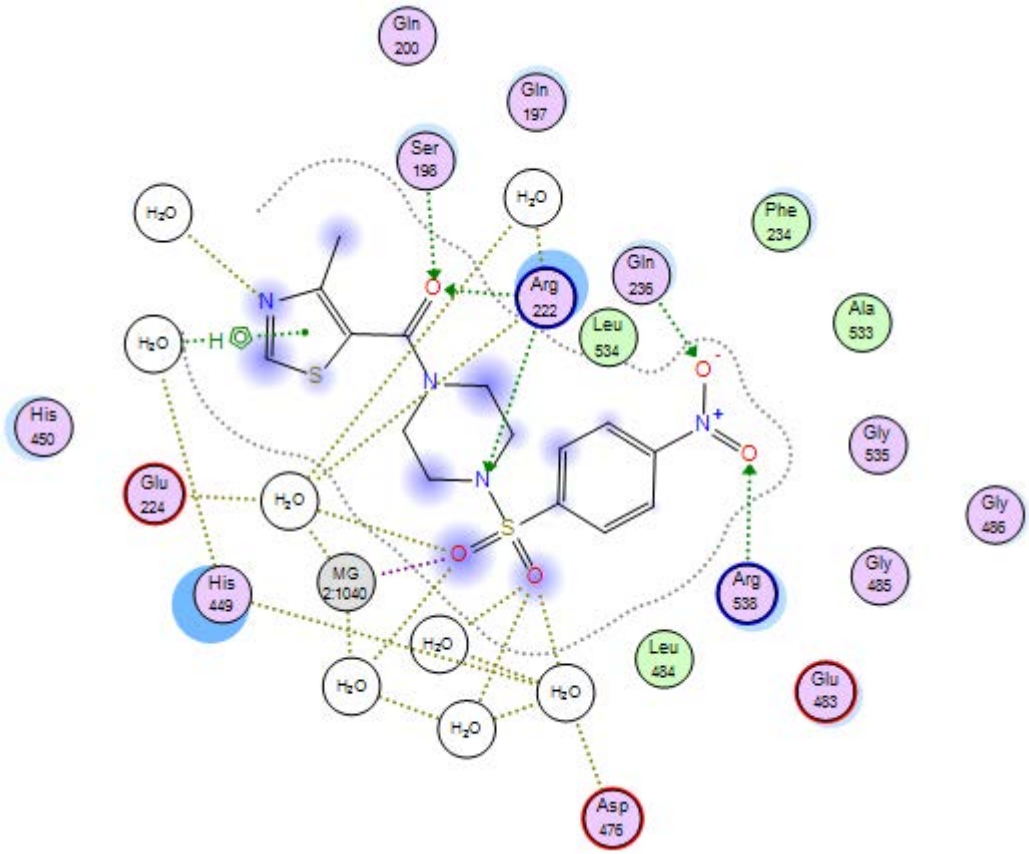

Figure 113: 2D binding interactions of compound **10b** with *E. faecalis* AspRS**.**

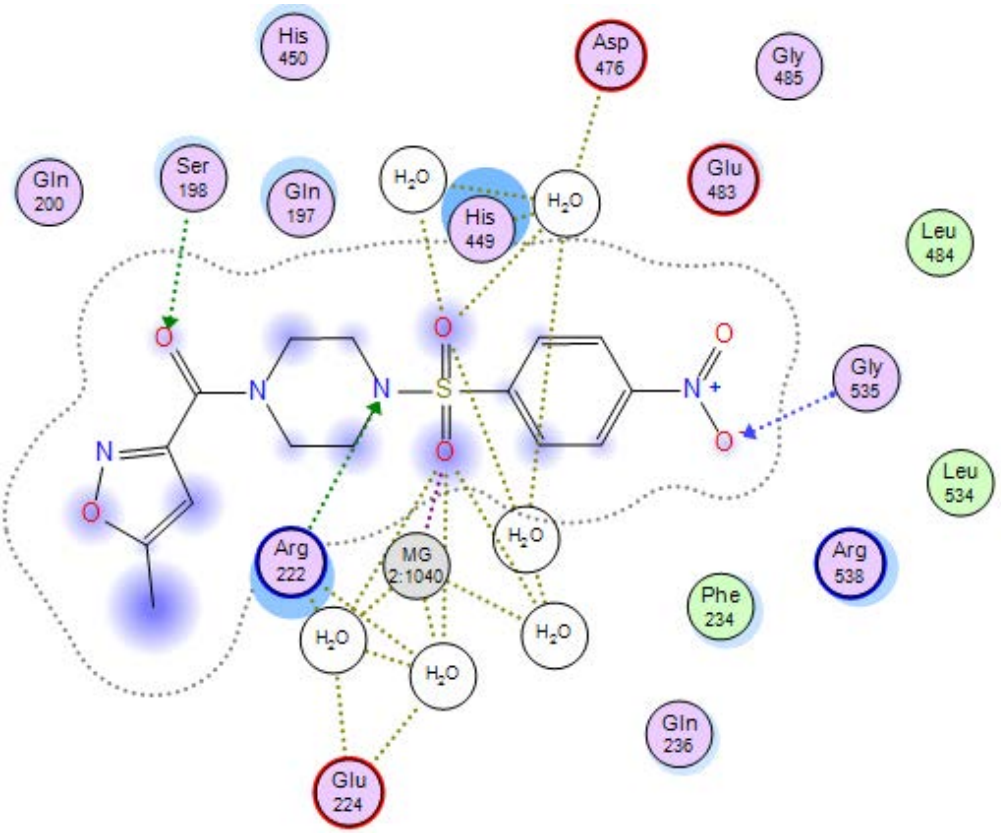

Figure 114: 2D binding interactions of compound **14b** with *E. faecalis* AspRS.

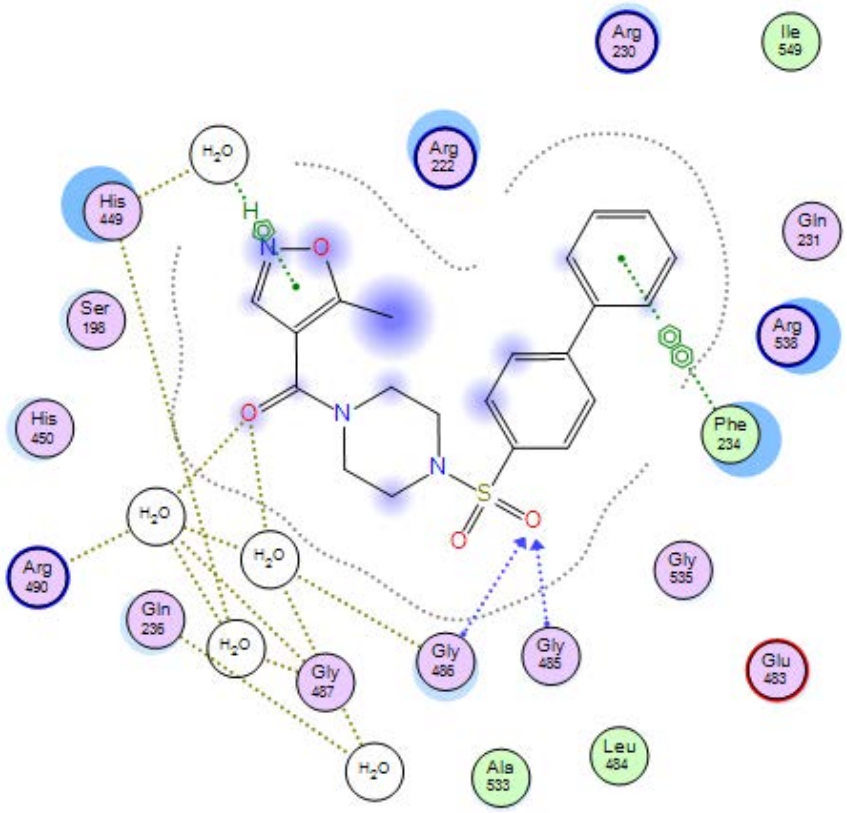

Figure 115: 2D binding interactions of compound **7c** with *E. faecalis* AspRS.

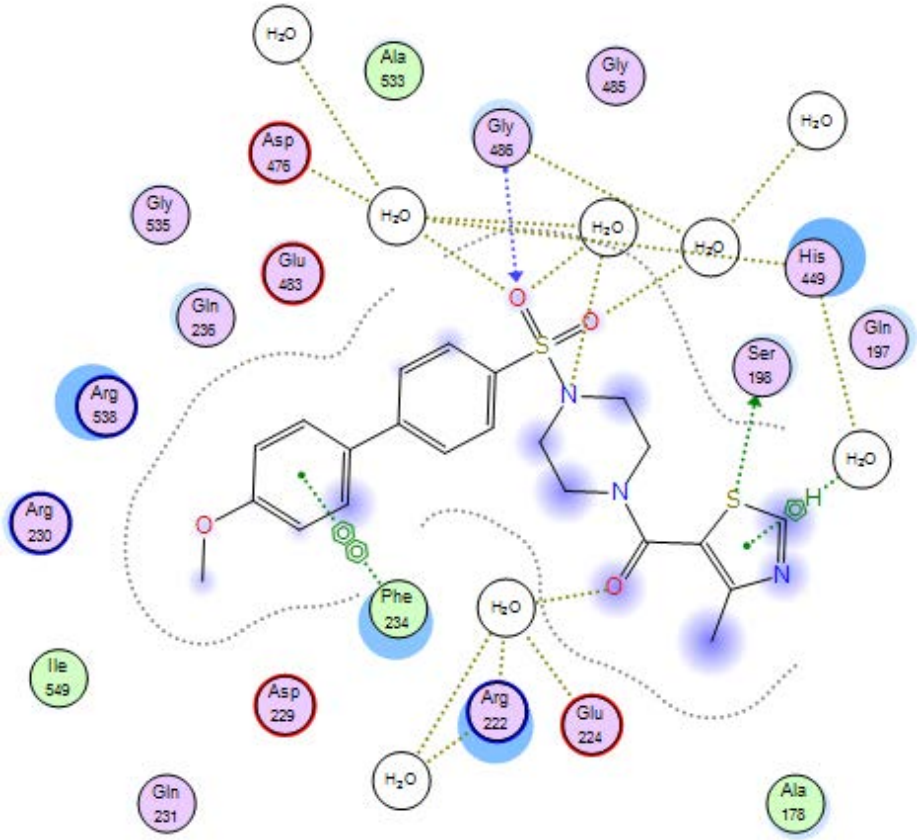

Figure 116: 2D binding interactions of compound **10d** with *E. faecalis* AspRS.

3.2.4. Docking studies of *E. faecalis* AsnRS.

Through alignment of series 1 compounds with asparaginyl adenylate inside the active sites of *E. faecalis* AsnRS, amino acid residues bound with the compounds were identified (Figure 117) (Table 25). In *E. faecalis* AsnRS, Phe234, the amino acid residue responsible for π-π stacking interaction with adenine in the natural substrate, made the same interaction with the benzene ring of series 1 compounds (Figure 118). In addition, the nitro group of compounds **7b** interacted via water molecules with Glu423 and Arg424 and directly with Leu231 in compound **14b** (Figures 119 and 120). Regarding the amino acid isosteric moiety, water-mediated interactions between Arg380 and the isosteric moiety, which is important in the recognition of asparagine in the natural substrate were observed in the docking study of compounds **7b**, **7c**, **7e**, **7f**, **10c** and **14a**-**c** with *E. faecalis* AsnRS (Figures 119, 121 and 122), however, the other key amino acid residue for asparagine recognition (Glu238) did not show any interaction with the amino acid isosteric moiety. There was no interaction observed for the methoxy, fluoro or chloro groups in the respective derivatives. Regarding Mg^{2+}

ion, the docking studies of series 1 compounds showed its role in sulfamoyl linkage stabilisation. For example, compounds **7a**, **7b**, **10c** and **14c** (Figures 118, 119, 121, 122). Lys346 and Asp364 contributed to the interaction with the cation through water molecules in compounds **10c** and **14c** (Figures 121 and 122) as observed in the docking study of asparaginyl adenylate with *E. faecalis* AsnRS in the presence of Mg^{2+} ion. These types of interactions are conserved in many AsnRSs.

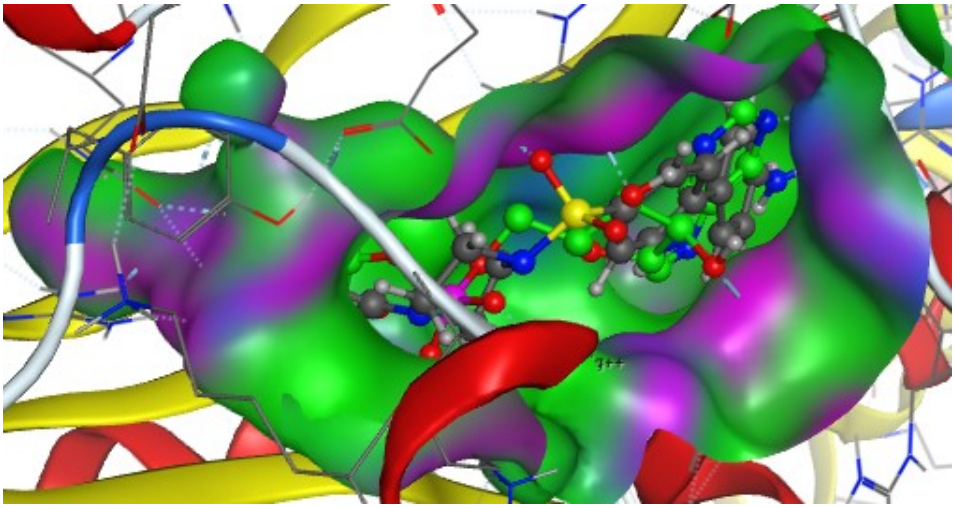

Figure 117: Alignment of compound **14a** (grey) with asparaginyl adenylate (green) in the active sites of *E. faecalis* AsnRS.

Table 25: Binding interactions of series 1 compounds with the amino acid residues of the binding sites of *E. faecalis* AsnRS.

Ligands	Asparagine pocket	AMP pocket
Asparaginyl-adenylate	Glu238 and Arg380	Arg221, Glu223, Arg229, His230, Phe234, Glu373, Gly376, Gly421 and Arg424
7a	Gln200	Glu178, His230, Phe234, Glu373, Glu423 and Arg424
7b	Gln200 and Arg380	Glu178, His230, Leu231, Phe234, Glu373, Glu423 and Arg424
7c	Gln200 and Arg380	Glu178, Phe234, Glu373, Glu423 and Arg424
7d	-	Arg221, His230 and Glu373

7e	Gln200 and Arg380	Arg221, His230, Phe234, Glu373, Gly376 and Arg424
7f	Gln200 and Arg380	Arg221, His230, Phe234 and Glu373
10a	Gln200	Glu178, His230, Phe234, Glu373, Glu423 and Arg424
10b	Gln200	Arg221, Glu223, Phe230, Leu231, Glu423, Arg424 and His230
10c	Gln200 and Arg360	Glu178, Arg221, Glu223 and Phe230
10d	-	Arg221, His230, Phe234 and Glu373
14a	Gln200 and Arg380	Phe234, Arg221, His230, Arg424, Glu373 and Gly376
14b	Gln200 and Arg380	Glu178, Arg221, Phe234, Leu231, Glu373, Glu423 and Arg424
14c	Gln200 and Arg380	Glu178, Arg221, Phe234, Glu373, Lys346, Asp364 and Arg424
14d	Gln200	Arg221, His230, Glu373, Glu423 and Arg424

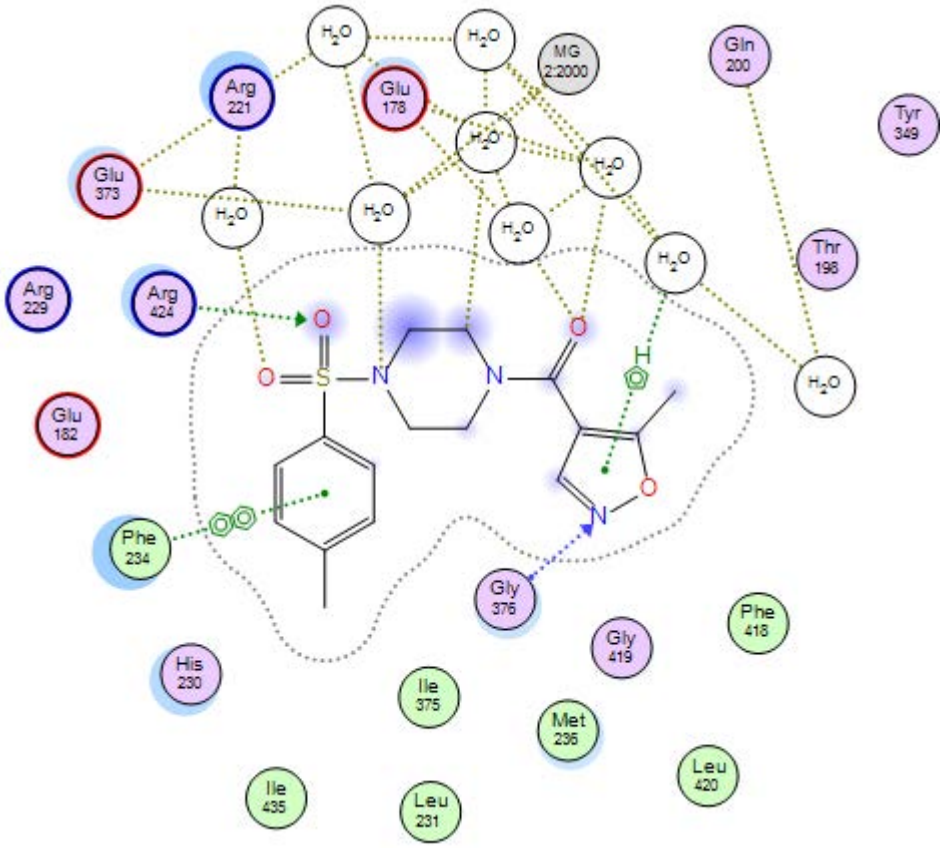

Figure 118: 2D binding interactions of compound **7a** with *E. faecalis* AsnRS.

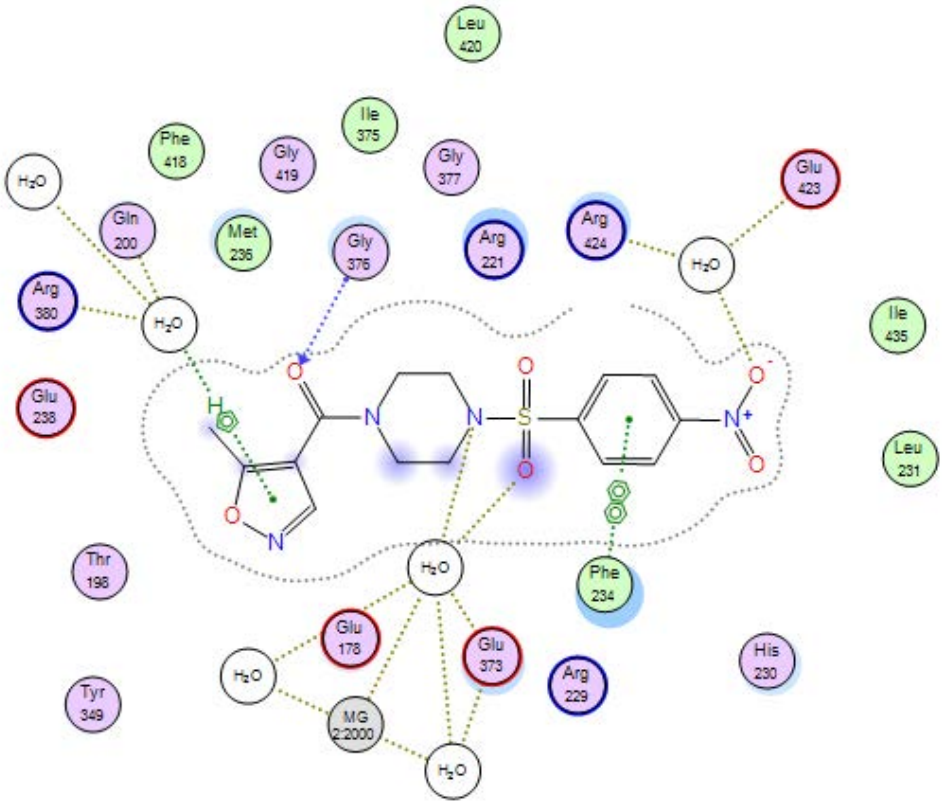

Figure 119: 2D binding interactions of compound **7b** with *E. faecalis* AsnRS.

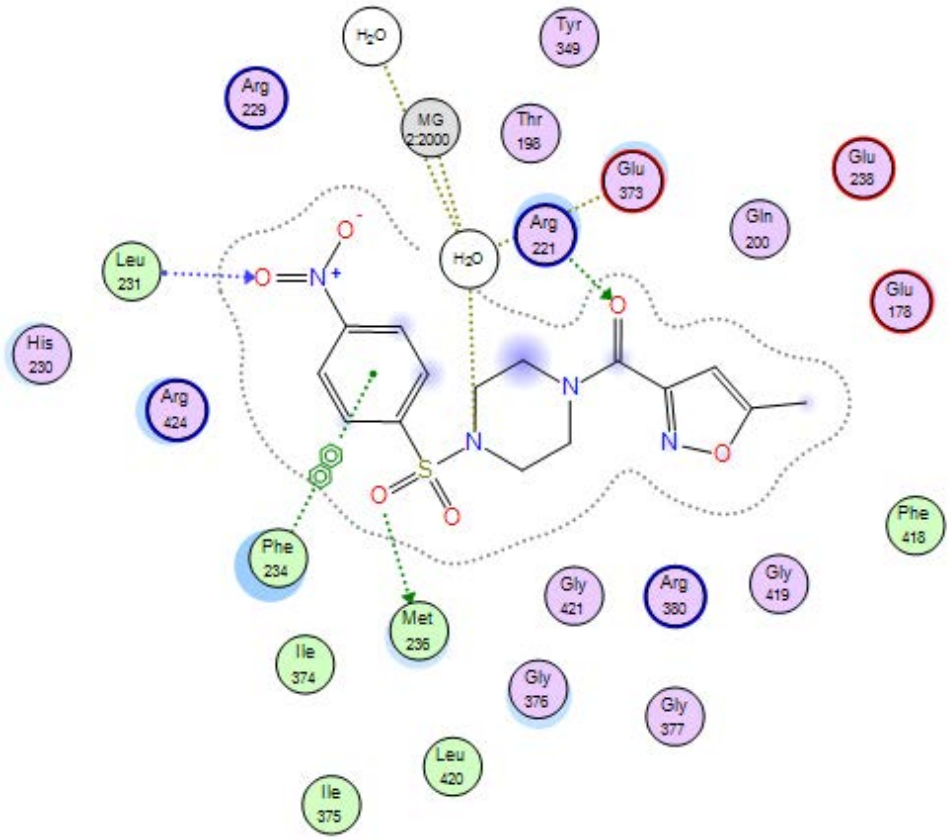

Figure 120: 2D binding interactions of compound **14b** with *E. faecalis* AsnRS.

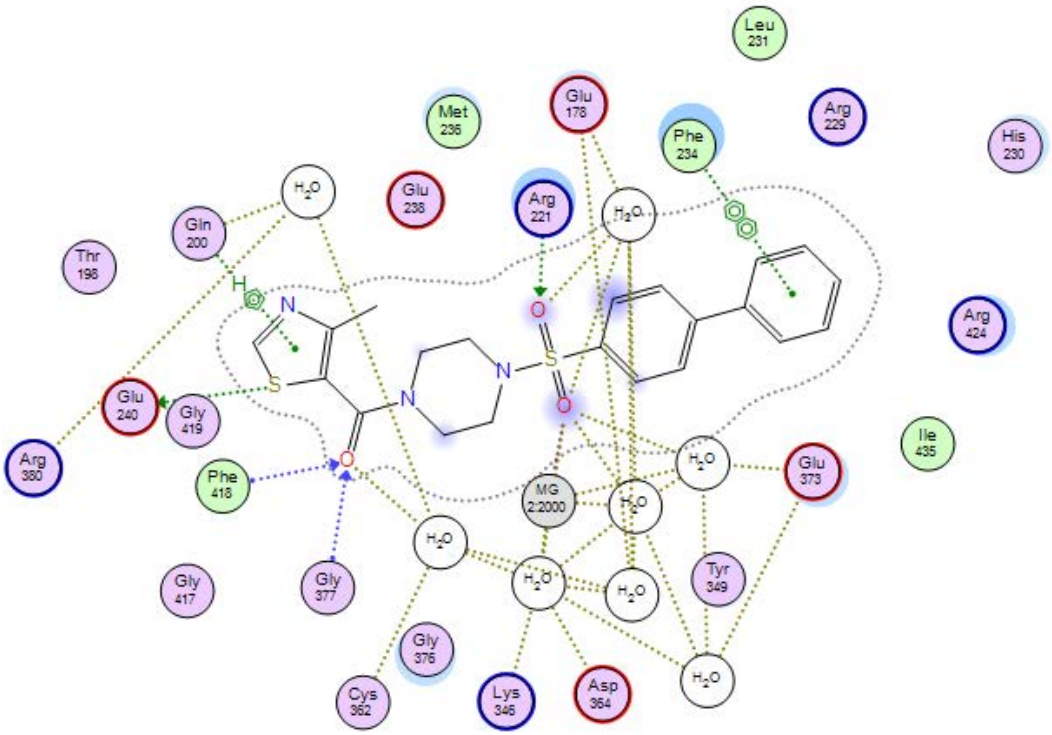

Figure 121: 2D binding interactions of compound **10c** with *E. faecalis* AsnRS.

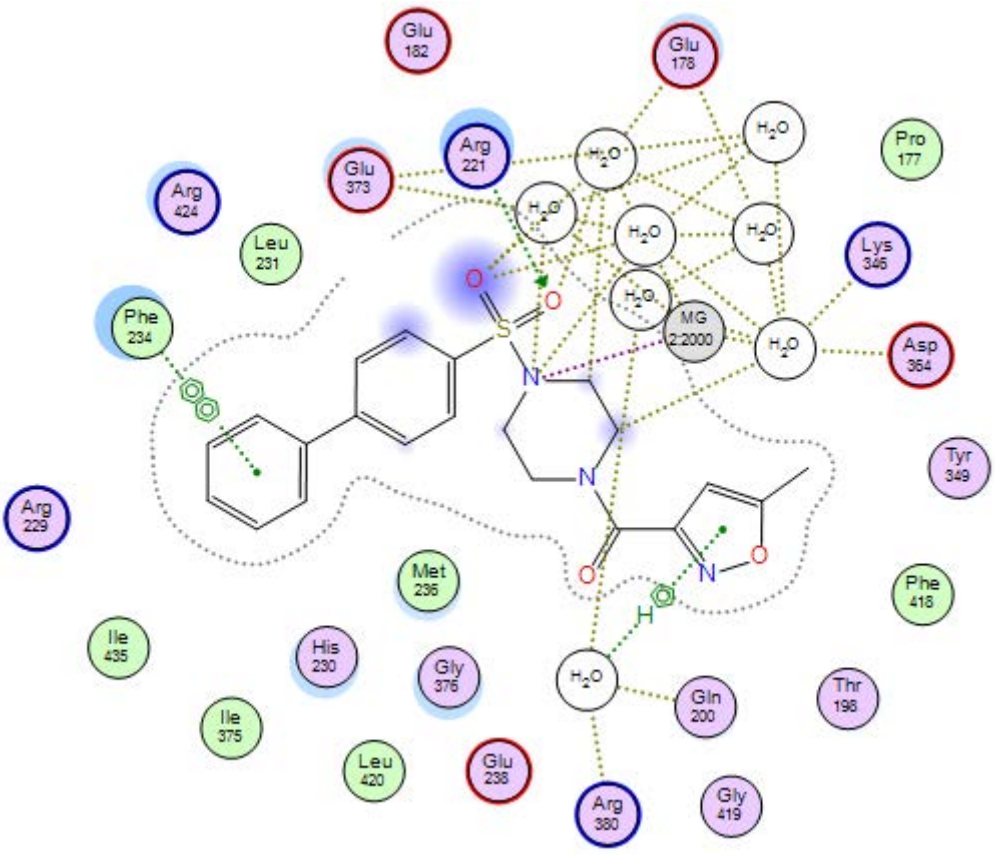

Figure 122: 2D binding interactions of compound **14c** with *E. faecalis* AsnRS.

3.3. Molecular dynamic studies

In the purpose of analysing the movement of compounds and the target enzymes, compound **7d** was selected for a molecular dynamic study using Schrödinger platform. In this study, the RMSD was monitored for each target enzymes with compound **7d** to identify how large the enzyme conformational change during 100 ns simulation time and how stable the compound is with respect to the protein and its binding pocket (Figures 123a-d). The RMSD plot of the molecular dynamic study of *S. aureus* AspRS with compound **7d** showed the largest conformational change of the enzyme in the first 30 nanosecond then it was equilibrated as the RMSD values stabilised around a fixed value between 5 and 6 Å. Also, it showed the stability of compound **7d** inside the binding pocket after the enzyme equilibration occurred (Figure 123a), while the RMSD plot of the molecular dynamic study of compound **7d** with *S. aureus* AsnRS showed less conformational change of AsnRS and more stability of the compound inside the binding pocket over all 100 nanoseconds of the simulation time (Figure 123b). In contrast, the conformational change of *E. faecalis* AspRS was large specifically, in last 20 nanoseconds during the molecular dynamic study of *E. faecalis* AspRS with compound **7d** but the compound was stabilised inside the binding pocket for 80 nanoseconds then diffused a way (Figure 123c). Regarding the molecular dynamic study of *E. faecalis* AsnRS with the same compound, the RMSD plot showed the stability of compound **7d** inside the binding pocket of the enzyme and the equilibration of the system was just in the first 30 nanoseconds of the simulation time then the enzyme subjected to large conformational changes with values between 5 and 10 Å (Figure 123d).

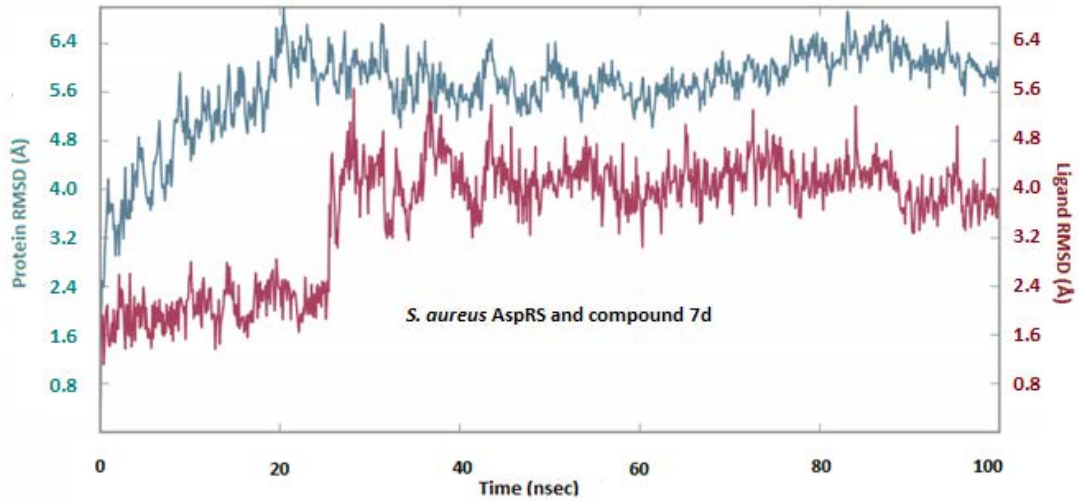

Figure 123a: RMSD (in angstrom) plot with respect to time in nanoseconds during 100 ns MD simulation of *S. aureus* AspRS with compound **7d**.

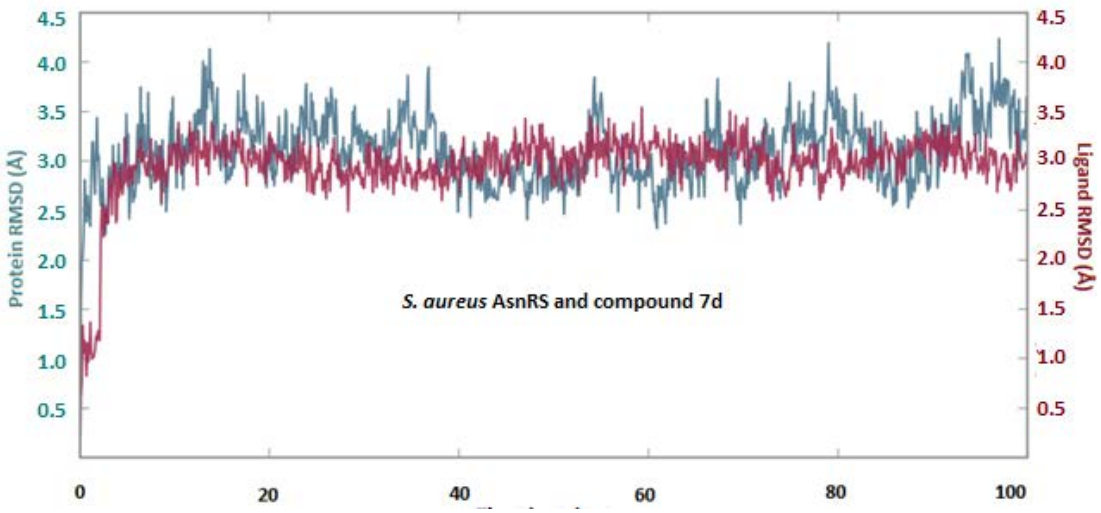

Figure 123b: RMSD (in angstrom) plot with respect to time in nanoseconds during 100 ns MD simulation of *S. aureus* AsnRS with compound **7d**.

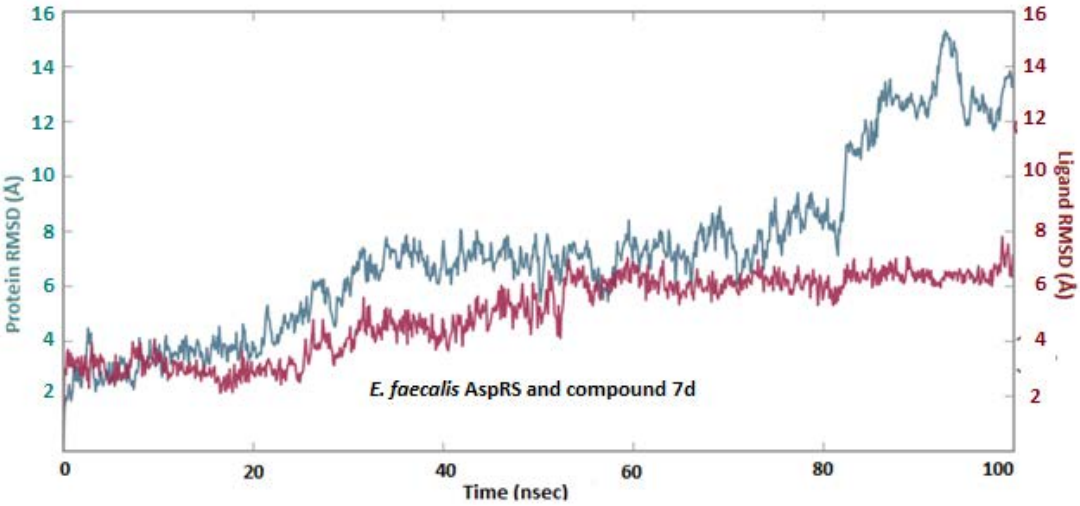

Figure 123c: RMSD (in angstrom) plot with respect to time in nanoseconds during 100 ns MD simulation of *E. faecalis* AspRS with compound **7d**.

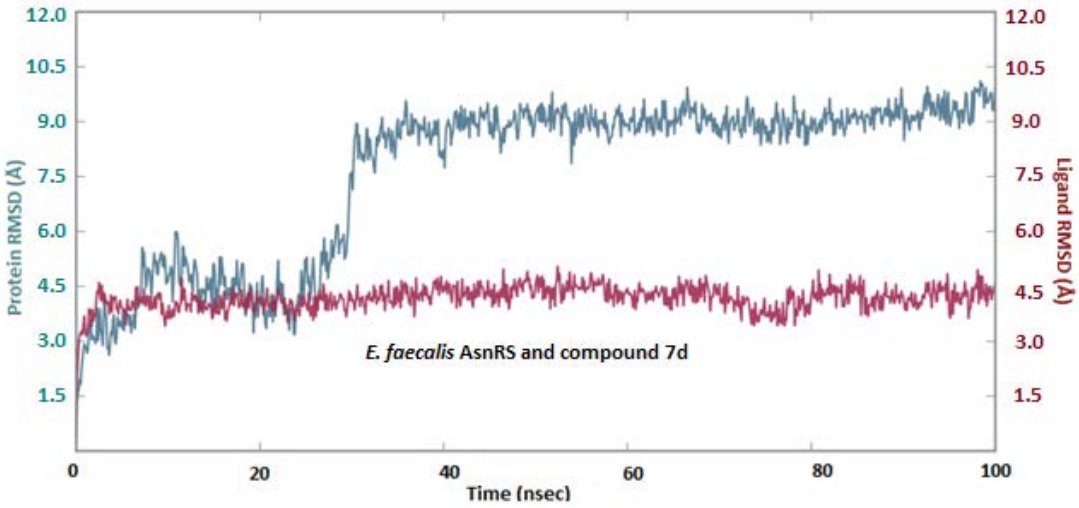

Figure 123d: RMSD (in angstrom) plot with respect to time in nanoseconds during 100 ns MD simulation of *E. faecalis* AsnRS with compound **7d**.

In addition, prime MM-GBSA tool was used to predict the binding energy of compound **7d** with *S. aureus* and *E. faecalis* AspRS and AsnRS enzymes and the results showed that compound **7d** was stronger bound to both enzymes of both microorganisms more than their natural substrates (Table 26 and 27).

Table 26: MM-GBSA binding energies of compound **7d** with *S. aureus* AspRS and AsnRS enzymes.

Binding affinity of compound **7d**	*S. aureus* AspRS	*S. aureus* AsnRS
ΔG range (kcal/mol)	-63.5689 to -38.8145	-53.9377 to -36.5909
ΔG average (kcal/mol)	-52.0794 ± 5.47	-44.0468 ± 4.03

Table 27: MM-GBSA binding energies of compound **7d** with *E. faecalis* AspRS and AsnRS enzymes.

Binding affinity of compound **7d**	*E. faecalis* AspRS	*E. faecalis* AsnRS
ΔG range (kcal/mol)	-77.7259 to -54.4728	-42.2914 to -7.6405
ΔG average (kcal/mol)	-68.0903 ± 4.50	-28.7793 ± 5.99

3.4. Biological assays

3.4.1. Microbiological screening

Microbiological screening of series 1 compounds was performed at the Antimicrobial Chemotherapy Unit in University Hospital of Wales (UHW) by Jennifer Richard and Mandy Wootton. Series 1 compounds **7a**-**f**, **10a**-**d** and **14a**-**d** were evaluated for antimicrobial activity against a broad panel of pathogens (sensitive and resistant strains) with ciprofloxacin as a standard for comparison. Isolates were tested by using clinical and NCTC/ATCC control organisms; *E. coli* (including (ATCC 25922) sensitive strain, ampicillin (ATCC 35218), nitrofurantoin/trimethoprim (353) and third generation cephalosporins (NCTC 13353) resistant strains), *Klebsiella pneumoniae* (including (21856) sensitive strain, carbapenems (NCTC 13443 and NCTC 13442) and fourth generation cephalosporins (ATCC 700603) resistant strains), *Proteus mirabilis* (NCTC 10975), *Pseudomonas aeruginosa* (ATCC 27853), *Salmonella enteritidis* (8204), *Acinetobacter baumanni* (572), *Burkholderia cepacian* (NCTC 10661), *Staphylococcus aureus* (including (ATCC 29213) sensitive strain, flucloxacillin (NCTC12493), erythromycin/clindamycin (ATCC BAA-977), vancomycin (ATCC 700698) and tetracycline (11051) resistant strains), *Enterococcus faecalis* (including (ATCC 29212) sensitive strain, vancomycin (NCTC 12201 (Van A) and ATCC 51299 (Van B)) resistant strains) and *Enterococcus faecium* (16568). MIC was measured for each compound using 2-fold doubling serial dilutions (log_2). From the MIC results of compounds **7a**-**f**, compound **7d** showed good inhibitory activity against the sensitive strain (ATCC 29212) and both vancomycin resistant strains (NCTC 12201 and ATCC 51299) of *E. faecalis* with MIC 4, 2 and 8 µg/mL respectively compared with ciprofloxacin (0.125 µg/mL against the sensitive strain of *E. faecalis* and 0.5 µg/mL against both resistant *E. faecalis* strains). However, compound **7d** showed low antimicrobial activity (64 µg/mL) against the sensitive strain of *S. aureus* and MRSA, while ciprofloxacin showed 0.25, 0.5, 0.25, 32 and 32 µg/mL MIC against *S. aureus* strains (Table 28). The difference between compound **7d** and **7e**-**f** derivatives is the presence of a methoxy group instead of fluoro and chloro groups. During the docking study of compounds **7d**-**f**, the methoxy group interacted with Arg540 and Leu216 of *S. aureus* AspRS and AsnRS respectively while there were no interactions with the fluoro and chloro groups of compounds **7e** and **7f**. In the case of the activity of these three compounds against *E.*

faecalis, the presence of the methoxy group in compound **7d** augmented the binding interactions of the biphenyl moiety inside the AMP pocket of AspRS (Table 24) and there was no difference between methoxy, fluoro and chloro groups in terms of their binding interactions inside the active site of AsnRS (Table 25). The lack of activity against *S. aureus* and *E. faecalis* of the other compounds may be owing to the smaller size of these compounds resulting in suboptimal occupancy of the active sites of the target enzymes.

For compounds **10a**-**d**, compound **10c** showed low antimicrobial activity (64, 32 and 64 µg/mL) against sensitive and both resistant strains of *E. faecalis* compared with the MIC of ciprofloxacin that showed 0.125 µg/mL against the sensitive strain and 0.5 µg/mL against the resistant strains of *E. faecalis*, while the MIC of compound **10d** was much better than **10c**, with MIC of 16 µg/mL against the sensitive strain of *E. faecalis* and 32 µg/mL against the resistant strains (Table 29). In the case of *S. aureus*, only compound **10b** showed MIC double the MIC of ciprofloxacin (32 µg/mL) against vancomycin resistant strain of *S. aureus* (Table 29). However, the MIC results of compounds **14a**-**d** showed that compounds **14c** and **14d** showed inhibitory activity against *E. faecalis* despite their low antimicrobial activity compared with the standard ciprofloxacin. Compound **14c** showed MIC of 64 µg/mL against vancomycin resistant of *E. faecalis*, while compound **14d** had a MIC of 64 µg/mL against the sensitive strain and vancomycin A resistant of *E. faecalis* (Table 30).

Among series 1 compounds, compound **7d** showed good inhibitory activity against the sensitive and resistant strains of *E. faecalis* and the similarity of **7d** with **10d** and **14d** is in the moiety that interacts with the amino acid residues in the AMP pocket, while the difference is in the bioisosteric amino acid (Asp/Asn) group. The isosteric moiety consists of 5-methyl isoxazole in compounds **7d** and **14d** but the carbonyl group of compound **7d** is linked to the fourth carbon atom of the isoxazole ring while it is linked to the third carbon atom in compound **14d** with the nitrogen atom closer to the carbonyl group that is important for class II aaRSs recognition. The proximity of the nitrogen atom could impair the binding of compound **14d** with target enzymes and reflect its low antimicrobial activity; the natural substrates contain an amine functional group on the α carbon next the carbonyl group, which is essential for the binding interactions. However, the isosteric moiety of the amino acid in compound

10d consists of 4-methyl thiazole and its antimicrobial activity against *S. aureus* and *E. faecalis* was lower than that of compound **7d** despite its good binding interactions with AspRS and AsnRS in the docking study. This may be owing to the increased lipophilicity of compound **10d** (log P = 3.3) compared with compound **7d** (log P = 2.3) resulting from the replacement of the oxygen atom in isoxazole ring with a sulfur atom in the thiazole ring.

Table 28: Microbiological data of compounds **7a-f.**

Organisms	MIC: (µg/mL)						
	Ciprofloxacin	**7a**	**7b**	**7c**	**7d**	**7e**	**7f**
Escherichia coli ATCC 25922	0.008	-	>128	>128	>128	>128	>128
Klebsiella pneumoniae 21856	0.03	-	>128	>128	>128	-	-
Proteus mirabilis NCTC 10975	0.015	-	>128	>128	>128	-	-
Pseudomonas aeruginosa ATCC 27853	0.25	128	>128	>128	>128	128	128
Salmonella enteritidis 8204	0.125	-	>128	>128	>128	-	-
Acinetobacter baumanni 572	0.25	-	>128	>128	>128	-	-
Burkholderia cepacian NCTC 10661	1	-	>128	>128	>128	-	-
Staphylococcus aureus ATCC 29213	0.25	>128	64	>128	64	>128	128

Enterococcus faecalis ATCC 29212	0.125	>128	128	>128	4	128	128
Enterococcus faecium 16568	>128	128	-	-	-	-	-
Escherichia coli							
ATCC 35218	0.008	-	>128	>128	>128	-	-
NCTC 13353	128	-	>128	>128	>128	-	-
353	64	-	>128	>128	>128	-	-
Klebsiella pneumoniae							
NCTC 13443	>128	-	>128	>128	>128	-	-
ATCC 700603	0.25	-	>128	>128	>128	>128	128
NCTC 13442	2	-	>128	>128	>128	-	-
Staphylococcus aureus							
NCTC 12493	0.5	128	128	>128	64	-	-
ATCC BAA-97	0.25	-	128	>128	128	-	-
ATCC 700698	32	-	128	>128	64	-	-
11051	32	-	128	>128	64	-	-
Enterococcus faecalis							
NCTC12201	0.5	-	128	>128	2	-	-
ATCC 51299	0.5	-	>128	>128	8	-	-

Table 29: Microbiological data of compounds **10a-d**.

Organisms	MIC: µg/mL				
	Ciprofloxacin	**10a**	**10b**	**10c**	**10d**
Escherichia coli ATCC 25922	0.008	-	>128	>128	>128
Klebsiella pneumoniae 21856	0.03	-	>128	>128	>128
Proteus mirabilis *NCTC 10975*	0.015	-	>128	>128	>128
Pseudomonas aeruginosa ATCC 27853	0.25	128	>128	>128	>128
Salmonella enteritidis 8204	0.125	-	>128	>128	>128
Acinetobacter baumanni 572	0.25	-	>128	>128	>128
Burkholderia cepacian NCTC 10661	1	-	>128	>128	>128
Staphylococcus aureus ATCC 29213	0.25	>128	>128	>128	>128
Enterococcus faecalis ATCC 29212	0.125	>128	>128	64	16
Enterococcus faecium 16568	>128	64	-	-	-
Escherichia coli ATCC 35218	0.008	-	>128	>128	>128
NCTC 13353	128	-	>128	>128	>128
353	64	-	>128	>128	>128
Klebsiella pneumoniae NCTC 13443	>128	-	>128	>128	>128

ATCC 700603	0.25	-	>128	>128	>128
NCTC 13442	2	-	>128	>128	>128
Staphylococcus aureus					
NCTC 12493	0.5	128	128	128	>128
ATCC BAA-97	0.25	-	64	>128	>128
ATCC 700698	32	-	64	>128	>128
11051	32	-	128	>128	>128
Enterococcus faecalis					
NCTC12201	0.5	-	128	32	32
ATCC 51299	0.5	-	>128	64	32

Table 30: Microbiological data of compounds **14a-d**.

Organisms	MIC µg/mL				
	Ciprofloxacin	**14a**	**14b**	**14c**	**14d**
Escherichia coli ATCC 25922	0.008	-	>128	>128	>128
Klebsiella pneumoniae 21856	0.03	-	>128	>128	>128
Proteus mirabilis NCTC 10975	0.015	-	>128	>128	>128
Pseudomonas aeruginosa ATCC 27853	0.25	128	>128	>128	>128
Salmonella enteritidis 8204	0.125	-	>128	>128	>128
Acinetobacter baumanni 572	0.25	-	>128	>128	>128
Burkholderia cepacian NCTC 10661	1	-	>128	>128	>128
Staphylococcus aureus ATCC 29213	0.25	>128	>128	>128	>128

Enterococcus faecalis ATCC 29212	0.125	128	>128	64	64
Enterococcus faecium 16568	>128	64	-	-	-
Escherichia coli					
ATCC 35218	0.008	-	>128	>128	>128
NCTC 13353	128	-	>128	>128	>128
353	64	-	>128	>128	>128
Klebsiella pneumoniae					
NCTC 13443	>128	-	>128	>128	>128
ATCC 700603	0.25	-	>128	>128	>128
NCTC 13442	2	-	>128	>128	>128
Staphylococcus aureus					
NCTC 12493	0.5	128	>128	>128	>128
ATCC BAA-97	0.25	-	>128	>128	>128
ATCC 700698	32	-	>128	>128	>128
11051	32	-	>128	>128	>128
Enterococcus faecalis					
NCTC12201	0.5	-	>128	64	64
ATCC 51299	0.5	-	>128	64	128

3.4.2. Aminoacylation assay

The antimicrobial assay was performed at the Department of Chemistry, University of Texas by Casey Hughes and James Bullard. The half maximal inhibitory concentration (IC_{50}) assay was performed for all compounds to measure their potencies in inhibiting 50% of the aminoacylation process. In this assay, *P. aeruginosa* AspRS was used and the control was EDTA in DMSO. All tested compounds did not show good IC_{50} results, even compound **7d**, which had an IC_{50} of 221.5 µM, while compounds **10d** and **14d** showed reduced inhibition with IC_{50} values of 249.1 and 253.1 µM respectively (Figure 124).

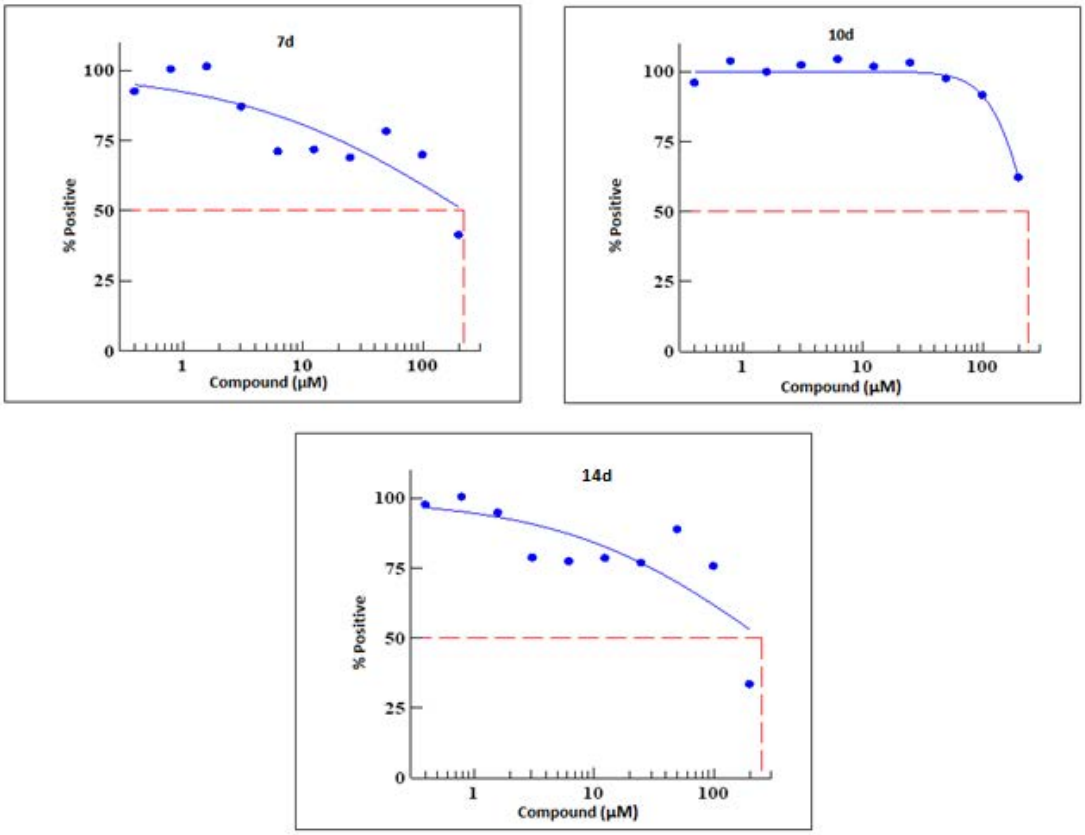

Figure 124: IC_{50} of compounds **7d**, **10d** and **14d**.

Ideally the compounds need to be tested against *S. aureus* and *E. faecalis* that they were designed to inhibit, however, only the *P. aeruginosa* AspRS assay was available. *P. aeruginosa* AspRS only has 50% similarity with the protein sequences of *S. aureus* and *E. faecalis* AspRSs (Figure 125) and *P. aeruginosa* AspRS is a non-discriminating enzyme, which can charge both $tRNA^{Asp}$ and $tRNA^{Asn}$. Further aminoacylation assays for **7d**, **10d** and **14d** against *S. aureus* and *E. faecalis* AspRS/ AsnRS are needed to confirm whether the design process was successful.

```
Percent Identity  Matrix - created by Clustal2.1

1: sp|Q51422|SYDND_PSEAE  100.00   53.28   51.55
2: sp|Q2FXU5|SYD_STAA8     53.28  100.00   63.82
3: sp|Q833I2|SYD_ENTFA     51.55   63.82  100.00
```

Figure 125: Percent identity matrix showing the percentage of identity in the protein sequence of *S. aureus*, *E. faecalis* and *P. aeruginosa* AspRSs.

In conclusion, 14 final compounds were successfully prepared in this series containing sulfamoyl piperazine derivatives bound to 4-carbonyl-5-methylthiazole, 3-carbonyl-5-methylisoxazole or 5-carbonyl-4-methylisoxazole. Compounds **7c**-**f**, **10c**-**d** and **14c**-**d** showed a good fit inside the active sites of *S. aureus* and *E. faecalis* AspRS/AsnRS and they formed hydrogen bonds and hydrophobic interactions with the key amino acid residues. However, compounds **7a**-**b**, **10a**-**b** and **14a**-**b** were easily flipping inside the pockets owing to their small sizes and inability to completely fill the pockets despite their abilities to form good binding interactions. The docking studies of these compounds also showed the contribution of Mg^{2+} ion in the stabilisation of the sulfamoyl linkage inside the active sites of the target enzymes. Compound **7d** showed good inhibitory activity (2-8 µg/ mL) against the sensitive and resistant strains of *E. faecalis* while compound **10d** showed MIC of 16 and 32 µg/mL against the same strains possibly owing to the increase in lipophilicity of compound **10d** resulting from the replacement of the isoxazole ring with a thiazole ring. However, compound **14d** did not show good inhibitory activity against the test microorganisms and this could be related to the proximity of the nitrogen atom to the carbonyl group, which impairs the recognition of the compound inside the active sites of the target enzymes. Any replacement of the amino acid isosteric moiety by an asparagine while retaining the same linker and aryl/biaryl moiety could increase the inhibitory activity against the target microorganisms.

3.5. Methods

3.5.1. Docking and molecular dynamic studies

All methods related to docking and molecular dynamic studies are described in the methods section in Chapter 2.

3.5.2. Biological assay

3.5.2.1. Antimicrobial screening test

The antimicrobial screening test was carried out at the Antimicrobial Chemotherapy Unit in University Hospital of Wales (UHW) by Jennifer Richard and Mandy Wootton. Antimicrobial activity was measured for compounds **7a**-**f**, **10a**-**d** and **14a**-**d** against a variety of clinically important pathogens alongside ciprofloxacin as the standard for comparison. Isolates were tested by using clinical and NCTC/ATCC control organisms; *E. coli* (including ampicillin, nitrofurantoin, trimethoprim and third generation cephalosporins resistant strains), *Klebsiella pneumoniae* (including carbapenems and fourth generation cephalosporins resistant strains), *Proteus mirabilis, Pseudomonas aeruginosa, Salmonella enteritidis, Acinetobacter baumannii, Burkholderia cepacian, Staphylococcus aureus* (including flucloxacillin, erythromycin, clindamycin, vancomycin and tetracycline resistant strains), *Enterococcus faecalis* (including vancomycin resistant strains). The tests were performed in microdilution trays and the preparation of the antimicrobial agents working solution is in 50 µL volumes per well with double the desired final concentration of designed inhibitors. Minimum inhibitory concentrations (MICs) were determined using dilution procedures which follow the international standard ISO/FDIS 20776-1:2006 (334). Briefly, compounds were dissolved in dimethyl sulfoxide (DMSO) to a concentration of 2560 µg/mL, and then diluted further in Mueller-Hinton Broth to achieve a range of log2 concentrations ranging from 0.008 µg/mL to 128 µg/mL. The presence of one well containing 50 µL of an inhibitor agent free medium as growth control for each strain is essential for reading results. The inoculum was prepared by diluting a broth culture or by suspending colonies from overnight culture on agar medium in broth. For both methods, three to five colonies of a pure nutritive agar medium were selected to be touched with loop and transferred to broth and incubated at 37 ^{o}C until the growth reaches turbidity equal to or greater than that of a 0.5 McFarland standard making the

final concentration of inoculum as 5 x 10^5 CFU/mL. Then the microdilution trays were inoculated within 30 minutes of standardising the inoculum saline suspension just to maintain the viable cell number concentration. To each well containing 50 µL of diluted proposed inhibitor in broth, a volume of 50 µL of bacterial suspension was added. Before reading results, the microdilution trays were incubated at 34 ^oC to 37 ^oC in ambient air for (18 ± 2) h. If there is no growth in the negative growth control, the amount of growth in each well is compared with that in the positive growth control and the MIC is registered as the lowest concentration of the agent that completely inhibits visible growth.

3.5.2.2. Aminoacylation assay

The aminoacylation assay was performed in the Department of Chemistry, University of Texas by Casey Hughes and James Bullard. Aminoacylation was carried out at 37 ^0C for 60 min and measured using a filter binding assay (50 µL) containing 50 mM Tris-HCl at pH 7.5, 10 mM $MgCl_2$, 2.5 mM ATP, 1mM DTT, 75 µM [^3H] aspartic acid and 0.015 µM *P. aeruginosa* AspRS comparable with the control which was 10 µL EDTA and 2 µL DMSO. The $tRNA^{Asp/Asn}$ concentrations were 0.4, 0.8, 1.6, 3.1, 6.25, 12.5, 25, 100 and 200 µM. Assays were stopped at time intervals between 1 and 5 min. Initial velocities for aminoacylation were calculated for all tRNA concentrations and the data of IC_{50} were plotted using Sigmoidal Dose-Response Model fit in XLfit software (335).

3.5.3. Chemistry

All chemicals, reagents and solvents were purchased from Sigma-Aldrich, Fisher Scientific, Alfa Aesar and Acros Organics and, where required, solvents were dried and stored over 4 Å molecular sieves under nitrogen. Gradient chromatography was performed with silica gel 60 nm (230-400) (Merck), and TLC was formed on precoated silica gel plates (Merck Kiesegel $60F_{245}$) and preparative TLC plates with 254 UV and dimension 20 x 20 cm (Analtech Inc.). Melting points were determined on an electrothermal instrument (GallenKamp) and are uncorrected. Compounds were visualised by irradiation with UV light at 254 nm and 366 nm. ^1H and ^{13}C NMR spectra were recorded on a Bruker A deviance DPX500 spectrometer operating at 500 MHz and 125 MHz respectively and auto calibrated to deuterated solvent reference peak. Chemical shifts are given in δ relative to tetramethylsilane (TMS), the coupling

constant (J) is given in Hertz. TMS, $CDCl_3$ and DMSO-d_6 were used as internal standards at 0, 7.26 and 2.50 ppm respectively for ^{1}H NMR while $CDCl_3$ and DMSO-d_6 were served as internal standards at 77.2 and 39.52 ppm respectively for ^{13}C NMR. Multiplicity is denoted as s (singlet), br s (broad singlet), d (doublet), t (triplet), br t (broad triplet), q (quartet), m (multiplet) or combinations thereof. Mass spectra were performed by the UK National Mass Spectrometry Facility of Engineering and Physical Science Research Council (EPSRC) in the Medical School of Swansea University (electron spray mass spectroscopy in positive mode). Elemental analysis was performed by Medac Ltd, Alpha 319, Chobham Business Centre. UV purity and LC-MS analyses were performed at Bath University using an Agilent QTOF 6545 with Jetstream ESI spray source coupled to an Agilent 1260 Infinity II Quat pump HPLC with 1260 autosampler, column oven compartment and variable wavelength detector (VWD). The MS was operated in positive ionisation mode with the gas temperature at 250°C, the drying gas at 12L/min and the nebuliser gas at 45 psi (3.10 bar). The sheath gas temperature and flow were set to 350°C and 12 L/min, respectively. The MS was calibrated using reference calibrant introduced from the independent ESI reference sprayer. Chromatographic separation was performed on a Zorbax Eclipse Plus C18 Rapid Resolution 2.1 x 50 mm, 1.8 µm using H20 (Merck, LC-MS grade) with 0.1 % formic acid (FA, Fluka) v/v and methanol (MeOH, VWR, HiPerSolv) with 0.1% FA v/v as mobile phase A and B, respectively. The column was operated at flow rate of 0.5 mL/min at 50°C starting with 5 % mobile phase B for 0.5 min, thereafter the gradient was started for 2 min to a final 100% B, held at 100% B for 1 min then returned to 5% B for 3.9 min in a total 7.5 min run time. The VWD was set to collect 254 and 320 nm wavelengths at 2.5 Hz. For HPLC purity determinations a 10 µL injection of a 50 µg/ml sample was made, thereafter for MS peak retention time and formula confirmation a 0.2 µL injection of the same sample was made. Data processing was automated in Qual B 07.00.

3.5.3.1. General procedure for the preparation of phenyl sulfonyl piperazines (**3a-f**) (329)

To a solution of piperazine (**1**) (10.49 mmol) in dry $CHCl_3$ (10 mL) was added EtN_3 (2.9 mL, 20.98 mmol). The reaction mixture was cooled to 0 °C followed by addition of phenyl sulfonyl chloride derivatives (**3a-f**) (5.25 mmol) in dry $CHCl_3$ (20 mL) dropwise over 30 min and the amount of $CHCl_3$ can be increased if the sulfonyl chloride

derivative is in suspension form. Then the reaction mixture was warmed slowly to room temperature and stirred for 3 h. The reaction was diluted with $CHCl_3$ (100 mL) and washed with saturated aqueous $NaHCO_3$ (3 x 50 mL). The organic layer was dried ($MgSO_4$) and evaporated under reduced pressure.

3.5.3.1.1. 1-Tosyl piperazine (**3a**) ($C_{11}H_{16}N_2O_2S$, Mol. Wt. 240.32)

Product obtained as white crystals, yield: 1.2g (96%), mp = 104 – 106 ^{0}C (Lit. mp = 101 ^{0}C, 110 ^{0}C (335, 336)). TLC: CH_3OH - CH_2Cl_2 1:9 v/v, (R_f = 0.7). ^{1}H NMR ($CDCl_3$) δ 2.15 (s, 1H, NH), 2.45 (s, 3H, CH_3), 2.98 (bs, 4H, CH_2, pip), 3.01 (bs, 4H, CH_2, pip), 7.35 (d, J = 7.8 Hz, 2H, CH, Ar), 7.65 (d, J = 8 Hz, 2H, CH, Ar).

3.5.3.1.2. 1-((4-Nitrophenyl)sulfonyl)piperazine (**3b**) ($C_{10}H_{13}N_3O_4S$, Mol. Wt. 271.29)

Product obtained after washed by CH_3CN as a yellow powder, yield: 0.91g (74%), mp = 150 – 152 ^{0}C. TLC: CH_3OH - CH_2Cl_2 1:9 v/v, (R_f = 0.8). ^{1}H NMR (DMSO-d_6) δ 2.72 (t, J = 4.93, 4.93 Hz, 4H, CH_2, pip), 2.85 (t, J = 4.22, 4.22 Hz, 4H, CH_2, pip), 7.99 (d, J = 8.9 Hz, 2H, CH, Ar), 8.46 (d, J = 8.9 Hz, 2H, CH, Ar), NH signal was not appeared. ^{13}C NMR (DMSO-d_6) δ 45.1, 47.2 (4 x CH_2, pip), 125.1, 129.6 (4 x CH, Ar), 141.1, 150.5 (2 x C, Ar). HPLC: 100% at RT: 3.5 min. HRMS (ES-TOF) m/z calculated mass: 272.0627 $[M + H]^+$, observed mass: 272.0702 $[M + H]^+$.

3.5.3.1.3. 1-([1,1'-Biphenyl]-4-yl)sulfonyl)piperazine (**3c**) ($C_{16}H_{18}N_2O_2S$, Mol. Wt. 302.39)

Product obtained as a white powder, yield: 1.2 g (96%), mp = 174 - 176 °C. TLC: CH_3OH - CH_2Cl_2 1:9 v/v, (R_F = 0.5). ^{1}H NMR ($CDCl_3$) δ 1.68 (s, 1H, NH), 2.98 (bs, 4H, CH_2, pip), 3.06 (bs, 4H, CH_2, pip), 7.46 (d, J = 8.3 Hz, 1H, CH, Ar), 7.51 (t, J = 8.3, 8.3 Hz, 2H, CH, Ar), 7.62 (d, J = 7.9 Hz, 2H, CH, Ar), 7.75 (d, J = 7.9 Hz, 2H, CH, Ar), 7.84 (d, J = 8.3 Hz, 2H, CH, Ar). ^{13}C NMR ($CDCl_3$) δ 45.5, 48.1 (4 x CH_2, pip), 114.8, 115.1, 126.6, 128.3 (8 x CH, Ar), 127.2 (CH, Ar) 130.9, 133.1, 144.7 (3 x C, Ar). HPLC: 100% at RT: 4.0 min. HRMS (ES-TOF) m/z calculated mass: 325.1089 $[M + Na]^+$, observed mass: 325.0984 $[M + Na]^+$.

3.5.3.1.4. 1-((4'-Methoxy-[1,1'-biphenyl]-4-yl)sulfonyl)piperazine (**3d**) ($C_{17}H_{20}N_2O_3S$, Mol. Wt. 332.42)

Product obtained as a white powder, yield: 1.2g (91%), mp = 175 – 177 °C. TLC: CH_3OH - CH_2Cl_2 1:9 v/v, (R_F = 0.4). ^1H NMR (DMSO-d_6) δ 2.28 (s, 1H, NH), 2.75 (br t, J = 4.6, 5.3 Hz, 4H, CH_2, pip), 2.83 (br t, J = 5.3, 4.6 Hz, 4H, CH_2, pip), 3.83 (s, 3H, OCH_3), 7.09 (d, J = 8.1 Hz, 2H, CH, Ar), 7.72 (d, J = 9.3 Hz, 2H, CH, Ar), 7.76 (d, J = 9.3 Hz, 2H, CH, Ar), 7.97 (d, J = 8.1 Hz, 2H, CH, Ar). ^{13}C NMR (DMSO-d_6) δ 45.5, 47.1 (4 x CH_2, pip), 55.8 (OCH_3), 114.8, 115.1, 125.9, 126.6, 127.2, 128.3, 128.8, 128.8 (8 x CH, Ar), 131.0, 133.1, 144.7, 160.3 (4 x C, Ar). HPLC: 98.4% at RT: 6.0 min. HRMS (ES-TOF) m/z calculated mass: 355.1195 $[M + Na]^+$, observed mass: 355.1090 $[M + Na]^+$.

3.5.3.1.5. 1-((4'-Fluoro-[1,1'-biphenyl]-4-yl)sulfonyl)piperazine (**3e**) ($C_{16}H_{17}FN_2O_2S$, Mol. Wt. 320.10)

Product obtained after washed by CH_3CN as a white powder, yield: 0.27g (46%), mp = 128 - 130 °C, TLC: CH_3OH - CH_2Cl_2 1:9 v/v, (R_F = 0.6). ^1H NMR ($CDCl_3$) δ 2.87 (bt, J = 4.7, 4.9 Hz, 4H, CH_2, pip), 2.96 (br t, J = 4.5, 4.9 Hz, 4H, CH_2, pip), 7.11 (t, J = 8.5, 8.8 Hz, 2H, CH, Ar), 7.49 (dd, J = 8.7, 5.2 Hz, 2H, CH, Ar), 7.61 (d, J = 8.3 Hz, 2H, CH, Ar), 7.73 (d, J = 8.3 Hz, 2H, CH, Ar), NH signal was not appeared. ^{13}C NMR ($CDCl_3$) δ 45.3, 46.9 (4 x CH_2, pip), 116.0, 116.2, 127.5, 127.8, 127.8, 128.4, 129.0, 129.1 (8 x CH, Ar), 134.1, 135.4, 135.4, 144.7, 162.2 (4 x C, Ar). HPLC: 96.9% at RT: 3.80 min. HRMS (ES-TOF) m/z calculated mass: 321.0995 $[M + H]^+$, observed mass: 321.1070 $[M + H]^+$.

3.5.3.1.6. 1-((4'-Chloro-[1,1'-biphenyl]-4-yl)sulfonyl)piperazine (**3f**) ($C_{16}H_{17}ClN_2O_2S$, Mol. Wt. 336.83)

Product obtained after washed by CH_3CN as a shiny white powder, yield: 0.6g (54%), mp = 168 - 170 ^{0} C, TLC: CH_3OH - CH_2Cl_2 1:9 v/v, (R_F = 0.5). ^1H NMR (DMSO-d_6) δ 2.29 (s, 1H, NH), 2.73 (br t, J = 4.8, 5.1 Hz, CH_2, Pip), 2.82 (br t, J = 4.8, J= 4.7Hz, CH_2, Pip) 7.59 (d, J = 8.6 Hz, 2H, CH, Ar), 7.79 (d, J = 1.8 Hz, 2H, CH, Ar), 7.81 (d, J = 1.8 Hz, 2H, CH, Ar), 7.96 (d, J = 8.6 Hz, 2H, CH, Ar). ^{13}C NMR (DMSO-d_6) δ 45.2, 47.2 (4 x CH_2, pip), 128.0, 128.8, 129.4, 129.6 (8 x CH, Ar), 134.1, 134.4, 137.6, 143.7 (4 x C, Ar). HPLC: 99.05% at RT: 3.94 min, HRMS (ES-TOF) m/z calculated mass: 337.0699 $[M + H]^+$, observed mass: 337.0775 $[M + H]^+$.

3.5.3.2. General procedure for the preparation of acid chlorides (**6** and **9**) (332).

To a solution of 5-methylisoxazol e-4-carboxylic acids (0.2g, 1.57 mmol) (**4**) or 4-methylthiazole-5-carboxylic acids (0.2g, 1.57 mmol) (**8**) in $SOCl_2$ (3 mL) (**5**) was heated at 50 °C for 2 h. The reaction mixture was cooled to ambient temperature and $SOCl_2$ was removed under reduced pressure to give the crude product that was used in the next step without purification.

3.5.3.2.1. 5-Methylisoxazole-4-carbonyl chloride (**6**) ($C_5H_4ClNO_2$, Mol. Wt. 145.54)

Product obtained as a yellow oil, yield: 0.19 g (79%). TLC: CH_3OH - CH_2Cl_2 1:9 v/v, (R_F = 1). ^1H NMR (DMSO-d_6) δ 2.64 (s, 3H, CH_3), 8.77 (s, 1H, CH).

3.5.3.2.2. 4-Methylthiazole-5-carbonyl chloride (**9**) (C_5H_4ClNOS, Mol. Wt. 161.60)

Product obtained as a white powder, yield: 0.3g (99%). TLC: CH_3OH - CH_2Cl_2 1:9 v/v, (R_F = 0.8). ^1H NMR (DMSO-d_6) δ 2.6 (s, 3H, CH_3), 9.12 (s, 1H, CH).

3.5.3.3. General procedure for the preparation of (5-methylisoxazol-4-yl)(4-((4-phenyl)sulfonyl)piperazin-1-yl)methanone derivatives (**7a-f**) and (4-methylthiazol-5-yl)(4-((4-phenyl)sulfonyl)piperazin-1-yl)methanone derivatives (**10a-d**).

To a solution of phenyl sulphonyl piperazine derivatives (**3a-f**) (1.3 mmol) in dry THF (15.6 mL) was added 5-methylisoxazole-4-carbonyl chloride (**6**) (0.23g, 1.57 mmol) or 4-methylthiazole-5-carbonyl chloride (**9**) (0.25g, 1.57 mmol) and reaction mixture was heated at 65 °C overnight. The mixture was cooled to ambient temperature and the solvent evaporated under reduced pressure. The residue was dissolved in CH_2Cl_2 (100 mL) and washed with saturated aqueous $NaHCO_3$ (50 mL) and H_2O (50 mL). The organic layer was dried over $MgSO_4$ and evaporated under reduced pressure. The crude product was purified by gradient chromatography or by recrystallisation.

3.5.3.3.1. (5-Methylisoxazol-4-yl)(4-tosylpiperazin-1-yl)methanone (**7a**) ($C_{16}H_{19}N_3O_4S$, Mol. Wt. 349.41)

Product obtained after purification by gradient chromatography and collected at 4:96 v/v CH_3OH - CH_2Cl_2 as a white powder, yield: 0.4 g (88%), mp = 138 – 140 °C. TLC: CH_3OH - CH_2Cl_2 0.5:9.5 v/v, (R_F = 0.5). ^1H NMR ($CDCl_3$) δ 2.44 (s, 3H, CH_3, Ar), 2.49 (s, 3H, CH_3, isoxazole), 3.03 (br s, 4H, CH_2, pip), 3.74 (br s, 4H, CH_2, pip), 7.42 (d, J = 8 Hz, 2H, CH_2, Ar), 7.61 (d, J = 8.2 Hz, 2H, CH_2, pip), 8.10 (s, 1H, CH, isoxazole). ^{13}C NMR

($CDCl_3$) δ 12.1 (CH_3, isoxazole), 21.6 (CH_3, Ar), 45.4, 46.0 (4 x CH_2, pip), 161.8 (CH, isoxazole), 127.5, 130.9 (4 x CH, Ar), 132.1, 144.4 (2 x C, Ar), 110.8, 176.6 (2 x C, isoxazole), 170.91 (C=O). HRMS (ES-TOF) m/z calculated mass: 350.1090 $[M + H]^+$, observed mass: 350.1169 $[M + H]^+$.

3.5.3.3.2. (5-Methylisoxazol-4-yl)(4-((4-nitrophenyl)sulfonyl)piperazin-1-yl)methanone (**7b**) ($C_{15}H_{16}N_4O_6S$, Mol. Wt. 380.38)

Product obtained after purification by recrystallisation from CH_3OH as a pale powder, yield: 0.48 g (99%), mp = 168 – 170 ^{0}C. TLC: CH_3OH - CH_2Cl_2 0.5:9.5 v/v, (R_f = 0.8). ^{1}H NMR (DMSO-d_6) δ 2.4 (s, 3H, CH_3, isoxazole), 3.05 (br s, 4H, CH_2, pip), 3.55 (br s, 4H, CH_2, pip), 8 (d, J = 8 Hz, 2H, CH_2, Ar), 8.4 (d, J = 8.2 Hz, 2H, CH_2, Ar), 8.6 (s, 1H, CH, isoxazole). ^{13}C NMR (DMSO-d_6) δ 12.1 (CH_3, isoxazole), 46.1 (4 x CH_2, pip), 152.2 (CH, isoxazole), 125.3, 129.6 (4 x CH, Ar), 141.3, 150.6 (2 x C, Ar), 111.4, 170.2 (2 x C, isoxazole), 161.5 (C=O). Elemental analysis: calculated for $C_{15}H_{16}N_4O_6S$ (380.38) C 47.37%, H 4.24%, N 14.73%. Found: C 47.32%, H 4.25%, N 14.77%.

3.5.3.3.3. (4-([1,1'-Biphenyl]-4-ylsulfonyl)piperazin-1-yl)(5-methylisoxazol-4-yl)methanone (**7c**) ($C_{21}H_{21}N_3O_4S$, Mol. Wt. 411.48)

Product obtained after purification by gradient column chromatography and collected at CH_3OH - CH_2Cl_2 4:96 v/v as a crystalline solid, yield: 0.39 g of (55%), mp = 158 - 160 °C. TLC: CH_3OH - CH_2Cl_2 1:9 v/v, (R_f = 1). ^{1}H NMR (DMSO-d_6) δ 2.45 (s, 3H, CH_3, isoxazole), 3.0 (s, 4H, CH_2, pip), 3.6 (s, 4H, CH_2, pip), 7.45 (t, J = 8, 8 Hz, 1H, CH, Ar), 7.55 (t, J = 9.7, 9.7 Hz, 2H, CH, Ar), 7.75 (d, J = 7.9 Hz, 2H, CH, Ar), 7.85 (d, J = 8 Hz, 2H, CH, Ar), 7.95 (d, J = 7.9 Hz, 2H, CH, Ar), 8.65 (s, 1H, CH, isoxazole). ^{13}C NMR (DMSO-d_6) δ 12.0 (CH3, isoxazole), 127.2, 127.8, 129.6, 129.8, 130.4 (9 x CH, Ar), 133.0, 137.9, 144.5 (3 x C, Ar), 151.5 (CH, isoxazole), 111.2, 169.9 (2 x C, isoxazole), 161.5 (C=O). Elemental analysis: calculated for $C_{21}H_{21}N_3O_4S$ (411.48): C 61.29%, H 5.14%, N 10.21%. Found: C 60.96%, H 4.85%, N 10.12%. HRMS (ES-TOF) m/z calculated mass: 412.1321 $[M + H]^+$, observed mass: 412.1321 $[M + H]^+$.

3.5.3.3.4. (4-((4'-Methoxy-[1,1'-biphenyl]-4-yl)sulfonyl)piperazin-1-yl)(5-methylisoxazol-4-yl)methanone (**7d**) ($C_{22}H_{23}N_3O_5S$, Mol. Wt. 441.50)

Product obtained after purification by recrystallisation from EtOAc as a white powder, yield: 0.33 g (57%), mp = 198 – 200 ^{0}C. TLC: CH_3OH - CH_2Cl_2: 1:9 v/v, (R_f = 0.9). ^{1}H NMR (DMSO-d_6) δ 2.44 (s, 3H, CH_3, isoxazole), 3.01 (s, 4H, CH_2, pip), 3.45 (s, 4H, CH_2, pip), 3.85 (s, 3H, OCH_3), 7.1 (d, J = 7.9 Hz ,2H, CH, Ar), 7.5 (d, J = 7.9 Hz,2H, CH, Ar), 7.79 (d, J = 8.1 Hz, 2H, CH, Ar), 7.9 (d, J = 8.1 Hz,2H, CH, Ar), 8.65 (s, 1H, CH, isoxazole). ^{13}C NMR (DMSO-d_6) δ 12.0 (CH_3, isoxazole), 46.2 (4 x CH_2, pip), 55.7 (OCH_3), 115.1, 127.4, 127.7, 128.7 (8 x CH, Ar), 131.3, 133.0, 145.9, 160.3 (4 x C, Ar), 111.5 (CH, isoxazole), 148.6, 170.1 (2 x C, isoxazole), 161.5 (C=O). Elemental analysis: calculated for $C_{22}H_{23}N_3O_5S$•0.1H_2O (443.30148) C 59.60% H 5.22%, N 9.48%. Found: C 59.42%, H 5.20%, N 9.38%.

3.5.3.3.5. (4-((4'-Fluoro-[1,1'-biphenyl]-4-yl)sulfonyl)piperazin-1-yl)(5-methylisoxazol-4-yl)methanone (**7e**) ($C_{21}H_{20}FN_3O_4S$, Mol. Wt. 429.47)

Product obtained after purification by preparative TLC using CH_3OH - CH_2Cl_2 1:9 v/v as colourless needles, yield: 120 mg (52%), mp = 172 - 174 ^{0}C. TLC: CH_3OH - CH_2Cl_2 1:9 v/v, (R_f = 0.9). ^{1}H NMR ($CDCl_3$) δ 2.52 (s, 3H, CH_3, isoxazole), 3.13 (br s, 4H, CH_2, pip), 3.75 (s, 4H, CH_2, pip), 7.20 (t, J = 9.8, 9.8 Hz, 2H, CH, Ar), 7.59 (d, J = 8.8 Hz, 2H, CH, Ar), 7.72 (d, J = 8.6 Hz, 2H, CH, Ar), 7.83 (d, J = 8.6 Hz, 2H, CH, Ar), 8.15 (s, 1H, CH, isoxazole). ^{13}C NMR ($CDCl_3$) δ 12.1 (CH_3, isoxazole), 46.0 (4 x CH_2, pip), 116.1, 116.3, 127.8, 128.3 (8 x CH, Ar), 133.9, 135.1, 162.3, 161.9 (4 x C, Ar), 148.6 (CH, isoxazole), 110.7, 171.1 (2 x C, isoxazole), 164.3 (C=O). HRMS (ES-TOF) m/z calculated mass: 452.1159 [M + Na]$^+$, observed mass: 452.1050 [M + Na]$^+$.

3.5.3.3.6. (4-((4'-Chloro-[1,1'-biphenyl]-4-yl)sulfonyl)piperazin-1-yl)(5-methylisoxazol-4-yl) methanone (**7f**) ($C_{21}H_{20}ClN_3O_4S$, Mol. Wt. 445.92)

Product obtained after purification by gradient column chromatography and collected at petroleum ether - EtOAc 20:80 v/v as a pale yellow crystalline solid, yield: 0.88g (59%), mp = 190 - 192 ^{0}C. TLC: petroleum ether - EtOAc 1:1 v/v, (R_f = 0.9). ^{1}H NMR ($CDCl_3$) δ 2.43 (s, 3H, CH_3, isoxazole), 3.04 (br s, 4H, CH_2, pip), 3.66 (s, 4H, CH_2, pip), 7.39 (d, J = 9 Hz ,2H, CH, Ar), 7.47 (d, J = 9 Hz,2H, CH, Ar), 7.65 (d, J = 10 Hz, 2H, CH, Ar), 7.74 (d, J = 10 Hz,2H, CH, Ar), 8.06 (s, 1H, CH, isoxazole). ^{13}C NMR ($CDCl_3$) δ 11.9 (CH_3, isoxazole), 46.1 (4 x CH_2, pip), 127.8, 128.4, 128.6, 129.4 (8 x CH, Ar), 134.2, 135.1, 137.4, 145.1 (4 x C, Ar), 148.6 (CH, isoxazole), 110.7, 171.1 (2 x C, isoxazole),

161.9 (C=O). HPLC: 98.2% at RT: 5.3 min. HRMS (ES-TOF) m/z calculated mass: 468.0863 $[M + Na]^+$, observed mass: 468.0749 $[M + Na]^+$.

3.5.3.3.7. (4-Methylthiazol-5-yl)(4-tosylpiperazin-1-yl)methanone (**10a**) ($C_{16}H_{19}N_3O_3S$, Mol. Wt. 365.47)

Product obtained after purification by gradient column chromatography and collected at 4:96 CH_3OH - CH_2Cl_2 v/v as a yellow powder, yield: 0.24 g (86%), mp = 143 - 144 ^{0}C. TLC: CH_3OH - CH_2Cl_2 1:9 v\v, (R_F = 0.5). ^{1}H NMR ($CDCl_3$) δ 2.35 (s, 3H, CH_3, thiazole) 2.38 (s, 3H, CH_3, Ar), 2.96 (br s, 4H, CH_2, pip) 3.58 (br s, 4H, CH_2, pip), 7.28 (d, J = 7.9 Hz, 2H, CH, Ar), 7.55 (d, J = 8 Hz, 2H, CH, Ar), 8.66 (s, 1H, CH, thiazole). ^{13}C NMR ($CDCl_3$) δ 16.3 (CH_3, thiazole), 21.6 (CH_3, Ar), 46.0 (4 x CH_2, pip), 152.9 (CH, thiazole), 127.7, 130.0 (4 x CH, Ar), 132.3, 144.3 (2 x C, Ar), 123.7, 152.9 (2 x C, thiazole), 162.7 (C=O). HRMS (ES-TOF) m/z calculated mass: 366.0941 $[M + H]^+$, observed mass: 366.0941 $[M + H]^+$.

3.5.3.3.8. (4-Methylthiazol-5-yl)(4-((4-nitrophenyl)sulfonyl)piperazin-1-yl)methanone (**10b**) ($C_{15}H_{16}N_4O_5S_2$, Mol. Wt. 396.44)

Product obtained after purification by gradient column chromatography and collected at 6:94 v/v CH_3OH - CH_2Cl_2 as yellow granules, yield: 0.4 g (73%), mp = 190 – 200 ^{0}C. TLC: CH_3OH - CH_2Cl_2 1:9 v/v, (R_F = 0.4).^{1}H NMR ($CDCl_3$) δ 2.44 (s, 3H, CH_3, thiazole), 3.13 (br s, 4H, CH_2, pip) 3.73 (br s, 4H, CH_2, pip), 7.95 (d, J = 9 Hz, 2H, CH, Ar), 8.42 (d, J = 8.9 Hz, 2H, CH, Ar), 8.76 (s, 1H, CH, thiazole). ^{13}C NMR ($CDCl_3$) δ 16.4 (CH_3, thiazole), 46.6 (4 x CH_2, pip), 154.9 (CH, thiazole), 125.3, 129.6 (4 x CH, Ar), 150.7, 152.0 (2 x C, Ar), 124.7, 141.4 (2 x C, thiazole), 162.4 (C=O). HRMS (ES-TOF) m/z calculated mass: 397.0561 $[M + H]^+$, observed mass: 397.0640 $[M + H]^+$.

3.5.3.3.9. (4-([1,1'-Biphenyl]-4-ylsulfonyl)piperazin-1-yl)(4-methylthiazol-5-yl)methanone (**10c**) ($C_{21}H_{21}N_3O_3S_2$, Mol. Wt. 427.54)

Product obtained after purification by gradient column chromatography and collected at 5:95 v/v CH_3OH - CH_2Cl_2 as a yellow oil, yield: 0.1 g (26%). TLC: CH_3OH - CH_2Cl_2 1:9 v\v, (R_F = 0.7). ^{1}H NMR ($CDCl_3$) δ 2.4 (s, 3H, CH_3, thiazole), 3.2 (br s, 4H, CH_2, pip) 3.7 (br s, 4H, CH_2, pip), 7.41 (t, J = 7.9, 7.9 Hz, 1H, CH, Ar), 7.48 (d, J = 7.9 Hz, 2H, CH, Ar), 7.6 (d, J = 8 Hz, 2H, CH, Ar), 7.75 (d, J = 7.9 Hz, 2H, CH, Ar), 7.8 (d, J = 8 Hz, 2H, CH, Ar), 8.71 (s, 1H, CH, thiazole). ^{13}C NMR ($CDCl_3$) δ 16.3 (CH_3, thiazole) 44.9, 45.5, 45.9, 46.0

(4 x CH_2, pip), 127.1, 127.6, 127.9, 128.2, 129.5, (9 x CH, Ar), 132.8, 133.9, 152.9 (3 x C, Ar), 138.9, 146.1 (2 x C, thiazole), 153.1 (CH, thiazole), 160.7 (C=O). HRMS (ES-TOF) m/z calculated mass: 428.1037 $[M + H]^+$, observed mass: 428.1116 $[M + H]^+$.

3.5.3.3.10. (4-((4'-Methoxy-[1,1'-biphenyl]-4-yl)sulfonyl)piperazin-1-yl)(4-methylthiazol-5-yl)methanone (**10d**) ($C_{22}H_{23}N_3O_4S_2$, Mol. Wt. 457.56)

Product obtained after purification by gradient column chromatography and collected at 6:94 v/v CH_3OH - CH_2Cl_2 as white crystals, yield: 0.46 g (78%), mp = 212 - 214 ^{0}C. TLC: CH_3OH - CH_2Cl_2 1:9 v\v, (R_F = 0.9). ^{1}H NMR (DMSO-d_6) δ 2.29 (s, 3H, thiazole CH_3), 3.0 (br s, 4H, CH_2, pip) 3.6 (br s, 4H, CH_2, pip), 3.85 (s, 3H, OCH_3), 7.05 (d, 2H, J = 7.9 Hz, 2H, CH, Ar), 7.75 (d, 2H, J = 8 Hz, 2H, CH, Ar), 7.79 (d, 2H, J = 8 Hz, 2H, CH, Ar), 7.91 (d, 2H, J = 7.9 Hz, 2H, CH, Ar), 9.09 (s, 1H, thiazole CH). ^{13}C NMR (DMSO-d_6) δ 16.4 (CH_3, thiazole), 46.2 (4 x CH_2, pip), 55.8 (OCH_3), 115.1, 127.4, 128.8, 128.6, (8 x CH, Ar), 124.7, 130.9, 133.4, 160.3 (4 x C, Ar), 144.9, 152.0 (2 x C, thiazole), 153.1 (CH, thiazole), 162.5 (C=O). Elemental analysis: calculated for $C_{22}H_{23}N_3O_4S_2$•0.3H_2O (462.964) C 57.08%, H 5.01%, N 9.07% Found: C 56.88%, H 5.09%, N 8.89%.

3.5.3.4. General procedure for the preparation of (5-methylisoxazol-3-yl)(4-((4-phenyl)sulfonyl)piperazin-1-yl)methanone derivatives (**14a-d**).

A solution of 5-methyl isoxazole-3-carboxylic acid (**11**) (0.2 g, 1.57 mmol) in dry DMF (6 mL) was combined with 1,1'-carbonyldiimidazole (**13**) (CDI) (0.31 g, 1.89 mmol). The reaction was stirred for 1 h at room temperature under nitrogen. After cooling the mixture to 0 ^{0}C, a solution of phenyl sulphonyl piperazine derivatives (**3a**-**d**) (1.57 mmol) in dry DMF (5mL) was added and the reaction stirred at room temperature for 48 h. On completion, the solvent was evaporated under reduced pressure then the residue was dissolved in CH_2Cl_2 (100 mL) and washed saturated aqueous $NaHCO_3$ (50 mL) and H_2O (50 mL). The organic layer was dried ($MgSO_4$) and evaporated under reduced pressure.

3.5.3.4.1. (5-Methylisoxazol-3-yl)(4-tosylpiperazin-1-yl)methanone (**14a**) ($C_{16}H_{19}N_3O_4S$, Mol. Wt. 349.41)

Product obtained after purification by gradient column chromatography and collected at 2:98 v/v CH_3OH - CH_2Cl_2 as a light brown crystalline solid, yield: 0.3g (68%), mp =

148 - 150 ^{0}C. TLC: CH_3OH- CH_2Cl_2 1:9 v/v (R_F = 0.8). ^{1}H NMR (DMSO-d_6) δ 2.7 (s, 3H, CH_3), 2.85 (s, 3H, CH_3, isooxazole), 2.96 (br s, 4H, CH_2, pip) 3.7 (s, 2H, CH_2, pip), 3.8 (s, 2H, CH_2, pip), 6.14 (s, 1H, CH, isoxazole), 7.24 (d, J = 7.9 Hz, 2H, CH, Ar), 7.52 (d, J = 8 Hz, 2H, CH, Ar). ^{13}C NMR (DMSO-d_6) δ 12.2 (CH_3, isoxazole), 21.5 (CH_3, Ar), 41.4, 46.1, 46.1, 46.6 (4 x CH_2, pip), 102.8 (CH, isoxazole), 128.1, 130.5 (4 x CH, Ar), 132.2, 144.4 (2 x C, Ar), 158, 170.9 (2 x C, isoxazole) 159.8 (CO). HRMS (ES-TOF) m/z calculated mass: 350.1090 $[M + H]^+$, observed mass: 350.1169 $[M + H]^+$.

3.5.3.4.2. (5-Methylisoxazol-3-yl)(4-((4-nitrophenyl)sulfonyl)piperazin-1-yl)methanone (**14b**) ($C_{15}H_{16}N_4O_6S$, Mol. Wt. 380.38)

Product obtained after purification by gradient column chromatography and collected at 94:6 v/v CH_3OH - CH_2Cl_2 as a pale yellow solid, yield: 0.146 g (99%), mp = 170 - 172 ^{0}C. TLC: CH_3OH - CH_2Cl_2 1:9 v/v (R_F = 0.9). ^{1}H NMR ($CDCl_3$) δ 2.49 (s, 3H, CH_3, isoxazole), 3.21 (s, 4H, CH_2, pip), 3.85 (s, 2H, CH_2, pip), 4.05 (s, 2H, CH_2, pip), 6.25 (s, 1H, CH, isoxazole), 7.95 (d, J = 7.9 Hz, 2H, CH, Ar), 8.4 (d, J = 7.9 Hz, 2H, CH, Ar). ^{13}C NMR ($CDCl_3$) δ 12.1 (CH_3, isoxazole), 41.9, 45.7, 46.3, 46.5 (4 x CH_2, pip), 103.1 (CH, isoxazole), 124.6, 128.9 (4 x CH, Ar), 141.4, 150.4 (2 x C, Ar), 158.2, 170.4 (2 x C, isoxazole), 159.5 (CO). Elemental analysis calculated for $C_{15}H_{16}N_4O_6S$ (380.38): C 47.37%, H 4.24%, N 14.72%. Found: C 47.25%, H 4.34%, N 14.54%.

3.5.3.4.3. (4-([1,1'-Biphenyl]-4-ylsulfonyl)piperazin-1-yl)(5-methylisoxazol-3-yl)methanone (**14c**) ($C_{21}H_{21}N_3O_4S$, Mol. Wt. 411.48)

Product obtained after purification by gradient column chromatography and collected at 6:94 v/v CH_3OH - CH_2Cl_2 as a white powder, yield: 0.146 g (26%), mp = 150 - 152 ^{0}C. TLC: CH_3OH - CH_2Cl_2 1:9 v/v (R_F = 0.9). ^{1}H NMR ($CDCl_3$) δ 2.49 (s, 3H, CH_3, isoxazole), 3.2 (s, 4H, CH_2, pip), 3.85 (s, 2H, CH_2, pip), 4.05 (s, 2H, CH_2, pip), 6.25 (s, 1H, CH, isoxazole), 7.49 (m, 1H, CH, Ar), 7.50 (d, J = 8 Hz, 2H, CH, Ar), 7.65 (d, J = 8 Hz, 2H, CH, Ar), 7.80 (d, J = 8 Hz, 2H, CH, Ar), 7.90 (d, J = 7.9 Hz, 2H, CH, Ar). ^{13}C NMR ($CDCl_3$) δ 12.1 (CH_3, isoxazole), 41.9, 45.8, 46.4, 46.6 (4 x CH_2, pip), 103.1 (CH, isoxazole), 127.4, 127.9, 128.3, 128.6, 129.1 (9 x CH, Ar), 133.8, 139.1 (2 x C, Ar), 158.3, 170.3 (2 x C, isoxazole), 159.6 (CO). Elemental analysis: calculated for $C_{21}H_{21}N_3O_4S$•0.1 H_2O (413.2814): C 61.03%, H 5.14%, N 10.21 %. Found: C 60.94%, H 5.09%, N 10.41%.

3.5.3.4.4. (4-((4'-Methoxy-[1,1'-biphenyl]-4-yl)sulfonyl)piperazin-1-yl)(5-methylisoxazol-3-yl)methanone (**14d**) ($C_{22}H_{23}N_3O_5S$, Mol. Wt. 441.50)

Product obtained after purification by gradient column chromatography and collected at 6:94 v/v CH_3OH - CH_2Cl_2 as a white powder, yield: 0.62 g (90%), mp = 198 - 200 ^{0}C, TLC: CH_3OH - CH_2Cl_2 0.5:9.5 v/v (R_F = 0.9). ^{1}H NMR ($CDCl_3$) δ 2.49 (s, 3H, CH_3, isoxazole), 3.23 (s, 4H, CH_2, pip), 3.32 (s, 2H, CH_2, pip), 3.81 (s, 3H, OCH_3), 4.05 (s, 2H, CH_2, pip), 6.25 (s, 1H, CH, isoxazole), 7.50 (d, J = 8 Hz, 2H, CH, Ar), 7.65 (d, J = 8 Hz, 2H, CH, Ar), 7.80 (d, J = 8 Hz, 2H, CH, Ar), 7.90 (d, J = 7.9 Hz, 2H, CH, Ar). ^{13}C NMR ($CDCl_3$) δ 12.1 (CH_3, isoxazole), 41.8, 45.7, 46.3, 46.5 (4 x CH_2, pip), 100.0 (CH, isoxazole), 114.6, 127.1, 127.1, 130.3 (8 x CH, Ar), 131.0, 138.3, 141.4, 150.4 (4 x C, Ar), 158.2, 170.4 (2 x C, isoxazole), 159.5 (CO). Elemental analysis: calculated for $C_{22}H_{23}N_3O_5S$•0.2H_2O (445.10296): C 59.37%, H 5.21%, N 9.44%. Found: C 59.20%, H 5.37%, N 9.25%.

Chapter 4: (S)-4-(4-phenyl-4-yl) sulfonyl)piperazin-1-yl)-3-amino-4-oxobutanamide derivatives

(Series 2)

4. Introduction

In this chapter, 4-(4-([1-phenyl]-4-yl)sulfonyl)piperazin-1-yl)-3-amino-4-oxobutanamide derivatives (**18**) were prepared retaining the same linker and substituted aryl/biaryl moieties as the adenine mimic but replacing the amino acid isoxazole or thiazole moiety with asparagine (Table 31). The rationale for the design of this series is based on exploiting the potency of the sulfamoyl linkage as well as mimicking asparaginyl adenylate, which is the natural substrate of AsnRS to increase the binding interactions with *S. aureus* and *E. faecalis* AsnRSs and to test the multitarget hypothesis in the case of binding with *S. aureus* and *E. faecalis* AspRSs.

Table 31: General chemical structures of scheme 2 AspRS and AsnRS inhibitors (**18**).

Series	General chemical structures	R groups
2	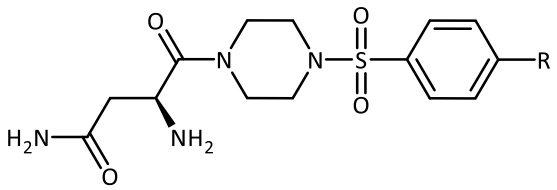	CH_3, NO_2, F, C_6H_5, $C_6H_4OCH_3$, C_6H_4F, C_6H_4Cl

This chapter is divided into four parts as follows:

- Results and discussion
- Docking studies
- Biological screening
- Methods

4.1. Synthetic pathway for (S)-4-(4-([1-phenyl]-4-yl)sulfonyl)piperazin-1-yl)-3-amino-4-oxobutanamide derivatives (18)

The methyl-thiazole or methyl-isoxazole rings as classical bioisosteres of Asp/Asn in series 1 were replaced by asparagine, combined with piperazine-sulfamoyl as the linker and substituted aryl or biaryl moieties instead of the adenine base. The synthetic pathways are shown in scheme 7 and involved the following steps:

- Nucleophilic reaction of piperazine with sulfonyl chloride derivatives (**3a**-**g**)
- Coupling reaction of sulfonyl piperazines with Boc-L-asparagine (**17a**-**g**)
- Deprotection of the Boc group (**18a**-**g**)

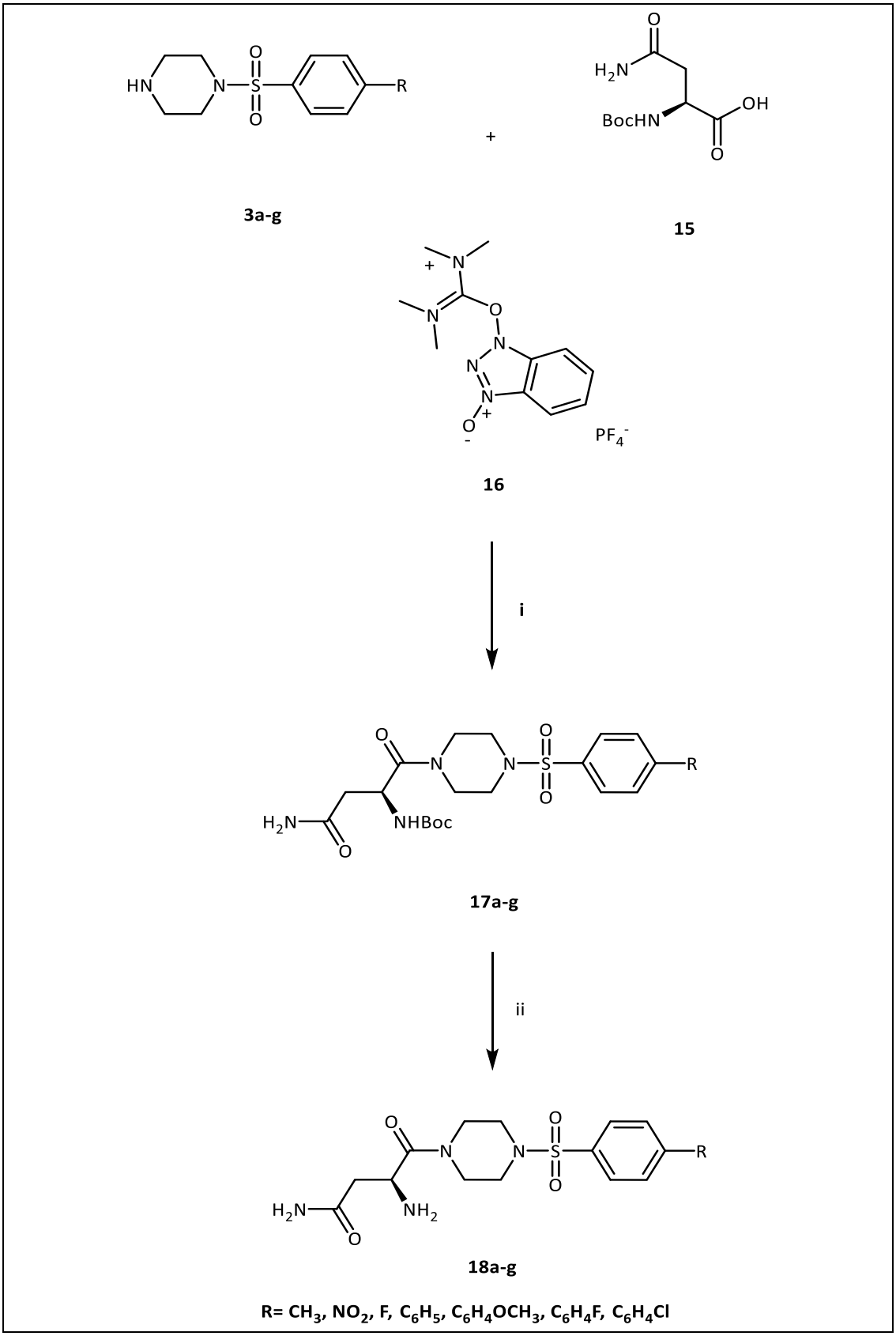

Scheme 7: Synthetic pathway for (S)-4-(4-phenyl-4-yl)sulfonyl)piperazin-1-yl)-3-amino-4-oxobutanamide derivatives (**18a-g**). *Reagents and conditions*: (i) Dry CH_2Cl_2, TBTU (**16**), Et_3N, rt, on, (ii) HCl/dioxane, 0 ^oC then rt, 3-24 h.

4.1.1. Synthesis of sulfonyl piperazine derivatives (3a-g)

The preparation of sulfonyl piperazine derivatives (**3a**-**g**) (327) was discussed in chapter 3.

4.1.2. Coupling reaction of phenyl-4-sulfonyl piperazine derivatives with N-Boc-L asparagine (17a-g)

To prepare the amide linkage directly from the carboxylic acid of asparagine (**15**) and the phenyl-4-sulfonyl piperazine derivatives (**3a**-**g**), coupling reagents were used as activating agents to form a good leaving group, which could then be displaced by the amine of the piperazine in compounds **3a**-**g** during nucleophilic substitution (327). In this synthetic step, propyl phosphonic anhydride (T_3P) and *O*-(benzotriazol-1-yl) N, N, *N´, N´*-tetramethyluranium tetrafluroborate (TBTU) were investigated as coupling agents. T_3P is an excellent and mild reagent for amide linkage formation (336) and the resulting propane phosphonic acid by-product is water-miscible, which is easily removed and non-hazardous (337), however, the reaction was unsuccessful. TBTU should be used in equimolar amounts relative to the carboxylic acid component of the coupling reaction to avoid reaction with the unprotected N-terminal of the amino acid (338). In this synthetic scheme, the protected L-asparagine (**15**) was used (Scheme 7) because unprotected asparagine has poor organic solubility and therefore slow coupling rates (339). It has been reported that the protection of the Asn side chain contributed to an increase in the coupling yield as well as conferring improved solubility of Asn derivatives through reducing the formation of hydrogen bonds that stabilise the structure (340). Using TBTU (**16**) in this synthetic step (Scheme 7) was successful to produce the coupled products (**17a**-**g**) in good yields (Table 32).

Table 32: Identification data for tert-butyl(4-amino-1-(4-phenyl)sulfonyl)piperazinyl)-1,4-dioxobutan-2-yl)carbamate derivatives (**17a-g**).

Compd	**R**	**Yield (%)**	**mp (^{0}C)**	**Appearance**
17a	CH_3	46	78-80	White solid
17b	NO_2	87	210-212	Yellow powder
17c	F	87	171-173	White solid
17d	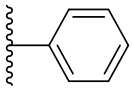	69	100-102	Colourless solid
17e	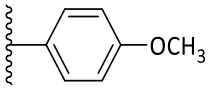	48	-	Colorless semisolid
17f	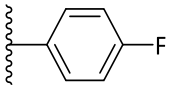	65	215-217	White powder
17g	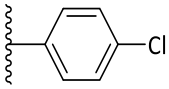	63	-	Colourless semisolid

The presence of Et_3N in this reaction is essential to deprotonate the Boc-L-asparagine to generate the carboxylate anion, which subsequently attacks TBTU to form the unstable *O*-acyl (tetramethyl) isouronium salt. The resulting anion attacked the electrophilic centre of the Boc-L-asparagine bearing the tetramethyl urea to afford the active ester and liberate tetramethyl urea. Consequently, this ester undergoes further nucleophilic attack by sulphonyl piperazine derivatives resulting in acylation of the coupled product (Scheme 8). ^{1}H and ^{13}C NMR spectra and either elemental analysis or HRMS confirmed the structures and purity. For example, the ^{1}H NMR spectra showed aromatic *CH* signals in the aromatic region as four doublet peaks, each integrated for 2 protons (Figure 126a), piperazine was observed as two broad multiplet peaks integrated for 4 protons each (Figure 126b), while Boc asparagine peaks showed as a singlet peak for $C(CH_3)_3$ integrated for nine protons, a doublet peak for CH_2, a quartet peak for *CH* and a singlet peak for *NH* (Figures 126c-d). The NH_2 peak was not observed

in the ^{1}H NMR spectra of compounds **17b** and **17e-g** while it was clearly observed in compounds **17a** and **17c-d**. High resolution mass spectrometry was used to check the molecular formula of the compounds.

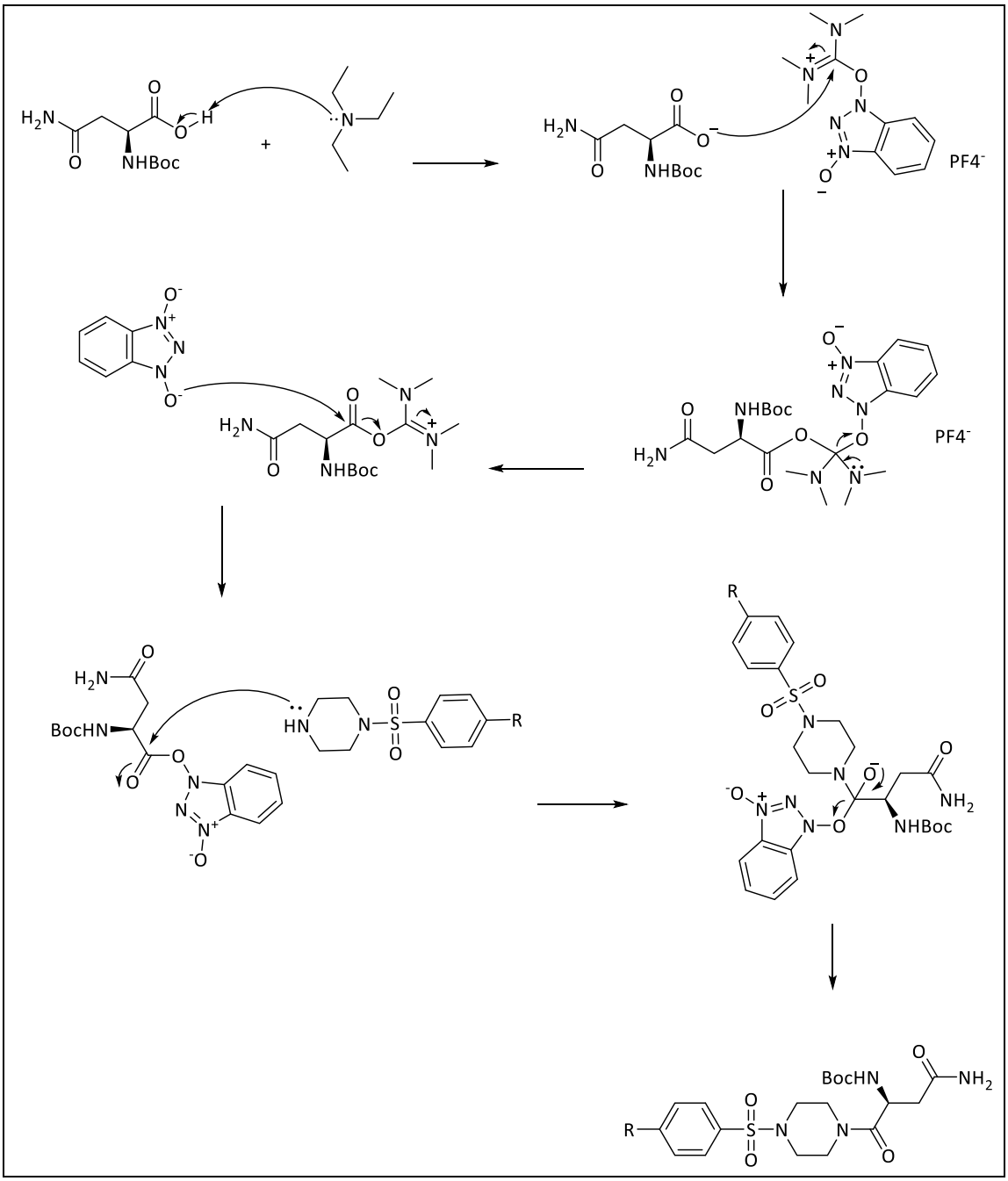

Scheme 8: Mechanism of the coupling reaction between phenyl sulfonyl piperazine derivatives (**3a-g**) and N-Boc-L-asparagine (**15**) using TBTU (**16**).

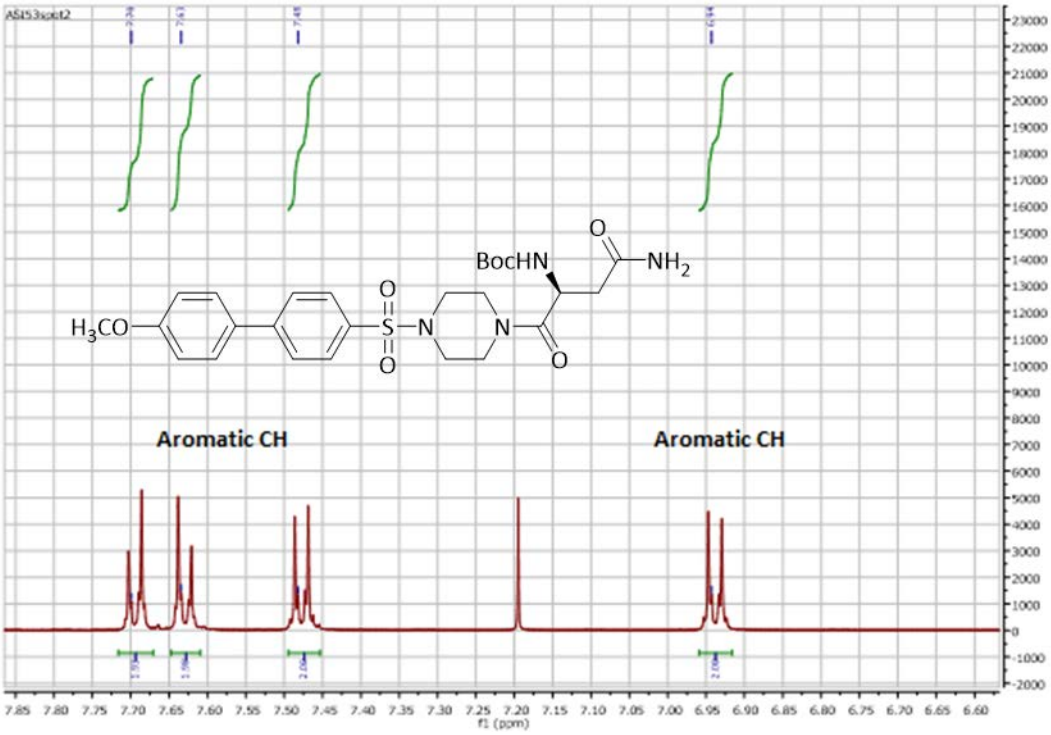

Figure 126a: ^{1}H NMR spectrum of compound **17e**. The spectrum shows aromatic CH as four peaks, each integrated for 2 protons.

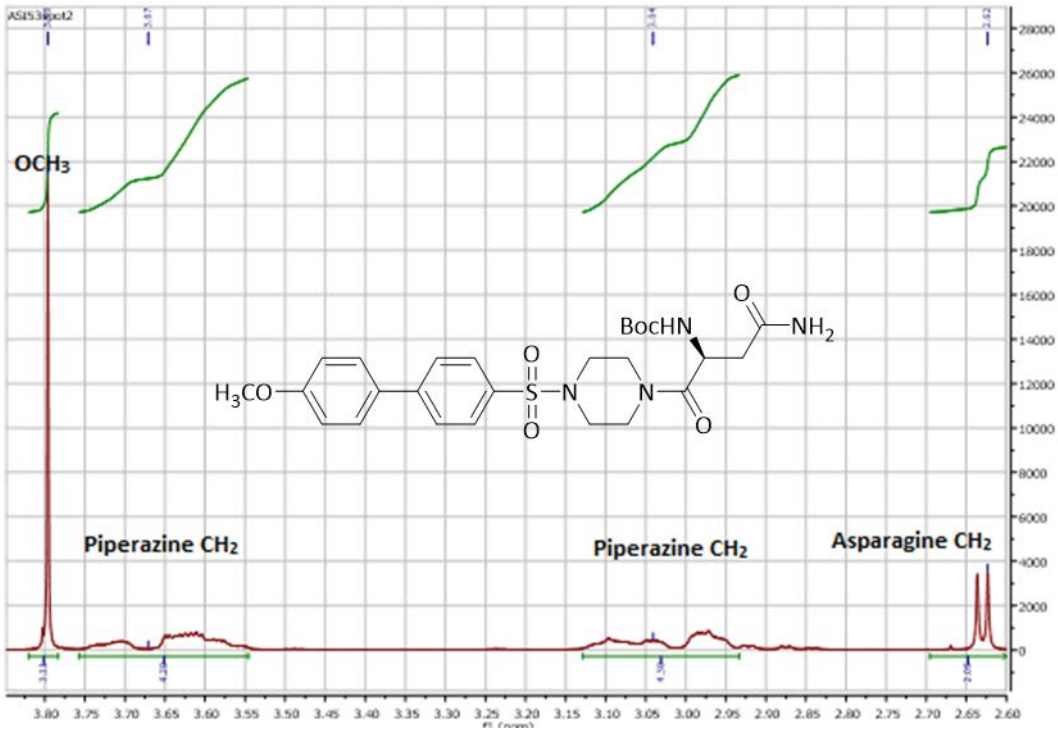

Figure 126b: ^{1}H NMR spectrum of compound **17e**. The spectrum shows OCH_3 peak as a singlet, two piperazine peaks and doublet peak of asparagine CH_2.

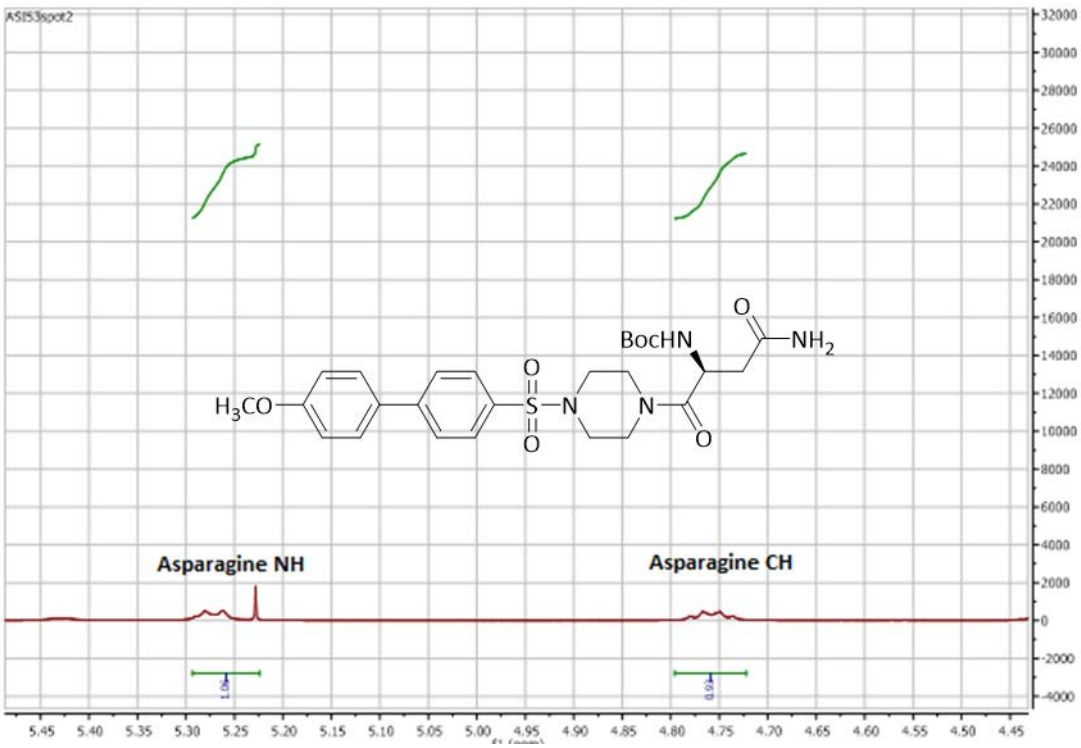

Figure 126c: ^{1}H NMR spectrum of compound **17e**. The spectrum shows the NH peak as a doublet and asparagine CH as a quartet peak.

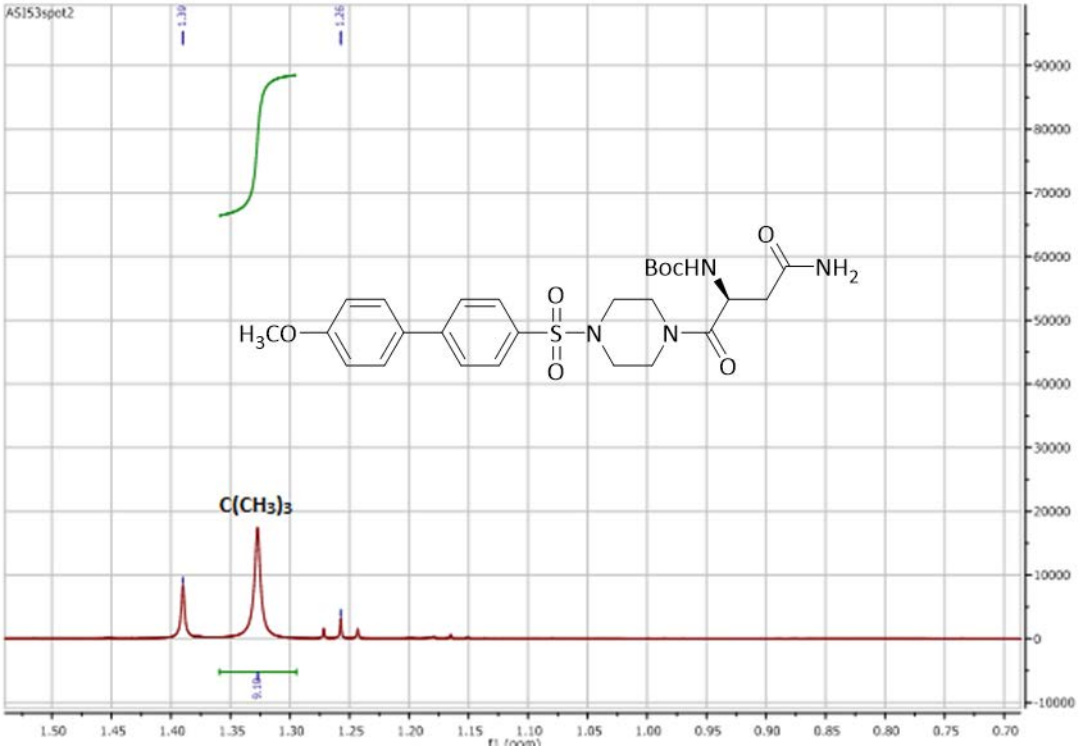

Figure 126d: ^{1}H NMR spectrum of compound **17e**. The spectrum shows $C(CH_3)_3$ peak as a singlet between ethanol peaks.

4.1.3. Boc deprotection for the preparation of (S)-4-(4-([1-phenyl]-4-yl)sulfonyl) piperazin-1-yl)-3-amino-4-oxobutanamide derivatives (18a-g)

The *tert*-butoxy carbonyl (Boc) group is an amine protecting group having acid and thermal sensitivity so can be easily removed using either concentrated acid or by heating at more than 80 ^{O}C (341, 342). In this synthetic pathway, the protected moiety is the asparagine amino acid and the removal of the Boc is particularly difficult in the N-terminal owing to the proximity of the free α-amino group, which under acidic conditions is in its protonated form (343). Deprotection using trifluoracetic acid (TFA) in CH_2Cl_2 (344), which is common method for amine deprotection, was attempted, however, it was unsuccessful owing to amide bond cleavage resulting in a complex mixture. However, deprotection of compounds **17a**-**g** using HCl in dioxane (345, 346) was successful generating the final products **18a**-**c** and **18e** in satisfactory yields (51-67%), and compounds **18d** and **18f**-**g** were obtained in lower yields (24-35%) (Table 33).

Table 33: Identification data for (S)-4-(4-([1-phenyl]-4-yl)sulfonyl)piperazin-1-yl)-3-amino-4-oxobutanamide hydrogen chloride derivatives (**18a**-**g**).

Compd	R	Yield (%)	mp (^{0}C)	Appearance
18a	CH_3	56	215-220	White solid
18b	NO_2	60	198-200	White solid
18c	F	51	175-177	White solid
18d	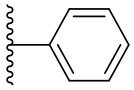	35	205-210	White crystalline solid
18e	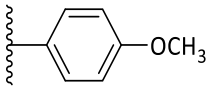	67	238-240	White powder
18f	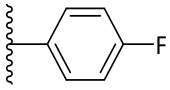	24	220-222	White powder
18g	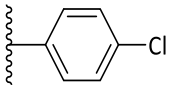	33	212-214	White solid

^{1}H, ^{13}C NMR spectra and HRMS confirmed the structures and purity. For example, the ^{1}H NMR spectra of compounds **18f** and **18g** showed the α amino group after deprotection as a singlet peak integrated for 3 protons (Figures 126 and 127).

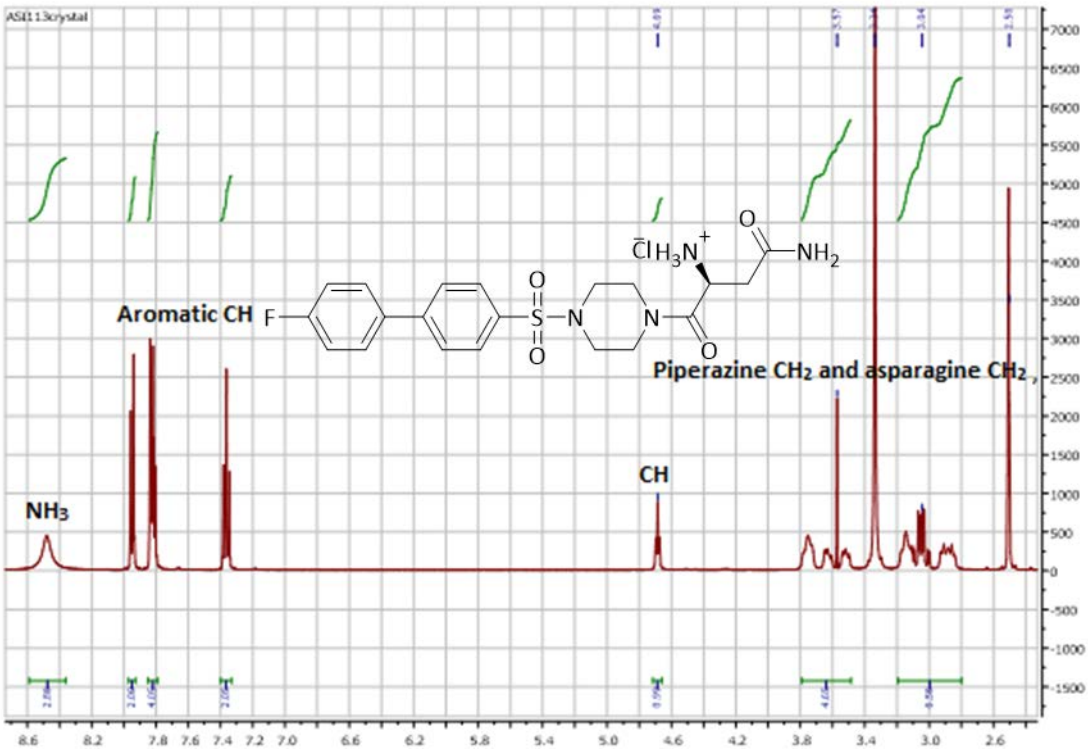

Figure 127: ^{1}H NMR spectrum of compound **18f**. The spectrum shows the NH_3 peak as a singlet peak, CH peak as a triplet and CH_2 as a doublet of doublet. It shows DMSO, H_2O and ethanol peaks.

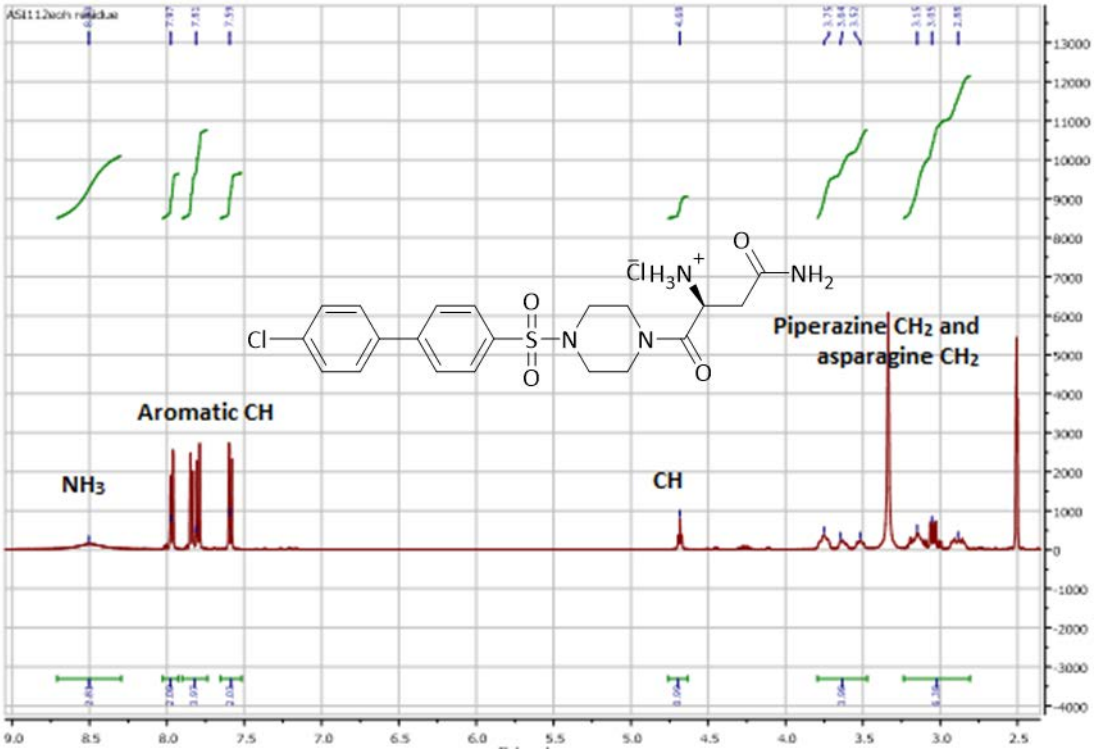

Figure 128: ^{1}H NMR spectrum of compound **18g**. The spectrum shows the NH_3 peak as a singlet, CH peak as a triplet and CH_2 as a doublet of doublet. It shows DMSO and H_2O peaks.

4.2 Docking studies

A docking study of the final compounds of series 2 with *S. aureus* and *E. faecalis* AspRSs and AsnRSs was performed to determine their binding interactions with the active sites of the respective aaRS enzymes. The docking study showed that the compounds interacted with some of the amino acid residues observed for the aa-AMP natural substrates binding interactions. Compounds **18a**-**c** showed good hydrogen bonding interactions, however, they were easily flipping inside the pockets owing to the smaller size and inability to completely fill the pocket. In contrast, the asparagine moiety of compounds **18d**-**g** did not show good interactions with the amino acid residues in the histidine and flipping loops of *S. aureus* and *E. faecalis* AspRS.

4.2.1. Docking studies of *S. aureus* AspRS

Through alignment of series 2 compounds with aspartyl adenylate in *S. aureus* AspRS, the amino acid residues responsible for binding interactions were identified (Figure 129) (Table 34). The asparagine moiety of series 2 compounds showed good hydrogen

binding interactions with the key amino acid residues in the Asp pocket, however, the flipping loop was not shown close to the asparagine moiety in compounds **18a-g** (Figures 130-132). As the interaction of Gln237 with the α -phosphate O and carbonyl atom of the aspartyl adenylate is a specific interaction for eubacteria AspRS enzymes (293), the docking study of compound **18c** showed that there was a hydrogen bond between Glu237 and the sulfamoyl O (Figure 130). Asp239, as an important amino acid residue formed a water mediated hydrogen bond with the Asp moiety of aspartyl adenylate formed the same interaction with the carbonyl group of Asn moiety in compound **18g** (Figure 132). However, not all key amino acid residues in the AMP pocket bound with aryl/biaryl moieties (Figures 130-132) and there was no binding interaction with methoxy, chloro and fluoro groups in compounds **18e**, **18f** and **18h** respectively.

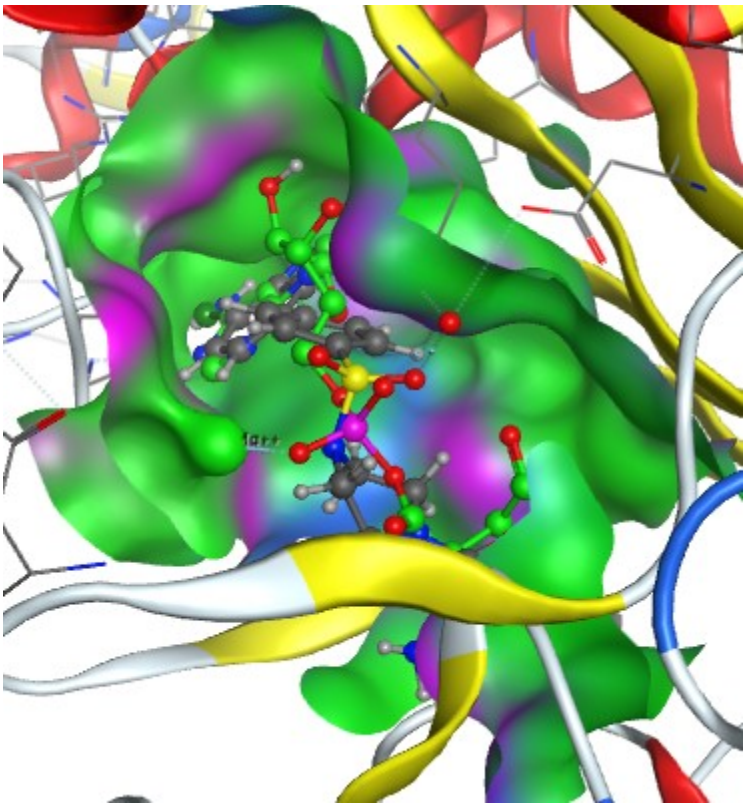

Figure 129: Alignment of compound **18g** (grey) with aspartyl adenylate (green) in the active sites of *S. aureus* AspRS**.**

Table 34: Binding interactions of series 2 compounds with the amino acid residues of the binding sites of *S. aureus* AspRS.

Ligands	Aspartic acid pocket	AMP pocket
Aspartyl-adenylate	Gln201, Lys204, His452, Gly488, Ser490, Arg492 and Asp239	Arg223, Phe235, Arg540, Gln232, Gln237 and Glu485
18a	Ser199, Arg231, Asp239, Gly488, His451 and His452	Arg223, Gln237, Asp478 and Glu485
18b	Ser199, Asp239, His451, His452 and Gly488	Glu485 and Gly487
18c	Ser199, Gln201, Asp239, His451, His452, Gly488, Arg492 and Gly489	Phe235, Arg540, Arg223, Gln237 and Glu485
18d	Gln198, Ser199, Gln237, His451, His452, Gly488 and Arg492	Arg231, Gln237, Asp478 and Glu485
18e	Ser199, Gln201, His451, His452, Gly488 and Arg492	Gln237, Glu485 and Arg540
18f	Ser199, Gln201, Asp239, Gly488 and His452	Gln237, Glu485 and Arg540
18g	Gln198, Ser199, Asp239, His451, His452, Gly488, Gly489 and Arg492	Gln237, Asp478 and Glu485

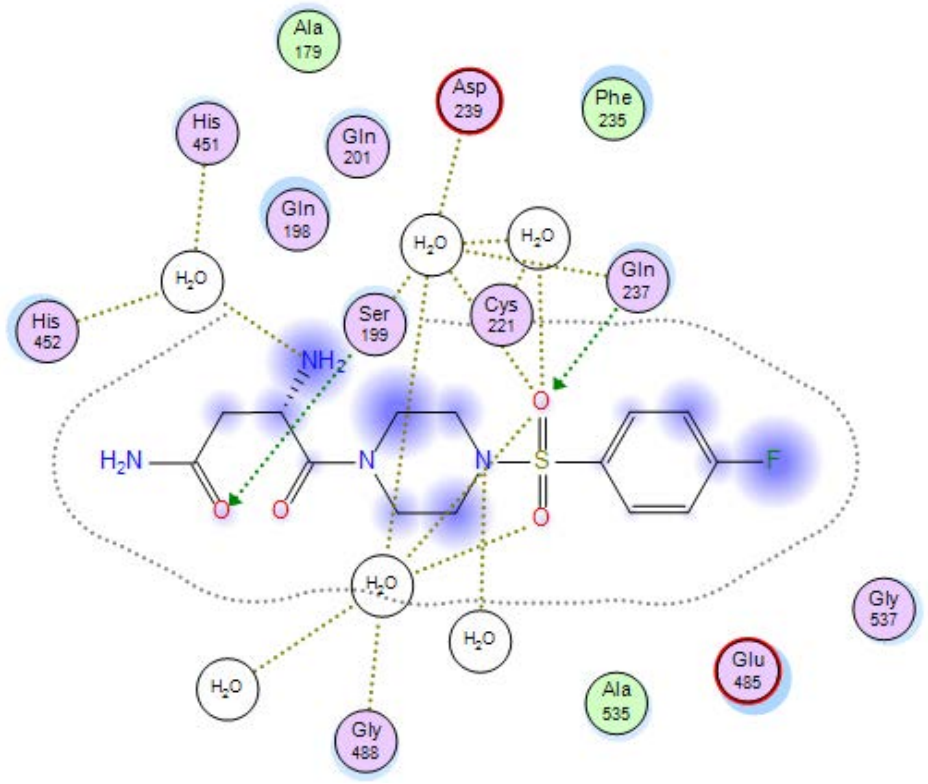

Figure 130: 2D binding interactions of compound **18c** with *S. aureus* AspRS.

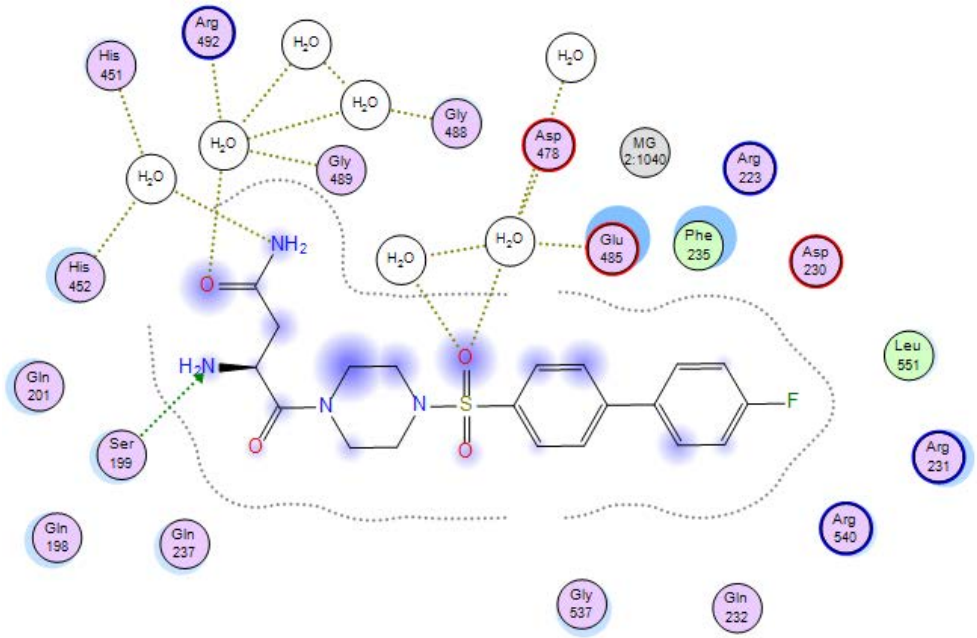

Figure131: 2D binding interactions of compound **18f** with *S. aureus* AspRS**.**

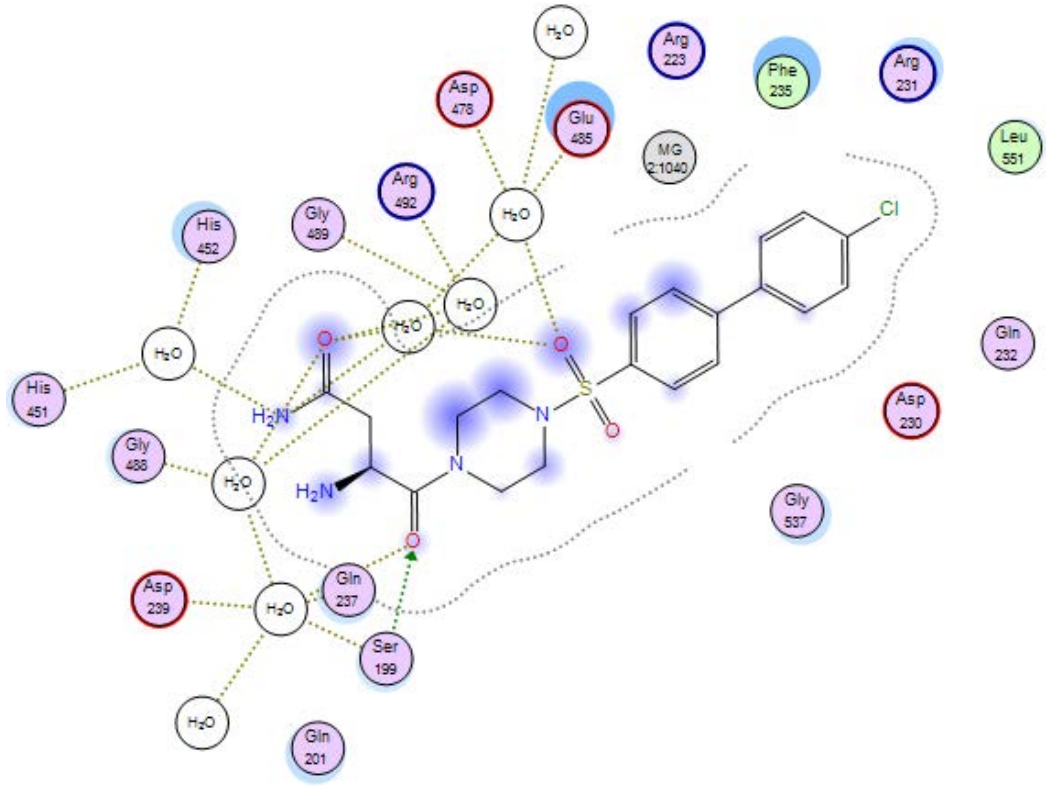

Figure 132: 2D binding interactions of compound **18g** with *S. aureus* AspRS.

4.2.2. Docking studies of *S. aureus* AsnRS

By alignment of series 2 compounds with asparaginyl adenylate in the *S. aureus* AsnRS, amino acid residues in asparagine and AMP pockets were determined (Figure 133) (Table 35). The aryl/biaryl moiety of compounds **18a**-**g** formed a π-π stacking interaction with Phe219 (Figures 134-138), while Arg206, Arg404 and Glu353 formed hydrogen bonding interactions directly or via water molecules with the sulfamoyl group and piperazine respectively (Figures 135, 136 and 138). The role of water molecule was observed in the interaction of Arg360 with the carbonyl oxygen of asparagine in compounds **18a**-**g** (Figures 134, 135, 137 and 138), while in compound **18g**, Arg360 made an additional direct hydrogen bond interaction with the same carbonyl oxygen (Figure 138). However, that role was not observed in the interaction with the second key amino acid residue (Glu223) for asparagine recognition. Glu223 formed a hydrogen bonding interaction with the amino group of the asparagine moiety in compounds **18b**, **18d**, **18e** and **18f** (Figures 135 and 137), however this interaction was not observed in compounds **18a** and **18c** (Figures 134 and 136). Only compound **18g** showed the interaction with both Glu223 and Arg360 via water

molecules with the amino and carbonyl groups of the asparagine moiety as observed in the binding interaction of the natural substrate with *S. aureus* AsnRS (Figure 138). The nitro and fluoro groups were bound with Leu216 in compounds **18b**, **18c** and **18f** (Figure 136). The docking studies of series 2 compounds showed the role of Mg^{2+} ion in stabilisation of the sulfamoyl linkage through its interaction via water molecules with the piperazine moiety of the sulfamoyl linkage in compounds **18a**-**c** (Figures 134-136). However, the sulfamoyl linkage was completely stabilised in the presence of the ion in compound **18g** as its structure is longer than compounds **18a**-**c** which could offer good fitting of *S. aureus* AsnRS active sites (Figure138). Compounds **18c**-**g** showed the interaction of Mg^{2+} ion bound with Lys326 and Asp344 via water molecules, the important amino acid residues responsible for Mg^{2+} ion binding interactions with asparaginyl adenylate intermediate in *S. aureus* AsnRS (Figures 136-138).

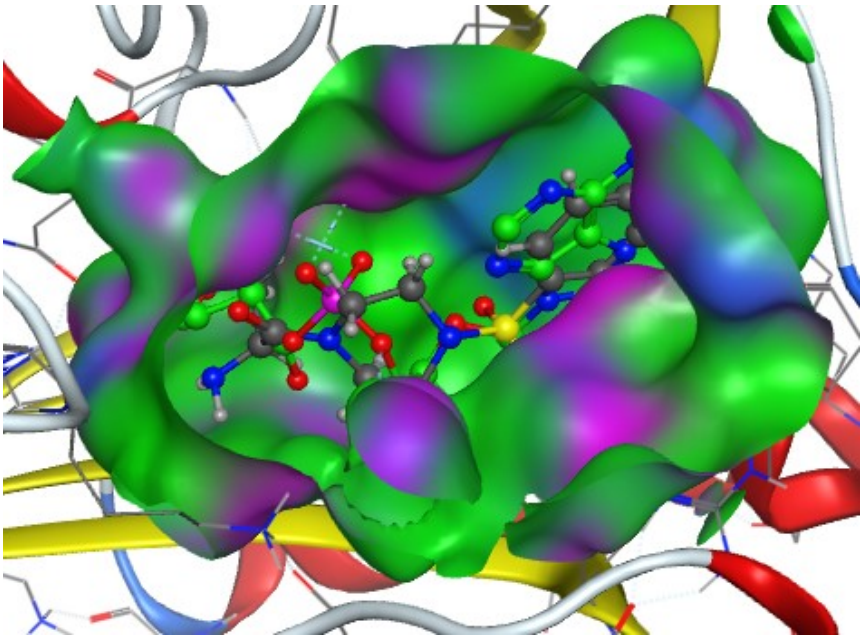

Figure 133: Alignment of compound **18a** (grey) with asparaginyl adenylate (green) in the active sites of *S. aureus* AsnRS.

Table 35: Binding interactions of series 2 compounds with the amino acid residues of the binding sites of *S. aureus* AsnRS.

Ligands	Asparagine pocket	AMP pocket
Asparaginyl-adenylate	Glu223 and Arg360	Arg206, Glu208, Arg214, His215, Phe219, Glu353, Gly356, Gly401 and Arg404
18a	Arg360	Arg206, Phe219, Glu353 and Arg404
18b	Glu223 and Arg360	Arg214, Lru216, Phe219, Glu353, Gly356 and Arg404
18c	Arg360	Leu216, Phe219, Glu353 and Arg404
18d	Glu223 and Arg360	Arg206, Phe219, Glu353, Gly356 and Arg404
18e	Glu223 and Arg360	Arg206, Phe219, Glu353, Gly356 and Arg404
18f	Glu223 and Arg360	Arg206, Leu216, Phe219, Glu353 and Arg404
18g	Glu223 and Arg360	Arg206, Leu216, Phe219, Glu353 and Arg404

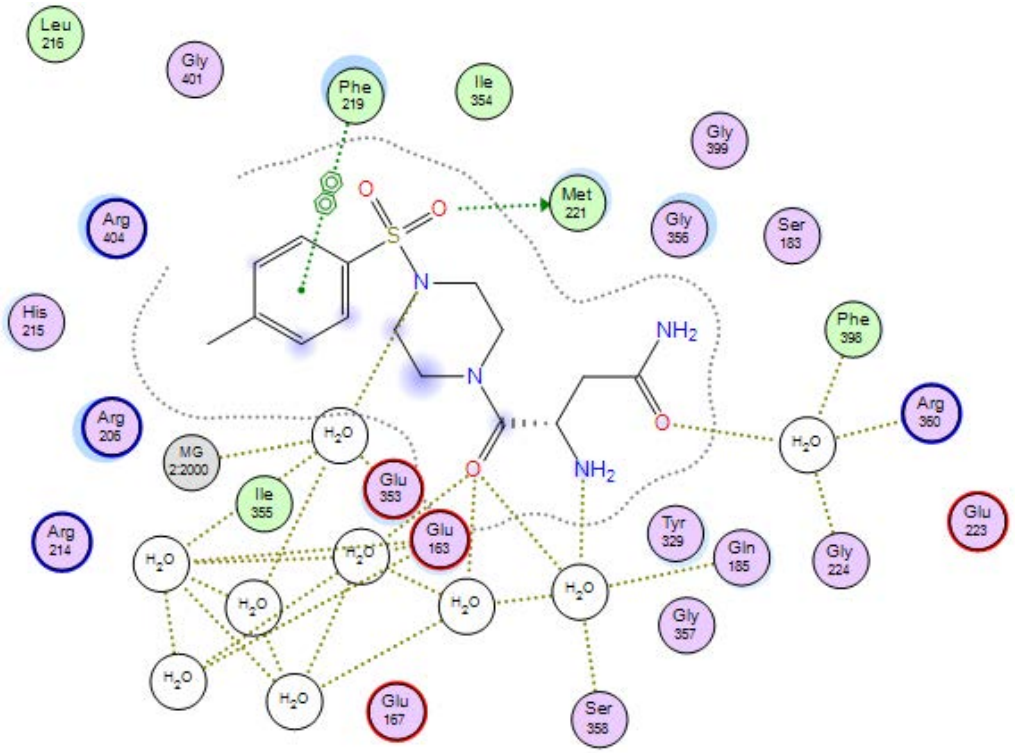

Figure 134: 2D binding interactions of compound **18a** with *S. aureus* AsnRS.

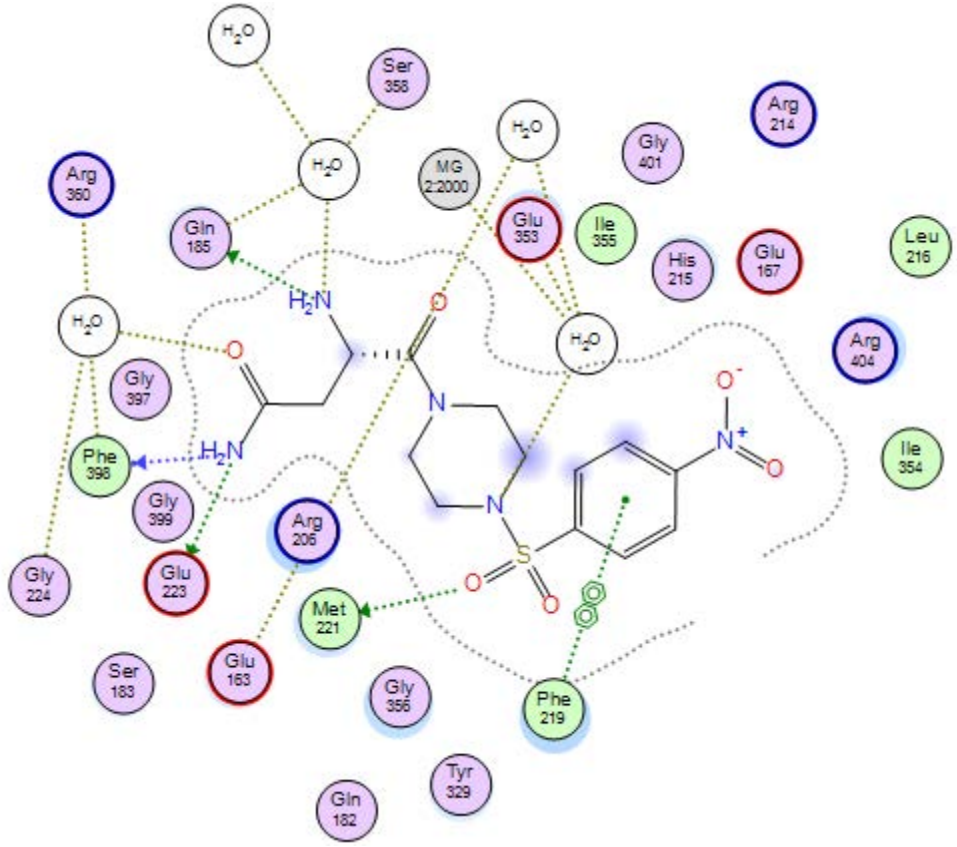

Figure 135: 2D binding interactions of compound **18b** with *S. aureus* AsnRS**.**

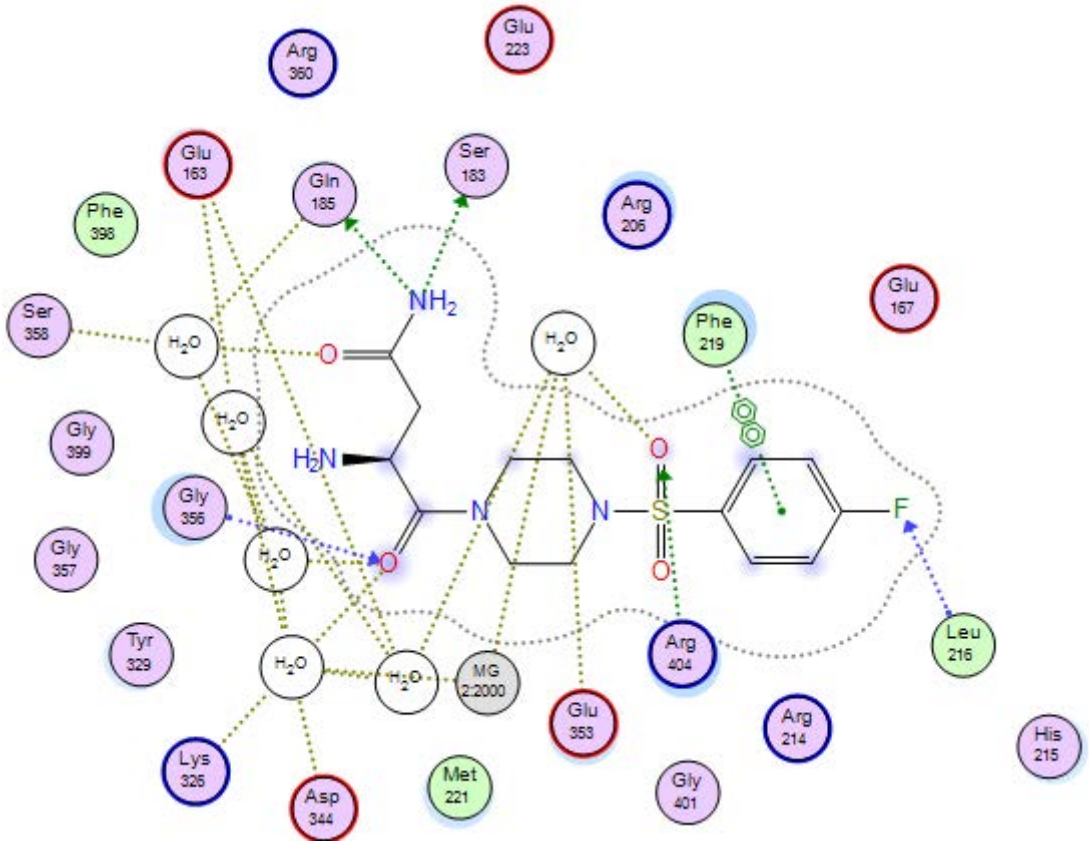

Figure 136: 2D binding interactions of compound **18c** with *S. aureus* AsnRS.

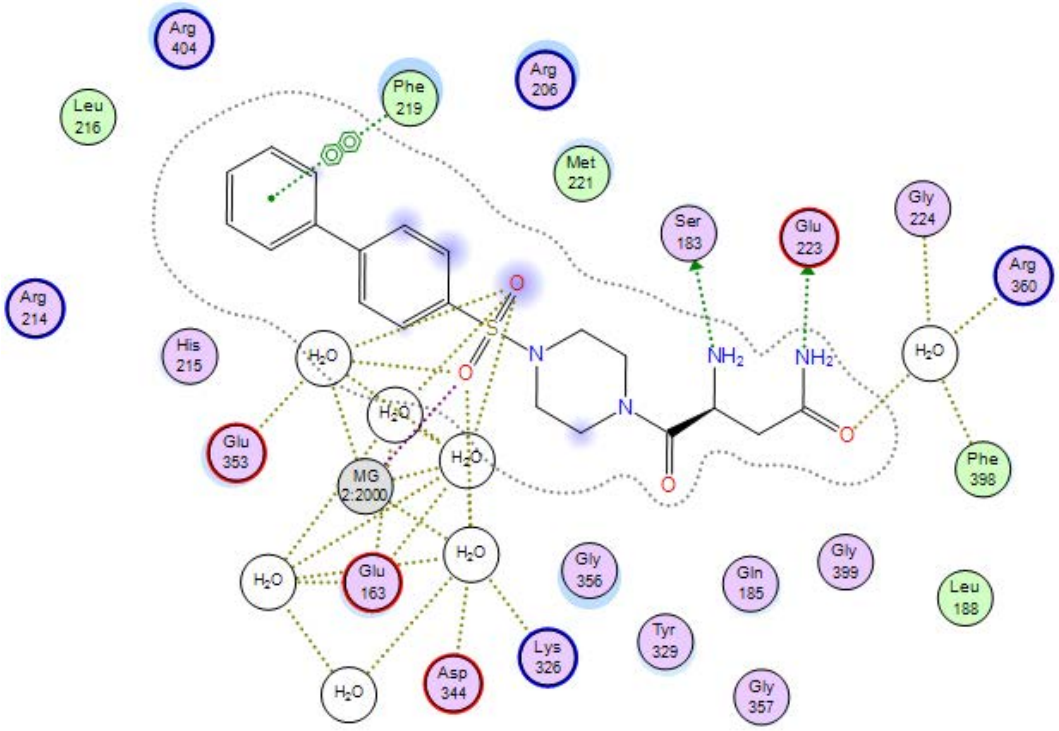

Figure 137: 2D binding interactions of compound **18d** with *S. aureus* AsnRS.

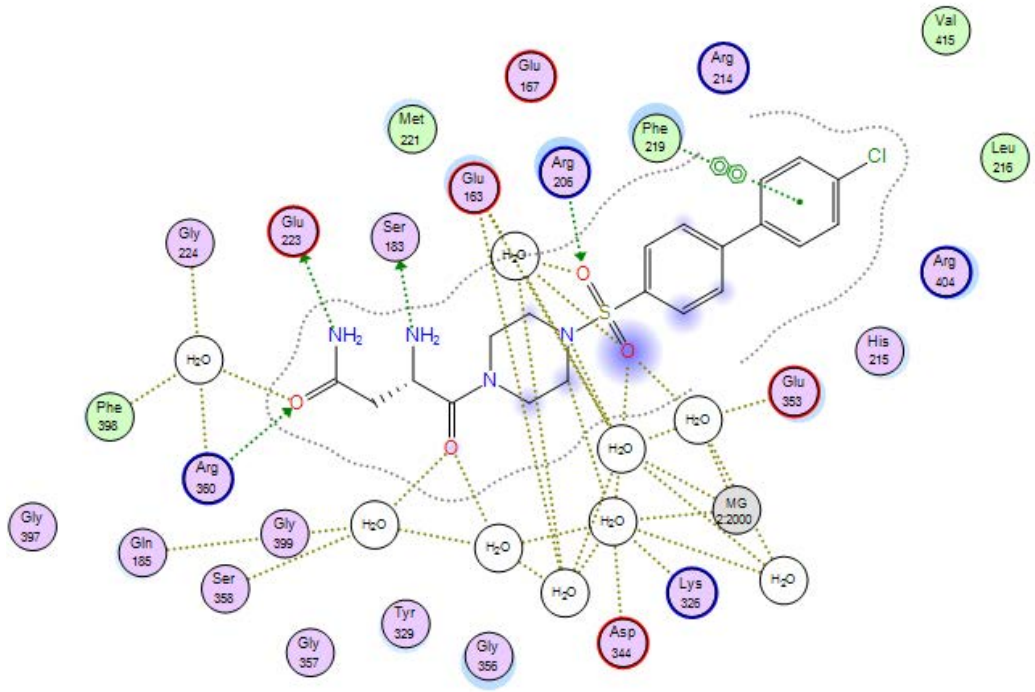

Figure 138: 2D binding interactions of compound **18g** with *S. aureus* AsnRS.

4.2.3. Docking studies of *E. faecalis* AspRS.

By alignment of series 2 compounds with aspartyl adenylate in *E. faecalis* AspRS, key amino acid residues in both amino acid and AMP pockets were determined (Figure 139) (Table 36). Most of amino acid residues in the AMP pocket made π-π stacking and hydrogen bonding interactions with aryl/biaryl and sulfamoyl piperazine moieties (Figures 140-143) For example, the interaction of Phe234 with the biphenyl moiety in Figures 142-144 and the interaction of Gln236 and Arg538 that formed hydrogen bonds with nitro group in compound **18b** (Figure 140), while Arg222 and Glu224 also formed hydrogen bonds via water molecules with piperazine in compound **18d** (Figure 141). The asparagine moiety interacted with some amino acid residues in the Asp pocket, however, not all key amino acid residues in the histidine and flipping loops interacted with the asparagine moiety as noted for compounds **18f** and **18g** (Figures 143 and 144). The docking studies of compounds **18a**-**g** showed the role of Mg^{2+} in stabilisation of the sulfamoyl linkage in compounds **18b**, **18d** and **18f** (Figures 140, 141 and 143). However, compounds **18e** and **18g** did not show any binding interactions with Mg^{2+} ion during docking studies (Figures 142 and 144).

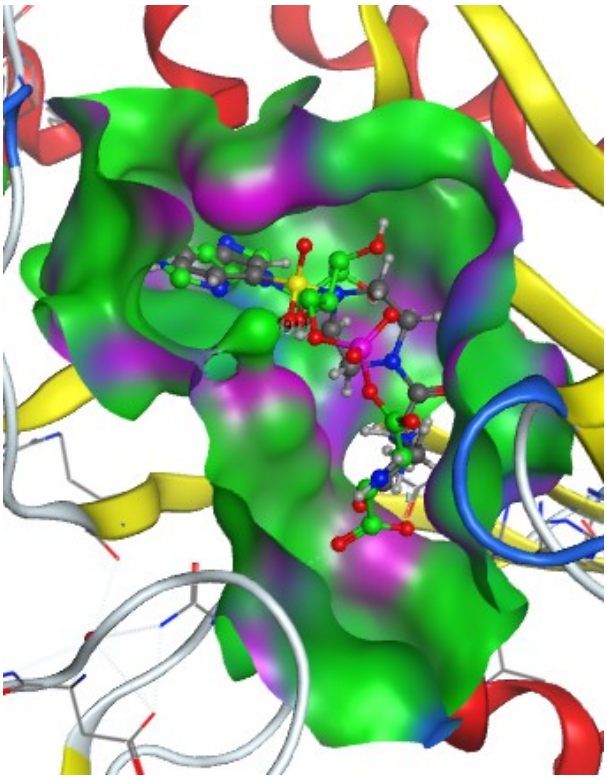

Figure 139: Alignment of compound **18d** (grey) with aspartyl adenylate (green) in the active sites of *E. faecalis* AspRS.

Table 36: Binding interactions of series 2 compounds with the amino acid residues of the binding sites of *E. faecalis* AspRS**.**

Ligands	Aspartic acid pocket	AMP pocket
Aspartyl-adenylate	Glu176, Arg230, His449, Arg490 and Asp238	Arg222, Phe234, Gln231, Gln236, Glu483 and Arg538
18a	Ser198, Arg230, Asp238, His449 and His450	Arg222, Glu224, Phe234, Gln236, Asp476 and Arg538
18b	Gln197, Ser198, Gln200, Asp238 and His449	Arg222, Phe234, Gln236, Glu483 and Arg538
18c	Ser198, Arg230 and His449	Arg222, Phe234, Gln236, Glu224, Glu483 and Arg538
18d	Ser198, Gln200, Asp238, His449 and Arg490	Arg222, Glu224 and Phe234
18e	Arg230 and His449	Arg222 and Gln236
18f	Asp238 and Arg490	Arg222 and Phe234
18g	Ser198, Arg230 and His449	Arg222, Phe234 and Gln236

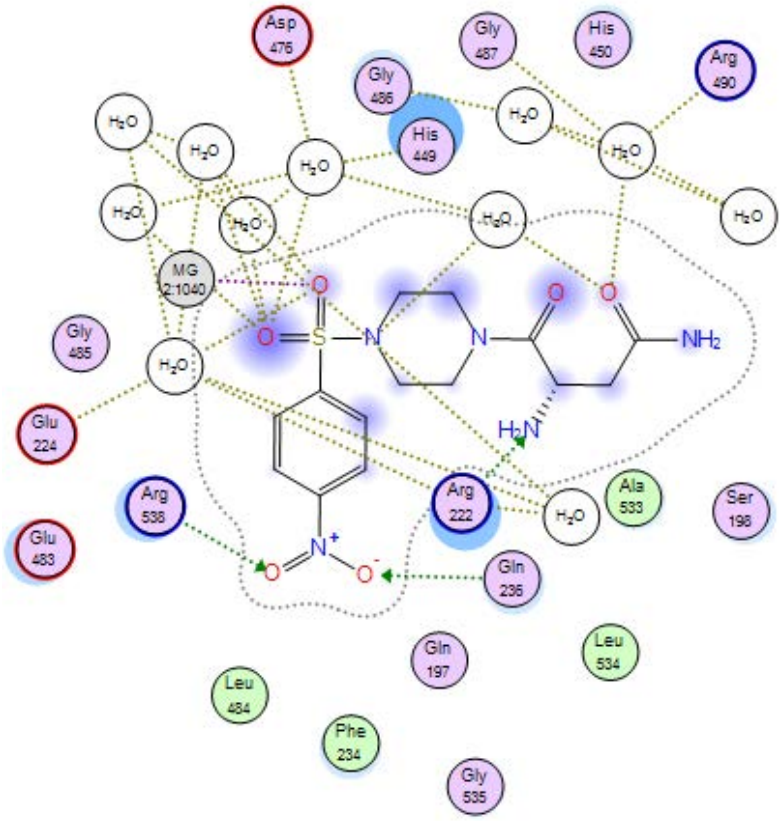

Figure 140: 2D binding interactions of compound **18b** with *E. faecalis* AspRS.

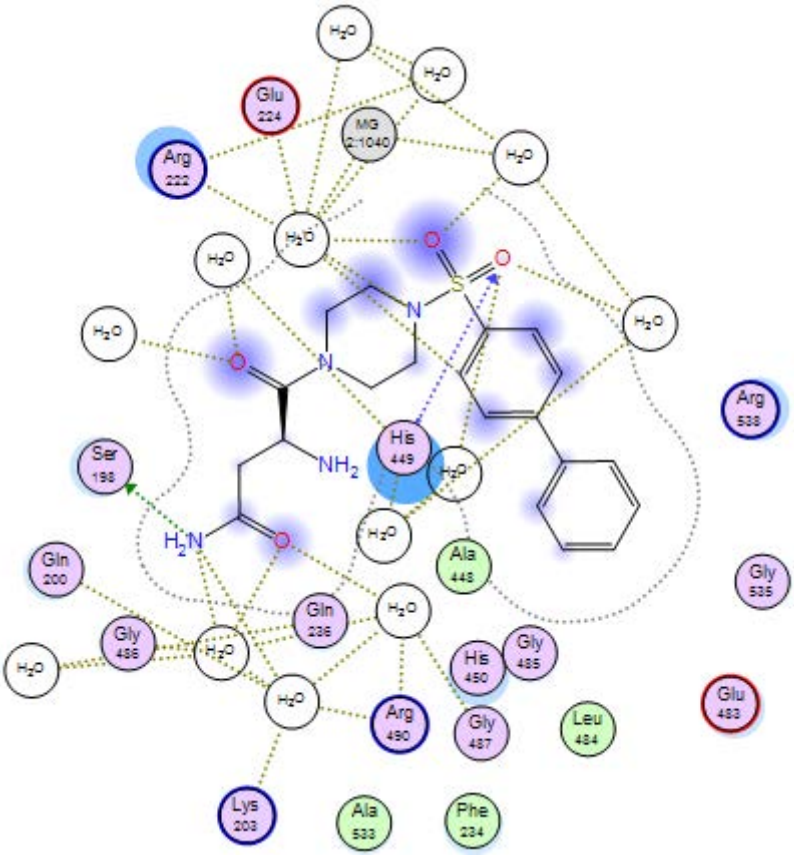

Figure 141: 2D binding interactions of compound **18d** with *E. faecalis* AspRS.

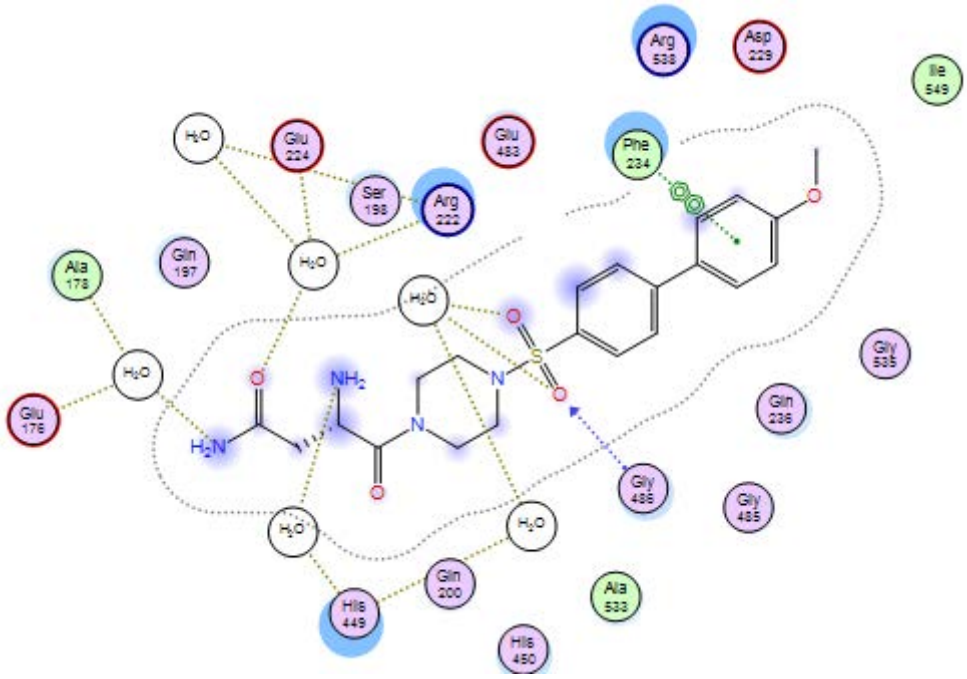

Figure 142: 2D binding interactions of compound **18e** with *E. faecalis* AspRS.

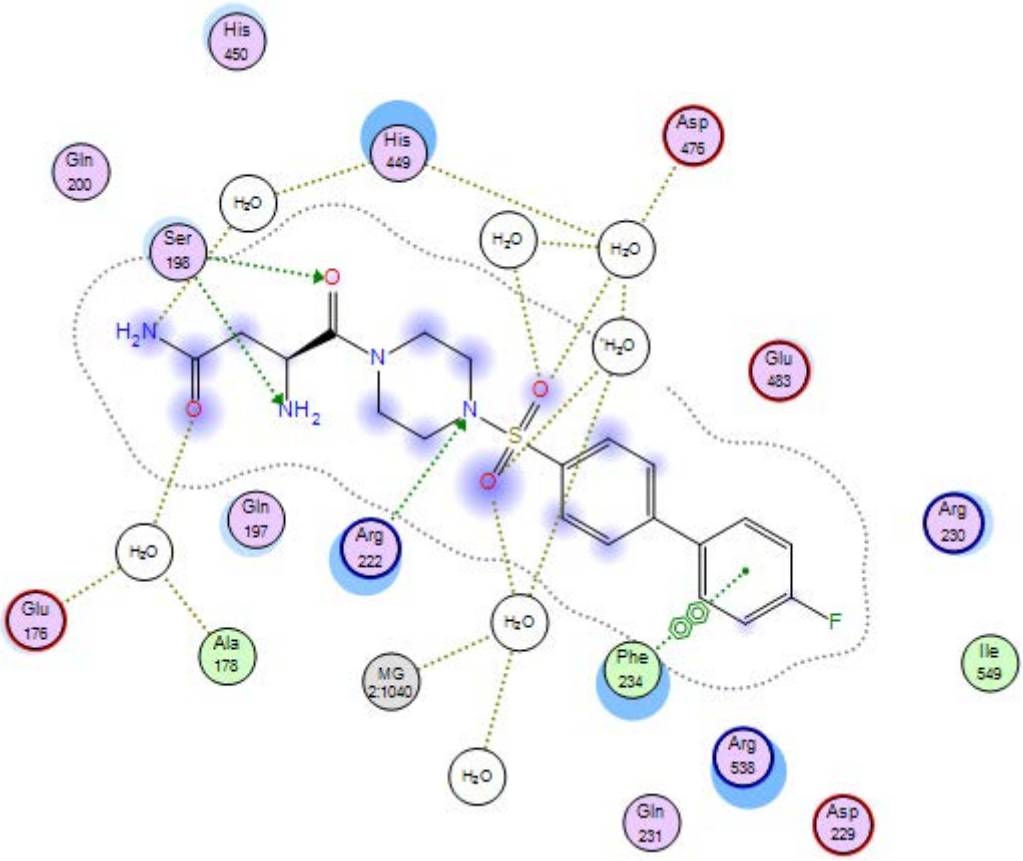

Figure 143: 2D binding interactions of compound **18f** with *E. faecalis* AspRS**.**

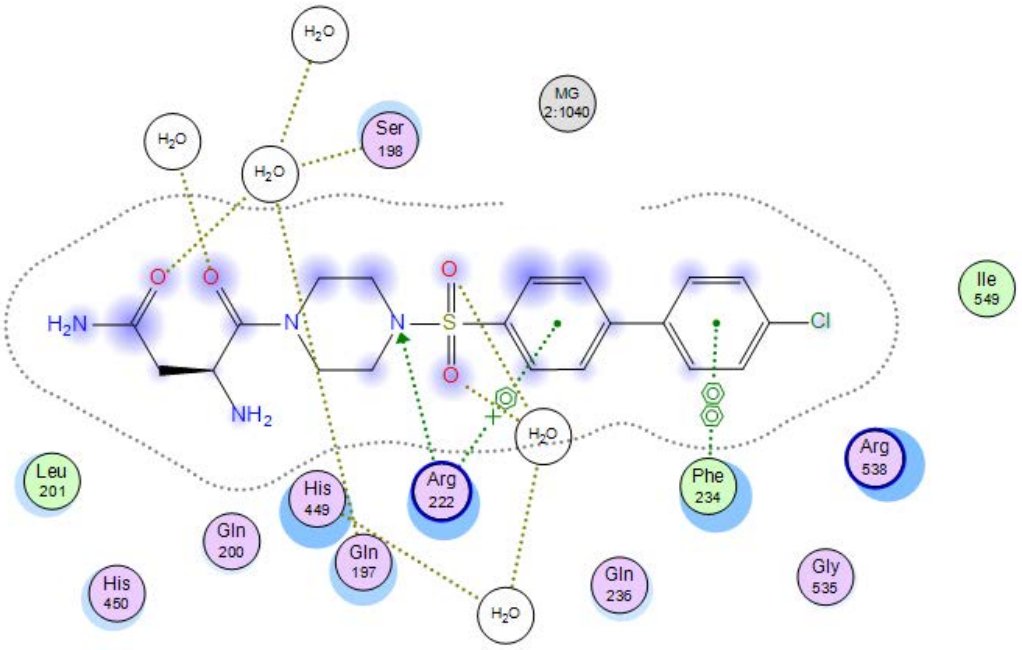

Figure 144: 2D binding interactions of compound **18g** with *E. faecalis* AspRS.

4.2.4. Docking studies of *E. faecalis* AsnRS

Through alignment of series 2 compounds with asparaginyl adenylate in *E. faecalis* AsnRS, amino acid residues in the Asn/AMP pockets that interacted with compounds were identified (Figure 145) (Table 37). The amino and carbonyl groups of the asparagine moiety of series 2 compounds made a hydrogen bond with Glu238 and Arg380 respectively, which are key amino acid residues responsible for asparagine recognition (Figures 146-150). The aryl/biaryl sulfamoyl piperazines made a π-π stacking interaction with Phe234 and hydrogen bonding interaction with several key amino acid residues such as Arg221, Glu223, Gly421 and Arg424 (Figures 146-150), while the nitro group of compounds **18b** made a hydrogen bond directly with Leu231 and via water molecule with Glu423 and Arg424 (Figure 147). Regarding Mg^{2+} ion, the docking studies of series 2 compounds showed its role in sulfamoyl linkage stabilisation in compounds **18d** and **18g** (Figures 149 and 150). Lys346 and Asp364 interacted with Mg^{2+} via water molecules in compound **18d** (Figure 149) as observed in the docking study of asparaginyl adenylate with *E. faecalis* AsnRS in the presence of Mg^{2+} ion.

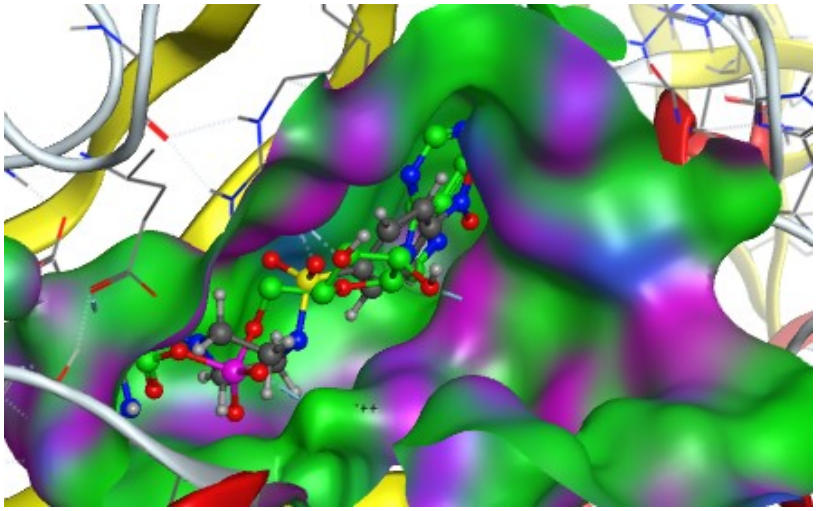

Figure 145: Alignment of compound **18b** (grey) with asparaginyl adenylate (green) in the active sites of *E. faecalis* AsnRS.

Table 37: Binding interactions of series 2 compounds with the amino acid residues of the binding sites of *E. faecalis* AsnRS.

Ligands	Asparagine pocket	AMP pocket
Asparaginyl-adenylate	Glu238 and Arg380	Arg221, Glu223, Arg229, His230, Phe234, Glu373, Gly376, Gly421 and Arg424
18a	Gln200, Glu238 and Arg380	Arg221, Phe234, Glu373, Gly376 and Arg424
18b	Gln200, Glu238 and Arg380	Arg221, Leu231, Phe234, Glu373, Gly376, Glu423 and Arg424
18c	Gln200, Glu238 and Arg380	Arg221, Leu231, Phe234, Glu373 and Arg424
18d	Gln200, Glu238 and Arg380	Arg221, His230, Phe234, Glu373 and Gly376
18e	Gln200, Glu238 and Arg380	Arg221, Arg229, Phe234, Glu373 and Arg424
18f	Gln200, Glu238 and Arg380	Arg221, Arg229, Phe234, Glu423, Glu373 and Arg424
18g	Gln200, Glu238 and Arg380	Arg221, Arg229, Leu231, Phe234, Glu423 and Glu373

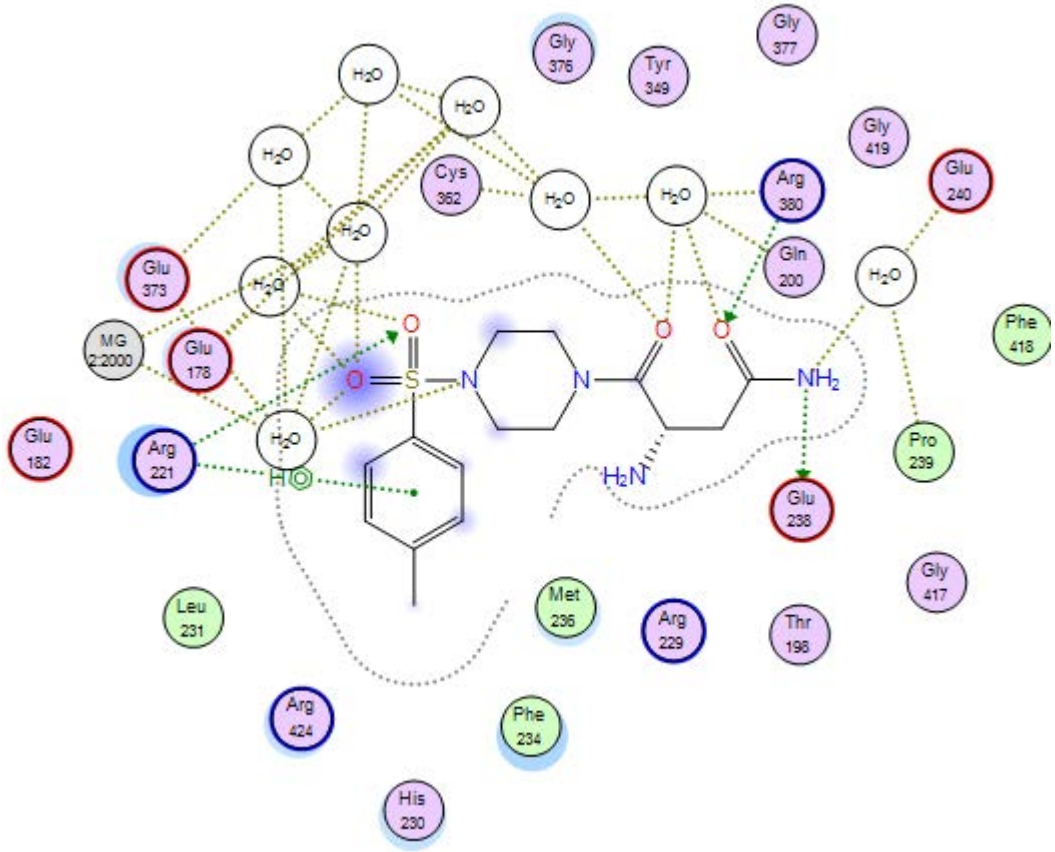

Figure 146: 2D binding interactions of compound **18a** with *E. faecalis* AsnRS.

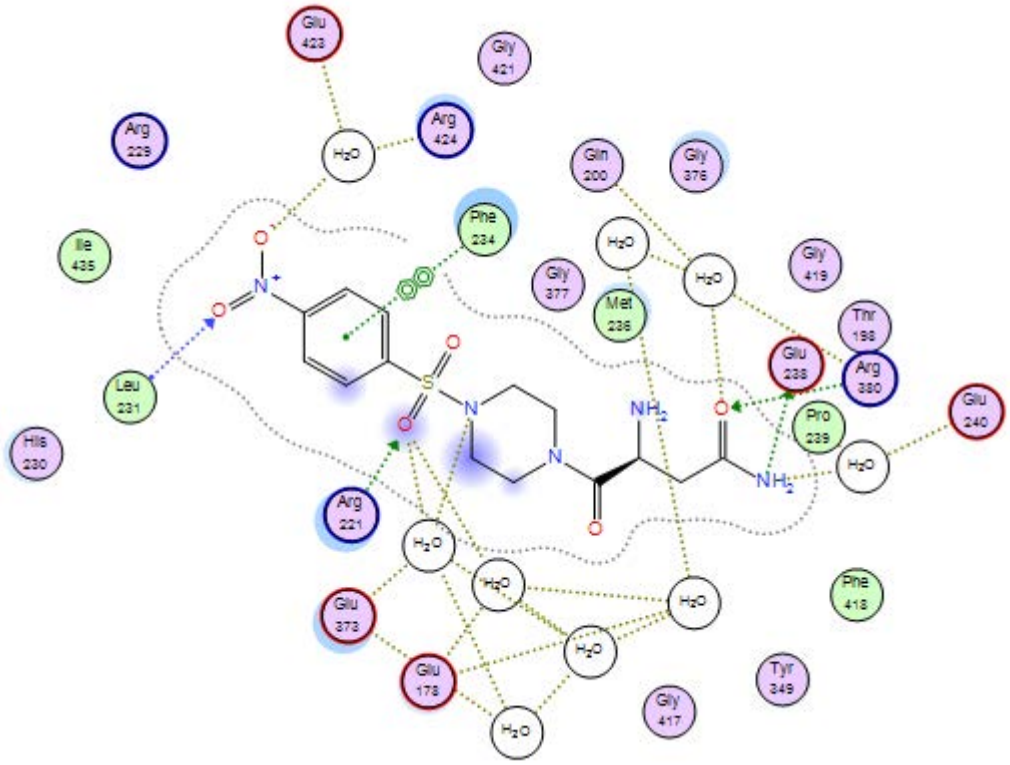

Figure 147: 2D binding interactions of compound **18b** with *E. faecalis* AsnRS.

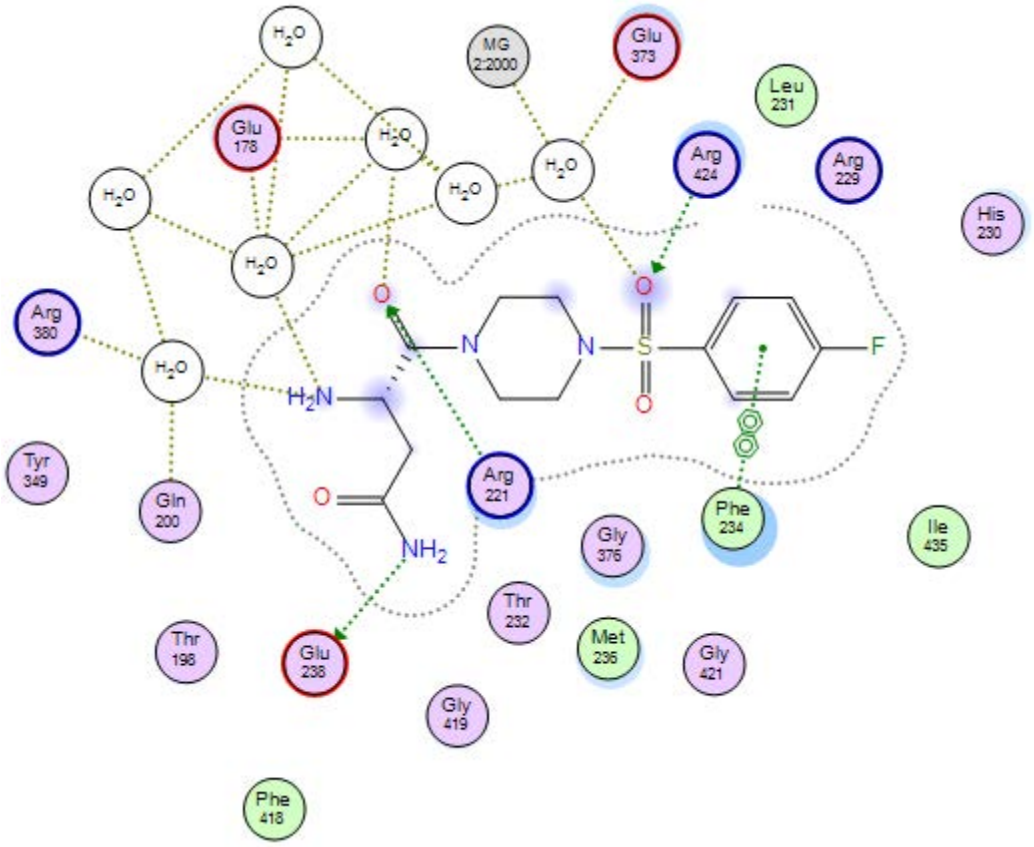

Figure 148: 2D binding interactions of compound **18c** with *E. faecalis* AsnRS.

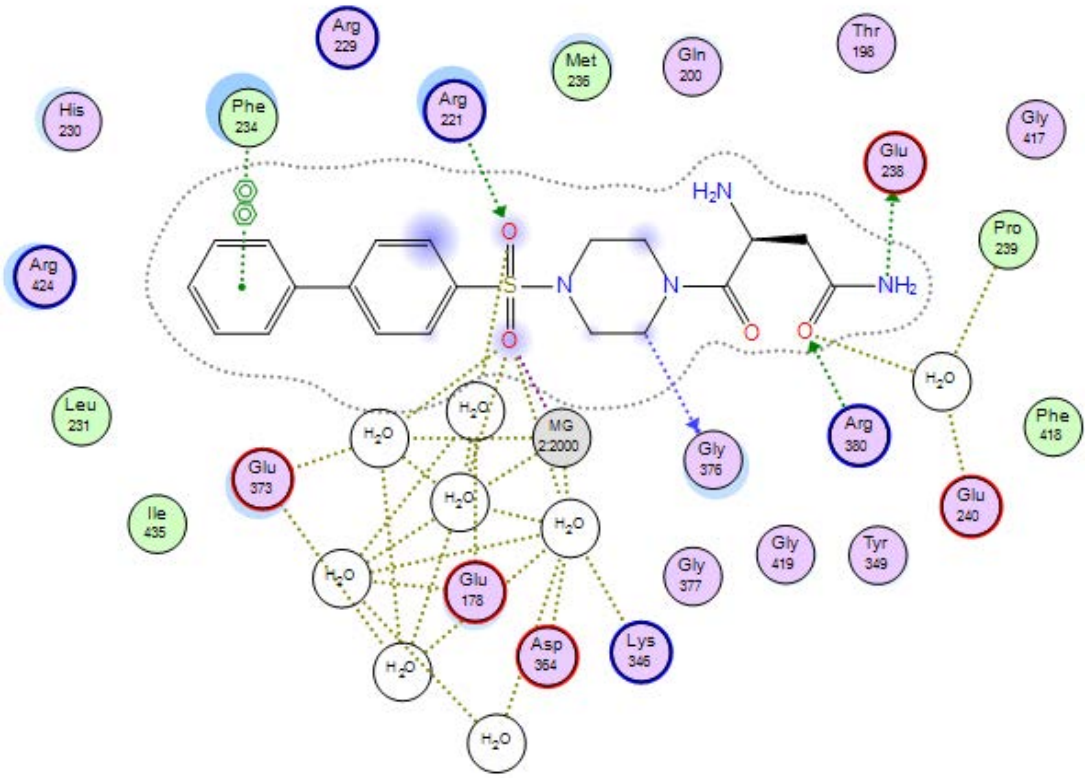

Figure 149: 2D binding interactions of compound **18d** with *E. faecalis* AsnRS.

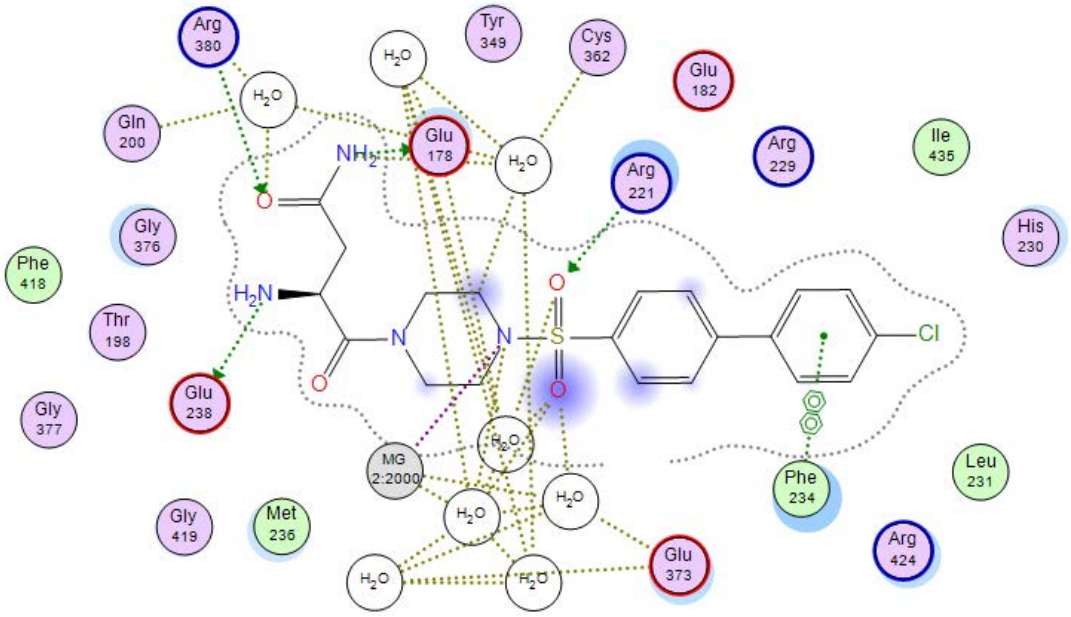

Figure 150: 2D binding interactions of compound **18g** with *E. faecalis* AsnRS.

4.3. Biological assays

4.3.1. Microbiological screening

Microbiological screening of series 2 compounds was performed at the Antimicrobial Chemotherapy Unit in University Hospital of Wales (UHW) by Jennifer Richard and Mandy Wootton. Series 2 compounds **18a**-**g** were evaluated for antimicrobial activity against a number of pathogens (sensitive and resistant strains) with ciprofloxacin as the standard for comparison. Isolates were tested by using clinical and NCTC/ATCC control organisms; *E. coli* (including ATCC 25922 sensitive strain), *Klebsiella pneumoniae* (including fourth generation cephalosporins (ATCC 700603) resistant strains), *Pseudomonas aeruginosa* (ATCC 27853), *Staphylococcus aureus* (including (ATCC 29213) sensitive strain and flucloxacillin (NCTC12493)), *Enterococcus faecalis* (including (ATCC 29212) sensitive strain), and *Enterococcus faecium* (16568). MIC was measured for each compound using 2-fold doubling serial dilutions (log_2). From the MIC results of compounds **18a**-**g** (Table 38), compound **18g** showed low antimicrobial activity (64 µg/mL) against the sensitive strain of *Enterococcus faecalis* (ATCC 29212) compared with ciprofloxacin (0.125 µg/mL), however, other compounds did not show good inhibitory activity against *S. aureus* and *E. faecalis* (Table 36). The lack of activity of compounds **18a**-**g** against *S. aureus* and *E. faecalis* AspRSs may be due to the presence of the asparagine moiety. As the specificity of AspRS is substrate assisted, the histidine and flipping loops reorganise once Asp binds to its pocket making a hydrogen bond between Asp and the key histidines in the histidine loop and bringing the negative glutamic acid close to the Asp ligand. From the docking study of series 2 compounds with *S. aureus* and *E. faecalis* AspRSs, compounds did not show good interactions with the histidine and flipping loops. In contrast, the results of the docking study of the compounds with *S. aureus* and *E. faecalis* AsnRSs showed good binding interactions with the key amino acid residues except **18a** and **18c**, which did not interact with Glu223 responsible for asparagine recognition in *S. aureus* AsnRS. These compounds were prepared in the form of salt except compound **18b** and their uptake across the cell wall into microorganisms may be impaired and this is reflected in the antimicrobial activity observed.

Table 38: Microbiological data of compounds **18a-g**.

Microorganisms	MIC: (µg/mL)							
	Ciprofloxacin	**18a**	**18b**	**18c**	**18d**	**18e**	**18f**	**18g**
Escherichia coli ATCC 25922	0.008	-	-	-	-	>128	>128	128
Pseudomonas aeruginosa ATCC 27853	0.25	128	128	128	128	128	128	128
Staphylococcus aureus ATCC 29213	0.25	>128	>128	>128	>128	>128	128	128
Enterococcus faecalis ATCC 29212	0.125	>128	128	>128	128	128	128	64
Enterococcus faecium 16568	>128	128	64	128	64	-	-	-
Klebsiella pneumoniae ATCC 700603	0.25	-	-	-	-	>128	128	128
Staphylococcus aureus NCTC 12493	0.5	128	128	128	128	-	-	-

4.3.2. Aminoacylation assay

The antimicrobial assay was performed at the Department of Chemistry, University of Texas by Casey Hughes and James Bullard. The half maximal inhibitory concentration (IC_{50}) assay was performed for the first four series 2 compounds to measure their activities in inhibiting 50% of the aminoacylation process. In this assay, *P. aeruginosa*

AspRS was used and the control was EDTA in DMSO. All tested compounds did not show good IC_{50} results. Ideally the compounds need to be tested against *S. aureus* and *E. faecalis* that they were designed to inhibit, however, only the *P. aeruginosa* AspRS assay was available.

In conclusion, series 2 compounds, which consisted of an asparagine and sulfamoyl piperazine linker connected with the aryl/biaryl moiety, were prepared in satisfactory yields in a salt form except compound **18b**. In the docking study of these compounds with *S. aureus* and *E. faecalis* AspRSs, they formed good binding interactions inside the AMP pockets while the asparagine group just formed hydrogen bonds with amino acid residues responsible for the histidine loop but not the flipping loop. However, they formed good binding interactions inside both active sites of *S. aureus* and *E. faecalis* AsnRSs. In the microbiological screening, none of compounds showed good inhibitory activity against the target microorganisms, possibly because they are salts and therefore the uptake inside the bacterial cell may be impaired. Thus, retaining the amino acid isosteric moiety in the next series could be better for bacterial uptake.

4.4. Methods

4.4.1. Docking studies

All methods related to docking studies are described in the methods section in Chapter 2.

4.4.2. Biological assay

4.4.2.1. Antimicrobial screening test

Method related to antimicrobial screening test is described in the methods section in Chapter 3.

4.4.2.2. Aminoacylation assay

Method related to aminoacylation assay is described in the methods section in Chapter 3.

4.4.3 Chemistry

4.4.3.1. General procedure for the preparation of phenyl sulfonyl piperazines (**3a**-**g**) (327)

The general procedure for the preparation of phenyl sulfonyl piperazines (**3a**-**g**) is described in the methods section in Chapter 3.

4.4.3.1.1. 1-(4 Fluorophenyl)sulfonyl)piperazine (**3g**) ($C_{10}H_{13}FN_2O_2S$, Mol. Wt. 244.28)

Product obtained after recrystallisation from EtOAc/petroleum ether as white crystalline needles, yield: 1.05 g (74%), mp = 108 - 110 ^oC (Lit. mp = not given (347)). TLC: CH_3OH - CH_2Cl_2 1:9 v/v, (R_f = 0.3). ^1H NMR (DMSO-d_6) δ 2.71 (br m, 4H, CH_2, pip), 2.78 (br m, 4H, CH_2, pip), 3.00 (br s, 1H, NH), 7.80 (dd, J = 5.2, 9.0 Hz, 2H, CH, Ar), 7.50 (t, J = 9.0 Hz, 2H, CH, Ar). HPLC: 100% at RT: 4.0 min, HRMS (ES-TOF) m/z calculated mass: 245.0682 $[M + H]^+$, observed mass: 245.0756 $[M + H]^+$.

4.4.3.2. General procedure for the preparation of tert-butyl(4-amino-1-(4-((4-phenyl)sulfonyl)piperazin-1-yl)-1,4-dioxobutan-2-yl)carbamate derivatives (**17a**-**g**) (327)

To an ice-cooled suspension of N-Boc-L-asparagine (**15**) (0.38 g, 1.65 mmol) and phenyl sulfonyl piperazine derivatives (**3a**-**g**) (1.65 mmol) in dry $CHCl_3$ (35 mL) was added TBTU (**16**) (1.06 g, 3.3 mmol) and Et_3N (0.92 mL, 6.6 mmol) dropwise then the reaction stirred at room temperature overnight. The clear reaction solution was diluted with $CHCl_3$ (65 mL) then washed with 0.1M aqueous HCl (50 mL) and H_2O (2 x 50 mL), dried over $MgSO_4$ and the solvent removed in vacuo. The crude product was purified by gradient column chromatography and/or recrystalisation from EtOH or stirring with Et_2O.

4.4.3.2.1. Tert-butyl(4-amino-1,4-dioxo-1-(4-tosylpiperazin-1-yl)butan-2-yl)carbamate (**17a**) ($C_{20}H_{30}N_4O_6S$, Mol. Wt. 454.54)

Product obtained after stirring with Et_2O and collected by filtration as a white solid, yield: 0.7 g (46%), mp = 78 - 80 ^OC. TLC: CH_3OH - CH_2Cl_2 1:9 v/v, (R_F = 0.8). ^1H NMR (DMSO-d_6) δ 1.32 (s, 9H, tBu), 2.41 (s, 3H, CH_3), 2.65 (br m, 2H, CH_2, pip), 2.65 (br m, 2H, CH_2, pip), 2.68 (m, 2H, CH_2CONH_2), 3.07 (br m, 2H, CH_2, pip), 3.32 (br m, 1H, CH, pip obscured by H_2O signal), 3.45 (br m, 1H, pip), 3.63 (br m, 1H, pip), 3.73 (br m, 1H,

pip), 4.64 (ddd, J = 7.4, 15.3, 22.9 Hz, 1H, *CH*NHBoc), 7.15 (br s, NH, *NH*Boc), 7.45 (d, J = 8.0 Hz, 2H, CH, Ar), 7.57 (s, 1H, CO*NH₂*), 7.59 (s, 1H, CO*NH₂*), 7.61 (d, J = 8.3 Hz, 2H, Ar). ^{13}C NMR (DMSO-d_6) δ 21.3 (CH_3), 28.4 (CH_3, $C(CH_3)_3$), 41.6, 49.2 (4 x CH_2, pip), 42.3 (CH_2, *CH_2*$CONH_2$), 49.1 (CH, *CH*NHBoc), 80.0 (C, $C(CH_3)_3$), 120.9, 130.0 (4 x CH, Ar), 115.9, 133.9 (2 x C, Ar), 150.1 (C=O), 145.1 (C=O, Boc), 165.6 (C=O, $CONH_2$). HPLC: 100 % at RT: 4.24 min. HRMS (ES-TOF) m/z calculated mass: 455.1886 $[M + H]^+$, observed mass: 455.1879 $[M + H]^+$.

4.4.3.2.2. Tert-butyl(4-amino-1-(4-((4-nitrophenyl)sulfonyl)piperazin-1-yl)-1,4-dioxobutan-2-yl)carbamate (**17b**) ($C_{19}H_{27}N_5O_8S$, Mol. Wt. 485.16)

Product obtained after purification by gradient column chromatography and collected at 4:96 v/v CH_3OH - CH_2Cl_2 then recrystalisation from EtOH to give a yellow powder, yield: 0.78 g (86.6%), mp = 210 - 212 ^{O}C. TLC: CH_3OH - CH_2Cl_2 1:9 v/v, (R_F = 0.5). ^{1}H NMR ($CDCl_3$) δ 1.34 (s, 9H, $(CH_3)_3$), 2.62 (d, J = 3.2 Hz, 1H, *CH_2*$CONH_2$), 2.63 (d, J = 2.5 1H, *CH_2*$CONH_2$), 3.09 (4H, CH_2, pip), 3.66 (4H, CH_2, pip), 7.86 (d, J = 5.2, 2H, CH, Ar), 8.32 (d, J = 5.2, 2H, CH, Ar), 4.76 (q, J = 7.6 Hz, 1H, *CH*NHBoc), 5.14 (br d, 1H, *NH*Boc), No NH_2 signal. ^{13}C NMR ($CDCl_3$) δ 28.2 (CH_3, $C(CH_3)_3$), 41.9 (CH_2, *CH_2*$CONH_2$), 45.9, 45.6, 45.3 (4 x CH_2, pip), 46.6 (CH, *CH*NHBoc), 79.3 (C, $C(CH_3)_3$), 124.6, 128.9 (4 x CH, Ar), 116.3 (C, Ar), 141.4 (C-NO_2), 150.5 (C=O, Boc), 154.5 (C=O), 167.5 (C=O, $CONH_2$). HPLC: 100 % at RT: 4.2 min. HRMS (ES-TOF) m/z calculated mass: 486.1580 $[M + H]^+$, observed mass: 486.1758 $[M + H]^+$.

4.4.3.2.3. Tert-butyl(4-amino-1-(4-((4-fluorophenyl)sulfonyl)piperazin-1-yl)-1,4-dioxobutan-2-yl)carbamate (**17c**) ($C_{19}H_{27}FN_4O_6S$, Mol. Wt. 458 .51)

Product obtained after purification by gradient column chromatography and collected at 4:96 v/v CH_3OH - CH_2Cl_2 and washing with Et_2O as a white solid, yield: 0.815 g (87%), mp = 171 - 173 ^{O}C. TLC: CH_3OH - CH_2Cl_2 1:9 v/v, (R_F = 0.5). ^{1}H NMR (DMSO-d_6) δ 1.32 (s, 9H, tBu), 2.69 (m, 4H, *CH_2*$CONH_2$ and CH_2, pip), 3.08 (br m, 2H, CH_2, pip), 3.37 (br m, 1H, pip partially obscured by H_2O signal), 3.47 (br m, 1H, pip), 3.64 (br m, 1H, pip), 3.73 (br m, 1H, pip), 7.16 (br s, *NH*Boc), 4.64 (ddd, J = 7.3, 15.2, 22.9 Hz, 1H, *CH*NHBoc), 7.50 (t, J = 8.9 Hz, 2H, CH, Ar), 7.57 (s, 1H, CO*NH₂*), 7.59 (s, 1H, CO*NH₂*), 7.82 (dd, J = 5.1, 8.9 Hz, 2H, Ar). ^{13}C NMR (DMSO-d_6) δ 20.7 (CH_2, *CH_2*$CONH_2$), 28.4 (CH_3, $C(CH_3)_3$),

41.6, 44.6, 46.2 (4 x CH_2, pip), 47.4 (CH, *CH*NHBoc), 79.3 (C, $C(CH_3)_3$), 117.1, 131.1, 131.2 (4 x CH, Ar), 118.8 (C, Ar), 131.5 (C=O), 155.1 (C=O, Boc), 167.6 (C-F), 166.3 (C=O, $CONH_2$). HPLC: 100 % at RT: 4.2 min. HRMS (ES-TOF) m/z calculated mass: 481.1635 $[M + Na]^+$, observed mass: 481.1572 $[M + Na]^+$.

4.4.3.2.4. Tert-butyl(1-(4-([1,1'-biphenyl]-4-yl)sulfonyl)piperazin-1-yl)-4-amino-1,4-dioxobutan-2-yl)carbamate (**17d**) ($C_{25}H_{32}N_4O_6S$ Mol. Wt. 516.61)

Product obtained after purification by gradient chromatography and collected at 1:1 v/v petroleum ether – EtOAc as a colourless solid, yield: 0.59 g, (69%), mp =100 - 102 ^{O}C. TLC: petroleum ether – EtOAc 1:1 v/v (R_f = 0.7). ^{1}H NMR (DMSO-d_6) δ 1.29 (s, 9H, tBu), 2.68 (d, J = 7.8 Hz, 2H, *CH*$_2$$CONH_2$), 2.75 (br m, 2H, CH_2, pip), 3.12 (br m, 2H, CH_2, pip), 3.40 (br m, 1H, CH, pip), 3.48 (br m, 1H, CH, pip), 3.65 (br m, 1H, CH, pip), 3.74 (br m, 1H, pip), 4.64 (dd, J = 7.1, 15.5 Hz, 1H, *CH*NHBoc), 7.16 (br s, 1H, *NH*Boc), 7.46 (t, J = 7.3 Hz, 1H, CH, Ar), 7.53 (m, 2H, CH, Ar), 7.57 (br s, 1H, NH_2), 7.59 (br s, 1H, NH_2), 7.75 (d, J = 7.2 Hz, 2H, CH, Ar), 7.81 (d, J = 8.7 Hz, 2H, CH, Ar), 7.95 (d, J = 8.6 Hz, 2H, CH, Ar). ^{13}C NMR (DMSO-d_6) δ 20.7 (CH_2, CH_2CONH_2), 28.4 (CH_3, $C(CH_3)_3$), 41.6, 44.7, 46.2 (4 x CH_2, pip), 47.5 (CH, *CH*NHBoc), 79.3 (C, $C(CH_3)_3$), 118.9, 133.9, 138.7 (3 x C, Ar), 127.6, 128.1, 128.7, 129.2, 129.7 (9 x CH, Ar), 145.3 (C=O), 155.1 (C=O, Boc), 167.6 (C=O, $CONH_2$). HPLC: 89.24 % at RT: 9.0 min.

4.4.3.2.5. Tert-butyl(4-amino-1-(4-((4'-methoxy-[1,1'-biphenyl]-4-yl)sulfonyl)piperazin-1-yl)-1,4-dioxobutan-2-yl)carbamate (**17e**) ($C_{26}H_{34}N_4O_7S$, Mol. Wt. 546.21)

Product obtained after purification by gradient chromatography and collected at 97:3 v/v CH_2Cl_2 - MeOH then recrystalisation from EtOH to give a colourless semisolid, yield: 0.24 g, (48%). TLC: CH_3OH - CH_2Cl_2 0.5:9.5 v/v, (R_F = 0.7). ^{1}H NMR ($CDCl_3$) δ 1.34 (s, 9H, $C(CH_3)_3$), 2.63 (d, J = 6.4 Hz, 2H, *CH*$_2$$CONH_2$), 3.79 (s, 3H, OCH_3), 3.65 (br m, 4H, CH_2, pip), 3.01 (br m, 4H, CH_2, Pip), 4.76 (q, J = 7.1 Hz, 1H, *CH*NHBoc), 5.27 (d, 1H, J= 9.3 Hz, *NH*Boc), 6.93 (d, 2H, J = 8.9 Hz, CH, Ar), 7.47 (d, 2H, J = 8.9 Hz, CH, Ar), 7.63 (d, 2H, J = 8.6 Hz, CH, Ar), 7.69 (d, 2H, J = 8.6 Hz, CH, Ar), no NH_2 peak was observed. ^{13}C NMR ($CDCl_3$) δ 28.2 ($C(CH_3)_3$), 41.9 (*CH*$_2$$CONH_2$), 46.7 (*CH*NHBoc), 55.4 (OCH_3), 45.3, 45.5, 45.7, 46.1 (4 X CH_2, pip), 114.6, 127.3, 128.2, 128.5 (8 X CH, Ar), 116.4, 131.3, 133.0,

154.5 (4 X C, Ar), 145.9 (C=O), 160.3(C=O, Boc), 167.3 (C=O, $CONH_2$). HPLC: 100 % at RT: 4.5 min. HRMS (ES-TOF) m/z calculated mass: 547.2148 $[M + H]^+$, observed mass: 547.2173 $[M + H]^+$.

4.4.3.2.6. *Tert*-butyl(4-amino-1-(4-((4'-fluoro-[1,1'-biphenyl]-4-yl)sulfonyl)piperazin-1-yl)-1,4-dioxobutan-2-yl)carbamate (**17f**) ($C_{25}H_{31}FN_4O_6S$, Mol. Wt. 534.60)

Product obtained after purification by gradient chromatography and collected at 97.5:2.5 v/v CH_2Cl_2 - MeOH then recrystalisation from EtOH to give a white powder, yield: 0.64 g, (65%), mp = 215 - 217 ^{O}C. TLC: CH_3OH - CH_2Cl_2 0.5:9.5 v/v, (R_F = 0.8). ^{1}H NMR ($CDCl_3$) δ 1.41 (s, 9H, $C(CH_3)_3$), 2.73 (d, J= 6.71 Hz, 2H, *CH_2*$CONH_2$), 3.13 (br m, 4H, CH_2, pip), 3.74 (br m, 4H, CH_2, pip), 4.86 (br q, 1H, *CH*NHBoc), 5.29 (br s, 1H, *NH*Boc), 7.20 (t, J = 7.9, 7.9 Hz, 2H, Ar), 7.59 (dd, J = 5.9, 7.9 Hz, 2H, Ar), 7.72 (d, J = 7.9 Hz, CH, Ar), 7.82 (d, J = 7.9 Hz, 2H, Ar). ^{13}C NMR ($CDCl_3$) δ 28.0 (C $(CH_3)_3$), 41.7 (*CH_2*$CONH_2$), 46.6 (*CH*NHBoc), 45.3, 45.7, 46.1 (4 x CH_2, pip), 116.1, 116.2, 127.8, 128.3, 129.0, 129.1 (8 x CH, Ar), 133.7, 134.2, 135.1, 162.3 (4 x C, Ar), 80.03 ($C(CH_3)_3$), 154.3 (C=O), 164.2 (C=O, Boc), 167.3 (C=O, $CONH_2$).

4.4.3.2.7. *Tert*-butyl(4-amino-1-(4-((4'-chloro-[1,1'-biphenyl]-4-yl)sulfonyl)piperazin-1-yl)-1,4-dioxobutan-2-yl)carbamate (**17g**) ($C_{25}H_{31}ClN_4O_6S$, Mol. Wt. 550.17)

Product obtained after purification by gradient chromatography and collected at 96.5:3.5 v/v CH_2Cl_2 - MeOH then recrystalisation from EtOH to give a colourless semisolid, yield: 0.32 g, (63%). TLC: CH_3OH - CH_2Cl_2 0.5:9.5 v/v, (R_F = 0.6). ^{1}H NMR ($CDCl_3$) δ 1.33 (s, 9H, $C(CH_3)_3$), 2.63 (d, J= 6.75 Hz, 2H, *CH_2*$CONH_2$), 3.02 (br m, 4H, CH_2, pip), 3.64 (br m, 4H, CH_2, pip), 4.77 (q, J =7.3 Hz, 1H, *CH*NHBoc), 5.26 (bs, 1H, *NH*Boc), 7.39 (d, J = 8.3 Hz, 2H, Ar), 7.46 (d, J = 8.95 Hz, 2H, Ar), 7.64 (d, J = 8.5 Hz, CH, Ar), 7.73 (d, J = 8.3 Hz, 2H, Ar). ^{13}C NMR: ($CDCl_3$) δ 28.2 ($C(CH_3)_3$), 41.9 (*CH_2*$CONH_2$), 46.7 (*CH*NHBoc), 45.3, 45.6, 45.7, 46.1 (4 x CH_2, pip), 127.7, 127.8, 128.3, 128.6, 128.6, 129.4 (8 X CH, Ar), 134.3, 134.2, 135.0, 137.4 (4 X C, Ar), 154.0 (C=O), 154.5 (C=O, Boc), 167.32 (C=O, $CONH_2$). HPLC: 100 % at RT: 4.6 min. HRMS (ES-TOF) m/z calculated mass: 551.1653 $[M + H]^+$, observed mass: 551.1844 $[M + H]^+$.

4.4.3.3. General procedure for the preparation of 1-(4-phenyl-4-ylsulfonyl)piperazin-1-yl)-4-amino-1,4-dioxobutan-2-aminium chloride derivatives (**18a**-**g**) (345)

To an ice-cooled solution of (**17a**-**g**) (0.33 mmol) in dry dioxane (2.5 mL) was added 4N HCl in dioxane (0.8 mL) dropwise. The colourless solution was stirred at 0 ^{O}C for 10 min then at room temperature for 50 min. The solvent was removed under vacuum to give a white glassy solid. CH_2Cl_2 (10 mL) was added and the solid/flask scratched to form a fine white powder, which was collected by vacuum filtration and washed with CH_2Cl_2 (3 x 5 mL). The crude solid was purified by recrystallisation to give the final product.

4.4.3.3.1. (S)-3-amino-4-oxo-4-(4-tosylpiperazin-1-yl)butanamide hydrogen chloride (**18a**) ($C_{15}H_{23}ClN_4O_4S$, Mol. Wt. 390.88)

Product obtained after washing with CH_2Cl_2, collected by filtration and dried (vacuum oven at 40 ^{o}C) as a white solid, yield: 0.144 g (56 %), mp. 215 - 220 ^{O}C. TLC: CH_3OH - CH_2Cl_2 1:9 v/v, (R_F = 0.6). ^{1}H NMR (DMSO-d_6) δ 2.41 (s, 3H, CH_3), 2.81 (br m, 2H, CH_2, pip), 3.07 (br m, 2H, CH_2, pip) overlapping 3.09 (ddd, J = 5.8, 17.5, 23.2 Hz, 2H, *CH_2*$CONH_2$), 3.47 (br m, 1H, pip), 3.60 (br m, 1H, pip), 3.72 (br m, 2H, CH_2, pip), 4.70 (t, J = 5.9 Hz, 1H, *CH*NH_3), 7.17 (br s, 1H, NH_2), 7.47 (d, J = 8.0 Hz, 2H, Ar), 7.64 (d, J = 8.3 Hz, 2H, Ar), 7.71 (br s, 1H, NH_2), 8.69 (br s, 3H, NH_3). ^{13}C NMR (DMSO-d_6) δ 19.8 (CH_2, CH_2CONH_2), 21.5 (CH_3), 41.9, 45.1 (2 x CH_2, pip), 45.7 (CH, *CH*NH_3), 46.0, 46.2 (4 x CH_2, pip), 128.1, 130.5 (2 x CH, Ar), 116.5,132.4 (2 x C, Ar), 144.4 (C=O), 165.6 (C=O, $CONH_2$). HPLC: 100% at RT: 3.43 min. HRMS (ES-TOF) m/z calculated mass: 355.1362 $[M + H]^+$, observed mass: 355.1435 $[M + H]^+$.

4.4.3.3.2. (S)-3-amino-4-(4-((4-nitrophenyl)sulfonyl)piperazin-1-yl)-4-oxobutanamide hydrogen chloride (**18b**) ($C_{14}H_{20}ClN_5O_6S$, Mol. Wt. 421.85)

Product obtained after washing with CH_2Cl_2 and collected the solution after filtration of impurities and evaporated the solvent to give a white solid as free amine, yield: 0.12 g (60%), mp: 198 - 200 ^{O}C. TLC: petroleum ether – EtOAc 1:1 v/v (R_f = 0.5). ^{1}H NMR (DMSO-d_6) δ 2.80 (br t, 4H, CH_2, pip), 3.57 (br t, 4H, CH_2, pip) 2.68 (d, J = 9.2 Hz, 2H, *CH_2*$CONH_2$), 4.64 (quintet, 1H, *CH*NH_2), 7.55 (d, J = 8.2, 1H, CH*NH*), 8.03 (d, J = 9 Hz, 2H, CH, Ar), 8.46 (d, J = 9 Hz, 2H, CH, Ar), 11.93 (s, 2H, NH_2). ^{13}C NMR (DMSO-d_6) δ 21.5 (CH_2, CH_2CONH_2), 40.5, 46.1 (4 x CH_2, pip), 47.4 (CH, $CHNH_3$), 125.2, 129.7, (4 x CH, Ar), 116.5, 146.9 (2 x C, Ar), 136.8 (C=O), 163.6 (C=O, $CONH_2$). HPLC: 100% at RT: 4.01 min.

HRMS (ES-TOF) m/z calculated mass: 408.1056 $[M + Na]^+$, observed mass: 408.0947 $[M + Na]^+$.

4.4.3.3.3. (S)-3-amino-4-(4-((4-fluorophenyl)sulfonyl)piperazin-1-yl)-4-oxobutanamide hydrogen chloride (**18c**) ($C_{14}H_{20}ClFN_4O_4S$, Mol. Wt. 394.85)

Product obtained after washing with CH_2Cl_2 and Et_2O, collected by filtration and dried (vacuum oven at 40 ^oC) as a white solid, yield: 0.132 g (51 %), mp. 175 - 177 ^OC. TLC: CH_3OH - CH_2Cl_2 1:9 v/v, (R_F = 0.5). ^1H NMR (DMSO-d_6) δ 2.90 (br m, 2H, CH_2, pip), 3.07 (br m, 2H, CH_2, pip) overlapping ~ 3.08 (ddd, J = 5.8, 17.5, 23.2 Hz, 2H, *CH_2*$CONH_2$) 3.52 (br m, 2H, CH_2, pip), 3.63 (br m, 1H, pip), 3.71 (br m, 2H, CH_2, pip), 4.71 (t, J = 5.7 Hz, 1H, *CH*NH_3), 7.17 (s, 1H, CO*NH_2*), 7.51 (t, J = 8.8 Hz, 2H, CH, Ar), 7.70 (s, 1H, CO*NH_2*), 7.84 (dd, J = 5.1, 8.9 Hz, 2H, CH, Ar), 8.70 (br s, 3H, NH_3). ^{13}C NMR (DMSO-d_6) δ 19.8 (CH_2, *CH_2*$CONH_2$), 41.9, 45.0, 46.0, 46.2 (4 x CH_2, pip), 45.6 (CH, *CH*NH_3), 117.2, 117,4, 131.1, 131.2 (4 x CH, Ar), 116.5 (C, Ar), 131.7 (C=O), 165.6 (C=O, $CONH_2$), 166.3 (C-F). HPLC: 100% at RT: 3.23 min. HRMS (ES-TOF) m/z calculated mass: 381.1111 $[M + Na]^+$, observed mass: 381.1006 $[M + Na]^+$.

4.4.3.3.4. (S)-4-(4-([1,1'-biphenyl]-4-ylsulfonyl)piperazin-1-yl)-3-amino-4-oxobutanamide hydrogen

chloride (**18d**) ($C_{20}H_{25}ClN_4O_4S$, Mol. Wt. 452.95)

Product obtained after recrystalisation from EtOH as a white crystalline solid, yield: 0.053 g (35 %), mp. 205 - 210 ^OC. TLC: CH_3OH - CH_2Cl_2 0.5:9.5 v/v, (R_F = 0.6). ^1H NMR (DMSO-d_6) δ 2.89 (br m, 2H, CH_2, pip), 3.08 (ddd, J = 6.0, 17.5, 23.4 Hz, 2H, *CH_2*$CONH_2$), 3.16 (br m, 2H, CH_2, pip), 3.52 (br m, 1H, pip), 3.63 (br m, 1H, pip), 3.76 (br m, 2H, CH_2, pip), 4.71 (t, J = 6.0 Hz, 1H, *CH*NH_3), 7.46 (t, J = 7.3 Hz, 1H, Ar), 7.53 (m, 2H, CH, Ar), 7.59 (br s, 1H, NH_2), 7.61 (br s, 1H, NH_2), 7.76 (d, J = 7.1 Hz, 2H, Ar), 7.83 (d, J = 8.6 Hz, 2H, CH, Ar), 7.96 (d, J = 8.7 Hz, 2H, CH, Ar), 8.63 (br s, 3H, NH_3). ^{13}C NMR (DMSO-d_6) δ 19.8 (CH_2, CH_2CONH_2), 41.9, 45.1, 46.0, 46.2 (4 X CH_2, pip), 45.7 (CH, *CH*NH_3), 127.6, 128.2, 128.7, 129.2, 129.7 (9 x CH, Ar), 116.5, 134.0, 138.7 (3 x C, Ar), 145.3 (C=O), 165.7 (C=O, $CONH_2$). HPLC: 100% at RT: 3.88 min. HRMS (ES-TOF) m/z calculated mass: 439.1518 $[M + Na]^+$, observed mass 439.1410 $[M + Na]^+$.

4.4.3.3.5. (S)-3-amino-4-(4-((4'-methoxy-[1,1'-biphenyl]-4-yl)sulfonyl)piperazin-1-yl)-4-oxobutanamide hydrogen chloride (**18e**) ($C_{21}H_{27}ClN_4O_5S$, Mol. Wt. 482.98)

Product obtained after washing with CH_2Cl_2, collected by filtration and dried (vacuum oven at 40 ^oC) then recrystalisation from EtOH to give a white powder, yield: 0.2 g (67 %), mp = 238 - 240 ^OC. TLC: petroleum ether – EtOAc 1:1 v/v (R_f = 0.4). ^1H NMR (DMSO-d_6) δ 3.03 (dd, J = 6.9, 10 Hz, 2H, *CH_2*$CONH_2$), 2.85 (br t, 2H, CH_2, pip), 3.14 (br t, 2H, CH_2, pip), 3.57 (br t, 2H, CH_2, pip), 3.76 (br t, 2H, CH_2, pip), 3.82 (s, 3H, OCH_3), 4.67 (t, J = 7.3, 7.3 Hz, 1H, *CH*NH_2), 7.08 (d, J = 9.8 Hz, 2H, Ar), 7.73 (d, J = 9.8 Hz, 2H, Ar), 7.79 (d, J = 9.8 Hz, 2H, Ar), 7.91 (d, J = 9.8 Hz, 2H, Ar), 8.38 (s, 3H, NH_3). ^{13}C NMR (DMSO-d_6) δ 30.7 (*CH_2*$CONH_2$), 27.0 (*CH*NH_2), 48.3, 48.7 (4 x CH_2, pip), 60.01 (OCH_3), 127.3, 127.8, 128.3, 129.0, 129.1, 131.9 (8 X CH, Ar), 133.7, 138.2, 135.1, 159.3 (4 X C, Ar), 173.3 (C=O), 167.3 (C=O, $CONH_2$). HPLC: 96% at RT: 4.2 min. HRMS (ES-TOF) m/z calculated mass: 447.1624 $[M + H]^+$, observed mass: 447.1697 $[M + H]^+$.

4.4.3.3.6. (S)-3-amino-4-(4-((4'-fluoro-[1,1'-biphenyl]-4-yl)sulfonyl)piperazin-1-yl)-4-oxobutanamide hydrogen chloride (**18f**) ($C_{20}H_{24}ClFN_4O_4S$, Mol. Wt. 470.94)

Product obtained after washing with CH_2Cl_2, collected by filtration and dried (vacuum oven at 40 ^oC) then recrystalisation from EtOH to give a white powder, yield: .0.13 g (67 %), mp. 220 - 222 ^OC. TLC: petroleum ether – EtOAc 1:1 v/v (R_f = 0.6). ^1H NMR (DMSO-d_6) δ 2.89 (br m, 2H, CH_2, pip), 3.03 (d, J = 6.6, 10 Hz, 1H, *CH_2*$CONH_2$), 3.06 (d, J = 6.6, 10 Hz, 1H, *CH_2*$CONH_2$), 3.14 (br s, 2H, CH_2, pip), 3.52 (br s, 2H, CH_2, pip), 3.62 (br s, 2H, CH_2, pip), 4.69 (t, J = 6.0, 6.0 Hz, 1H, *CH*NH_2), 7.36 (t, J = 9.6, 9.6 Hz, 2H, Ar), 7.82 (m, 2H, Ar), 7.96 (d, J = 9.8 Hz, 2H, Ar), 8.48 (s, 3H, NH_3). ^{13}C NMR (DMSO-d_6) δ 20,0 (*CH_2*$CONH_2$), 41.0 (*CH*NH_2), 45.8, 48.7 (4 x CH_2, pip), 127.3, 127.8, 128.3, 129.0, 129.1, 131.9 (8 X CH, Ar), 133.7, 138.2, 135.1, 159.3 (4 X C, Ar), 173.3 (C=O, $CONH_2$), 172.6 (C=O). HPLC: 100% at RT: 4.2 min. HRMS (ES-TOF) m/z calculated mass: 435.1424 $[M + H]^+$, observed mass: 435.1512 $[M + H]^+$.

4.4.3.3.7. (S)-3-amino-4-(4-((4'-chloro-[1,1'-biphenyl]-4-yl)sulfonyl)piperazin-1-yl)-4-oxobutanamide hydrogen chloride (**18g**) ($C_{20}H_{24}Cl_2N_4O_4S$, Mol. Wt. 486.09)

Product obtained after washing with CH_2Cl_2, collected by filtration and dried (vacuum oven at 40 ^oC) then recrystalisation from EtOH to give a white solid, yield: 0.2 g (33 %),

mp. 212 - 214 ^{O}C. TLC: petroleum ether – EtOAc 1:1 v/v (R_f = 0.5). ^{1}H NMR (DMSO-d_6) δ 2.88 (br m, 2H, CH_2, pip), 3.03 (d, J = 6.9, 6.9 Hz, 1H, *CH_2*$CONH_2$), 3.06 (d, J = 6.6, 10 Hz, 1H, *CH_2*$CONH_2$), 3.14 (br s, 2H, CH_2, pip), 3.55 (br s, 2H, CH_2, pip), 3.75 (br s, 2H, CH_2, pip), 4.69 (t, J = 6.0, 6.0 Hz, 1H, *CH*NH_2), 7.59 (d, J = 8.4 Hz, 2H, Ar), 7.79 (d, J = 8.4 Hz, 2H, Ar), 7.83 (d, J = 8.4 Hz, 2H, Ar), 7.97 (d, J = 8.4 Hz, 2H, Ar), 8.52 (s, 3H, NH_3). ^{13}C NMR (DMSO-d_6) δ 20.2 (*CH_2*$CONH_2$), 41.8 (*CH*NH_2), 45.1, 46.0, 46.2 (4 x CH_2, pip), 128.0, 128.6, 129.4, 129.6, (8 X CH, Ar), 134.2, 134.3, 137.5, 143.9 (4 X C, Ar), 165.7 (C=O, $CONH_2$), 171.4 (C=O). HPLC: 100% at RT: 4.3 min. HRMS (ES-TOF) m/z calculated mass: 473.1129 $[M + Na]^+$, observed mass: 473.1011 $[M + Na]^+$.

Chapter 5: N-(3,4-dimethylisoxazol-5-yl)-4-(phenyl)sulfonyl)piperazine-1-carboxamide derivatives

(Series 3)

5. Introduction

In this chapter, *N*-(3,4-dimethylisoxazol-5-yl)-4-(phenyl)sulfonyl)piperazine-1-carboxamide derivatives (**24**) were prepared retaining the same substituted aryl/biaryl moieties as the adenine mimic and the amino acid moiety was replaced by 3,4-dimethylisoxazole, while the linker in this series consists of an amide group connected with a sulfamoyl linkage through a piperazine ring (Table 39). The rational for the design of this series was to mimic the sulfamoyl linkage using an amide bond to test the hypothesis, in the literature, that the amide linkage is an effective in aa-AMP replacement (321).

Table 39: General chemical structures of scheme 3 AspRS and AsnRS inhibitors (**24**).

Series	General chemical structures	R groups
3	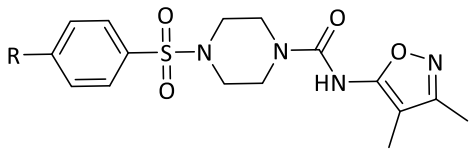	CH_3, NO_2, C_6H_5, $C_6H_4OCH_3$, C_6H_4F, C_6H_4Cl

This chapter is divided into four parts as follows:

- Results and discussion
- Docking studies
- Biological screening
- Methods

5.1. Synthetic pathway for *N*-(3,4-dimethylisoxazol-5-yl)-4-(phenyl)sulfonyl) piperazine-1-carboxamide derivatives (24)

The asparagine moiety of Asp/Asn series 2 inhibitors was replaced by 3,4-dimethylisoxazole, combined with an amide piperazine-sulfamoyl linker and substituted aryl/biaryl moieties instead of the adenine base. The synthetic pathways are shown in scheme 9 and involved the following steps:

- Nucleophilic reaction of piperazine with sulfonyl chloride derivatives (**3a**-**f**)
- Amide linkage formation between 3,4-dimethyl isoxazole amine and trichloroethyl carbonochloridate (**21**)
- Nucleophilic substitution reaction of sulfonyl piperazine derivatives with 2,2,2-trichloroethyl(3,4-dimethylisoxazol-5-yl)carbamate (**24a**-**f**)

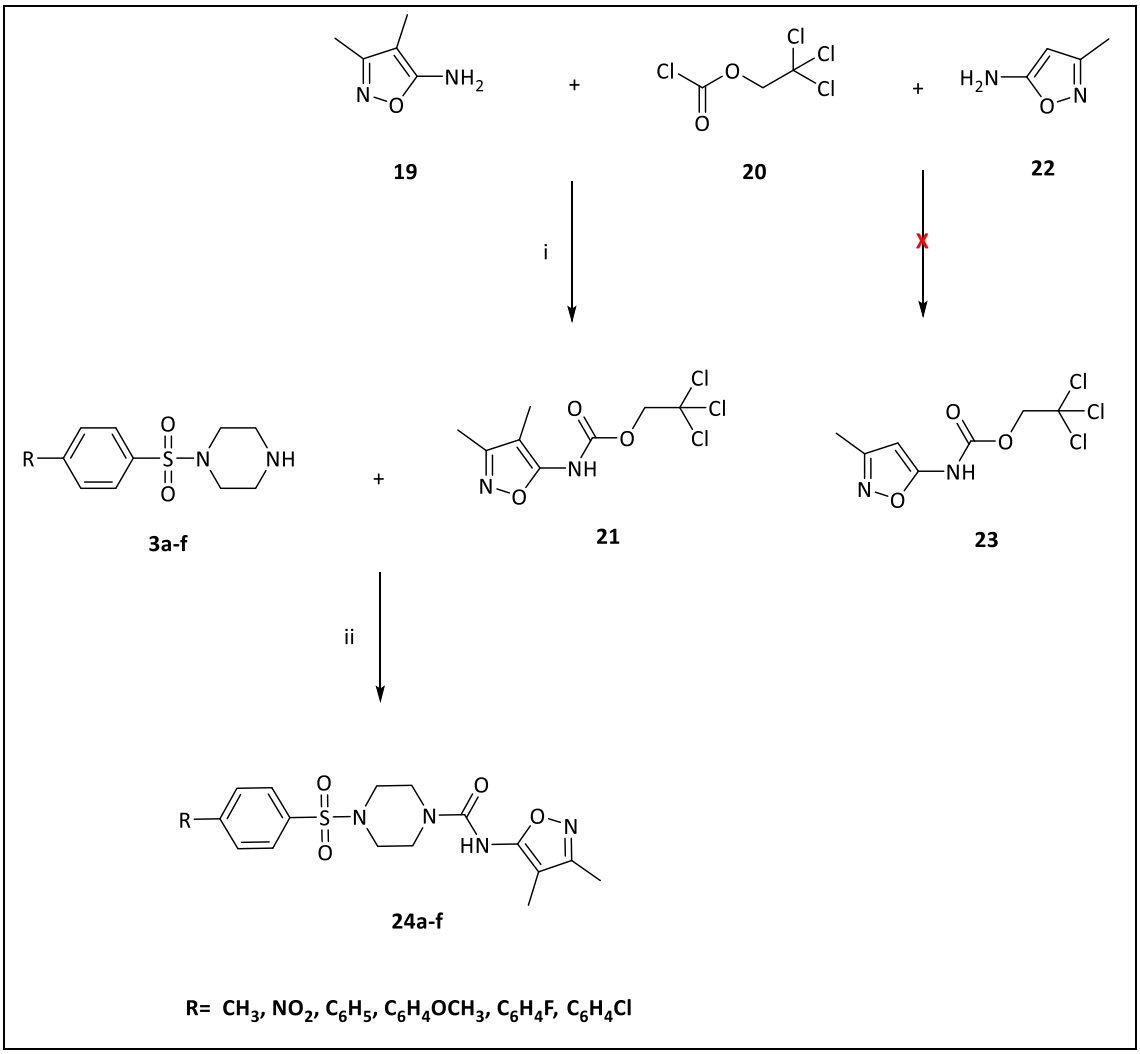

Scheme 9: Synthetic pathway for *N*-(3,4-dimethylisoxazol-5-yl)-4-(phenyl) sulfonyl) piperazine-1-carboxamide derivatives (**24a**-**f**). *Reagents and conditions*: (i) Pyridine, dry THF, 0 ^{O}C, 1 h. (ii) *N*-ethyl-diisopropylamine, dry DMF, 70 ^{O}C, 2-24 h.

5.1.1. Synthesis of sulfonyl piperazine derivatives 3a-f

The preparation of sulfonyl piperazine derivatives (**3a**-**f**) (327) was discussed in chapter 3.

5.1.2. Synthesis of 2,2,2-trichloroethyl (3,4-dimethylisoxazol-5-yl)carbamate (21)

2,2,2-Trichloroethoxycarbonyl chloride (**20**) was used to introduce the 2,2,2-trichloroethoxycarbonyl (Troc) group to 3,4-dimethylisoxazol-5-amine (**19)** in the presence of pyridine as a base and THF as solvent (Scheme 9) (347). This group is widely used as a protecting group for amines (348) and the reaction takes just 1h at 0 ^{O}C producing compound **21** in a good yield (Table 40). However, using the same reaction with 3-methylisoxazole-5-amine (**22**) to produce 2,2,2-trichloroethyl (3-methylisoxazol-5-yl)carbamate (**23**) was unsuccessful owing to its reduced nucleophilicity.

Table 40: Identification data for 2,2,2-trichloroethyl (3,4-dimethylisoxazol-5-yl) carbamate (**21**).

Compd	**Yield (%)**	**mp (^{O}C)**	**Appearance**
21	90	78-80	Colourless solid

5.1.3. Synthesis of *N*-(3,4-dimethylisoxazol-5-yl)-4-(phenyl)sulfonyl)piperazine-1-carboxamide derivatives (24a-f)

2,2,2-Trichloroethyl (3,4-dimethylisoxazol-5-yl)carbamate (**21**) was reacted with sulfonyl piperazine derivatives (**3a-f**) using *N*-ethyldiisopropylamine as base and DMF as solvent and the reaction mixture heated at 70 ^{O}C for a period of time ranging from 2- 24 h (347) (Scheme 9). The products (**22a-f**) were obtained in satisfactory yields (41-66%), however, compound **24e** was obtained in lower yield (26%) (Table 41) as the reaction did not reach completion resulting in a lower yield after recrystallisation.

Table 41: Identification data for *N*-(3,4-dimethylisoxazol-5-yl)-4-(phenyl)sulfonyl) piperazine-1-carboxamide derivatives (**24a**-**f**).

Compd	**R**	**Yield (%)**	**mp (^{o}C)**	**Appearance**
24a	CH_3	66	-	Pale yellow semisolid
24b	NO_2	52	196-198	White solid
24c	C_6H_5	41	176-178	White shiny solid
24d	$C_6H_4OCH_3$	60	-	White semisolid
24e	C_6H_4F	26	194-196	White crystal
24f	C_6H_4Cl	51	206-208	White solid

^{1}H and ^{13}C NMR spectra and either elemental analysis or HRMS confirmed the structures and purity. For example, the ^{1}H NMR spectrum of compound **24d** showed aromatic *CH* signals in the aromatic region as four doublet peaks, each integrated for 2 protons and the NH peak was observed as a broad singlet peak (Figure 151a), OCH_3 was observed as a singlet peak and piperazine as two broad singlet peaks integrated for 4 protons each (Figure 151b), while isoxazole CH_3 peaks showed as two singlet peaks integrated for three protons each (Figures 151c).

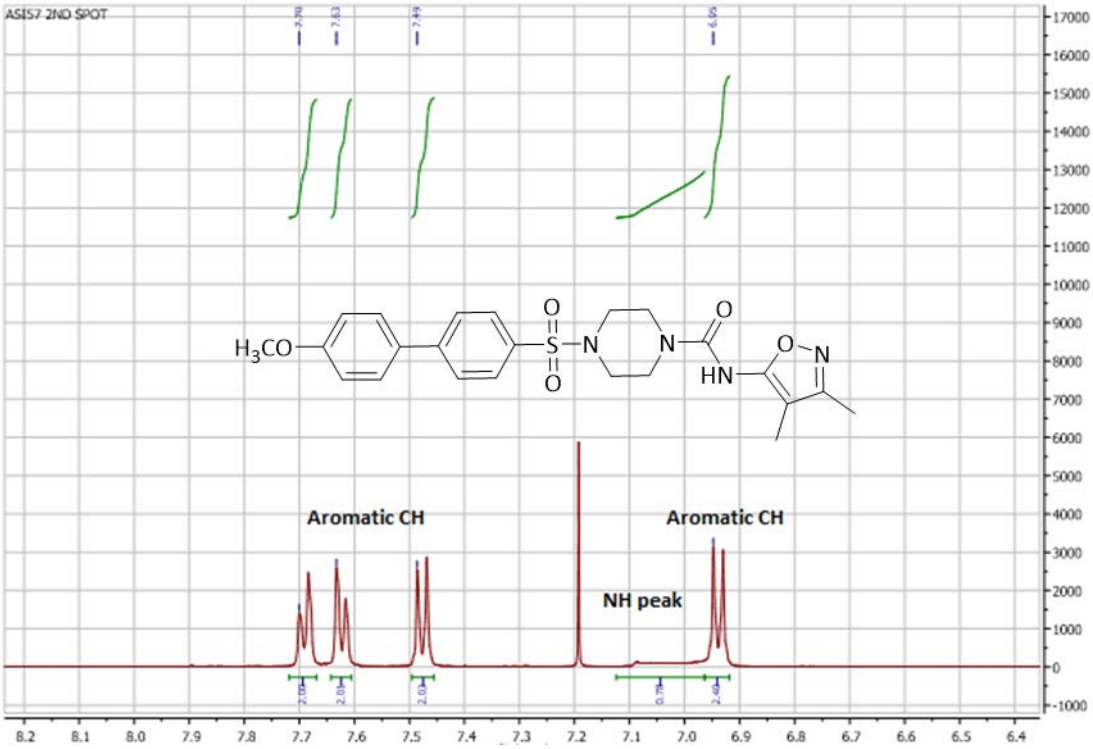

Figure 151a: ^{1}H NMR spectrum of compound **24d**. The spectrum shows aromatic CH as four doublet peaks, each integrated for 2 protons and NH as a singlet peak.

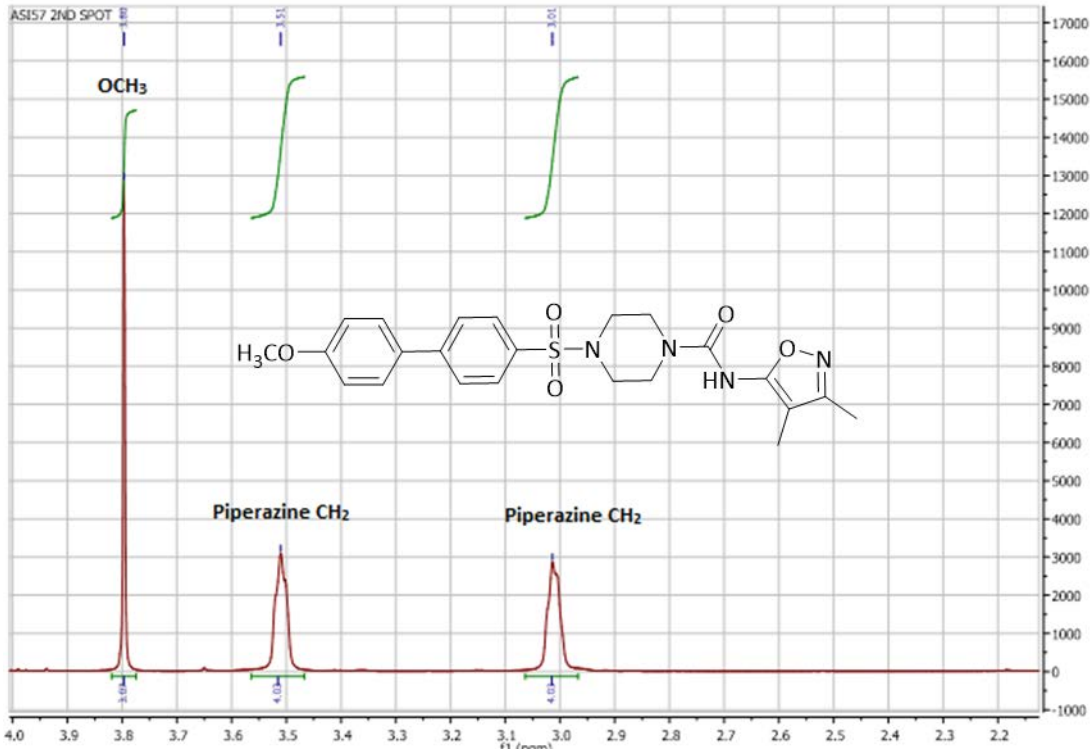

Figure 151b: ^{1}H NMR spectrum of compound **24d**. The spectrum shows the OCH_3 peak as a singlet and piperazine CH_2 as two broad singlet peaks.

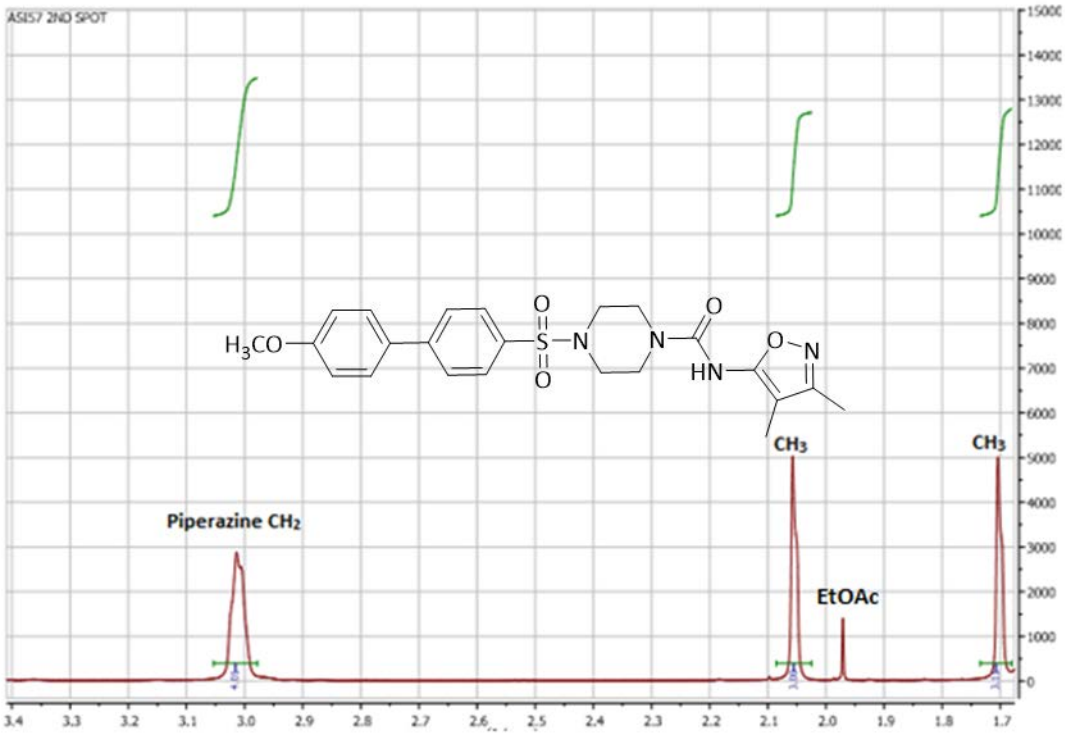

Figure 151c: ^{1}H NMR spectrum of compound **24d**. The spectrum shows the two isoxazole CH_3 as two singlet peaks.

5.2. Docking studies

A docking study of the final compounds of series 3 with *S. aureus* and *E. faecalis* AspRS and AsnRS enzymes was performed to determine their binding interactions with the active sites of the respective aaRS enzymes. The docking study showed that the compounds interacted with some of the amino acid residues observed for the aa-AMP natural substrates. Compounds **24a**-**b** were too short to fill the Asp and Asn pockets of the target enzymes while the interactions of their sulfamoyl piperazine aryl moieties were good with the amino acid residues responsible for AMP pocket of both enzymes. The docking studies of compounds **24c**-**f** showed good fitting inside the active sites and good binding interactions. However, the amino acid isosteric moiety of compounds **24a**-**f** interacted with only one key amino acid residue (Arg360) responsible for the Asn pocket of *S. aureus* and *E. faecalis* AsnRSs.

5.2.1. Docking studies of *S. aureus* AspRS

By alignment of series 3 compounds with aspartyl adenylate inside the active site of *S. aureus* AspRS (Figure 152), the amino acid residues responsible for binding

interactions were identified (Table 42). The aryl/biaryl sulfamoyl piperazine moiety of compounds **24a**-**f** formed hydrogen bonds with the same amino acid residues that interacted with AMP. Because of the reduced length of compounds **24a** and **24b**, the binding interactions of the amino acid isosteric moiety with the amino acid residues responsible for the Asp pocket were not good despite the close approach of the histidine and flipping loops (Figures 153 and 154). The docking study of compound **24c**-**f** showed good hydrogen binding interactions with the amino acid residues in both pockets (Figure 155 and 156). There was no interaction with the methoxy, fluoro and chloro groups of the respective compounds. In addition, the hydrophobic interactions were not formed with the replacement part of the adenine base in compounds **24a**-**f**. The docking studies of series 3 compounds with *S. aureus* AspRS showed the role of Mg^{2+} ion in stabilisation of the sulfamoyl linkage. (Figures 153-156).

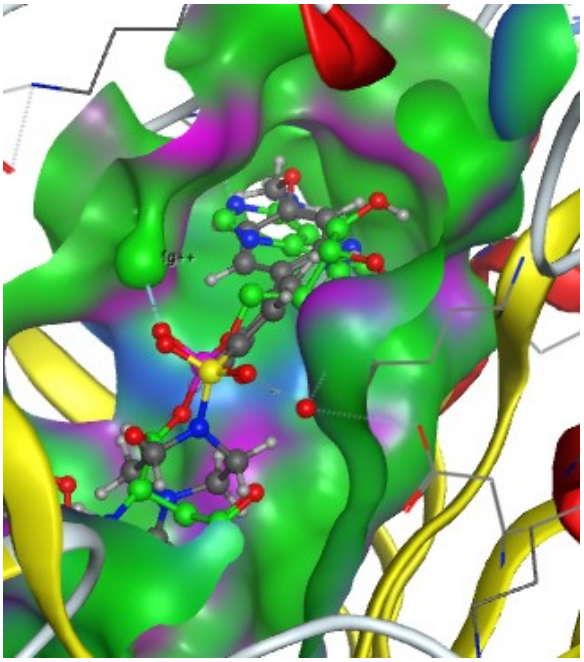

Figure 152: Alignment of compound **24d** (grey) with aspartyl adenylate (green) in the active sites of *S. aureus* AspRS.

Table 42: Binding interactions of series 3 compounds with the amino acid residues of the binding sites of *S. aureus* AspRS.

Ligands	Aspartic acid pocket	AMP pocket
Aspartyl-adenylate	Gln201, Lys204, His452, Gly488, Ser490, Arg492 and Asp239	Arg223, Phe235, Gln232, Arg540 and Glu485
24a	Ser199, Arg231 and His452	Phe235, Gln237, Glu485 and Arg540
24b	Gln237, Arg231 and Asp239	Arg223, Asp478, Glu485 and Arg540
24c	Ser199, Gln237, His452, Gly488 and Asp239	Asp478, Glu485 and Arg540
24d	Ser199, Gln201, Gln237, His451, His452, Gly488 and Asp239	Arg223, Asp478, Glu485 and Arg540
24e	Ser199, Gln201, Gln237, His451, His452, Gly488, Gly489, Arg492 and Asp239	Arg223, Gln232, Asp478 and Glu485
24f	Ser199, Gln237, His451, His452, Gly488 and Asp239	Gln232, Phe235 and Glu485

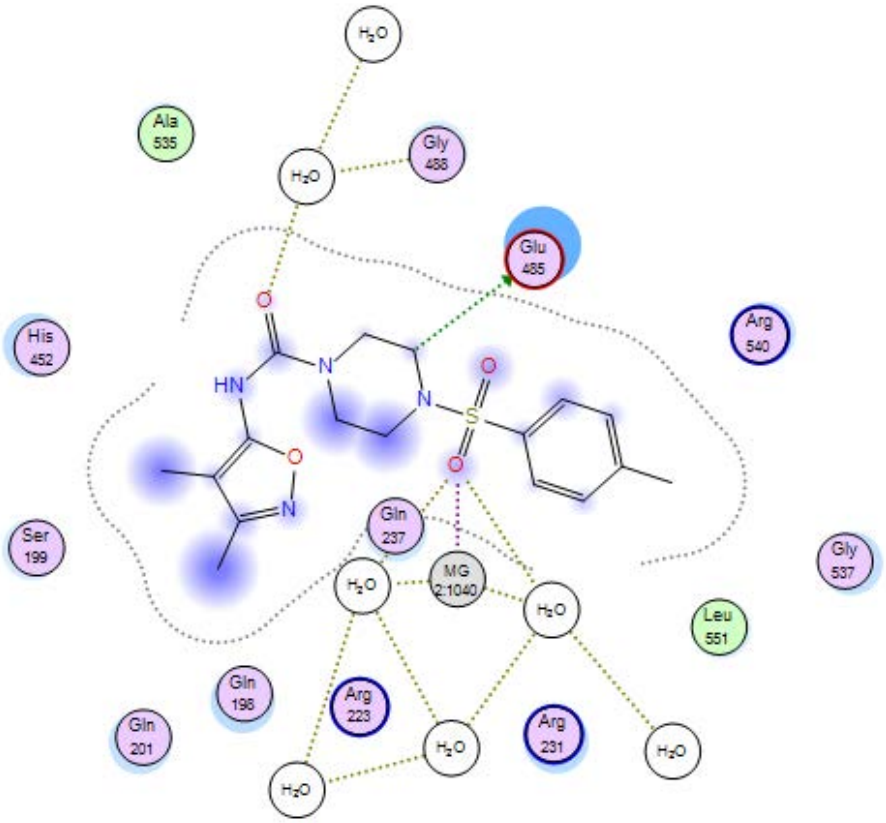

Figure 153: 2D binding interactions of compound **24a** with *S. aureus* AspRS.

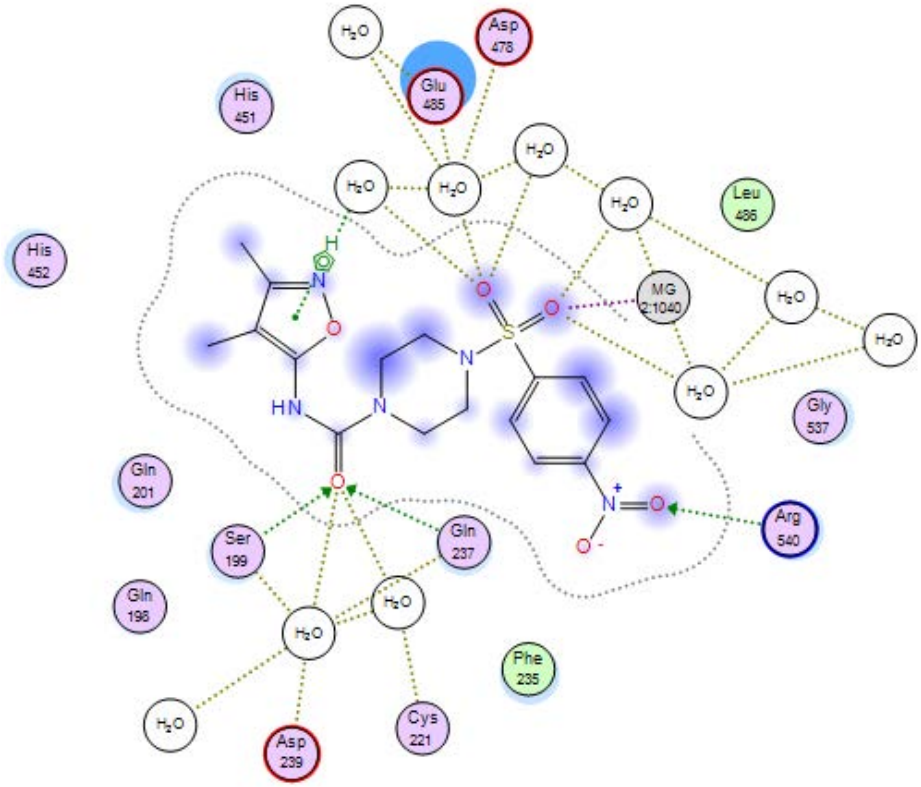

Figure 154: 2D binding interactions of compound **24b** with *S. aureus* AspRS.

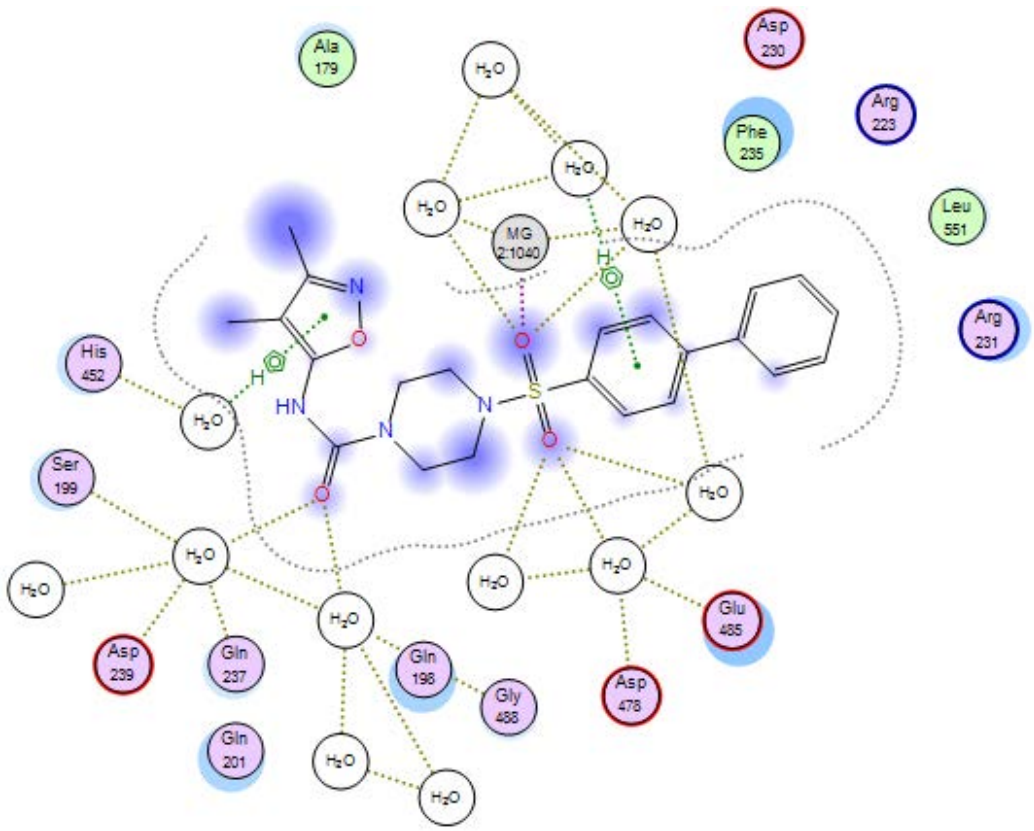

Figure 155: 2D binding interactions of compound **24c** with *S. aureus* AspRS.

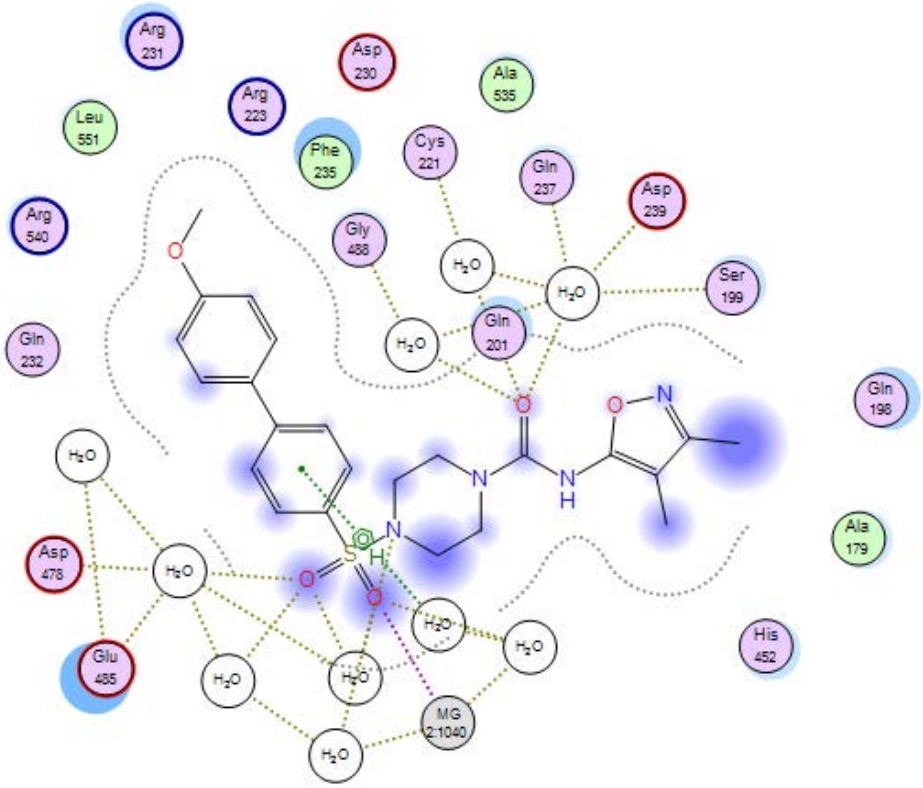

Figure 156: 2D binding interactions of compound **24d** with *S. aureus* AspRS.

5.2.2. Docking studies of *S. aureus* AsnRS

By alignment of series 3 compounds with asparaginyl adenylate inside the active site of *S. aureus* AspRS (Figure 157), the amino acid residues responsible for binding interactions were identified (Table 43). Compounds **24a** and **24b** were too short to occupy the Asn pocket, but they formed hydrophobic and hydrogen binding interactions with the amino acid residues responsible for the AMP pocket. The docking studies of compounds **24a-f** showed good binding interactions of the sulfamoyl piperazine biaryl moieties with the same amino acid residues observed for binding of AMP. For example, a π-π stacking interaction of the biphenyl moiety with Phe219 was shown in compounds **24c**-**d** and **24f** (Figures 158, 159 and 161). The interaction of Glu223 and Arg360 as key amino acid residues for asparagine recognition and the assistant role of water molecules were not observed for compounds **24a-f** during the docking study. However, the 3,4 -dimethyl isoxazole of compound **24c** and **24e** formed a water mediated hydrogen bond with Arg360 (Figure 158 and 160) while in compound **24f**, two hydrogen bonds were observed, one via a water molecule and the second directly with the nitrogen atom of the amino acid isosteric moiety (Figure 161). The role of Mg^{2+} ion in stabilisation of the sulfamoyl linkage was clear in the binding interactions of series 3 compounds with S. *aureus* AsnRS model (Figures 158-161).

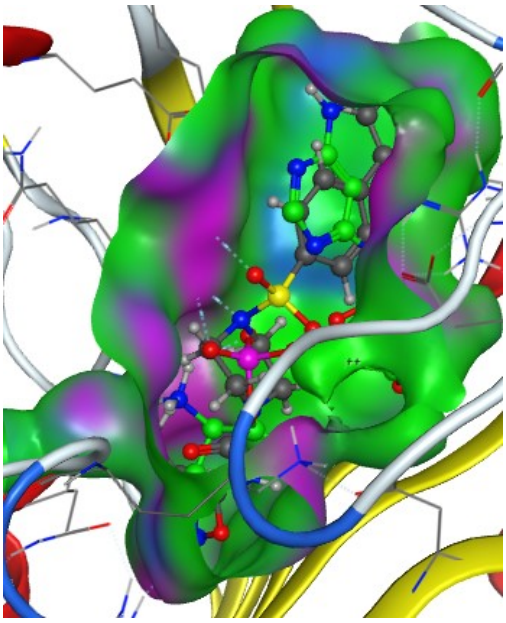

Figure 157: Alignment of compound **24c** (grey) with asparaginyl adenylate (green) in the active sites of *S. aureus* AsnRS.

Table 43: Binding interactions of series 3 compounds with the amino acid residues of the binding sites of *S. aureus* AsnRS.

Ligands	Asparagine pocket	AMP pocket
Asparaginyl-adenylate	Glu223 and Arg360	Arg206, Glu208, Arg214, His215, Phe219, Glu353, Gly356, Gly401 and Arg404
24a	-	Arg206, Phe219, Glu353, Gly356 and Arg404
24b	-	Arg206, Phe219, Glu353 and Arg404
24c	Arg360	Glu163, Glu167, Arg206, Phe219, Glu353, Gly356 and Arg404
24d	Arg360	Glu163, Glu167, Arg206, His215, Phe219, Glu353 and Arg404
24e	Arg360	Glu163, Glu167, Arg206, Phe219, Glu353, Gly356 and Arg404
24f	Arg360	Glu163, Glu167, Arg206, His215, Phe219, Glu353 and Arg404

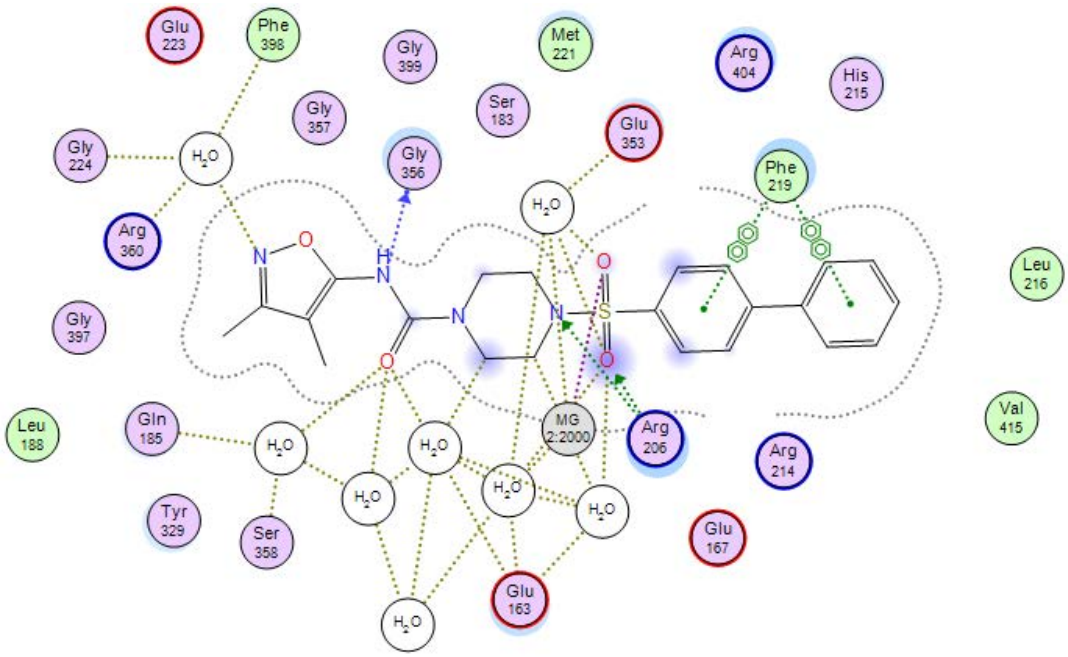

Figure 158: 2D binding interactions of compound **24c** with *S. aureus* AsnRS.

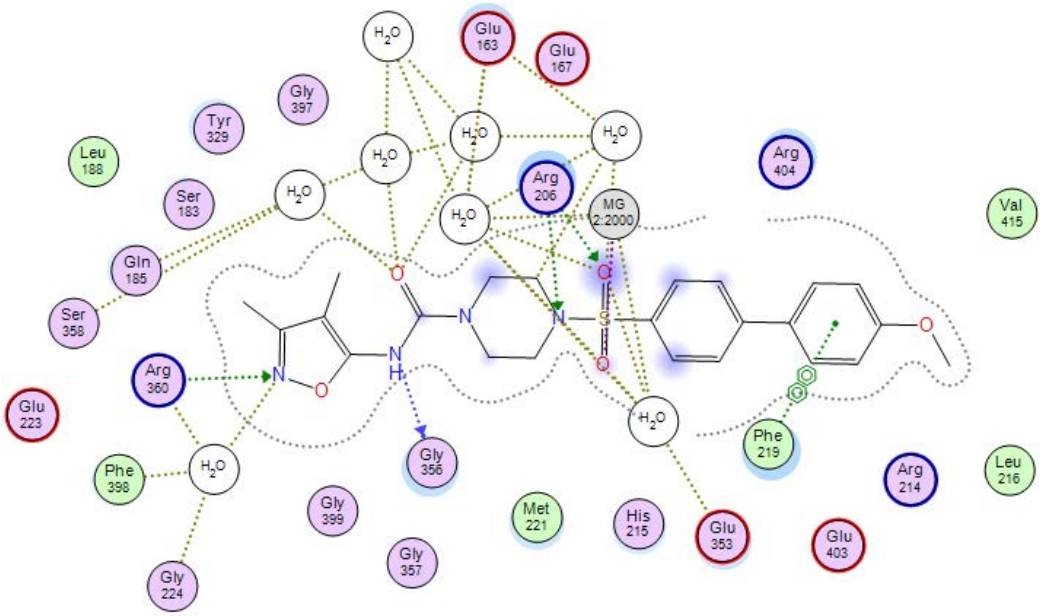

Figure 159: 2D binding interactions of compound **24d** with *S. aureus* AsnRS**.**

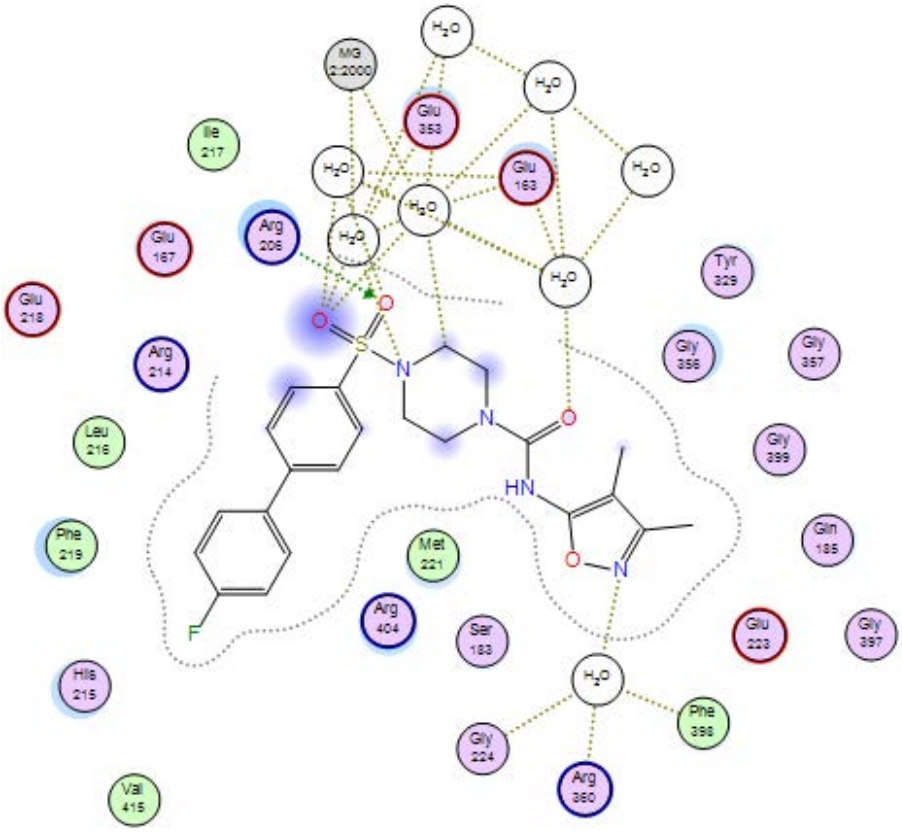

Figure 160: 2D binding interactions of compound **24e** with *S. aureus* AsnRS.

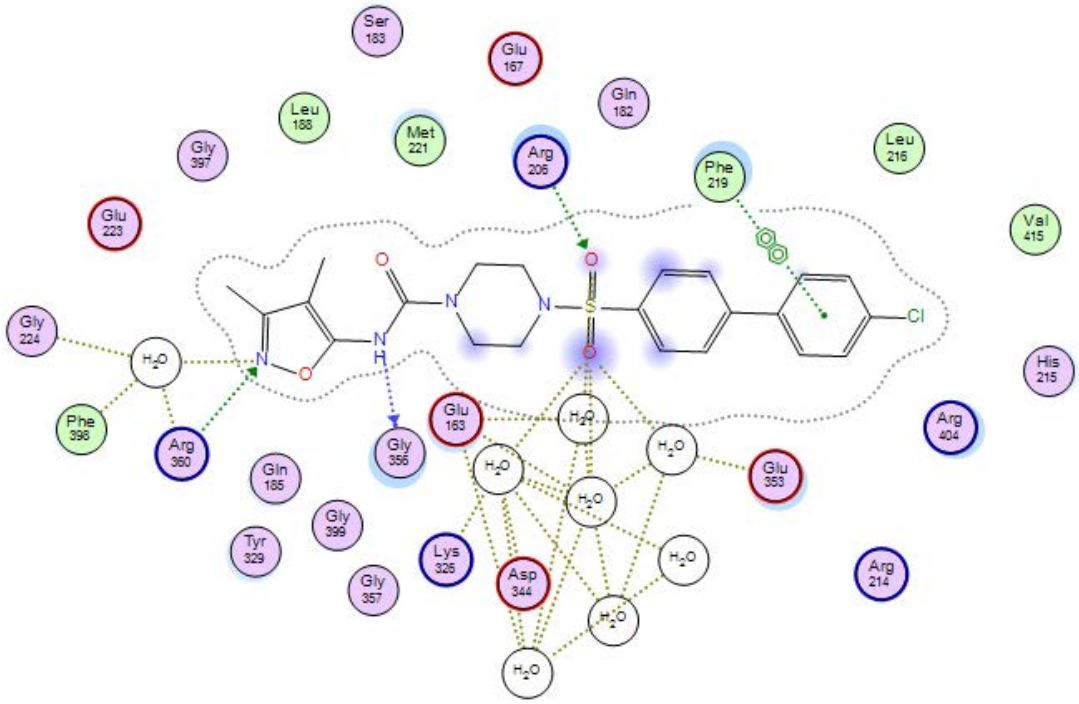

Figure 161: 2D binding interactions of compound **24f** with *S. aureus* AsnRS.

5.2.3. Docking studies of *E. faecalis* AspRS.

The amino acid residues responsible for binding interactions with series 3 compounds were identified through alignment with aspartyl adenylate inside the active sites of *E. faecalis* AspRS (Figure 162) (Table 44). The docking study of compounds **24a**-**f** showed good binding interactions inside both pockets. For example, the benzene ring of compounds **24a**-**b** and **24d** formed a π-π stacking interaction with Phe234 and the nitro group of compound **24b** formed hydrogen bonds directly with Gln231 and via water molecule with Asp537 (Figures 163-166). In spite of the good fitting of compounds **24d** and **24e** inside the pockets and with the histidine and flipping loops close to the amino acid isosteric moiety, the Mg^{2+} ion did not show any role in stabilising the sulfamoyl linkage (Figures 165 and 166). The docking study of compound **24f** showed good binding interactions with the key amino acid residues of the Asp pocket but the role of Mg^{2+} was absent in the poses that showed good fitting inside the active sites (Figure 167).

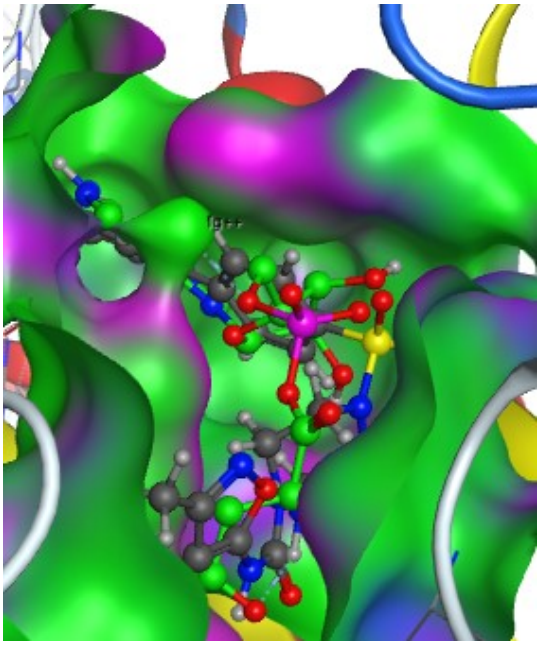

Figure 162: Alignment of compound **24d** (grey) with aspartyl adenylate (green) in the active sites of *E. faecalis* AspRS.

Table 44: Binding interactions of series 3 compounds with the amino acid residues of the binding sites of *E. faecalis* AspRS.

Ligands	Aspartic acid pocket	AMP pocket
Aspartyl-adenylate	Glu176, Arg230, His449, Arg490 and Asp238	Arg222, Phe234, Gln231, Gln236, Glu483 and Arg538
24a	Gln236, Gly486 and His449	Arg222, Phe234, Glu483 and Arg538
24b	Ser198, Gln200, Gln236, His449 and Arg490	Arg222, Phe234, Glu483 and Arg538
24c	Ser198 and His449	Arg222, Phe234, Glu483 and Arg538
24d	Ser198, Gln200, Gln236, His449 and Arg490	Phe234 and Asp476
24e	His449 and Glu224	Arg222, Phe234 and Gly486
24f	Ser198, Gln200, Gln236, Asp239, His449 and Arg490	Arg222, Phe234, Glu483 and Arg538

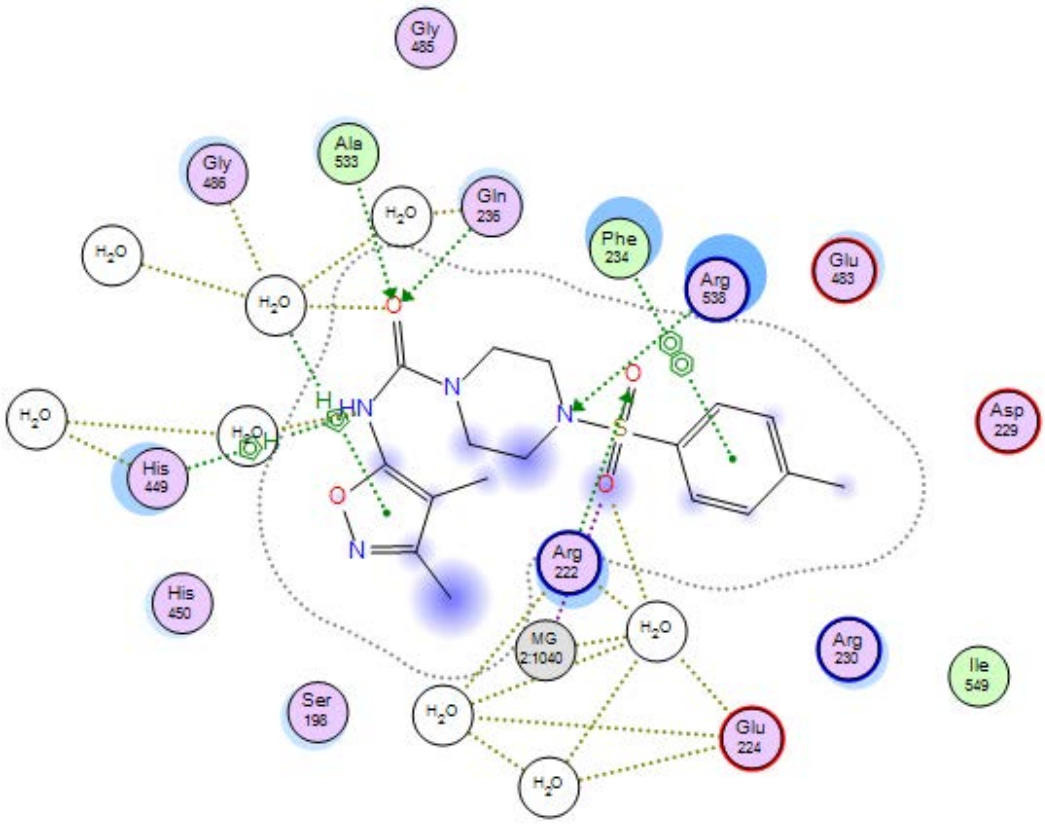

Figure 163: 2D binding interactions of compound **24a** with *E. faecalis* AspRS.

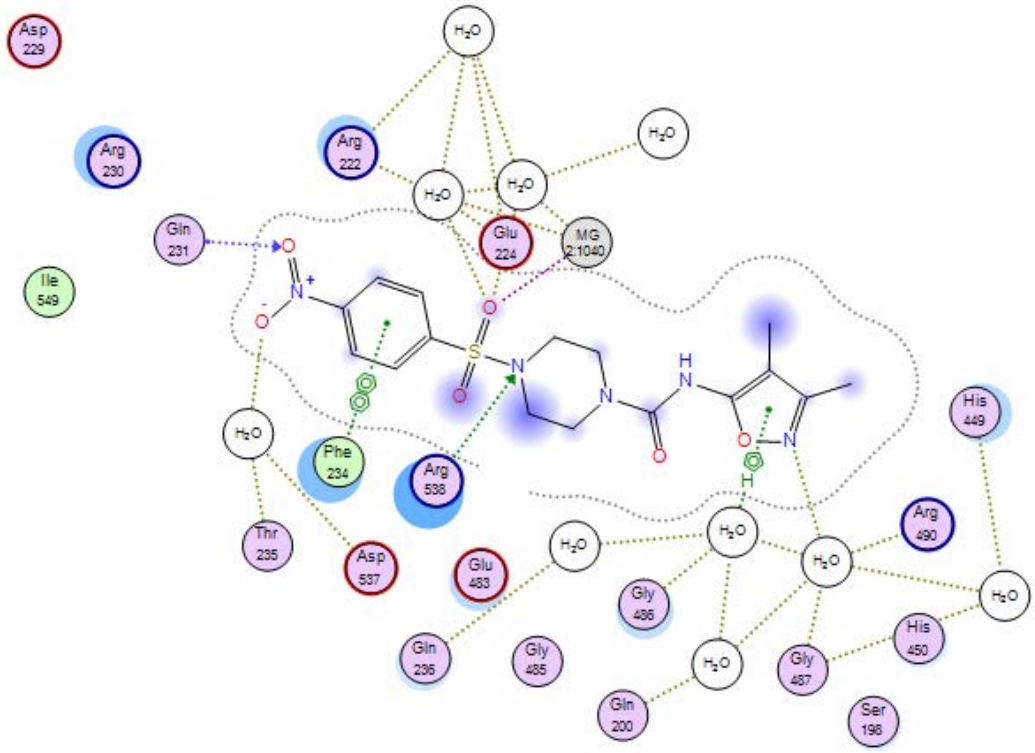

Figure 164: 2D binding interactions of compound **24b** with *E. faecalis* AspRS.

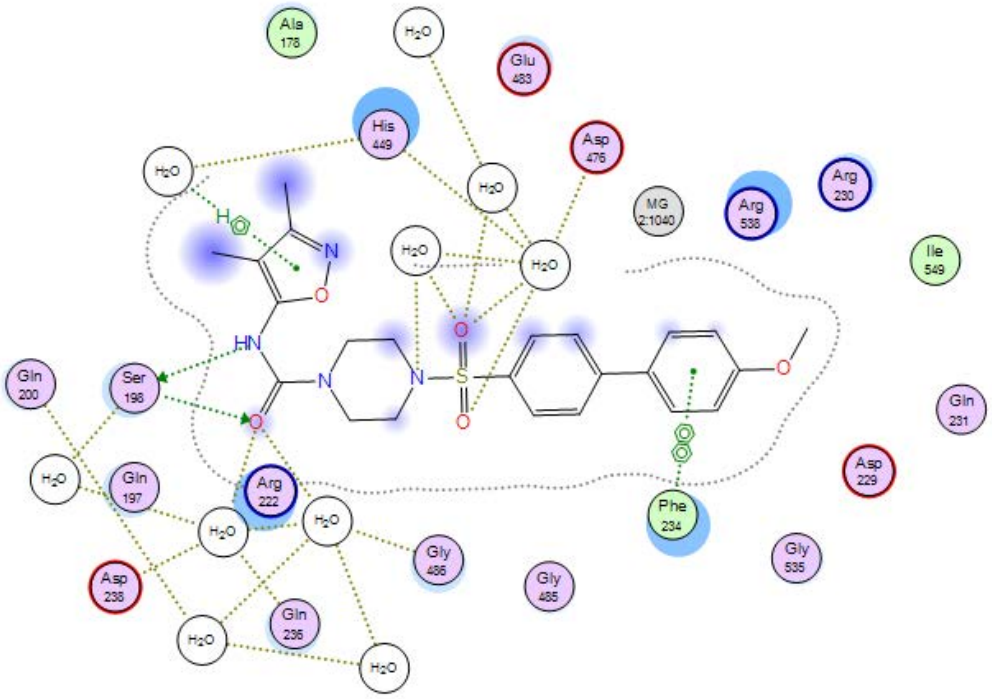

Figure 165: 2D binding interactions of compound **24d** with *E. faecalis* AspRS.

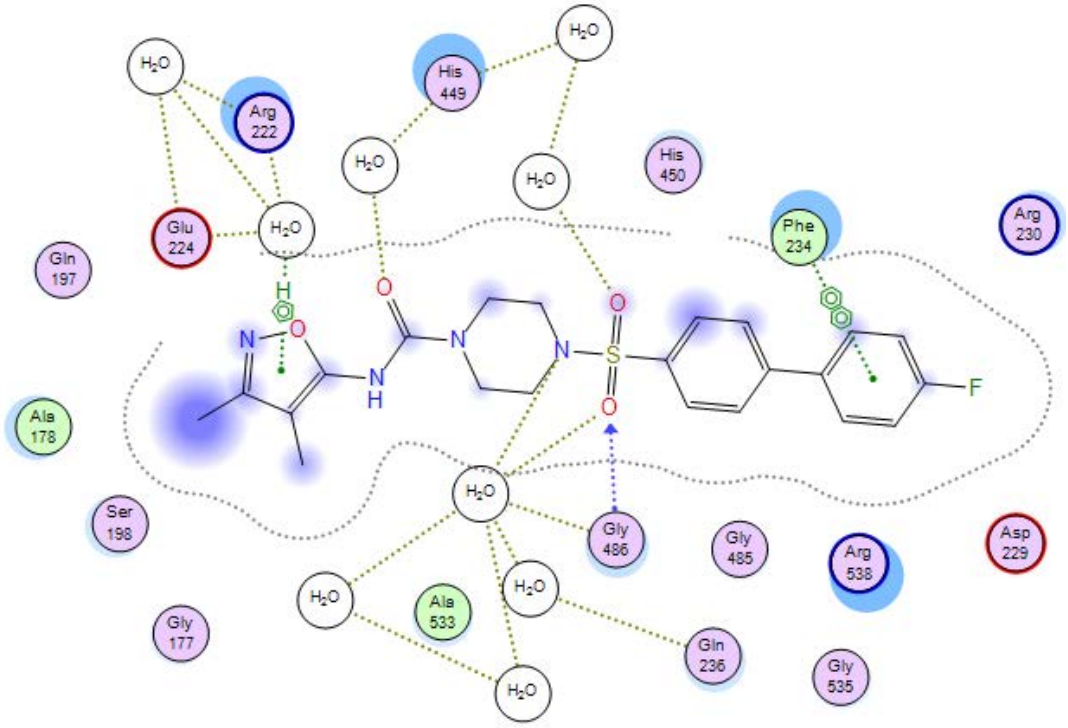

Figure 166: 2D binding interactions of compound **24e** with *E. faecalis* AspRS.

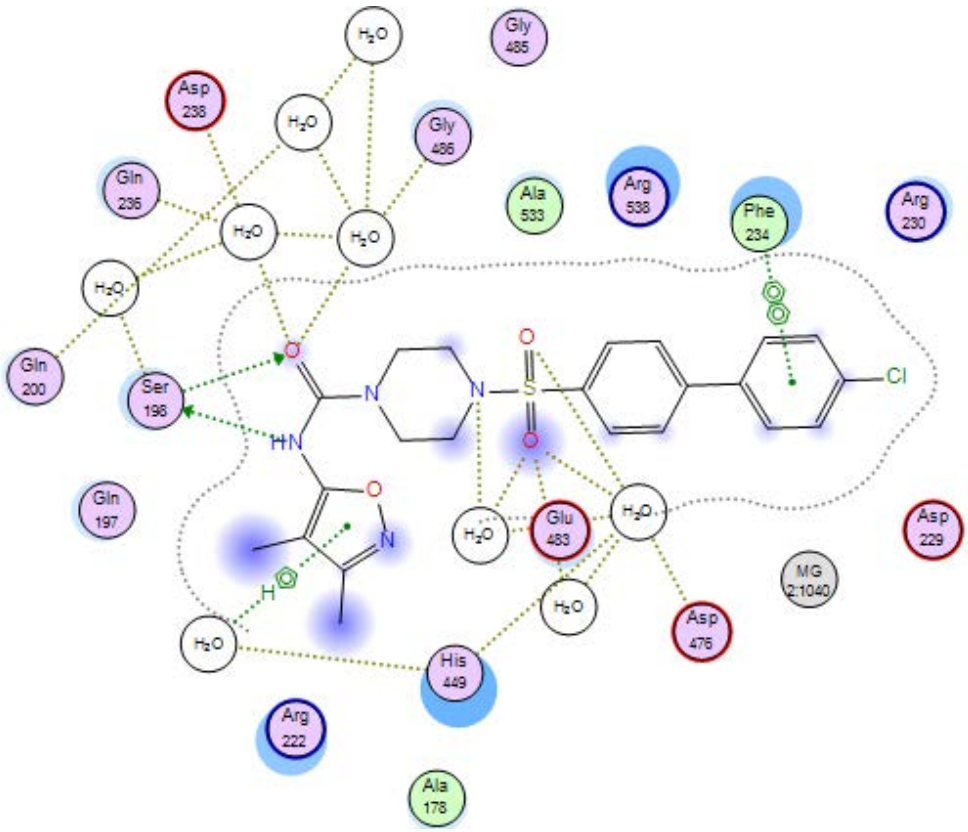

Figure 167: 2D binding interactions of compound **24f** with *E. faecalis* AspRS.

5.2.4. Docking studies of *E. faecalis* AsnRS.

The amino acid residues responsible for binding interactions with series 3 compounds were identified through alignment with asparaginyl adenylate inside the active sites of *E. faecalis* AsnRS (Figure 168) (Table 45). In general, the docking studies of this series showed that compounds **24a**-**f** flipped in most of the poses. Glu373, a key amino acid residue that participates in the formation of a water mediated hydrogen bond in the AMP pocket, was observed in the docking study of compounds **24a**-**f** (Figures 169-171). Phe234 formed a π-π stacking interaction with the benzene ring of compounds **24a** and **24c** (Figures 169 and 171). Regarding the asparagine pocket, Arg380, the key amino acid residue responsible for Asn recognition in *E. faecalis* AsnRS, formed the same hydrogen bond with the 3, 4-dimethyl isoxazole moiety in compounds **24a**-**f**, while Glu238 did not show any type of interactions with series 3 compounds (Figures 169-171). The role of Mg^{2+} ion in stabilisation of the sulfamoyl linkage was clear in the docking studies of these compounds. The binding interactions of compounds **24a**-**f** with *E. faecalis* AsnRS were not as good as those observed with the natural substrate.

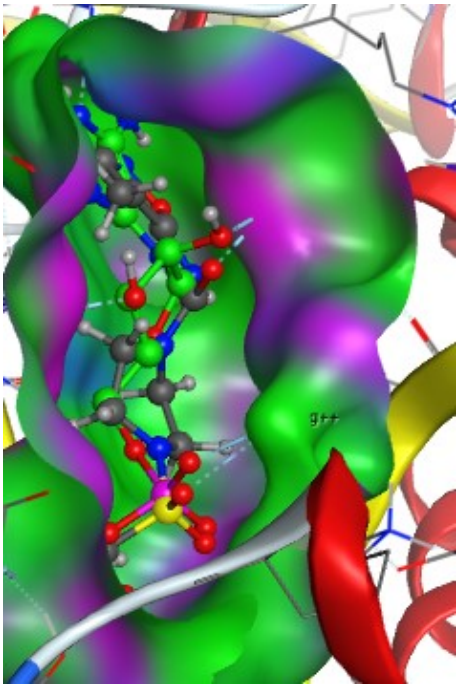

Figure 168: Alignment of compound **24b** (grey) with asparaginyl adenylate (green) in the active sites of *E. faecalis* AsnRS.

Table 45: Binding interactions of series 3 compounds with the amino acid residues of the binding sites of *E. faecalis* AsnRS.

Ligands	Asparagine pocket	AMP pocket
Asparaginyl-adenylate	Glu238 and Arg380	Arg221, Glu223, Arg229, His230, Phe234, Glu373, Gly376, Gly421 and Arg424
24a	Gln200 and Arg380	Arg221, Phe234, Glu373 and Arg424
24b	-	Arg229, Glu373 and Arg424
24c	Gln200 and Arg380	Glu173, Arg221, Phe234 and Glu373
24d	Gln200 and Arg380	Glu173, Arg221 and Glu373
24e	Gln200 and Arg380	Glu373 and Arg424
24f	Gln200 and Arg380	Glu373 and Arg424

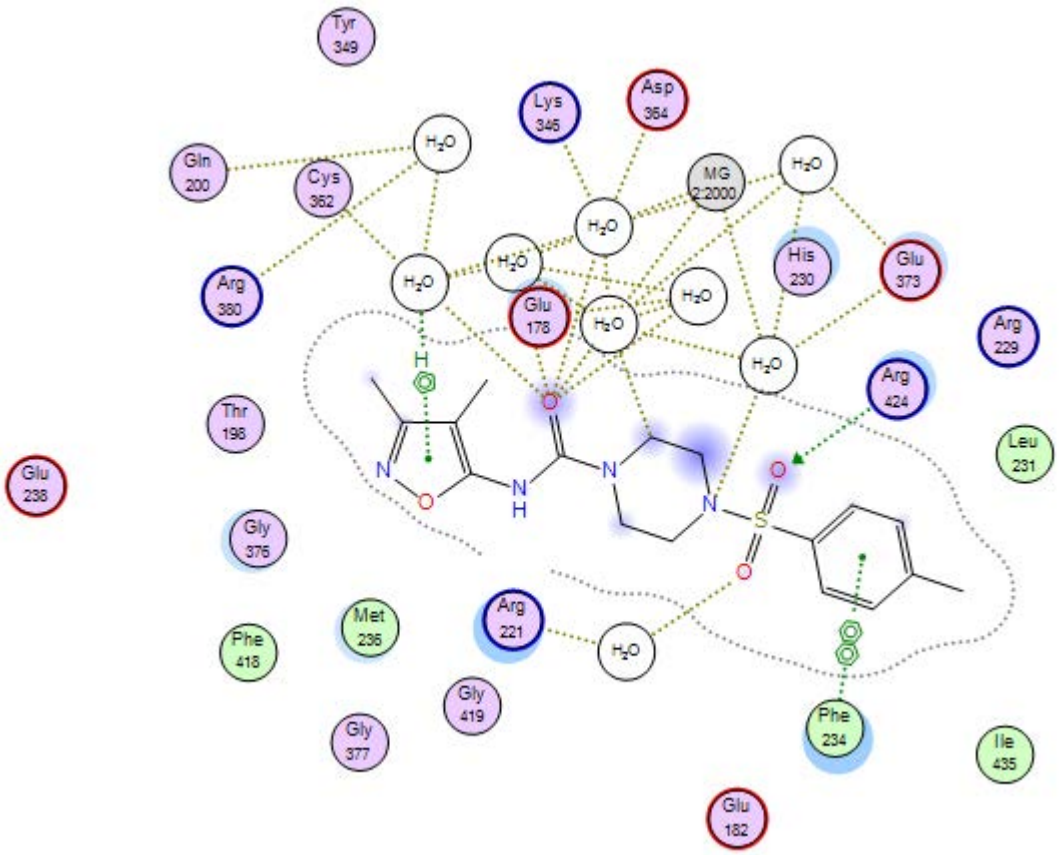

Figure 169: 2D binding interactions of compound **24a** with *E. faecalis* AsnRS.

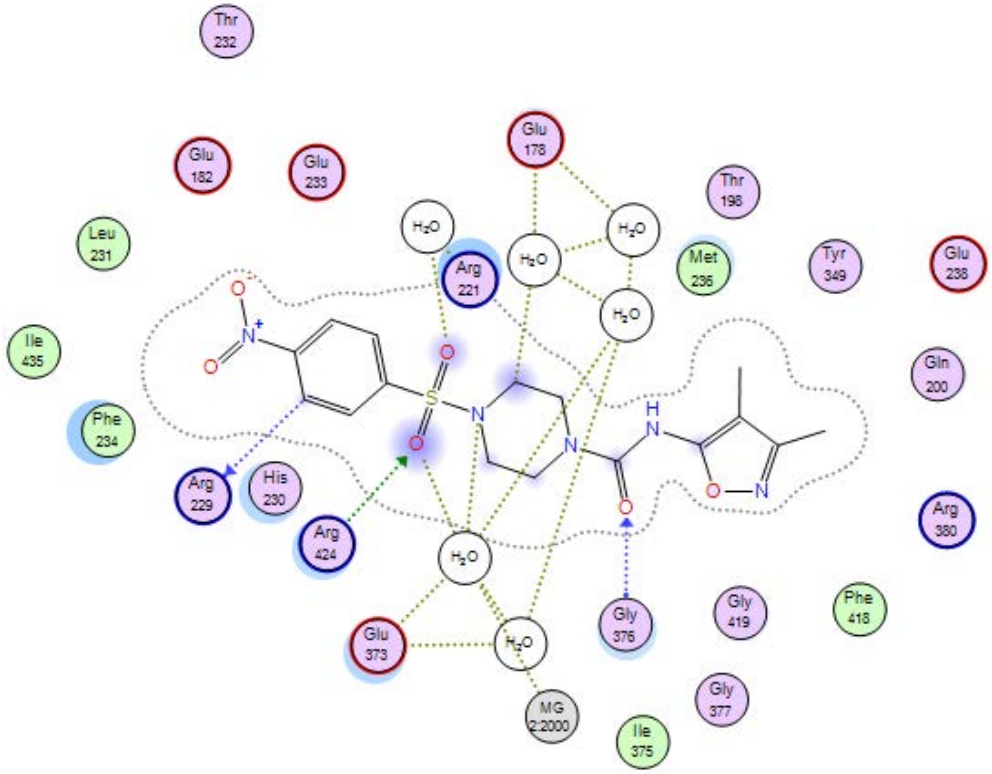

Figure 170: 2D binding interactions of compound **24b** with *E. faecalis* AsnRS.

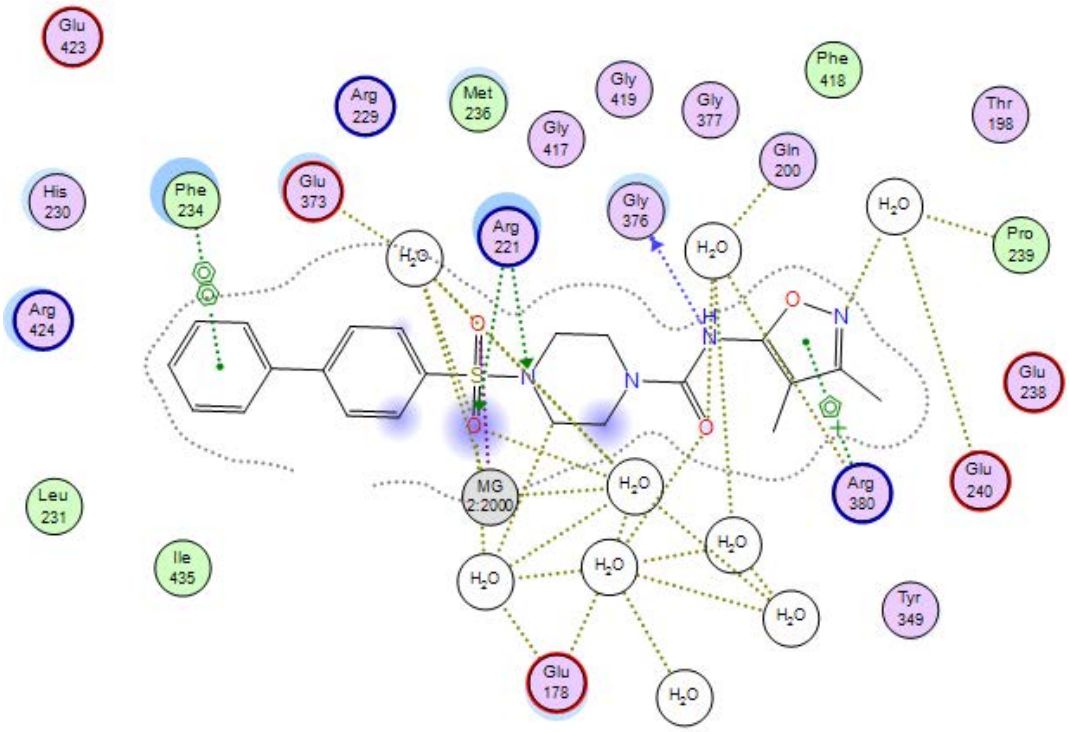

Figure 171: 2D binding interactions of compound **24c** with *E. faecalis* AsnRS.

5.3. Biological assays

5.3.1. Microbiological screening

Microbiological screening of series 3 compounds was performed at the Antimicrobial Chemotherapy Unit in University Hospital of Wales (UHW) by Jennifer Richard and Mandy Wootton. Series 3 compounds **24a**-**f** were evaluated for antimicrobial activity against a number of pathogens (sensitive and resistant strains) with ciprofloxacin as the standard for comparison. Isolates were tested by using clinical and NCTC/ATCC control organisms; *Pseudomonas aeruginosa* (including ATCC 27853 and 26739 sensitive strains), *Staphylococcus aureus* (including (ATCC 29213) sensitive strain and flucloxacillin (NCTC12493)), *Enterococcus faecalis* (including (ATCC 29212) sensitive strain), and *Enterococcus faecium* (16568). MIC was measured for each compound using 2-fold doubling serial dilutions (log_2). From the MIC results of compounds **24a**-**f** (Table 46), compound **24b** showed moderate antimicrobial activity (32 µg/mL) against the sensitive and resistant strains of *Staphylococcus aureus* compared with ciprofloxacin (0.25 and 0.5 µg/mL) respectively. However, its antimicrobial activity against the sensitive strain of *Enterococcus faecium* (32 µg/mL) was high compared with the inhibitory activity of ciprofloxacin against the same microorganism (>128 µg/mL). In comparison of the standard activity against the sensitive strain of *Enterococcus faecium,* compounds **24d-f** showed good antimicrobial activity (64 µg/mL) and compound **24f** showed the same inhibitory activity against the resistant strain of *S. aureus*. None of the compounds showed good inhibitory activity (≥ 128 µg/mL) against the sensitive strain of *Enterococcus faecalis* (ATCC 29212) compared with ciprofloxacin (0.125 µg/mL). The lack of inhibitory activity of compounds **24a**-**f** against *S. aureus* and *E. faecalis* AspRS and AsnRS enzymes may be due to the presence of the amide linkage next to the sulfamoyl linkage leading to impairment of the stability of these compounds inside the pockets of the target enzymes. The docking study of series 3 compounds with the target enzymes showed that amide linkage formed good binding interactions with several key amino acid residues including those bound with Mg^{2+} ion causing a shift in the interactions from the sulfamoyl to the amide linkage. This resulted in Mg^{2+} stabilisation preferentially with the amino acid isosteric moiety. Despite the close proximity of the histidine and flipping loops to the amino

acid isosteric moiety in the docking studies of compounds **24a**-**f** with *S. aureus* and *E. faecalis* AspRS enzymes, the binding interactions were not satisfied and the Mg^{2+} ion was not able to stabilise the sulfamoyl linkage of compounds **24d**-**f** in the docking studies of *E. faecalis* AspRS. By contrast, compounds **24a**-**f** did not show good binding interactions with the key amino acid residues responsible for Asn recognition in the AsnRS enzymes of both microorganisms.

Table 46: Microbiological data of compounds **24a**-**f**.

Microorganisms	MIC: (µg/mL)						
	Ciprofloxacin	**24a**	**24b**	**24c**	**24d**	**24e**	**24f**
Pseudomonas aeruginosa ATCC 27853	0.25	128	128	128	128	128	128
26739	0.06	128	128	128	128	128	128
Staphylococcus aureus ATCC 29213	0.25	>128	32	>128	>128	>128	>128
Enterococcus faecalis ATCC 29212	0.125	128	>128	128	128	128	128
Enterococcus faecium 16568	>128	128	32	128	64	64	64
Staphylococcus aureus NCTC 12493	0.5	128	32	128	128	128	64

5.3.2. Aminoacylation assay

The antimicrobial assay was performed at the Department of Chemistry, University of Texas by Casey Hughes and James Bullard. The half maximal inhibitory concentration (IC_{50}) assay was performed for the first four series 3 compounds to measure their activities in inhibiting 50% of the aminoacylation process. In this assay, *P. aeruginosa* AspRS was used and the control was EDTA in DMSO. All tested compounds did not show good IC_{50} results. Ideally the compounds need to be tested against *S. aureus* and *E. faecalis* that they were designed to inhibit, however, only the *P. aeruginosa* AspRS assay was available.

In conclusion, series 3 compounds consist of 3,4-dimethyl isoxazole as the amino acid isosteric moiety and the same aryl/biaryl moiety while the linker was extended by adding an amide group to the sulfamoyl linkage. The docking studies of these compounds with the target enzymes showed good binding interactions but the stabilisation of the sulfamoyl linkage by the interaction with Mg^{2+} ion was impaired by the presence of the amide group and this could reflect on the microbiological screening results. However, compound **24b** showed inhibitory activity higher than that of ciprofloxacin against *E. faecium*. Thus, any modification of the linker may improve the binding and stabilisation of the compounds inside the active sites.

5.4. Methods

5.4.1 Docking studies

All methods related to docking studies are described in the methods section in Chapter 2.

5.4.2 Biological assay

5.4.2.1. Antimicrobial screening test

Method related to antimicrobial screening test is described in the methods section in Chapter 3.

5.4.2.2. Aminoacylation assay

Method related to aminoacylation assay is described in the methods section in Chapter 3.

5.4.3 Chemistry

5.4.3.1. General procedure for the preparation of phenyl sulfonyl piperazines **3a**-**f** (327)

The general procedure for the preparation of phenyl sulfonyl piperazines (**3a**-**f**) is described in the methods section in Chapter 3.

5.4.3.2. General procedure for the preparation of 2,2,2-trichloroethyl(3,4-dimethyl isoxazol-5-yl)carbamate (**21**) (347) ($C_8H_9Cl_3N_2O_3$, Mol. Wt. 287.52)

To a stirred solution of 5-amino-3,4-dimethylisoxazole (**19**) (0.5 g, 4.46 mmol) and pyridine (0.44 mL, 5.35 mmol) in dry THF (15 mL) was added 2,2,2-trichloroethyl chloroformate (**20**) (0.74 mL, 5.35 mmol) dropwise at 0 ^{O}C. The mixture was stirred at 0 ^{O}C for 1 h, poured into water (20 mL), and extracted with EtOAc (3 x 50 mL). The organic layer was washed with water (20 mL), dried over anhydrous $MgSO_4$, and concentrated in vacuo. The residue was purified by gradient column chromatography and the product was collected at 60:40 v/v petroleum ether – EtOAc as a colourless solid, yield: 0.78 g (60%) mp = 78 – 80 ^{O}C. TLC: petroleum ether – EtOAc 1:1 v/v, (R_f = 0.8). ^{1}H NMR ($CDCl_3$) δ 1.85 (s, 3H, CH_3), 2.15 (s, 3H, CH_3), 4.75 (s, 2H, CH_2), 7.33 (br s, 1H, NH).

5.4.3.3. General procedure for the preparation of *N*-(3,4-dimethylisoxazol-5-yl)-4-(phenyl)sulfonyl)piperazine-1-carboxamide derivatives (**24a**-**f**) (347)

A mixture of phenyl sulfonyl piperazines (**3a**-**f**) (0.66 mmol), 2,2,2-trichloroethyl(3,4-dimethylisoxazol-5-yl)carbamate (**21**) (0.19 g, 0.66 mmol), *N*-ethyldiisopropylamine (0.17 mL, 0.99 mmol), and DMF (5 mL) was stirred at 70 ^{O}C overnight, poured into water (5 mL), and extracted with EtOAc (3 x 50 mL). The organic layer was washed with H_2O (50 mL), dried over anhydrous $MgSO_4$ and concentrated in *vacuo*. The residue was purified by gradient column chromatography.

5.4.3.3.1. *N*-(3,4-dimethylisoxazol-5-yl)-4-tosylpiperazine-1-carboxamide (**24a**) ($C_{17}H_{22}N_4O_4S$, Mol. Wt. 378.45)

Product obtained after purification by gradient column chromatography and collected at 4:96 v/v CH_3OH - CH_2Cl_2 to give a pale yellow semisolid, yield: 0.33 g (66%). TLC: CH_3OH - CH_2Cl_2 1:9 v/v, (R_F = 0.4). ^1H NMR ($CDCl_3$) δ 1.72 (s, 3H, CH_3), 2.09 (s, 3H, CH_3), 2.43 (s, 3H, CH_3), 2.97 (br s, 4H, CH_2, pip), 3.54 (br s, 4H, CH_2, pip), 7.33 (d, J = 8.2 Hz, 2H, CH, Ar), 7.59 (d, J = 8.2 Hz, 2H, CH, Ar), 7.93 (s, 1H, NH). ^{13}C NMR ($CDCl_3$) δ 6.9, 10.7, 21.6 (3 x CH_3), 43.2, 43.6, 45.4, 45.7 (4 x CH_2, pip), 127.6, 127.7, 129.9, 130.2 (4 x CH, Ar), 102.9, 157.8, 161.8 (3 x isoxazole C) 132.4, 144.3 (2 x C, Ar), 153.1 (C=O). HPLC: 100% at RT: 4.10 min. HRMS (ES-TOF) m/z calculated mass: 379.1362 $[M + H]^+$, observed mass: 379.1401 $[M + H]^+$.

5.4.3.3.2. *N*-(3,4-dimethylisoxazol-5-yl)-4-((4-nitrophenyl)sulfonyl)piperazine-1-carboxamide (**24b**) ($C_{16}H_{19}N_5O_6S$, Mol. Wt. 409.42)

Product obtained after purification by gradient column chromatography and collected at 10:90 v/v petroleum ether - EtOAc and recrystallisation from EOH to give a white solid, yield: 0.26 g (52%), mp = 196 – 198 ^OC. TLC: petroleum ether - EtOAc 1:1 v/v, (R_F = 0.3). ^1H NMR ($CDCl_3$) δ 2.06 (s, 3H, CH_3), 1.69 (s, 3H, CH_3), 3.04 (br s, 4H, CH_2, pip), 3.52 (br s, 4H, CH_2, pip), 7.10 (s, 1H, NH), 7.89 (d, J = 8.95 Hz, 2H, CH, Ar), 8.32 (d, J = 8.95 Hz, 2H, CH, Ar). ^{13}C NMR ($CDCl_3$) δ 6.9, 10.7 (2 x CH_3), 43.8, 45.6 (4 x CH_2, pip), 124.6, 128.9 (4 x CH, Ar), 102.9, 157.1, 162.1 (3 x isoxazole C), 141.5 (C-S), 150.5 (C-NO_2), 152.6 (C=O). HPLC: 99.3% at RT: 3.98 min. HRMS (ES-TOF) m/z calculated mass: 410.1056 $[M + H]^+$, observed mass: 410.1130 $[M + H]^+$.

5.4.3.3.3. *N*-(3,4-dimethylisoxazol-5-yl)-4-([1,1'-biphenyl]-4-ylsulfonyl)piperazine-1-carboxamide (**24c**) ($C_{22}H_{24}N_4O_4S$, Mol. Wt. 440.52)

Product obtained after purification by gradient column chromatography and collected at 4:96 v/v CH_3OH - CH_2Cl_2 and recrystallisation from EOH to give a white shiny solid, yield: 0.29 g (41%), mp = 176 – 178 ^OC. TLC: CH_3OH - CH_2Cl_2 1:9 v/v, (R_F = 0.7). ^1H NMR ($CDCl_3$) δ 1.73 (s, 3H, CH_3), 2.08 (s, 3H, CH_3), 3.06 (t, J = 5, 5.1 Hz, 4H, CH_2, pip), 3.53 (t, J = 4.9, 5.2 Hz, 4H, CH_2, pip), 6.47 (s, 1H, NH), 7.37 (d, J = 7.55 Hz, 2H, CH, Ar), 7.43 (t, J = 8, 8 Hz, 1H, CH, Ar), 7.54 (d, J = 7.55 Hz, 2H, CH, Ar), 7.69 (d, J = 8.45 Hz, 2H, CH, Ar), 7.75 (d, J = 7.55 Hz, 2H, CH, Ar). ^{13}C NMR ($CDCl_3$) δ 7.1, 10.7 (2 x CH_3), 43.9, 45.7 (4 x CH_2), 127.4, 127.9, 128.3, 128.7, 129.1 (9 x CH, Ar), 102.9, 156.8, 162.1 (isoxazole C),

133.8, 139.1, 146.3 (3 x C, Ar), 152.3 (C=O). HPLC: 99.1% at RT: 4.37 min. HRMS (ES-TOF) m/z calculated mass: 463.1518 $[M + Na]^+$, observed mass: 463.1411 $[M + Na]^+$.

5.4.3.3.4. *N*-(3,4-dimethylisoxazol-5-yl)-4-((4'-methoxy-[1,1'-biphenyl]-4-yl)sulfonyl)piperazine-1-carboxamide (**24d**) ($C_{23}H_{26}N_4O_5S$, Mol. Wt. 470.54)

Product obtained after purification by gradient column chromatography and collected at 10:90 v/v petroleum ether - EtOAc to give a white semisolid, yield: 0.24 g (60%). TLC: petroleum ether - EtOAc 1:1 v/v, (R_F = 0.2). ^{1}H NMR ($CDCl_3$) δ 1.70 (s, 3H, CH_3), 2.06 (s, 3H, CH_3), 3.79 (s, 3H, OCH_3), 3.51 (br s, 4H, CH_2, pip), 3.01 (br s, 4H, CH_2, pip), 6.94 (d, J = 8.4 Hz, 2H, CH, Ar), 7.07 (s, 1H, NH), 7.48 (d, J = 8.4 Hz, 2H, CH, Ar), 7.62 (d, J = 8.25 Hz, 2H, CH, Ar), 7.69 (d, J = 8.25 Hz, 2H, CH, Ar). ^{13}C NMR ($CDCl_3$) δ 7.0, 10.7 (2 x CH_3), 43.8, 45.7 (4 x CH_2, pip), 55.4 (OCH_3), 114.6, 127.3, 128.3, 128.5 (8 x CH), 102.9, 160.3, 162.0 (3 x isoxazole C), 131.3, 132.9, 152.7, 157.3 (4 x C, Ar), 152.7 (C=O). HPLC: 100% at RT: 4.35 min. HRMS (ES-TOF) m/z calculated mass: 493.1624 $[M + Na]^+$, observed mass: 493.1517 $[M + Na]^+$.

5.4.3.3.5. *N*-(3,4-dimethylisoxazol-5-yl)-4-((4'-fluoro-[1,1'-biphenyl]-4-yl)sulfonyl) piperazine-1-carboxamide (**24e**) ($C_{22}H_{23}FN_4O_4S$, Mol. Wt. 458.51)

Product obtained after purification by recrystallisation from EOH to give white crystals, yield: 0.1 g (26%), mp = 194 – 196 ^{O}C. TLC: CH_3OH - CH_2Cl_2 1:9 v/v, (R_F = 0.3). ^{1}H NMR (CD_3OD): 1.88 (s, 3H, CH_3), 2.20 (s, 3H, CH_3), 3.12 (br s, 4H, CH_2, pip), 3.61 (bs, 4H, CH_2, pip), 6.77 (s, 1H, NH), 7.21 (t, J = 8.7 Hz, 2H, CH, Ar), 7.60 (t, J = 6.9 Hz, 2H, CH, Ar), 7.73 (d, J = 7.2 Hz, 2H, CH, Ar), 7.82 (d, J = 7.9 Hz, 2H, CH, Ar). ^{13}C NMR (CD_3OD) : 5.3, 9.1 (2 x CH_3), 43.6, 45.7 (4 x CH_2, pip), 127.4, 128.2, 128.9, 129.0 (8 x CH), 103.2, 158.4, 161.6 (3 x isoxazole C), 134.0, 135.4, 144.9 (3 x C, Ar), 154.2 (C=O) 162.3 (C-F). HPLC: 100% at RT: 4.40 min. HRMS (ES-TOF) m/z calculated mass: 481.1424 $[M + Na]^+$, observed mass: 481.1346 $[M + Na]^+$.

5.4.3.3.6. *N*-(3,4-dimethylisoxazol-5-yl)-4-((4'-chloro-[1,1'-biphenyl]-4-yl)sulfonyl) piperazine-1-carboxamide (**24f**) ($C_{22}H_{23}ClN_4O_4S$, Mol. Wt. 474.96)

Product obtained after purification by gradient column chromatography and collected at 10:90 v/v petroleum ether - EtOAc and recrystallisation from EOH to give a white solid, yield: 0.2 g (51%), mp = 206 – 208 ^{O}C. TLC: petroleum ether - EtOAc 1:1 v/v, (R_F

= 0.3). ^{1}H NMR ($CDCl_3$) δ 1.72 (s, 3H, CH_3), 2.07 (s, 3H, CH_3), 3.53 (t, J = 5.35, 5.35 Hz, 4H, CH_2, pip), 3.04 (t, J= 5.35, 5.35 Hz, 4H, CH_2, pip), 6.70 (s, 1H, NH), 7.74 (d, J = 8.45 Hz, 2H, CH, Ar), 7.64 (d, J = 9.2 Hz, 2H, CH, Ar), 7.47 (d, J = 9.2 Hz, 2H, CH, Ar), 7.39 (d, J = 8.45 Hz, 2H, CH, Ar). ^{13}C NMR ($CDCl_3$) δ 7.0, 10.7 (2 x CH_3), 43.8, 45.7 (4 X CH_2, pip), 127.8, 128.4, 128.6, 129.4 (8 x CH), 102.9, 156.9, 162.1 (3 x isoxazole C), 134.1, 135.0, 137.5, 145.0 (4 x C, Ar), 152.45 (C=O). HPLC: 100% at RT: 4.50 min. HRMS (ES-TOF) m/z calculated mass: 497.1129 $[M + Na]^+$, observed mass: 497.1021 $[M + Na]^+$.

Chapter 6: 1-(3,4-dimethylisoxazol-5-yl)-3-(2-(4-(phenyl)sulfonyl)piperazin-1-yl)-2-oxoethyl) urea derivatives (Series 4)

6. Introduction

In this chapter, 1-(3,4-dimethylisoxazol-5-yl)-3-(2-(4-(phenyl)sulfonyl)piperazin-1-yl)-2-oxoethyl) urea derivatives (**30**) were prepared retaining the same substituted aryl/biaryl moieties as the adenine mimic and the same amino acid isosteric moiety in chapter 5 while the linker in this series consisted of an oxoethyl urea linked to the piperazine of the sulfamoyl linkage (Table 47). The rational for the design of this series is to extend the linker to improve the fitting of designed compounds inside the active sites of the target enzymes.

Table 47: General chemical structures of scheme 4 AspRS and AsnRS inhibitors (**30**).

Series	General chemical structures	R groups
4	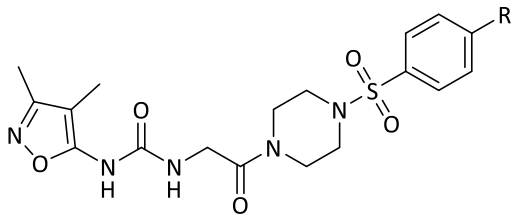	CH_3, NO_2, C_6H_5, $C_6H_4OCH_3$, C_6H_4F, C_6H_4Cl

This chapter is divided into four parts as follows:

- Results and discussion
- Docking studies
- Biological screening
- Methods

6.1. Synthetic pathway for 1-(3,4-dimethylisoxazol-5-yl)-3-(2-(4-(phenyl) sulfonyl)piperazin-1-yl)-2-oxoethyl)urea derivatives (30)

Series 4 compounds consists of an oxoethyl urea sulfamoyl piperazine linked to the same aryl/biaryl moieties and 3,4-dimethylisoxazole instead of Asp and Asn amino acids and the synthetic pathways are shown in scheme 10 and involved the following steps:

- Coupling reaction of sulfonyl piperazine derivatives with Boc-glycine (**28a**-**f**)
- Deprotection reaction for Boc group removal (**29a**-**f**)

- Nucleophilic substitution reaction of 2-amino-1-(4-(phenyl)sulfonyl)piperazin-1-yl)ethan-1-one derivatives with 2,2,2-trichloroethyl(3,4-dimethylisoxazol-5-yl)carbamate for urea derivatives formation (**30a-f**)

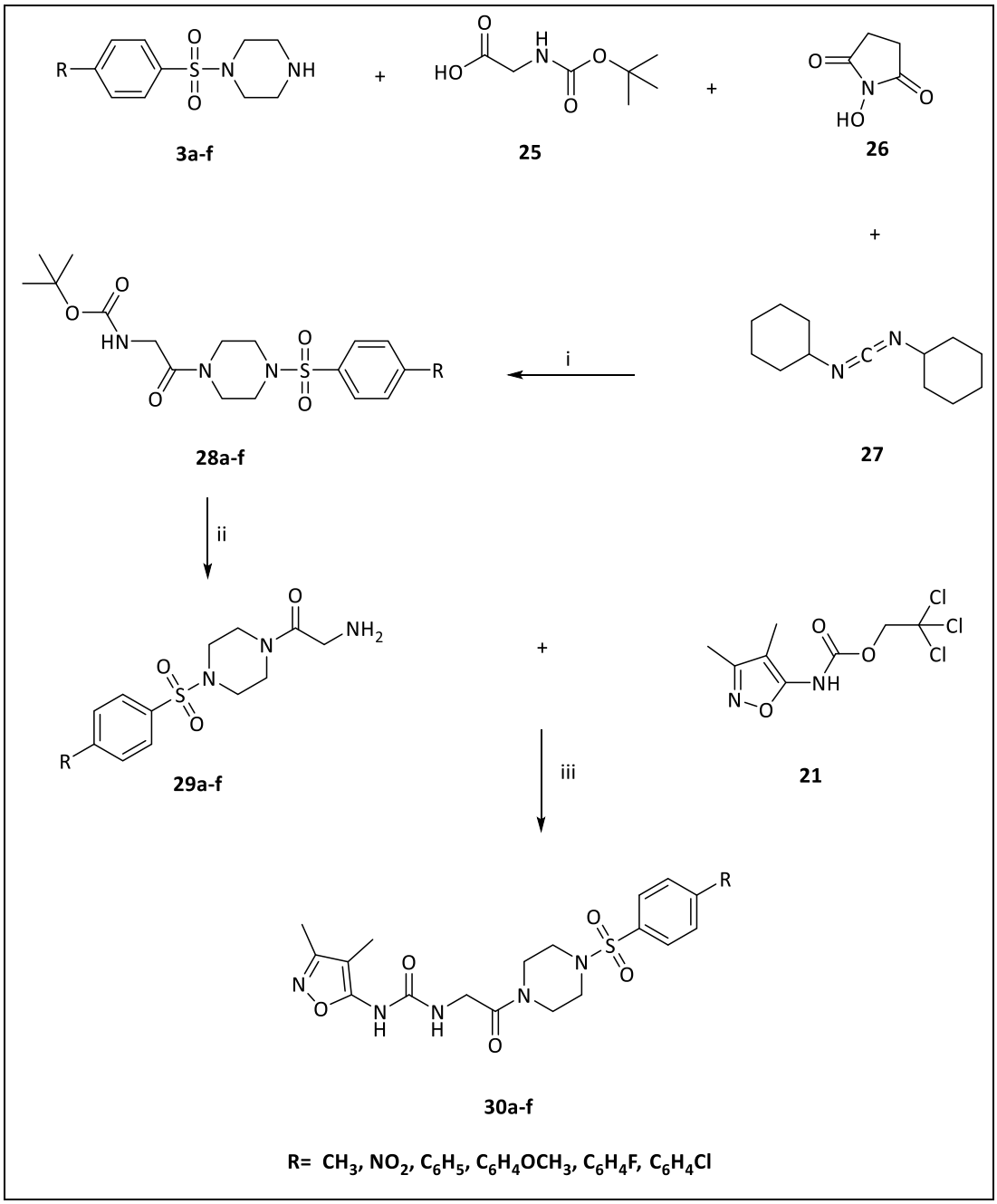

Scheme 10: Synthetic pathway for 1-(3,4-dimethylisoxazol-5-yl)-3-(2-(4-(phenyl)sulfonyl)piperazin-1-yl)-2-oxoethyl)urea derivatives. *Reagent and conditions*: (i) *N*-hydroxysuccinimide (**26**), *N*, *N'*-dicyclohexylcarbodiimide (**27**), dry CH_2Cl_2, 0 ^{O}C then rt, o/n. (ii) TFA/CH_2Cl_2, o/n or 4N HCl/dioxane, 0 ^{O}C then rt, o/n (iii) *N*-ethyldiisopropylamine, DMF, 70 ^{O}C, o/n.

6.1.1. Synthesis of tert-butyl (2-(4-(phenyl)sulfonyl)piperazin-1-yl)-2-oxoethyl) carbamate derivatives (28a-f)

N, *N*'-Dicyclohexyl carbodiimide (DCC) (**27**) as a coupling reagent was used for amide linkage formation between sulfonyl piperazine derivatives (**3a**-**f**) and N-Boc glycine (**25**) in the presence of *N*-hydroxy succinimide (NHS) (**26**) as an activating agent for the carboxylic acid group (349) (Scheme 10) (160). Compounds **28a**-**f** were successfully prepared in good yields (Table 48). The mechanism of reaction was started by the reaction of DCC with Boc glycine to form an *O*-acylisourea intermediate, which has the same reactivity as the corresponding carboxylic acid anhydride. Consequently, the hydroxyl group of NHS makes a nucleophilic attack on the electrophilic centre of the *O*-acylisourea intermediate forming 1,3-dicyclohexylurea (DHU) and succinimidyl ester, which can then be attacked by the lone pair of electrons of the nitrogen atom of the sulfonyl piperazine derivatives, resulting in the amide products (**28a**-**f**) and regenerating NHS (Scheme 11). *N*-acylurea is an undesired side product, which is observed when DCC is used alone owing to transposition of *O*-acylurea to *N*-acylurea resulting from a competing intramolecular reaction to give the energetically more favored compound. *N*-acylurea is stable and unreactive towards amines, thus using a nucleophile additive such as NHS suppresses the formation of the stable *N*-acylurea through protonation of the *O*-acylisourea intermediate (Scheme 12) (350-352). In addition, this type of reaction should be done under dry conditions as hydrolysis of the *O*-acylurea intermediate is more likely to happen in the presence of H_2O than formation of the amide linkage. The molar amount of DCC used in the reaction is higher than that of carboxylic acid to avoid forming an acid anhydride after *O*-acylurea formation despite its ability to form the desired amide (353), while the molar amount of NHS should not exceed that of the carboxylic group (354). Regarding by-products, NHS is water soluble, and can be removed in the aqueous layer on extraction of the product with CH_2Cl_2 and washing with H_2O. However, DHU has poor solubility in water and most organic solvents and the best way to eliminate DHU is by dissolving the desired product and filtration using celite or charcoal or by column chromatography (354, 355).

Table 48: Identification data for *tert*-butyl (2-(4-(phenyl)sulfonyl)piperazin-1-yl)-2-oxoethyl)carbamate derivatives (**28a**-**f**).

Compd	R	Yield (%)	Mp (^{O}C)	Appearance
28a	CH_3	50	-	Colourless semisolid
28b	NO_2	85	96-98	White powder
28c	C_6H_5	78	162-164	White solid
28d	$C_6H_4OCH_3$	75	188-190	White solid
28e	C_6H_4F	59	90-92	White solid
28f	C_6H_4Cl	90	198-200	White solid

^{1}H and ^{13}C NMR spectra and either elemental analysis or HRMS confirmed the structures and purity. For example, the ^{1}H NMR spectrum of compound **28b** showed aromatic *CH* signals in the aromatic region as two doublet peaks, each integrated for 2 protons (Figure 172a), while the aromatic protons of compound **28c** appeared as five peaks in the ^{1}H NMR spectrum, two of them were triplet peaks and the others were doublet peaks. The integration of the peak with lowest chemical shift was 1 proton while other peaks integrated for 2 protons (Scheme 173a). The *NH* proton coupled with CH_2 protons in compound **28b** was observed as a triplet peak and a doublet peak respectively (Figure 172a and 172b). However, the resonance of electrons between O and N atoms of the amide linkage in compound **28c** resulted in singlet signals for *NH* and CH_2 (Figure 173a and 173b). Piperazine was observed as two broad multiplet peaks integrated for 4 protons each in compound **28b** (Figure 172b) and three broad singlet peaks integrated for 4, 2 and 2 protons respectively in compound **28c** (Figure 173b), while the Boc group was observed in the ^{1}H NMR spectra of both compounds as a singlet peak for $C(CH_3)_3$ integrated for nine protons (Figures 172b and 173b).

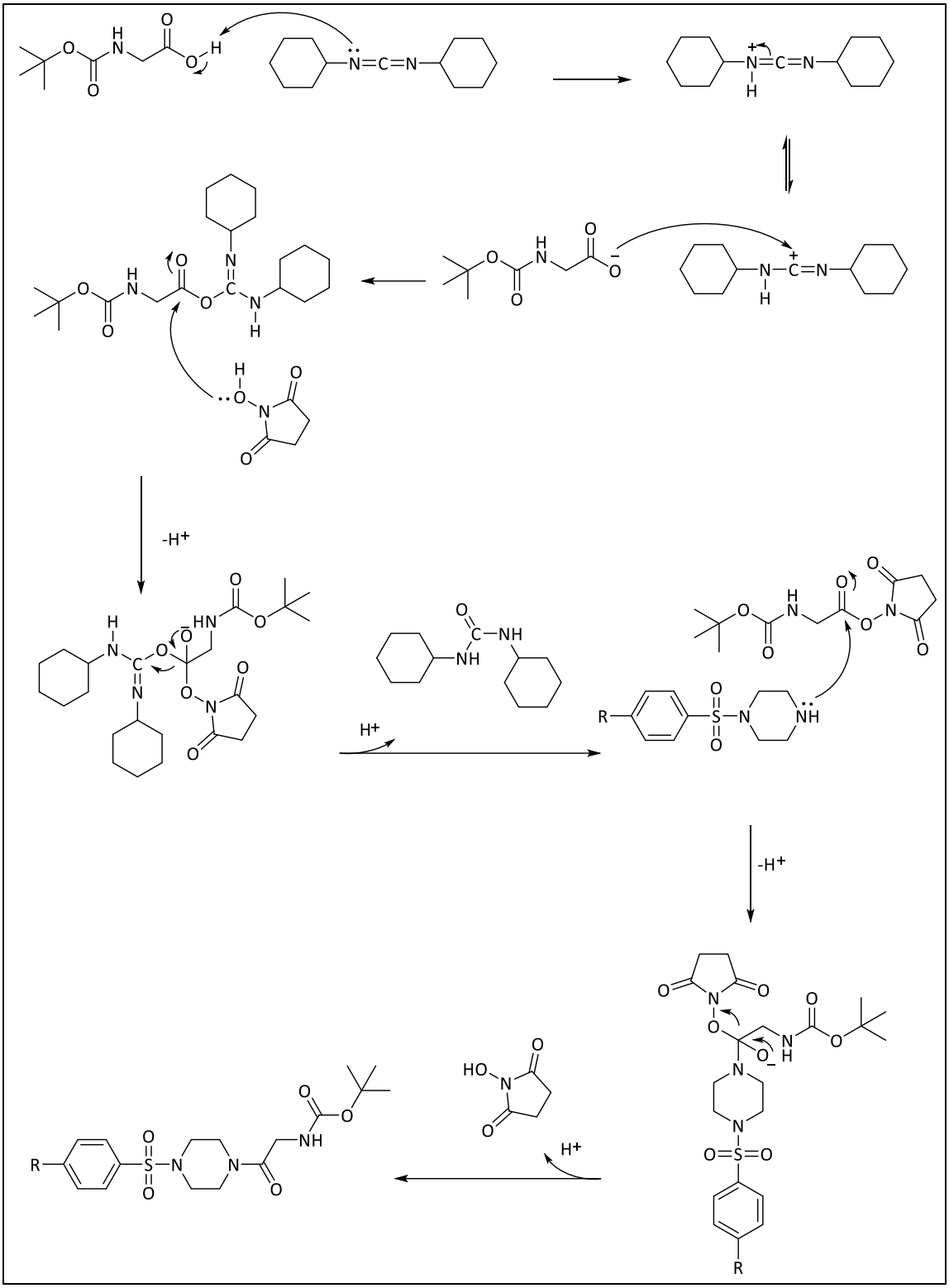

Scheme 11: Mechanism of coupling reaction using DDC.

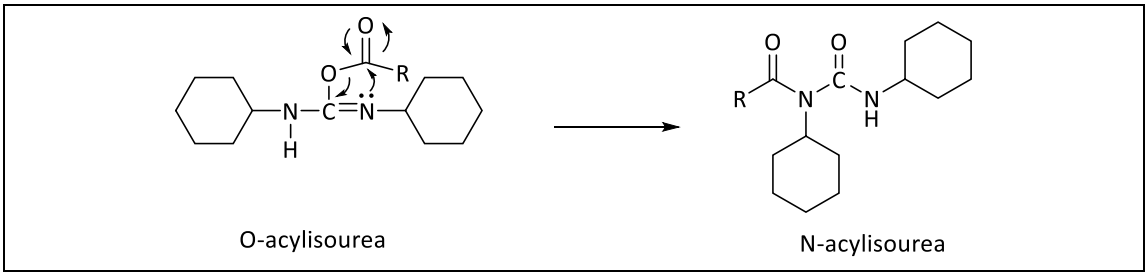

Scheme 12: Intramolecular reaction of transposition *O* to *N* acylisourea.

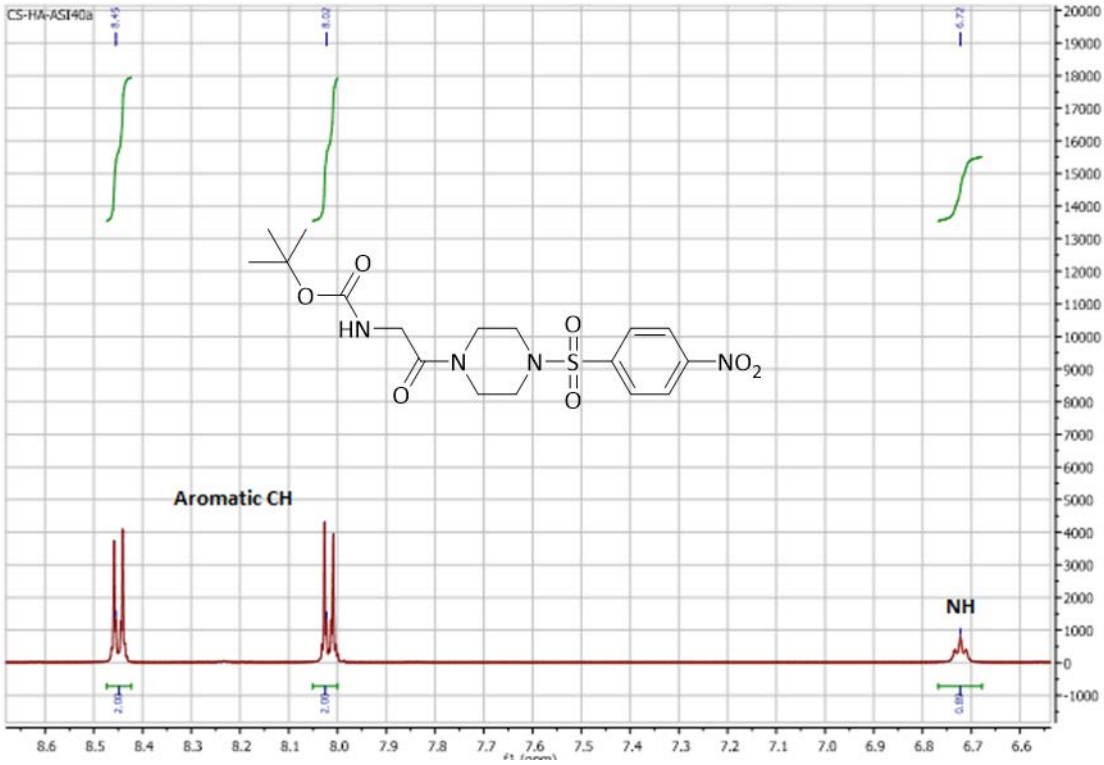

Figure 172a: ^{1}H NMR spectrum of compound **28b**. The spectrum shows aromatic CH as two peaks, each integrated for 2 protons and NH signal as a triplet peak.

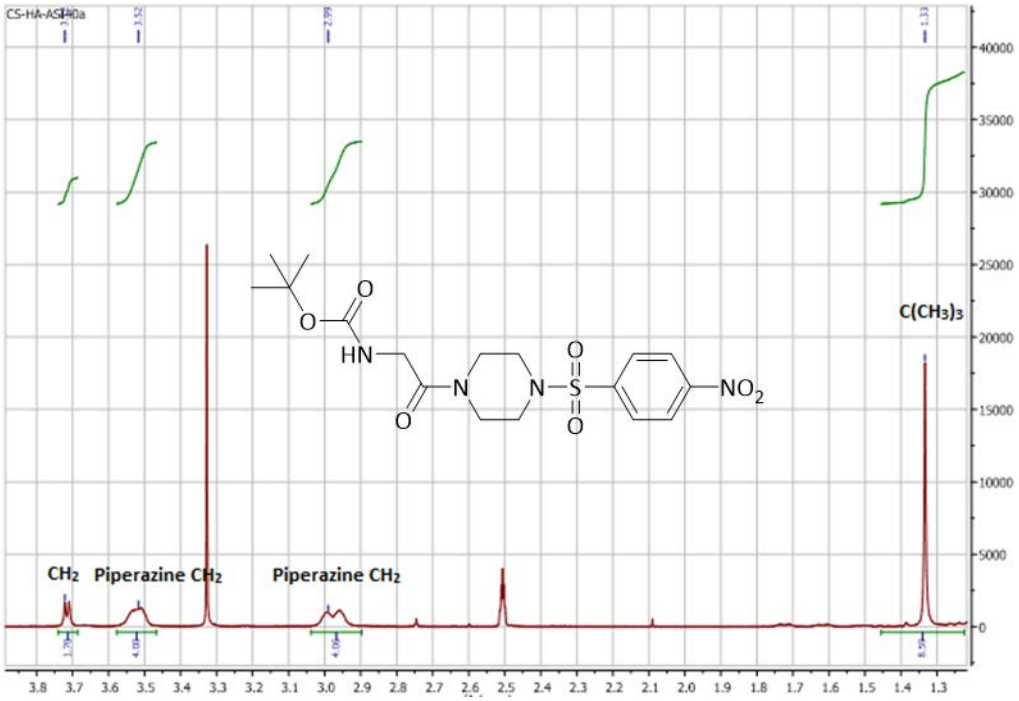

Figure 172b: ^{1}H NMR spectrum of compound **28b**. The spectrum shows $C(CH_3)_3$ as a singlet peak, piperazine CH_2 as two broad peaks, each integrated for 4 protons and CH_2 signal as a doublet peak.

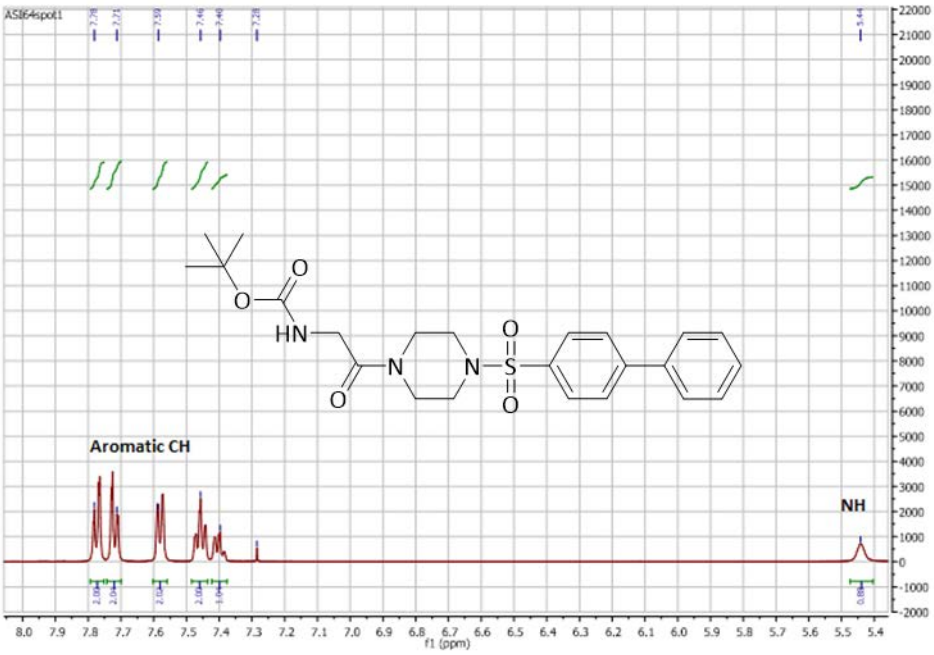

Figure 173a: ^{1}H NMR spectrum of compound **28c**. The spectrum shows aromatic CH as five peaks, four of them integrated for 2 protons and one integrated for 1 proton and NH signal as a singlet peak.

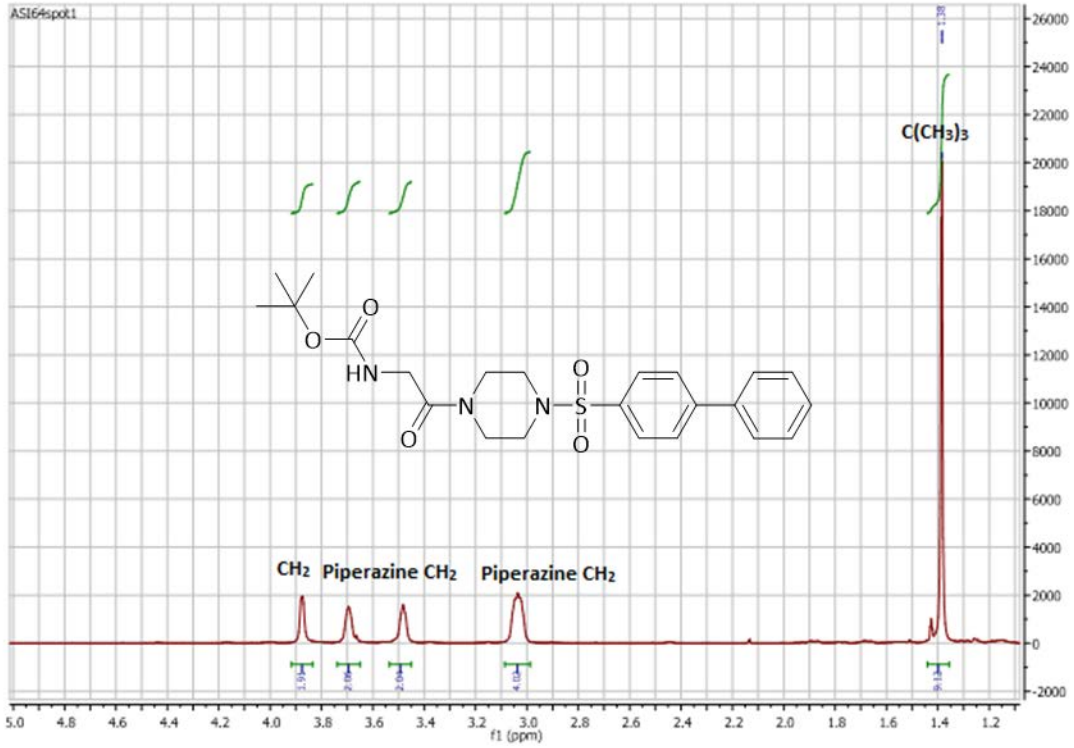

Figure 173b: ^{1}H NMR spectrum of compound **28c**. The spectrum shows $C(CH_3)_3$ as a singlet peak, piperazine CH_2 as three broad peaks, one integrated for 4 protons while others integrated for 2 protons and CH_2 signal as a singlet peak.

6.1.2. Synthesis of 2-amino-1-(4-(phenyl)sulfonyl)piperazin-1-yl)ethan-1-one (29a-f)

The deprotection methods for Boc group removal were previously described in Chapter 5 (341, 342). In this synthetic pathway, deprotection was performed using TFA in CH_2Cl_2 (344) or using HCl in dioxane (345) generating successfully the final products (**29a**-**f**) in good yields (344, 345) (Table 49). ^{1}H and ^{13}C NMR spectra and HRMS confirmed the structures and purity. The Boc group and NH peaks disappeared from the spectra of compounds **29a**-**f**. For example, the ^{1}H NMR spectra of compounds **29c** and **29d** showed the NH_3^+ protons as a singlet peak integrated for 3 protons (Figures 174 and 175). The NH_3^+ peak observed in compounds **29a**, **29c** and **29d** while it was not visible in the ^{1}H NMR spectra of compounds **29b**, **29e** and **29f** owing to the use of deuterium methanol solvent in the NMR. However, using high resolution mass spectrometry was a useful tool to check their molecular formulas and the success of the preparation of next step proved the formation of the desired compounds.

Table 49: Identification data for *tert*-butyl (2-(4-(phenyl)sulfonyl)piperazin-1-yl)-2-oxoethyl)carbamate derivatives (**29a**-**f**).

Compd	R	Yield (%)	mp (^{O}C)	Appearance
29a	CH_3	93	170-172	White solid
29b	NO_2	90	230-232	White powder
29c	C_6H_5	56	135-137	White solid
29d	$C_6H_4OCH_3$	46	258-260	White solid
29e	C_6H_4F	54	250-252	White powder
29f	C_6H_4Cl	73	268-270	White solid

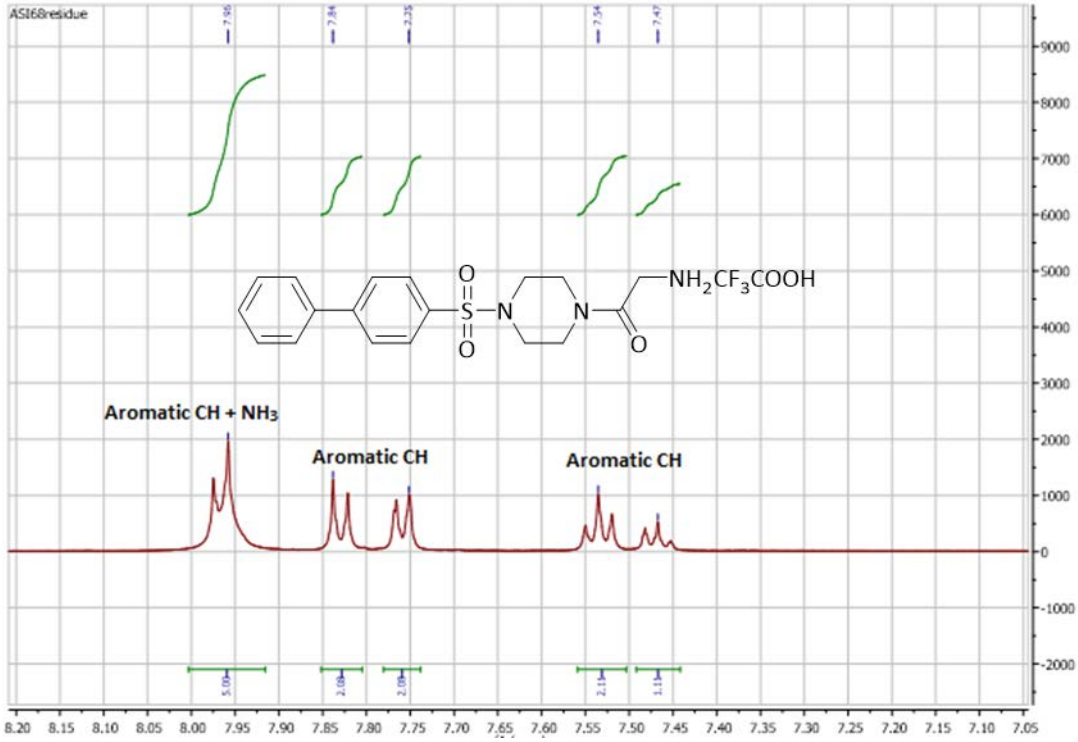

Figure 174a: ^{1}H NMR spectrum of compound **29c.** The spectrum shows aromatic CH as five peaks, three of them integrated for 2 protons, one integrated for 1 proton and the one has higher chemical shift integrated for five protons, 2 protons are for aromatic CH while 3 protons are for the NH_3^+ signal.

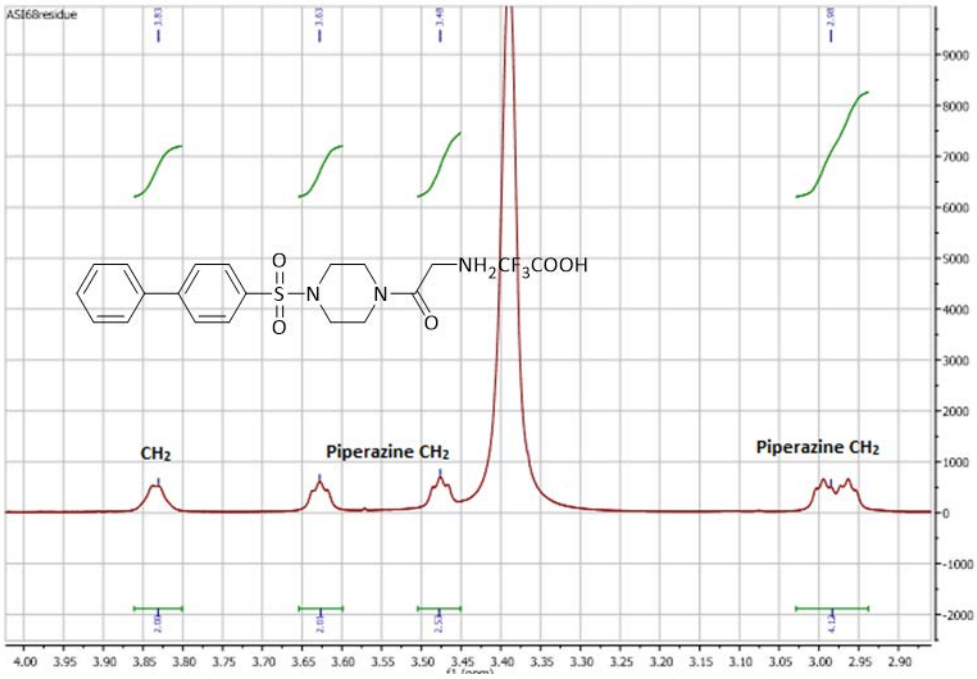

Figure 174b: ^{1}H NMR spectrum of compound **29c**. The spectrum shows piperazine CH_2 as three broad peaks, one integrated for 4 protons while the others integrated for 2 protons and the CH_2 signal as a singlet peak. H_2O peak from DMSO-d_6 solvent was observed in the spectrum.

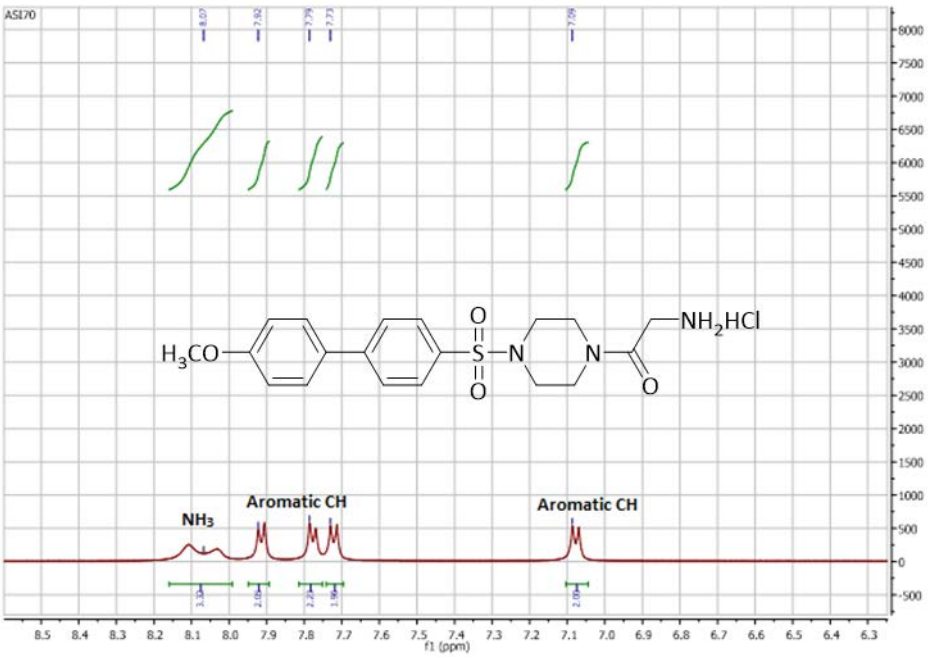

Figure 175a: ^{1}H NMR spectrum of compound **29d.** The spectrum shows aromatic CH as four peaks, each integrated for 2 protons and NH_3 signal as a doublet peak.

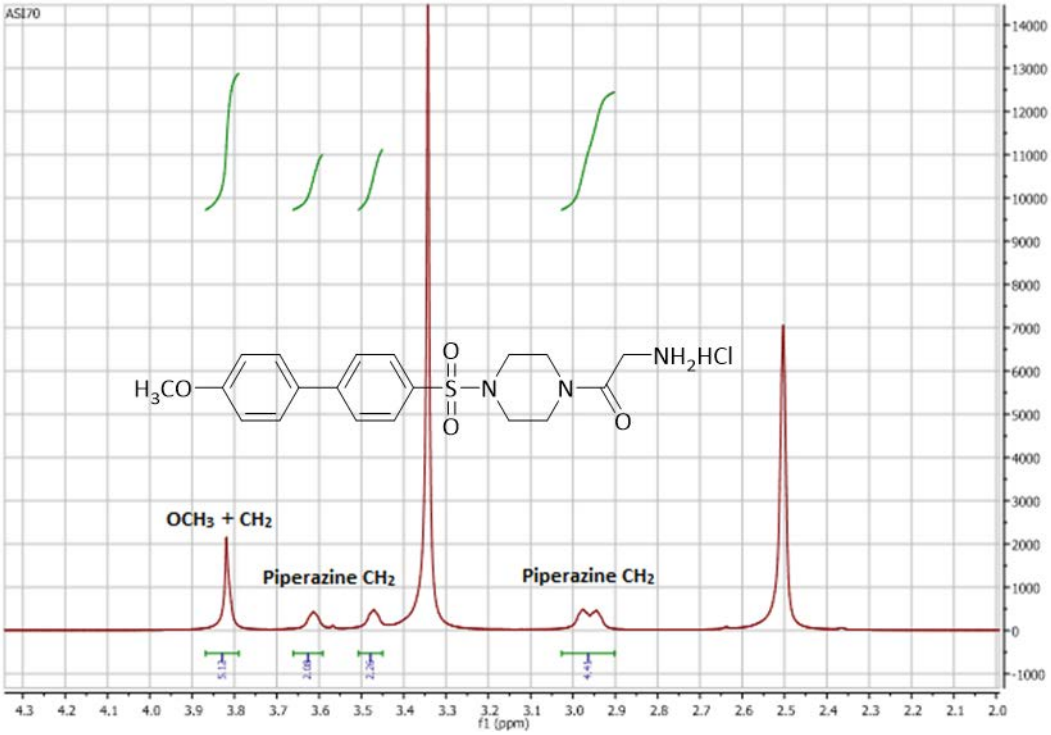

Figure 175b: ^{1}H NMR spectrum of compound **29d**. The spectrum shows piperazine CH_2 as three broad peaks, one integrated for 4 protons while others integrated for 2 protons and OCH_3 and CH_2 signals observed as a singlet peak integrated for 5 protons. The solvent and H_2O peaks showed in the spectrum.

6.1.3. Synthesis of 1-(3,4-dimethylisoxazol-5-yl)-3-(2-(4-(phenyl)sulfonyl)piperazin-1-yl)-2-oxoethyl)urea (30a-f)

2, 2, 2-Trichloroethyl(3,4-dimethylisoxazol-5-yl)carbamate (**21**) was reacted with 2-amino-1-(4-(phenyl)sulfonyl)piperazin-1-yl)ethan-1-one (**29a**-**f**) using *N*-ethyldiisopropylamine as base and DMF as solvent and the reaction mixture heated at 70 ^{O}C for a period of time ranging from 2-24 h (Scheme 10) (349). The final products (**30a**-**d**) were obtained in satisfactory yields (Table 50). ^{1}H and ^{13}C NMR spectra and HRMS confirmed the structures and purity. For example, the ^{1}H NMR spectrum of compound **30b** showed two peaks for the urea NH protons, each integrated for a proton, one was a singlet peak while the other was a triplet peak coupled with CH_2 protons (Figures 176a and 176b). However, for compounds **30e** and **30f**, although NMR indicated the presence of the products, all purification attempts were unsuccessful and even after column chromatography, recrystalisation and preparative

thin layer chromatography (TLC), compound **30f** was impure and the HPLC recorded about 6% of purity for the formula.

Table 50: Identification data for 1-(3,4-dimethylisoxazol-5-yl)-3-(2-(4-(phenyl) sulfonyl)piperazin-1-yl)-2-oxoethyl)urea (**30a**-**f**).

Compd	R	Yield (%)	mp (^{o}C)	Appearance
30a	CH_3	65	124-126	White solid
30b	NO_2	34	228-230	White solid
30c	C_6H_5	25	-	White semisolid
30d	$C_6H_4OCH_3$	62	-	Colourless semisolid
30e	C_6H_4F	-	-	Impure product
30f	C_6H_4Cl	-	-	Impure product

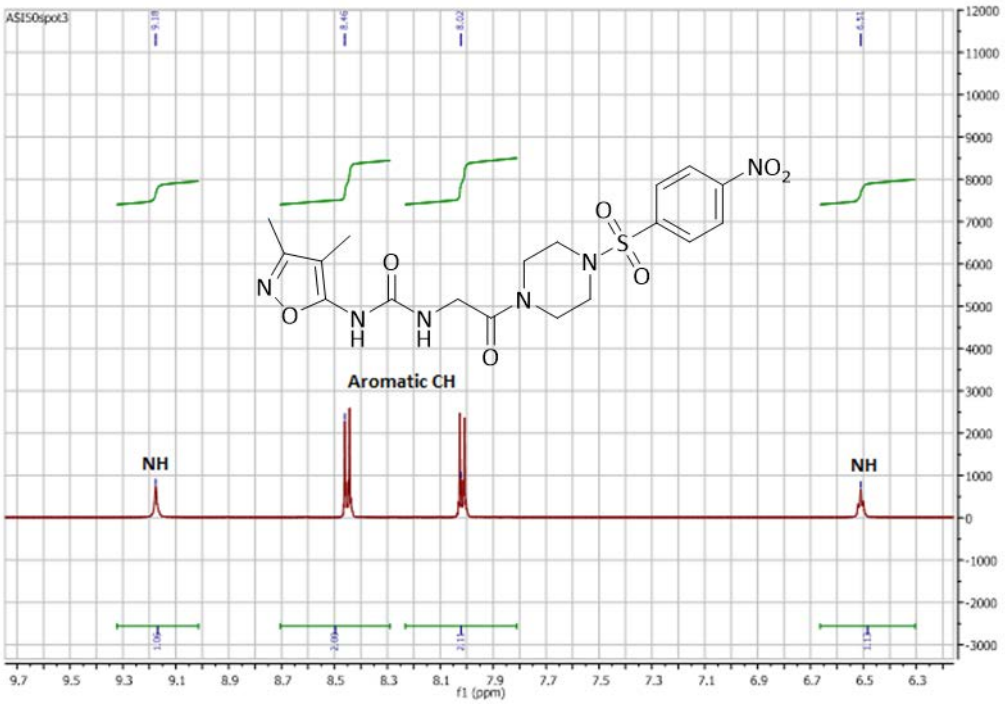

Figure 176a: ^{1}H NMR spectrum of compound **30b**. The spectrum shows aromatic CH as two peaks, each integrated for 2 protons and two peaks for NH, one was a singlet while the other was a triplet peak.

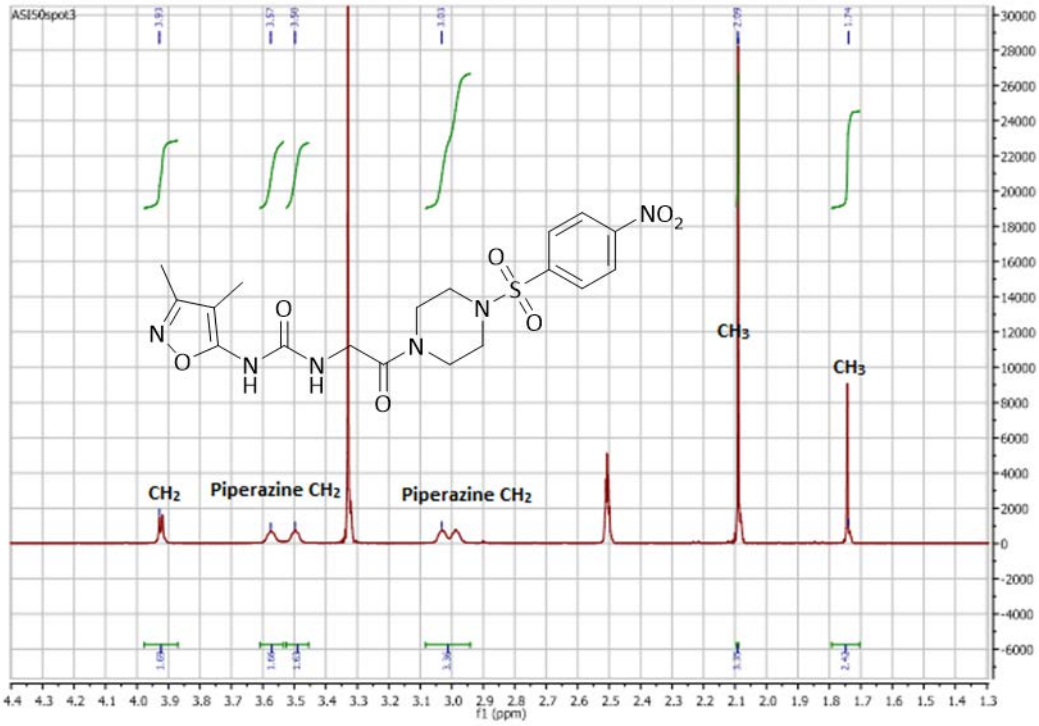

Figure 176b: ^{1}H NMR spectrum of compound **30b**. The spectrum shows piperazine CH_2 as three broad peaks, one integrated for 4 protons and two integrated for 2 protons, CH_2 was observed as a doublet peak and two singlet peaks for dimethyl protons.

6.2. Docking studies

A docking study of the final compounds of series 4 with *S. aureus* and *E. faecalis* AspRS and AsnRS enzymes was performed to determine their binding interactions with the active sites of the respective aaRS enzymes. The docking study of compounds **30a**-**f** with *S. aureus* AspRS showed that compounds **30a**-**c** were a good fit inside the Asp and AMP pockets without flipping and formed hydrogen bonds with the key amino acid residues while the docking study of compounds **30a**-**f** with *S. aureus* AsnRS showed the good fitting of the aryl/biaryl moieties inside the AMP pocket and Arg360 as one of the key amino acid residue responsible for Asn recognition formed a water mediated hydrogen bond with the amino acid isosteric moiety in compounds **30a**-**b** and **f.** Regarding *E. faecalis* AspRS and AsnRS enzymes, the aryl/biaryl sulfamoyl piperazine showed good interactions inside the AMP pockets. The amino acid isosteric moiety showed good interactions in the Asp pocket of compounds **30a**-**c,** but this moiety did not fit well in the same pocket in compounds **30d**-**f**. Furthermore, these

compounds did not interact well inside the Asn pocket and interacted with only Arg380 in some compounds.

6.2.1. Docking studies of *S. aureus* AspRS

By alignment of series 4 compounds with aspartyl adenylate inside the active site of *S. aureus* AspRS (Figure 177), the amino acid residues responsible for binding interactions were identified (Table 51). The amino acid isosteric moiety and urea fit well inside the Asp pocket forming hydrogen bonds with several amino acid residues such as Ser199, Gln237, Gly488, Gly489, Arg492 and Asp239. In addition, the histidine and flipping loops were close to the amino acid isosteric moiety indicating the correct recognition inside the Asp pocket (Figures 178-182). The docking studies of compounds **30a**-**f** showed that the length of compounds **30a**-**c** was enough to fill both active sites and form binding interactions with the key amino acid residues (Figures 178-180). However, compounds **30d**-**f** were too long to fit both pockets, thus the amino acid isosteric moiety with the linker showed good hydrogen binding interactions inside the Asp pocket and less binding interactions inside AMP pocket (Figures 181-182). The docking study of series 4 compounds did not show any hydrophobic interactions with Phe235 and the presence of urea in this series was effective at enhancing the binding interactions inside the Asp pocket while Mg^{2+} ion stabilised the sulfamoyl linkage via a network of hydrogen bonds (Figures 178-182).

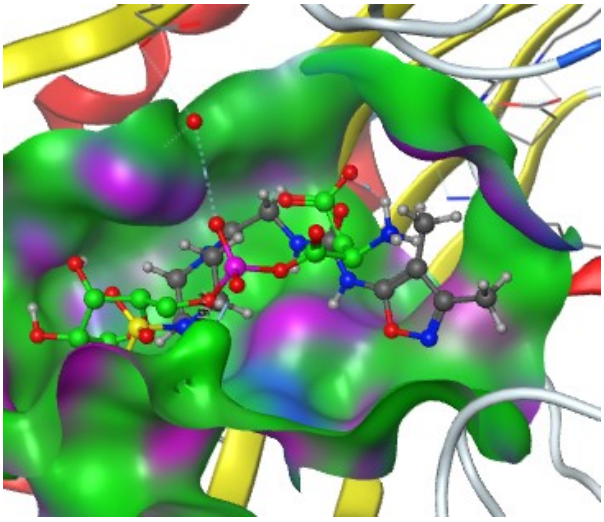

Figure 177: Alignment of compound **30b** (grey) with aspartyl adenylate (green) in the active sites of *S. aureus* AspRS.

Table 51: Binding interactions of series 4 compounds with the amino acid residues of the binding sites of *S. aureus* AspRS.

Ligands	Aspartic acid pocket	AMP pocket
Aspartyl-adenylate	Gln201, Lys204, His452, Gly488, Ser490, Arg492 and Asp239	Arg223, Phe235, Gln232, Arg540 and Glu485
30a	Ser199, Gln237, Gly488, Gly489, Arg492 and Asp239	Arg223, Glu485 and Arg540
30b	Ser199, Gln237, His452, Gly488, Gly489, Arg492 and Asp239	Glu485, Asp539 and Arg540
30c	Ser199, Gln237, His451, His452, Gly488, Gly489, Arg492 and Asp239	Asp478, Glu485 and Arg540
30d	Ser199, Gln237, His451, His452, Gly488 and Asp239	Glu485 and Arg540
30e	Ser199, His451 and His452	Arg231, Asp478, Glu485 and Arg540
30f	Ser199, Gln237, Asp239, Gly488 and Arg492	Asp478 and Glu485

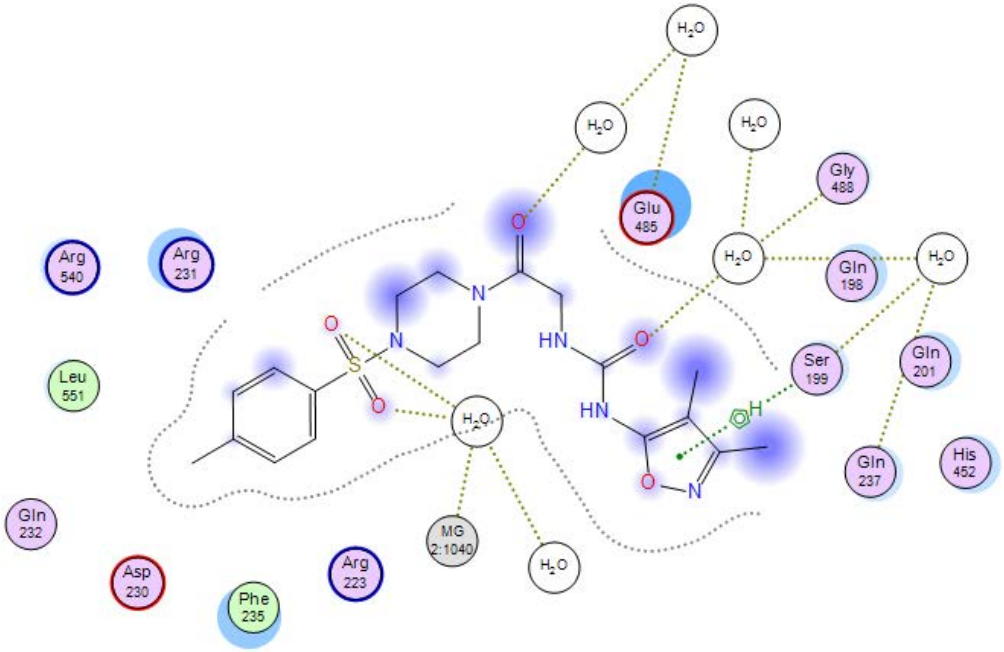

Figure 178: 72D binding interactions of compound **30a** with *S. aureus* AspRS.

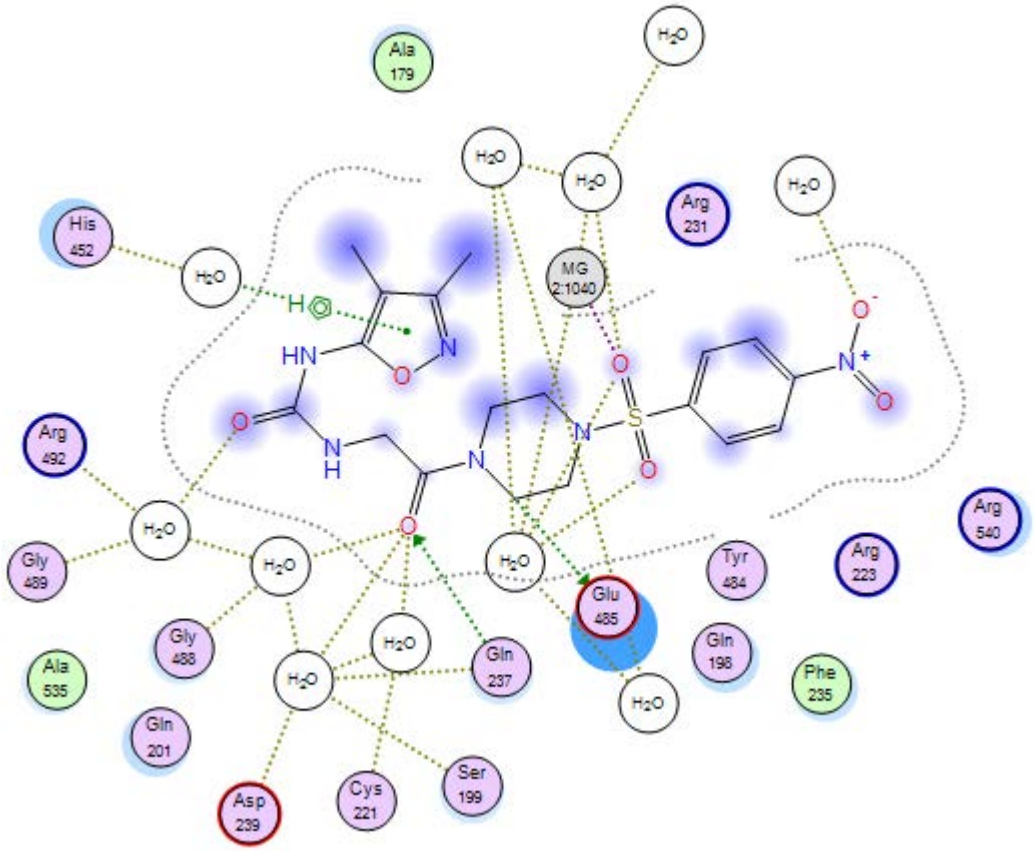

Figure 179: 2D binding interactions of compound **30b** with *S. aureus* AspRS.

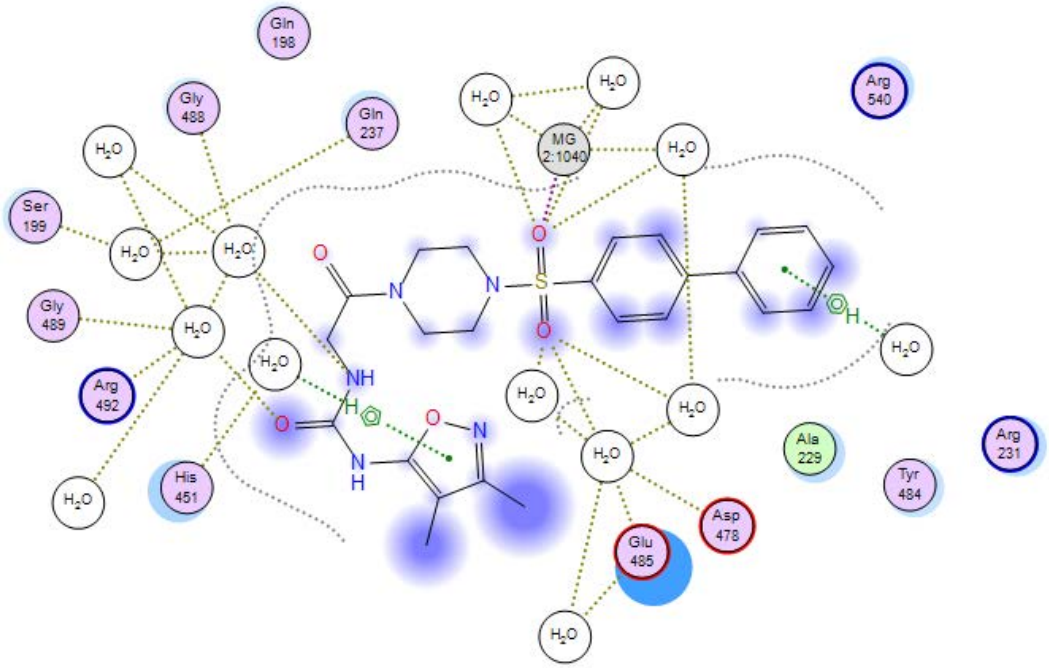

Figure 180: 2D binding interactions of compound **30c** with *S. aureus* AspRS.

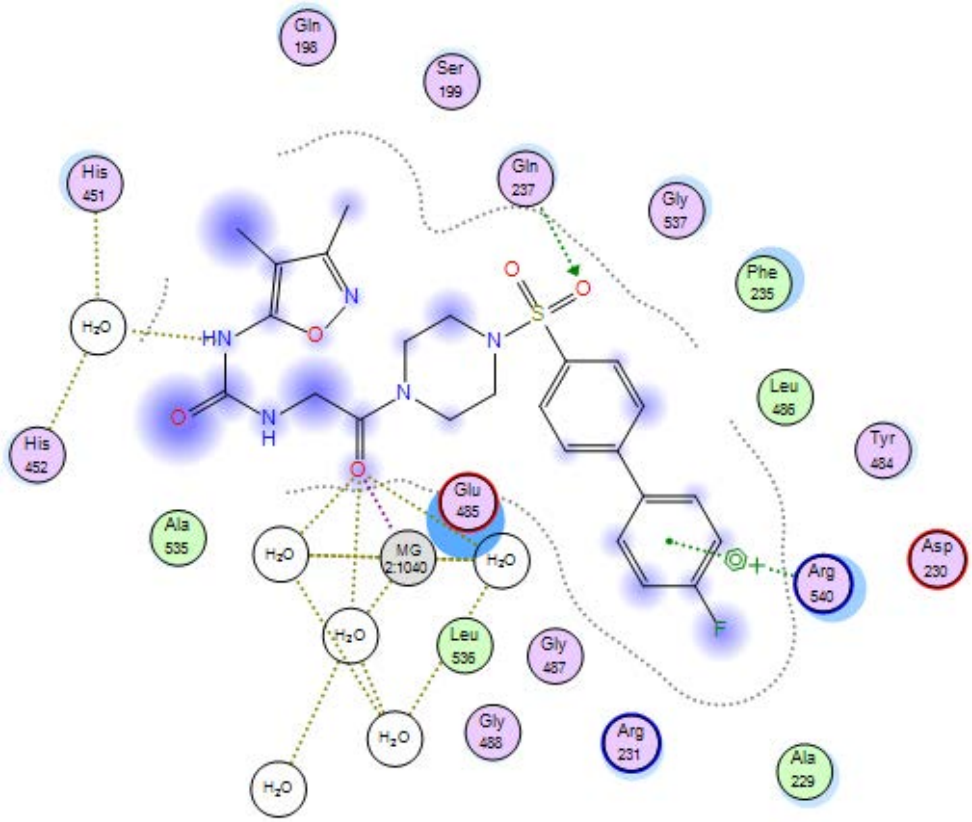

Figure 181: 2D binding interactions of compound **30e** with *S. aureus* AspRS.

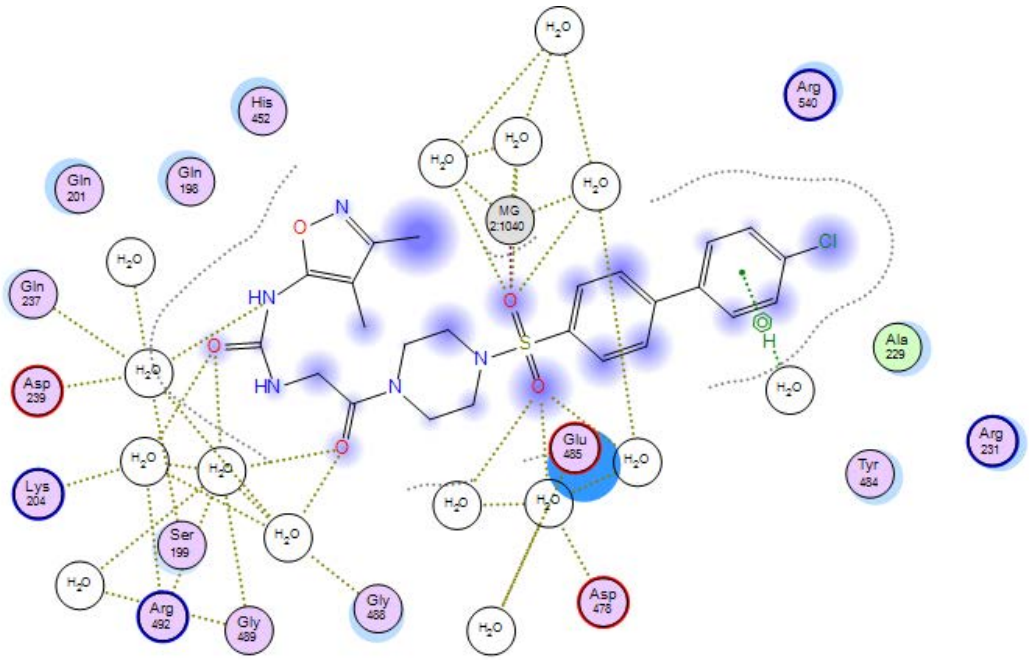

Figure 182: 2D binding interactions of compound **30f** with *S. aureus* AspRS.

6.2.2. Docking studies of *S. aureus* AsnRS

By alignment of series 4 compounds with asparaginyl adenylate inside the active site of *S. aureus* AspRS (Figure 183), the amino acid residues responsible for binding interactions were identified (Table 52). The docking study of compound **30a**-**f** showed that the aryl/biaryl sulfamoyl piperazine moiety occupied the AMP pocket of AsnRS forming a π-π stacking interaction between the benzene ring and Phe219, for examples, compound **30a** and **30d** (Figures 184 and 185). His215 formed two types of hydrophobic interactions with the biphenyl group of compound **30d**, π-π stacking interaction with one benzene ring and π-H with the other one (Figure 185). Water molecules contributed to the stabilisation of the sulfamoyl piperazine linkage through a network of hydrogen bonds with Mg^{2+} ion and key amino acid residues such as Glu353, Gly356 and Arg404 (Figures 184-186). In the docking study of compound **30a** (Figure 184), the sulfamoyl and urea linkage were stabilised by the presence of Mg^{2+} ion, thus the fitting of the amino acid isosteric moiety inside the Asn pocket was better than the same moiety in compounds **30d**-**f** (Figure 184 and 186). Arg360, as a key amino acid residue for Asn recognition, formed a water mediated hydrogen bond with the N atom of the dimethyl isoxazole while the second key, Glu223, did not interact (Figure 184). In spite of the interaction of Arg360 with the N atom of the urea linkage

in compound **30f**, the biphenyl moiety did not form any hydrophobic interactions inside the AMP pocket (Figure 186).

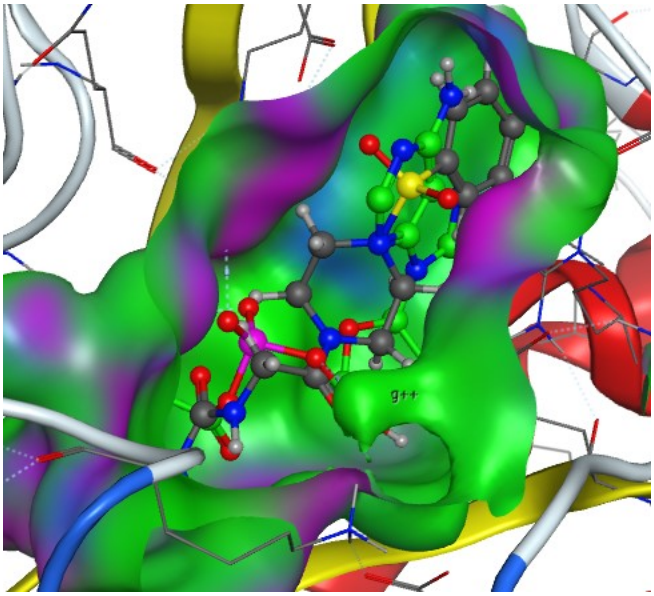

Figure 183: Alignment of compound **30a** (grey) with asparaginyl adenylate (green) in the active sites of *S. aureus* AsnRS.

Table 52: Binding interactions of series 4 compounds with the amino acid residues of the binding sites of *S. aureus* AsnRS.

Ligands	Asparagine pocket	AMP pocket
Asparaginyl-adenylate	Glu223 and Arg360	Arg206, Glu208, Arg214, His215, Phe219, Glu353, Gly356, Gly401, Arg404
30a	Arg360	Arg206, Glu208, Arg214, His215, Phe219, Glu353, Gly356, Gly401, Arg404
30b	Arg360	Glu163, Glu167, Arg206, Phe219, Glu353, Gly356, Arg404
30c	-	Glu163, Glu167, Arg206, Phe219, Glu353, Gly356, Arg404
30d	-	Glu163, Glu167, Arg206, Phe219, Glu353, Gly356, Arg404
30e	-	Glu163, Glu167, Arg206, Phe219, Glu353, Gly356, Arg404
30f	Arg360	Glu163, Glu167, Arg206, Phe219, Glu353, Gly356, Arg404

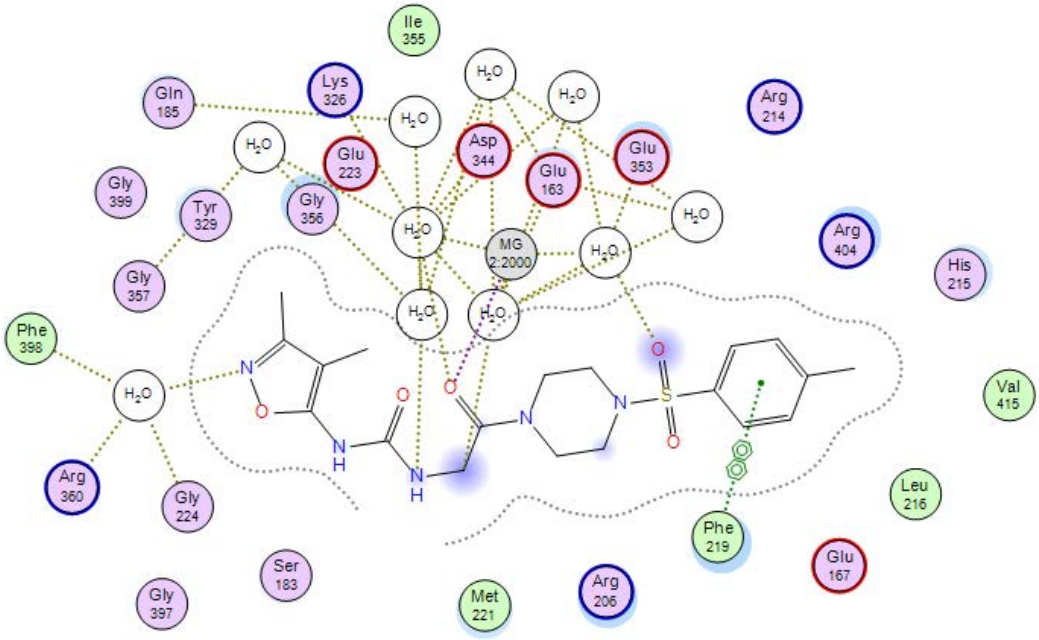

Figure 184: 2D binding interactions of compound **30a** with *S. aureus* AsnRS.

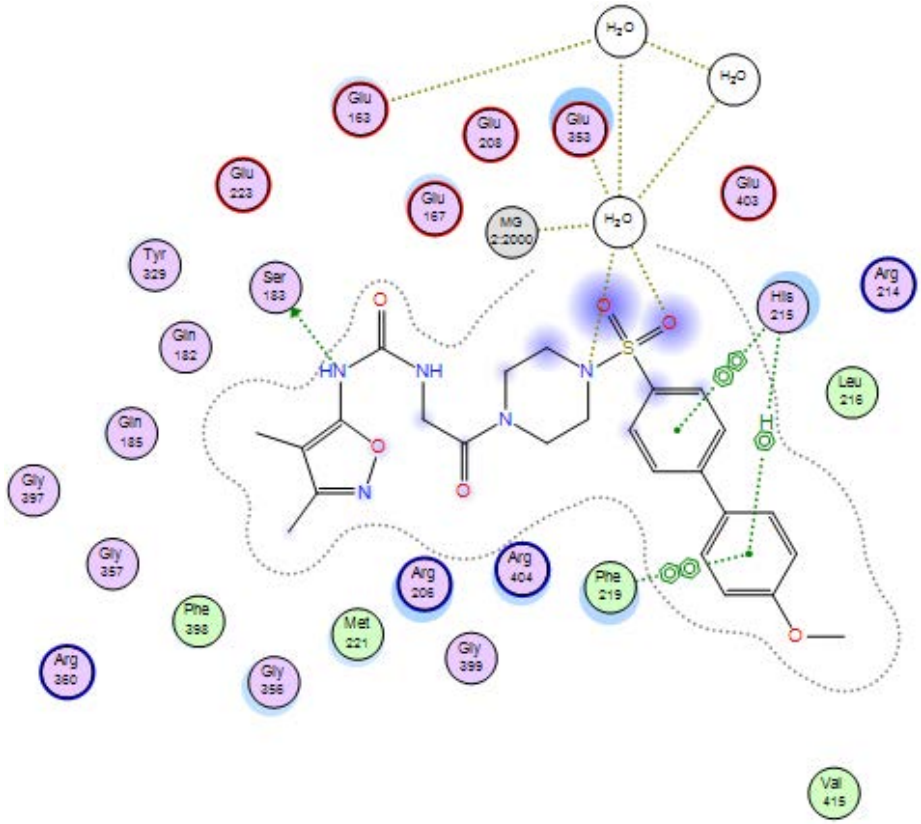

Figure 185: 2D binding interactions of compound **30d** with *S. aureus* AsnRS.

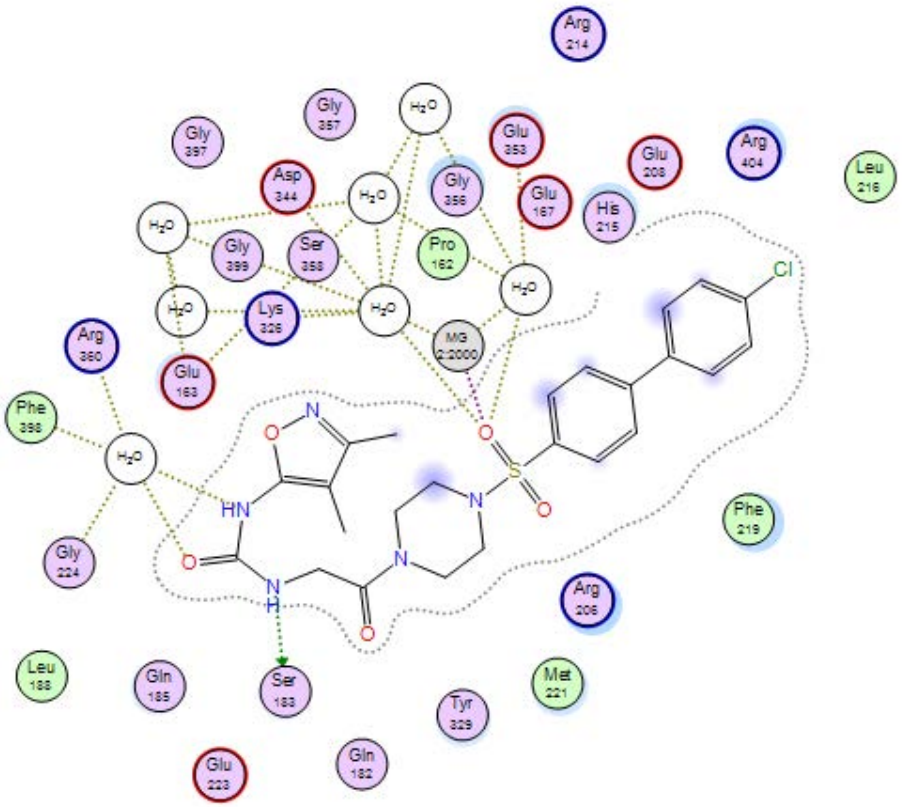

Figure 186: 2D binding interactions of compound **30f** with *S. aureus* AsnRS.

6.2.3. Docking studies of *E. faecalis* AspRS

The amino acid residues responsible for binding interactions with series 4 compounds were identified through alignment with aspartyl adenylate inside the active sites of *E. faecalis* AspRS (Figure 187) (Table 53). The docking studies of compounds **30a**-**f** showed good fitting and binding interactions of the aryl/biaryl sulfamoyl piperazine moiety inside the AMP pocket forming a π-π stacking interaction with Phe234 and a hydrogen bond either directly or via water molecules with several key amino acid residues such as Arg222, Glu224, Gln236 and Arg538 (Figures 188-191). Mg^{2+} ion stabilised the sulfamoyl linkage in compounds **30a**-**c** owing to their good length inside both pockets (Figure 188). However, compounds **30d**-**f** were too long and not able to form good binding interactions especially in the Asp pocket even though the histidine loop was in close proximity. This could impair the ability of Mg^{2+} ion in the stabilisation of the sulfamoyl linkage (Figures 190 and 191). The nitro group of compound **30b** formed a direct hydrogen bond with Gln231 (Figure 189) while the methoxy , fluoro and chloro groups of the respective compounds did not show any interactions with the key amino acid residues responsible for the AMP active site of *E. faecalis* AspRS (Figures 190 and 191).

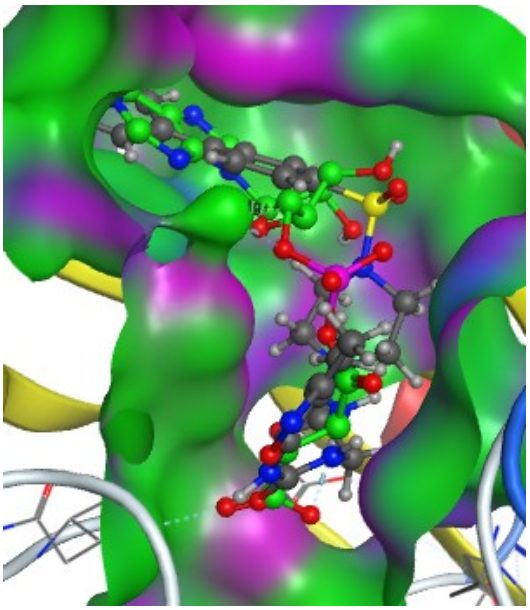

Figure 187: Alignment of compound **30e** (grey) with aspartyl adenylate (green) in the active sites of *E. faecalis* AspRS.

Table 53: Binding interactions of series 4 compounds with the amino acid residues of the binding sites of *E. faecalis* AspRS.

Ligands	Aspartic acid pocket	AMP pocket
Aspartyl-adenylate	Glu176, Arg230, His449, Arg490 and Asp238	Arg222, Phe234, Gln231, Gln236, Glu483 and Arg538
30a	Glu176, His449 and His450	Arg222, Glu224, Phe234, Gln236 and Arg538
30b	Glu176, His449 and Arg490	Arg222, Glu224, Phe234, Gln231, Gln236 and Arg538
30c	Asp238	Arg222, Glu224, Phe234, Gln231, Gln236
30d	His449, Arg490 and Asp238	Arg222, Glu224, Phe234, Gln236 and Arg538
30e	Glu176 and His449	Arg222, Glu224, Phe234, Gln236 and Arg538
30f	Glu176 and His449	Arg222, Glu224, Phe234 and Gln236

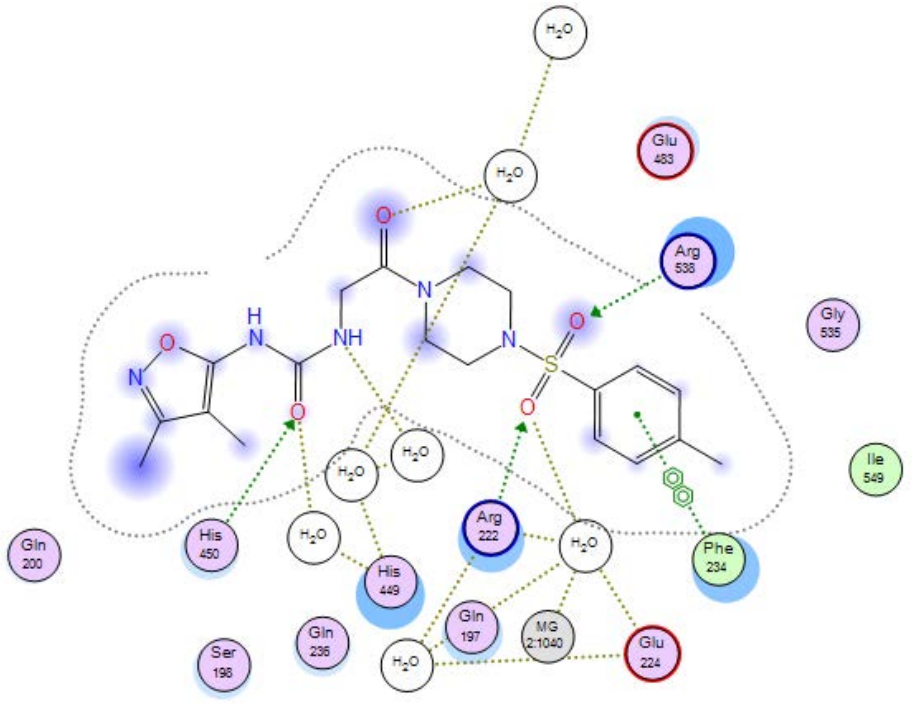

Figure 188: 2D binding interactions of compound **30a** with *E. faecalis* AspRS.

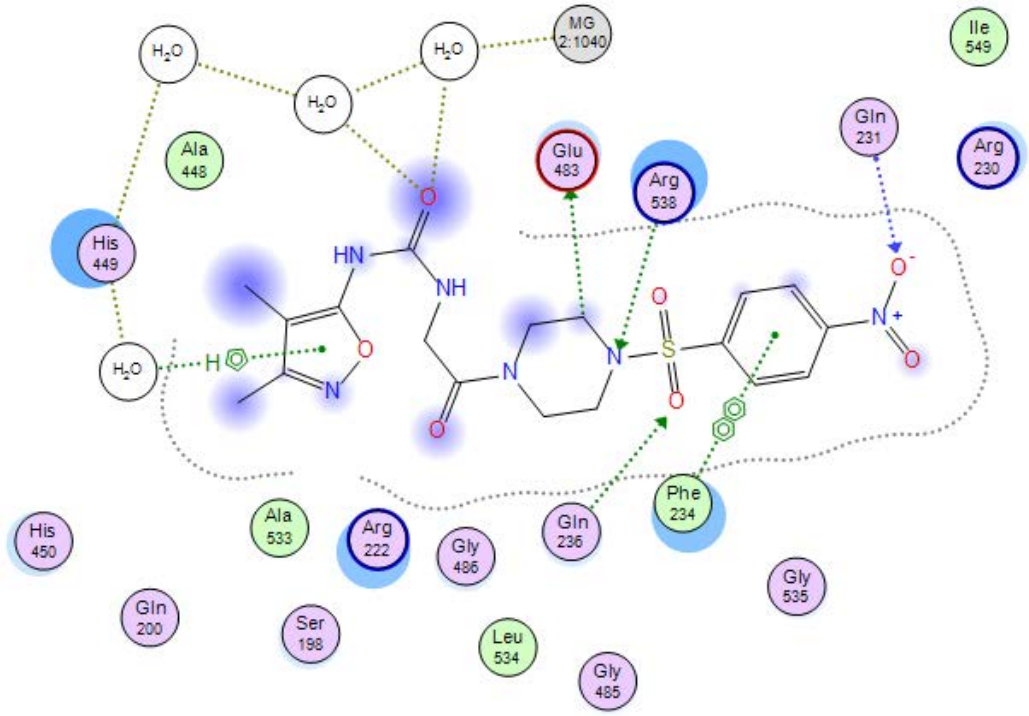

Figure 189: 2D binding interactions of compound **30b** with *E. faecalis* AspRS.

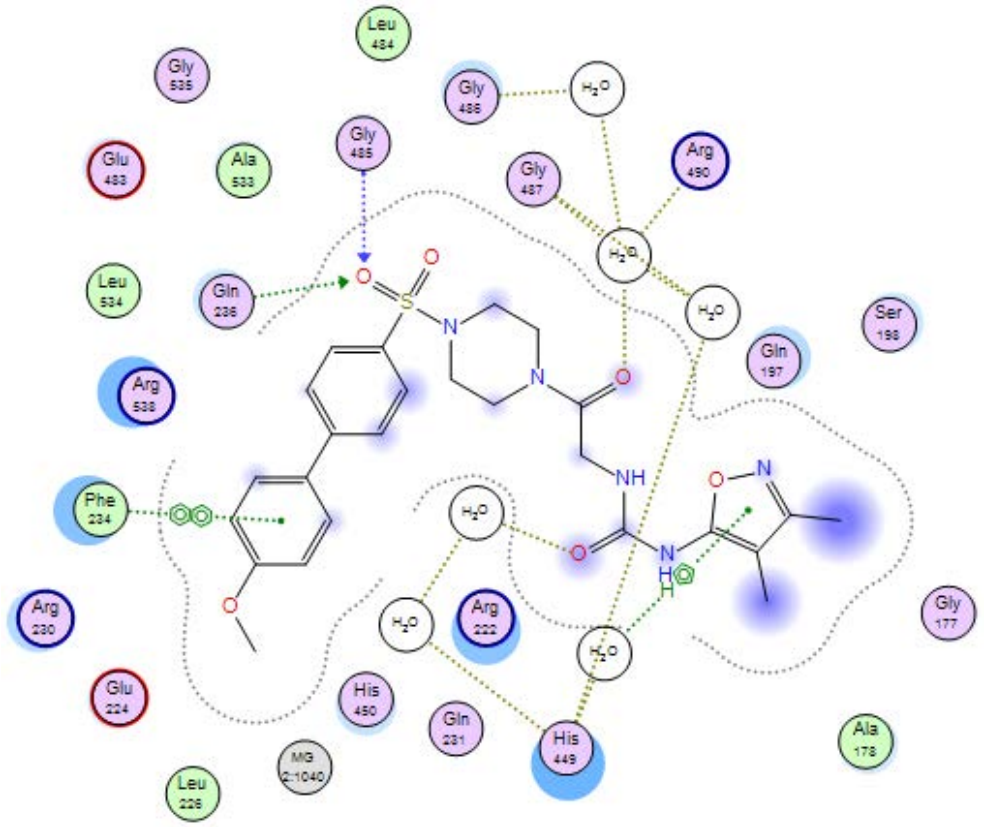

Figure 190: 2D binding interactions of compound **30d** with *E. faecalis* AspRS.

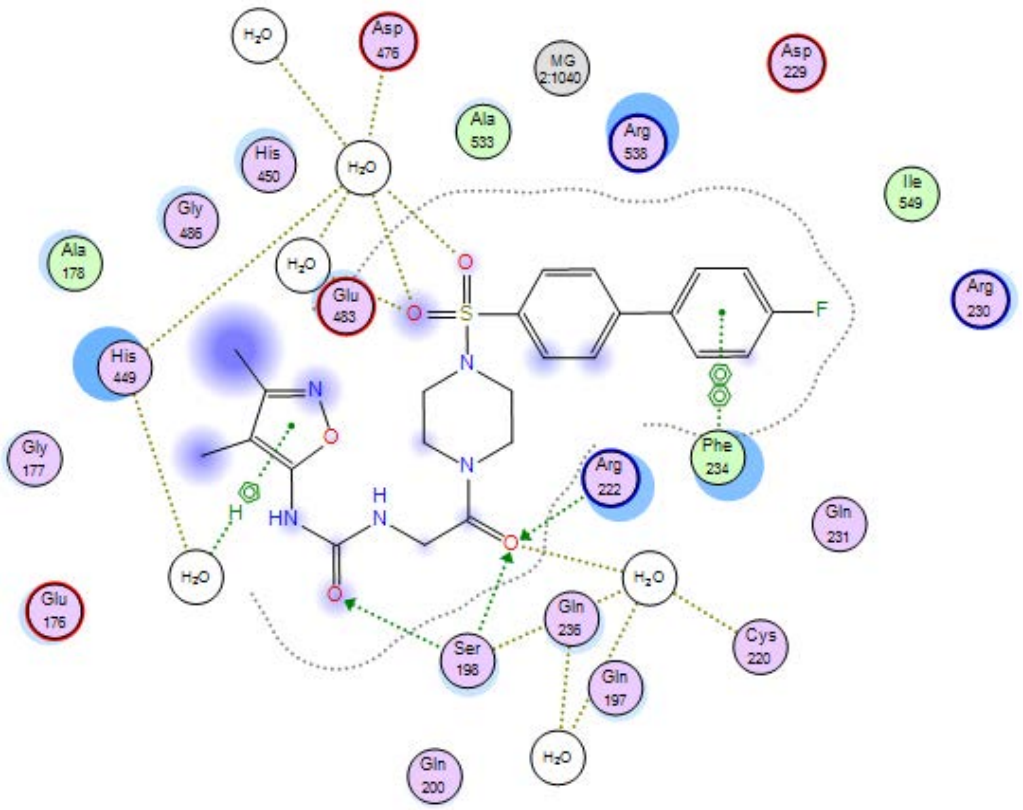

Figure 191: 2D binding interactions of compound **30e** with *E. faecalis* AspRS.

6.2.4. Docking studies of *E. faecalis* AsnRS.

The amino acid residues responsible for binding interactions with series 4 compounds were identified through alignment with asparaginyl adenylate inside the active sites of *E. faecalis* AsnRS (Figure 192) (Table 54). The docking studies of this series compounds showed that compounds **30a**-**f** were flipping inside both active sites in most of the poses and because they were too long, part of compounds **30d**-**f** were little bit outside the AMP pocket if the amino acid isosteric moiety fitted well in the Asn pocket. The aryl/biaryl sulfamoyl piperazine moiety of compounds **30a**-**c** formed a π-π stacking interaction with Phe234 and hydrogen bonds with Arg221, His230, Glu373 and Arg424 (Figure 193). However, the methoxy, fluoro and chloro biphenyl sulfamoyl derivatives did not show good fitting inside the AMP pocket if the amino acid isosteric moiety fitted well inside the Asn pocket and vice versa during the docking study (Figures 194 and 195). In addition, the binding interactions with Glu238 and Arg380 observed with asparaginyl-adenylate, were not observed for series 4, and only Arg380 formed a water mediated hydrogen bond with the carbonyl group of urea linkage in compound **30a** and with dimethyl isoxazole in compounds **30d** and **f** (Figures 193-195).

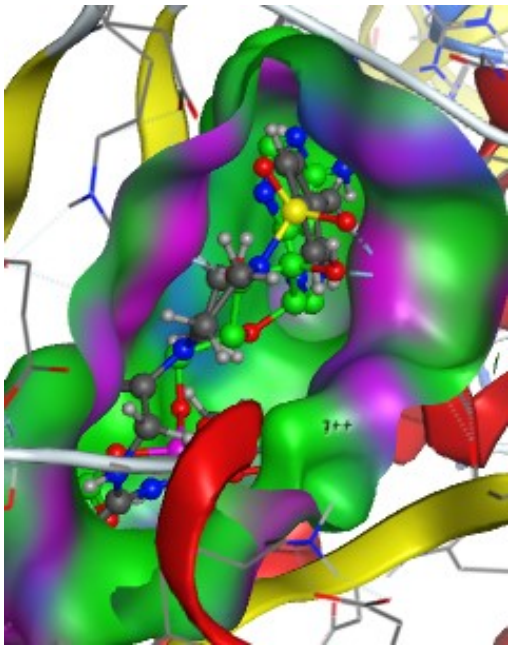

Figure 192: Alignment of compound **30b** (grey) with asparaginyl adenylate (green) in the active sites of *E. faecalis* AsnRS.

Table 54: Binding interactions of series 4 compounds with the amino acid residues of the binding sites of *E. faecalis* AsnRS.

Ligands	Asparagine pocket	AMP pocket
Asparaginyl-adenylate	Glu238 and Arg380	Arg221, Glu223, Arg229, His230, Phe234, Glu373, Gly376, Gly421 and Arg424
30a	Gln200 and Arg380	Arg221, His230, Phe234, Glu373 and Arg424
30b	-	Arg221, Arg229, His230, Glu373 and Arg424
30c	Gln200 and Arg380	Glu173, Arg221 and Glu373
30d	Gln200 and Arg380	Glu173, Arg221, His230 and Glu373
30e	-	Arg221, Glu373 and His230
30f	Gln200 and Arg380	Arg221, Glu373 and Arg424

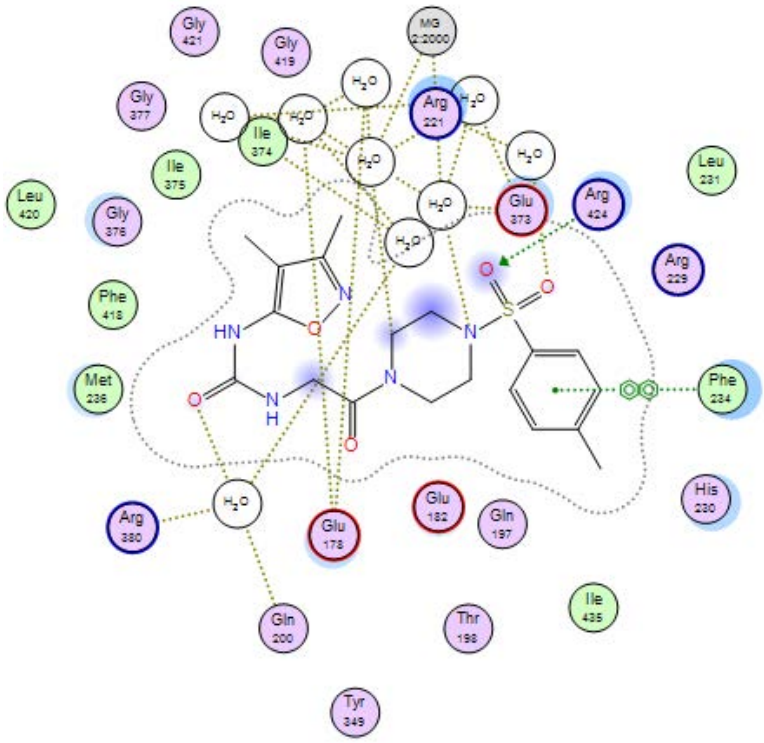

Figure 193: 2D binding interactions of compound **30a** with *E. faecalis* AsnRS.

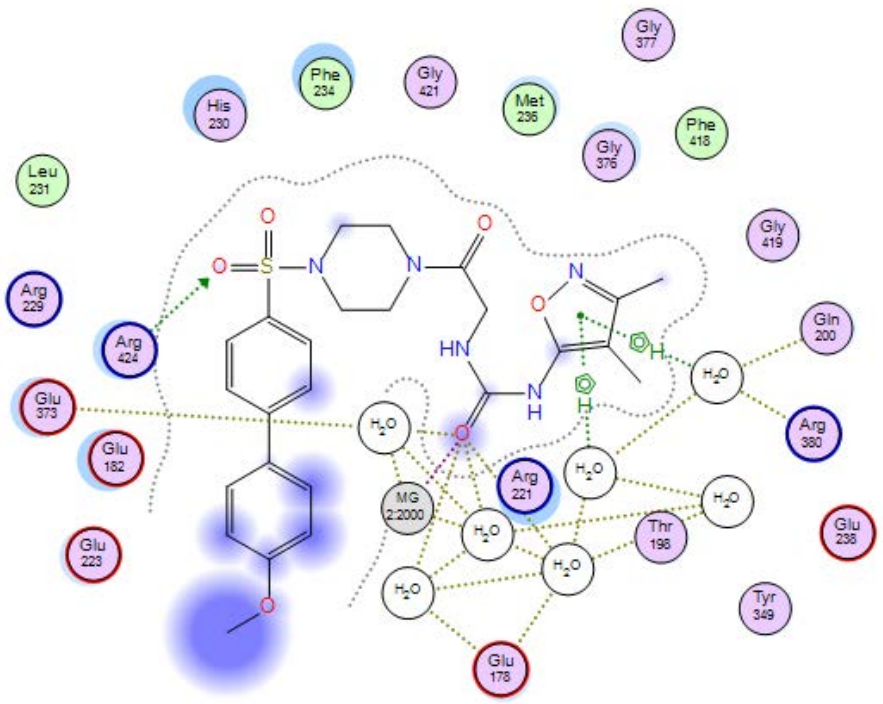

Figure 194: 2D binding interactions of compound **30d** with *E. faecalis* AsnRS.

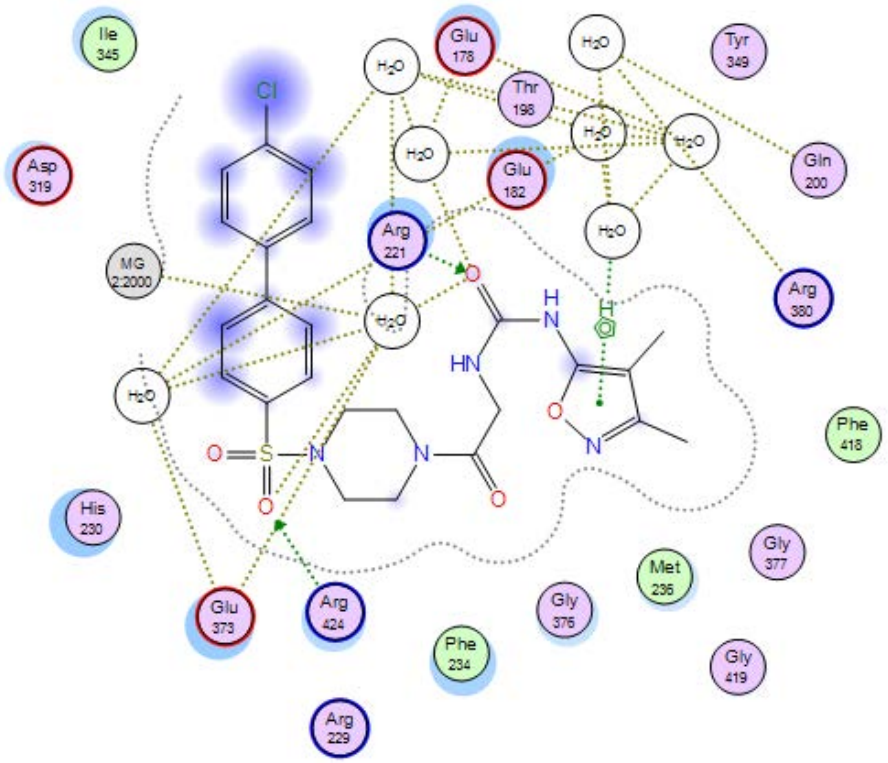

Figure 195: 2D binding interactions of compound **30e** with *E. faecalis* AsnRS.

6.3. Biological assays

6.3.1. Microbiological screening

Microbiological screening of series 4 compounds was performed at the Antimicrobial Chemotherapy Unit in University Hospital of Wales (UHW) by Jennifer Richard and Mandy Wootton. Series 4 compounds **30a**-**d** were evaluated for antimicrobial activity against the same microorganisms mentioned in chapter 5. From the MIC results of compounds **30a**-**d** (Table 55), compounds **30c** and **30d** showed low inhibitory activity (64 µg/mL) against *Enterococcus faecalis* compared with ciprofloxacin (0.125 µg/mL) but that inhibitory activity is higher than that of ciprofloxacin against *Enterococcus faecium* (>128 µg/mL). Compounds **30b**-**d** showed some inhibitory activity against the resistant strain of *Staphylococcus aureus*, which was 64 µg/mL for compound **30b** and 32 µg/mL for compounds **30c** and **30d**. The presence of the urea linkage next to the amino acid isosteric moiety showed more binding interactions in the Asp pocket of both microorganisms target AspRS enzymes during the docking study while it formed good binding interactions with some of the key amino acid residues responsible for the AMP pocket of *S. aureus and E. faecalis* AsnRS. The easy flipping of compounds **30a** and **30b** inside the active sites of AspRS enzymes would suggest they are too short to completely fill the pocket which may be in turn their abilities in binding the enzymes and exert their inhibitory activities. However, the MIC values of compounds **30c** and **30d** against *E. faecalis* and the resistant strain of *S. aureus* indicate the good fitting compared with compounds **30a** and **30b**.

Table 55: Microbiological data of compounds **30a**-**d**.

Microorganisms	MIC: (µg/mL)				
	Ciprofloxacin	**30a**	**30b**	**30c**	**30d**
Pseudomonas aeruginosa					
ATCC 27853	0.25	128	128	128	128
26739	0.06	128	128	128	128
Staphylococcus aureus					
ATCC 29213	0.25	>128	>128	128	128
Enterococcus faecalis					
ATCC 29212	0.125	128	>128	64	64
Enterococcus faecium					
16568	>128	128	>128	64	64
Staphylococcus aureus					
NCTC 12493	0.5	128	64	32	32

6.3.2. Aminoacylation assay

The antimicrobial assay was performed at the Department of Chemistry, University of Texas by Casey Hughes and James Bullard. IC_{50} assay was performed for the series 4 compounds as previously described for series 1. None of the compounds in series 3 showed good inhibitory activity.

In conclusion, only four compounds from this series were successfully prepared in satisfactory yields. In the docking study, these compounds formed many binding interactions in both active sites of the target enzymes. The presence of the ethoxy

urea next to the sulfamoyl linkage improved the microbiological screening results of compounds **30c**-**d** compared with series 3 compounds against *S. aureus* and *E. faecalis*. The design of new series containing urea, amide or amino sulfonamide linker with piperazine, ethyl diamine or benzyl instead of ribose could be effective in optimising the fit inside the active sites which may exert good inhibitory activity.

6.4. Methods

6.4.1 Docking studies

All methods related to docking studies are described in the methods section in Chapter 2.

6.4.2 Biological assay

6.4.2.1. Antimicrobial screening test

The methods related to antimicrobial screening test is described in the methods section in Chapter 3.

6.4.2.2. Aminoacylation assay

The methods related to the aminoacylation assay is described in the methods section in Chapter 3.

6.4.3 Chemistry

6.4.3.1. General procedure for the preparation of *tert*-butyl (2-(4-(phenyl)sulfonyl)piperazin-1-yl)-2-oxoethyl)carbamate (**28a**-**f**)

N-Hydroxy succinamide (**26**) (0.2 g, 1.85 mmol) and DCC (**27**) (0.42 g, 2.03 mmol) were added to a cold solution of *N*-Boc glycine (**25**) (0.32 g, 1.85 mmol) in CH_2Cl_2 (5 mL). The reaction mixture was stirred at 0 ^{0}C for 1 h, then at room temperature overnight. After filtration, the solution was cooled to 0 ^{o}C and 1 equivalent of sulfonyl piperazine derivative (**3a**-**f**) (1.85 mmol) was added. The reaction mixture was stirred overnight at room temperature. CH_2Cl_2 (5 mL) was added and the solution washed with water (3 x 20 mL), dried over anhydrous $MgSO_4$ and the solvent evaporated under reduced pressure.

6.4.3.1.1. *Tert*-butyl(2-oxo-2-(4-tosylpiperazin-1-yl)ethyl)carbamate (**28a**) ($C_{18}H_{27}N_3O_5S$, Mol. Wt. 397.49)

Product obtained after gradient column chromatography and collected at 2.5:97.5 v/v CH_3OH – CH_2Cl_2 to give a colourless semisolid, yield: 0.4 g (50%). TLC: CH_3OH - CH_2Cl_2 0.5:9.5 v/v, (R_F = 0.8). ^{1}H NMR ($CDCl_3$) δ 1.38 (s, 9H, $C(CH_3)_3$), 2.41 (s, 3H, CH_3), 2.96 (quintet, 4H, CH_2, pip), 3.48 (br t, J = 4.7, 5.3 Hz, 2H, CH_2, pip), 3.79 (br t, J = 4.7, 5.3 Hz, 2H, CH_2, pip), 3.89 (d, J = 3.9 Hz, 2H, CH_2), 5.39 (s, 1H, NH), 7.36 (d, J = 8 Hz, 2H, CH, Ar), 7.63 (d, J = 8 Hz, 2H, CH, Ar). ^{13}C NMR ($CDCl_3$) δ 21.6 (CH_3), 28.3 (CH_3, $C(CH_3)_3$), 42.1 (CH_2), 42.9, 43.9, 45.5, 45.7 (4 x CH_2, pip), 79.9 (C, $C(CH_3)_3$), 127.7, 129.9 (4 x CH, Ar), 132.2 (C, Ar), 144.3 (C-S), 155.73 (C=O), 166.9 (C=O). HPLC: 100% at RT: 4.28 min. HRMS (ES-TOF) m/z calculated mass: 420.1671 $[M + Na]^+$, observed mass: 420.1577 $[M + Na]^+$.

6.4.3.1.2. *Tert*-butyl(2-(4-((4-nitrophenyl)sulfonyl)piperazin-1-yl)-2-oxoethyl) carbamate (**28b**) ($C_{17}H_{24}N_4O_7S$, Mol. Wt. 428.46)

Product obtained after gradient column chromatography and collected at 5:95 v/v CH_3OH – CH_2Cl_2 to give a white powder, yield: 0.67 g (85%), mp = 96 – 98 ^{O}C. TLC: CH_3OH - CH_2Cl_2 1:9 v/v, (R_F = 0.5). ^{1}H NMR (DMSO-d_6) δ 1.44 (s, 9H, $C(CH_3)_3$), 3.11 (br s, 4H, CH_2, pip), 3.55 (br s, 2H, CH_2, pip), 3.76 (br s, 2H, CH_2, pip), 3.92 (d, J = 5.8 Hz, 2H, CH_2), 6.72 (t, J = 5.8, 5.8 Hz, 1H, NH), 7.96 (d, J = 8.9 Hz, 2H, CH, Ar), 8.43 (d, J = 8.9 Hz, 2H, CH, Ar). ^{13}C NMR (DMSO-d_6) δ 28.4 (CH_3, $C(CH_3)_3$), 42.5 (CH_2), 43.8, 45.6 (4 x CH_2, pip), 79.3 (C, $C(CH_3)_3$), 124.6, 128.9 (4 x CH, Ar), 143.5 (C-S), 150.5 (C-NO_2), 156.6 (C=O), 163.2 (C=O). HRMS (ES-TOF) m/z calculated mass: 451.1258 $[M + Na]^+$, observed mass: 451.1298 $[M + Na]^+$.

6.4.3.1.3. *Tert*-butyl(2-(4-([1,1'-biphenyl]-4-ylsulfonyl)piperazin-1-yl)-2-oxoethyl) carbamate (**28c**) ($C_{23}H_{29}N_3O_5S$, Mol. Wt. 459.56)

Product obtained after gradient column chromatography and collected at 3:97 v/v CH_3OH – CH_2Cl_2 to give a white solid, yield: 0.6 g (78%), mp = 162 – 164 ^{O}C. TLC: CH_3OH - CH_2Cl_2 1:9 v/v, (R_F = 0.9). ^{1}H NMR ($CDCl_3$) δ 1.38 (s, 9H, $C(CH_3)_3$), 3.04 (br s, 4H, CH_2, pip), 3.48 (s, 2H, CH_2, pip), 3.69 (s, 2H, CH_2, pip), 3.88 (br d, 2H, CH_2), 5.44 (s, 1H, NH), 7.39 (t, J = 6.6, 7.2 Hz, 1H, CH, Ar), 7.46 (t, J = 6.6, 7.4 Hz, 2H, CH, Ar), 7.58 (d, J = 7.4

Hz, 2H, CH, Ar), 7.72 (d, J = 8.4 Hz, 2H, CH, Ar), 7.77 (d, J = 8.4 Hz, 2H, CH, Ar). ^{13}C NMR ($CDCl_3$) δ 28.6 (CH_3, $C(CH_3)_3$), 40.8 (CH_2), 42.1, 43.8, 45.8, 45.9 (4 x CH_2, pip), 79.7 (C, $C(CH_3)_3$), 127.3, 127.9, 128.4, 128.7, 129.1 (9 x CH, Ar), 133.6, 133.7, 138.9 (3 x C, Ar), 155.8 (C=O), 167.0 (C=O). HPLC: 100% at RT: 4.55 min.

6.4.3.1.4. *Tert*-butyl(2-(4-((4'-methoxy-[1,1'-biphenyl]-4-yl)sulfonyl)piperazin-1-yl)-2-oxoethyl)carbamate (**28d**) ($C_{24}H_{31}N_3O_6S$, Mol. Wt. 489.59)

Product obtained after gradient column chromatography and collected at 3:97 v/v CH_3OH – CH_2Cl_2 to give a white solid, yield: 0.3 g (75%), mp = 188 – 190 ^{O}C. TLC: CH_3OH - CH_2Cl_2 0.5:9.5 v/v, (R_F = 0.8). ^{1}H NMR ($CDCl_3$) δ 1.33 (s, 9H, $C(CH_3)_3$), 2.98 (quintet, 4H, CH_2, pip), 3.42 (br t, J = 5, 5.6 Hz, 2H, CH_2, pip), 3.66 (br t, J = 5, 5.6 Hz, 2H, CH_2, pip), 3.79 (s, 3H, OCH_3), 3.82 (d, J = 3 Hz, 2H, CH_2), 5.30 (s, 1H, NH), 6.94 (d, J = 8.6 Hz, 2H, CH, Ar), 7.48 (d, J = 8.6 Hz, 2H, CH, Ar), 7.63 (d, J = 8.6 Hz, 2H, CH, Ar), 7.77 (d, J = 8.4 Hz, 2H, CH, Ar). ^{13}C NMR ($CDCl_3$) δ 28.3 (CH_3, $C(CH_3)_3$), 41.3 (CH_2), 42.1, 43.9, 45.7, 45.9 (4 x CH_2, pip), 55.4 (OCH_3), 79.9 (C, $C(CH_3)_3$), 114.6, 114.8, 127.3, 127.6, 128.3, 128.4, 128.5, 128.8 (8 x CH, Ar), 131.4, 132.8, 145.9 (3 x C, Ar), 160.2 (C-O), 155.7 (C=O), 166.9 (C=O). HPLC: 100% at RT: 4.53 min. HRMS (ES-TOF) m/z calculated mass: 490.1934 $[M + H]^+$, observed mass: 490.2020 $[M + H]^+$.

6.4.3.1.5. *Tert*-butyl (2-(4-((4'-fluoro-[1,1'-biphenyl]-4-yl)sulfonyl)piperazin-1-yl)-2-oxoethyl)carbamate (**28e**) ($C_{23}H_{28}FN_3O_5S$, Mol. Wt. 477.55)

Product obtained after gradient column chromatography and collected at 70:30 v/v petroleum ether – EtOAc to give a white solid, yield: 0.4 g (59%), mp = 90 – 92 ^{O}C. TLC: petroleum ether – EtOAc 3:1 v/v, (R_F = 0.8). ^{1}H NMR ($CDCl_3$) δ 1.34 (s, 9H, $C(CH_3)_3$), 2.99 (quintet, 4H, CH_2, pip), 3.44 (br t, J = 3.6, 6.5 Hz, 2H, CH_2, pip), 3.67 (br t, J = 3.6, 6.5 Hz, 2H, CH_2, pip), 3.82 (s, 2H, CH_2), 5.30 (s, 1H, NH), 7.12 (t, J = 8.6, 8.6 Hz, 2H, CH, Ar), 7.51 (dd, J = 3.6, 9 Hz, 2H, CH, Ar), 7.63 (d, J = 8.6 Hz, 2H, CH, Ar), 7.72 (d, J = 9 Hz, 2H, CH, Ar). ^{13}C NMR ($CDCl_3$) δ 28.3 (CH_3, $C(CH_3)_3$), 41.3 (CH_2), 42.1, 42.9, 43.1, 43.9 (4 x CH_2, pip), 79.9 (C, $C(CH_3)_3$), 116.3, 127.7, 127.9, 128.0 128.1, 128.3, 129.0, 129.1, (8 x CH, Ar), 133.7, 145.3, 155.7 (3 x C, Ar), 164.2 (C-F), 162.2 (C=O), 166.9 (C=O). HPLC: 100% at RT: 3.83 min. HRMS (ES-TOF) m/z calculated mass: 478.1734 $[M + H]^+$, observed mass: 478.1810 $[M + H]^+$.

6.4.3.1.6. *Tert*-butyl (2-(4-((4'-chloro-[1,1'-biphenyl]-4-yl)sulfonyl)piperazin-1-yl)-2-oxoethyl)carbamate (**28f**) ($C_{23}H_{28}ClN_3O_5S$, Mol. Wt. 493.14)

Product obtained after gradient column chromatography and collected at 70:30 v/v petroleum ether – EtOAc to give a white solid, yield: 0.7 g (90%), mp = 198 – 200 ^{O}C. TLC: petroleum ether – EtOAc 3:1 v/v, (R_F = 0.7). ^{1}H NMR ($CDCl_3$) δ 1.34 (s, 9H, $C(CH_3)_3$), 2.99 (quintet, 4H, CH_2, pip), 3.44 (br t, J = 4, 4.7 Hz, 2H, CH_2, pip), 3.67 (br t, J = 4, 4.7 Hz, 2H, CH_2, pip), 3.82 (s, 2H, CH_2), 5.29 (s, 1H, NH), 7.39 (d, J = 8.4 Hz, 2H, CH, Ar), 7.46 (d, J = 8.8 Hz, 2H, CH, Ar), 7.64 (d, J = 8.8 Hz, 2H, CH, Ar), 7.73 (d, J = 8.4 Hz, 2H, CH, Ar). ^{13}C NMR ($CDCl_3$) δ 28.3 (CH_3, $C(CH_3)_3$), 41.3 (CH_2), 42.1, 43.9, 45.5, 45.9 (4 x CH_2, pip), 79.9 (C, $C(CH_3)_3$), 127.8, 127.9, 128.4, 128.6, 129.3, 129.4 (8 x CH, Ar), 135.0, 137.5, 145.1 (3 x C, Ar), 134.0 (C-Cl), 166.9 (C=O), 167.6 (C=O). HPLC: 100% at RT: 4.68 min. HRMS (ES-TOF) m/z calculated mass: 516.1438 $[M + Na]^+$, observed mass: 516.1452 $[M + Na]^+$.

6.4.3.2. General procedure for the preparation of 2-amino-1-(4-(phenyl)sulfonyl)piperazin-1-yl)ethan-1-one (**29a**-**f**)

Procedure 1: a solution of protected compound **28a**-**f** (0.15 mmol) in TFA/ CH_2Cl_2 (20 mL, 75:25 v/v) was stirred o/n at room temperature. The solvent was then evaporated and the residue co-evaporated with ethanol three times. Then the residue was saturated with Et_2O (75 mL), stirred for 2 h to afford a solid TFA salt, which was collected by filtration in quantitative yield.

Procedure 2: 4N HCl in dioxane method is described in Chapter 4.

6.4.3.2.1. 2-Amino-1-(4-tosylpiperazin-1-yl)ethan-1-one trifluoroacetic acid (**29a**) ($C_{15}H_{20}F_3N_3O_5S$, Mol. Wt. 411.40)

Product obtained after washed with Et_2O and collected by filtration as a white powder, yield: 0.28 g (93%), mp = 170 – 172 ^{O}C. TLC: CH_3OH – CH_2Cl_2 1:9 v/v, (R_F = 0.1). ^{1}H NMR (DMSO-d_6) δ 2.41 (s, 3H, CH_3), 2.88 (m, 4H, CH_2, pip), 3.64 (m, 4H, CH_2, pip, overlapped by 3.30 (H_2O peak), 3.82 (br s, 2H, CH_2), 7.48 (d, J = 7.5 Hz, 2H, CH, Ar), 7.64 (d, J = 7.5 Hz, 2H, CH, Ar), 8.03 (s, 3H, NH_3). ^{13}C NMR (DMSO-d_6) δ 21.4 (CH_3), 41.1 (CH_2), 43.9, 46.2 (4 x CH_2, pip), 128.3, 130.3 (4 x CH, Ar), 132.3, 144.6 (2 x C, Ar), 165.4 (C=O). HPLC:

100% at RT: 3.27 min. HRMS (ES-TOF) m/z calculated mass: 411.1076 $[M]^+$, observed mass: 411.0980 $[M]^+$.

6.4.3.2.2. 2-Amino-1-(4-((4-nitrophenyl)sulfonyl)piperazin-1-yl)ethan-1-one trifluoroacetic acid (**29b**) ($C_{14}H_{17}F_3N_4O_7S$, Mol. Wt. 442.37)

Product obtained after washed with Et_2O and collected by filtration as a white powder, yield: 0.3 g (90%), mp = 230 – 232 ^{O}C. TLC: CH_3OH – CH_2Cl_2 1:9 v/v, (R_F = 0.14). ^{1}H NMR (CD_3OD) δ 3.15 (m, 4H, CH_2, pip), 3.55 (br t, J = 4.7, 5.5 Hz, 2H, CH_2, pip), 3.74 (br t, J = 4.7, 5.5 Hz, 2H, CH_2, pip), 3.91 (s, 2H, CH_2), 8.07 (d, J = 8.8 Hz, 2H, CH, Ar), 8.48 (d, J = 8.8 Hz, 2H, CH, Ar). ^{13}C NMR (CD_3OD) δ 42.2 (CH_2), 45.9, 46.2 (4 x CH_2, pip), 124.6, 128.1 (4 x CH, Ar), 145.4, 150.9 (2 x C, Ar), 164.2 (C=O). HPLC: 100% at RT: 3.08 min. HRMS (ES-TOF) m/z calculated mass: 351.0841 $[M + Na]^+$, observed mass: 351.0746 $[M + Na]^+$.

6.4.3.2.3. 1-(4-([1,1'-Biphenyl]-4-yl)sulfonyl)piperazin-1-yl)-2-aminoethan-1-one trifluoroacetic acid (**29c**) ($C_{20}H_{22}F_3N_3O_5S$, Mol. Wt. 437.47)

Product obtained after washed with Et_2O and collected by filtration as a white solid, yield: 0.5 g (56%), mp = 135 – 137 ^{O}C. TLC: CH_3OH – CH_2Cl_2 1:9 v/v, (R_F = 0). ^{1}H NMR (DMSO-d_6) δ 2.96 (br t, J = 4.4, 5.1 Hz, 2H, CH_2, pip), 2.99 (br t, J = 4.4, 5.1 Hz, 2H, CH_2, pip), 3.48 (br t, J = 4.4, 5.1 Hz, 2H, CH_2, pip), 3.63 (br t, J = 4.4, 5.1 Hz, 2H, CH_2, pip), 3.84 (s, 2H, CH_2), 7.47 (t, J = 6.7, 7.1 Hz, 1H, CH, Ar), 7.54 (t, J = 6.7, 7.1 Hz, 2H, CH, Ar), 7.76 (d, J = 7.1 Hz, 2H, CH, Ar), 7.83 (d, J = 8.3 Hz, 2H, CH, Ar), 7.97 (d, J = 8.3 Hz, 2H, CH, Ar) overlapped by 8.03 NH_3 (s, 3H, NH_3). ^{13}C NMR (DMSO-d_6) δ 41.2 (CH_2), 43.9, 46.2 (4 x CH_2, pip), 127.6, 128.1, 128.7, 129.2, 129.7 (9 x CH, Ar), 133.9, 138.7, 145.4 (3 x C, Ar), 165.2 (C=O). HPLC: 98.1% at RT: 3.78 min. HRMS (ES-TOF) m/z calculated mass: 382.1304 $[M + Na]^+$, observed mass: 382.1209 $[M + Na]^+$.

6.4.3.2.4. 2-Amino-1-(4-((4'-methoxy-[1,1'-biphenyl]-4-yl)sulfonyl)piperazin-1-yl)ethan-1-one hydrogen chloride (**29d**) ($C_{19}H_{24}ClN_3O_4S$, Mol. Wt. 425.93)

Product obtained after washing with CH_2Cl_2, collected by filtration and dried (vacuum oven at 40 ^{o}C) as a white solid, yield: 0.26 g (46%), mp = 258 – 260 ^{O}C. TLC: CH_3OH – CH_2Cl_2 1:9 v/v, (R_F = 0.1). ^{1}H NMR (DMSO-d_6) δ 2.98 (br d, J = 2.9 Hz, 4H, CH_2, pip), 3.47 (br s, 2H, CH_2, pip), 3.61 (br s, 2H, CH_2, pip), 3.81 (s, 3H, OCH_3) overlapped by 3.82 (s,

2H, CH_2), 7.09 (d, J = 7.7 Hz, 2H, CH, Ar), 7.73 (d, J = 7.7 Hz, 2H, CH, Ar), 7.79 (d, J = 7.9 Hz, 2H, CH, Ar), 7.92 (d, J = 7.9 Hz, 2H, CH, Ar), 8.07 (s, 3H, NH_3). ^{13}C NMR (DMSO-d_6) δ 41.2 (CH_2), 43.9, 46.1 (4 x CH_2, pip), 55.8 (OCH_3), 115.1, 127.4, 128.7, 128.8 (8 x CH, Ar), 130.8, 132.9, 144.9 (3 x C, Ar), 160.4 (C-OCH_3), 165.2 (C=O). HPLC: 100% at RT: 3.84 min. HRMS (ES-TOF) m/z calculated mass: 425.1176 $[M]^+$, observed mass: 425.1142 $[M]^+$.

6.4.3.2.5. 2-Amino-1-(4-((4'-fluoro-[1,1'-biphenyl]-4-yl)sulfonyl)piperazin-1-yl)ethan-1-one hydrogen chloride (**29e**) ($C_{18}H_{21}ClFN_3O_3S$, Mol. Wt. 413.89)

Product obtained after washing with CH_2Cl_2, collected by filtration and dried (vacuum oven at 40 ^oC) as a white solid, yield: 0.14 g (54%), mp = 250 – 252 ^OC. TLC: CH_3OH – CH_2Cl_2 1:9 v/v, (R_F = 0). ^{1}H NMR (CD_3OD) δ 3.09 (br t, J = 4.9, 4.9 Hz, 2H, CH_2, pip), 3.12 (br t, J = 4.9, 5.4 Hz, 2H, CH_2, pip), 3.56 (br t, J = 4.5, 4.9 Hz, 2H, CH_2, pip), 3.74 (br t, J = 4.5, 5.4 Hz, 2H, CH_2, pip), 3.91 (s, 2H, CH_2) 7.26 (t, J = 8.6, 9 Hz, 2H, CH, Ar), 7.74 (dd, J = 5.4, 8.6 Hz, 2H, CH, Ar), 7.88 (s, 4H, CH, Ar). ^{13}C NMR (CD_3OD) δ 41.2 (CH_2), 39.5, 43.9, 45.6, 45.7 (4 x CH_2, pip), 115.3, 115.7, 127.4, 128.2, 128.8, 128.9 (8 x CH, Ar), 133.9, 135.2, 144.9 (3 x C, Ar), 164.3 (C-F), 167.6 (C=O). HPLC: 100% at RT: 3.82 min. HRMS (ES-TOF) m/z calculated mass: 400.1209 $[M + Na]^+$, observed mass: 400.1107 $[M + Na]^+$.

6.4.3.2.6. 2-Amino-1-(4-((4'-chloro-[1,1'-biphenyl]-4-yl)sulfonyl)piperazin-1-yl)ethan-1-one hydrogen chloride (**29f**) ($C_{18}H_{21}Cl_2N_3O_3S$, Mol. Wt. 430.34)

Product obtained after washing with CH_2Cl_2, collected by filtration and dried (vacuum oven at 40 ^oC) as a white solid, yield: 0.4 g (73%), mp = 268 – 270 ^OC. TLC: CH_3OH – CH_2Cl_2 1:9 v/v, (R_F = 0.1). ^{1}H NMR (CD_3OD) δ 3.11 (m, 4H, CH_2, pip), 3.55 (br t, J = 5, 5.2 Hz, 2H, CH_2, pip), 3.74 (br t, J = 4.6, 5,2 Hz, 2H, CH_2, pip), 3.91 (s, 2H, CH_2) 7.26 (d, J = 8.5 Hz, 2H, CH, Ar), 7.71 (d, J = 8.7 Hz, 2H, CH, Ar), 7.89 (br s, 4H, CH, Ar). ^{13}C NMR (CD_3OD) δ 41.2 (CH_2), 39.5, 43.8, 45.6, 45.7 (4 x CH_2, pip), 127.4, 128.3, 128.5, 128.9 (8 x CH, Ar), 134.4, 137.6, 144.7 (3 x C, Ar), 164.3 (C-Cl), 167.6 (C=O). HPLC: 100% at RT: 3.98 min. HRMS (ES-TOF) m/z calculated mass: 416.0914 $[M + Na]^+$, observed mass: 416.0783 $[M + Na]^+$.

6.4.3.3. General procedure for the preparation of 1-(3,4-dimethylisoxazol-5-yl)-3-(2-(4-(phenyl)sulfonyl)piperazin-1-yl)-2-oxoethyl)urea (**30a**-**f**)

The general procedure for the preparation of 1-(3,4-dimethylisoxazol-5-yl)-3-(2-(4-(phenyl)sulfonyl)piperazin-1-yl)-2-oxoethyl)urea (**30a**-**f**) is described in the methods section in Chapter 5.

6.4.3.3.1. 1-(3,4-Dimethylisoxazol-5-yl)-3-(2-oxo-2-(4-tosylpiperazin-1-yl)ethyl)urea (**30a**) ($C_{19}H_{25}N_5O_5S$, Mol. Wt. 435.50)

Product obtained after gradient column chromatography and collected at 6:94 v/v CH_3OH – CH_2Cl_2 to give a white solid, yield: 0.17 g (65%), mp = 124 – 126 ^{O}C. TLC: CH_3OH – CH_2Cl_2 1:9 v/v, (R_F = 0.5). ^{1}H NMR ($CDCl_3$) δ 1.84 (s, 3H, CH_3), 2.14 (s, 3H, CH_3), 2.44 (s, 3H, CH_3), 3.02 (m, 4H, CH_2, pip), 3.53 (br t, J = 4.9, 4.9 Hz, 2H, CH_2, pip), 3.68 (br t, J = 4.9, 4.9 Hz, 2H, CH_2, pip), 4.06 (s, 2H, CH_2), 6.69 (br s, 1H, NH), 7.34 (d, J = 8.1 Hz, 2H, CH, Ar), 7.62 (d, J = 8.1 Hz, 2H, CH, Ar), 8.38 (s, 1H, NH). ^{13}C NMR ($CDCl_3$) δ 6.7 (CH_3), 10.7 (CH_3), 21.6 (CH_3), 41.2 (CH_2), 41.9, 42.8, 44.1, 45.9 (4 x CH_2, pip), 100.2, 153.7, 157.1 (3 x C, isoxazole), 127.8, 130.2 (4 x CH, Ar), 132.1, 144.3 (2 x C, Ar), 161.8 (C=O), 167.4 (C=O). HPLC: 100% at RT: 4.04 min. HRMS (ES-TOF) m/z calculated mass: 458.1576 $[M + Na]^+$, observed mass: 458.1474 $[M + Na]^+$.

6.4.3.3.2. 1-(3,4-Dimethylisoxazol-5-yl)-3-(2-(4-((4-nitrophenyl)sulfonyl)piperazin-1-yl)-2-oxoethyl)urea (**30b**) ($C_{18}H_{22}N_6O_7S$, Mol. Wt. 466.47)

Product obtained after gradient column chromatography and collected at 4:96 v/v CH_3OH – CH_2Cl_2 to give a white solid, yield: 0.1 g (34%), mp = 228 – 230 ^{O}C. TLC: CH_3OH – CH_2Cl_2 1:9 v/v, (R_F = 0.7). ^{1}H NMR (DMSO-d_6) δ 1.74 (s, 3H, CH_3), 2.12 (s, 3H, CH_3), 2.99 (s, 2H, CH_2, pip), 3.03 (s, 2H, CH_2, pip), 3.50 (s, 2H, CH_2, pip), 3.57 (s, 2H, CH_2, pip), 3.92 (d, J = 4.8 Hz, 2H, CH_2), 6.51 (t, J = 4.8, 4.8 Hz, 1H, NH), 8.01 (d, J = 8.6 Hz, 2H, CH, Ar), 8.45 (d, J = 8.6 Hz, 2H, CH, Ar), 9.18 (s, 1H, NH). ^{13}C NMR (DMSO-d_6) δ 6.9 (CH_3), 10.7 (CH_3), 41.1 (CH_2), 43.5, 43.7, 46.0, 46.1 (4 x CH_2, pip), 100.3, 153.6, 158.6 (3 x C, isoxazole), 125.3, 129.6 (4 x CH, Ar), 141.1, 150.7 (2 x C, Ar), 161.5 (C=O), 167.7 (C=O). HPLC: 100% at RT: 3.98 min. HRMS (ES-TOF) m/z calculated mass: 489.1271 $[M + Na]^+$, observed mass: 489.1139 $[M + Na]^+$.

6.4.3.3.3. 1-(2-(4-([1,1'-Biphenyl]-4-ylsulfonyl)piperazin-1-yl)-2-oxoethyl)-3-(3,4-dimethylisoxazol-5-yl)urea (**30c**) ($C_{24}H_{27}N_5O_5S$, Mol. Wt. 497.57)

Product obtained after gradient column chromatography and collected at 7:93 v/v CH_3OH – CH_2Cl_2 to give a white semisolid, yield: 0.05 g (25%), TLC: CH_3OH – CH_2Cl_2 0.25:9.75 v/v, (R_F = 0.3). ^{1}H NMR ($CDCl_3$) δ 1.76 (s, 3H, CH_3), 2.07 (s, 3H, CH_3), 3.01 (m, 4H, CH_2, pip), 3.46 (br t, J = 4.7, 4.7 Hz, 2H, CH_2, pip), 3.64 (br t, J = 4.7, 4.7 Hz, 2H, CH_2, pip), 3.98 (s, 2H, CH_2), 6.53 (br s, 1H, NH), 7.35 (t, J = 7.4, 7.4 Hz, 1H, CH, Ar), 7.41 (t, J = 7.4, 7.4 Hz, 2H, CH, Ar), 7.52 (d, J = 7.4 Hz, 2H, CH, Ar), 7.66 (d, J = 8.7 Hz, 2H, CH, Ar), 7.72 (d, J = 8.7 Hz, 2H, CH, Ar), 7.91 (s, 1H, NH). ^{13}C NMR ($CDCl_3$) δ 6.7 (CH_3), 10.5 (CH_3), 41.5 (CH_2), 42.0, 44.2, 45.7, 45.9 (4 x CH_2, pip), 100.3, 153.7, 157.1 (3 x C, isoxazole), 127.4, 127.9, 128.3, 128.7, 129.1 (9 x CH, Ar), 133.6, 183.8, 146.2 (3 x C, Ar), 161.9 (C=O), 167.3 (C=O). HPLC: 100% at RT: 4.35 min. HRMS (ES-TOF) m/z calculated mass: 520.1733 $[M + Na]^+$, observed mass: 520.1626 $[M + Na]^+$.

6.4.3.3.4. 1-(3,4-Dimethylisoxazol-5-yl)-3-(2-(4-((4'-methoxy-[1,1'-biphenyl]-4-yl)sulfonyl)piperazin-1-yl)-2-oxoethyl)urea (**30d**) ($C_{25}H_{29}N_5O_6S$, Mol. Wt. 527.60)

Product obtained after gradient column chromatography and collected at 3.5:96.5 v/v CH_3OH – CH_2Cl_2 to give a colourless semisolid, yield: 0.08 g (62%), TLC: CH_3OH – CH_2Cl_2 1:9 v/v, (R_F = 0.3). ^{1}H NMR ($CDCl_3$) δ 1.76 (s, 3H, CH_3), 2.07 (s, 3H, CH_3), 2.99 (m, 4H, CH_2, pip), 3.46 (br t, J = 4.5, 5.2 Hz, 2H, CH_2, pip), 3.63 (br t, J = 4.9, 5.2 Hz, 2H, CH_2, pip), 3.79 (s, 3H, OCH_3), 3.97 (s, 2H, CH_2), 6.52 (br s, 1H, NH), 6.93 (d, J = 8.5 Hz, 2H, CH, Ar), 7.47 (d, J = 7.8 Hz, 2H, CH, Ar), 7.62 (d, J = 8.5 Hz, 2H, CH, Ar), 7.68 (d, J = 7.9 Hz, 2H, CH, Ar), 7.92 (s, 1H, NH). ^{13}C NMR ($CDCl_3$) δ 6.7 (CH_3), 10.6 (CH_3), 41.5 (CH_2), 42.0, 42.1, 44.2, 45.9 (4 x CH_2, pip), 55.4 (OCH_3), 100.3, 153.6, 157.0 (3 x C, isoxazole), 114.6, 127.3, 130.2, 128.5 (8 x CH, Ar), 131.2, 131.3, 132.9, 160.2 (4 x C, Ar), 161.9 (C=O), 167.3 (C=O). HPLC: 97.7% at RT: 4.33 min. HRMS (ES-TOF) m/z calculated mass: 528.1839 $[M + H]^+$, observed mass: 528.1924 $[M + H]^+$.

Chapter 7: Miscellaneous compounds (Series 5 and 6)

7. Introduction

This chapter discusses the preparation of 1-(3,4-dimethylisoxazol-5-yl)-3-(2-((3-phenyl-1,2,4-thiadiazol-5-yl)amino)ethyl)urea (**44**) and *N*-(3,4-dimethylisoxazol-5-yl)-4-(3-phenyl-1,2,4-thiadiazol-5-yl)piperazine-1-carboxamide (**45**) 3-methyl or 3,4-dimethyl-(4-(4-chlorophenoxypiperidin-1-yl)benzylamine)isoxazole-sulphonamide derivatives (**60a** and **60b**), presented in scheme 5 and scheme 6 respectively. In both series, the amino acid isosteric moiety was the same as that in series 3 and 4 (3,4-dimethyl isoxazole), while for series 5, the adenine base was an aryl moiety and the linker consisted of piperazine or ethyl diamine linked to a thiadiazole ring but in series 6, the adenine base was replaced by phenoxy piperidine linked to benzyl sulphonamide (Table 56). The rational for the design of series 5 and 6 was to improve the fitting of designed compounds through adding thiadiazole or benzyl rings as mimics of the ribose sugar of AMP.

Table 56: General chemical structures of schemes 5 and 6 AspRS and AsnRS inhibitors.

Series	Chemical structures
5	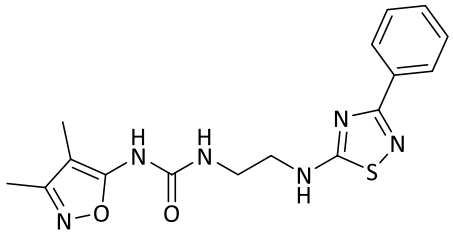
5	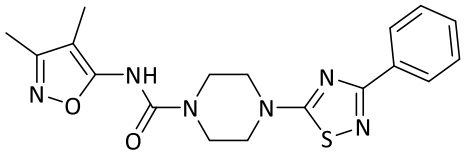
6	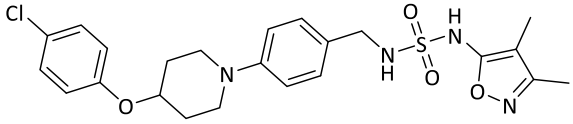
6	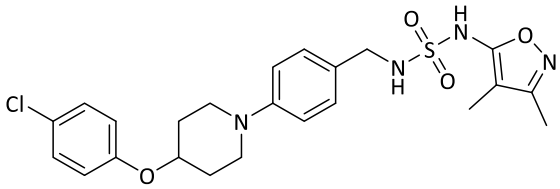

This chapter is divided into four parts as follows:

▪ Results and discussion

▪ Docking studies

▪ Biological screening

▪ Methods

7.1. Synthetic pathway for 1-(3,4-dimethylisoxazol-5-yl)-3-(2-((3-phenyl-1,2,4-thiadiazol-5-yl)amino)ethyl)urea (44) and *N*-(3,4-dimethylisoxazol-5-yl)-4-(3-phenyl-1,2,4-thiadiazol-5-yl)piperazine-1-carboxamide (45) (Series 5)

The synthetic pathways for the preparation of compounds (**44**) and (**45**) are shown in scheme 13a and 13b and involved the following steps:

- Protection reaction of ethylenediamine (**33**).
- Nucleophilic substitution reaction of 2,2,2-trichloroethyl (3,4-dimethylisoxazol-5-yl)carbamate with *tert*-butyl (2-aminoethyl)carbamate or tert-butyl piperazine-1-carboxylate (**34**) and (**37**).
- Deprotection of the Boc group using HCl/dioxane (**35**) and (**38**).
- Pinner reaction for ethyl benzimidate hydrochloride preparation (**41**).
- Nucleophilic substitution for benzamidines hydrochloride preparation (**42**).
- Cyclisation reaction for 5-chloro-3-phenyl-1,2,4- thiadiazole preparation (**43**).
- Nucleophilic substitution reaction of 5-chloro-3-phenyl-1,2,4-thiadiazol with 1-(2-aminoethyl)-3-(3,4-dimethylisoxazol-5-yl)urea hydrochloride or *N*-(3,4-dimethylisoxazol-5-yl)piperazine-1-carboxamide hydrochloride (**44**) and (**45**).

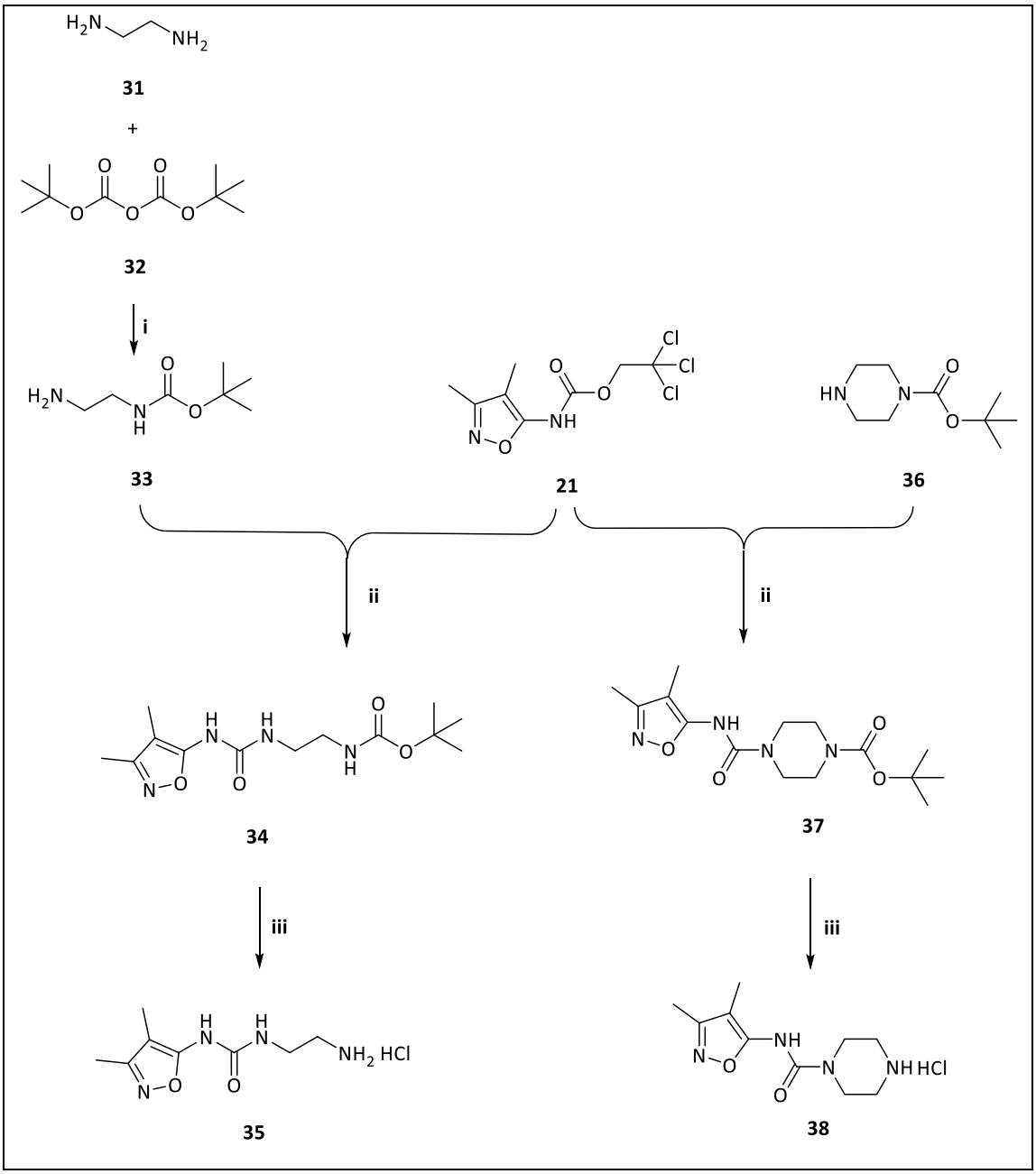

Scheme 13a: Synthetic pathway for 1-(2-Aminoethyl)-3-(3,4-dimethylisoxazol-5-yl)urea hydrochloride (**35**) and *N*-(3,4-Dimethylisoxazol-5-yl)piperazine-1-carboxamide 2,2,2-trifluoroacetic acid (**38**). *Reagents and conditions*: (i) dry CH_2Cl_2, 0 ^{O}C, 1 h, then rt o/n. (ii) *N*-ethyldiisopropylamine, DMSO, 70 ^{O}C 2-24 h. (iii) HCl/dioxane 0 ^{O}C 10 min, then rt 50 min.

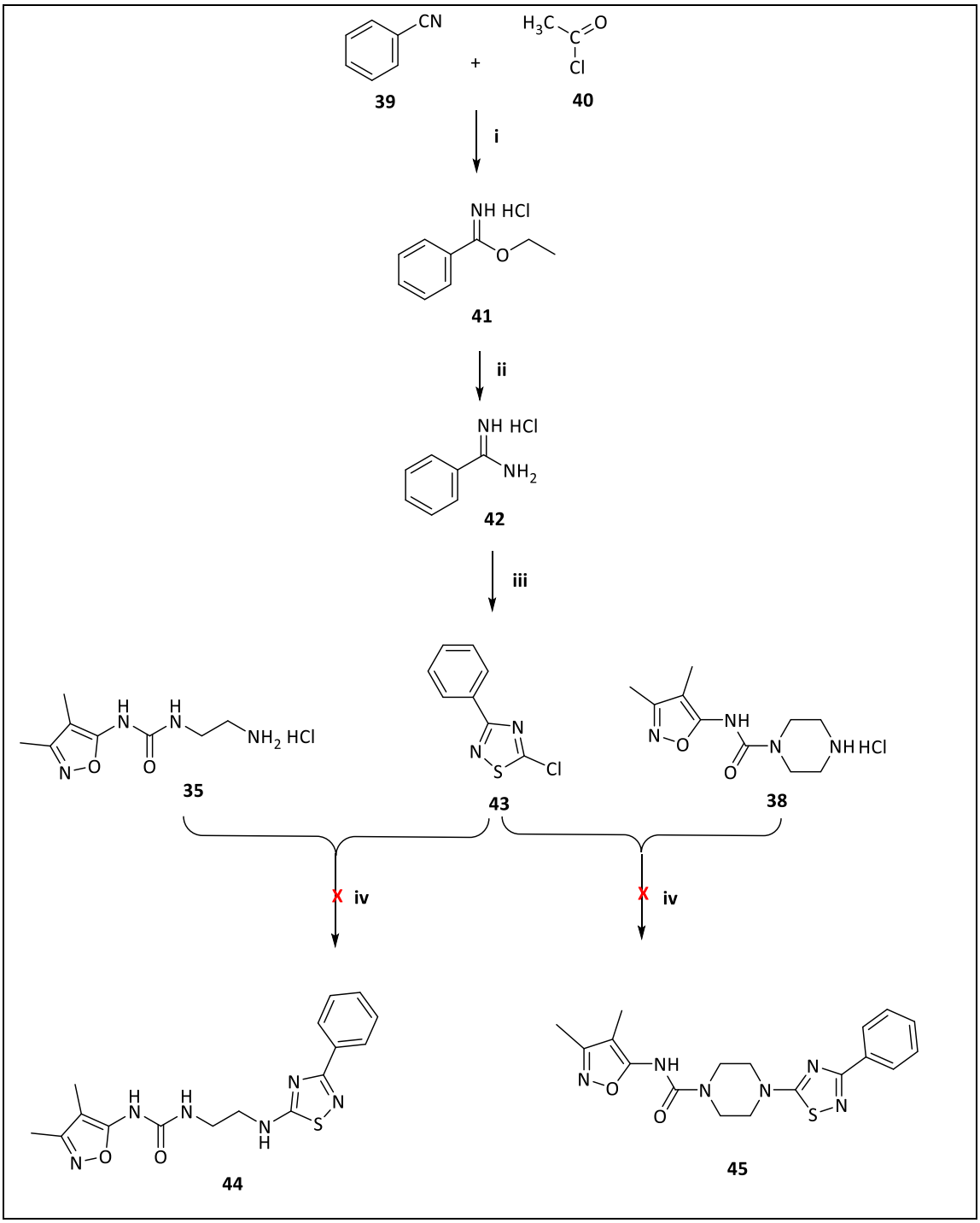

Scheme 13b: Synthetic pathway for 1-(3,4-dimethylisoxazol-5-yl)-3-(2-((3-phenyl-1,2,4-thiadiazol-5-yl)amino)ethyl)urea (**44**) and *N*-(3,4-dimethylisoxazol-5-yl)-4-(3-phenyl-1,2,4-thiadiazol-5-yl)piperazine-1-carboxamide (**45**). *Reagents and conditions*: (i) Acetyl chloride (**40**), benzonitrile (**39**), EtOH, 10 ^{O}C then rt 48 h. (ii) EtOH, ammonia in MeOH rt, 24 h. (iii) perchloromethyl mercaptan, CH_2Cl_2, aq. NaOH, 0 ^{O}C, 1 h then rt, 2 h. (iv) Et_3N, NaI, MeCN, 90 ^{O}C o/n.

7.1.1. Synthesis of *tert*-butyl (2-aminoethyl)carbamate (33)

Di-*tert*-butyl dicarbonate (**32**) is widely used in organic synthesis as a reagent to protect amino groups and the preparation of *tert*-butyl (2-aminoethyl)carbamate (**33**) was successfully performed with ethylenediamine (**31**) in CH_2Cl_2 (356) producing the product in a good yield (Table 57).To avoid the protection of both amino groups, the quantity of ethylenediamine (**31**) used in this reaction was much higher than that of di-*tert*-butyl dicarbonate (**32**) and the excess ethylenediamine removed by aqueous extraction.^{1}H NMR confirmed the formation of the product.

Table 57: Identification data for *tert*-butyl (2-aminoethyl)carbamate (**33**).

Compd	Yield (%)	mp (^{O}C)	Appearance
33	77	110-112	White powder

7.1.2. Synthesis of *tert*-butyl (2-(3-(3,4-dimethylisoxazol-5-yl)ureido)ethyl)carbamate (34)

2,2,2-Trichloroethyl(3,4-dimethylisoxazol-5-yl)carbamate (**21**) was reacted with *tert*-butyl (2-aminoethyl)carbamate (**33**) in the presence of *N*-ethyldiisopropylamine as a base and DMSO as solvent to give a good yield of *tert*-butyl (2-(3-(3,4-dimethylisoxazol-5-yl)ureido)ethyl)carbamate (**34**) after stirring the reaction at 70 ^{O}C overnight (347) (Table 58). The ^{1}H NMR spectrum of compound **34** showed the $C(CH_3)_3$ protons as a singlet peak, integrated for 9 protons, two CH_3 protons as two singlet peaks, two CH_2 as quartet peaks and the three NH protons as singlets (Figure 196).

Table 58: Identification data for *tert*-butyl (2-(3-(3,4-dimethylisoxazol-5-yl) ureido) ethyl)carbamate (**34**).

Compd	Yield (%)	Mp (^{O}C)	Appearance
34	54	142-144	White solid

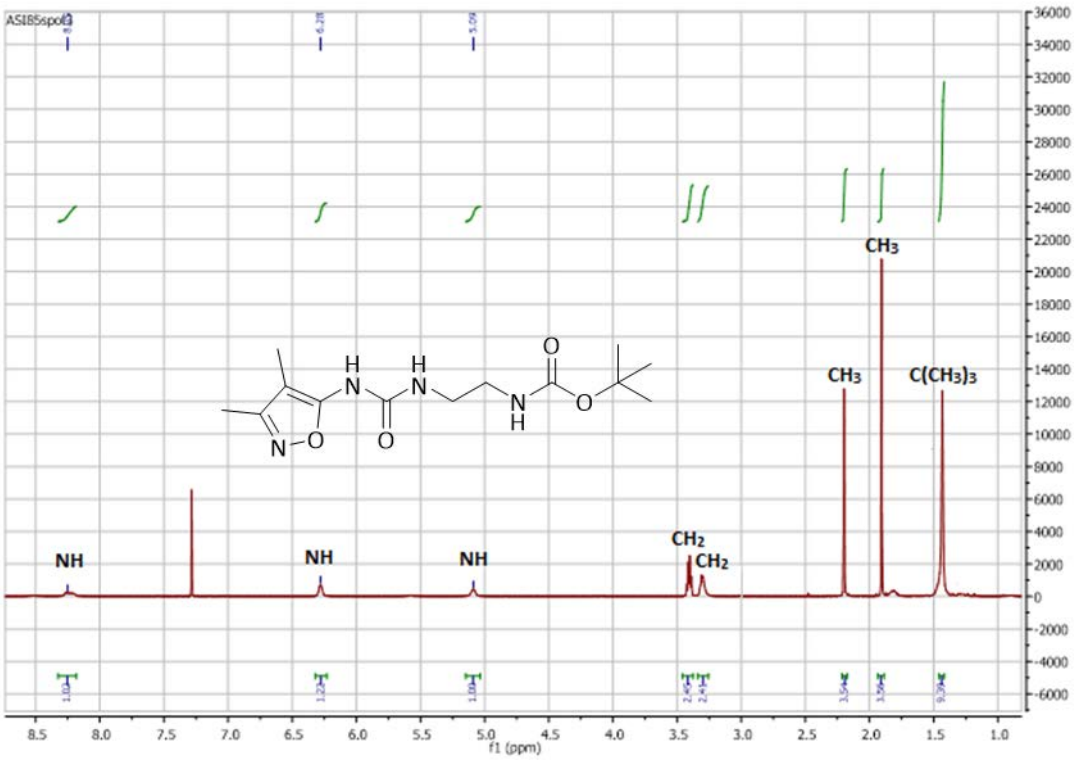

Figure 196: ^{1}H NMR spectrum of compound **34**. The spectrum shows the $C(CH_3)_3$, two CH_3, two CH_2 and three NH protons peaks.

7.1.3. Synthesis of **1-(2-aminoethyl)-3-(3,4-dimethylisoxazol-5-yl)urea hydrochloride** (35)

The deprotection method of Boc group by using HCl/dioxane was described in Chapter 4. In this synthetic pathway, using HCl in dioxane was successful in generating the product (**35**) in a good yield (345) (Table 59). The ^{1}H NMR spectrum confirmed the deprotected structure which showed the two CH_3 signals of 3,4-dimethylisoxazole as two singlet peaks, ethyl protons as two broad quartet peaks, two NHs as two broad singlet peaks and singlet peak for NH_3 (Figure 197).

Table 59: Identification data for 1-(2-aminoethyl)-3-(3,4-dimethylisoxazol-5-yl)urea hydrochloride (**35**).

Compd	Yield (%)	Mp (^oC)	Appearance
35	89	210-212	White solid

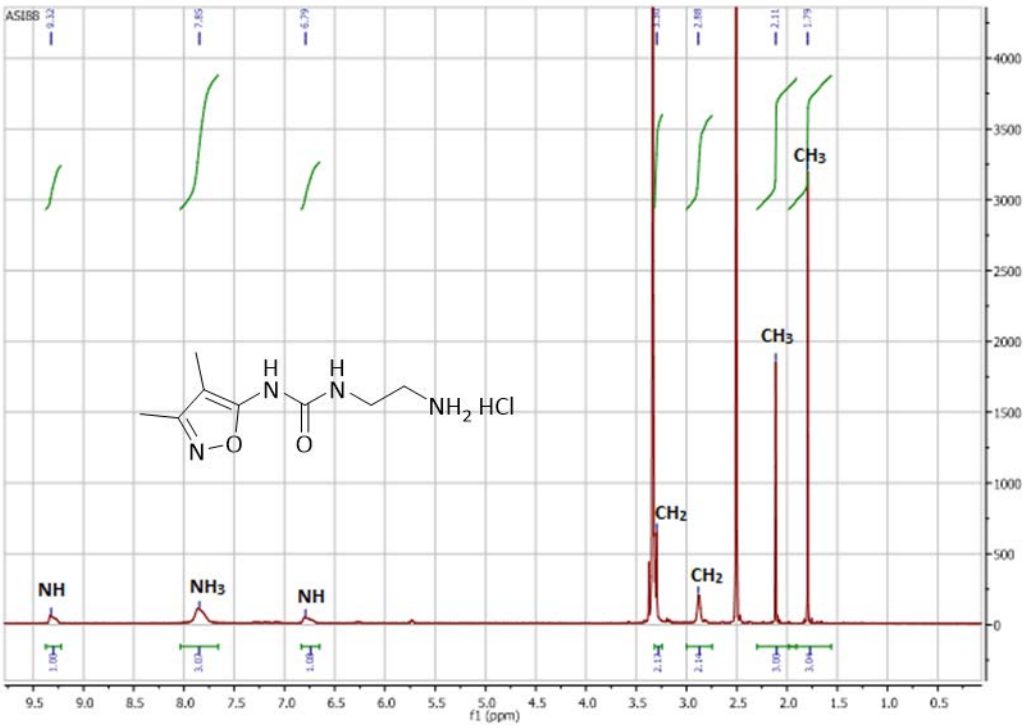

Figure 197: ^{1}H NMR spectrum of compound **35**. The spectrum shows the NH_3 as a singlet peak and disappearance of the Boc group.

7.1.4. Synthesis of *tert*-butyl 4-((3,4-dimethylisoxazol-5-yl)carbamoyl)piperazine-1-carboxylate (37)

Using the same procedure described for compound **34**, compound **37** was prepared in a good yield from *tert*-butyl piperazine and 2,2,2-trichloroethyl (3,4-dimethylisoxazol-5-yl)carbamate (**21**) under the same reaction condition (347) (Table 60). The ^{1}H NMR spectrum confirmed the structure of compound **37**, which showed $C(CH_3)_3$ protons as a singlet peak, the two CH_3 signals of 3,4-dimethylisoxazole as two singlet peaks, piperazine protons as two broad triplet peaks and NH proton as a singlet peak (Figure 198).

Table 60: Identification data for *tert*-butyl 4-((3,4-dimethylisoxazol-5-yl)carbamoyl)piperazine-1-carboxylate (**37**).

Compd	Yield (%)	mp (^{O}C)	Appearance
37	74	164-166	Needle crystals

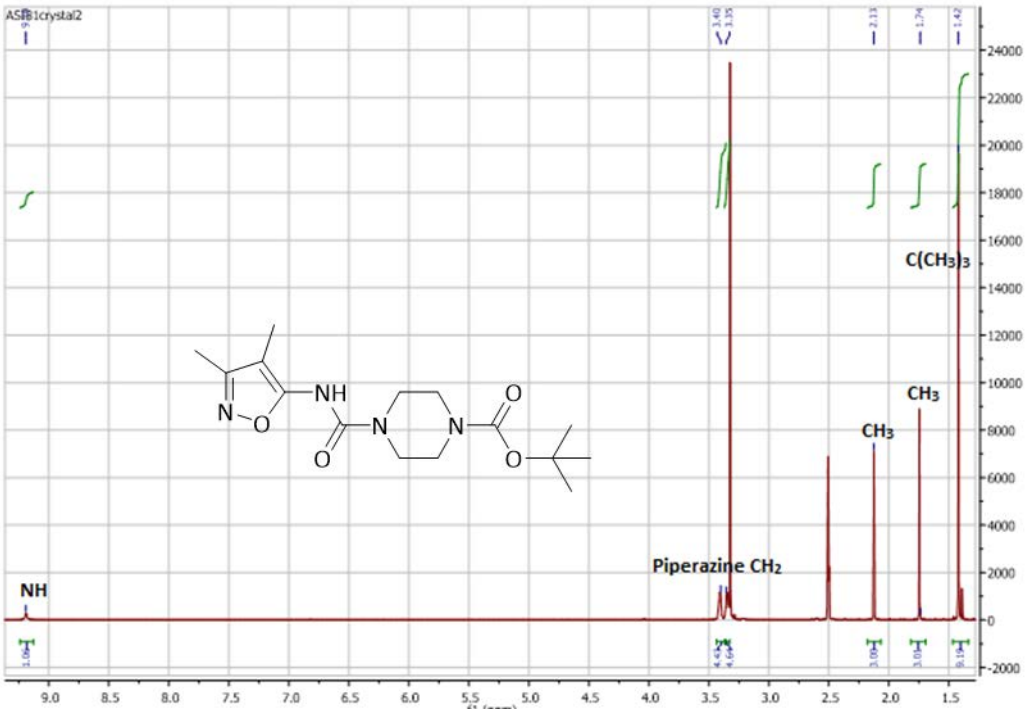

Figure 198: ^{1}H NMR spectrum of compound **37**. The spectrum shows $C(CH_3)_3$, the two CH_3, piperazine CH_2 and NH protons.

7.1.5. Synthesis of *N*-(3,4-dimethylisoxazol-5-yl)piperazine-1-carboxamide hydrochloride (38)

Boc deprotection (HCl/dioxane) was successful in generating the products (**38**) in a good yield (345) (Table 61). The ^{1}H NMR spectrum confirmed the deprotected structure which showed the two CH_3 signals of 3,4-dimethylisoxazole as two singlet peaks, piperazine protons as two broad triplet peaks, NH as a singlet peak and broad singlet peak for NH_2 (Figure 199).

Table 61: Identification data for *N*-(3,4-dimethylisoxazol-5-yl)piperazine-1-carboxamide hydrogen chloride (**38**).

Compd	Yield (%)	Mp (^{o}C)	Appearance
38	90	222-224	White solid

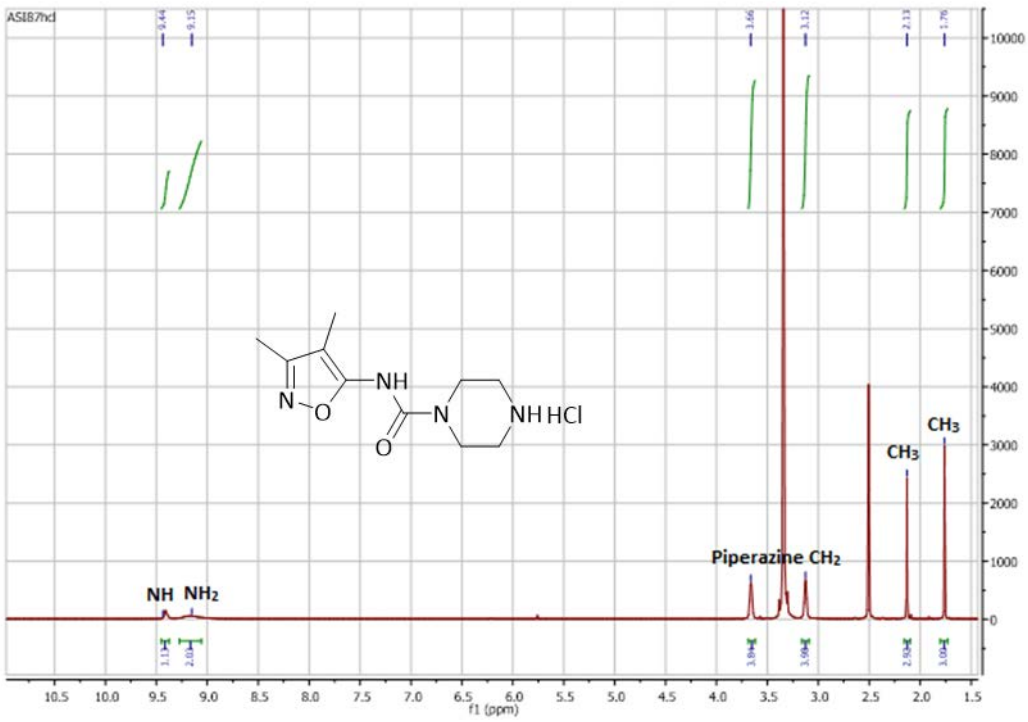

Figure 199: ^{1}H NMR spectrum of compound **38**. The spectrum shows NH_2 protons as a singlet peak and disappearance of the Boc group.

7.1.6. Synthesis of ethyl benzimidate hydrochloride (41)

The Pinner reaction was used to synthesise ethyl benzimidate hydrochloride from benzonitrile (**39**), ethanol and acetyl chloride (**40**) (357, 358 and 359). Benzonitrile (**39**) was dissolved in anhydrous ethanol and, to the cooled solution (0 ^{O}C), acetyl chloride (**40**) was added dropwise to the reaction mixture then stirred at room temperature for 48 h to obtain the product in a good yield (Table 62). In this reaction, the quantity used of acetyl chloride and ethanol was more than that of benzonitrile to generate HCl as a result of esterification reaction between acetyl chloride and ethanol. The generated HCl catalysed the Pinner reaction of benzonitrile with ethanol to form an imino ester salt (Scheme 14). Ethyl benzimidate HCl was successfully prepared, ^{1}H and ^{13}C NMR confirmed formation of the product, although the NH signal was not observed as CD_3OD was used as the NMR spectrum, however the success of the next step confirmed compound **41**.

Table 62: Identification data for ethyl benzimidate hydrochloride (**41**).

Compd	Yield (%)	mp (^{o}C)	Appearance
41	82	122-124	White solid

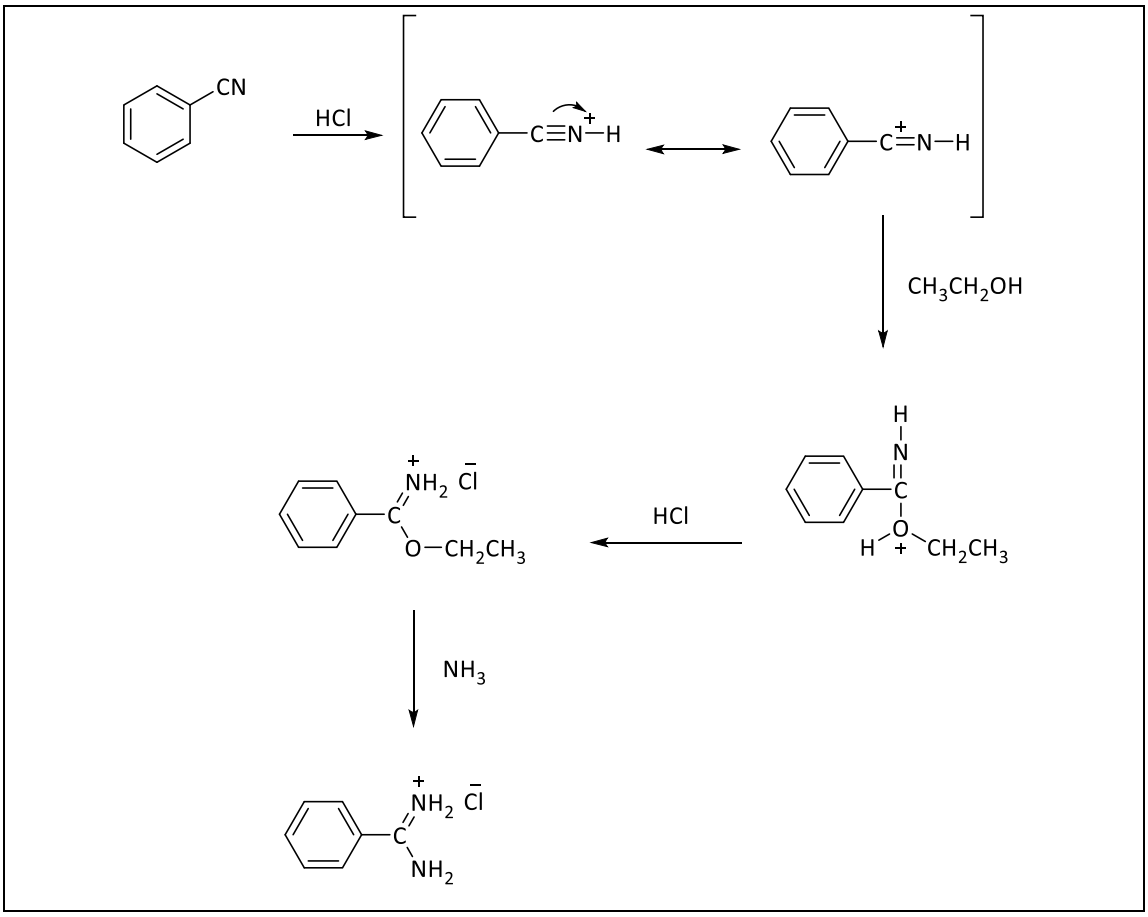

Scheme 14: Suggested mechanism of the Pinner reaction.

7.1.7. Synthesis of benzimidamide hydrochloride (42)

The Pinner salt, ethyl benzimidate hydrochloride (**41**), was reacted with NH_3 generating benzimidamide hydrochloride (**42**) in a good yield (Scheme 14) (Table 63). This reaction was placed in a sealed tube and stirred at room temperature for 24 h. In the ^{1}H NMR spectrum, the NH and NH_3 protons were observed as two singlet peaks integrated for 1 and 3 protons, respectively.

Table 63: Identification data for benzimidamide hydrochloride (**42**).

Compd	Yield (%)	mp (^{O}C)	Appearance
42	90	230-232	White semisolid

7.1.8. Synthesis of 5-chloro-3-phenyl-1,2,4- thiadiazole (43)

This thiadiazole compound (**43**) was obtained from the cyclisation reaction of benzamidine hydrochloride (**42**) with perchloromethyl mercaptan in CH_2Cl_2, followed by addition of a solution of NaOH at low temperature in a yield of 48% (348) (Table 64). Compound **43** was used for the next step without any purification.

Table 64: Identification data for 5-chloro-3-phenyl-1,2,4- thiadiazole (**43**).

Compd	Yield (%)	mp (^{O}C)	Appearance
43	48	-	Yellow semisolid

7.1.9. Synthesis of *N*-(3,4-dimethylisoxazol-5-yl)-4-(3-phenyl-1,2,4-thiadiazol-5-yl) piperazine-1-carboxamide (45)

The Finklestein reaction was used to prepare *N*-(3,4-dimethylisoxazol-5-yl)-4-(3-phenyl-1,2,4-thiadiazol-5-yl) piperazine-1-carboxamide (**45**) from *N*-(3,4-dimethylisoxazol-5-yl)piperazine-1-carboxamide hydrochloride (**38**) and 5-chloro-3-phenyl-1,2,4- thiadiazole (**43**) in the presence of sodium iodide, triethylamine and CH_3CN (347), however it was not successful. This may due to the presence of compound **38** in a salt form, thus, the scheme was reordered to make the Finklestein reaction between *tert*-butyl piperazine (**36**) and 5-chloro-3-phenyl-1,2,4- thiadiazole (**43**) under the same condition and this successfully produced *tert*-butyl 4-(3-phenyl-1,2,4-thiadiazol-5-yl)piperazine-1-carboxylate (**46**) in a satisfactory yield (Scheme 15) (Table 62). Then, the Boc deprotection of compound **46** using HCl/dioxane generated 3-phenyl-5-(piperazin-1-yl)-1,2,4-thiadiazole hydrochloride (**47**) in a good yield (Table 65). Compound **47** was then reacted with 2,2,2-trichloroethyl (3,4-dimethylisoxazol-5-yl)carbamate (**21**) in the last step under nucleophilic substitution reaction to finally prepared *N*-(3,4-dimethylisoxazol-5-yl)-4-(3-phenyl-1,2,4-thiadiazol-5-yl) piperazine-1-carboxamide (**45**) in a lower yield (Table 65) owing to incomplete reaction of **47** with

2,2,2-trichloroethyl (3,4-dimethylisoxazol-5-yl)carbamate (**21**). The reaction mixture was purified by preparative TLC and the purity of the final product (**45**) was confirmed by ^{1}H and ^{13}C NMR and HPLC. The ^{1}H NMR spectrum showed the piperazine protons as a broad singlet peak integrated for 8 protons, aromatic protons as two multiplet peaks integrated for 2 and 3 protons respectively and one singlet peak for NH (Figure 200). However, the preparation of 1-(3,4-dimethylisoxazol-5-yl)-3-(2-((3-phenyl-1,2,4-thiadiazol-5-yl)amino)ethyl)urea (**44**) was not successful using this synthetic scheme.

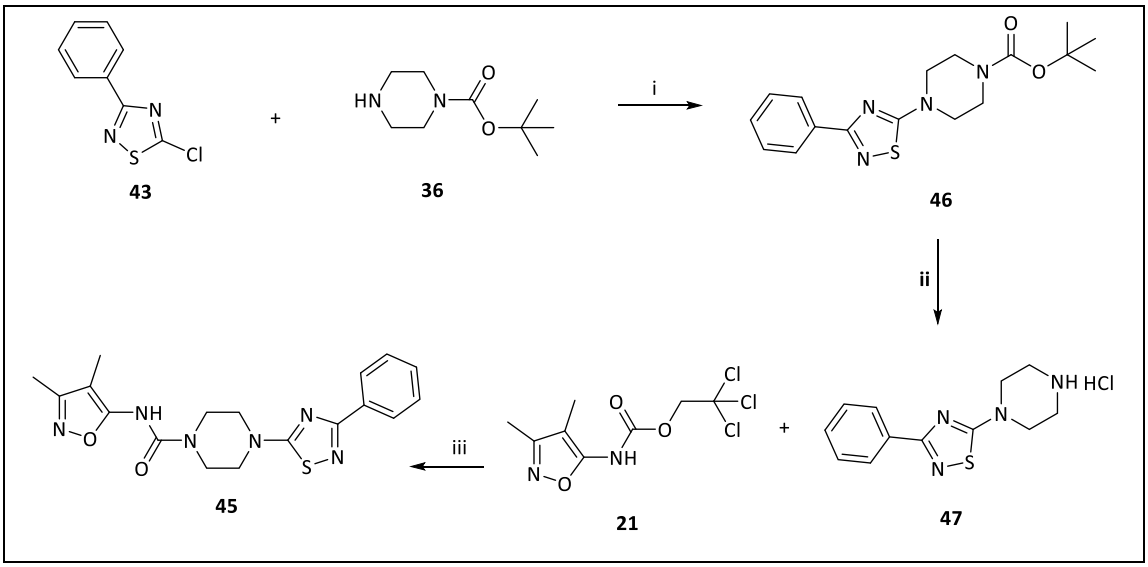

Scheme 15: Synthetic pathway for *N*-(3,4-dimethylisoxazol-5-yl)-4-(3-phenyl-1,2,4-thiadiazol-5-yl)piperazine-1-carboxamide (**45**).

Table 65: Identification data for tert-butyl 4-(3-phenyl-1,2,4-thiadiazol-5-yl)piperazine-1-carboxylate (**46**), 3-phenyl-5-(piperazin-1-yl)-1,2,4-thiadiazole hydrochloride (**47**) and *N*-(3,4-dimethylisoxazol-5-yl)-4-(3-phenyl-1,2,4-thiadiazol-5-yl) piperazine-1-carboxamide (**45**).

Compd	**Yield (%)**	**Mp (^{o}C)**	**Appearance**
46	34	-	white semisolid
47	69	190-192	Pale yellow solid
45	16	-	White semisolid

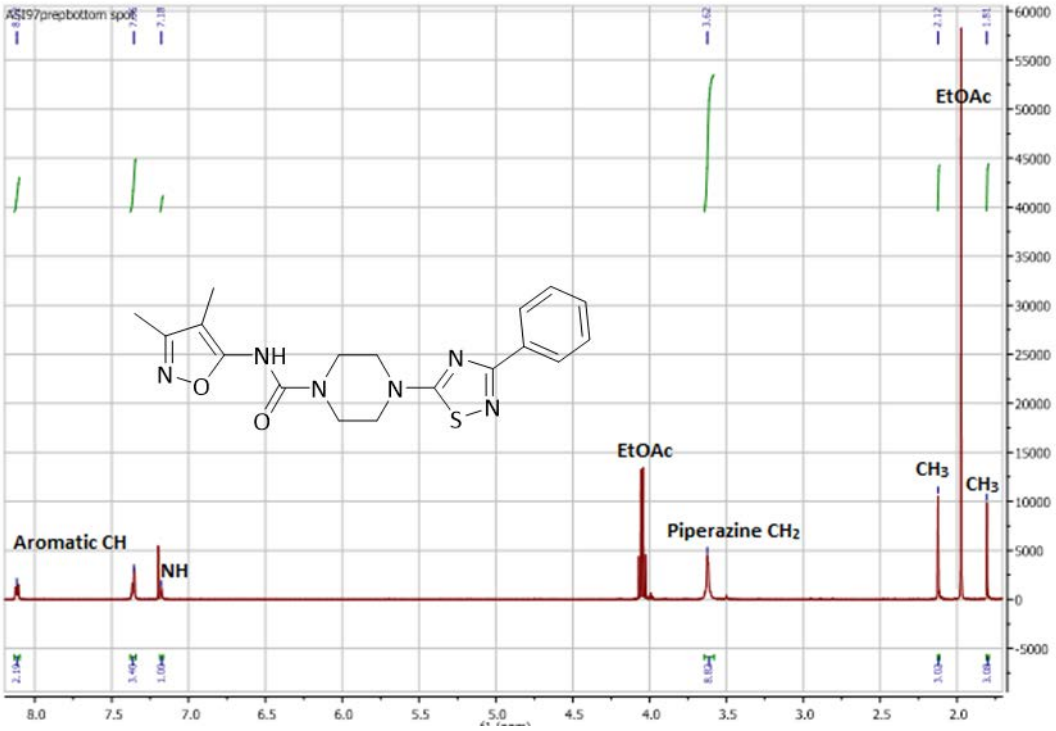

Figure 200: ^{1}H NMR spectrum of compound **45**. The spectrum shows two CH_3, piperazine, NH and aromatic protons.

7.2. Synthetic pathway for 1-(3-methyl or 3,4-dimethylisoxazol-5-yl)-3-(4-(4-chlorophenoxypiperidin-1-yl)benzyl) sulfuric diamide (Series 6)

Due to the importance of the piperidine heterocycle in the wide range of its therapeutic applications, synthesising scaffolds containing this moiety may generate the highest therapeutic efficacy (360). Series 6 compounds consists of phenoxy piperidine linked to benzyl sulphonamide and 3-methyl or 3,4-dimethylisoxazole instead of Asp and Asn amino acids and the synthetic pathways are shown in scheme 16 and involved the following steps:

- Nucleophilic reaction of 4-fluorobenzonitril with hydroxy piperidine (**50**).
- Mitsunobu reaction for 4-(4-phenoxypiperidin-1-yl)benzonitrile derivatives (**52**).
- Reduction reaction for methaneamine formation (**55**).
- Nucleophilic substitution for synthesis of 2-oxo-N-(4-(4-phenoxypiperidin-1-yl) benzyl) oxazolidine-3-sulfonamide derivatives (**57**).
- Nucleophilic reaction for sulphonamide derivatives synthesis (**58**).

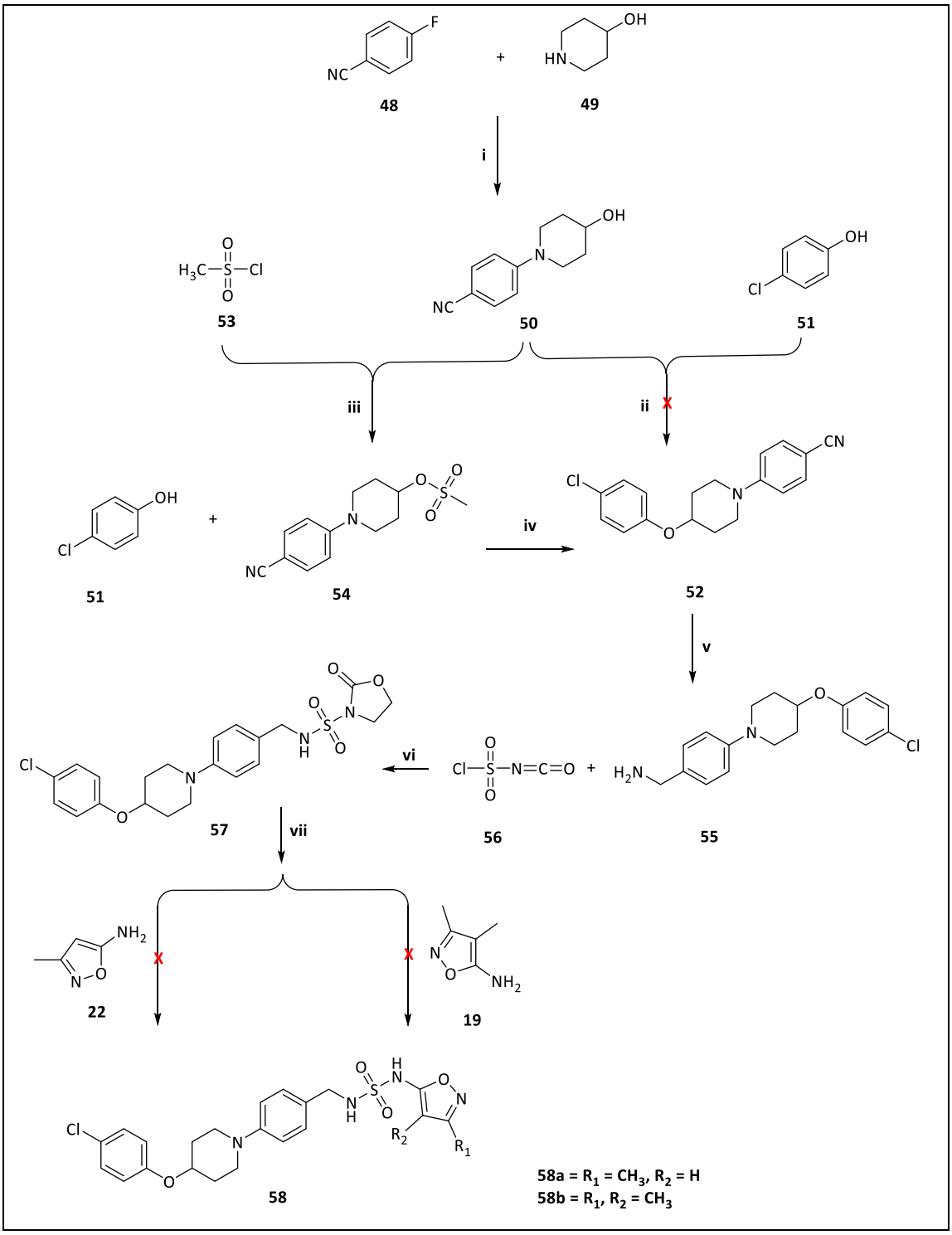

Scheme 16: Synthetic pathway for 3-methyl or 3,4-dimethyl-(4-(4-chlorophenoxypiperidin-1-yl) benzylamine) isoxazole sulphonamides (**58**). *Reagents and condition*: (i) K_2CO_3, DMF, 150 ^{O}C, 6 h, (ii) diisopropyl azodicarboxylate (DIAD), triphenyl phosphine (PPh_3), CH_2Cl_2, rt, o/n, (iii) Et_3N, CH_2Cl_2, rt, 1 h, (iv) K_2CO_3, *tert*-butyl ammonium bromide (v) $LiAlH_4$, THF, 0 ^{O}C, then rt, 2 h. (vi) 2-bromoethanol, chlorosulfonyl isocyanate (**56**), benzylamine derivatives (**57**), Et_3N, CH_2Cl_2, rt, (vii) 5-amino-3,4-methylisoxazole (**19**) or 5-amino-3-methylisoxazole (**22**), Et_3N, CH_3CN.

7.2.1. Synthesis of 4-(4-hydroxypiperidin-1-yl)benzonitrile (50)

4-Hydroxy-piperidine benzonitrile (**50**) was prepared in a good yield by the reaction of 4-flouorobenzonitrile (**48**) and 4-hydroxypiperidine (**49**) in the presence of the activated potassium carbonate as a base and DMF as solvent (361) (Scheme 16) (Table 66). ^{1}H NMR spectrum proved the structure of compound **50** through disappearance of NH signal of 4-hydroxypiperidine (**49**), while the piperidine ring, OH and aromatic protons were shown in the spectrum as three multiplet signals, singlet and two doublet peaks respectively (Figure 201). Compound **52** was pure enough to be used in the next step.

Table 66: Identification data for 4-(4-hydroxypiperidin-1-yl)benzonitrile (**50**).

Compd	Yield (%)	Mp (^{O}C)	Appearance
50	82	86-88	Pale shiny powder

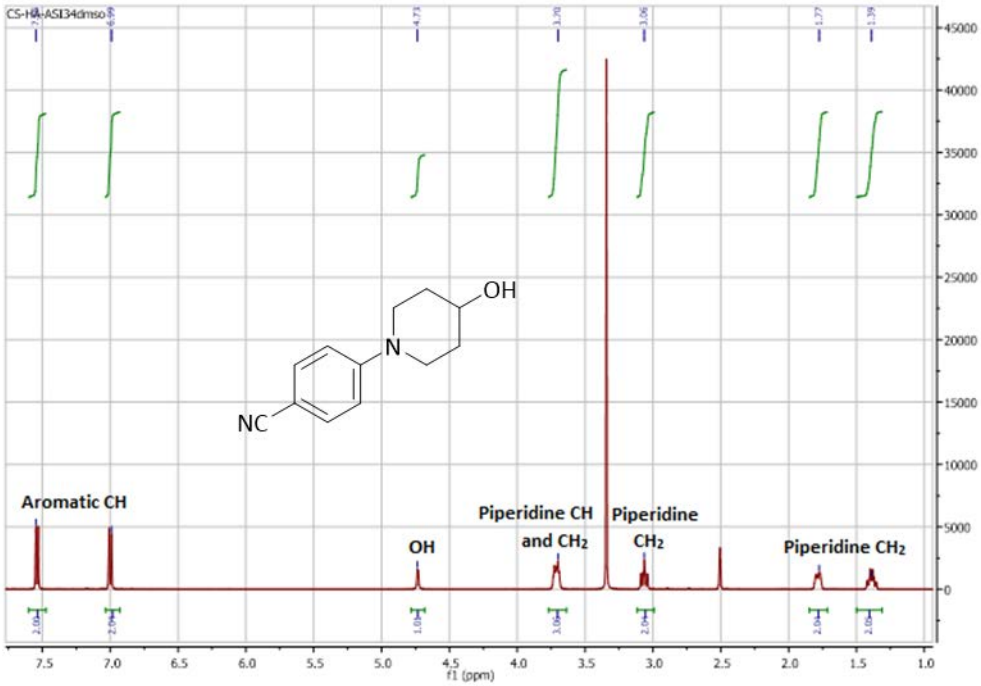

Figure 201: ^{1}H NMR spectrum of compound **50**. The spectrum shows piperidine ring, aromatic and OH protons.

7.2.2. Synthesis of 4-(4-(4-chlorophenoxy)piperidin-1-yl)benzonitrile (52)

4-(4-(4-Chlorophenoxy)piperidin-1-yl)benzonitrile (**52**) was prepared by the reaction of 4-chlorophenol (**53**) and 4-(4-hydroxypiperidine-1-yl)benzonitrile (**52**) in the presence of diisopropyl azodicarboxylate (DIAD) and triphenyl phosphine (PPh_3) as reagents and CH_2Cl_2 as a solvent in a Mitsunobu reaction (Scheme 17) (362-365). The Mitsunobu reaction is a dehydrative coupling of a primary or secondary alcohol to a pronucleophile, which results in a hydrazine derivative as a reduced product of the azo species and phosphine oxide as an oxidised product of phosphine. Both by-products are difficult to remove during the purification process (366). The Mitsunobu reaction can be done under mild condition, generally at 0 ^{0}C to room temperature, using standard solvents such as THF, diethyl ether, dichloromethane, ethyl acetate, acetonitrile and DMF (367, 368). In this synthetic step, 4-chlorophenol (**51**) was used as the pronucleophile with a pKa 9.26. Acidity is one of limitations to the reaction success with the final product depending on the acidic reagent and the used nucleophile, which must have a pKa lower than 11 as the resulting betaine from the reaction of DIAD and PPh_3 is about 13, and therefore removes the acidic proton from the pronucleophile, otherwise alkylation of DIAD will occur (364, 366). The mechanism of the reaction is started by attack of PPh_3 on DIAD to form a zwitterionic intermediate, followed by deprotonation of the acidic compound normally by the action of the intermediate, to afford the anionic nucleophile. Then, 4-(4-(4-chlorophenoxy)piperidin-1-yl)benzonitrile (**50**) binds to the phosphonium ion and the nucleophile performs a SN2 attack to yield the final substitution product **52** and triphenyl phosphine oxide ($Ph_3P=O$) (Scheme 13). This step was not reproducible to prepare a high percentage yield of pure compound **52** and after purification process its yield was 28%.

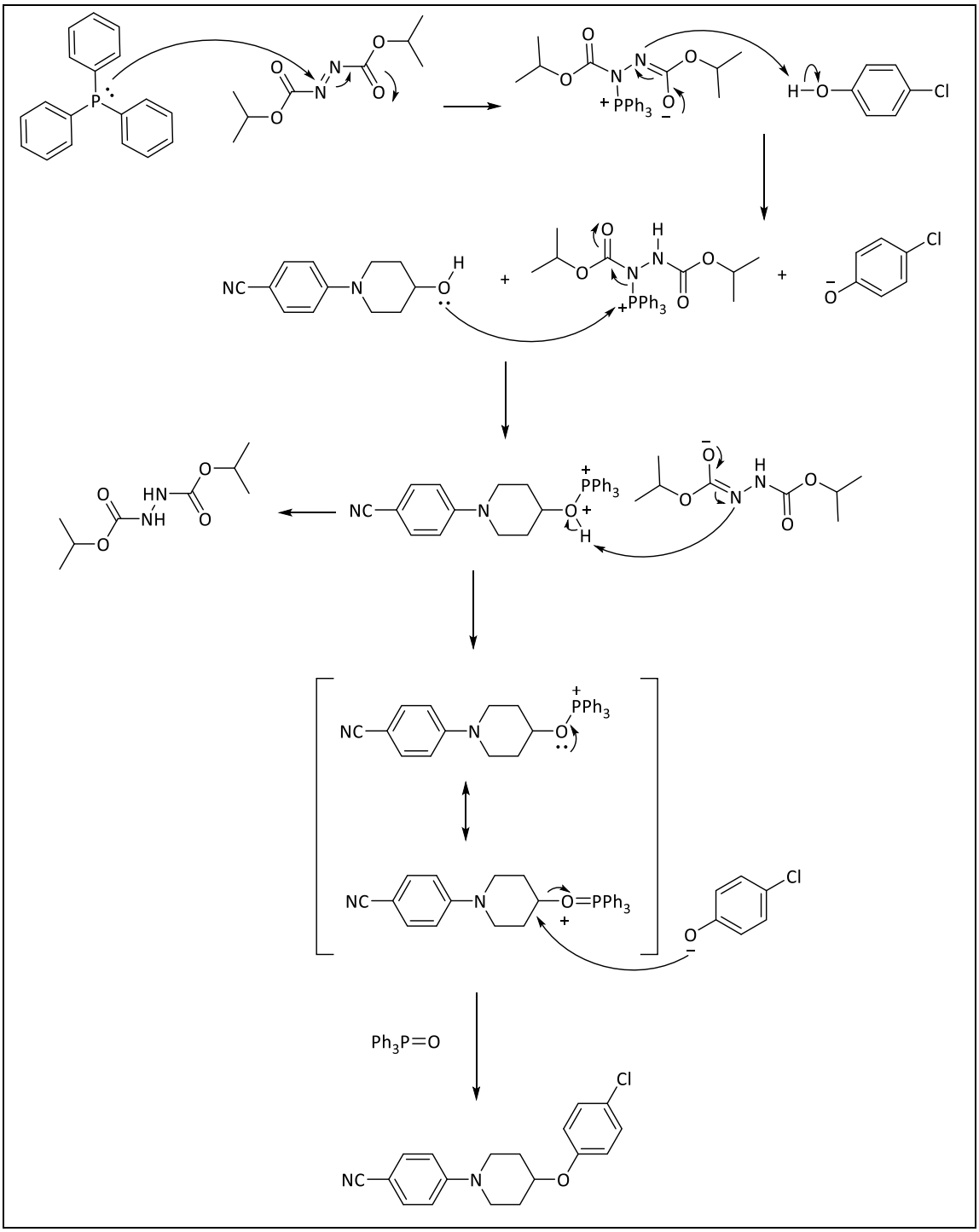

Scheme 17: Mechanism of the Mitsunobu reaction.

To prepare 4-(4-(4-chlorophenoxy)piperidin-1-yl)benzonitrile (**52**) in a good yield, 1-(4-cyanophenyl)piperidin-4-yl-methanesulfonate (**54**) was prepared by the reaction of 4-hydroxy-piperidine benzonitrile (**50**) and methane sulfonyl chloride (**53**) in the presence of Et_3N and CH_2Cl_2 (363). Compound **54** was produced in a good yield (Table 67). Then, it was reacted with 4-chlorophenol (**51**) in the presence of sodium hydride and DMF to obtain 4-(4-(4-chlorophenoxy)piperidin-1-yl)benzonitrile (**52**) in a yield

higher than that of Mitsunobu reaction (363) (Table 67). The ^{1}H NMR spectrum confirmed the structure of the compound which showed all aromatic and piperidine protons (Figure 202).

Table 67: Identification data for 1-(4-cyanophenyl)piperidin-4-yl-methanesulfonate (**54**) and 4-(4-(4-chlorophenoxy)piperidin-1-yl)benzonitrile (**52**).

Compd	Yield (%)	mp (^{o}C)	Appearance
54	98	-	Colourless semisolid
52	76	138-140	White crystal

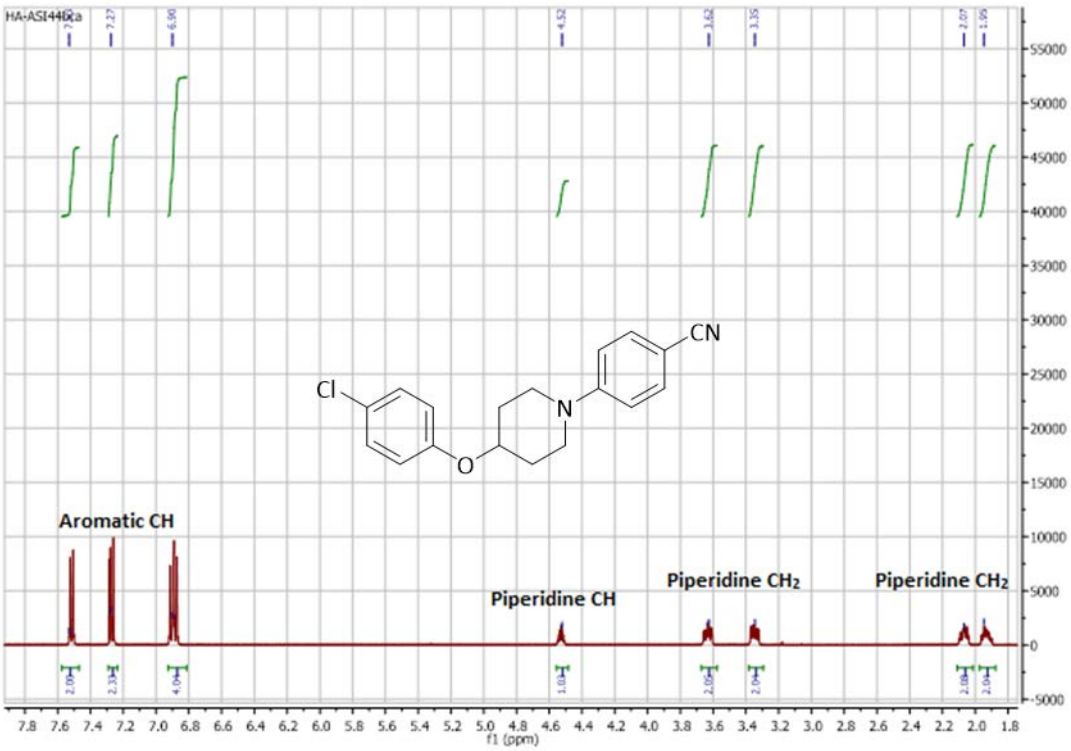

Figure 201: ^{1}H NMR spectrum of compound **52**. The spectrum shows piperidine protons and aromatic protons for biaryl moieties as three peaks integrated for 4, 2 and 2 respectively.

7.2.3. Synthesis of (4-(4-(4-chlorophenoxy)piperidin-1-yl)phenyl)methanamine (55)

(4-(4-(4-Chlorophenoxy)piperidin-1-yl)phenyl)methanamine (**55**) was prepared by the reaction of 4-(4-(4-chlorophenoxy)piperidin-1-yl)benzonitrile (**52**) with $LiAlH_4$ in THF (Scheme 12), to convert the nitrile group to amine (369). Aqueous workup was used as an essential step in this reduction reaction to remove any ionic intermediates. Compound **55** was used in the next step without further purification.

7.2.4. Synthesis of *N*-(4-(4-(4-chlorophenoxy)piperidin-1-yl)benzyl)-2-oxooxazolidine-3-sulfonamide (57)

N-(4-(4-(4-Chlorophenoxy)piperidin-1-yl)benzyl)-2-oxooxazolidine-3-sulfonamide (**57**) was prepared by the reaction of chlorosulfonyl isocyanate, 2-bromoethanol, (4-(4-(4-chlorophenoxy)piperidin-1-yl)phenyl)methanamine (**55**) and Et_3N as a base in CH_2Cl_2 (Scheme 16) (369). After adjusting the pH of the reaction to 2, the crude product was purified by gradient column chromatography and obtained in a good yield (Table 68).

Table 68: Identification data for *N*-(4-(4-(4-chlorophenoxy)piperidin-1-yl)benzyl)-2-oxooxazolidine-3-sulfonamide (**57**).

Compd	Yield (%)	Mp (^{O}C)	Appearance
57	64	134–138	Red fine powder

The mechanism of this reaction begins with attack of the oxygen atom of 2-bromoethanol on the electrophilic carbon of chlorosulfonyl isocyanate, with cyclisation through attack of the nitrogen atom at the second carbon of bromoethanol releasing HBr. Using Et_3N as a base to neutralise the generated HBr, the free amine of (4-(4-(4-chlorophenoxy)piperidin-1-yl)phenyl)methanamine (**55**) attacks the sulfur atom of 2-oxooxazolidine-3-sulfonyl chloride forming the final product **57** and releasing HCl (Scheme 18).

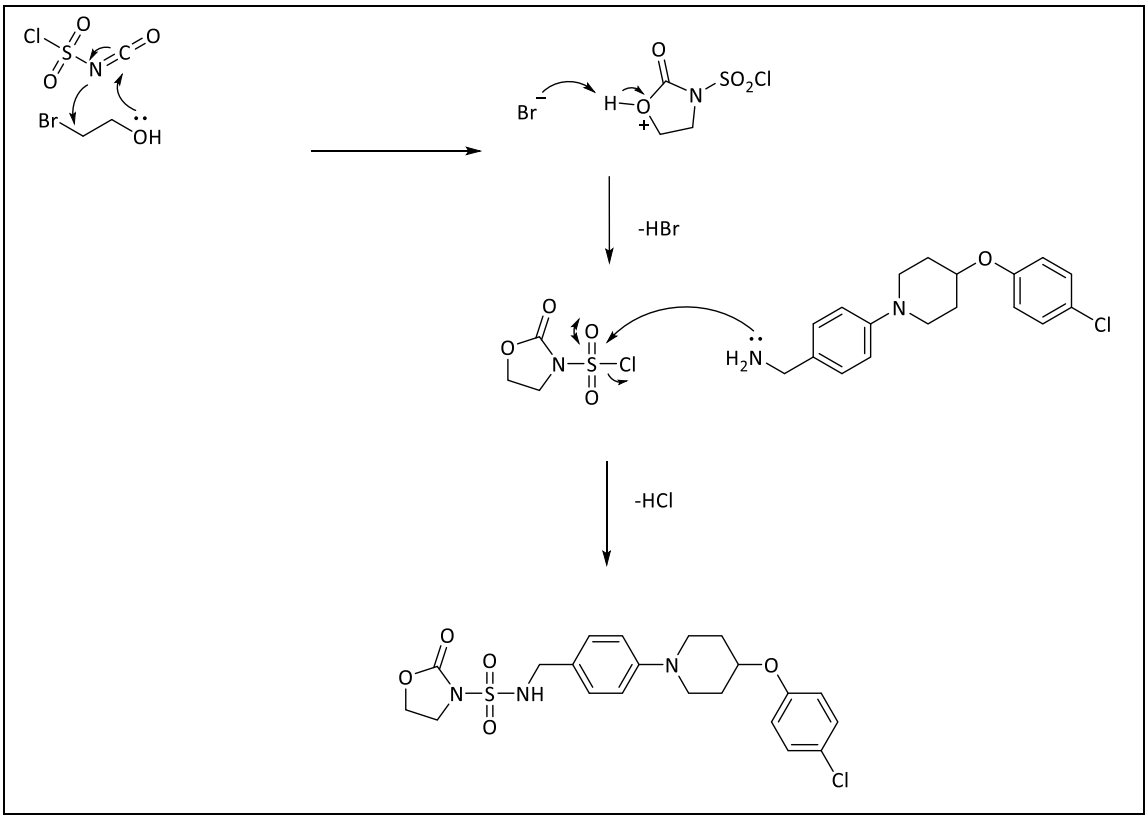

Scheme 18: Mechanism of *N*-(4-(4-(4-chlorophenoxy)piperidin-1-yl)benzyl)-2-oxooxazolidine-3-sulfonamide formation (**57**).

7.2.5. Synthesis of 3-methyl- or 3,4-dimethyl-(4-(4-chlorophenoxypiperidin-1-yl)benzyl)isoxazole-sulphondiamide (58a-b)

To prepare 3-methyl- or 3,4-dimethyl-(4-(4-chlorophenoxypiperidin-1-yl)benzyl)isoxazole-sulphondiamide (**58**), Et_3N was added to a solution of 3-methylisoxazol-5-amine (**22**) or 3,4-dimethylisoxazol-5-amine (**19**) in CH_3CN followed by addition of compound **57**. As the oxooxazolidine ring that exists next to the sulfonamide group is chemically unstable, it can be easily attacked by good nucleophiles but using 3-methylisoxazol-5-amine (**22**) or 3,4-dimethylisoxazol-5-amine (**19**) was not successful to form the desired final products **58a-b**.

7.3. Docking studies

A docking study of the final compounds of series 5 and 6 with *S. aureus* and *E. faecalis* AspRS and AsnRS enzymes was performed to determine their binding interactions with the active sites of the respective aaRS enzymes.

7.3.1. Docking studies of *S. aureus* AspRS

By alignment of series 5 and 6 compounds with aspartyl adenylate inside the active site of *S. aureus* AspRS (Figure 203), the amino acid residues responsible for binding interactions were identified (Table 69). Compound **44** was easily flipping inside the pockets and formed many binding interactions with the key amino acid residues if it was in the right position. The histidine and flipping loops were close to the amino acid isosteric part (Figure 204). The docking studies of compound **45** showed good fitting inside the pockets forming good binding interactions with the key amino acid residues but Mg^{2+} ion did not participate in any binding interactions with compound **45**. For example, Arg537 formed a π- cation interaction with the thiadiazole ring in the AMP pocket (Figure 205). Compounds **58a-b** were too long to be accommodated inside the AMP pocket despite the good interactions of the sulfonamide linkage and the amino acid isosteric part (Figure 206). The chloro atom of the phenoxy moiety in compound **58b** formed a hydrogen bond with Gln232 (Figure 207).

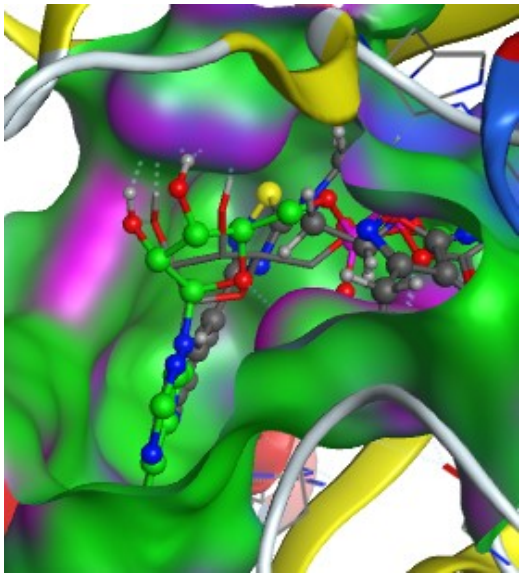

Figure 203: Alignment of compound **45** (grey) with aspartyl adenylate (green) in the active sites of *S. aureus* AspRS.

Table 69: Binding interactions of series 5 and 6 compounds with the amino acid residues of the binding sites of *S. aureus* AspRS.

Ligands	Aspartic acid pocket	AMP pocket
Aspartyl-adenylate	Gln201, Lys204, His452, Gly488, Ser490, Arg492 and Asp239	Arg223, Phe235, Gln232, Arg540 and Glu485
44	Ser199, Gln237, Gly488, His452, Arg492 and Asp239	Arg231, Glu485 and Arg540
45	Ser193, Gln237, His451, His452, Gly488, Gly489 and Arg492	Phe222, Phe235, Glu485, Arg537 and Arg540
58a	Ser193, Gln237, His451, His452, Gly488, Gly489, Arg490 and Asp239	Arg231, Glu485 and Arg540
58b	Ser193, Gln237, Asp239, His451, His452, Gly488, Gly489 and Arg492	Gln232, Glu485 and Arg540

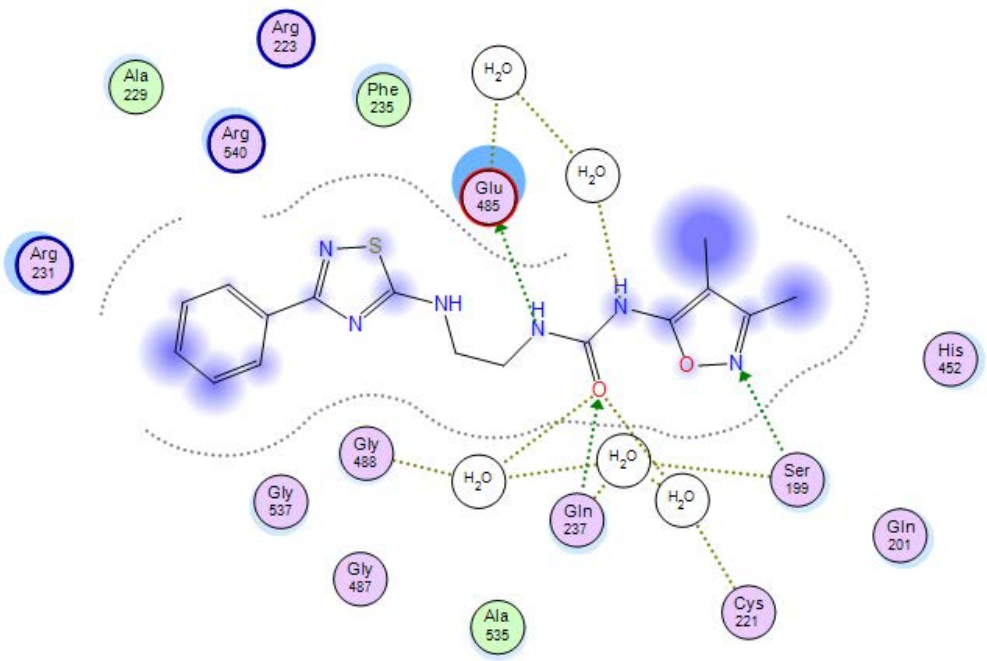

Figure 204: 2D binding interactions of compound **44** with *S. aureus* AspRS.

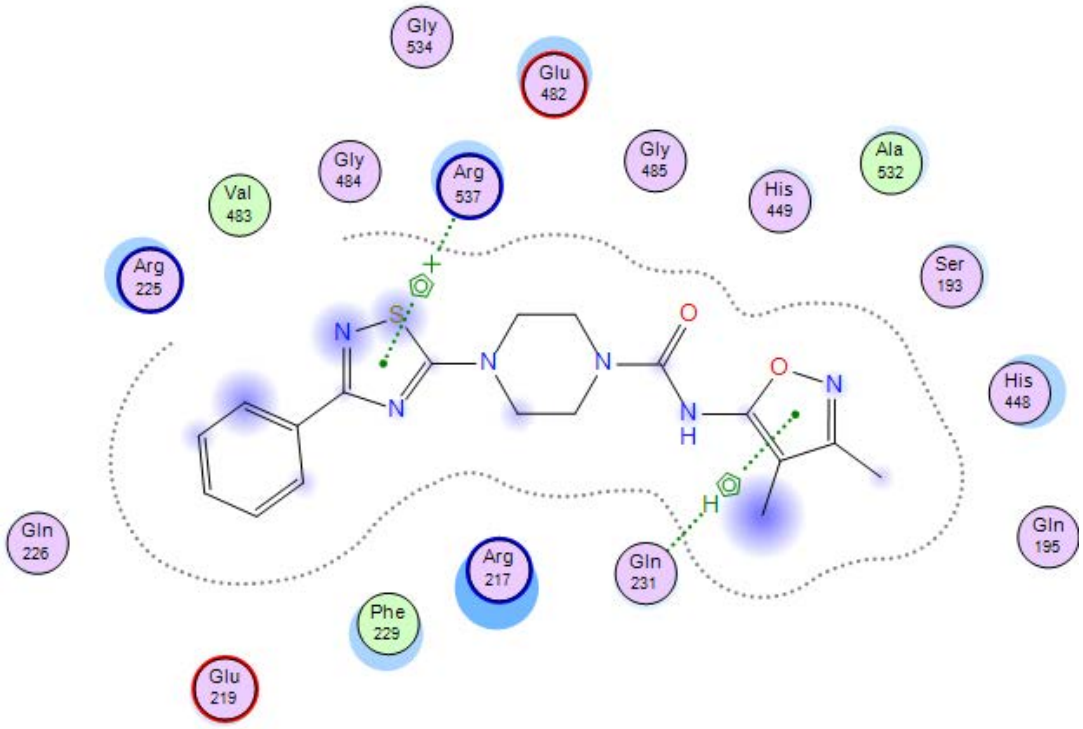

Figure 205: 2D binding interactions of compound **45** with *S. aureus* AspRS.

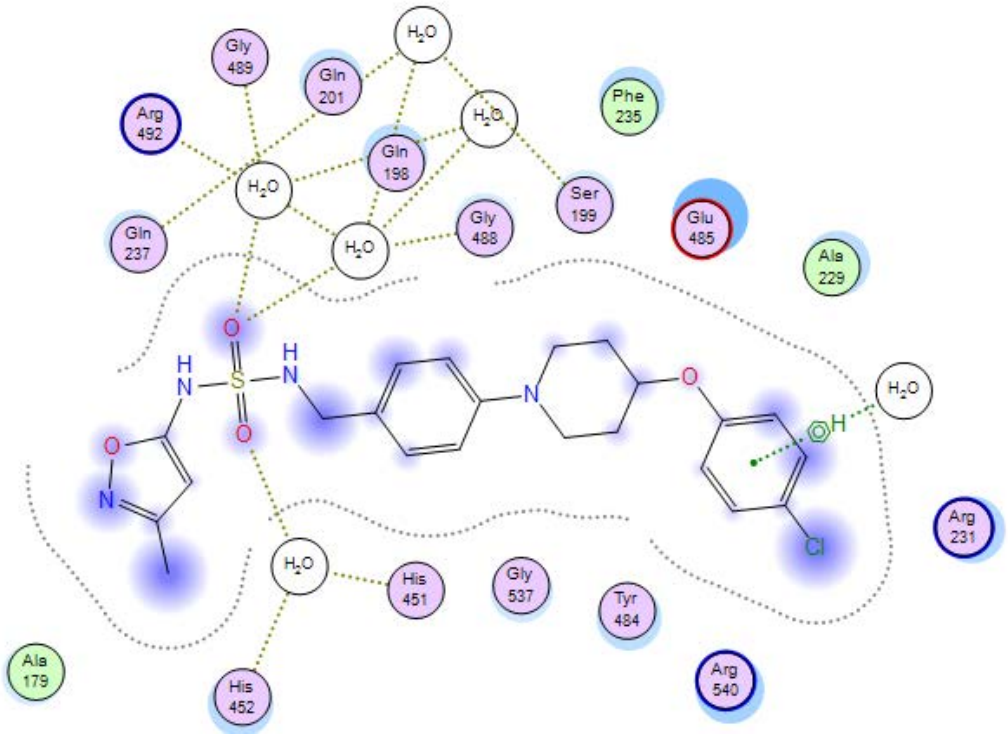

Figure 206: 2D binding interactions of compound **60a** with *S. aureus* AspRS.

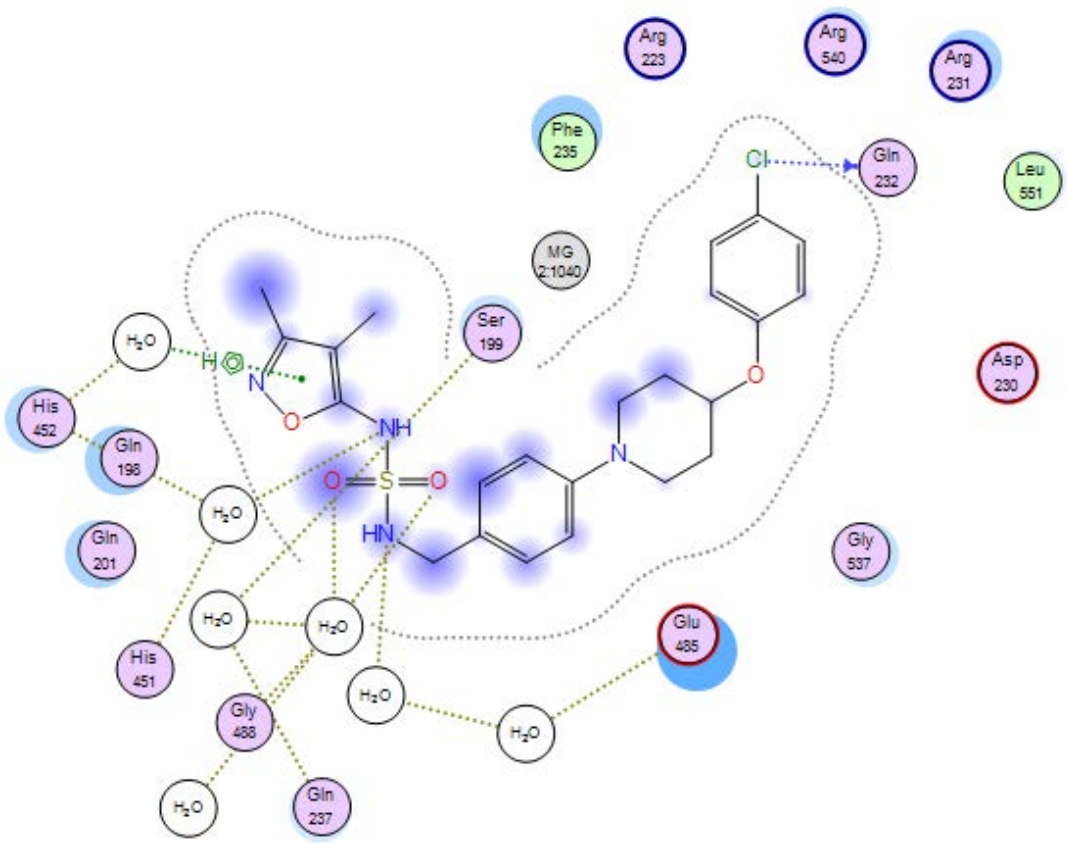

Figure 207: 2D binding interactions of compound **60b** with *S. aureus* AspRS.

7.3.2. Docking studies of *S. aureus* AsnRS

By alignment of series 5 and 6 compounds with asparaginyl adenylate inside the active site of *S. aureus* AspRS (Figure 208), the amino acid residues responsible for binding interactions were identified (Table 70). The docking study of compounds **44**, **45** and **58a**-**b** showed good binding interactions with the key amino acid residues responsible for the AMP pocket. For example, Phe219 formed a π-π stacking interaction with the aryl moiety of series 5 and 6 compounds (Figures 209-213). By contrast, compounds **44** and **45** did not form any interactions with the key amino acid responsible for asparagine recognition (Figure 209-210). In the docking study of compounds **58a** and **58b**, Arg360 showed two types of interactions, one was a water mediated hydrogen bond with the nitrogen atom of 3-methyl-isoxazole moiety and the second was π-cation interaction with the isoxazole ring in another pose (Figure 211-213).

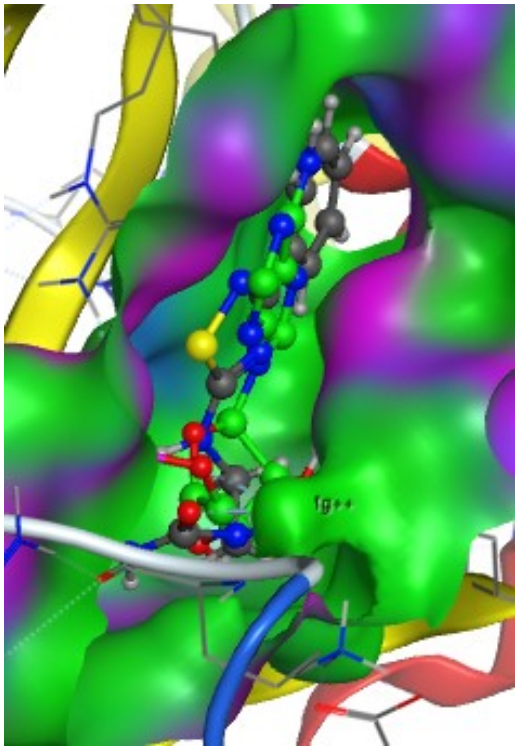

Figure 208: Alignment of compound **44** (grey) with asparaginyl adenylate (green) in the active sites of *S. aureus* AsnRS.

Table 70: Binding interactions of series 5 and 6 compounds with the amino acid residues of the binding sites of *S. aureus* AsnRS.

Ligands	Asparagine pocket	AMP pocket
Asparaginyl-adenylate	Glu223 and Arg360	Arg206, Glu208, Arg214, His215, Phe219, Glu353, Gly356, Gly401 and Arg404
44	-	Arg206, Glu163, Gln189, Phe219, Glu353, Lys326, Asp344 and Arg404
45	-	Glu163, Arg206, Phe219, Glu353, Gly356 and Arg404
58a	Arg360	Glu163, Glu167, Phe219, Glu353, Lys326, Asp344 Gly356 and Arg404
58b	Arg360	Glu163, Glu167, Gln189, Arg206, Phe219, Glu353, Gly356 and Arg404

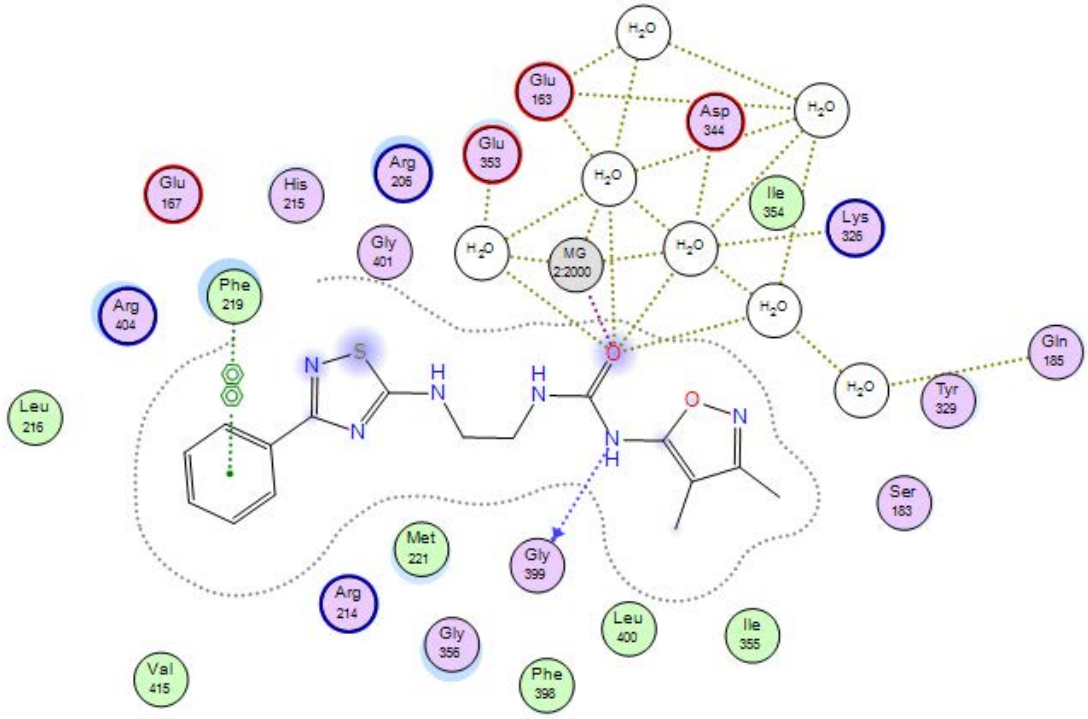

Figure 209: 2D binding interactions of compound **44** with *S. aureus* AsnRS.

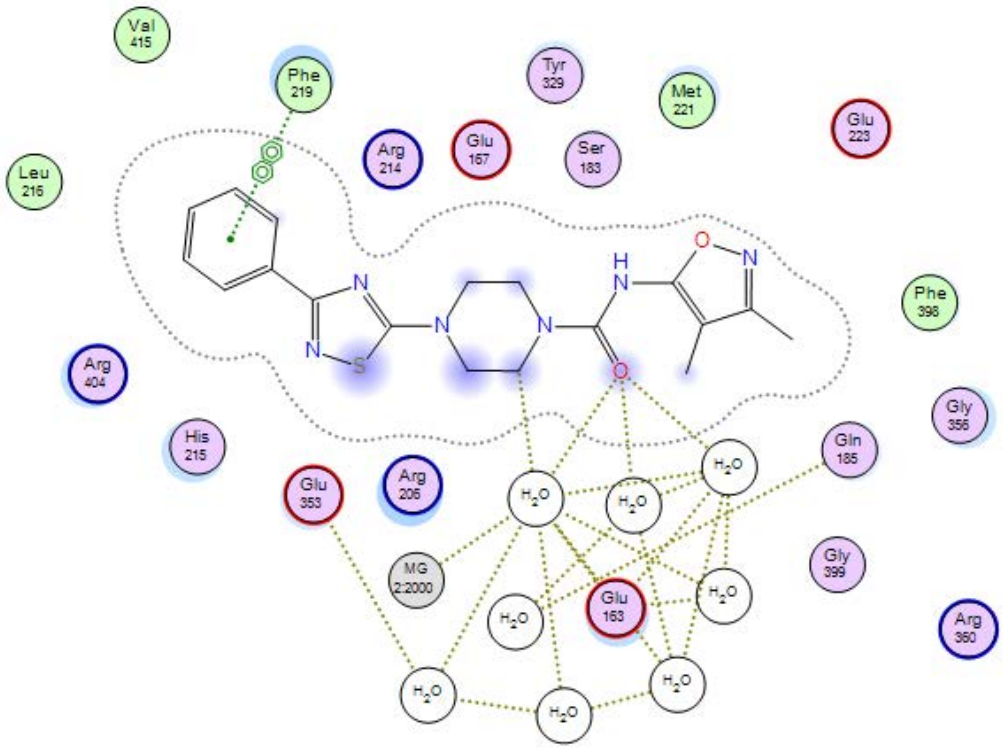

Figure 210: 2D binding interactions of compound **45** with *S. aureus* AsnRS.

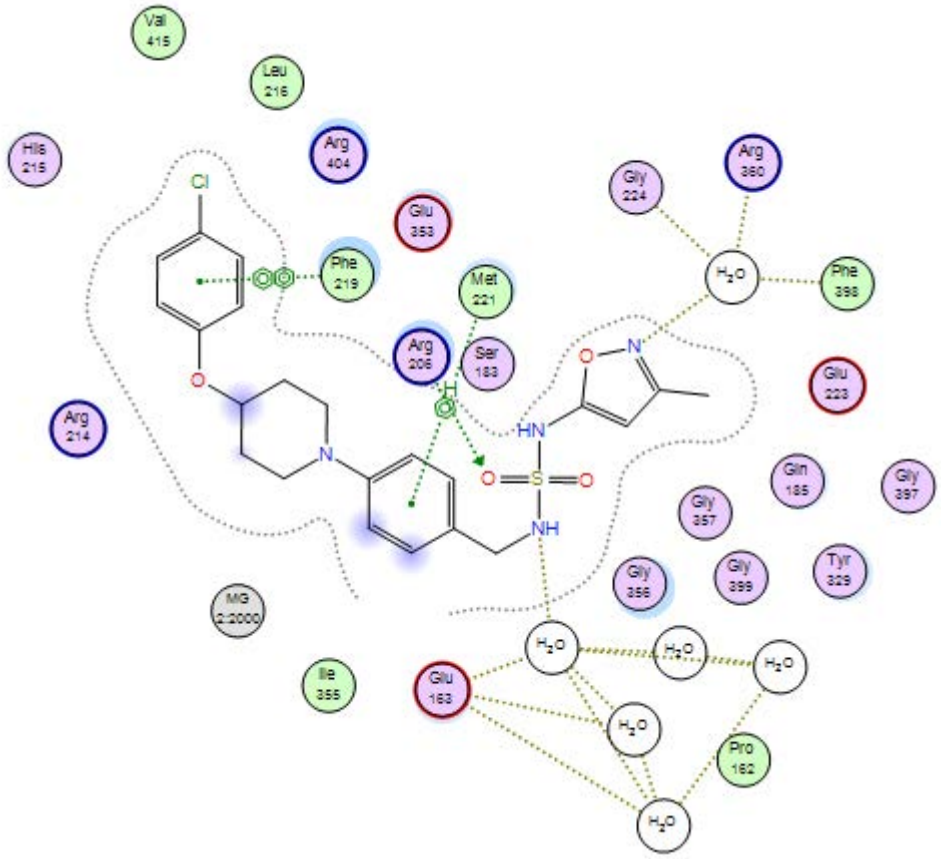

Figure 211: 2D binding interactions of compound **60a** with *S. aureus* AsnRS.

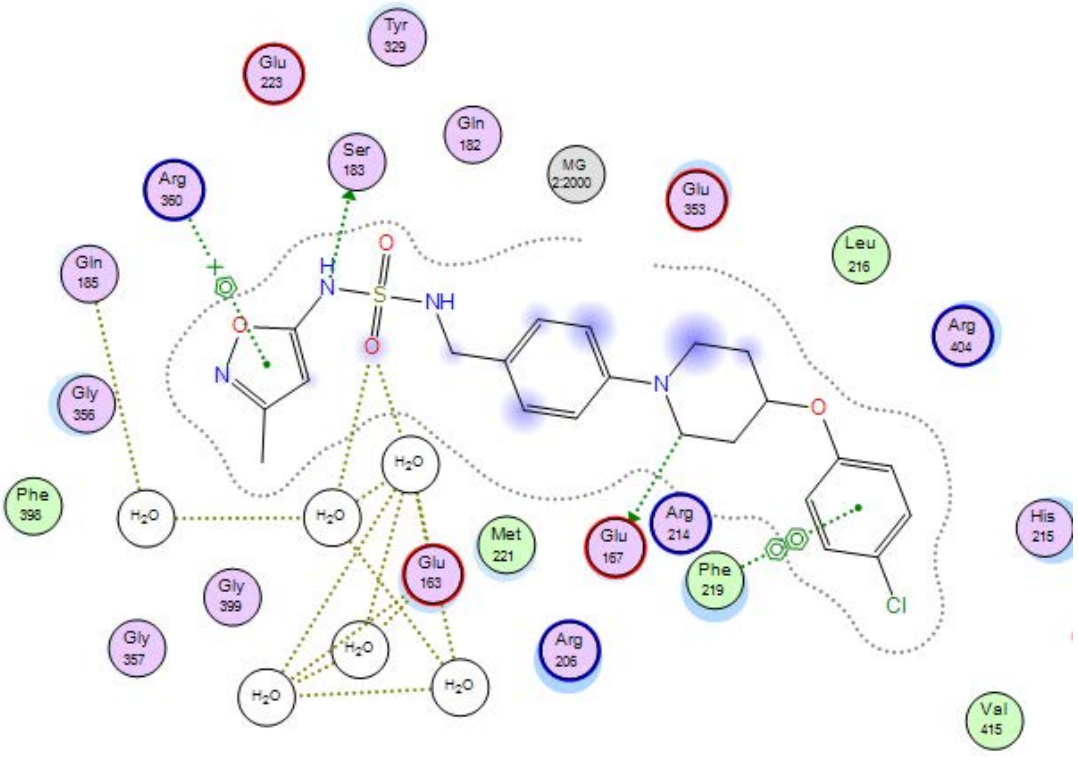

Figure 212: 2D binding interactions of compound **60a** with *S. aureus* AsnRS.

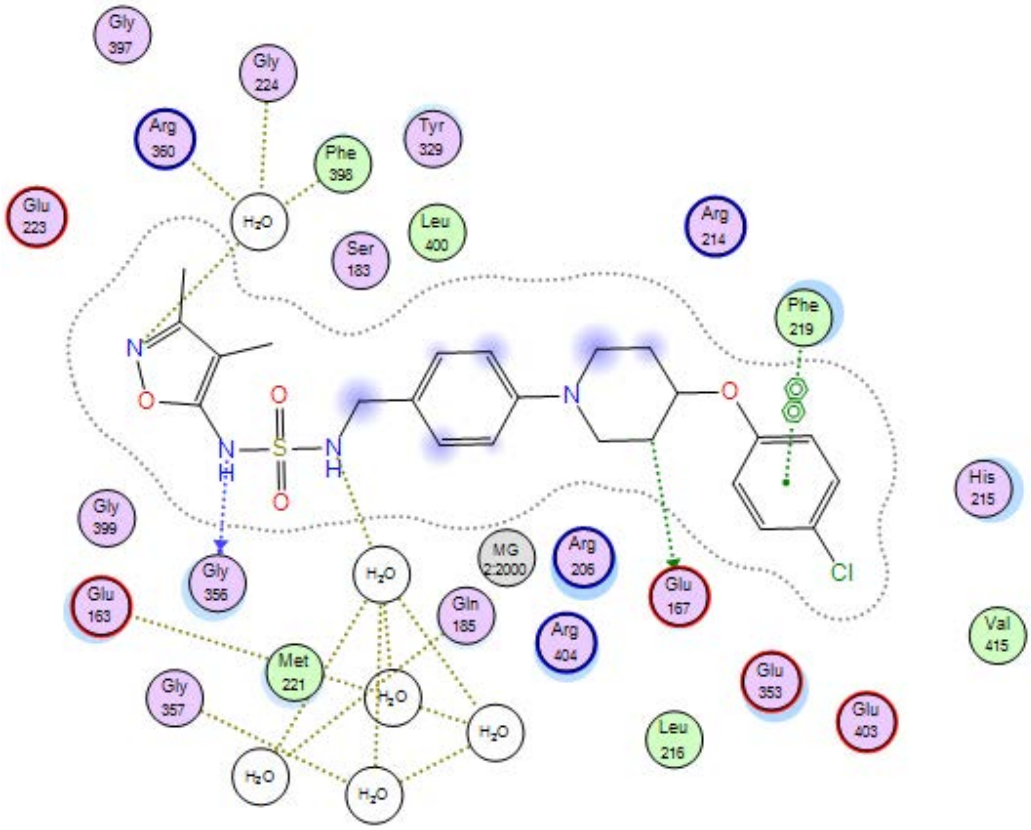

Figure 213: 2D binding interactions of compound **60b** with *S. aureus* AsnRS.

7.3.3. Docking studies of *E. faecalis* AspRS.

The amino acid residues responsible for binding interactions with series 5 and 6 compounds were identified through alignment with aspartyl adenylate inside the active sites of *E. faecalis* AspRS (Figure 214) (Table 71). The docking studies of compounds **44** and **45** did not show good interactions inside the Asp pocket despite the close distance of histidine loop to the isosteric moiety of the amino acid in compound **45** while the flipping loop was not shown close to the amino acid pocket during the docking studies (Figure 215). Compounds **58a**-**b** were too long to fit well in both pockets, but they formed several good interactions, and the histidine loop was close to the Asp pocket. For example, Phe234 formed a π-π stacking interaction with the chloro aryl moiety in the AMP pocket. The sulphonamide linkage was furthermore a good source for forming several hydrogen bonds either water mediated or direct (Figure 216-217).

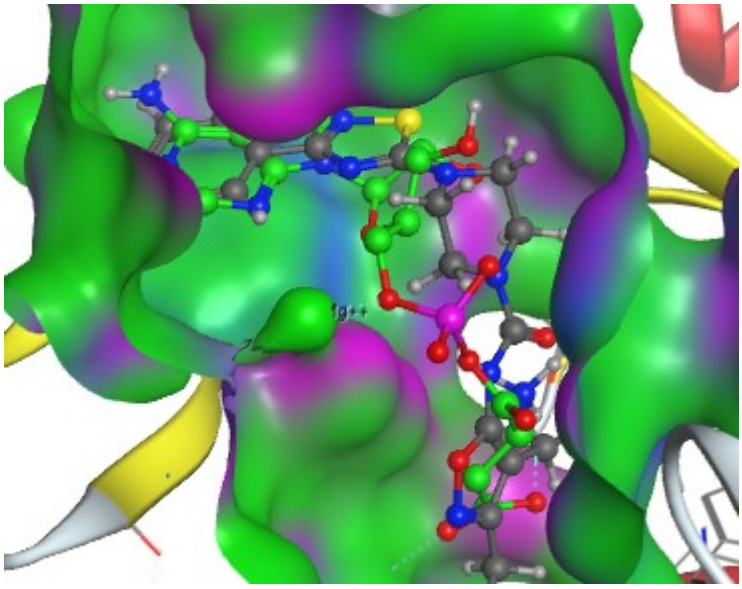

Figure 214: Alignment of compound **45** (grey) with aspartyl adenylate (green) in the active sites of *E. faecalis* AspRS.

Table 71: Binding interactions of series 5 and 6 compounds with the amino acid residues of the binding sites of *E. faecalis* AspRS.

Ligands	Aspartic acid pocket	AMP pocket
Aspartyl-adenylate	Glu176, Arg230, His449, Arg490 and Asp238	Arg222, Phe234, Gln231, Gln236, Glu483 and Arg538
44	His449,	Arg222, Glu224 and Phe234
45	Glu176, Ser198, His449, Gln236 and Arg490	Arg222, Glu224, Phe234, Gln236 and Arg538
58a	Gln200, His449 and Arg490	Arg222, Glu224 and Phe234
58b	Arg230, His449, Arg490 and Asp238	Arg222, Glu224, Phe234 and Arg538

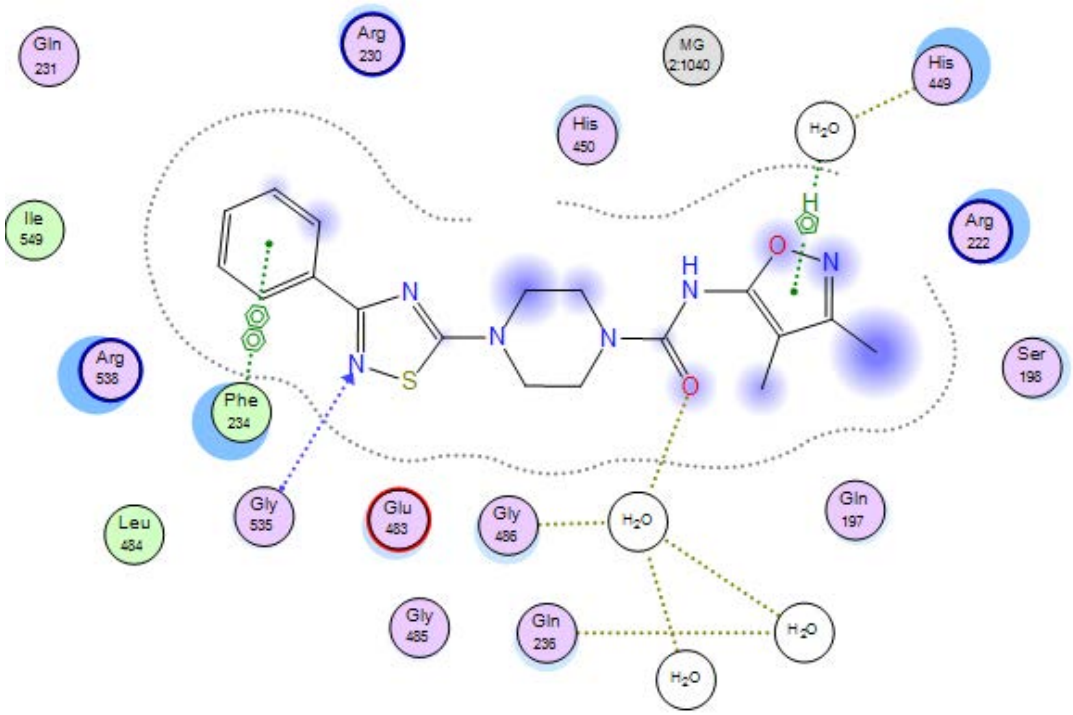

Figure 215: 2D binding interactions of compound **45** with *E. faecalis* AspRS.

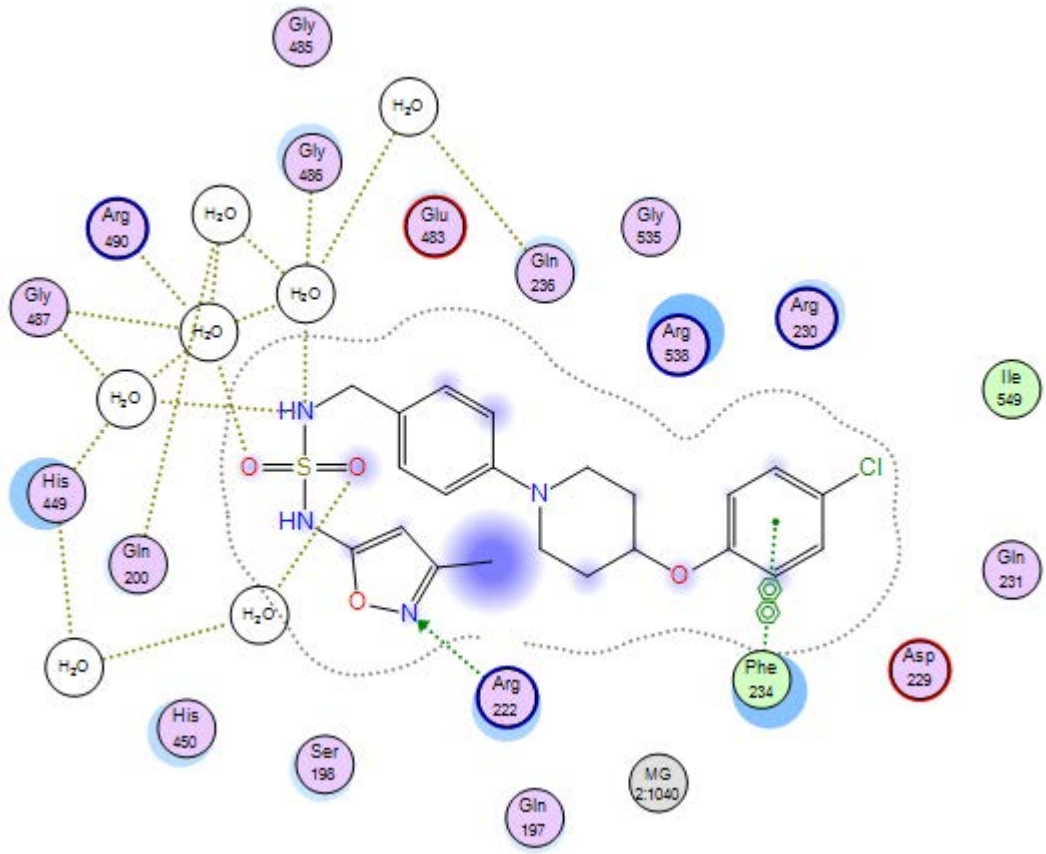

Figure 216: 2D binding interactions of compound **60a** with *E. faecalis* AspRS.

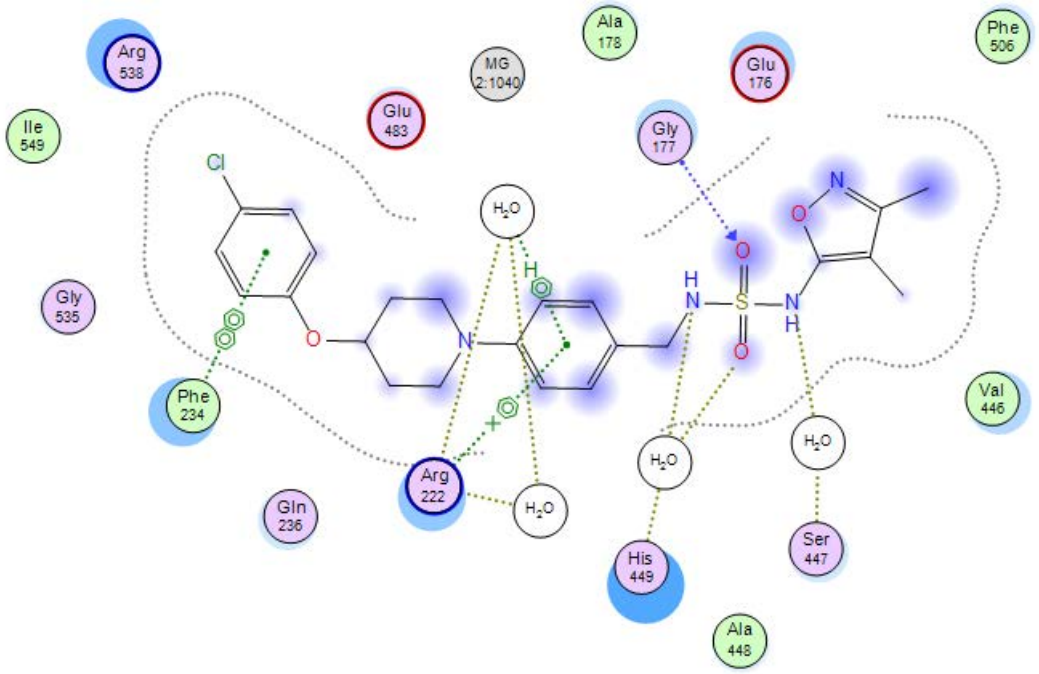

Figure 217: 2D binding interactions of compound **60b** with *E. faecalis* AspRS.

7.3.4. Docking studies of *E. faecalis* AsnRS.

The amino acid residues responsible for binding interactions with series 5 and 6 compounds were identified through alignment with asparaginyl adenylate inside the active sites of *E. faecalis* AsnRS (Figure 218) (Table 72). The docking studies of compound **45** showed that the amino acid isosteric moiety formed a direct hydrogen bond with the key Arg380 and this amino acid residue also participated in another hydrogen bond via water molecule to stabilise the CO of the amide moiety while the same moiety in compound **44** did not show any interactions with the key amino acid residues responsible for Asn (Figure 219-220). Compounds **58a** and 58**b** were too long to fit both pocket and easy to flip inside the active sites. They did not interact well inside the AMP pocket. The key amino residue (Arg380) formed a water mediated hydrogen bond with the isoxazole ring in compound **58a** and with sulphondiamide linkage in compound **58b** (Figure 221-222).

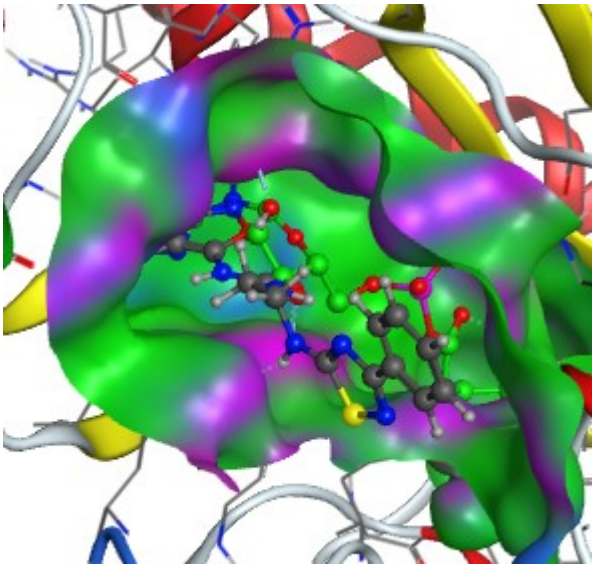

Figure 218: Alignment of compound **24b** (grey) with asparaginyl adenylate (green) in the active sites of *E. faecalis* AsnRS.

Table 72: Binding interactions of series 5 and 6 compounds with the amino acid residues of the binding sites of *E. faecalis* AsnRS.

Ligands	Asparagine pocket	AMP pocket
Asparaginyl-adenylate	Glu238 and Arg380	Arg221, Glu223, Arg229, His230, Phe234, Glu373, Gly376, Gly421 and Arg424
44	-	Arg221, Phe234, Glu373 and Arg424
45	Gln200 and Arg380	His230, Glu373 and Arg424
58a	Gln200 and Arg380	Glu173, Arg221 and Glu373
58b	Gln200 and Arg380	Arg221 and Glu373

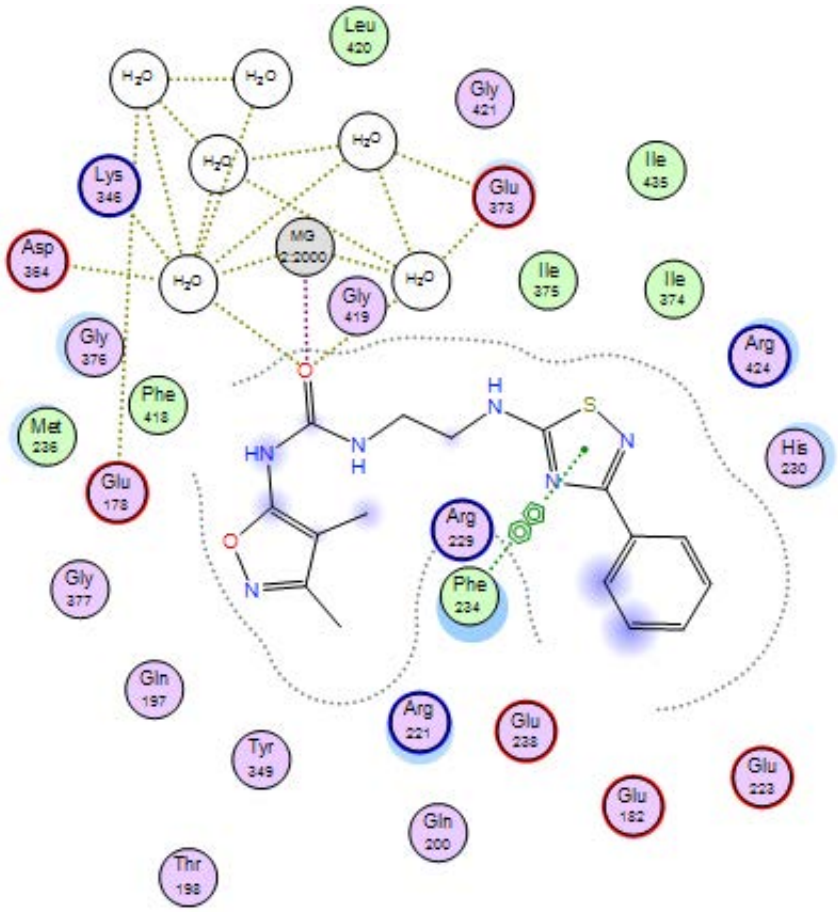

Figure 219: 2D binding interactions of compound **44** with *E. faecalis* AsnRS.

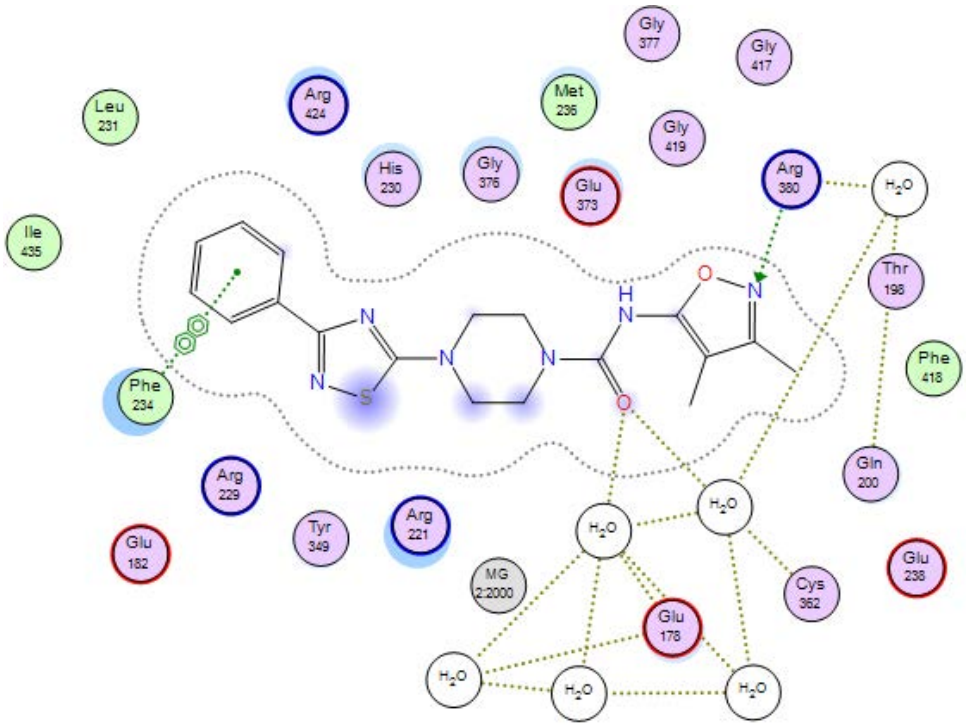

Figure 220: 2D binding interactions of compound **45** with *E. faecalis* AsnRS.

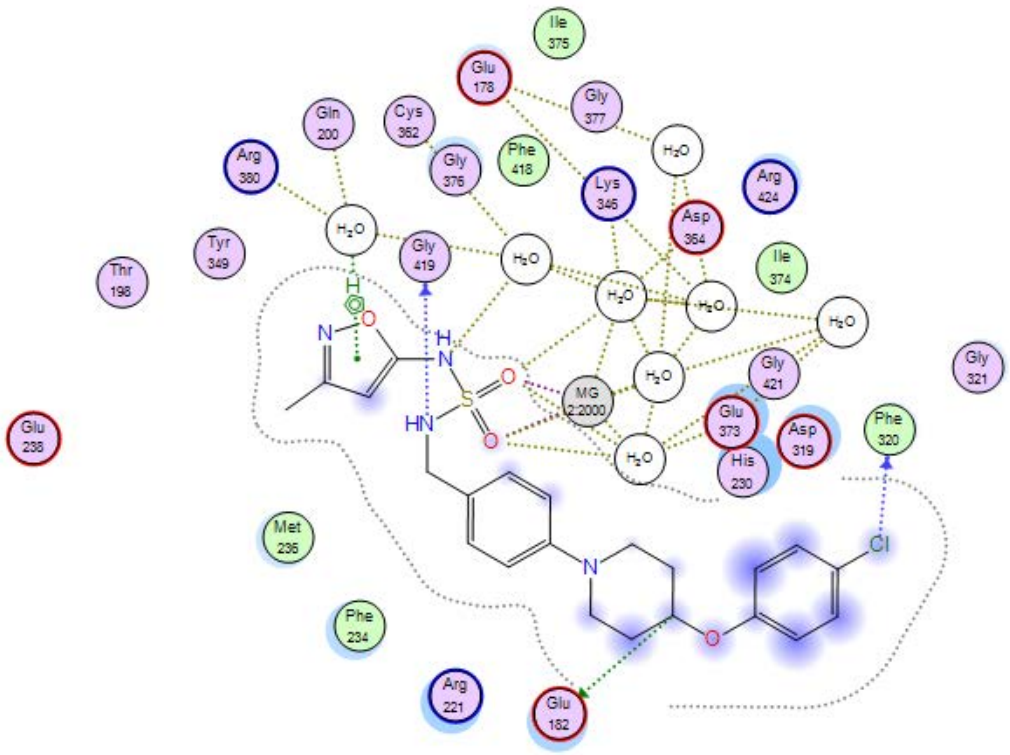

Figure 221: 2D binding interactions of compound **60a** with *E. faecalis* AsnRS.

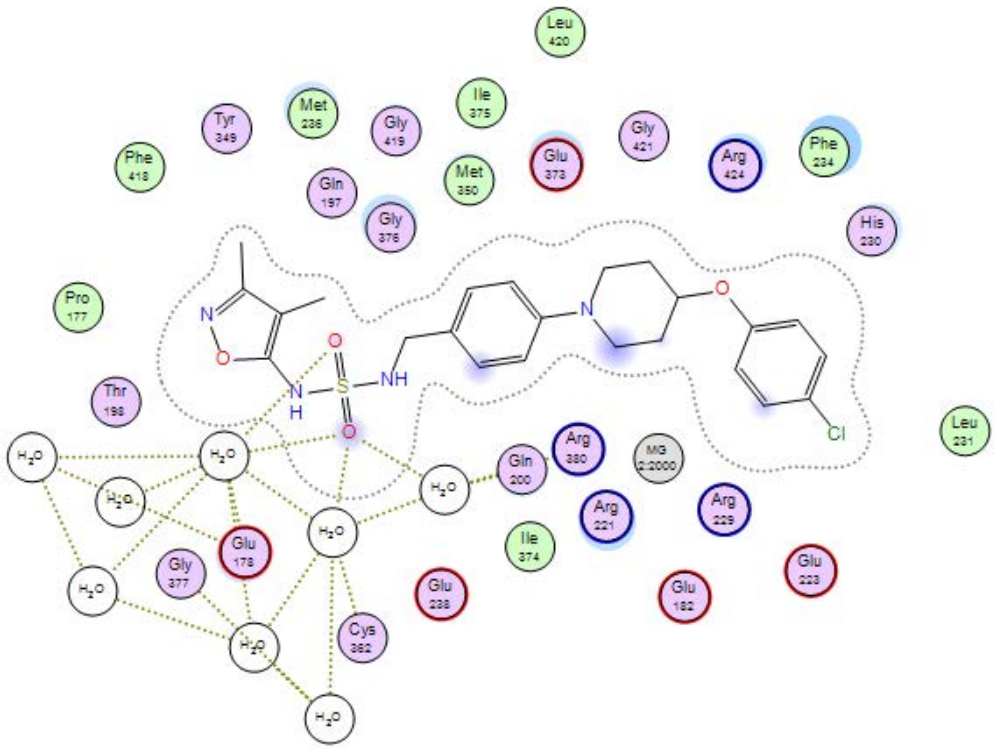

Figure 222: 2D binding interactions of compound **60b** with *E. faecalis* AsnRS.

7.4. Biological assays

7.4.1. Microbiological screening

Microbiological screening of *N*-(3,4-dimethylisoxazol-5-yl)-4-(3-phenyl-1,2,4-thiadiazol-5-yl) piperazine-1-carboxamide (**45**) was performed at the Antimicrobial Chemotherapy Unit in University Hospital of Wales (UHW) by Jennifer Richard and Mandy Wootton. Series 5 compound **45** was evaluated for antimicrobial activity against the same microorganisms mentioned in chapter 5. From the MIC results of compounds **45** (Table 73), compound **45** showed very low inhibitory activity (128 µg/mL) against all tested microorganisms compared with ciprofloxacin (0.008 - 0.25 µg/mL). The docking study of compound **45** showed that Mg^{2+} as an essential element in the interactions, did not participate in any interactions with compound **45** inside the active sites of *S. aureus* AspRS while in *E. faecalis* AspRS, the flipping loop was not close to the Asp pocket indicating the failed recognition of the compound. By contrast, the easy flipping of compound **45** inside the active sites of AsnRS enzymes during the docking study would suggest that it was not stable enough to form good binding interactions in both pockets which may explain its inability to exert inhibitory activity against the target microorganism.

Table 73: Microbiological data of compound **45**.

Microorganisms	MIC: (µg/mL)	
	Ciprofloxacin	**45**
Pseudomonas aeruginosa ATCC 27853	0.25	128
Staphylococcus aureus ATCC 29213	0.25	128
Enterococcus faecalis ATCC 29212	0.125	128
Escherichia coli ATCC 25922	0.008	>128
Klebsiella pneumoniae ATCC 700603	0.25	>128

In conclusion, compound **45** consisted of 3,4- dimethyl isoxazole as the amino acid isosteric moiety and piperazine amide linked to phenyl thiadiazole, was the only compound successfully prepared. In the docking study, compound **45** showed good binding interactions inside the active sites of the target enzymes. However, Mg^{2+} ion did not participate in any binding interactions indicating that the amide linkage was not enough to stabilise the compound inside the pockets. Furthermore, the lack of a carbonyl group next to the amino acid isosteric moiety may disrupt the stabilisation of the compound and its recognition by the enzymes and this could reflect on its inhibitory activity.

7.5. Methods

All methods are described in the methods section in Chapter 3.

7.5.1 Chemistry

7.5.1.1. *Tert*-butyl (2-aminoethyl)carbamate (**33**) ($C_7H_{16}N_2O_2$, Mol. Wt. 160.22)

A solution of Boc_2O (**32**) (0.4 g, 1.66 mmol) in dry CH_2Cl_2 (5 mL) was added dropwise to a solution of ethylenediamine (**31**) (1 g, 16.6 mmol) in dry CH_2Cl_2 (10 mL) at 0 ^{O}C. The reaction mixture was stirred at 0 ^{O}C for 1h then o/n at room temperature. H_2O (5 ml) was added, and the organic layer was washed with H_2O (2 x 10 mL), dried over anhydrous $MgSO_4$ and the solvent as removed under vacuum to obtain the product as a white powder, yield: 0.2 g (77%), mp = 110 – 112 ^{O}C. TLC: CH_3OH - CH_2Cl_2 1:9 v/v, (R_F = 0.3). ^{1}H NMR ($CDCl_3$) δ 1.34 (br s, 2H, NH_2), 1.38 (s, 9H, $C(CH_3)_3$), 2.73 (t, J = 5.8 Hz, 2H, CH_2), 3.11 (q, J = 6.1 Hz, 2H, CH_2), 4.80 (br s, 1H, NH). ^{13}C NMR ($CDCl_3$) δ 28.4 (CH_3, $C(CH_3)_3$), 41.9 (CH_2), 43.4 (CH_2), 79.1 (C, $C(CH_3)_3$), 156.2 (C=O).

7.5.1.2 *Tert*-butyl (2-(3-(3,4-dimethylisoxazol-5-yl)ureido)ethyl)carbamate (**34**) ($C_{13}H_{22}N_4O_4$, Mol. Wt. 298.34)

A mixture of *tert*-butyl (2-aminoethyl)carbamate (**33**) (0.2 g, 1.25 mmol), 2,2,2-trichloroethyl (3,4-dimethylisoxazol-5-yl)carbamate (**21**) (0.4 g, 1.50 mmol), *N*-ethyldiisopropylamine (0.3 mL, 1.50 mmol), and DMSO (20 mL) was stirred at 70 ^{O}C o/n. After cooling the reaction was, poured into water (10 mL), and extracted with EtOAc (3 x 50 mL). The organic layer was washed with water (2 x 50 mL), dried over anhydrous $MgSO_4$, and concentrated in *vacuo*. The crude product was purified by

gradient column chromatography and collected at 10:90 v/v petroleum ether – EtOAc to obtain the product as a white solid, yield: 0.2 g (54%), mp = 142 – 144 ^{O}C. TLC: petroleum ether – EtOAc 1:1 v/v, (R_F = 0.1). ^{1}H NMR ($CDCl_3$) δ 1.42 (s, 9H, $C(CH_3)_3$), 1.89 (s, 3H, CH_3), 2.21 (s, 3H, CH_3), 3.31 (q, J = 4.6, 5.3 Hz, 2H, CH_2), 3.40 (q, J = 5.3, 5.3 Hz, 2H, CH_2), 5.09 (s, 1H, NH), 6.27 (s, 1H, NH), 8.23 (s, 1H, NH). ^{13}C NMR ($CDCl_3$) δ 6.3 (CH_3), 10.4 (CH_3), 28.5 (CH_3, $C(CH_3)_3$), 41.6 (CH_2), 42.4 (CH_2), 79.3 (C, $C(CH_3)_3$), 100.2, 158.9, 160.0 (3 x C, isoxazole), 154.9 (C=O), 155.2 (C=O).

7.5.1.3. 1-(2-Aminoethyl)-3-(3,4-dimethylisoxazol-5-yl)urea hydrochloride (**35**) ($C_8H_{15}ClN_4O_2$, Mol. Wt. 234.68)

The Boc deprotection using HCl/dioxane was described in Chapter 4. Product obtained as a white solid, yield: 0.6 g (98%), mp = 210 – 212 ^{O}C. TLC: CH_3OH – CH_2Cl_2 1:9 v/v, (R_F = 0.1). ^{1}H NMR (DMSO-d_6) δ 1.79 (s, 3H, CH_3), 2.12 (s, 3H, CH_3), 2.88 (br q, 2H, CH_2), 3.29 (br q, 2H, CH_2) overlapped by 3.30 (H_2O peak), 6.77 (s, 1H, NH), 7.85 (br s, 3H, NH_3), 9.30 (s, 1H, NH). ^{13}C NMR (DMSO-d_6) δ 7.1 (CH_3), 10.7 (CH_3), 43.2 (CH_2), 49.6 (CH_2), 106.1, 156.9, 160.4 (3 x C, isoxazole), 154.5 (C=O).

7.5.1.4. *Tert*-butyl 4-((3,4-dimethylisoxazol-5-yl)carbamoyl)piperazine-1-carboxylate (**37**) ($C_{15}H_{24}N_4O_4$, Mol. Wt. 324.38)

A mixture of *tert*-butyl piperazine-1-carboxylate (**36**) (0.39 g, 2.09 mmol), 2,2,2-trichloroethyl (3,4-dimethylisoxazol-5-yl)carbamate (**21**) (0.3 g, 1.04 mmol), *N*-ethyldiisopropylamine (0.18 mL, 1.04 mmol), and DMSO (5 mL) was stirred at 70 ^{O}C for 2 h, poured into water (5 mL), and extracted with EtOAc (3 x 50 mL). The organic layer was washed with water (2 x 50 mL), dried over anhydrous $MgSO_4$, and concentrated in *vacuo*. The oversaturation of the crude product in EtOAc and adding drops of hexane resulted in the formation of the product as needle like crystals, yield: 0.25 g (74%), mp = 164 – 166 ^{O}C. TLC: petroleum ether – EtOAc 1:3 v/v, (R_F = 0.2). ^{1}H NMR (DMSO-d_6) δ 1.42 (s, 9H, $C(CH_3)_3$), 1.75 (s, 3H, CH_3), 2.13 (s, 3H, CH_3), 3.35 (br t, 4H, CH_2, pip), 3.41 (br t, 4H, CH_2, pip), 9.19 (s, 1H, NH). ^{13}C NMR (DMSO-d_6) δ 7.1 (CH_3), 10.1 (CH_3), 28.7 (CH_3, $C(CH_3)_3$), 44.2 (4 x CH_2, pip), 79.9 (C, $C(CH_3)_3$), 102.8, 159.4, 161.5 (3 x C, isoxazole), 153.7 (C=O), 154.2 (C=O).

7.5.1.5. *N*-(3,4-Dimethylisoxazol-5-yl)piperazine-1-carboxamide 2,2,2-trifluoroacetic acid (**38**) ($C_{10}H_{17}ClN_4O_4$, Mol. Wt. 260.72)

The Boc deprotection using HCl/dioxane was described in Chapter 4. Product obtained as a white solid, yield: 0.2 g (99%), mp = 222 – 224 ^{O}C. TLC: CH_3OH – CH_2Cl_2 1:9 v/v, (R_F = 0.1). ^{1}H NMR (DMSO-d_6) δ 1.76 (s, 3H, CH_3), 2.13 (s, 3H, CH_3), 3.08 (br t, 4H, CH_2, pip), 3.41 (br t, 4H, CH_2, pip), 9.15 (s, 2H, NH_2), 9.44 (s, 1H, NH). ^{13}C NMR (DMSO-d_6) δ 7.1 (CH_3), 11.2 (CH_3), 41.6, 42.5 (2 x CH_2, pip), 102.8, 159.1, 161.4 (3 x C, isoxazole), 154.5 (C=O).

7.5.1.6. Ethyl benzimidate hydrochloride (**41**) ($C_9H_{12}ClNO$, Mol. Wt. 185.65)

Acetyl chloride (**40**) (2.8 mL, 38.8 mmol) was added dropwise to a solution of benzonitrile (**39**) (0.5 mL, 4.85mmol) in ethanol (3.4 mL, 58.2 mmol) at 10 ^{O}C. The reaction mixture was stirred at room temperature for 48 h. then evaporated in *vacuo* and the crude product washed with Et_2O (10 mL) and petroleum ether (10 mL). The product was recrystallised from ethanol as a white solid, yield: 0.7 g (82%), mp = 122 – 124 ^{O}C (Lit. mp = 122 – 123 ^{O}C (360)). TLC: CH_3OH – CH_2Cl_2 1:9 v/v, (R_F = 0.6). ^{1}H NMR (CD_3OD) δ 1.64 (t, J = 7.4 Hz, 3H, CH_3), 4.67 (q, J = 7.4 Hz, 2H, CH_2), 7.68 (t, J = 7.4 Hz, 2H, CH, Ar), 7.85 (t, J = 7.4 Hz, 1H, CH, Ar), 8.07 (d, J = 7.4 Hz, 2H, CH, Ar). ^{13}C NMR (CD_3OD) δ 17.0 (CH_3), 57.0 (CH_2), 128.2, 128.6, 129.2 (5 x CH), 130.0 (C, Ar), 152.5 (C=N).

7.5.1.7. Benzimidamide hydrochloride (**42**) ($C_7H_9ClN_2$, Mol. Wt. 156.61)

Ethyl benzimidate hydrochloride (**41**) (0.5 g, 2.69 mmol) was dissolved in ethanol (3 mL) and placed in a sealed tube. Then, ammonia in methanol (3 mL) was added to the reaction mixture, which was stirred at room temperature for 24 h. After evaporation in *vacuo*, the crude product was purified by recrystallisation from ethanol to obtain a white powder, yield: 0.38 g (90%), mp = 230 – 232 ^{O}C. TLC: CH_3OH – CH_2Cl_2 1:9 v/v, (R_F = 0.3). ^{1}H NMR (DMSO-d_6) δ 7.63 (t, J = 7.8 Hz, 2H, CH, Ar), 7.75 (t, J = 7.6 Hz, 2H, CH, Ar), 7.83 (d, J = 7.8 Hz, 2H, CH, Ar), 8.36 (s, 1H, NH), 9.15 (br s, 3H, NH_3). ^{13}C NMR (DMSO-d_6) δ 128.5, 129.5, 134.3 (5 x CH), 128.6 (C, Ar), 166.3 (C=N).

7.5.1.8. 5-Chloro-3-phenyl-1,2,4-thiadiazole (**43**) ($C_8H_5ClN_2S$, Mol. Wt. 196.65)

To a stirred solution of benzamidine hydrochloride (0.2 g, 1.47 mmol) and perchloromethyl mercaptan (0.2 mL, 1.47 mmol) in CH_2Cl_2 (5 mL) was added a solution of NaOH (0.3 g, 7.31mmol) in H_2O (2.5 mL) dropwise at 0 ^{O}C. The mixture was stirred

at 0 ^{O}C for 1 h and then at room temperature for 2 h. The organic layer was washed with water (10 mL), dried over anhydrous $MgSO_4$, and concentrated in *vacuo* to obtain the product as a pale yellow semisolid, yield: 0.2 g. This product was used for next step without further purification.

7.5.1.9. *N*-(3,4-dimethylisoxazol-5-yl)-4-(3-phenyl-1,2,4-thiadiazol-5-yl)piperazine-1-carboxamide (**45**) ($C_{18}H_{20}N_6O_2S$, Mol. Wt. 384.46)

Compound **45** was prepared as described for **34** and purified using preparative TLC to obtain a white semisolid, yield: 20 mg (16%). TLC: CH_3OH – CH_2Cl_2 1:9 v/v, (R_F = 0.2). ^{1}H NMR ($CDCl_3$) δ 3.62 (br s, 8H, CH_2, pip), 7.18 (s, 1H, NH), 7.35 (m, 3H, CH, Ar), 8.13 (m, 2H, CH, Ar). ^{13}C NMR ($CDCl_3$) δ 7.12 (CH_3), 10.7 (CH_3), 43.5, 48.3 (4 x CH_2, pip), 102.9, 157.3, 162.1 (3 x C, isoxazole), 123.0, 128.5, 130.1 (5 x CH, Ar), 133.2 (1 x C, Ar), 152.92 (C=O), 170.4, 185.1 (2 x C, thiadiazol). HPLC: 98 % at RT: 6.0 min. HRMS (ES-TOF) m/z calculated mass: 407.1262 $[M + Na]^+$, observed mass: 407.1368 $[M + Na]^+$.

7.5.1.10. *Tert*-butyl 4-(3-phenyl-1,2,4-thiadiazol-5-yl)piperazine-1-carboxylate (**46**) ($C_{17}H_{22}N_4O_2S$, Mol. Wt. 346.45)

A mixture of 5-chloro-3-phenyl-1,2,4-thiadiazole (**43**) (0.34 g, 1.73 mmol), *tert*-butyl piperazine-1-carboxylate (**36**) (0.32 g, 1.73 mmol), Et_3N (0.48 mL, 3.46 mmol), sodium iodide (0.26 g, 1.73 mmol) and MeCN (18 mL) was stirred at 90 ^{O}C o/n. After completion, the solvent was concentrated in *vacuo* and the residue was purified by gradient column chromatography and collected at 70:30 v/v petroleum ether – EtOAc as a white semisolid, yield: 0.2 g, (34%), TLC: petroleum ether – EtOAc 1:1 v/v, (R_F = 0.5). ^{1}H NMR ($CDCl_3$) δ 1.39 (s, 9H, $C(CH_3)_3$), 3.47 (s, 8H, CH_2, pip), 7.30 (br d, 3H, CH, Ar), 8.08 (m, 2H, CH, Ar). ^{13}C NMR ($CDCl_3$) δ 28.6 (CH_3, $C(CH_3)_3$), 44.2, 45.6 (4 x CH_2, pip), 79.8 (C, $C(CH_3)_3$), 127.5, 129.3, 132.1 (5 x CH, Ar), 130.1 (1 x C, Ar), 161.5, 169.9 (2 x C, thiadiazol), 154.2 (C=O). HPLC: 98.26 % at RT: 9.17 min.

7.5.1.11. 3-Phenyl-5-(piperazin-1-yl)-1,2,4-thiadiazole hydrochloride (**47**) ($C_{12}H_{22}ClN_4S$, Mol. Wt. 282.79)

The Boc deprotection using HCl/dioxane was described in Chapter 4. Product obtained as a pale yellow solid, yield: 0.1 g (69.2%), mp = 190 -192 ^{O}C. TLC: petroleum ether – EtOAc 1:1 v/v, R_F = 0.1. ^{1}H NMR (DMSO-d_3) δ 3.29 (br t, 4H, CH_2, pip), 3.83 (br t, 4H,

CH_2, pip), 7.90 (br d, 3H, CH, Ar), 8.12 (m, 2H, CH, Ar), 9.35 (s, 2H, NH_2). ^{13}C NMR (DMSO-d_3) δ 42.3, 45.8 (4 x CH_2, pip), 128.0, 129.2, 130.7 (5 x CH, Ar), 133.1 (1 x C, Ar), 169.6, 176.6 (2 x C, thiadiazol). HPLC: 100 % at RT: 6.86 min.

7.5.1.12. 4-(4-Hydroxypiperidin-1-yl)benzonitrile (**50**) ($C_{12}H_{14}N_2O$, Mol. Wt. 202.26)

A mixture of 4-fluorobenzonitrile (**48**) (1 g, 8.26 mmol), 4-hydroxy piperidine (**49**) (1.1 g, 9.08 mmol) and K_2CO_3 (3.4 g, 24.8 mmol) in DMF (10 mL) was heated to 150 ^{O}C for 6 h. The reaction was cooled slowly at room temperature then poured onto cold H_2O (10 mL). The resulting solid was collected by filtration, washed with H_2O (10 mL), and dried to obtain the product as a pale shiny powder, yield: 1.4 g (82%), mp = 86 – 88 ^{O}C. (Lit. mp = 102 -103) (361) TLC: CH_3OH – CH_2Cl_2 0.5:9.5 v/v, (R_F = 0.7). ^1H NMR (DMSO-d_6) δ 1.39 (m, 2H, CH_2, piperidine), 1.79 (m, 2H, CH_2, piperidine), 3.06 (m, 2H, CH_2, piperidine), 3.71 (m, 3H, CH_2 and CH, piperidine), 4.73 (s, 1H, OH), 7.01 (d, J = 9.8 Hz, 2H, CH, Ar), 7.55 (d, J = 9.8 Hz, 2H, CH, Ar).

7.5.1.13. 4-(4-(4-Chlorophenoxy)piperidin-1-yl)benzonitrile (**52**) ($C_{18}H_{17}ClN_2O$, Mol. Wt. 312.80)

To a suspension of sodium hydride (60% in mineral oil) (0.1 g, 1.28 mmol) in dry DMF (10 mL) was added 4-chlorophenol (**51**) (0.2 g, 1.28 mmol) at room temperature and the reaction was stirred for 15 min. 1-(4-Cyanophenyl)piperidin-4-yl methanesulfonate (**54**) (0.3 g, 1.07 mmol) was added and the reaction mixture stirred at 80 ^{O}C for 8 h. After cooling, the reaction mixture was poured into H_2O (10 mL) and extracted with EtOAc (2 x 50 mL). The organic layer was washed with H_2O (20 mL), dried over anhydrous $MgSO_4$ and the solvent was removed by evaporation. The product was obtained after gradient column chromatography and collected at 30:70 v/v petroleum ether – EtOAc to give a white crystalline solid, yield: 0.25 g (76%), mp = 138 – 140 ^{O}C. TLC: petroleum ether – EtOAc 1:1 v/v, (RF = 0.8). ^1H NMR ($CDCl_3$) δ 1.93 (m, 2H, CH_2, piperidine), 2.07 (m, 2H, CH_2, piperidine), 3.35 (m, 2H, CH_2, piperidine), 3.63 (m, 2H, CH_2, piperidine), 4.53 (m, 1H, CH, piperidine), 6.89 (m, 4H, CH, Ar), 7.27 (d, J = 9.6 Hz, CH, Ar), 7.52 (d, J = 9.6 Hz, CH, Ar). ^{13}C NMR ($CDCl_3$) δ 30.9, 48.6 (4 x CH_2, piperidine), 77.1 (CH, piperidine), 117.6, 119.8, 130.9, 133.7 (8 x CH, Ar), 101.5, 125.9, 152.7, 155.1 (4 x C, Ar) 118.1 (CN). HRMS (ES-TOF) m/z calculated mass: 313.1102 $[M + H]^+$, observed mass: 313.1131 $[M + H]^+$.

7.5.1.14. 1-(4-Cyanophenyl)piperidin-4-yl methanesulfonate (**54**) ($C_{13}H_{16}Cl_3N_2O_3$, Mol. Wt. 280.34)

Et_3N (1.03 mL, 7.42 mmol) was added to a stirred and cooled suspension of 4-(4-hydroxypiperidin-1-yl)benzonitrile (**50**) (0.5 g, 2.47 mmol) in CH_2Cl_2 (5 mL) followed by methansulfonyl chloride (0.58 mL, 7.42 mmol) dropwise and stirred at 0 ^{O}C 1 h. The reaction was then quenched with ice-cold water (20 mL), washed with H_2O (20 mL), dried over anhydrous $MgSO_4$ and concentrated under reduced pressure. The product obtained after gradient column chromatography and collected at 30:70 v/v petroleum ether – EtOAc to give a colourless semisolid, yield: 0.68 g (98%), TLC: petroleum ether – EtOAc 1:1 v/v, (R_F = 0.3). ^{1}H NMR ($CDCl_3$) δ 2.01 (m, 2H, CH_2, piperidine), 2.13 (m, 2H, CH_2, piperidine), 3.32 (m, 2H, CH_2, piperidine), 3.63 (m, 2H, CH_2, piperidine CH_2), 3.08 (s, 3H, CH_3), 4.99 (m, 1H, CH, piperidine), 6.89 (d, J = 9.4 Hz, 2H, CH, Ar), 7.52 (d, J = 9.4 Hz, 2H, CH, Ar). ^{13}C NMR ($CDCl_3$) δ 30.9, 31.0 (2 x CH_2, piperidine), 38.9 (CH_3), 44.3, 44.6 (2 x CH_2, piperidine), 76.8 (CH, piperidine), 119.9 (CN), 100.5, 152.7 (2 x C, Ar), 114.3, 114.6, 133.40, 133.4, 133.9 (4 x CH, Ar).

7.5.1.15. (4-(4-(4-Chlorophenoxy)piperidin-1-yl)phenyl)methanamine (**55**) ($C_{18}H_{21}ClN_2O$, Mol. Wt. 316.83)

To a solution of 4-(4-(4-chlorophenoxy)piperidin-1-yl)benzonitrile (**52**) (0.25 g, 0.79 mmol) in THF (5 mL) at 0 ^{o}C was added $LiAlH_4$ and then the resulting mixture was heated at 80 ^{O}C for 2 h. The reaction mixture was cooled to room temperature and quenched with H_2O (5 mL). The insoluble solid was removed by filtration using celite and the filtrate was diluted with saturated Na_2CO_3 (15 mL) and extracted with EtOAc (2 x 50 mL). The organic phase was washed with brine (2 x 50 mL), dried over anhydrous $MgSO_4$ and concentrated under reduced pressure to obtain the product as a yellow semisolid, yield: 0.1 g (40%). TLC: CH_3OH – CH_2Cl_2 1:9 v/v, (R_F = 0.1). This product was used for next step without further purification.

7.5.1.16. *N*-(4-(4-(4-Chlorophenoxy)piperidin-1-yl)benzyl)-2-oxooxazolidine-3-sulfonamide (**57**) ($C_{21}H_{24}ClN_3O_5S$, Mol. Wt. 465.95)

To a cooled (0 ^{o}C) solution of chlorosulfonyl isocyanate (0.91 g, 0.72 mmol) in dry CH_2Cl_2 (1 mL) was added a solution of 2-bromoethanol (0.1 mL, 0.72 mmol) in CH_2Cl_2 (0.5 mL) dropwise while maintaining the temperature between 0 and 10 ^{O}C. The

reaction mixture was stirred at the same temperature for 1 h. A mixture of (4-(4-(4-chlorophenoxy)piperidin-1-yl)phenyl)methenamine (**55**) (0.25 g, 0.79 mmol) and Et_3N (0.25 mL, 1.79 mmol) in CH_2Cl_2 (0.7 mL) was then added dropwise while maintaining the temperature between 0 and 10 ^{O}C. Aqueous HCl (12.5 mL, 0.2 M) was added and the pH of the reaction was adjusted to 2 with concentrated HCl if necessary. The reaction mixture was decanted, and the separated organic layer washed with 0.2 M aqueous HCl (12.5 mL) and H_2O (12.5 mL). The organic layer was diluted with H_2O (12.5 mL) and as much as possible of CH_2Cl_2 was removed under vacuum at a temperature below 25 ^{O}C. Et_2O (15 mL) was added to the suspension, which was stirred at room temperature. The resulting solid was collected by filtration, washed with H_2O, and dried under vacuum at 60 ^{O}C o/n. The crude product was purified by gradient column chromatography and collected at 30:70 v/v petroleum ether – EtOAc, to give the product as a red fine powder, yield: 0.24 g (64%), mp = 134 – 138 ^{O}C. TLC: petroleum ether – EtOAc 1:1 v/v, (R_F = 0.5). ^{1}H NMR (DMSO) δ 1.69 (m, 2H, CH_2, piperidine), 2.02 (m, 2H, CH_2, piperidine), 3.05 (m, 2H, CH_2, piperidine), 3.51 (m, 2H, CH_2, piperidine), 4.57 (m, 1H, CH, piperidine), 3.75 (t, J = 8.4 Hz, 2H, CH_2, oxooxazolidine), 4.15 (t, J = 7.8 Hz, 2H, CH_2, oxooxazolidine), 4.10 (d, J = 6.3 Hz, 2H, CH_2), 7.32 (d, J = 4.3 Hz, CH_2, Ar), 7.18 (d, J = 4.6 Hz, CH_2, Ar), 7.02 (d, J = 4.3 Hz, CH_2, Ar), 6.94 (d, J = 4.6 Hz, CH_2, Ar), 8.82 (t, J = 6.2 Hz, 1H, NH). ^{13}C NMR (DMSO) δ 30.1, 30.2, 44.5 (4 x CH_2, piperidine), 45.5 (CH_2), 46.5, 62.7 (2 x CH_2, oxooxazolidine), 72.9 (1 x CH, piperidine), 113.8, 116.2, 118.1, 129.1, (8 x CH, Ar), 129.8, 151.0, 156.3 (3 x C, Ar), 124.7 (C-Cl), 152.82 (C=O). HPLC: 100 % at RT: 4.51 min. HRMS (ES-TOF) m/z calculated mass: 466.1125 $[M + H]^+$, observed mass: 466.1199 $[M + H]^+$.

Conclusion

In conclusion, antimicrobial resistance is a global public health issue affecting humanity causing prolonged hospital stays, higher medical costs, and increased mortality (1, 2). Thus, the WHO has paid attention and has made tackling the rise of AMR a priority through endorsement of five strategic objectives that represent the global action plan (10). Improving awareness and understanding of antimicrobial resistance worldwide is one of the objectives to ensure the best practices among health employees, general public and policy makers and every year, the world antimicrobial awareness week (WAAW) takes place from 18 -24 November under the slogan of Antimicrobials: Handle with care (370). In addition, the WHO is taking into consideration the optimisation of antimicrobial medicines use, reduction in the incidence of infection, strong surveillance, and investment in research (10, 16). As antibiotic resistance is part of AMR (18-25), this project focused on that through exploring aaRSs dual inhibitors as novel antibacterial agents and testing the multitarget hypothesis, through a computational approach, the aim of which is to reduce the development of microbial resistance on treatment with the designed aaRS dual inhibitors (371).

Bactroban ® and Kerydin ® (190-194) are examples of approved dual inhibitors acting competitively with the normal substrate of IleRS and LeuRS respectively for the treatment of MRSA infection and onychomycosis. As there is a percentage of similarity in the protein sequences between aaRS enzymes belong to each subclass, *S. aureus* and *E. faecalis* AspRS and AsnRS were selected to be targets in this project for the design of multitarget inhibitors. MOE and SWISS-MODEL server were used for computational analysis. *Thermus thermophilus* AspRS (pdb: 1EFW) (277) and *Pyrococcus horikoshii* AsnRS (pdb: 1X54) (282) were used as templates for homology model building of *S. aureus* AspRS and AsnRS with 51% and 46% respective similarity in their protein sequences and the same templates were used for building *E. faecalis* AspRS and AsnRS homology models with 51% and 46% of sequences identity. All models of the target enzymes were validated using Ramachandran plot, ProSA and Verify 3D and docked with their natural substrates to identify the binding interactions inside the active sites. Molecular dynamic study and binding affinity measurements were performed using the Desmond programme of Schrödinger to create a platform for the design of AspRS/AsnRS inhibitors.

Different series of AspRS/AsnRS inhibitors were designed based on mimicking the aminoacyl sulfamoyladenosine structure as the sulfamoyl link is more stable than the normal substrates and generally has improved binding within the active sites (124). Thus, the designed compounds consisted of three components; amino acid or its bioisosteres, nonpolar moiety instead of adenine to increase selectivity toward bacterial aaRSs and sulfamoyl linker with variation in the length depending on its ability to completely fill the active sites of the modelled enzyme while keeping the carbonyl group next to the amino acid for AspRS/AsnRS recognition (316, 317, 321, 322). The different series of compounds were prepared after optimisation of the synthetic routes and ^{1}H and ^{13}C NMR, mass spectrometry, elemental analysis and HPLC were used to confirm the structure of compounds and their purities. Then, the synthesised compounds were evaluated for antimicrobial activity against a broad panel of sensitive and resistant strains of pathogens with ciprofloxacin as a standard for comparison. An aminoacylation assay was performed for some of the compounds using *P. aeruginosa* AspRS assay.

Series 1 compounds **7a**-**f**, **10a**-**d** and **14a**-**d** consisted of a sulfamoyl piperazine derivatives bound to 5-carbonyl-4-methylthiazole, 3-carbonyl-5-methylisoxazole or 4-carbonyl-5-methylisoxazole instead of Asp/Asn and substituted aryl/biaryl moiety. Compound **7d** showed good inhibitory activity against the sensitive strain (ATCC 29212) and both vancomycin resistant strains (NCTC 12201 and ATCC 51299) of *E. faecalis* with MIC values of 4, 2 and 8 µg/mL respectively, while compounds **10c** and **10d** showed 32 µg/mL against the resistant strains of *E. faecalis* (NCTC12201). The difference between compounds **7d** and **10c**-**d** is in the bioisosteric amino acid (Asp/Asn) group. The presence of a sulfur atom in the thiazole ring of compounds **10c-d** instead of an oxygen atom in the isoxazole ring of compound **7d** decreases their inhibitory activity against *E. faecalis*, although they showed good binding interactions in the docking study with the target enzymes. However, derivatives **14a**-**d** did not show good MIC values owing to the presence of the nitrogen atom next to the carbonyl group leading to impaired recognition of AspRS/AsnRS.

Series 2 compounds **18a**-**g** consisted of asparagine and the same linker and substituted aryl/biaryl moiety of series 1 compounds, in an attempt to test the multitarget hypothesis. However, the MIC results of compounds **18a**-**g** did not show good

inhibitory activity against the tested microorganisms, which may be due to poor uptake of the compounds through the bacterial cell walls as the compounds were synthesised in salt forms. The aminoacylation assay was not useful to clarify the binding affinity of compounds **18a**-**g** with the target enzymes because it was performed by using *P. aeruginosa* AspRS assay not *S. aureus* and *E. faecalis* AspRS and AsnRS assays.

Series 3 compounds **24a**-**f** retained the same substituted aryl/biaryl moieties and the amino acid moiety was replaced by 3,4-dimethylisoxazole, while the linker in this series consisted of an amide group connected with a sulfamoyl linkage through a piperazine ring. The MIC results of compounds **24a**-**f** showed some inhibitory activity (32 µg/mL) of compound **24b** against flucloxacillin resistant strain of *S. aureus* (NCTC12493). The presence of an amide next to the sulfamoyl linkage contributed to forming good binding interactions with the amide linker, however this resulted in a shift of the sulfamoyl group and loss of interaction with Mg^{2+} ion, which subsequently reduces the stabilisation of the sulfamoyl group. Although the histidine and flipping loops were in close proximity to the Asp binding pocket, the shift of the compound inside the active sites of the target enzymes also resulted in no interaction with the key amino acid residues in the Asp pocket. Likewise the shift observed in AspRS was also observed with AsnRS, the result of which was that none of the key amino acid resides responsible for Asn recognition formed any binding interactions with the amino acid isosteric moiety.

Series 4 compounds **30a**-**d** have the same substituted aryl/biaryl moieties and the same amino acid isosteric moiety of compounds **24a**-**f**, while the linker in this series consisted of an oxoethyl urea linked to the piperazine of the sulfamoyl linkage to improve the fitting and stabilisation of the compounds inside the active sites. From the MIC results of compounds (**30a**-**d**), compounds **30c** and **30d** showed 32 µg/mL inhibitory activity against flucloxacillin resistant strain of *S. aureus* (NCTC12493), while others showed low inhibitory activity against the tested microorganisms. However, just one compound **45** was prepared from series 5 and 6 containing the same amino acid bio-isosteric moiety next to an amide bond while the adenine base was replaced by an aryl moiety and the linker consisted of piperazine connected with a thiadiazole ring instead of ribose to test if the fitting of the compound was improved or not but

this compound did not show good inhibitory activity against the tested microorganisms.

This project faced many challenges and limitations and due to the lack of available information about AspRS and AsnRS enzymes, the lack of crystal structures of both enzymes and no lead compounds for inhibitors design, it was not possible to rely on the background of these enzymes to establish the research. However, based on the available research on others aaRS enzymes and the similarity in their protein sequences, the computational studies have assisted in creating a good platform for the design of AspRS/AsnRS inhibitors, which showed good inhibitory activity against *S. aureus* and *E. faecalis* specifically compound **7d**. The results related to MIC measurement of all designed inhibitors did not give a full perception of the competitive binding of the compounds with the natural substrates of the target enzymes as the uptake through the cell membrane may have limited the effectiveness of the designed compounds. Thus, a competitive binding assay of *S. aureus* and *E. faecalis* AspRS and AsnRS is required to accurately measure the efficacy and potency of the designed compounds. Some of compounds were investigated using the aminoacylation assay of *P. aeruginosa* AspRS owing to its availability and this is another limitation because the difference in the protein sequences of *P. aeruginosa* AspRS and *S. aureus* and *E. faecalis* AspRSs is high. Many studies reported that the recognition of the same natural substrate by the same aaRS in different microorganisms is different as the identity elements for the recognition is varied as a result of evolutionary history of these enzymes.

From the docking studies, microbiological screening results and published aaRSs published research, the presence of a carbonyl group next to the amino acid or amino acid isosteric moiety is essential for AspRS/AsnRS recognition and also, for the stabilisation of compounds inside the active sites. Replacement the phosphoanhydride linkage with a sulfamoyl linkage was effective and the latter linkage takes the same role in stabilisation of the compounds inside the pockets through its binding interactions with Mg^{2+} ions. Any replacement of the phosphoanhydride linkage with an amide or urea, resulted in loss of the binding interactions required for stabilisation of the compounds inside the active sites of the target enzymes despite their binding interactions with other key amino acid residues. There is no main binding

interaction with the ribose moiety, and it can be replaced by any moiety having a similar 5-ring structure. The presence of donating groups on the biphenyl ring, such as a methoxy group in compound **7d**, augmented the biding interactions of the biphenyl moiety inside the AMP pocket, which was reflected by its inhibitory activity. However, compounds **7e**-**f** did not show good inhibitory activity as their biphenyl rings contained fluoro and chloro substitutions.

References

[1] World Health Organization, Global antimicrobial resistance surveillance system (GLASS) report. https://apps.who.int/iris/bitstream/handle/10665/259744/9789241513449eng.pdf;jsessionid=E9766ED0A0A0481007723B1989CB163A?sequence=1 , 2017 (accessed 1 December 2019).

[2] S. Barber, K. Swaden-Lewis, Antimicrobial resistance. House of Commons library. https://researchbriefings.parliament.uk/ResearchBriefing/Summary/CBP-8141 , 2017 (accessed 30 September 2019).

[3] V.M. KateKhaye, G.S. Kohli, R.R. Uchil, O.S. Swami, Strategies to combat antimicrobial resistance, J Clin Diagn Res. 8 (7) (2014) 1-4. https://www.ncbi.nlm.nih.gov/pmc/articles/PMC4149102/ .

[4] D.S. Davies, R. Sugden, what if antibiotics were to stop working? https://www.kingsfund.org.uk/reports/thenhsif/what-if-antibiotics-stopped-working/ , 2016 (accessed 2 April 2020).

[5] R.B. Fugitt, R.W. Luckenbaugh, 5-Halomethyl-3-phenyl-2-oxazolidinones. https://patents.google.com/patent/US4128654A/en , 1978 (accessed 2 April 2020).

[6] M. Debono, M. Barnhart, C.B. Carrell, J.A. Hoffmann, J.L. Occolowitz, B.J. Abbott, D.S. Fukuda, R.L. Hamill, K. Biemann, W.C. Herlihy, A21978C, a complex of new acidic peptide antibiotics: isolation, chemistry, and mass spectral structure elucidation, J Antibiot. 40 (1987) 761–777. https://pubmed.ncbi.nlm.nih.gov/3610833/ .

[7] R. Novak, D.M. Shlaes, The pleuromutilin antibiotics: a new class for human use. Curr Opin Investig Drugs. 11 (2010) 182–191. https://pubmed.ncbi.nlm.nih.gov/20112168/ .

[8] National Center for Biotechnology Information. PubChem compound summary for CID 446596, Mupirocin. https://pubchem.ncbi.nlm.nih.gov/compound/Mupirocin , 1988 (accessed 2 April 2020).

[9] J. O'Neill, Antimicrobial Resistance: Tackling a crisis for the health and wealth of nations. https://amr-review.org/sites/default/files/AMR%20Review%20Paper%20%20Tackling%20a%20cr

isis%20for%20the%20health%20and%20wealth%20of%20nations_1.pdf , 2014 (accessed 2 April 2020).

[10] Antibiotic Research UK, Chief Medical Officer calls for new action on antibiotic resistance. 2017 https://www.antibioticresearch.org.uk/chief-medical-officer-calls-new-action-antibiotic-resistance/ , 2017 (accessed 1 September 2018).

[11] World Health Organisation, WHO multi-country survey reveals widespread public misunderstanding about antibiotic resistance. https://www.who.int/en/news-room/detail/16-11-2015-who-multi-country-survey-reveals-widespread-public-misunderstanding-about-antibiotic-resistance , 2015 (accessed 29 March 2020).

[12] Wellcome Trust, Understanding of antibiotics. https://wellcome.ac.uk/sites/default/files/antibiotic-resistance-graphic-wellcome-apr16.pdf , 2016 (accessed 29 March 2020).

[13] NHS Choices, The antibiotic awareness campaign. https://www.nhs.uk/conditions/antibiotics/ , 2015 (accessed 29 March 2029).

[14] K. Lay, Three quarters of doctors take a guess on antibiotics. https://www.thetimes.co.uk/article/three-quarters-of-doctors-take-a-guess-on-antibiotics-mbdsl395x , 2017 (accessed 29 March 2020) .

[15] J. O'Neill, Antimicrobials in agriculture and the environment: reducing unnecessary use and waste. https://ec.europa.eu/health/amr/sites/amr/files/amr_studies_2015_am-in-agri-and-env.pdf , 2015 (accessed 29 March 2020).

[16] J. Wentworth, Antibiotic resistance in the environment. Parliamentary office of science and technology, 2013 https://post.parliament.uk/research-briefings/post-pn-446/ , (accessed 29 March 2020).

[17] L.L. Silver, Challenges of antibacterial discovery, Clin. Microbiol. Rev. 24 (1) (2011) 71-109. https://www.ncbi.nlm.nih.gov/pmc/articles/PMC3021209/ .

[18] L.E. Bryan, Two forms of antimicrobial resistance: bacterial persistence and positive function resistance, J. Antimicrob. Chemother. 23 (1989) 817– 820. https://pubmed.ncbi.nlm.nih.gov/2668250/ .

[19] P. Courvalin, Predictable and unpredictable evolution of antibiotic resistance, J. Intern. Med. 264 (2008) 4–16. https://pubmed.ncbi.nlm.nih.gov/18397243/ .

[20] V.M. D'Costa, K.M. McGrann, D.W. Hughes, G.D. Wright. 2006. Sampling the antibiotic resistome, Science. 311 (2006) 374–377. https://pubmed.ncbi.nlm.nih.gov/16424339/ .

[21] J. Davies, Inactivation of antibiotics and the dissemination of resistance genes, Science. 264 (1994) 375–382. https://science.sciencemag.org/content/264/5157/375.

[22] J.M.T. Hamilton-Miller, The emergence of antibiotic resistance: myths and facts in clinical practice, Intensive Care Med. 16 (1990) 206–211. https://link.springer.com/article/10.1007/BF01709702 .

[23] J.L. Martinez, F. Baquero. 2000. Mutation frequencies and antibiotic resistance, Antimicrob. Agents Chemother. 44 (2000) 1771–1777. https://pubmed.ncbi.nlm.nih.gov/10858329/ .

[24] J.L. Martinez, F. Baquero, D.I. Andersson, Predicting antibiotic resistance, Nat. Rev. Microbiol. 5 (2007) 958–965. https://pubmed.ncbi.nlm.nih.gov/18007678/ .

[25] L.L. Silver, K. A. Bostian, Discovery and development of new antibiotics: the problem of antibiotic resistance, Antimicrob. Agents Chemother. 37 (1993) 377–383. https://www.ncbi.nlm.nih.gov/pmc/articles/PMC187680/ .

[26] K. Garima, S. Saigal, A. Elongavan, Action and resistance mechanisms of antibiotics: A guide for clinicians, J. Anaesthesiol. Clin. Pharmacol. 33 (3) (2017) 300–305. https://www.ncbi.nlm.nih.gov/pmc/articles/PMC5672523/ .

[27] H.C. Neu, The crisis in antibiotic resistance, Science. 257 (1992) 1064-1073. https:// 10.1126/science.257.5073.1064. .

[28] M.C. McManus, Mechanism of bacterial resistance to antimicrobial agents, Am J Health Syst Pharm. 54 (12) (1992) 1064-1073. https://doi.org/10.1093/ajhp/54.12.1420.

[29] P.A. Lambert, Bacterial resistance to antibiotics: modified target sites, Adv. Drug Deliv. Rev. 57(10) (2005) 1471-85. https://doi.org/10.1016/j.addr.2005.04.003.

[30] K. Drlica, X. Zhao, DNA gyrase, topoisomerase IV, and the 4-quinolones, Microbiol Mol Biol Rev 61 (1997) 377-392. PMCID: PMC232616.

[31] J. Yao, R.J. Moellering, Antibacterial agents, in: P.R. Murray, E.J. Baron, J.H. Jorgensen, M.A. Pfaller, R.H. Yolken (Eds.), Manual of clinical microbiology, DC:ASM press, Washington, 2003, pp. 1039-1073.

[32] W.A.J. Petri, Antimicrobial agents: sulphonamides, trimethoprim-sulfamethoxazole, quinolones, and agents for urinary tract infection, in: L.L. Brunton, J.S. Lazo, K.L. Parker, (Eds.), Goodman and Gilman 's the pharmacological basis of therapeutics, McGrawhill, New York, 2006, pp. 1111-1126.

[33] D.R. Storm, K.S. Rosenthal, P.E. Swanson, Polymyxin and related peptide antibiotics, Annu. Rev. Biochem. 46 (1977) 723-763. https://doi.org/10.1146/annurev.bi.46.070177.003451.

[34] C.F. Carpenter, H.F. Chambers, Daptomycin: another novel agent for treating infections due to drug-resistant gram-positive pathogen, Clin Infect Dis. 38 (7) (2004) 994-1000. https://doi.org/10.1086/383472.

[35] H.M. Dockrell, R.V. Goering, I. Roitt, D. Wakelin, M. Zuckerman, Attacking the enemy: antimicrobial agents and chemotherapy, in: C. Mims, H.M. Dockrell, R.V. Goering, I. Roitt, D. Wakelin, M. Zuckerman (Eds.), Medical Microbiology, Elsevier Mosby, Netherlands, 2004, pp. 473–507.

[36] M.N. Alekshun, S.B. Levy, Molecular mechanisms of antibacterial multidrug resistance. Cell. 128 (6) (2007) 1037-1050. https://doi.org/10.1016/j.cell.2007.03.004.

[37] G.A. Jacoby, L.S. Munoz-Price, The new beta-lactamases, N Engl J Med. 352(4) (2005) 380-91. http://10.1056/NEJMra041359.

[38] B.A. Rasmussen, k. Bush, Carbapenem-hydrolyzing beta-lactamases, Antimicrob. Agents Chemother. 41 (2) (1997) 223-32. http://10.1128/AAC.41.2.223.

[39] G.V. Crichlow, A.P. Kuzin, M. Nukaga, K. Mayama, T. Sawai, J.R. Knox, Structure of the extended-spectrum class C beta-lactamase of Enterobacter cloacae GC1, a natural mutant with a tandem tripeptide insertion, Biochemistry. 38 (32) (1999) 10256-10261. http://10.1021/bi9908787.

[40] T. Naas, P. Nordmann, OXA-type beta-lactamases. Curr Pharm Des. 5 (11) (1999) 865-79. PMID: 10539993.

[41] F. Maurice, I. Broutin, I. Podglajen, P. Benas, E. Collatz, F. Dardel, Enzyme structural plasticity and the emergence of broad-spectrum antibiotic resistance, EMBO Rep. 9 (4) (2008) 344-349. https://doi.org/10.1038/embor.2008.9.

[42] T. Strateva, D. Yordanov, Pseudomonas aeruginosa - a phenomenon of bacterial resistance. J. Med. Microbiol. 58 (9) (2009) 1133-48. https://doi.org/10.1099/jmm.0.009142-0.

[43] M.E. Tolmasky, Bacterial resistance to aminoglycosides and beta-lactams: the Tn1331 transposon paradigm, Front Biosci. 5 (2000) 20-29. http://doi.10.2741/tolmasky.

[44] P.A. Lambert, Mechanisms of antibiotic resistance in *Pseudomonas aeruginosa*, J. R. Soc. Med. 41 (2002) 22-26. PMID: 12216271.

[45] F.C. Tenover, Mechanisms of antimicrobial resistance in bacteria, Am. J. Med. 119 (6) (2006) 3-70. http://doi.org.10.1016/j.amjmed.2006.03.011.

[46] B. Weisblum, Erythromycin resistance by ribosome modification, Antimicrob. Agents Chemother. 39 (3) (1995) 577-585. PMID: 7793855.

[47] K. Hiramatsu, L. Cui, M. Kuroda, T. Ito, The emergence and evolution of methicillin-resistant *Staphylococcus aureus*, Trends Microbiol. 9 (10) (2001) 486-493. http://doi.10.1016/s0966-842x(01)02175-8.

[48] A. Giedraitienė, A. Vitkauskienė, R. Naginienė, A. Pavilonis, Antibiotic resistance mechanisms of clinically important bacteria, Medicina (Kaunas). 47(3) (2011) 137-146. PMID: 21822035.

[49] S. Džidic, J. Šuškovic, B. Kos, Antibiotic resistance mechanisms in bacteria: Biochemical and genetic aspects. Food Technol. Biotechnol. 46 (1) (2008) 11–21. file:///C:/Users/amena/Downloads/46_11.pdf.

[50] Y.H. Kim, C.J Cha, C.E. Cerniglia, Purification and characterization of an erythromycin esterase from an erythromycin-resistant Pseudomonas sp., FEMS

Microbiol. Lett. 210 (2) (2002) 239-244. https://doi.org/10.1111/j.1574-6968.2002.tb11187.x.

[51] R.I. Aminov, R.I. Mackie, Evolution and ecology of antibiotic resistance genes, FEMS Microbiol. Lett. 271 (2) (2007) 147–161. https://doi.org/10.1111/j.1574-6968.2007.00757.x.

[52] A.H. Delcour, Outer membrane permeability and antibiotic resistance, Biochem Biophys Acta. 1794 (5) (2009) 808-816. https://doi.org/10.1016/j.bbapap.2008.11.005.

[53] R.J. Henry, The mode of action of sulfonamides, Bacteriol. Rev. 7 (4) (1943) 175–262. PMID: 16350088.

[54] G.A. Naik, L.N. Bhat, B.A. Chpoade, J.M. Lynch, Transfer of broad-host-range antibiotic resistance plasmids in soil microcosms, Curr. Microbiol. 28 (4) (1994) 209–215. http://doi.10.1007/BF01575963.

[55] M. Varga, L. Kuntova, R. Pantucek, I. Maslanova, V. Ruzickova, J. Doskar, Efficient transfer of antibiotic resistance plasmids by transduction within methicillin-resistant *Staphylococcus aureus* USA300 clone, FEMS Microbiol. Lett. 332 (2) (2012) 146–152. http://doi.10.1111/j.1574-6968.2012.02589.x.

[56] I. Chen, D. Dubnau, DNA uptake during bacterial transformation, Nat. Rev. Microbiol. 2 (3) (2004) 241–249. http://doi.10.1038/nrmicro844.

[57] O. Johnsborg, V. Eldholm, L.S. Håvarstein, Natural genetic transformation: prevalence, mechanisms and function, Microbiol. Res. 158 (10) (2007) 767–778. http://doi.10.1016/j.resmic.2007.09.004.

[58] K.M. Derbyshire, T.A. Gray, Distributive conjugal transfer: new insights into horizontal gene transfer and genetic exchange in mycobacteria, Microbiol. Spectr. 2 (1) (2014) 61–79. http://doi.10.1016/j.resmic.2007.09.004.

[59] W. Bereket, K. Hemalatha, B. Getenet, T. Wondwossen, A. Solomon, A. Zeynudin, S. Kannan, Update on bacterial nosocomial infections, Eur. Rev. Med. Pharmacol. Sci. 16 (8) (2012) 1039–1044. PMID: 22913154.

[60] S. Sacar, K.S. Sayin, H. Turgut, N. Cevahir, C.D. Hircin, K. Tekin, Epidemiology and associated factors for nosocomial methicillin-resistant *Staphylococcus aureus* infection in a tertiary-care hospital, Epidemiol. Infect. 138 (5) (2010) 697–701. http://doi.10.1017/S0950268809991063.

[61] S. Santajit, N. Indrawattana, Mechanisms of antimicrobial resistance in ESKAPE pathogens, Biomed Res Int. (2016) 1-8. http://doi.10.1155/2016/2475067.

[62] J.N. Pendleton, S.P. Gorman, B.F. Gilmore, Clinical relevance of the ESKAPE pathogens, Expert Rev Anti Infect Ther. 11 (3) (2013) 297–308. http://doi.10.1586/eri.13.12.

[63] A. Molander, C. Reit, G. Dahlén, T. Kvist, Microbiological docks of root-filled teeth with apical periodontitis, Int Endod J. 31 (1) (1998) 1–7. PMID: 9823122.

[64] K.J. Ryan, C.G. Ray, Sherris medical microbiology: an introduction to infectious diseases, fourth ed., McGraw Hill, New York, 2004.

[65] P. Courvalin, Vancomycin resistance in Gram-positive cocci, Clin. Infect. Dis. 42 (1) (2006) S25–34. http://doi.10.1086/491711.

[66] H.F. Wertheim, D.C. Melles, M.C. Vos, L.W. Van, B.A. Van, H.A. Verbrugh, J.L. Nouwen, The role of nasal carriage in *Staphylococcus aureus* infections, Lancet. Infect. Dis. 5 (12) (2005) 751–762. http://doi.10.1016/S1473-3099(05)70295-4.

[67] S.Y. Tong, J.S. Davis, E. Eicenberger, T.L. Holland, V.G. Foweler, *Staphylococcus aureus* infections: epidemiology, pathophysiology, clinical manifestations, and management, Clin. Microbiol. Rev. 28 (3) (2015) 603-661. http://doi.10.1128/CMR.00134-14.

[68] F.D. Lowy, *Staphylococcus aureus* Infections, N Engl J Med. 339 (8) (1998) 520-532. http://doi.10.1056/NEJM199808203390806.

[69] J.G. Rachel, D.L. Franklin, Pathogenesis of methicillin-resistant *Staphylococcus aureus* infection, Clin Infect Dis. 46 (5) (2008) S350-359. http://doi.10.1086/533591.

[70] H. Patel, Y. Vashasiya, B.R. Vyas, S. Chanda, Antibiotic-resistant *Staphylococcus aureus*: a challenge to researchers and clinicians. J. Bacteriol. 2 (2) (2012), 23-45. http://doi.10.3923/bj.2012.23.45.

[71] R.C. Simon, J.F. Simon, Surface adhesins of *Staphylococcus aureus*, Adv. Microb. Physiol. 51 (2006) 187–224. http://doi.10.1016/S0065-2911(06)51004-5.

[72] F. Timothy, *Staphylococcus*, in: S. Baron, (Ed.), Medical Microbiology, Galveston (TX): University of Texas Medical Branch, Galveston, 1996, Chapter 12.

[73] G.J. Tortora, B.R. Funke, L. Christine, Microbiology: An Introduction, Eleventh ed., Pearson Education Inc., 2013.

[74] M. Bukowski, B. Wladyka, D.G. Grzegorz, Exfoliative toxins of *Staphylococcus aureus*, Toxins. 2 (5) (2010) 1148-1165. http://doi.10.3390/toxins2051148.

[75] J.T. Weber, Community-associated methicillin-resistance *Staphylococcus aureus*, Clint. Infect. Dis. 2005, 41 (2005) 269-272. http://doi.10.1086/430788.

[76] Centers for Disease Control and Prevention, General information about MRSA in community. https://www.cdc.gov/mrsa/community/index.html , (accessed 15 April 2018).

[77] D.E. Gonzalez, G. Martinez-Aguilar, K.G. Hulten, W.A. Hammerman, J. Coss-Bu, Severe *Staphylococcal* sepsis in adolescents in the era of community-acquired methicillin-resistant *Staphylococcus aureus*, Pediatrics. 115 (3) (2005) 642-648. http://doi.10.1542/peds.2004-2300.

[78] S.E. Cosgrove, Y. Qi, K.S. Kaye, S. Harbarth, A.W. Karchmer, Y. Carmeli, The impact of methicillin-resistant in *Staphylococcus aureus* bacteremia on patient outcomes: mortality, length of stay and hospital charge, Infect Control Hosp Epidemiol. 26 (2) (2005) 166-174. http://doi.10.1086/502522.

[79] C. Kassis, R. Hachem, I.I. Raad, C.A. Perego, T. Dvorak, Outbreak of community-acquired methicillin-resistant *Staphylococcus aureus* skin infections among health care workers in a cancer centre, Am. J. Infect. Control. 39 (12) (2011) 112-117. http://doi.10.1016/j.ajic.2010.04.220.

[80] J.P. Jeannon, A. Orabi, A. Manganaris, R. Simo, Methicillin-resistant *Staphylococcus aureus* infection as a causative agent of fistula formation following total laryngectomy for advanced head and neck cancer, Head Neck Oncol. 2 (14) (2010). http://doi10.1186/1758-3284-2-14.

[81] T.P. Lodise, J. Graves, A. Evans, E. Graffunder, M. Helmecke, B.M. Lomaestro, K. Stellrecht, Relationship between vancomycin MIC and failure among patients with methicillin-resistant *Staphylococcus aureus* bacteremia treated with vancomycin, Antimicrob. Agents Chemother. 52 (9) (2008) 3315. http://doi10.1128/AAC.00113-08.

[82] S. Shurland, M. Zhan. D.D. Bradham, M.C. Roghmann, Comparison of mortality risk associated with bacteremia due to methicillin-resistant and methicillin-susceptible *Staphylococcus aureus*, Infect Control Hosp Epidemiol. 28 (3) (2007) 273-279. http://doi.10.1086/512627.

[83] K.B. Laupland, O. Lyytikainen, M. Sogaard, K.J. Kennedy, J.D. Knudsen, C. Ostergaard, J.C. Galbraith, L. Valiquette, G. Jacobsson, P. Collignon, H.C. Schonheyder, International bacteremia surveillance collaborative: the changing epidemiology of *Staphylococcus aureus* bloodstream infection: a multinational population-based surveillance study, Clin Microbiol Infect. 19 (5) (2013) 465– 471. http://doi.10.1111/j.1469-0691.2012.03903.x.

[84] MRSA Action UK, MRSA & Clostridium Difficile Trends. http://mrsaactionuk.net/monthlystatistics.html , 2016, (accessed 13 April 2018).

[85] National Statistics, MRSA bacteremia: monthly data by post infection review assignment, https://www.gov.uk/government/statistics/mrsa-bacteraemia-monthly-data-by-post-infection-review-assignment , 2016, (accessed 13 April 2018).

[86] Annual epidemiological commentary: Gram-negative bacteraemia, MRSA bacteraemia, MSSA bacteraemia and *C. difficile* infections, up to and including financial year April 2018 to March 2019. https://assets.publishing.service.gov.uk/government/uploads/system/uploads/attachment_data/file/843870/Annual_epidemiological_commentary_April_2018-March_2019.pdf, 2019, (accessed 13 May 2018).

[87] Office for National Statistics, Deaths involving MRSA: 2008 to 2012. https://www.ons.gov.uk/peoplepopulationandcommunity/birthsdeathsandmarriages/deaths/bulletins/deathsinvolvingmrsa/2013-08-22 , 2012, (accessed 13 April 2018).

[88] V.G. Fowler, J.M. Miro, J.M. Hoen, B. Cabell, C.H. Abrutyn, E. Rubinstein, E. Corey, G.R. Spelman, D. Bradley, S.F. Barsic, B. Pappas, P.A. Anstrom , K.J. Wray, D. Fortes,

C.Q. Anguera, I. Athan, E. Jones, E.P. Meer, J.T. Elliott, T.S. Levine, D.P. Bayer, *Staphylococcus aureus* endocarditis: a consequence of medical progress, JAMA. 293 (24) (2005) 3012–3021. http://doi.10.1001/jama.293.24.3012.

[89] Z.A. Kanafani, T.H. Mahfouz, S.S. Kanj, Infective endocarditis at a tertiary care centre in Lebanon: predominance of *streptococcal* infection, J Infect. 45 (3) (2002) 152–159. http://doi.10.1016/s0163-4453(02)91041-8.

[90] M.S. Ikama, M. Nkalla-Lambi, G. Kimbally-Kaky, M.L. Loumouamou, J.L. Nkoua, Profile of infective endocarditis at Brazzaville University Hospital, Med. Sante Trop. 23 (2013) 89–92. http://doi.10.1684/mst.2013.0151.

[91] N.V. Yameogo, K.J. Kologo, A.A. Yameogo, C. Yonaba, G.R. Millogo, S.A. Kissou, B.J. Toguyeni, A.K. Samadoulougou, S. Pignatelli, J. Simpore, P. Zabsonre, Infective endocarditis in sub-Saharan African children, cross-sectional study about 19 cases in Ouagadougou at Burkina Faso. Ann Cardiol. Angeiol. 63 (1) (2013) 7–10. http://doi.10.1016/j.ancard.2013.02.004.

[92] R.S. TrabelsiI, A. Znazen, I. Maaloul, D. Abid, A. Maalej, I. Kharrat, M. Ben -Jemaa, A. Hammemi, A. Kammoun, Native valve infective endocarditis in a tertiary care center in a developing country (Tunisia), Am. J. Cardiol. 102 (9) (2008) 1247–1251. https://doi.org/10.1016/j.amjcard.2008.06.052.

[93] A. Letaief, E. Boughzala, N. Kaabia, S. Ernez, F. Abid, T.B. Chaabane, M. Jemaa, R. Boujnah, M. Chakroun, M. Daoud, R. Gaha, N. Kafsi, A. Khalfallah, L. Slimane, M. Zaouali, Epidemiology of infective endocarditis in Tunisia: a 10-year multicenter retrospective study, Int. J. Infect. Dis. 11 (5) (2007) 430– 433. https://doi.org/10.1016/j.ijid.2006.10.006.

[94] American Thoracic Society, Infectious Diseases Society of America, Guidelines for the management of adults with hospital-acquired, ventilator associated, and healthcare-associated pneumonia. Am J Respir Crit Care Med. 171 (4) (2005) 388– 416. http://doi.10.1164/rccm.200405-644ST.

[95] M.S. Lee, V. Walker, L.F. Chen, D.J. Sexton, D.J. Anderson, The epidemiology of ventilator-associated pneumonia in a network of community hospitals: a prospective

multicentre study, Infect Control Hosp Epidemiol. 34 (7) (2013) 657– 662. http://doi.10.1086/670991.

[96] R.G. Wunderink, How important is methicillin-resistant *Staphylococcus aureus* as a cause of community-acquired pneumonia and what is best antimicrobial therapy, Infect. Dis. Clin. North Am. 27 (1) (2013) 177–188. http://doi.10.1016/j.idc.2012.11.006.

[97] S. Esposito, G. Pennoni, V. Mencarini, N. Palladino, L. Peccini, N. Principi, Antimicrobial treatment of *staphylococcus aureus* in patients with cystic fibrosis, Front Pharmacol. 10 (2019) 849. http://doi.10.3389/fphar.2019.00849.

[98] R.M. Klevens, M.A. Morrison, J. Nadle, S. Petit, K. Gershman, S. Ray, L.H. Harrison, R. Lynfield, G. Dumyati, J.M. Townes, A.S. Craig, E.R. Zell, G.E. Fosheim, L.K. McDougal, R.B. Carey, S.K. Fridkin, Invasive methicillin-resistant S*taphylococcus aureus* infections in the United States, JAMA. 298 (15) (2007)1763–1771. http://doi.10.1001/jama.298.15.1763.

[99] W.J. Peppard, A. Daniels, L. Fehrenbacher, J. Winner, Evidence based approach to the treatment of community-associated methicillin-resistant *Staphylococcus aureus*, Infect Drug Resist. 2 (2009) 27-40. https://doi.org/10.2147/IDR.S3794.

[100] Minnesota Department of Health fact sheet, *Staphylococcus aureus*, Infectious Disease Epidemiology, Prevention and Control, www.health.state.mn.us , 2010, (accessed 13 April 2018).

[101] S. Saxena, P. Thompson, R. Birger, A. Bottle, N. Spyridis, I. Wong, A.P. Johnson, R. Gilbert, M. Sharland, Improving children's antibiotic prescribing group: increasing skin infections and *Staphylococcus aureus* complications in children, England, 1997-2006, Emerg. Infect. Dis. 16 (3) (2010) 530–533. http://doi.10.3201/eid1603.090809.

[102] V.L. Vaska, G.R. Nimmo, M. Jones, K. Grimwood, D.L. Paterson, Increases in Australian cutaneous abscess hospitalisations: 1999-2008, Eur. J. Clin. Microbiol. Infect. Dis. 31 (1) (2011) 93–96. http://doi.10.1007/s10096-011-1281-1283.

[103] S.H. Sheehy, B.A. Atkins, P. Bejon, I. Byren, D. Wyllie, N.A. Athanasou, A.R. Berendt, M.A. McNally, The microbiology of chronic osteomyelitis: prevalence of

resistance to common empirical anti-microbial regimens, J. Infect. 60 (5) (2010) 338–343. http://doi.10.1016/j.jinf.2010.03.006.

[104] O. Clerc, G. Prod'hom, G. Greub, G. Zanetti, L. Senn, Adult nativeseptic arthritis: a review of 10 years of experience and lessons for empirical antibiotic therapy, J. Antimicrob. Chemother. 66 (5) (2011) 1168–1173. http://doi.10.1093/jac/dkr047.

[105] T.N. Peel, A.C. Cheng, P.F. Choong, K.L. Buising, Early onset prosthetic hip and knee joint infection: treatment and outcomes in Victoria, Australia, J. Hosp. Infect. 82 (4) (2012) 248–253. http://doi.10.1016/j.jhin.2012.09.005.

[106] F.A. Waldvogel, G. Medoff, M.N. Swartz, Osteomyelitis: a review of clinical features, therapeutic considerations and unusual aspects, N Eng J Med. 1970, 282 (1970) 198–206. http://doi.10.1056/NEJM197001222820406.

[107] T. Akiyama, H. Chikuda, H. Yasunaga, Y. Horiguchi, K. Fushimi, K. Saita, Incidence and risk factors for mortality of vertebral osteomyelitis: a retrospective analysis using the Japanese diagnosis procedure combination database, BMJ. 3 (3) (2013). http://doi.10.1136/bmjopen-2012-002412.

[108] W.S. Chang, M.W. Ho, P.C. Lina, C.M. Ho, C.H. Choua, M.C. Luac, Y.J. Chenbcd, H.T. Chenb, J.H. Wanga, C.Y. Chi, Clinical characteristics, treatments, and outcomes of hematogenous pyogenic vertebral osteomyelitis, 12-year experience from a tertiary hospital in central Taiwan, J. Micro. 51 (2) (2018) 235-242. http://doi.10.1016/j.jmii.2017.08.002.

[109] M. McHenry, K. Easly, G. Locker, Vertebral osteomyelitis: long term outcome for 253 patients from 7 Cleveland-area hospitals, Clin. Infect. Dis. 34 (10) (2002) 1342–1350. http://doi.10.1086/340102.

[110] E. Mylona, M. Samarkos, E. Kakalou, P. Fanourgiakis, A. Skoutelis, Pyogenic vertebral osteomyelitis: a systematic review of clinical characteristics, Semin. Arthritis Rheum. 39 (1) (2009) 10–17. http://doi.10.1016/j.semarthrit.2008.03.002.

[111] N. Stoesser, J. Pocock, C.E. Moore, S. Soeng, P. Hor, P. Sar, D. Limma-thurotsakul, N. Day, V. Kumar, S. Khan, V. Sar, C.M. Parry, The epidemiology of paediatric bone and

joint infections in Cambodia, 2007-11, J. Trop. Pediatr. 59 (2013) 36–42. http://doi.10.1093/tropej/fms044.

[112] S.M. Kurtz, K.L. Ong, E. Lau, K.J. Bozic, D. Berry, J. Parvizi, Prosthetic joint infection risk after TKA in the Medicare population, Clin Orthop Relat Res. 468 (1) (2010) 52–56. http://doi.10.1007/s11999-009-1013-1015.

[113] D. Bouras, A. Doudoulakakis, M. Tsolia, I Vaki, N. Giormezis, N. Petropoulou, E. Lebessi, V. Gennimata, A.Tsakris, I.Spiliopoulou, A. Michos, *Staphylococcus aureus* osteoarticular infections in children: an 8-year review of molecular microbiology, antibiotic resistance and clinical characteristics, J. Med. Microbiol. 67 (12) (2018) 1753–1760. http://doi.10.1099/jmm.0.000859.

[114] B.E. Murray, The life and times of the *Enterococcus,* Clin. Microbiol. Rev. 3 (1) (1990) 46–65. http://doi.10.1128/cmr.3.1.46.

[115] K. J. Christopher, R.B. Louis, A.A. Cesar, *Enterococcal* infection—treatment and antibiotic resistance, in: M.S. Gilmore, D.B. Clewell, Y. Ike, N. Shankar, (Eds.), *Enterococci*: from commensals to leading causes of drug resistant infection, Boston, 2014, pp. 123-180.

[116] J.F. Mohr, L.V. Friedrich, S. Yankelev, K.C. Lamp, Daptomycin for the treatment of *enterococcal* bacteraemia: results from the Cubicin Outcomes Registry and Experience (CORE), Int. J. Antimicrob. Agents. 33 (6) (2009) 543–548. http://doi.10.1016/j.ijantimicag.

[117] S.F. Ataide, M. Ibba, Small molecules: big players in the evolution of protein synthesis, ACS Chem. Biol. 1 (5) (2006) 285-297. http://doi.10.1021/cb600200k.

[118] Biology Forums, Aminoacyl-tRNA synthetase charging a tRNA. http://biology-forums.com/index.php?action=gallery;sa=view;id=430 , 2011 (accessed 14 April 2020).

[119] J.G. Arnez, D. Moras, Structural and functional considerations of the aminoacylation reaction, Trends Biochem. Sci. 22 (6) (1997) 211-216. http://doi.10.1016/s0968-0004(97)01052-9.

[120] M. Mirande, Processivity of translation in the eukaryote cell: role of aminoacyl-tRNA synthetases, FEBS Lett. 584 (2) (2010) 443-447. https://doi.org/10.1016/j.febslet.2009.11.027.

[121] M. Ibba, D. Soll, Aminoacyl-tRNA synthesis, Annu. Rev. Biochem. 69 (2000) 617–650. http://doi.10.1146/annurev.biochem.69.1.617.

[122] G. Eriani, M. Delarue, O. Poch, J. Gangloff, D. Moras, Partition of tRNA synthetases into two classes based on mutually exclusive sets of sequence motifs, Nature, 347 (1990) 203-206. https://doi.org/10.1038/347203a0.

[123] V. Rajendran, P. Kalita, H. Shukla, A. Kumar, T. Tripathi, Aminoacyl-tRNA synthetases: structure, function, and drug discovery, Int. J. Biol. Macromol. 111 (2018) 400–414. http://doi.10.1016/j.ijbiomac.2017.12.157.

[124] H.M. Gaston, V.A. Arthur, Aminoacyl-tRNA synthetase inhibitors as potential antibiotics, Eur. J. Med. Chem. 46 (11) (2011) 5227-5236. http://doi.10.1016/j.ejmech.2011.08.049.

[125] M. Mirande, Aminoacyl-tRNA synthetase family from prokaryotes and eukaryotes: structural domains and their implications, in: W.E. Cohn, (Eds.), progress in nucleic acid research and molecular biology, 40 (1991) 95-142. https://doi.org/10.1016/S0079-6603(08)60840-5.

[126] S. Dutta, K. Choudhury, S.D. Banik, N. Nandi, Active site nanospace of aminoacyl tRNA synthetase: difference between the class I and class II synthetases, J. Nanosci. Nanotechnol. 14 (3) (2014) 2280-2298. http://doi.10.1166/jnn.2014.8534.

[127] S.T. Rao, M.G. Rossmann, Comparison of super-secondary structures in proteins, J Mol Biol. 76 (2) (1973) 241-256. http://doi.10.1016/0022-2836(73)90388-4.

[128] G. Eriani, J. Cavarellitt, F. Martin, G. Dirheimer, D. Morast, J. Gangloff, Role of dimerization in yeast aspartyl-tRNA synthetase and importance of the class II invariant proline, Proc Natl Acad Sci. 90 (22) (1993) 10816-10820. http://doi.10.1073/pnas.90.22.10816.

[129] M. Szymañski, M. Deniziak, J. Barciszewski, The new aspects of aminoacyl-tRNA synthetases, Acta Biochim. Pol. 47 (3) (2000) 821-834. https://doi.org/10.18388/abp.2000_4000.

[130] J.G. Hurdle, A.J. O'Neill, I. Chopra, Prospects for aminoacyl-tRNA synthetase inhibitors as new antimicrobial agents, Antimicrob. Agents Chemother. 49 (12) (2005) 4821-4833. http://doi.10.1128/AAC.49.12.4821-4833.2005.

[131] P. Donoghue, Z.L. Schulten, On the evolution of structure in aminoacyl-tRNA synthetases, Microbiol Mol Biol Rev. 67(4) (2003) 550-573. http://doi.10.1128/mmbr.67.4.550-573.2003.

[132] R. Giege, M. Springer, Aminoacyl-tRNA synthetases in the bacterial world, EcoSal Plus. 5 (1) (2012) 1-77. http://doi.10.1128/ecosalplus.4.2.1.

[133] U.A. Ochsner, X. Sun, T.I. Jarvis, I. Critchley, N. Janjic, Aminoacyl-tRNA synthetases: essential and still promising targets for new anti-infective agents, Expert Opin. Investig. Drugs. 2007, 16 (5) (2007) 573-593. http://doi.10.1517/13543784.16.5.573.

[134] K.J. Newberry, Y.M. Hou, J.J Perona, Structural origins of amino acids selection without editing by cysteinyl-tRNA synthetase, EMBO J. 21 (2002) 2778-2787. http://doi.10.1093/emboj/21.11.2778.

[135] T.J. Bullwinkle, M. Ibba, Emergence and evolution, Top Curr Chem. 344 (2014) 43-87. http://doi.10.1007/128_2013_423.

[136] O. Nureki, D.G. Vassylyev, K. Katayanagi, T. Shimizu, S. Sekine, T. Kigawa, T. Miyazawa, S. Yokoyama, K. Morikawa, Architecture of class-defining and specific domains of glutamyl-tRNA synthetase, Science. 267 (5206) (1995) 1958-1965. http://doi.10.1126/science.7701318.

[137] P. Brick, T.N. Bhat, D.M. Blow, Structure of tyrosyl-tRNA synthetase refined at 2.3 A resolution: Interaction of the enzyme with tyrosyl adenylate intermediate, J. Mol. Biol. 208 (1) (1989) 83-98. https://doi.org/10.1016/0022-2836(89)90090-9.

[138] J.J. Perona, I. Cruic-Sovulj, Synthetic and editing mechanisms of aminoacyl tRNA synthetases. Top Curr Chem. 344 (2014) 1-41. http://doi.10.1007/128_2013_456.

[139] S. Cusack, Aminoacyl-tRNA synthetases, Curr Opin Struct Biol. 7 (6) (1997) 881–889. http://doi.10.1016/s0959-440x(97)80161-3.

[140] J.J. Perona, I. Gruic-Sovulj, Synthetic and editing mechanisms of aminoacyl-tRNA synthetases, in: S., Kim, (Eds.), Aminoacyl-tRNA synthetases in biology and medicine, Springer Netherlands, Dordrecht, 2014, pp. 1–41.

[141] T. Terada, O. Nureki, R. Ishitani, A. Ambrogelly, M. Ibba, D. Söll, S. Yokoyama, Functional convergence of two lysyl-tRNA synthetases with unrelated topologies, Nat. Struct. Biol. 9 (4) (2002) 257–262. http://doi.10.1038/nsb777.

[142] M. Ibba, H.C. Losey, Y. Kawarabayasi, H. Kikuchi, S. Bunjun, D. Soll, Substrate recognition by class I Lysyl-tRNA synthetase: a molecular basis for gene displacement, Proc Natl Acad Sci. 96 (2) (1999) 418-423. https://doi.org/10.1073/pnas.96.2.418.

[143] J. Chen, N. Guo, T. Li, E. Wang, Y. Wang, CP1 domain in *Escherichia coli* leucyl-tRNA synthetase is crucial for its editing function, J. Biochem. 39 (22) (2000) 6726-6731. https://doi.org/10.1021/bi000108r.

[144] S. Cusack, tRNA (Pro) anticodon recognition by *Thermus thermophilus* prolyl-tRNA synthetase, Structure. 6 (1) (1998) 101-108. https://doi.org/10.1016/S0969-2126(98)00011-2.

[145] G. Srinivasan, C.M. James, J.A. Krzycki, Pyrrolysine encoded by UAG in archaea: charging of a UAG-decoding specialized tRNA, Science. 296 (5572) (2002) 1459–1462. http://doi.10.1126/science.1069588.

[146] M.G. Klotz, D.J. Arp, P.S.G. Chain, A.F. El-Sheikh, L.J. Hauser, N.G. Hommes, F.W. Larimer, S.A. Malfatti, J.M. Norton, A.T. Poret-Peterson, L.M. Vergez, B.B. Ward, The complete genome sequence of the marine, chemolithoautotrophic, ammonia-oxidizing bacterium *Nitrosococcus oceani* ATCC 19707, Appl. Environ. Microbiol. 72 (9) (2006) 6299-6315. https://digitalcommons.usu.edu/psc_facpub/330/.

[147] B.C. Jester, J.D. Levengood, H. Roy, M. Ibba, K.M. Devine, Nonorthologous replacement of lysyl-tRNA synthetase prevents addition of lysine analogues to the genetic code, Proc Natl Acad Sci. 100 (24) (2003) 14351–14356. https://doi.org/10.1073/pnas.2036253100.

[148] T.J. Bullwinkle, M. Ibba, Emergence and evolution, Top Curr Chem. 344 (2014) 3–87. http://doi.10.1007/128_2013_423.

[149] J.D. Levengood, H. Roy, R. Ishitani, D. Soll, O. Nureki, M. Ibba, Anticodon recognition and discrimination by the α-helix cage domain of class I lysyl-tRNA synthetase, Biochemistry. 46 (39) 2007, 11033–11038. http://doi.10.1021/bi700815a.

[150] S.F. Ataide, M. Ibba, Discrimination of cognate and noncognate substrates at the active site of class II lysyl-tRNA synthetase, Biochemistry. 43 (37) (2004) 11836–11841. http://doi.10.1021/bi0490542.

[151] S. Wang, M.P. Ibba, S.F. Ataide, H. Roy, Discrimination of cognate and noncognate substrates at the active site of class I lysyl-tRNA synthetase, Biochemistry. 45 (11) (2006) 3646–3652. http://doi.10.1021/bi0523005.

[152] S. Onesti, A.D. Miller, P. Brick, The crystal structure of the Lysyl-tRNA synthetase (LysU) from *Escherichia coli*, Structure. 3 (2) (1995) 163-176. http://doi.10.1016/s0969-2126(01)00147-2.

[153] M.H. Mazauric, G. Keith, D. Logan, R. Kreutzer, R. Giege, D. Kern, Glycyl-tRNA synthetase from *Thermus thermophilus* – wide structural divergence with other prokaryotic glycyl-tRNA synthetases and functional inter-relation with prokaryotic and eukaryotic glycylation systems, Eur J Biochem. 251 (1998) 744–757. http://doi.10.1046/j.1432-1327.1998.2510744.x.

[154] S. Tanga, J. Huang. Evolution of different oligomeric glycyl-tRNA synthetases, FEBS Lett. 579 (6) (2005) 1441–1445. http://10.1016/j.febslet.2005.01.045.

[155] T.F. Smith, H. Hartman, The evolution of class II aminoacyl-tRNA synthetases and the first code, FEBS Letters 589 (23) (2015) 3499–3507. https://doi.org/10.1016/j.febslet.2015.10.006.

[156] E.L. Sonnhammer, S.R. Eddy, R. Durbin, Pfam: a comprehensive database of protein domain families based on seed alignments, Proteins. 28 (3) (1997) 405–420. http://doi.10.1002/(sici)1097-0134(199707)28:3<405::aid-prot10>3.0.co;2-l.

[157] L. Conte, S.E. Brenner, T.J. Hubbard, C. Chothia, A.G. Murzin, Lo SCOP database in 2002: refinements accommodate structural genomics, Nucleic Acids Res. 30 (1) (2002) 264–267. http://doi.10.1093/nar/30.1.264.

[158] P. Fang, M. Guo, Evolutionary limitation and opportunities for developing tRNA synthetase inhibitors with 5-binding-mode classification, MDPI. 5 (4) (2015) 1703-25. https://doi.org/10.3390/life5041703.

[159] P. Yao, P.L. Fox, Aminoacyl-tRNA synthetases in medicine and disease, EMBO Mol Med. 5 (3) (2013) 332-343. http://doi.10.1002/emmm.201100626.

[160] J.W. Lee, K. Beebe, L.A. Nangle, J. Jang, C.M. Longo-Guess, S.A. Cook, M.T. Davisson, J.P. Sundberg, P. Schimmel, S.L. Ackerman, Editing defective tRNA synthetase causes protein misfolding and neurodegeneration, Nature. 443 (7107) (2006) 50–55. http://doi.10.1038/nature05096.

[161] V.A. Karkhanis, A.P. Mascarenhas, S.A. Martinis, Amino acid toxicities of *Escherichia Coli* that are prevented by leucyl-tRNA synthetase amino acid editing, J. Bacteriol. 189 (23) (2007) 8765–8768. http://doi.10.1128/jb.01215-07.

[162] M. Guo, P. Schimmel, Structural analyses clarify the complex control of mistranslation by tRNA synthetases. Curr Opin Struct Biol. 22 (1) (2012) 119–126. http://doi.10.1016/j.sbi.2011.11.008.

[163] R. Fukunaga, S. Yokoyama, Structural basis for substrate recognition by the editing domain of isoleucyl-tRNA synthetase, J. Mol. Biol. 359 (4) (2006) 901–912. http://doi.10.1016/j.jmb.2006.04.025.

[164] A.R. Fersht, C. Dingwall, Evidence for the double-sieve editing mechanism in protein synthesis. Steric exclusion of isoleucine by valyl-tRNA synthetases, Biochemistry. 18 (12) (1979) 2627–2631. https://doi.org/10.1021/bi00579a030.

[165] O. Nureki, D.G. Vassylyev, M. Tateno, A. Shimada, T. Nakama, S. Fukai, M. Konno, T.L. Hendrickson, P. Schimmel, S. Yokoyama, Enzyme structure with two catalytic sites for double-sieve selection of substrate, Science. 280 (5363) (1998) 578–582. http://doi.10.1126/science.280.5363.578.

[166] J. Wilson, T. Hunt, B.E.A. Alberts, Molecular Biology of the Cell, Sixth ed., Taylor and Francis, USA, 2015.

[167] S.A. Martinis, M.T. Boniecki, The balance between pre- and post-transfer editing in tRNA synthetases, FEBS Lett. 584 (2) (2010) 455–459. http://doi.10.1016/j.febslet.2009.11.071.

[168] A.P. Mascarenhas, S. An, A.E. Rosen, S.A. Martinis, K. Musier-Forsyth, Fidelity mechanisms of the aminoacyl-tRNA synthetases, in: C.R. Bhandary (Eds.), Protein Engineering, Springer-Verlag, Berlin, 2008, pp. 155–203.

[169] A. Palencia, T. Crépin, M. Vu, T.J. Lincecum, S.A. Martinis, S. Cusack, Structural dynamics of the aminoacylation and proofreading functional cycle of bacterial leucyl-tRNA synthetase, Nat. Struct. Mol. Biol. 19 (2012) 677-684. http://doi.10.1038/nsmb.2317.

[170] I. Ahel, D. Korencic, M. Ibba, D. Söll, Trans-editing of mischarged tRNAs, PNAS. 100 (26) (2003) 15422-15427. https://doi.org/10.1073/pnas.2136934100.

[171] R. Giege, M. Springer, Aminoacyl-tRNA synthetases in the bacterial world, EcoSal Plus. 7 (1) (2016) 1-9. http://0.1128/ecosalplus.ESP-0002-2016.

[172] F.C. Wong, P.J. Beuning, C. Silvers, K. Musier-Forsyth, An isolated class II aminoacyl tRNA synthetase insertion domain is functional in amino acid editing, J Biol Chem. 278 (52) (2003) 52857-52864. http://doi.10.1074/jbc.M309627200.

[173] S. Dwivedi, S.P. Kruparani, R. Sankaranarayanan, A D-amino acid editing module coupled to the translational apparatus in archaea, Nat Struct Mol Biol. 12 (6) (2005) 556–557. http://doi.10.1038/nsmb943.

[174] M. Guo, Y.E. Chong, K. Beebe, R. Shapiro, X.L. Yang, P. Schimmel, The C-Ala domain brings together editing and aminoacylation functions on the tRNA, Science. 325 (5941) (2009) 744-747. http://doi.10.1126/science.1174343.

[175] K. Beebe, L.R.D. Pouplana, P. Schimmel, Elucidation of tRNA-dependent editing by a class II tRNA synthetase and significance for cell viability, EMBO J. 22 (3) (2003) 668-675. http://doi.10.1093/emboj/cdg065.

[176] S. An, K. Musier-Forsyth, Trans-editing of Cys-tRNAPro by Haemophilus influenzae YbaK protein, J Biol Chem. 279 (41) (2004) 42359–42362. http://doi.10.1074/jbc.C400304200.

[177] B. Ruan, D. Soll, The bacterial YbaK protein is a Cys-tRNAPro and Cys-tRNA Cys deacylase, J Biol Chem. 280 (27) (2005) 25887–25891. http://doi.10.1074/jbc.M502174200.

[178] B.R. So, S. An, S. Kumar, M. Das, D.A. Turner, C.M. Hadad, K. Musier-Forsyth, Substrate-mediated fidelity mechanism ensures accurate decoding of proline codons, J Biol Chem. 286 (36) (2011) 31810–31820. http://doi.10.1074/jbc.m111.232611.

[179] J. Ling, N. Reynolds, M. Ibba, Aminoacyl-tRNA synthesis and translational quality control, Annu Rev Microbiol. 63 (2009) 61–78. http://doi.10.1146/annurev.micro.091208.073210.

[180] W. Yan, M. Tan, G. Eriani, E.D. Wang, Leucine-specific domain modulates the aminoacylation and proofreading functional cycle of bacterial leucyl-tRNA synthetase, Nucleic Acids Res. 41 (9) (2013) 4988–4998. http://doi.10.1093/nar/gkt185.

[181] M. Ibba, S. Dieter, Aminoacyl-tRNA synthesis, Annu. Rev. Biochem. 69 (2000) 617–650. https://doi.org/10.1146/annurev.biochem.69.1.617.

[182] J. Lapointe, L. Duplain, M. Proulx, A single glutamyl-tRNA synthetase aminoacylates tRNAGlu and tRNAGln in *Bacillus subtilis* and efficiently misacylates *Escherichia coli* tRNAGln1 in vitro, J Bacteriol. 165 (1) (1986) 88–93. http://doi.10.1128/jb.165.1.88-93.1986.

[183] H.D. Becker, J. Reinbolt, R. Kreutzer, R. Giege, D. Kern, Existence of two distinct aspartyl-tRNA synthetases in *Thermus thermophilus*. Structural and biochemical properties of the two enzymes, Biochemistry. 36 (29) (1997) 8785–8797. https://doi.org/10.1021/bi970392v.

[184] P. Chuawong, T.L. Hendrickson, The non-discriminating aspartyl-tRNA synthetase from *Helicobacter pylori*: anticodon-binding domain mutations that impact tRNA specificity and heterologous toxicity, Biochemistry. 45 (26) (2006) 8079–8087. http://doi.10.1021/bi060189c.

[185] M. Guo, X.L. Yang, P. Schimmel, New functions of aminoacyl-tRNA synthetases beyond translation, Nat Rev Mol. Cell Biol. 11 (9) (2010) 668-674. http://doi.10.1038/nrm2956.

[186] S. Kim, S. You, D. Hwang, Aminoacyl-tRNA synthetases and tumorigenesis: more than housekeeping, Nat Rev Cancer. 11 (10) (2011) 708-718. http://doi.10.1038/nrc3124.

[187] Y.W. Kim, C. Kwon, J.L. Liu, S.H. Kim, S. Kim, Cancer association study of aminoacyl-tRNA synthetase signalling network in glioblastoma. PLoS One. 7 (8) (2012) 40960. http://doi.10.1371/journal.pone.0040960.

[188] A.J. Sanju, S.S. Kopula, K.K. Palra, Screening for mupirocin resistance in *staphylococcus*, J Clin Diagn Res. 9 (10) (2015) 9–10. http://doi.10.7860/JCDR/2015/15230.6678.

[189] N. Sharma, D. Sharma, An upcoming drug for onychomycosis: tavaborole, J Pharmacol Pharmacother. 6 (4) (2015) 236–239. http://doi.10.4103/0976-500X.171870.

[190] B.D. Cookson, The emergence of mupirocin resistance: a challenge to infection control and antibiotic prescribing practice, J Antimicrob Chemother. 41 (1) (1998) 11-18. http://doi.10.1093/jac/41.1.11.

[191] J. Sphoorthi, S. Finch, Spotlight on tavaborole for the treatment of onychomycosis, Drug Des Devel Ther. 9 (2015) 6185–6190. http://doi.10.2147/DDDT.S81944.

[192] S. Kim, S.W. Lee, E.C. Choi, S.Y. Choi, Aminoacyl-tRNA synthetases and their inhibitors as a novel family of antibiotics, Appl Microbiol Biotechnol. 61 (4) (2003) 278-288. http://doi.10.1007/s00253-003-1243-5.

[193] E. Boni, M.D. Elewski, A. Raza, L. Sheryl, R.N. Baldwin, F. Remigio, S. González, R. Phoebe, M. Weisfeld, H. Wiltz, L.T. Zane, R. Pollak, Efficacy and safety of tavaborole topical solution, 5%, a novel boron-based antifungal agent, for the treatment of toenail onychomycosis: Results from 2 randomized phase-III studies, JAAD. 73 (1) (2015) 62–69. http://doi.10.1016/j.jaad.2015.04.010.

[194] F.L Rock, W. Mao, A. Yaremchuk, M. Tukalo, T. Crepin, H. Zhou, Y.k. Zhang, V. Hernandez, T. Akama, S.J. Baker, J.J. Plattner, L. Shapiro, S.A. Martinis, S.J. Benkovic, S. Cusack, M.R. Alley, An antifungal agent inhibits an aminoacyl-tRNA synthetase by trapping tRNA in the editing site, Science. 316 (5832) (2007) 1759-1761. http://doi.10.1126/science.

[195] Z. Yaxue, M. Qingqing, In silico discovery of aminoacyl tRNA synthetase inhibitors, Int J Mol Sci. 15 (1) (2014) 1358-1373. http://doi.10.3390/ijms15011358.

[196] P. Schimmel, J. Tao, J. Hill, Aminoacyl tRNA synthetases as target for new anti-infective, FASEB J. 12 (1998) 1599-1609. https://doi.org/10.1096/fasebj.12.15.1599.

[197] J.M. Hill, G. Yu, Y.K. Shue, T.M. Zydowski, J. Rebek, Aminoacyl adenylate mimics as novel antimicrobial and antiparasitic agents. https://www.lens.org/lens/patent/169-730-606-954-401 , Cubist Pharmaceuticals, 1998, (accessed 02 May 2020).

[198] R. Petraitiene, V. Petraitis, A.M. Kelaher, A.A. Sarafandi, D. Mickiene, A.H. Groll, T. Sein, J. Bacher, T.J. Walsh, Efficacy, plasmapharmacokientics and safety of icofungipen an inhibitor of candida Isoleucyl tRNA synthetase in treatment of experimental disseminated candiasis in persistently neutropenic rabbits, Antimicrob Agents Chemother. 49 (5) (2005) 2084-2092. http://doi.10.1128/AAC.49.5.2084-2092.2005.

[199] C.S. Houge-Frydrych, M.L. Gilpin, P.W. Skett, J.W. Tyler, SB-203207 and SB-203208, two novel Isoleucyl tRNA synthetase inhibitors from a *Streptomyces* sp. II. Structure determination, J Antibiot. 53 (4) (2000) 364-372. http://doi.10.7164/antibiotics.53.364.

[200] A.L. Stefanska, M. Fulston, C.S. Houge-Frydrych, J.J. Jones, S.R. Warr, A potent Seryl tRNA synthetase inhibitor SB-217452 isolated from a *Streptomyces* species, J Antibiot. 53 (12) (2000) 1346-1353. http://doi.10.7164/antibiotics.53.1346.

[201] K. Tanaka, M. Tamaki, S. Watanabe, Effect of furanomycin on the synthesis of isoleucyl-tRNA, Biochem Biophys Acta. 195 (1) (1969) 244-245. http://doi.10.1016/0005-2787(69)90621-2.

[202] R. Meyer-Schuman, A. Antonellis, Emerging mechanisms of aminoacyl tRNA synthetase mutations in recessive and dominant human disease, Hum. Mol. Genet. 26 (R2) (2017) 114-127. https://doi.org/10.1093/hmg/ddx231.

[203] H. Shiozawa, T. Kagasaki, T. Kinoshita, H. Haruyama, H. Domon, Y. Utsui, K. Kodama, S. Takahashi, Thiomarinol, a new hybrid antimicrobial antibiotic produced by a marine bacterium. Fermentation, isolation, structure and antimicrobial activity, J Antibiot. 46 (12) (1993) 1834-1842. http://doi.10.7164/antibiotics.46.1834.

[204] H. Shiozawa, T. Kagasaki, A. Torikata, N. Tanaka, K. Fujimoto, T. Hata, Y. Furukawa, S. Takahashi, Thiomarinols B and C, new antimicrobial antibiotics produced by a marine bacterium, J Antibiot. 48 (8) (1995) 907-909. http://doi.10.7164/antibiotics.48.907.

[205] J.S. Pharm, K.L. Dawson, K.E. Jackson, E.E. Lim, C.F. Pasaje, K.E. Turner, S.A. Ralph, Aminoacyl tRNA synthetase as drug targets in eukaryotic parasites, Int J Parasitol Drugs Drug Resist. 4 (1) (2014) 1-13. http://doi.10.1016/j.ijpddr.2013.10.001.

[206] E.S. Istvan, N.V. Dharia, S.E. Bopp, I. Gluzman, E.A. Winzeler, D.E. Goldberg, Validation of isoleucine utilization targets in *Plasmodium falciparum*, Proc Natl Acad Sci. 108 (4) (2011) 1627-1632. http://doi.10.1073/pnas.1011560108.

[207] S. Bernier, D.Y. Dubois, M. Therrien, J. Lapointe, R. Chenevert, Synthesis of glutaminyl adenylate analogues that are inhibitors of glutaminyl-tRNA synthetase, Bioorganic Med. Chem. Lett. 10 (21) (2000) 2441-2444. http://doi.10.1016/s0960-894x(00)00478-9.

[208] J.S. Reader, P.T. Ordoukhanian, J.G. Kim, V.D. Crecy-Lagard, I. Hwang, S. Farrand, P. Schimmel, Major biocontrol of plant tumors targets tRNA synthetase, Science. 309 (5740) (2005) 1533. http://doi.10.1126/science.1116841.

[209] S. Chopra, A. Palencia, C. Virus, A. Tripathy, B.R. Temple, A. Velazquez-Campoy, S. Cusack, J.S. Reader, Plant tumor biocontrol agent employs a tRNA-dependent mechanism to inhibit leucyl-tRNA synthetase, Nat. Commun. 4 (1417) (2013). http://doi.10.1038/ncomms2421.

[210] J.G. Kim, B.K. Park, S.U. Kim, D. Choi, B.H. Nahm, J.S. Moon, J.S. Rreader, S.K. Farrand, I. Hwang, Bases of biocontrol: sequence predicts synthesis and mode of action of agrocin 84, the Trojan horse antibiotic that control crown gall, Proc Natl Acad Sci. 103 (23) (2006) 8846-8851. http://doi.10.1073/pnas.0602965103.

[211] P. Heinstein, Mechanism of action of granaticin: inhibition of ribosomal RNA maturation and cell cycle specificity, J. Pharm. Sci. 71(2) (1982) 197-200. https://doi.org/10.1002/jps.2600710215.

[212] D. Ding, Q. Meng, G. Gao, Y. Zhao, Q. Wang, B. Nare, R. Jacobs, F. Rock, M.R. Alley, J.J. Plattner, G. Chen, D. Li, H. Zhou, Design, synthesis, and structure-activity relationship of *Trypanosoma brucei* leucyl-tRNA synthetase inhibitors as antitrypanosomal agents, J. Med. Chem. 54 (5) (2011) 1276-1287. http://doi.10.1021/jm101225g.

[213] R.E. Mendes, M.R. Alley, H.S. Sader, D.J. Biedenbach, R.N. Jones, Potency and spectrum of activity of AN3365, a novel boron-containing protein synthesis inhibitor, tested against clinical isolates of *Enterobacteriaceae* and non-fermentative Gram-negative *bacilli*, Antimicrob Agents Chemther. 57 (6) (2013) 2849-2857. http://doi.10.1128/AAC.00160-13.

[214] R.G. Werner, L.F. Thorpe, W. Reuter, K.H. Nierhaus, Indolmycin inhibits prokaryotic tryptophanyl-tRNA ligase, Eur J Biochem. 68 (1) (1976) 1-3. http://doi.10.1111/j.1432-1033.1976.tb10758.x.

[215] J.G. Hurdle, A.J. O'Neill, I. Chopra, Anti-*Staphylococcal* activity of indolmycin: a potential topical agent for control of *Staphylococcal* infections, J. Antimicrob. Chemother. 54 (2) (2004) 549-552. https://doi.org/10.1093/jac/dkh352.

[216] Z.P. Xiao, X.B. He, Z.Y. Peng, T.J. Xiong, J. Peng, L.H. Chen, H.L. Zhu, Synthesis, structure, molecular docking and structure activity relationship analysis of enamines: 3-aryl-4-alkylaminofuran-2 (5H)- ones as potential antibacterials, Bioorg. Med. Chem. 19 (2011) 1571-1579. http://doi.10.1016/j.bmc.2011.01.051.

[217] H. Osada, K. Isono, Mechanism of action and selective toxicity of ascamycin: a nucleoside antibiotic, Antimicrob Agents Chemother. 27 (2) (1985) 230-233. http://doi.10.1128/aac.27.2.230.

[218] M. Ubukata, H. Osada, K. Isono, Synthesis and biological activity of nucleoside antibiotics, ascamycin and its amino acid analogs, Nucleic Acids Symp. Ser. 16 (1985) 81-83. PMID: 3841391.

[219] C. Zhao, J. Qi, W. Tao, L. He, W. Xu, J. Chen, Z. Deng, Characterisation of biosynthetic genes of ascamycin/dealanylascamycin featuring a 5`-O-sulfonamide moiety in *Streptomyces* sp. JCM9888, PloS One. 9 (2014) 114722. https://doi.org/10.1371/journal.pone.0114722.

[220] C.W. Carter, Cognition mechanism and evolutionary relationships in aminoacyl tRNA synthetases, Annu Rev Biochem. 62 (1993) 715-748. http://10.1146/annurev.bi.62.070193.003435.

[221] I. Konrad, R. Roschenthaler, Inhibition of phenylalanine tRNA synthetase from *Bacillus subtilis* by ochratoxin A, FEBS Lett. 83 (2) (1977). http://10.1016/0014-5793(77)81037-5.

[222] T. Oki, M. Hirano, K. Tomatsu, K. Numata, H. Kamei, Cispentacin, a new antifungal antibiotic. II. In vitro and in vivo antifungal activities, J Antibiot. 42 (12) (1989) 1756-1762. http://10.7164/antibiotics.42.1756.

[223] M. Uramoto, C.J. Kim, K. Shin-YA, H. Kusakabe, K. Isono, D.R. Phillips, J.A. McClosky, Isolation and characterisation of phosmidosine. A new anti-fungal nucleotide antibiotic, J. Antibiot. 44 (4) (1991) 375-381. http://doi.10.7164/antibiotics.44.375.

[224] J. Finn, J. Tao, Anminoacyl tRNA synthetases and diseases, in: M. Ibba, C. Franckly, S. Cusack (Eds.), Aminoacyl-tRNA synthetases, Lndes Biosciences, Georgetown, Texas, 2003, pp. 405-411.

[225] J.B. Koepfli, J.F. Mead, J.A. Brochman, Alkaloids of dichroa febrifuga; isolation and degradative studies, J Am Chem Soc. 71 (3) (1949). http://doi.10.1021/ja01171a080.

[226] M. Guo, P. Schimmel, Essential non-translational functions of tRNA synthetases, Nat Chem Biol. 9 (3) (2013) 145-153. http://doi.10.1038/nchembio.1158.

[227] M.S. Sundrud, S.B. Koralov, M. Feuerer, D.P Calaso, A.E. Kozhaya, A. Rhule-Smith, R.E. Lefebvre, D. Unutmaz, R. Mazitschek, H. Waldner, M. Whitman, T. Keller, A. Rao, Halofuginone inhibits TH17 cell differentiation by activating the amino acid starvation response, Science. 324 (5932) (2009) 1334-1338. http://doi.10.1126/science.1172638.

[228] B. Ruan, M.L. Bovee, M. Sacher, C. Stathopoulos, K. Poralla, C.S. Francklyn, D.A. Soll, A unique hydrophobic cluster near the active site contributes to differences in borrelidin inhibition among threonyl-tRNA synthetases, J Biol Chem. 280 (1) (2005) 571-577. http://doi.10.1074/jbc.M411039200.

[229] C. Olano, B. Wilkinson, C. Sanchez, S.J. Moss, R. Sheridan, V. Math, A.J. Weston, A.F. Brana, C.J. Martin, M. Oliynyk, C. Mendez, P.F. Leadlay, J.A. Salas, Biosynthesis of the angiogenesis inhibitor borrelidin by *Streptomyces parvulus* Tu4055: cluster analysis and assignment of functions, Chem Biol. 11 (1) (2004) 87-97. http://doi.10.1016/j.chembiol.2003.12.018.

[230] M. Lumb, P.E. Macey, J. Spyvee, J.M. Whitmarsh, R.D. Wright, Isolation of vivomycin and borrelidin, two antibiotics with antiviral activity, from a species of *Streptomyces* (C2989), Nature. 206 (1965) 263-265. https://doi.org/10.1038/206263a0.

[231] B. Wilkinson, M.A. Gregory, S.J. Moss, I. Carletti, R.M. Sheridan, A. Kaja, M. Ward, C. Olano, C. Mendez, J.A. Salas, P.F. Leadlay, R. vanGinckel, M.Q. Zhang, Separation of anti-angiogenic and cytotoxic activities of borrelidin by modification at the C17 side chain, Bioorganic Med Chem Lett. 16 (22) (2006) 5814-5817. http://doi.10.1016/j.bmcl.2006.08.073.

[232] I.A. Critchley, C.L. Young, K. C. Stone, U.A. Ochsner, J. Guiles, T. Tarasow, N. Janjic, Antibacterial activity of REP8839, a new antibiotic for topical use, Antimicrob Agents Chemother. 49 (10) (2005) 4247-4252. http://doi.10.1128/AAC.49.10.4247-4252.2005.

[233] R.L. Jarvest, J.M. Berge, V. Berry, H.F. Boyd, M.J. Brown, J.S. Elder, A.K. Forrest, A.P Fosberry, D.R. Gentry, M.J. Hibbs, D.D. Jaworski, P.J. O'Hanlon, A.J. Pope, S. Rittenhouse, R.J. Sheppard, C. Slater-Raosti, A. Worby, Nanomolar inhibitors of

staphylococcal aureus methionyl tRNA synthetase with potent antibacterial activity against gram positive pathogens, J Med Chem. 45 (10) (2002) 1959-1962. http://doi.10.1021/jm025502x.

[234] M.A.R. Gomez, M. Ibba, Aminoacyl-tRNA synthetases, RNA. 26 (8) (2020) 910-939. http://doi.10.1261/rna.071720.119.

[235] Y. Zeng, A. Kulkarni, Z. Yang, P.B. Patil, W. Zhou, X. Chi, S.V. Lanen, S. Chen, Biosynthesis of albomycin delta δ2 provides a template for assembling siderophore and aminoacyl-tRNA synthetases inhibitor conjugates, ACS Chem Biol. 7 (9) (2012)1565-1575. http://doi.10.1021/cb300173x.

[236] R. Ushimaru, Z. Chen, H. Zhao, F. Po-hsun, L. Hung-wen, Identification of the enzymes mediating the maturation of the Seryl tRNA synthetase inhibitor SB-217452 during the biosynthesis of albomycins, Angew. Chem. Int. Ed. 59 (9) (2020) 3558–3562. https://doi.org/10.1002/anie.201915275.

[237] A. Pramanik, V. Braun, Albomycin uptake via a ferric hydroxamate transport system of *Streptococcus pneumoniae* R6, J Bacteriol. 188 (11) (2006) 3878–3886. http://doi.10.1128/JB.00205-06.

[238] G.F. Gause, Recent studies on albomycin, a new antibiotic, Br Med J. 2 (4949) (1955) 1177–1179. http://doi.10.1136/bmj.2.4949.1177.

[239] Z. Lin, X. Xu, S. Zhao, X. Yang, J. Guo, Q. Zhang, C. Jing, S. Chen, Y. He, Total synthesis and antimicrobial evaluation of natural albomycins against clinical pathogens, Nat Commun. 9 (3445) (2018) 1-8. https://doi.org/10.1038/s41467-018-05821-1.

[240] P.M. Scott, W.V. Walbeek, W.M. MacLean, Cladosporin, a new antifungal metabolite from Cladosporium cladosporioides, J Antibiot. 24 (11) (1971) 747-755. http://10.7164/antibiotics.24.747.

[241] D. Hoepfner, C.W. McNamara, C.S. Lim, C. Studer, R. Riedl, T. Aust, S.L. McCormack, D.M. Plouffe, S. Meister, S. Schuierer, U. Plikat, N. Hartmann, F. Staedtler, S. Cotesta, E.K. Schmitt, F. Petersan, F. Supek, R.J. Glynne, J.A. Tallarico, J.A. Porter, M.C. Fishman, C. Bodenreider, T.T. Diagana, N.R. Movva, E.A. Winzeler, Selective and

specific inhibition of the *plasmodium falciparum* lysyl tRNA synthetase by the fungal secondary metabolite cladosporin, Cell Host Microbe. 11 (6) (2012) 654-663. http://doi.10.1016/j.chom.2012.04.015.

[242] D.G. Kim, J.W. Choi, J.Y. Lee, H. Kim, Y.S. Oh, J.W.Lee, Y.K. Tak, J.M. Song, E. Razin, S.H.Yun, S. Kim, Interaction of two translational components, lysyl-tRNA synthetase and p40/37LRP, in plasma membrane promotes laminin-dependent cell migration, FASEB J. 26 (10) (2012) 4142-4159. https://doi.org/10.1096/fj.12-207639.

[243] D.G. Kim, J.Y. Lee, N.H. Kwon, P. Fang, Q. Zhang, J. Wang, N.L. Young, M. Guo, H.Y. Cho, A.U. Mushtaq, Y.H. Jeon, J.W. Choi, J.M. Han, H.W. Kang, J.E. Joo, Y. Hur, W. Kang, H. Yang, D.H. Nam, M.S. Lee, J.W. Lee, E.S. Kim, A. Moon, K. Kim, D. Kim, E.J. Kang, Chemical inhibition of prometastatic lysyl tRNA synthetase-laminin receptor interaction, Nat. Chem. Biol. 10 (1) (2014) 29-34. http://10.1038/nchembio.1381.

[244] A. Corona, S.O. Palmer, R. Zamacona, B. Mendez, F. B. Dean, J.M. Bullard, Discovery and characterisation of chemical compounds that inhibit the function of aspartyl-tRNA synthetase from *Pseudomonas aeruginosa*, SLAS Discov. 23 (3) (2018) 294-301. http://doi.10.1177/2472555217744559.

[245] J.S. Pham, K. L. Dawson, K.E. Jackson, E.E. Lim, C. F.A. Pasaje, K.E.C. Turner, S.A. Ralph, Aminoacyl-tRNA synthetases as drug targets in eukaryotic parasites, Int J Parasitol Drugs Drug Resist. 4(1) (2014) 1–13. http://doi.10.1016/j.ijpddr.2013.10.001.

[246] S. Khan, A. Sharma, A. Jamwal, V. Sharma, A.K. Pole, K.K. Thakur, Uneven spread of cis- and trans-editing aminoacyl-tRNA synthetase domains within translational compartments of *P. falciparum*, Sci Rep. 1 (2011) 188. http://doi.10.1038/srep00188.

[247] M.Y. Rybak, A.V. Rayevsky, O.I. Gudzera, M.A. Tukalo, Stereospecificity control in aminoacyl-tRNA-synthetases: new evidence of D-amino acids activation and editing, Nucleic Acids Res. 47 (18) (2019) 9777–9788. http://doi.10.1093/nar/gkz756.

[248] S.M. Shiadeh, A. Pormohammad, A. Hashemi, P. Lak, Global prevalence of antibiotic resistance in blood-isolated *Enterococcus faecalis* and *Enterococcus faecium*: a systematic review and meta-analysis, Infect Drug Resist. 12 (2019) 2713–2725. http://doi.10.2147/IDR.S206084.

[249] Z. Munn, S. Moola, D. Riitano, K. Lisy, The development of a critical appraisal tool for use in systematic reviews addressing questions of prevalenc, Int J Health Policy Manag. 3 (3) (2014) 123-128. http://doi.10.15171/ijhpm.2014.71.

[250] R.A. Lewis, The development of molecular modelling programs: the use and limitations of physical models. In: D.J. Livingstone, A.M. Davis, (Eds.), Drug design strategies: quantitative approaches, RSCPublishing, London, 2011, pp. 88–107.

[251] K. Awanish, J. Anubhuti, Drug development strategies, in: Elsevier Inc. (Eds.), Anticandidal agents, Academic Press, 2017, pp. 63-71.

[252] O. Osakwe, The significance of discovery screening and structure optimization studies, social aspects of drug discovery, development and commercialization, in: Elsevier Inc. (eds.), Social aspects of drug discovery, development and commercialization, Academic Press, 2016, pp. 109-128.

[253] Y. Wenbo, A.D. Mackerell, Computer-aided drug design methods, Methods Mol Biol. 1520 (2017) 85-106. http://doi.10.1007/978-1-4939-6634-9_5.

[254] D.A. Rio, G. Varchi, Molecular design of compounds targeting histone methyltransferases, in: Epi-Informatics (Eds.), Discovery and development of small molecule epigenetic drugs and probes, 2016, pp. 257-272.

[255] Y. Tua, A. Laaksonen, Implementing quantum mechanics into molecular mechanics—combined QM/MM modeling methods, in: J.R. Sabin, E. Brändas, (Eds.), Advances in quantum chemistry, Elsevier Inc, San Diego, USA, 2010, pp. 1-15.

[256] A. Fiser, Template-based protein structure modeling method, Methods Mol Biol. 673 (2010) 73-94. http://doi.10.1007/978-1-60761-842-3_6.

[257] M.A. Marti-renom, A.C. Stuart, A. Fiser, R. Sanchez, F. Melo, A. Sali, Comparative protein structure modeling of genes and genomes, Annu Rev Biophys Biomol Struct. 29 (2009) 291. http://doi.10.1146/annurev.biophys.29.1.291.

[258] A.M. Lesk, C. Chothia, How different amino acid sequences determine similar protein structures: the structure and evolutionary dynamics of the globins, J. Mol. Biol. 136 (3) (1980) 225. https://doi.org/10.1016/0022-2836(80)90373-3.

[259] A. Andreeva, D. Howorth, J.M. Chandonia, S.E. Brenner, T.J. Hubbard, C. Chothia, A.G. Murzin, Data growth and its impact on the SCOP database: new developments, Nucleic Acids Res. 36 (2008) 419-425. http://doi.10.1093/nar/gkm993.

[260] J.C. Faver, M.N. Ucisik, W. Yang, K.M. Merz, Computer-aided drug design: using numbers to your advantage. ACS Med Chem Lett. 4 (9) (2013) 812−814. http://doi.10.1021/ml4002634.

[261] J. Singh, C.E. Chuaqui, P.A. Boriack-Sjodin, W.C. Lee, T. Pontz, M.J. Corbley, H.K. Cheung, R.M. Arduini, J.N. Mead, M.N. Newman, J.L. Papadatos, S. Bowes, S. Josiah, L.E. Ling, Successful shape-based virtual screening: the discovery of a potent inhibitor of the type I TGF beta receptor kinase (TbetaRI), Bioorg. Med. Chem. Lett. 13 (24) (2003) 4355–4359. http://doi.10.1016/j.bmcl.2003.09.028.

[262] O.M. Becker, D.S. Dhanoa, Y. Marantz, D. Chen, S. Shacham, S. Cheruku, A. Heifetz, P. Mohanty, M. Fichman, A. Sharadendu, R. Nudelman, M. Kauffman, S. Noiman, An integrated in silico 3D model-driven discovery of a novel, potent, and selective amidosulfonamide 5-HT1A agonist (PRX-00023) for the treatment of anxiety and depression, J. Med. Chem. 49 (11) (2006) 3116–3135. http://doi.10.1021/jm0508641.

[263] Molecular Operating Environment (MOE 2014.0901), Chemical computing group Inc, Montreal Quebec Canada, https://www.chemcomp.com/ , 2014 (accessed 30 September 2017).

[264] H.R. Charles, 2010. Computer-aided drug design: a practical guide to protein structure-based modeling, in: C.H. Reynolds, K.M. Merz, D. Ringe (Eds.), Drug design: structure- and ligand-based approaches, Cambridge University Press, 2010, PP. 181-193.

[265] D.A. Erlanson, R.S. McDowell, T. O'Brien, Fragment-based drug discovery, J Med Chem. 47 (14) (2004) 3463-3482. http://doi.10.1021/jm040031.

[266] T. Schwede, J. Kopp, N. Guex, M.C. Peitsch, SWISS-MODEL: an automated protein homology-modeling server, Nucleic Acids Res. 31 (13) (2003) 3381–3385. http://doi.10.1093/nar/gkg520.

[267] Model building, SWISS-MODEL help. https://swissmodel.expasy.org/docs/help , (accessed 17 February 2020).

[268] D. Vlachakis, E. Bencurova, N. Papangelopoulos, S. Kossida, Current state-of-the-art molecular dynamics methods and application, in: R. Donev (eds.), Advances in protein chemistry and structural biology, Elsevier Inc., Academic Press, Burlington, 2014, pp.269-313.

[269] The UniProt Consortium, UniProt: a worldwide hub of protein knowledge, Nucleic Acids Res. 47 (D1) (2019) 506–515. https://www.uniprot.org/help/publications.

[270] S.F. Altschul, T.L. Madden, A.A. Schäffer, J. Zhang, Z. Zhang, W. Miller, D.J. Lipman, Gapped BLAST and PSI-BLAST: a new generation of protein database search programs, Nucleic Acids Res. 25 (17) (1997) 3389–3402. http://doi.10.1093/nar/25.17.3389.

[271] Clustal Omega tool, https://www.ebi.ac.uk/Tools/msa/clustalo/ , (accessed 1 December 2019).

[272] F. Madeira, Y.M. Park, J. Lee, N. Buso, T. Gur, N. Madhusoodanan, P. Basutkar, A.R.N. Tivey, S.C. Potter, R.D. Finn, R. Lopez, The EMBL-EBI search and sequence analysis tools APIs in 2019, 47 (W1) (2019) 636-641. http://doi.10.1093/nar/gkz268.

[273] National Center for Biotechnology Information, BLAST: Basic Local Alignment Tool Search. https://blast.ncbi.nlm.nih.gov/Blast.cgi?PAGE_TYPE=BlastSearch&BLAST_SPEC=blast2seq&LINK_LOC=align2seq , (accessed 1 December 2020).

[274] A.A. Schäffer, L. Aravind, T.L. Madden, S. Shavirin, J.L. Spouge, Y.I. Wolf, E.V. Koonin, S.F. Altschul, Improving the accuracy of PSI-BLAST protein database searches with composition-based statistics and other refinements, Nucleic Acids Res. 29 (14) (2001) 2994–3005. http://doi.10.1093/nar/29.14.2994.

[275] E. Gasteiger, A. Gattiker, C. Hoogland, I. vanyi, R.D. Appel, Bairoch, ExPASy: the proteomics server for in-depth protein knowledge and analysis, Nucleic Acids Res. 31 (13) (2003) 3784-3788. https://doi.org/10.1093/nar/gkg563.

[276] RCSB, Protein Data Bank. https://www.rcsb.org/pdb , (accessed 1 December 2016).

[277] C. Briand, A. Poterszman, S. Eiler, G. Webster, J. Thierry, D. Moras, An intermediate step in the recognition of $tRNA^{Asp}$ by aspartyl-tRNA synthetase, J Mol Biol 299 (4) (2000) 1051-1060. https://doi.org/10.1006/jmbi.2000.3819.

[278] B. Rees, G. Webster, M. Delarue, M. Boeglin, D. Moras, Aspartyl tRNA-synthetase from *Escherichia coli :*flexibility and adaptability to the substrates, J Mol Biol. 299 (5) (2000) 1157-1164. http://doi.10.1006/jmbi.2000.3792.

[279] T. Suzuki, A. Nakamura, K. Kato, D. Soll, I. Tanaka, K. Sheppard, M. Yao, Structure of the *Pseudomonas aeruginosa* transamidosome reveals unique aspects of bacterial tRNA-dependent asparagine biosynthesis, Proc Natl Acad Sci. 112 (2) (2015) 382-387. https://doi.org/10.1073/pnas.1423314112.

[280] B. Min, J.T. Pelaschier, D.E. Graham, D. Tumbula-Hansen, D. Söll, Transfer RNA-dependent amino acid biosynthesis: An essential route to asparagine formation, Proc Natl Acad Sci. 99 (5) (2002) 2678-2683. http://doi.10.1073/pnas.012027399.

[281] 5ZG8, Crystal structure of TtNRS. https://www.rcsb.org/structure/5zg8 , 2018 (accessed January 2016).

[282] I. Wataru, S. Shun-ichi, K. Chizu, K. Seiki, S. Mikako, Y. Shigeyuki, Structural basis of the water-assisted asparagine recognition by aspariginyl-tRNA synthetase, J Mol Biol. 360 (2) (2006) 329-342.

[283] S. Squizzato, Y.M. Park, N. Buso, T. Gur, A. Cowley, W. Li, M. Uludag, S. Pundir, J.A. Cham, H. McWilliam, R. Lopez, The EBI Search engine: providing search and retrieval functionality for biological data from EMBL-EBI, Nucleic Acids Res. (43) (2015) 585–588. http://doi:10.1093/nar/gkv316.

[284] S.F. Ataide, M. Ibba, Small molecules: big players in the evolution of protein synthesis, ACS Chem. Biol. 1 (5) (2006) 285-297. http://doi.10.1021/cb600200k.

[285] D.T. Jones, Protein secondary structure prediction based on position-specific scoring matrices, J. Mol .Biol. 292 (2) (1999) 195-202. http://doi.10.1006/jmbi.1999.3091.

[286] The UniProt Consortium, UniProt: the universal protein knowledgebase, Nucleic Acids Res. 46 (5) (2018) 2699. https://doi.org/10.1093/nar/gky092.

[287] A.F. Gillaspy, V. Worrell, J. Orvis, B.A. Roe, D.W. Dyer, J.J. Iandolo, 2006. The *staphylococcus aureus* NCTC 8325 genome, in: v. Fischetti, R. Novick, J. Ferretti, D. Portnoy, J. Rood (Eds.), Gram positive pathogens, ASM Press, Washington, 2006, pp. 381-412.

[288] RAMPAGE Server, Ramachandran plot, http://mordred.bioc.cam.ac.uk/~rapper/rampage.php , (accessed 11 February 2020).

[289] R. Lüthy, J.U. Bowie, D. Eisenberg, Assessment of protein models with three-dimensional profiles, Nature. 356 (6364) (1992) 83-85. http://doi.10.1038/356083a0.

[290] M. Wiederstein, M.J. Sipp, ProSA-web: interactive web service for the recognition of errors in three-dimensional structures of proteins, Nucleic Acids Res. 35 (2) (2007) 407-410. https://doi.org/10.1093/nar/gkm290.

[291] S.C. Lovell, I.W. Davis, W.B. Arendall, P.I.W. de Bakker, J.M. Word, M.G. Prisant, J.S. Richardson, D.C. Richardson, Structure validation by Calpha geometry: phi,psi and Cbeta deviation, Proteins. 50 (3) (2003) 437-450. http://doi.10.1002/prot.10286.

[292] F. Sievers, D.G. Higgins, Clustal Omega for making accurate alignments of many protein sequences, Protein Sci. 27 (1) (2018) 135-145. http://doi.10.1002/pro.3290.

[293] S. Eiler, A.C. Dock-Bregeon, L. Moulinier, J.C. Thierry, D. Moras, Synthesis of aspartyl-tRNA (Asp) in *Escherichia coli*--a snapshot of the second step, EMBO J. 18 (22) (1999) 6532-6541. http://doi.10.1093/emboj/18.22.6532.

[294] K.R. KIM, S.H. PARK, H.S. Kim, K.H. Rhee, B. Kim, D.G. Kim, M.S. Park, H. Kim, S. Kim, B.W. Han, Crystal structure of human cytosolic aspartyl-tRNA synthetase, a component of multi-tRNA synthetase complex, Proteins. 81 (10) (2013) 1840-1846. http://doi.10.1002/prot.24306.

[295] D. Kern, H. Roy, H.D. Becker, Asparaginyl-tRNA synthetases. https://www.ncbi.nlm.nih.gov/books/NBK6048/ , 2000-2013 (accessed 11 February 2020).

[296] K. Shiba, H. Motegi, M. Yoshida, T. Noda, Human aspariginyl-tRNA synthetase: molecular cloning and inference of the evolutionary history of Asx-tRNA synthetase family, Nucleic Acids Res. 26 (22) (1998) 5045-5051. http://doi.10.1093/nar/26.22.5045.

[297] T. Yamane, J.J. Hopfield, Experimental evidence for kinetic proofreading in the aminoacylation of tRNA by synthetase, Proc Natl Acad Sci. 74 (6) (1977) 2246-2250. http://doi.10.1073/pnas.74.6.2246.

[298] C. Berthet-Colominas, L. Seignovert, M. Hartlein, M. Greti, S. Cusack, R. Leberman, The crystal structure of aspariginyl-tRNA synthetase from *Thermus thermophilus* and its complexes with ATP and aspariginyl-adenylate: the mechanism of discrimination between asparagine and aspartic acid, ENBO J. 17 (10) (1998) 2947-2960. http://doi.10.1093/emboj/17.10.2947.

[299] G. Archontis, T. Simonson, D. Moras, M. Karplus, Specific amino acid recognition by aspartyl-tRNA synthetase studied by free energy simulations, J. Mol. Biol. 275 (5) (1998) 823-846. http://doi.10.1006/jmbi.1997.1470.

[300] L. Ador, S. Jaeger, R. Geslain, F. Martin, J. Cavarelli, G. Eriani, Mutation and evolution of the magnesium-binding site of a class II aminoacyl-tRNA synthetase, Biochemistry. 43 (22) (2004) 7028–7037. http://doi.10.1021/bi049617.

[301] D. Thompson, T. Simonson, Molecular dynamics simulation show that bound mg^{2+} contributes to amino acid and aminoacyl adenylate binding specificity in AspRS through long range electrostatic interactions, J. Biol. chemist. 281 (2006) 23792-23803. http://doi.10.1074/jbc.M602870200.

[302] E. Schmitt, L. Moulinier, S. Fujiwara, T. Imanaka, J.C. Thierry, D. Moras, Crystal structure of aspartyl-tRNA synthetase from *pyrococcus kodakaraensis* KOD: archaeon specificity and catalytic mechanism of adenylate formation, EMBO J. 17 (1998) 5227–5237. http://doi.10.1093/emboj/17.17.5227.

[303] L. Moulinier, S. Eiler, G. Eriani, J. Gangloff, J.C. Thierry, K. Gabriel, W.H. McClain, D. Moras, The structure of an AspRS-$tRNA^{Asp}$ complex reveals a tRNA-dependent control mechanism, EMBO J. 20 (18) (2001) 5290-5301. http://doi.10.1093/emboj/20.18.5290.

[304] D. Thompson, P. Plateau, T.T. Simonson, Free-energy simulations and experiments reveal long-range electrostatic interactions and substrate-assisted specificity in an aminoacyl-tRNA synthetase, ChemBioChem. 7 (2) (2006) 337–344. http://doi.10.1002/cbic.200500364.

[305] J.D. Durrant, J.A. McCammon, Molecular dynamics simulations and drug discovery, BMC Biol. 9 (71) (2011) 1-9. http://doi10.1186/1741-7007-9-71.

[306] Schrodinger, Drug discovery. https://www.schrodinger.com/drug-discovery , (accessed 2 March 2020).

[307] L. Martinez, Automatic identification of mobile and rigid substructures in molecular dynamics simulations and fractional structural fluctuation analysis, PLoS One. 10 (3) (2015) 1-10. https://doi.org/10.1371/journal.pone.0119264.

[308] T. Hou, J. Wang, Y. Li, W. Wang, Assessing the performance of the MM/PBSA and MM/GBSA methods. 1. The accuracy of binding free energy calculations based on molecular dynamics simulations, J. Chem. Inf. Model. (51) (1) (2001) 69–82. https://doi.org/10.1021/ci100275a.

[309] L. Pang, M. Nautiyal, S. De Graef, B. Gadakh, V. Zorzini, A. Economou, S.V. Strelkov, A. Van Aerschot, S.D. Weeks, Structural insights into the binding of natural pyrimidine-based inhibitors of class II aminoacyl-tRNA synthetases, ACS Chem Biol. 15 (2) (2020) 407-415. http://doi.10.1021/acschembio.9b00887.

[310] I.T. Paulsen, L. Banerjei, G.S.A. Myers, K.E. Nelson, R. Seshadri, T.D. Read, D.E. Fouts, J.A. Eisen, S.R. Gill, J.F. Heidelberg, H. Tettelin, R.J. Dodson, L.A. Umayam, L.M. Brinkac, M.J. Beanan, S.C. Daugherty, R.T. DeBoy, S.A. Durkin, C.M. Fraser, Role of mobile DNA in the evolution of vancomycin-resistant *Enterococcus faecal*, Science. 299 (5615) (2003) 2071-2074. http://doi.10.1126/science.1080613.

[311] A. Neuenfeldt, B. Lorber, E. Ennifar, A. Gaudry, C. Sauter, M. Sissler, C. Floentz, Thermodynamic properties distinguish human mitochondrial aspartyl-tRNA synthetase from bacterial homolog with same 3D architecture, Nucleic Acids Res. 41 (4) (2013) 2698-2708. https://doi.org/10.1093/nar/gks1322.

[312] J.S. Park, M.C. Park, K.L. Lee, P.C. Goughnour, S.J. Jeong, H.S. Kim, H.J. Kim, B.J. Lee, S. Kim, B.W. Han, Unique N-terminal extension domain of human asparaginyl-tRNA synthetase elicits CCR3-mediated chemokine activity, Int J Biol Macromol. (120) (2018) 835-845. http://doi:10.1016/j.ijbiomac.2018.08.171.

[313] M. Blaise, M. Fréchin, V. Oliéric, C. Charron, C. Sauter, B. Lorber, H. Roy, D. Kern, Crystal structure of the archaeal asparagine synthetase: interrelation with aspartyl-tRNA and asparaginyl-tRNA synthetases, J Mol Biol. 412 (3) (2011) 437-452. http://http://doi.10.1016/j.jmb.2011.07.050.

[314] M.C. Peitsch, ProMod and Swiss-Model: Internet-based tools for automated comparative protein modelling, Biochem Soc Trans. (1) (1996) 274-279. http://doi.10.1042/bst0240274.

[315] M.C. Peitsch, Large scale protein modelling and model repository, Proc Int Conf Intell Syst Mol Biol. (5) (1997) 234-236. PMID: 9322042.

[316] H. Ueda, Y. Shoku, N. Hayashi, J. Mitsunaga, Y. In, M. Doi, M. Inoue, T. Ishida, X-ray crystallographic conformational study of 5'-O-[N-(L-alanyl)-sulfamoyl]adenosine, a substrate analogue for alanyl-tRNA synthetase, Biochim Biophys et Acta. 1080 (2) (1991) 126-134. https://doi.org/10.1016/0167-4838(91)90138-P.

[317] H. Belrhali, A. Yaremchuk, M. Tukalo, K. Larsen, C. Berthet-Colominas, R. Leberman, B. Beijer, B. Sproat, J. Als-Nielsen, G. Grubel, Crystal structures at 2.5 angstrom resolution of seryl-tRNA synthetase complexed with two analogs of seryl adenylate, Science. 263 (5152) (1994) 1432-1436. http://doi.10.1126/science.8128224.

[318] S. Bernier, D.Y. Dubois, M. Therrien, J. Lapointe, R. Chenevert, Synthesis of glutaminyl adenylate analogues that are inhibitors of glutaminyl-tRNA synthetase, Bioorganic Med Chem Lett. 10 (21) (2000) 2441-2444. http://doi.10.1016/s0960-894x(00)00478-9.

[319] A.K. Forrest, R.L. Jarvest, L.M. Mensah, P.J. O'Hanlon, A.J. Pope, R.J. Sheppard, Aminoalkyl adenylate and aminoacyl sulfamate intermediate analogues differing greatly in affinity for their cognate *Staphylococcus aureus* aminoacyl tRNA

synthetases, Bioorganic Med Chem Lett. 10 (16) (2000) 1871-1874. http://doi.10.1016/s0960-894x(00)00360-7.

[320] P. Brown, C.M. Richardson, L.M. Mensah, P.J. O'Hanlon, N.F. Osborne, A.J. Pope, G. Walker, Molecular recognition of tyrosinyl adenylate analogues by prokaryotic tyrosyl tRNA synthetases. Bioorg. Med. Chem. 7 (11) (1999) 2473-2485. https://doi.org/10.1016/S0968-0896(99)00192-3.

[321] J. Lee, S.U. Kang, M.K. Kang, M.W. Chun, Y.J. Jo, J.H. Kwak, S. Kim. Methionyl adenylate analogues as inhibitors of methionyl-tRNA synthetase, Bioorg. Med. Chem. Lett. 9 (10) (1999) 1365-1370. http://doi.10.1016/s0960-894x(99)00206-1.

[322] M. Ora, M. Murtola, S. Aho, M. Oivanen, Hydrolytic reactions of 3'-*N*-phosphoramidate and 3'-*N*-thiophosphoramidate analogs of thymidylyl-3', 5'-thymidine. Org. Biomol. Chem. 2 (4) (2004) 593-600. https://doi.org/10.1039/B313470A.

[323] T. Moriguchi, N. Asai, T. Wada, M. Sekine, Synthesis of nucleotide antibiotics having *N*-acyl phosphoramidate linkages. Nucleic Acids Symp. Ser. 42 (1) (1999) 15-16. https://doi.org/10.1093/nass/42.1.15.

[324] X.Y. Yu, G.M. Hill, G. Yu, W. Wang, A.F. Kluge, P. Wendler, P. Gallant, Synthesis and structure-activity relationships of a series of novel thiazoles as inhibitors of aminoacyl-tRNA synthetases. Bioorg. Med. Chem. Lett. 9 (3) (1999) 375-380. https://doi.org/10.1016/S0960-894X(98)00738-0.

[325] Y. Winum, A. Scozzafava, J.L. Montero, C.T. Supuran, Sulfamates and their therapeutic potential, Med. Res. Rev. (25) (2) (2005) 186-228. http://doi.10.1002/med.20021.

[326] W. Marc, Harrold, R.M. Zavod, Basic concepts in medicinal chemistry, 1st ed., Amer Soc of Health-System Pharm, Wisconsin, 2013.

[327] J.J. Marugan, W. Zheng, O. Motabar, N. Southall, E. Goldin, W. Westbroek, B.K. Stubblefield, E. Sidransky, R. Aungst, W. Lea, A. Simeonov, W. Leist, C. Austin, Evaluation of quinazoline analogues as glucocerebrosidase inhibitors with chaperone activity, J. Med. Chem. 54 (4) (2011) 1033–1058. https://doi.org/10.1021/jm1008902.

[328] T. Moore, B. Sidney, M. Thorn, M. Vera, *N*-Substituted derivatives of piperazine and ethylenediamine. Part I. The Preparation of *N*-monosubstituted derivatives, J. Chem. Soci. (1929) 39-51. https://doi.org/10.1039/JR9290000039.

[329] R. Baltzly, J.S. Buck, E. Lorz, W. Schon, The preparation of N-mono-substituted and unsymmetrically disubstituted piperazines, J. Am. Chem. Soc. 66 (2) (1944) 263-266. https://doi.org/10.1021/ja01230a031.

[330] D. Im, K. Jung, S. Yang, W. Aman, J.M. Hah, Discovery of 4-aryl amido 3-methyl isoxazole derivatives as novel FMS kinase inhibitors, Eur. J. Med. Chem. 102 (2015) 600-610. http://10.1016/j.ejmech.2015.08.031.

[331] C.A.G. Montalbrtt, V. Falque, Amide bond formation and peptide coupling, Tetrahedron. 61 (2005) 10827- 10825. http://doi.0.1016/j.tet.2005.08.031.

[332] A. Armstrong, L. Wenju, *N*, *N'*-Carbonyldiimidazole. https://doi.org/10.1002/9780470842898.rc024.pub2 , 2007 (accessed 15 June 2020).

[333] H.K. Hall, Field and inductive effects on the base strengths of amines. J. Am. Chem. Soci. 78 (1956) 2570-2572. https://doi.org/10.1021/ja01592a066.

[334] Clinical laboratory testing and in vitro diagnostic test systems, Susceptibility testing of infectious agents and evaluation of performance of antimicrobial susceptibility devices- Part 1: Reference methods for testing the in vitro activity of antimicrobial agents against bacteria involved in infectious diseases, ISO/FDIS 20776-1:2006. https://www.iso.org/standard/41630.html , (accessed 18 April 2020).

[335] T.T. Nguyen, K. Song, Y. Tsoy, J.Y. Kim, Y.J. Kwon, M. Kang, M.A.E. Hansen, Robust dose-response curve estimation applied to high content screening data analysis, Source Code Biol Med. 9 (1) (2014) 27. http://doi.10.1186/s13029-014-0027-x.

[336] T. Daniel, Prodrugs of pyridone amides useful as modulator of sodium channels. Patent Reference: WO2015089361, 75 https://app.dimensions.ai/details/patent/WO-2015089361-A1 , (accessed 30 May 2020).

[337] A.A. Waghmare, R.M. Hindupur, H.N. Pati, Propylphosphonic anhydride (T3P®): an expedient reagent for organic synthesis, Rev. J. Chem. 4 (2) (2014) 53-131. http://doi.org/10.1134/S2079978014020034.

[338] I. Abdelmoty, F. Albericio, L.A. Carpino, B.M. Foxman, S.A. Kates, Structural studies of reagents for peptide bond formation: crystal and molecular structures of HBTU and HATU, Lett. Pept. Sci. 1 (1994) 57-67. http://doi.org/10.1007/BF00126274.

[339] F. Albericio, M. Cases, J. Alsina, S.A. Triolo, L.A. Carpino, S.A. Kates, On the Use of PyAOP, a phosphonium salt derived from HOAt, in Solid-Phase Peptide Synthesis, Tetrahedron Lett. 38 (27) (1997) 4853-4856. https://doi.org/10.1016/S0040-4039(97)01011-3.

[340] R.D. Dimarchi, J.P. Tam, S.B.H. Kent, R.B. Merrifield, Solid phase synthesis of the protected 43–55 tridecapeptide of the heavy chain of myeloma immunoglobin M603, employing cyclohexyl ester protection for glutamic acid, Int. J. Pept. Protein Res. 19 (3) (1982) 80-88. http://doi.10.1111/j.1399-3011.1982.tb03038.x.

[341] International union of pure and applied chemistry, Compendium of chemical terminology gold book. http://goldbook.iupac.org/pdf/goldbook.pdf , 2014 (accessed 6 June 2020).

[342] R.M. Williams, P.J. Sinclair, E. Duane, D. Mong, D, Chen, D. Zhai, Asymmetric synthesis of *N-tert*-Butoxycarbonyl α-Amino Acids. Synthesis of (5S,6R)-4-tert-Butoxycarbonyl-5,6-diphenylmorpholin-2-one (4-Morpholinecarboxylic acid, 6-oxo-2,3-diphenyl-, 1,1-dimethylethyl ester, (2S,3R)-)], Organic Synthesis. 2003. https://doi.org/10.1002/0471264180.os080.03.

[343] X. ZHONG, C. Liren, T. Mengqun, T. Shengbin, M.A. Zhike, Benzenesulfonyl piperazine compounds or benzoyl piperazine compounds, preparation methods and uses thereof. https://patents.google.com/patent/CN102838567B/en , 2014 (accessed on 10 June 2020).

[344] B.J.P. Quesnel, Incomplete trifluoroacetic acid deprotection of asparagine-trityl-protecting group in the vicinity of a reduced peptide bond, J Pept Res. 52 (2) (1998) 107-111. http://doi.10.1111/j.1399-3011.1998.tb01364.x.

[345] G. Han, M. Tamaki, V.J. Hrubyfast, efficient and selective deprotection of the *tert*-butoxycarbonyl (BOC) group using HCl/ dioxane (4 M). J pept Res. 58(4) (2001) 338-341. https://doi.org/10.1034/j.1399-3011.2001.00935.x.

[346] B.J. Henderson, D.J. Carper, T.F. González-Cestari, K. Mahasenan, R.E. Pavlovicz, M.L. Dalefield, R.S. Coleman, L. Chenglong, D.B. McKay, Structure–activity relationship studies of sulfonylpiperazine analogues as novel negative allosteric modulators of human neuronal nicotinic receptors. J. Med. Chem. 54 (24) (2011) 8681-8692. http://doi.10.1021/jm201294r.

[347] M. Konoa, T. Matsumoto, T. Kawamura, A. Nishimura, Y. Kiyota, H. Oki, J. Miyazaki, S. Igaki, C.A. Behnke, M. Shimojo, M. Kori, Synthesis, SAR study, and biological evaluation of a series of piperazine ureas as fatty acid amide hydrolase (FAAH) inhibitors. Bioorg. Med. Chem. 21 (1) (2013) 28–41. http://doi.10.1016/j.bmc.2012.11.006.

[348] T.B. Windholz, D.B.R. Johnston, Trichloroethoxycarbonyl: a generally applicable protecting group. Tetrahedron Lett. 8 (27) (1967) 2555-2557. https://doi.org/10.1016/S0040-4039(00)70346-7 .

[349] E. Scapecchi, E. Martini, D. Manetti, C. Ghelardini, C. Martelli, S. Dei, N. Galeotti, L. Guandalini, M.N. Romanellia, E. Teodori, Structure–activity relationship studies on unifiram (DM232) and sunifiram (DM235), two novel and potent cognition enhancing drugs, Bioorg. Med. Chem. 12 (1) (2004) 71–85. http://http://doi.10.1016/j.bmc.2003.10.025.

[350] J.C. Sheehan, G.P. Hess, A new method of forming peptide bonds (carbodiimide). J. Am. Chem. Soc. 77 (4) (1955) 1067-1068. https://doi.org/10.1021/ja01609a099.

[351] D.H. Rich, J. Singh, The carbodiimide method in E Gross, in: J. Meienhofer (Eds.), The Peptides: analysis, synthesis, biology, Academic Press, New York, 1979, pp. 241-261.

[352] A.H.M. Schotman, Mechanism of the reaction of carbodiimides with carboxylic acids, Wiley Online Library. 110 (7) (1991) 319-324. https://doi.org/10.1002/recl.19911100704.

[353] N. Nakajima, Y. Ikada, Mechanism of amide formation by carbodiimide for bioconjugation in aqueous media, Bioconjugate Chem. 6 (1) (1995) 123-130. https://doi.org/10.1021/bc00031a015.

[354] J.V. Staros, R.W. Wright, D.M. Swingle, Enhancement by *N*-hyroxysulfosuccinimide of water soluble carbodiimide- mediated coupling reaction, Anal Biochem. 156 (1) (1986) 220-226. http://doi.10.1016/0003-2697(86)90176-4.

[355] A.G.N. Montalbeti, F. Virginie, Amide bond formation and peptide coupling, Tetrahedron. 61 (46) (2005) 10827-10852. https://doi.org/10.1016/j.tet.2005.08.031.

[356] D.S. Gaillard, S. Ward, T.R. Renaud, Achiral cyclopentadienone iron tricarbonyl complexes embedded in streptavidin: an access to artificial iron hydrogenases and application in asymmetric hydrogenation, Catal Lett. 146 (3) (2016) 564-569. https://doi.org/10.1007/s10562-015-1681-6.

[357] K. Sudheendran, D. Schmidt, W. Frey, J. Conrad, Facile synthesis of 3,5-diaryl-1,2,4-triazoles via copper-catalyzed domino nucleophilic substitution/oxidative cyclisation using amidines or imidates as substrates, Tetrahedron. 70 (2014) 1635-1645. http://doi.10.1016/j.tet.2014.01.019.

[358] J.A. Smith, H. Taylor, Synthesis of *N*-substituted amidines of potential pharmacological activity. J. Pharm. Pharmaol. 15 (1) (1963) 548-551. https://doi.org/10.1111/j.2042-7158.1963.tb12832.x.

[359] Z. Xu, L.K. Thompson, Fundamentals: ligands, complexes, synthesis, purification and structure, in: A. McCleverty, T.J. Meyer, (Eds.), Comprehensive coordination chemistry II, Elsevier Science, 2003.

[360] P. Bibek, B. Subhasis, Importance of piperidine moiety in medicinal chemistry research: a review. J. Pharm. Res. 5 (12) (2012) 5493-5509. https://scholar.google.com/scholar_lookup?title=Importance%20of%20piperidine%20moiety%20in%20medicinal%20chemistry%20research%3A%20a%20review&journal=J%20Pharm%20Res&volume=5&pages=5493-5509&publication_year=2012&author=Pati%2CB&author=Banerjee%2CS.

[361] S. Kang, Y.M. Kim, R.Y. Kim, M.J. Seo, Z. No, K. Nam, Synthesis and structure activity studies of side chain analogues of the antitubercular agent Q203. Eur. J. Med. Chem. 125 (2017) 807-815. http://doi.10.1016/j.ejmech.2016.09.082.

[362] D.F. Bruhn, M.S. Scherman, L.K. Woolhiser, D.B. Madhura, M.M. Maddox, A.P. Singh, R.B. Lee, J.G. Hurdle, M.R. McNeil, Pentacyclic nitrofurans with in vivo efficacy and activity against nonreplicating *Mycobacterium tuberculosis*. PLoS One. 9 (2) (2014) 87909. http://doi.10.1371/journal.pone.0087909.

[363] K. Kaneyoshi, Preparation of indolylpropanoyltetrahydroquinoline derivatives with inhibition binding of somatostatin. PCT Int. Appl. 2001025228. (2001).

[364] O. Mitsunobu, M. Yamada, T.B. Mukaiyama, Preparation of esters of phosphoric acid by the reaction of trivalent phosphorus compound with diethyl azodicarboxylate in the presence of alcohols, Chem. Soc. Jpn. 40 (4) (1967) 935–939. https://doi.org/10.1246/bcsj.40.935.

[365] O. Mitsunobu, M.B. Yamada, Preparation of esters of carboxylic and phosphoric acid via quaternary phosphonium salts, Chem. Soc. Jpn. 40 (10) (1967) 2380–2382. https://doi.org/10.1246/bcsj.40.2380.

[366] S. Fletcher, The Mitsunobu reaction in the 21 century, Org. Chem. Front. 2 (2015) 739-752. https://doi.org/10.1039/C5QO00016E.

[367] K.C. Kumara, N.N. Swamy, K. Bhuvan, E. Balaraman, K.V.P. Kumar, Mitsunobu and related reactions: advances and applications, Chem. Rev. 109 (6) (2009) 2551-2651. https://doi.org/10.1021/cr800278z.

[368] T.Y.S. But, P.H. Toy, The Mitsunobu reaction: origin, mechanism, improvements, and applications, Chem.–Asian J. 2 (11) (2007) 1340-1355. http://doi.10.1002/asia.200700182.

[369] H.J. Shine, A.K.M. Hoque, Formation of 1,2,4-triazoles by cation radical induced oxidative addition of aryl hydrazones of benzaldehyde and butyraldehyde to nitriles, J. Org. Chem. 53 (18) (1988) 4349-4353. https://doi.org/10.1021/jo00253a029.

[370] World Health Organization, Antibiotic resistance. WWW.who.int , 2020 (accessed 29 November 2020).

[371] D.A. Gray, M. Wenzel, Multitarget approaches against multiresistant superbugs, ACS infect. Dis. 6 (6) (2020) 1346-1365. https://doi.org/10.1021/acsinfecdis.0c00001.